Universitá di Genova

Tesi di dottorato in Fluidodinamica e Processi dell'Ingegneria Ambientale

On Rayleigh's criterion of thermo-acoustics

Rationale, generalisation and connection with thermodynamics

Author:
Andrea Di Vita

Supervisor:
Prof. Alessandro Bottaro

Reviewer:
Prof. Giampiero Colonna

Et ignem regunt numeri (*Numbers rule fire too*)

Jean Baptiste Joseph Fourier (quoting Plato) *Théorie analytique de la chaleur* (1822)

Acknowledgements

It is impossible to recall the names of all those people who made this work possible. To start with, my wife and my daughter have put up with my mumbling strange words and obscure computations: their patience is equal to their love.

I am indebted to my supervisor and my reviewer for their time and conscientiousness in thoroughly examining this paper. They helped mold it into form and removed hopefully all the errors. Their continuous support and encouragement were key factors in the completion of this work.

In particular, I would like to express my special thanks to Prof. A. Bottaro for bearing my endless monologue on thermodynamics, stability and the like while trying to introduce me to the beauty of fluid dynamics. Also, I owe Prof. G. Colonna a deeper insight in the intricacies of electric conduction in premixed flames.

Ansaldo Sviluppo Energia -the firm I am currently employed- is a unique environment where innovation meets the needs of production in the world of heavy-duty gas turbines. The present work is the final outcome of three years of person-power -no tiny effort indeed from the point of view of the payroll office, an effort authorised by the valiant decision of Dr. F. Bonzani. I hope it was worth it.

One of the results of practical interest of the present work -the possible stabilisation of humming with the help of electromagnetic waves in the GHz frequency range- is the result of a collaboration with CNR - IMIP (Consiglio Nazionale delle Ricerche - Istituto di Metodologie Inorganiche e dei Plasmi)

I would like to thank Dr. V. Anisimov for providing me with information both on precessing vortex core and on the work of Rauschenbach, usually overlooked in today's thermoacoustic community, as well as for his sharp criticism of my initial approach to the slippery concept of flame thickness.

Dr. G. D. Barbarino has provided me with many pictures of gas turbines.

Dr. G. Campa has often acted as a fast, on-line specialised dictionary.

Dr. C. Coppola has supplied the input data for the computation of electric conductivity.

Dr. F. Dacca′ has called my attention on the possible effect of electric fields on pollution.

Dr. D. Iurashev has provided me with bibliography concerning swirled flames.

I owe Dr. A. Pesenti all information concerning the behaviour of humming vs. environment humidity in heavy-duty gas turbines.

Dr. C. Piana has stressed the weak points in my discussion of Le Châtelier's principle.

Dr. S. Rizzo has discussed with me some practical issues concerning active control of humming.

And to conclude this far-from-complete list, no work about the impact of electromagnetic fields on the stability of flames, as described by Rayleigh's criterion, would have been possible without the ceaseless encouragement and the productive critique of Dr. E. Cosatto.

Contents

List of variables and acronyms

Latin [1]

a, b	generic quantities
$\overline{a}$	Fourier transform of a
$\widehat{a}$	non-oscillating, time-dependent multiplicative factor in a
a_*	maximum value attained by a in the flame in a period τ
a_M	maximum value attained by a everywhere in a period τ
$(a)_n$	when computing a, all Y_k's are kept fixed
$\langle a \rangle$	average of a on time
$\langle a \rangle_f$	average of a on the flame surface and weighted by the Rayleigh index
$\langle a \rangle_s$	local, turbulent-surface-average of a (see eq. (5.79) of Ref. [4])
$a\|_u^d$	$a_d - a_u$
$\mathbf{a}$	generic vector quantity
$\mathbf{a}_\perp$	$(\mathbf{a} \cdot \mathbf{n})\,\mathbf{n}$
$\mathbf{a}_\parallel$	$\mathbf{a} - \mathbf{a}_\perp$
a_b, a_c	generic, bilinear quantities in the a_0's and the a_1's
A	positive constant quantity
A_b	boundary surface of the system (i.e. of a combustor)
A_f	flame area
A_ψ	surface bounded by iso-ψ surfaces in the meridian plane

[1] Some symbols have different meanings in different Chapters, due to the different formalism of different bibliographical references. In case, all meanings are listed. However, it turns out that the meaning of each variable is always obvious from the context.

$ALFA$	$\dfrac{\lvert\mathbf{m}\rvert}{\pi R_b^2}\sqrt{\dfrac{1}{2\cdot\rho_u\cdot\lvert p\rvert_{u\rvert}^{d}}}$
B	positive constant quantity
B	$\int_V d\mathbf{x}\left(\dfrac{p_1^2}{2\rho_0 c_{s0}^2}\right)$
c	speed of light in vacuum
c_n	coefficient multiplying ϕ_n
c_N	dimensionless curvature
c_p	specific heat per unit mass at constant pressure
c_s	speed of sound
c_v	specific heat per unit mass at constant volume
$c_1, c_2, c_3, c_4, c_5, c_6, c_\mu$	constant quantities
C	$K+B$
$d\mathbf{a}$	surface element vector
d_0	thickness of RF absorption region
D	Rayleigh's index
D_b	diameter of the combustor, $= 2\cdot R_b$
D_f	positive quantity, such that $D = D_f\cdot\delta\left(G\right)$
D_ξ	$-\mathbf{m}_1\cdot\zeta_1 - \langle\mathbf{m}_1\cdot\zeta_1\rangle$
D_s	$-\left(\mathbf{m}_1 s_1\right)\cdot\nabla\langle T\rangle + \langle\mathbf{m}\rangle\cdot\left(s_1\nabla T_1\right) - \langle\mathbf{m}_1 s_1\rangle\cdot\nabla T + \mathbf{m}\cdot\langle s_1\nabla T_1\rangle$
D_{Q_*}	$T_1 Q_{*1} + \langle T_1 Q_{*1}\rangle$
D_{Q^*}	$T_1 Q_1^* + \langle T_1 Q_1^*\rangle$
D_ψ	$\mathbf{m}_1\cdot\psi_1 + \langle\mathbf{m}_1\cdot\psi_1\rangle$
D_{ψ^*}	$\mathbf{m}_1\cdot\psi_1^* + \langle\mathbf{m}_1\cdot\psi_1^*\rangle$
D_{Y_k}	$g_1\nabla\cdot\mathbf{m}_1 + \langle g_1\nabla\cdot\mathbf{m}_1\rangle + \sum_{k=1}^{N-1}\left(g_{1k}\Omega_{1k} + \langle g_{1k}\Omega_{1k}\rangle\right)$
Da	Damkoehler number on the length scale l_T
e	$1.6\cdot 10^{-19}C$
$\mathbf{e}_\chi$	unit vector in the azimuthal direction

E	argument of the partial time derivative in Rayleigh's criterion and Myers' corollary
E_{thr}	threshold on E_{RF}
E_{RF}	RF electric field
f	shape-related quantity, generatrix of an axisymmetric flame
f	$\int^s ds'\zeta \exp\left(\frac{s'}{c_p}\right)$
f_{FTF}	flame transfer function
F	function of ψ; $\equiv rv_\chi$
F_{max}	constant quantity
Fr	Froude number
g	Gibbs' free energy per unit mass, $\equiv h - Ts$
g	shape-related quantity, $\equiv \ln F$
g_k	chemical potential per unit mass of the k-th chemical species
g_r	growth rate
g_{max}	maximum growth rate
G	function of $\mathbf{x}$; $G =$ const. at the flame
G	constant quantity, lower-bounded everywhere at all times
H	enthalpy
h	$u + \frac{p}{\rho}$
h	typical elongation length $\frac{\varphi}{\frac{d\varphi}{dz}}$
h_k	enthalpy per unit mass of the k-th chemical species
H	$h + \frac{\lvert\mathbf{v}\rvert^2}{2}$
H_{LHV}	lower heating value
He	Helmholtz number
I	$\int_V d\mathbf{x}\frac{\rho_0}{2}\lvert\xi\rvert^2$
I_σ	dimensionless, monotonically increasing function of T
$\Im\{a\}$	imaginary part of a

J	Jacobian
k	function of T which plays the role of Arrhenius' coefficient
k	swirl-related quantity $\equiv \dfrac{\sqrt{3}S_w D_b}{h}$
k_B	$1.38 \cdot 10^{-23} J \cdot K^{-1}$
k_{cr}	value of the swirl-related k at commutation
k_{cr-A}	value of the swirl-related k at anticommutation
k_{Ra}	constant, dimensionless quantity
$\mathbf{k}$	wave number vector
$\mathbf{k}_{RF}$	RF wave number vector
K	curvature of an axisymmetric flame in the meridian plane
K	$\int_V d\mathbf{x}\rho_0 \lvert\dfrac{\partial \xi}{\partial t}\rvert^2$
K^b	reverse Arrhenius coefficient
K^f	Arrhenius coefficient
K	$F_{max}T_{0max}$
K_{tot}	total curvature
l	arc length
l_{tip}	arc length at the flame tip
l_T	$\dfrac{Re_T \nu}{u'}$
L	Lagrangian density
L	typical linear dimension of the system
L_r	reduced Lagrangian density
m_{air}	$2.8 \cdot 10^{-2} Kg$
m_e	$9.1 \cdot 10^{-31} Kg$
$\mathbf{m}$	$\rho\mathbf{v}$
m_N	dimensionless impinging mass flow
M	Mach number

M_v	auxiliary Lagrangian density
Ma	Markstein number
n	number of chemical species
n_e	density of free electrons
n_{FTF}	parameter in a $n-\tau$ transfer function
n_n	density of neutrals
$\mathbf{n}$	unit vector, perpendicular to the flame ($\mathbf{n}\cdot\mathbf{v}_u<0$)
$\mathbf{n}_N$	$-\mathbf{n}$
N_{Av}	Avogadro number
p	pressure
p_N	dimensionless pressure
P	$P_h-\nabla\cdot\mathbf{q}$
P_a	density of RF power absorbed in the flame
P_i	density of RF power impinging on the flame
P_r	density of RF power reflected by the flame
P_t	density of RF power transmitted across the flame
Pe	Peclet number
P_0	positive constant quantity
P_h	$Q+\Phi$
P^*	function of $\mathbf{x}$; $\int d\mathbf{x}P^*=\dfrac{W_c}{P_0}$
$\mathbf{q}$	heat flux due to conduction (and, possibly, radiation)
q_{RF}	quality factor of the RF cavity
q	$\dfrac{1}{2\pi}\dfrac{d\varphi}{d\psi}$
$\mathbf{q}$	heat flow due to heat conduction and radiation
Q	amount of heat produced by combustion per unit time and volume
Q_C	total amount of heat which flows into a cold body per unit time
Q_H	total amount of heat which flows out from a hot body per unit time

Q_*	$\frac{1}{T}\left[-\nabla\cdot(\lambda\nabla T)+\rho\nabla\cdot\left(\sum_{k=1}^{n}h_kY_k\mathbf{V}_k\right)+\Phi+Q\right]$
Q^*	$-\frac{1}{T}\left[\sum_{k=1}^{n}g_k\omega_k+\sum_{k=1}^{n}g_k\nabla\cdot(\rho\mathbf{V}_kY_k)\right]$
r	c_p-c_v
r	radial coordinate
r_1	radial coordinate of a flame anchor point
r_A	lower bound on the range of integration in dr
r_B	upper bound on the range of integration in dr
r_{max}	upper bound on the integration range for computation of W_c
R_b	radius of the combustor
R_f	RF reflection coefficient
R_{in}	distance of upstream flow pattern from symmetry axis
R_v	axial average of R_{vort}
R_{vort}	half radial size of upstream flow pattern
Re	Reynolds' number
Re_T	turbulent Reynolds' number
$\Re\{a\}$	real part of a
s	entropy per unit mass
s_d	displacement speed
s_L	laminar flame velocity
s_T	turbulent flame velocity
S	entropy
S_{max}	maximum value of S_{tot} during an oscillation
S_{min}	minimum value of S_{tot} during an oscillation
S_{tot}	total amount of entropy inside the combustor
S_w	swirl-related quantity, $\equiv\sqrt{2\pi q\left(\psi_0\right)\frac{1}{\psi_b-\psi_0}\int_{\psi_0}^{\psi_b}q\,d\psi}$
S_N	swirl number
St	Strouhal number

t	time
t_0	initial time
T	temperature
T_f	estimate of T inside the flame, $\dfrac{\int d\mathbf{x} P_h}{\int d\mathbf{x} \dfrac{P_h}{T}}$
T_f	function of $\mathbf{x}$, temperature inside the flame, $T_u \leq T_f \leq T_d$
T_f	estimate of T inside the reaction zone of the flame, $\approx T_d$
T_{ref}	constant addictive factor
u	internal energy per unit mass
u'	typical amplitude of turbulent velocity fluctuations
$\mathbf{u}$	velocity of a point on the boundary of Ω
U	total energy of an isentropic perturbation of a fluid initially at rest
U	total internal energy
U_{RF}	total RF energy
v_{ave}	mean velocity of free electrons
v_r	radial component of velocity
v_z	axial component of velocity
v_χ	azimuthal component of velocity
$\mathbf{v}$	velocity
$\mathbf{v}_k$	diffusion velocity of the k-th chemical species
V	volume
V_b	combustor volume
V_d	volume of the downstream region, occupied by unburnt gases
V_f	flame volume
V_{max}	maximum value of V_u during an oscillation
V_{min}	minimum value of V_u during an oscillation
V_r	$A_f \cdot \dfrac{\delta_L}{Ze}$

V_u	volume of the upstream region, occupied by burnt gases
$\mathbf{V}$	constant, uniform velocity
W_{ant}	power at the RF antenna
W_c	heat release
W_{loss}	RF power losses
W_{RF}	total RF power absorbed at the flame
$W_{threshold}$	threshold value for W_c
$\mathbf{x}$	position vector
Y_k	mass fraction of the k-th chemical species
$\mathbf{W}$	integrand in the surface integral in Rayleigh's criterion and Myers' corollary
z	axial coordinate
Ze	Zel'dovich number

Greek

α	function of T_u
β	opening angle
β_c	auxiliary scalar quantity
β_{swirl}	angle between a swirler blade and the axis of symmetry
γ	$\frac{c_p}{c_v}$
Γ	swirl-related quantity $\left(\frac{S_w}{h}\right)^2 \frac{(2\pi\psi_0)}{s_L}$
δ_L	laminar flame thickness
δ_T	turbulent flame thickness (according to Ref. [112])
ΔA_q	flame area element
$\Delta h^0_{f,k}$	formation enthalpy per unit mass at 300 K of the k-th chemical species
Δp	pressure perturbation amplitude
ΔS	net amount of entropy flowing per unit time
ΔV	$V_{max} - V_{min}$
ϵ	dimensionless quantity, $0 < \lvert\epsilon\rvert \leq 1$
ϵ_{turb}	mechanical power per unit mass dissipated in turbulence
ϵ_0	$8.85 \cdot 10^{-12} F \cdot m^{-1}$
ζ	function of $\mathbf{x}$, Lagrange multiplier
ζ	normalised pressure drop across the flame
ζ	constant, positive quantity
ζ	$(\nabla \wedge \mathbf{v}) \wedge \mathbf{v}$
η	$\tan(\eta)$ slope of axisymmetric flame in the meridian plane
η	initial condition on ξ
η_K	Kolmogorov length
ϑ	function of $\mathbf{x}$, Lagrange multiplier
θ	Lagrange multiplier; $\nabla\theta = 0$

Θ	auxiliary vector field; $P_h = \nabla \cdot \Theta$
ι	$\frac{4\pi^2\theta}{s_L}\,(1+\varpi)$
κ_{st}	flame stretch
λ	thermal conductivity
λ	function of $\mathbf{x}$, Lagrange multiplier
λ_D	Debye length
λ_{RF}	RF wavelength
μ	function of $\mathbf{x}$, Lagrange multiplier
μ	reciprocal of typical length, $\equiv -\frac{\theta}{2\pi s_L}$
ν	kinematic viscosity
ν	function of $\mathbf{x}$, Lagrange multiplier
ν	electron collision frequency
ν_{RF}	frequency of RF field
ξ	displacement of a small element of fluid
ξ	function of $\mathbf{x}$, Lagrange multiplier
Ξ	wrinkling factor, $\equiv \frac{s_T}{s_L}$
ϖ	shape-related quantity, $\equiv \min\left(\lvert f'\rvert^2\right)$
Π	viscous stress tensor
ρ	mass density
σ	electric conductivity of the flame
$\overline{\sigma}$	spatial average of σ on the reaction zone of thickness $\frac{\delta_L}{Ze}$
ς	shape-related, qconstant quantity
σ_{coll}	total electron-neutral cross-section
Σ	arbitrary surface
τ	oscillation period
τ_{FTF}	parameter in a $n-\tau$ transfer function

τ_K	reciprocal of stretch of turbulent eddies on the Kolmogorov scale
τ_L	value of τ_{res} for a laminar flame
τ_{res}	residence time of the flow across the flame
τ_{RF}	duration of one RF burst
τ_T	value of τ_{res} for a turbulent flame
τ_1	lower bound on τ
τ_2	upper bound on τ
τ_σ	time-scale of the ramp-up of σ
υ	shape-related, constant quantity
ϕ	equivalence ratio
ϕ	function of $\mathbf{x}$; auxiliary scalar field
ϕ_n	eigenfunction
φ	flux of υ_χ across A_ψ
Φ	viscous power density
χ	azimuthal coordinate
χ	function of $\mathbf{x}$, progress variable, $0 \le \chi \le 1$
ψ	stream function
ψ_i	$\dfrac{1}{\rho}\dfrac{\partial \Pi_{ij}}{\partial x_i}$
ψ_0	extremum of integration
ψ^*	$\sum_{k=1}^{n} g_k \nabla Y_k$
ω	oscillation pulsation
ω_k	production rate of the k-th chemical species
ω_n	eigenfrequency corresponding to ϕ_n
ω_{n0}	value of ω_n computed for $\frac{\partial Q_1}{\partial t} = 0$
ω_p	electron plasma frequency
ω_{RF}	$2\pi\nu_{RF}$
Ω	domain of integration in three-dimensional space
Ω_k	$\omega_k - \nabla \cdot (\rho \mathbf{V}_k Y_k) - \nabla \cdot (\mathbf{m} Y_k)$

Superscripts and subscripts

$_0$	quantity in the unperturbed state (unless otherwise defined)
$_1$	perturbation
$_+$	quantity in the open configuration
$_-$	quantity in the closed configuration
$_{air}$	quantity referred to air
$_{amb}$	quantity referred to the environment
$_b$	quantity in the boundary of the system combustor + flame + fluid
$_c$	quantity referred to a cold body
$_d$	quantity referred to the downstream side of the premixed flame (burnt gases)
$_f$	quantity in the flame
$_{fuel}$	quantity referred to the fuel
$_h$	quantity referred to a hot body
$_{inlet}$	quantity referred to the inlet
$_k$	quantity referred to the k-th chemical species
$_s$	quantity referred to a slot
$_u$	quantity referred to the upstream side of the premixed flame (unburnt gases)
$_w$	quantity referred to a wall
^{K}	quantity in the frame of reference moving at velocity $\mathbf{V}$ with respect to the lab
∇_N	$L \cdot \nabla$

Part I

The problem

Chapter 1

Combustion instability

The words *combustion instability* refer to a broad range of processes giving rise to oscillations in heat release and resonant coupling between combustion and acoustics and resulting in sound emission, structural vibrations, intensified heat fluxes to the walls of the combustor [1].

Combustion instability is a current research topic of *thermo-acoustics*, which investigates sound in fluids where thermal processes occur. In particular, combustion instability raises difficult issues and constitutes a challenging area in combustion research. Under normal operating conditions (often affected by turbulence), flames [1] generate heat-release rate fluctuations that seem to be essentially incoherent. Under unstable operation, a resonant loop is established among the flow (which may carry various types of disturbances), combustion (which feeds the oscillation with energy), and the acoustic modes of the system (which are responsible for sound emission). This feedback synchronizes heat-release rate and pressure perturbations of pressure and temperature. For example, Fig. 1.1 displays such feedback in a combustor with a *premixed* flame [2]. In the following, we are going to consider premixed flames only.

The above described feedback can give rise to large oscillation levels that may have detrimental consequences. Enhanced heat fluxes to the combustor walls and intense vibrations lead to mechanical failure and in extreme cases to destruction of the system. Such phenomena are specifically damaging in devices with large power densities, a situation prevailing in high-pressure systems (gas turbines, aeroengines, liquid propellant rockets). Combustion instability seems to be particularly dangerous in *lean* combustion, i.e. whenever the relative fraction of oxidizer in the mixture of unburnt gases which impinges on the flame is more than enough to ensure complete combustion of all the available fuel [3]. Recent issues in combustion instability are found in modern *(heavy-duty) gas turbines for power production* (GT), which rely on lean, premixed combustion to reduce polluting

[1] A *flame* is a self-sustaining propagation of a localised combustion zone at subsonic velocities [2].

[2] In *premixed combustion*, fuel and oxidizer are mixed before they undergo combustion.

[3] An equivalent definition of *lean combustion* is that $\phi < 1$, where the *equivalence ratio* ϕ is defined as the ratio between the value of the ratio of fuel mass fraction and oxidyzer mass fraction and the corresponding value in stoichiometric combustion [4]. In lean combustion, no fuel remains in the burnt gases. In contrast, *stoichiometric* combustion (no oxidizer and no fuel remains in the burnt gases) and *rich* combustion correspond to $\phi = 1$ and $\phi > 1$ respectively.

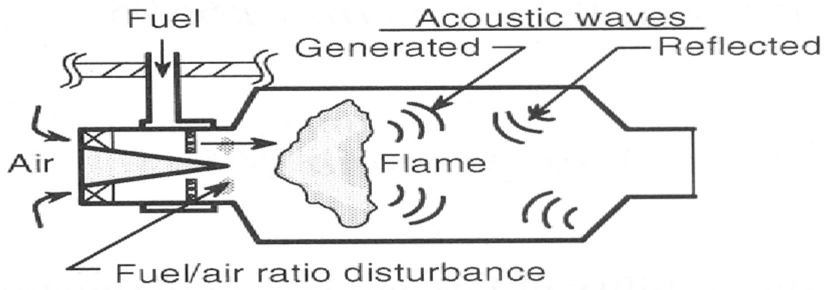

Figure 1.1: *An example of feedback in thermo-acoustics. The fuel/air mixture flows from the inlet (on the left) towards the flame. It may carry perturbations of fuel/air ratio, which affect the heat release due to combustion at the flame. The resulting oscillations of heat release produce acoustic waves, which start from the flame are reflected on the combustor walls. This occurs both downstream (in the region of burnt gases) and upstream (in the region of unburnt gases). In turn, acoustic flames reflecting on the upstream side, near the fuel/air inlet, may trigger perturbations of fuel/air ratio [3], and a feedback is established. Other perturbations carried by the flow towards the flame are perturbations of vorticity, which affect the shape -hence the heat release- of swirl-stabilised flames. Vorticity perturbations may be e.g. produced by upstream reflection of acoustic waves on the inclined swirler blades [1].*

emissions -see e.g. Fig. 1.2- but are more sensitive to resonant coupling, leading to instability [1]. The present work focusses on GT, while still having in mind possible connections of the combustion instability problem with other problems of physics and engineering.

In order to help the reader to figure out what we are speaking about, here are some information about GT. Before entering the turbine, the air -previously compressed- gets heated by one or more combustors. Fig. 1.3 displays the core of a typical GT. Some GT include 24 combustors, symmetrically located all around the symmetry axis (Fig. 1.4). Each combustor is fed with air and fuel; it includes a burner, a plenum, and a combustion chamber which embeds a flame. Fig. 1.5 displays a conceptual lay-out of one combustor. Fig. 1.6 displays a cross section of a GT, where the location of one burner and of the corresponding combustion chamber are highlighted. Typical values for the combustors of the displayed GT are $p_0 = 17.7$ bar, total (air + fuel) mass flow 28.2 Kg/s, temperature at the inlet 882 K and fuel molar fraction 0.04.

In the GT community, the popular nickname for a destructive combustion instability

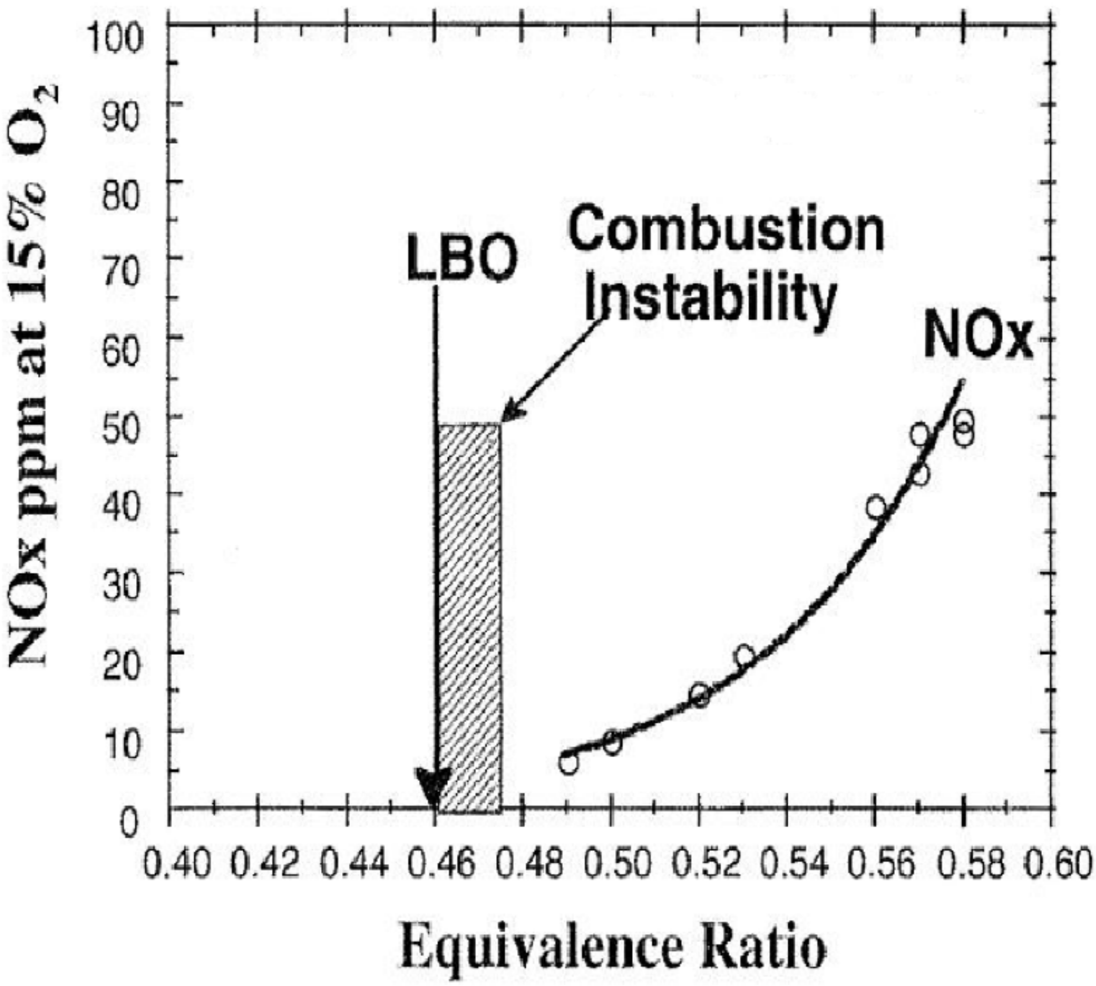

Figure 1.2: *As the equivalence ratio decreases, NO_x formation reduces - from Ref. [5]. In lean combustion the flame temperature is reduced due to an excess of air, as combustion occurs at low equivalence ratios. A decrease in (thermal) NO_x formation follows. Below the lean blow-out (LBO) limit there is just no fuel enough to sustain combustion.*

is *humming* [4]. Fig. 1.7 displays a typical signal $\dfrac{\Delta p}{p_0}$ as a function of time when humming occurs in a GT combustor. Here Δp and p_0 are humming amplitude and unperturbed pressure respectively. Typically a cycle has a duration $\tau \approx 1 - 10$ ms. As for the order of magnitude, $p_0 \approx O\left(10\right)$ bar $\approx O\left(10^6\right)$ Pa, then $\dfrac{\Delta p}{p_0} = 0.01$ corresponds to $\Delta p \approx O\left(100\right)$ mbar $\approx O\left(10^4\right)$ Pa.

In order to grasp the physical implications of Fig. 1.7, we recall that sound is understood in terms of pressure variations accompanied by an oscillating motion of a medium.

[4] A common witness' remark is that the system 'hums' when the catastrophe occurs.

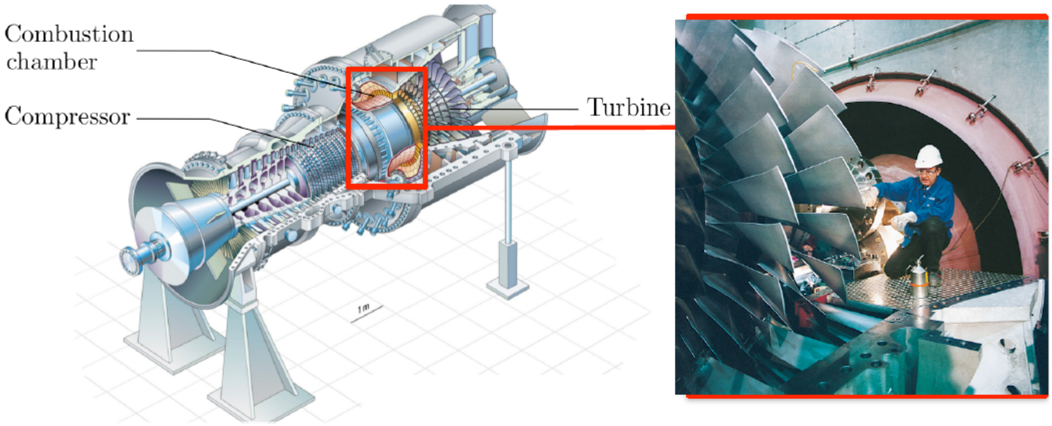

Figure 1.3: *The core of a typical GT. Air flows in the direction from the compressor (on the left) to the turbine (on the right). Before entering the turbine, it gets heated by the combustors, symmetrically located all around the symmetry axis (not displayed here; they are connected to the yellow region in the figure).*

Generally speaking, compression and rarefaction lead to heating and cooling respectively. Thus, sound propagation is *always* involved with heat -as a matter of principle at least- even if no net source of heat is present. When it comes to ordinary speech, however, pressure variations are about 0.05 Pa, and correspond to temperature variations and displacements of small mass elements of air of $\approx 40\mu$K and $\approx 0.2\mu$m respectively. So, the thermal effects of sound cannot be observed in daily life. Since such effects are commonly related to irreversible processes like e.g. heat transport, hence to growth of entropy, a common approximation is that sound propagation is adiabatic, i.e. it leaves entropy unchanged. Remarkably, if we apply the same approximation when $\Delta p = 3 \cdot 10^4$ Pa we get 24 K and 10 cm respectively. These variations are due to sound propagation only, as we have taken in account no oscillation of the heat source. This result casts doubt on the relevance of the adiabatic approximation when it comes to humming in GT. It shows also that humming severely affects the flow inside the combustor, as even the oscillation velocity of a small fluid mass element undergoing a 1-cm oscillation at $\tau \approx 10$ ms is of the same order of magnitude of the velocity of the flow in a GT combustor without humming.

Fig. 1.8 displays the effect of humming on the combustor walls. If the combustion chamber which embeds the flame has a linear size ≈ 1 m, then 10^4-Pa humming leads to a mechanical stress $\approx 10^4$ N ≈ 1000 tons on the chamber walls, oscillating with period

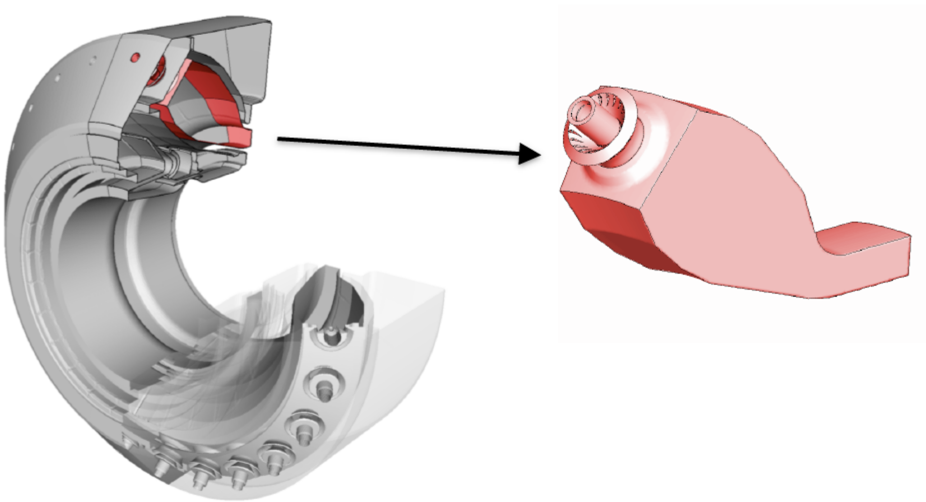

Figure 1.4: *Each combustor (rose) is part of a ring-shaped structure (grey) which encircles the symmetry axis of the GT.*

τ. This is enough to induce severe damage in most cases -let alone the thermal stresses. From the financial point of view, a rough estimate of humming-related costs over all the world (including repair and substitution of damaged components) is $>$ 1 billion \$/yr.

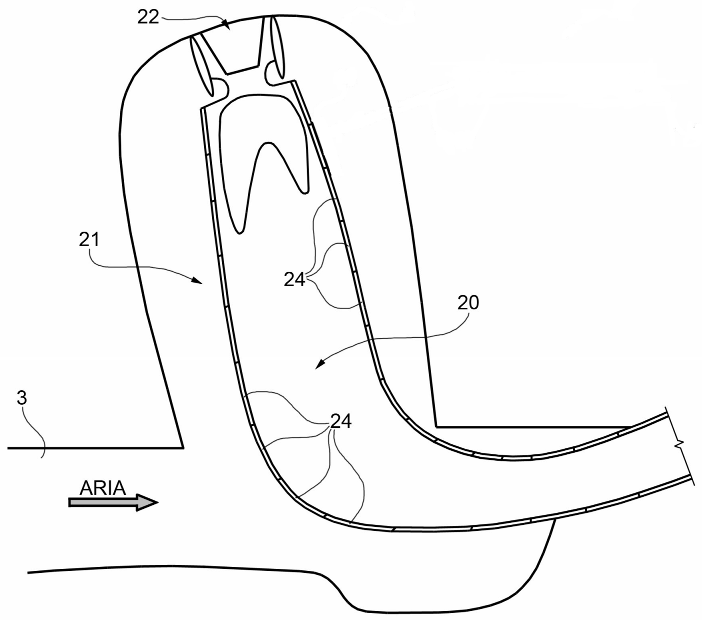

Figure 1.5: *Conceptual lay-out of a combustor in a GT (from an Ansaldo Energia patent). Combustion occurs in a combustion chamber (20) embedded in a plenum (21). The latter feeds the former with air, which comes from an air intake (3). The inner walls of the combustion chamber are coated with ceramic tiles (24). Fuel enters the system through (22). The C-shaped figure inside the combustion chamber stands for the flame.*

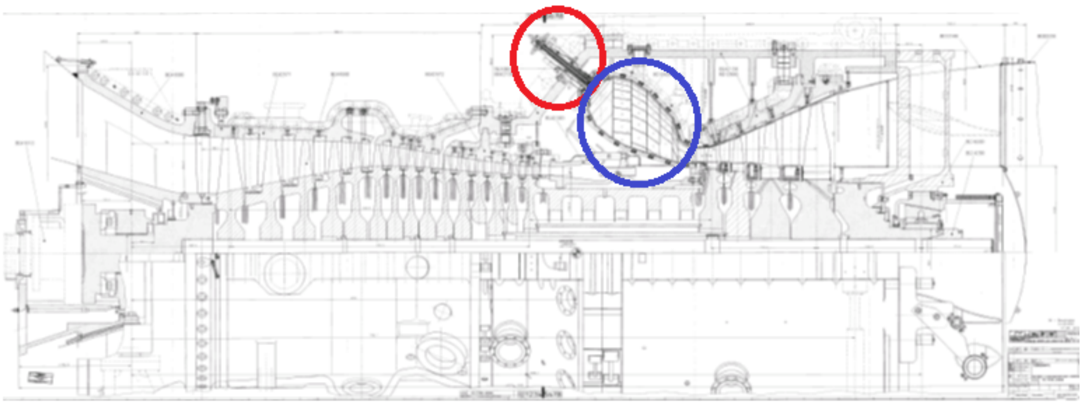

Figure 1.6: *An example of GT cross section. The red and the blue circles embed a burner and the corresponding combustion chamber respectively.*

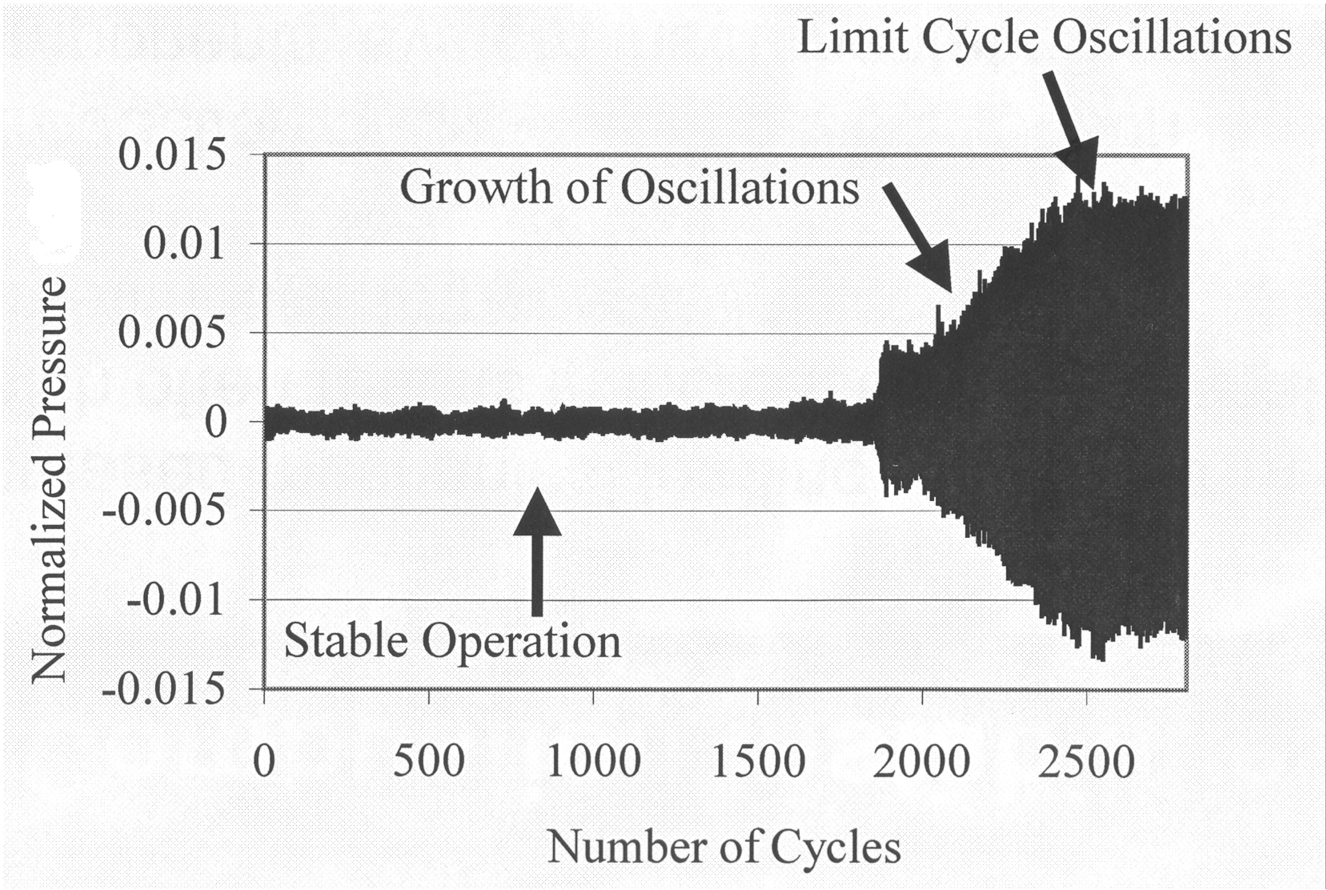

Figure 1.7: $\dfrac{\Delta p}{p_0}$ *(dimensionless) vs. time (number of cycles). Some non-linear models describe humming as a limit cycle -basically, a stable, periodic oscillation- hence the title. Remarkably, the ramp-up has no clear exponential dependence on time, in contrast with the predictions of a widely popular class of linear models.*

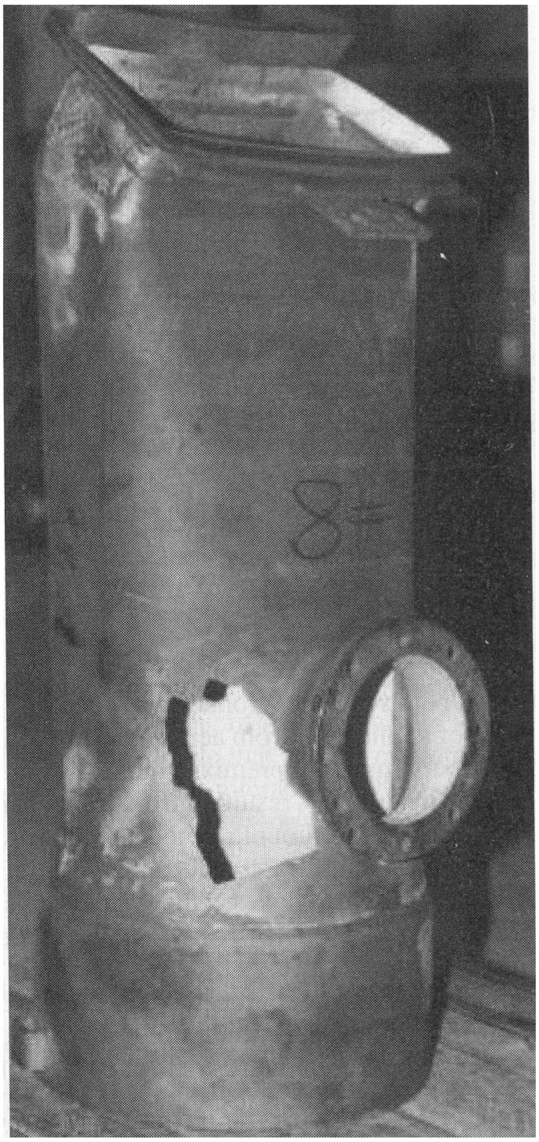

Figure 1.8: *A component of a combustor after humming has occurred.*

Chapter 2

A bit of taxonomy

Before further discussion, we recall that combustion instability is definitely far from being the only instability which may affect premixed flames. For example, even if:

- the combustion processes have been properly ignited [1];
- the flame is described as a mathematical surface in space, or, more generally, as a volume with negligible thickness [2], as $Da >> 1$, $He << 1$, and $Pe >> 1$,

the temperature jump across the flame, the combined effects of heat and particle diffusion and gravity may still trigger Darrieus-Landau [8] (Fig. 2.1), thermo-diffusion (Fig. 2.2) and Rayleigh-Taylor instability respectively [9].

And even if

[1] This requires that the relative abundance of fuel and air lies in the so-called *flammability limit*. No flame is ignited if either too few fuel or too few air is present. Of course, GT manufacturers are supposed to be able to fix this problem effectively.

[2] This is typically the case where both $Da >> 1$, $Pe >> 1$ (*thin* flame), and $He << 1$ (*acoustically thin* flame) Da, Pe and He and being the Damkoehler number [4], i.e. the ratio of convective time-scale and chemical time-scale, the Peclet number [6], i.e. the ratio of the typical linear size L of the combustor and the flame thickness, and the Helmholtz number [7], i.e. the ratio the flame thickness and the typical wavelength of combustion instability.

- As for $Da >> 1$, it implies that combustion and other chemical reactions are so fast that they allow the flame where they occur to be much thinner than the typical flow structures. If turbulence occurs and if many chemical reactions are simultaneously taken into account, rigorously speaking a Damkoehler number is to be defined for each chemical reaction and each length-scale involved in the turbulent spectrum separately. Usually, the condition $Da \gg 1$ is not true for the tiniest turbulent whirls at the Kolmogorov length-scale, but the typical convective time-scale of the latter is so short with respect to τ that their effect are seldom explicitly taken into account when discussing combustion instability. As for the value of Da referred to in the text, it is reasonable to compute it for whirls at the typical turbulence length l_T, the *integral length* of the Appendix on the impact of flame velocity.
- As for $Pe >> 1$, the typical linear size L of the combustor is ≈ 1 m and the flame thickness lies in the range from 0.1 mm to 1 mm.
- As for $He << 1$, usually the typical wavelength of combustion instability and the flame thickness lie in the ranges from 0.1 m to 1 m and from 0.1 mm to 1 mm respectively.

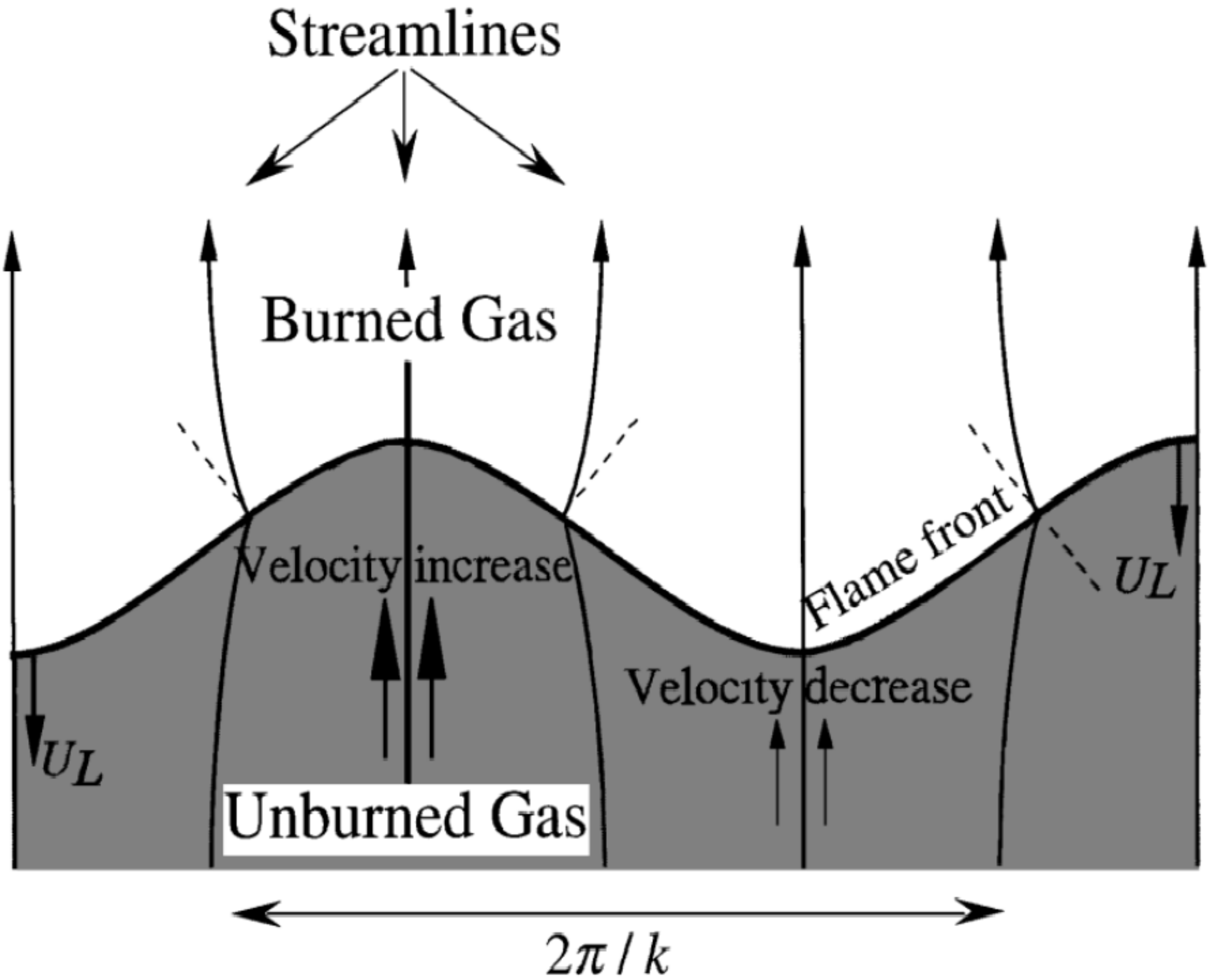

Figure 2.1: *The Darrieus-Landau instability, or hydrodynamic instability, can occur in exothermal reacting flows due to the acceleration of the burning gases. A small disturbance can alter the flame front and cause flame wrinkling. Therefore, with respect to the reactants, convex and concave regions will be present. These gases accelerate normal to the flame front. In convex regions, the streamlines have to diverge toward the flame front and converge after the flame front. The opposite is true for the concave region of the flame. Because the reactants velocity drops as approaching the flame and the burning velocity stays approximately constant, the convex parts tend to grow - from Ref. [5]. Stabilisation is possible provided that the flame velocity depends on the flame curvature, in order to compensate the displacement of the flame. Accordingly, Darrieus-Landau instability may be particularly dangerous for perturbations with large wavelengths, where the flame curvature remains relatively low everywhere [6].*

- Darrieus-Landau instability plays no role [3], e.g. as $Ma \gg 1$,

[3]For uniform impinging flow, this stabilisation requires that the flame is not perfectly flat, and that its radius of curvature is shorter than a typical (*Markstein*) length [6]. (To this purpose, other researchers

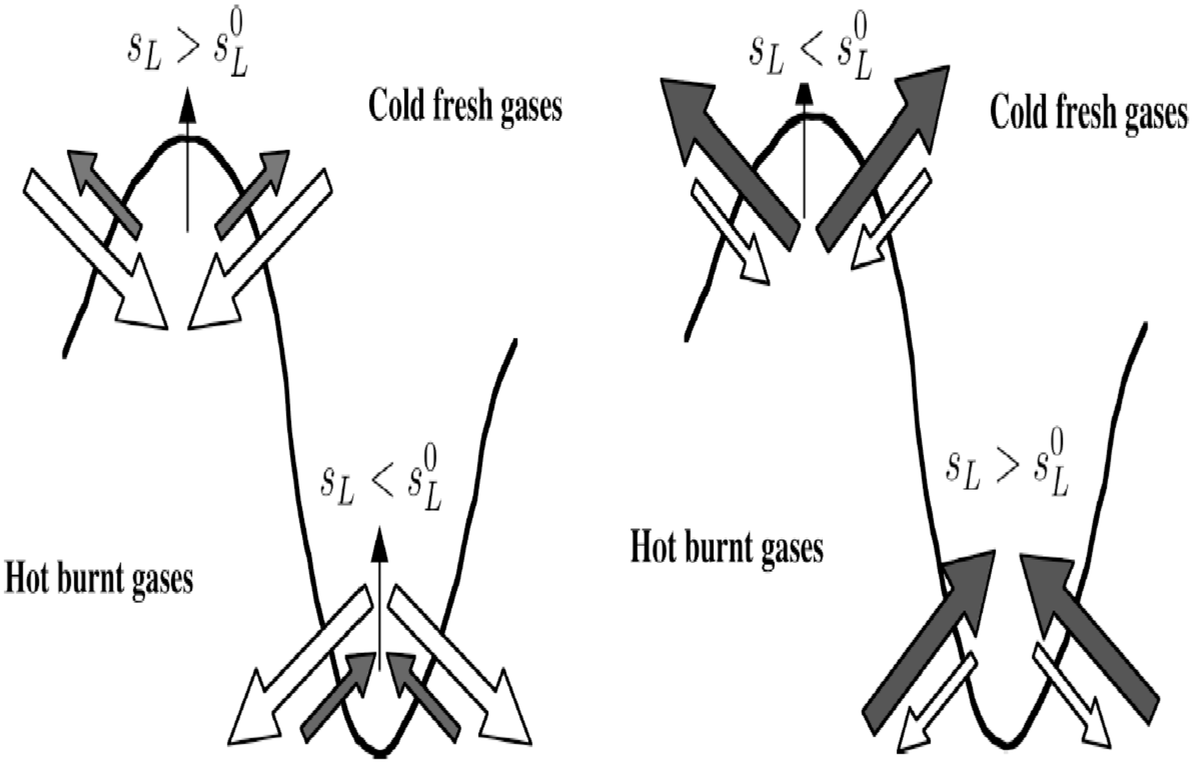

Figure 2.2: *Thermo-diffusion instability. Unstable (stable) regime on the left (right) for $Le < Le_{cr}$ ($Le > Le_{cr}$). - from Ref. [4]. In the unstable regime, when the flame front is convex towards the fresh gases reactants diffuse towards burnt gases faster than heat diffuse towards cold fresh gases. These reactants are heated and then burn faster, increasing the local flame speed with respect to the flame speed of the unperturbed flame. On the other hand, for fronts convex towards the burnt gases, reactants diffuse in a large zone and the flame velocity is decreased compared to the flame speed of the unperturbed flame. This situation is unstable, and the flame front wrinkling (as well as the flame surface) increases. In the stable regime, a similar analysis shows that the flame is stable, and the flame surface decreases.*

- thermo-diffusion instability is suppressed [4], e.g. as $Le = 1$,

[10] would rather refer to the role of flame *stretch* -see Appendix on flame velocity for a definition). The larger the latter, the easier the stabilisation. A dimensionless measure of Markstein length is the *Markstein number* Ma, i.e. the ratio of Markstein length and flame thickness

[4] This requires that the stabilising effect of heat diffusion, which aims at suppressing the destabilising jump of temperature across the flame, overcomes the effect of particle diffusion, which feeds the hot region of burnt gases with further fresh, unburnt gases and sustains therefore the temperature jump [9]. Formally, this implies that $Le > Le_{cr}$, where the *Lewis number* Le and Le_{cr} are the dimensionless ratio between heat diffusion coefficient and particle diffusion coefficient and a numerical threshold slightly smaller than 1 respectively. As for laminar flames, see e.g. equation (1.16) and Figs. 1.4, 2.31 of [4]. Again, different chemical species may have different value of Le. A universal, simplifying assumption is just $Le = 1$ for most practical purposes. An alternative, equivalent definition of the Lewis number is $Le \equiv \frac{Sc}{Pr}$, where the Schmidt number Sc and the Prandtl number Pr are the dimensionless ratio of kinematic viscosity and particle diffusion coefficient and of kinematic viscosity and heat diffusion coefficient respectively.

- and Rayleigh-Taylor instability is not relevant [5], e.g. as $Fr >> 1$,

as it is usually assumed in GT flames, the location of the GT flame as a whole may change abruptly due to flashback [6], lift-off [7] and blow-off [8], depending on the flame shape, the flow of unburnt gases impinging on the flame and the flame velocity, which in turn are strongly affected by turbulence [2]. In fact, GT high power density implies large bulk velocities which can compromise the anchoring of the flame. In all cases, GT flames cease to burn in a predictable manner compatible with the purposes of commercially competitive energy production [9]. This is why GT designers are primarily concerned with stabilisation against undesired motions of flame location.

In industrial combustors, such stabilisation usually relies on refractory burner tiles (see Fig. 2.3), bluff (i.e. unstreaming) bodies and swirlers - see Fig. 2.4 for an example of swirler. Tiles represent a nearly adiabatic boundary, reradiating back to the flame and then maintaining locally the flame velocity at a desired level. Bluff bodies and swirlers act on the flow of the unburnt gases and create *recirculation zones* in it, i.e. vortices which spread burnt gases (Fig. 2.5), leading both to easier ignition of unburnt gases, lower emission of NO_x in premixed combustion and better local matching of flame speed and inflow velocity - see Fig. 2.6. In particular, recirculation zones make available a region where the flow velocity is sufficiently low and comparable to the characteristic turbulent burning rate (defined as the volumetric rate of reactant consumption per unit mean flame cross-sectional area) which in turn is related to the turbulent flame velocity) [11]. Here we anticipate that swirl allows the flame to satisfy a condition satisfied by stable, steady flames, i.e. (the turbulent counterpart of) equation (13.21) below.

Swirl-induced stabilisation is commonly used in today's GT [2]. If sufficiently high swirl is given to the flow of reactants, then *vortex breakdown* occurs (Fig. 2.7), i.e. a *Inner Recirculation Zone* (IRZ) appears right along the axis of the swirler and acts as an aerodynamic flameholder [12]. IRZ is a recirculation bubble which results from the radial pressure gradient generated by the guided rotating flow (large tangential velocity component of the flow) and the flow expansion through a nozzle at the chamber inlet. The radial pressure gradient and axial velocity components decay producing a negative axial pressure gradient and a reverse flow or IRZ (Fig. 2.8). In confined configurations, the sudden expansion of the flow at the chamber inlet is partly controlled by flow recirculating bubbles present at the outer edges. Such bubbles are usually referred to as *Corner Recirculating Zones* (CRZ) or *Outer Recirculating Zones* (ORZ) - see e.g. the vortex in Fig. 2.5. Thin regions with highly non-uniform flow separate the IRZ from the ORZ, often referred to as the Inner Shear Layer (ISL) and the Outer Shear Layer (OSL) respectively

[5]The dimensionless ratio between convective and gravitational terms in the equation of motion is related to the so called Froude number Fr. If $Fr >> 1$ then gravity-related effects like Rayleigh-Taylor instability are negligible.

[6]*Flashback* means that the flame suddenly moves towards the fuel inlet.

[7]*Lift-off* means that the flame suddenly starts floating inside the combustor, far from all walls.

[8]*Blow-off* means that the flame suddenly moves away from the fuel inlet.

[9]Correspondingly, when it comes to flame stabilisation we have to specify *against what*. This is very important when looking e.g. for information in the literature, as the same words *flame stabilisation* are given different meanings by different authors.

- see Fig. 2.9. Usually, swirl-stabilised flames are located not too far from these layers [13] [12].

Under specific conditions (still not clearly mastered) the the IRZ becomes unstable giving rise to the *Precessing Vortex Core*(PVC), a vorticity tube of helical shape located at the outer rim of the IRZ. This thin vortex tube has a helicoidal shape can be co- or counter-rotative to swirl, i.e. it can turn around the swirler axis in the swirl or opposite direction (Fig. 2.10). In some cases several vortex tubes may coexist at the same time [13]. PVC is commonly retrieved in swirled flows when no flame occurs, both in experiments and in the results of computational fluid dynamics (*CFD*). When combustion occurs, however, the situation is far less clear, as combustion may suppress PVC [14]. Indeed, according to common wisdom a conservative assumption is to neglect PVC altogether, but for fully detached flames. We are going to refer to PVC-free, swirl-stabilised flames in the following, unless otherwise specified.

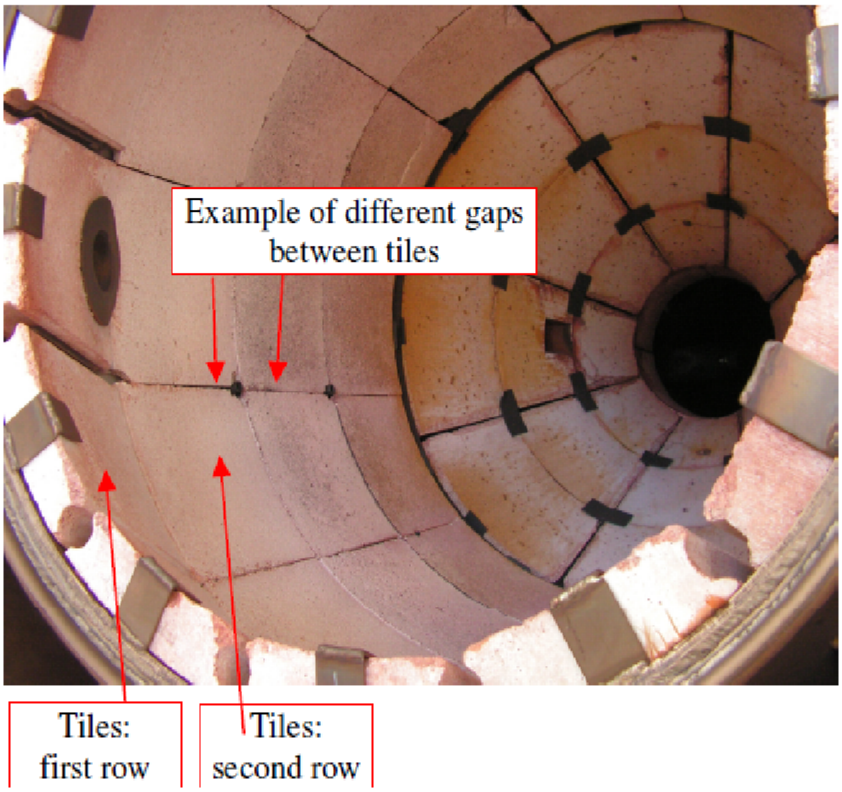

Figure 2.3: *Tile rows on the inner wall of a test rig - from Ref. [15].*

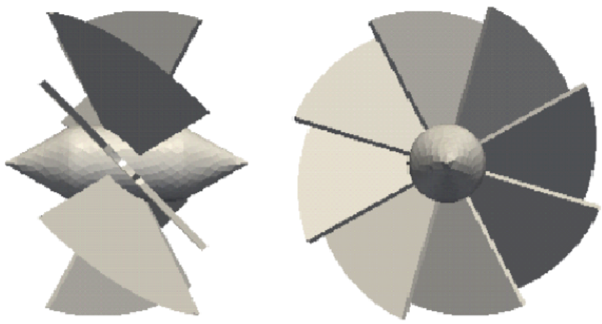

Figure 2.4: *Axial eight-vane swirler, side view (left) and front view (right) - from Ref. [16].*

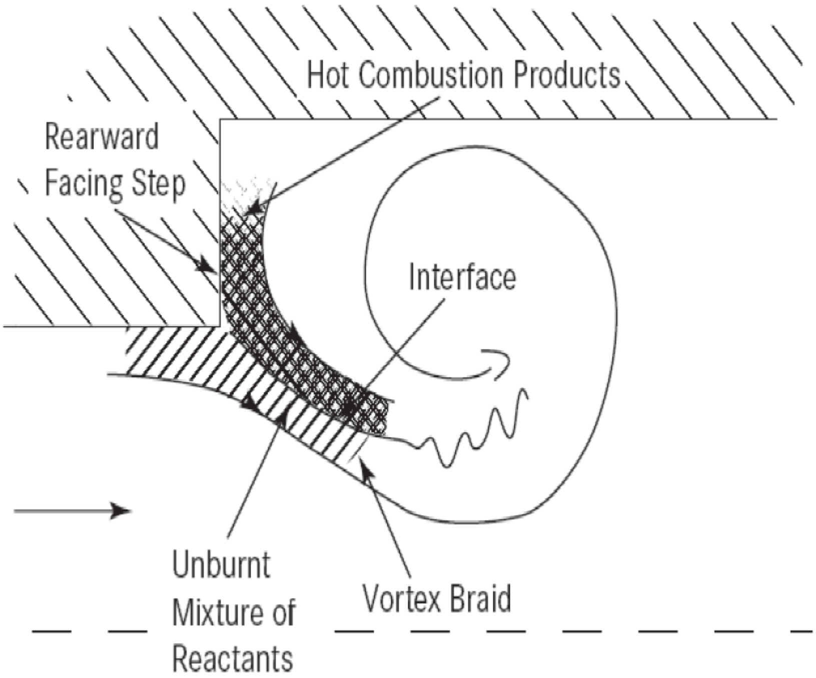

Figure 2.5: *A simple example of vortex which spreads burnt gases. The fresh gases inside are convected by the mean flow downstream and are also simultaneously mixed with the burnt product gases. - from Ref. [5].*

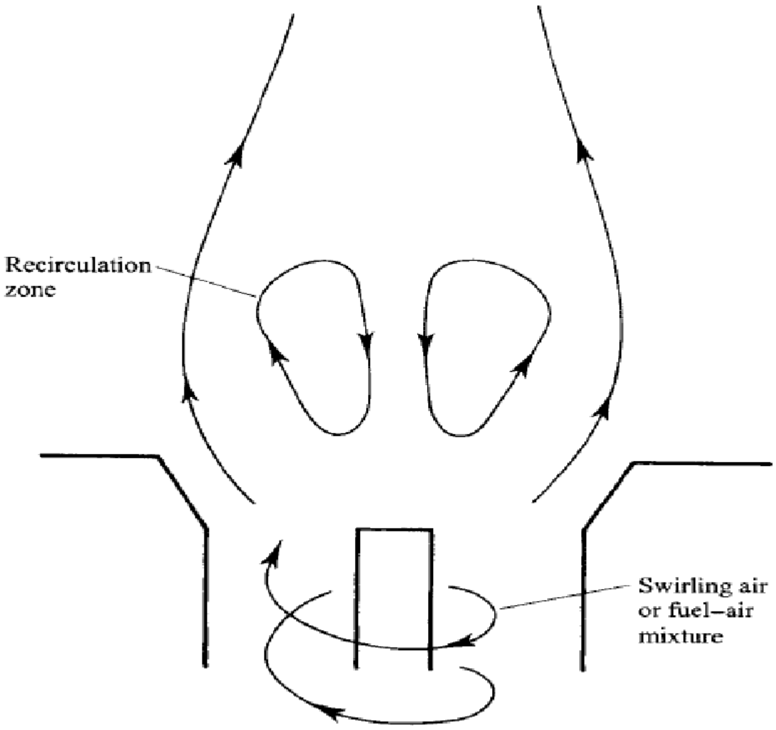

Figure 2.6: *Artist's view of the flow patterns for a flame with inlet swirl - from Ref. [2].*

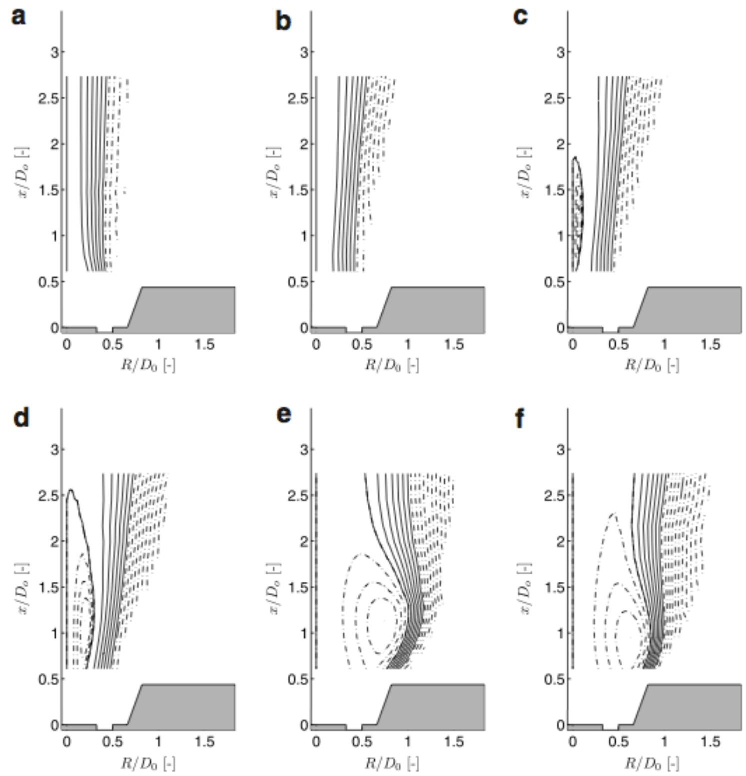

Figure 2.7: *A simple example of VB for increasingly swirled flow without combustion (swirl increases from a. to f.) - from Ref. [14]. Meridian cross section in cylindrical coordinates. VB occurs at c.*

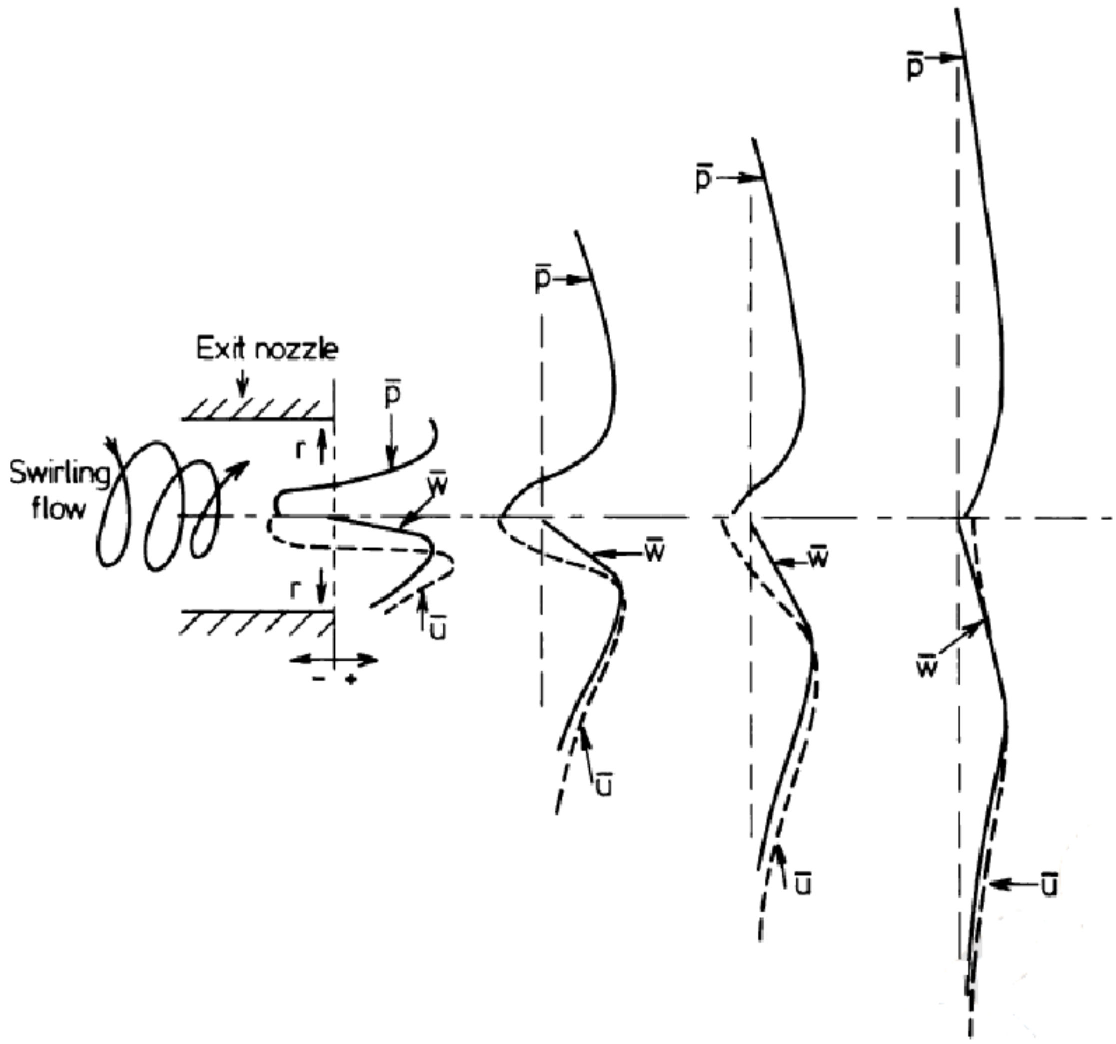

Figure 2.8: *Schematic diagram of processing leading to CRZ formation at atmospheric unperturbed pressure: (1) tangential velocity profile creates a centrifugal pressure gradient and sub-atmospheric pressure near the central axis; (2) axial decay of tangential velocity causes decay of radial distribution of centrifugal pressure gradient in axial direction; (3) thus, an axial pressure gradient is set up in the central region towards the swirl burner, causing reverse flow - from Ref. [17].*

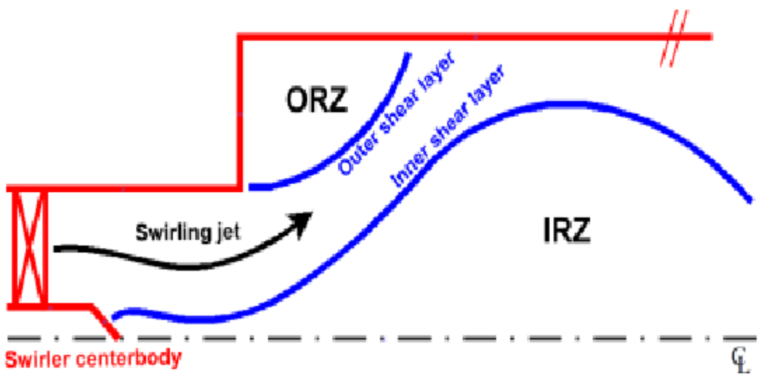

Figure 2.9: *Meridian cross-section of an axisymmetric combustor. The upstream swirled flow (black arrow) is embedded between an inner recirculation zone (IRZ) and an outer recirculation zone (ORZ). The flame surface lies not too far from the shear layers displayed in blue - from Ref. [16].*

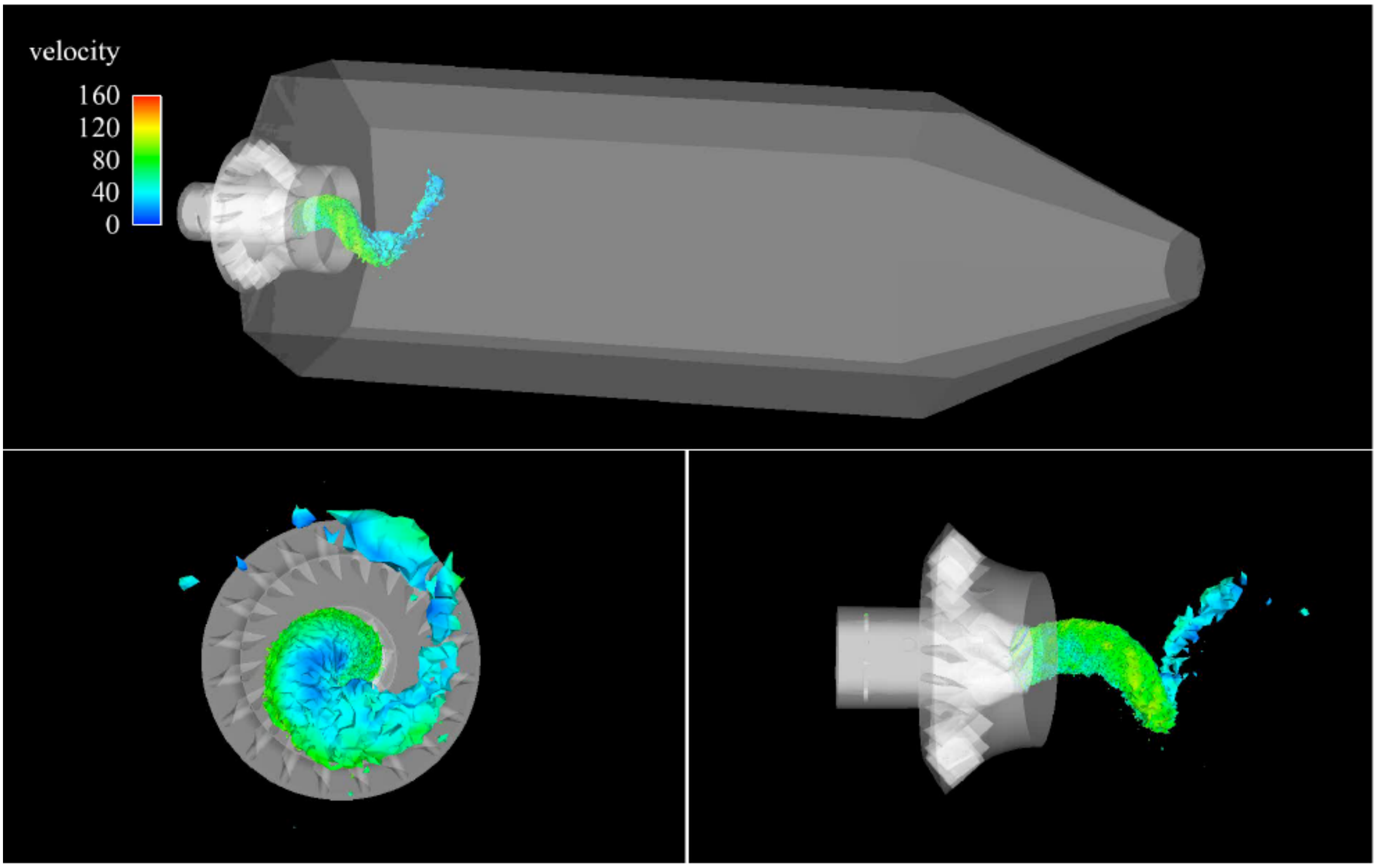

Figure 2.10: *Computed velocity field in PVC - from Ref. [14].*

Chapter 3

The Holy Grail

A common misconception deserves further attention here. The misconception lies in the academic vision of humming as an unwanted perturbation of an otherwise quiet system (possibly affected by noise). Combustion instability cannot be properly described as *humming* in all cases. Basically, combustion instability is ubiquitous in GT and involves a whole spectrum of well-peaked frequencies -see Fig. 3.1 for an example. Unavoidably, both manufacturers and users have to cope with them. This academic vision has been correctly called *poetic* by a senior GT designer. It is even possible that some mild combustion instability spontaneously develops and saturates at a far-from-dangerous level, thus subtracting energy from the really dangerous modes and preventing the occurrence of humming. Unfortunately, most popular available models based on linearisation of the conservation equations of the fluid are unable to describe this highly desirable condition, as the latter requires energy exchange among modes, which is usually a nonlinear phenomenon.

The well-peakedness of the frequencies in the humming spectrum means that each mode has its own τ, which is usually not far from the period of oscillation of the acoustic eigenfrequency of the combustor. Physically, this is likely to be due to the fact that the typical wavelength of humming and the linear size of the combustor are often of the same order of magnitude. Since humming involves sound, its onset requires efficient transmission of acoustic energy from one side of the combustor to another side, and such transmission is possible only at frequencies near the acoustic eigenfrequencies. Luckily, GT combustion is strongly subsonic, i.e. the Mach number M of the flow of unburnt gases impinging on the flame is $\ll 1$; it follows that Mach-related, *Doppler* corrections to the eigenfrequencies may be safely neglected. Once the combustor geometry is known and the speed of sound is known everywhere across the system [1], eigenfrequencies are an output of numerical codes which solve the (*Helmholtz*) wave equation for acoustic waves.

Thus, we sort of know at which frequency humming may occur, *provided that it actually occurs.* To date, what we do not know is precisely if humming will occur or not in a given GT combustor. To put it in other words, the still unsolved problem, our Holy Grail, is to predict when and why the amplitude of a given mode grows up to dangerous

[1] This is basically equivalent to know the temperature everywhere, a piece of information routinely delivered in output even by commercial CFD codes.

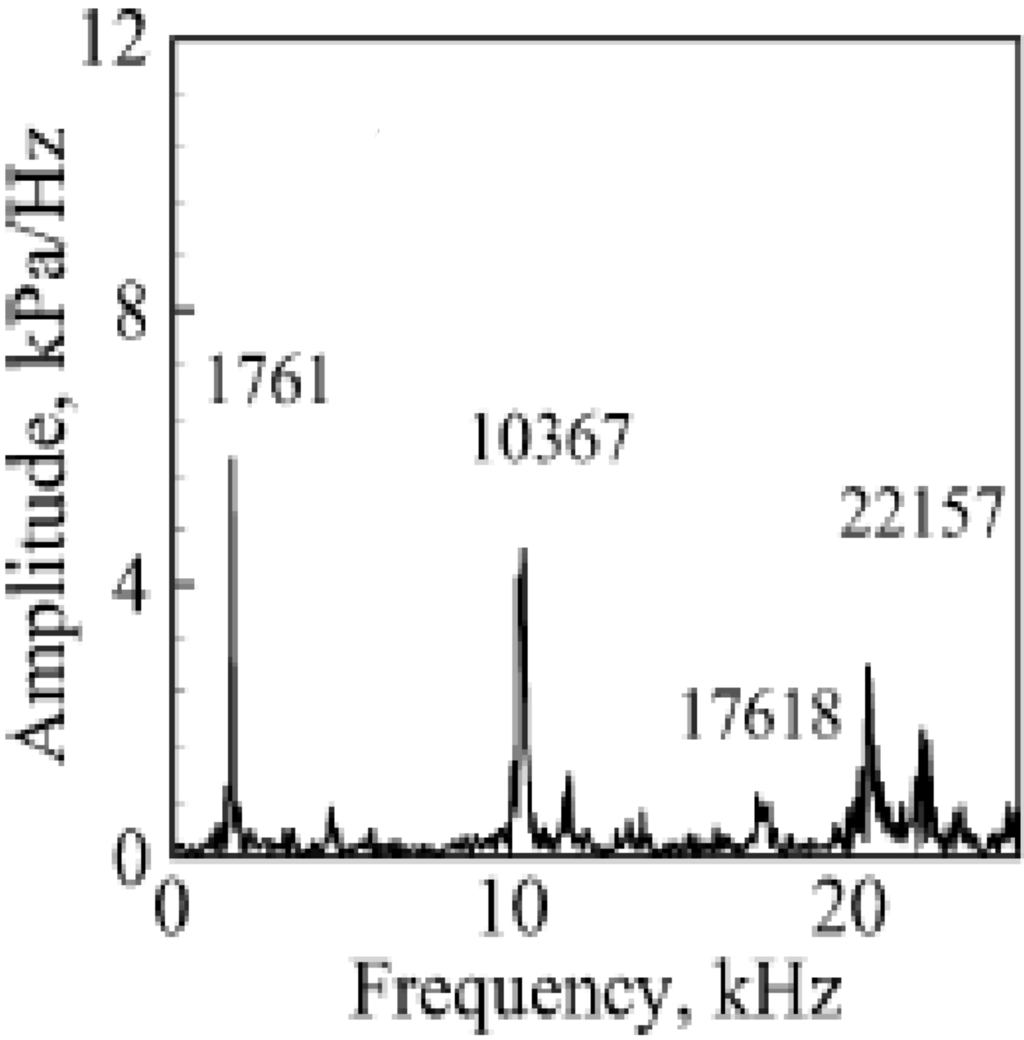

Figure 3.1: *Power spectral densities of pressure fluctuations for a swirl-stabilised combustor - from Ref. [18].*

levels, like those displayed in Fig. 1.7. In the following, we refer to this problem as to *humming prediction*. The problem has been successfully solved in very particular cases only [19] [20] [21], whose relevance to real-life GT is not always obvious.

This time, the fact that

$$M << 1$$

makes things worse, as it makes the convective time-scale (related to the fluid motion) to differ considerably from the acoustic time-scale (related to the propagation of sound). Usually, coexistence of phenomena with vastly different time-scales makes predictions difficult. This is true also in the (by now) well-known case of swirl-stabilised combustion well within the limits of the flammability domain, and where the simplifying assumptions

$$Da >> 1, \quad He << 1, \quad Pe >> 1, \quad Fr >> 1, \quad Ma >> 1, \quad Le = 1$$

hold. As we shall see, it is tempting to assume that -just as Doppler corrections to the eigenfrequences are small- convection plays no role at all in the onset of humming. We are going to see that this simplification is as attractive as dangerous.

As it usually happens in fluid dynamics, we have introduced many dimensionless quantities above. Humming too has its own dimensionless quantity, the so-called *Strouhal number* St: it is defined as the humming frequency $\frac{1}{\tau}$ multiplied by some typical length and divided by some typical velocity. Usually, it is said that humming starts whenever $St > 1$, so that humming-free combustors correspond to $St < 1$. Not surprisingly, there is no unambiguous, generally accepted definition of St -for an example, see e.g. Ref. [22]. This lack corresponds precisely to the absence of a generally accepted physical model for the onset of humming.

A somehow intermediate goal exists between the relatively simple computation of eigenfrequencies and the Holy Grail. Once experimental data are available for different burners with and without humming, it is still possible to interpolate between them and predict the behaviour of burners which do not differ considerably from the older ones. As we are going to see, the involved mathematics is not too cumbersome and leads to many useful information. As for the difference between different possible goals of simulation in humming-related research, namely computation of frequencies, interpolation and prediction we refer to Fig. 3.2.

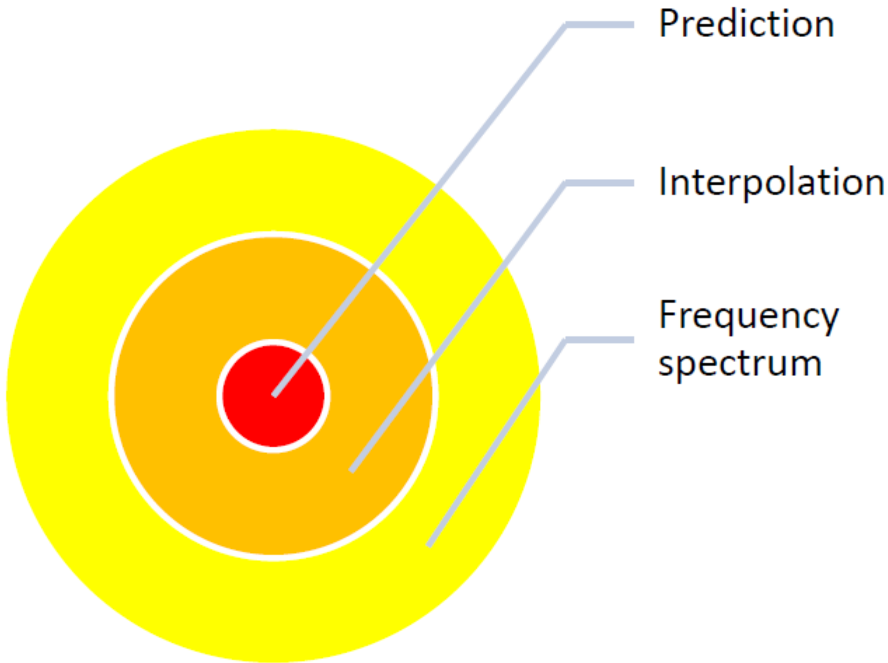

Figure 3.2: *Goals of humming-related research. To predict if humming will affect a combustor which is still in its design phase, starting from first principles, is the most difficult goal (red). To compare results of computation with experimental data in different combustors with and without humming and to interpolate the results is somehow easier (orange). By far, the most common results found in the available literature focus on computing the frequencies of possible humming excitations (yellow).*

Chapter 4

Rayleigh, and beyond

The onset of humming is an example of spontaneous birth of self-sustaining pressure oscillations in a fluid, driven by a source of heat - in this case, combustion. Experiments by Sondhauss [23], Rijke [24], Riess [26], Taconis [27], Biwa et al. [28], Meija et al [29] and Hong et al. [30] have shown that it is the energy exchange between the fluid and the source of heat, rather than the detailed nature of this source, which plays a fundamental role. Back in the XIX century Rayleigh has summarised this fact in a work [31] which contains the by now well-known words:

> *If heat be given to the air at the moment of greatest condensation, or be taken from it at the moment of greatest rarefaction, the vibration is encouraged. On the other hand, if heat be given at the moment of greatest rarefaction, or abstracted at the moment of greatest condensation, the vibration is discouraged*

The similarity with a GT Brayton thermodynamical cycle is striking: maximum efficiency in converting heat into acoustic energy is obtained whenever heating (cooling) occurs at the time of maximum compression (expansion). Many authors [32] [33] [34] have translated Rayleigh's works in rigorous mathematical form - *Rayleigh's criterion* - in different ways. Basically, Rayleigh's criterion is a time-averaged and space-averaged energy balance of the perturbation, and allows us to describe stability against humming as the outcome of a balance between a stabilising and a destabilising term.

The main advantage of Rayleigh's criterion is that it depends on no detailed microscopic model of the flame and of the fluid around it. Accordingly, our poor knowledge of turbulent combustion in GT leaves the validity of the Rayleigh-based predictions unaffected. Nevertheless, Rayleigh's criterion is far from being a common tool in GT manufacturers' R & D on humming, partly because of its convoluted mathematical structure which requires full knowledge of the acoustic spectrum across the combustor volume for utilisation, partly because of the unphysical assumptions it relies upon, which include e.g. the lack of any motion of the fluid mixture inside the combustor when no humming occurs.

The present work aims at:

- discussing different forms of Rayleigh's criterion, as well as its generalisation, Myers' corollary;

- highlighting the connection between Rayleigh's criterion and thermodynamics;
- deriving results relevant to GT.

Fig. 4.1 displays the corresponding workflow. Part II is dedicated to the first goal. We start from the constitutive equations for a fluid mixture of reacting gases inside a GT combustor. Then, derive different forms of Rayleigh's criterion in a particular case, in order to show its range of validity and its limits. A short review of conventional tools for humming analysis and prediction, namely modal analysis and flame transfer function, is also presented for comparison. Finally, we discuss a generalisation of Rayleigh's criterion, Myers' corollary. We show how Rayleigh's criterion and Myers' corollary provide us with formally similar, necessary conditions of stability for steady and unsteady unperturbed states respectively.

We have seen that Rayleigh's criterion is somehow connected to Brayton's cycle. Indeed, the connection to thermodynamics goes still deeper. From the point of view of thermodynamics, humming is connected to many experiments in thermo-acoustics even outside the domain of combustion. Moreover, the constitutive equations both Rayleigh's criterion and Myers' corollary are based on include the first principle of thermodynamics, applied to a small mass element of the fluid. If we apply the *second* principle of thermodynamics too, then a number of further results follow. These results include Le Châtelier's principle of thermodynamics. We show in Part III that flames which are stable according to Rayleigh's criterion are also stable according to Le Châtelier's principle, that formulations of the stability problem exist which are equivalent to Rayleigh's criterion, and that similar results hold also for unsteady unperturbed states, in agreement with the results on Myers' corollary. Finally, our discussion on thermodynamics allows us to retrieve many results of thermo-acoustics, as a benchmark.

Three Chapters in Part IV are dedicated to the third goal. The first chapter deals with flames without humming. We apply the formulations of stability quoted above to the conservation equations of mass, momentum and energy in the particular case of axisymmetric, swirl-stabilised flames where infinitely fast, one-step combustion is assumed. It turns out that even humming-free flames may abruptly switch from one shape to another, depending on the heat release, the switch number and the flame velocity. Usually, hysteresis occurs when the flame reverts to the original state. Even if scarcely relevant to GT, we retrieve also the condition of stability against thermo-diffusion instability for quasi-flat flames, including the well-known Bunsen flame, as a further benchmark.

The second chapter deals with the onset of humming. We show that only some models -out of those available in the literature- are actually compatible with thermodynamics. Moreover, we start from Myers' corollary and work out an expression for a dimensionless quantity which can play the role of Strouhal number.

The third chapter deals with stabilisation of humming. Starting from the results of previous Chapters, and in agreement with experimental data available in the liteature, we suggest a new, competitive, patented approach to stabilisation of humming, based on electromagnetic waves in the GHz range. The corresponding computations have been the subject of a collaboration between Ansaldo Energia and CNR-IMIP, Bari, Italy.

The final Parts include the conclusions, the bibliography and some Appendices.

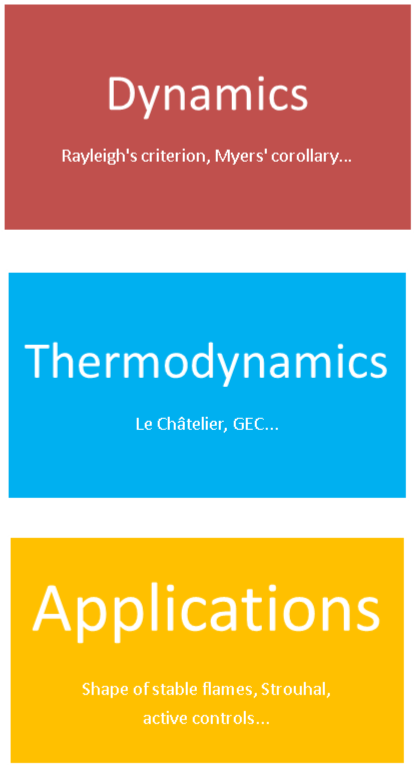

Figure 4.1: *To start with, we review classical results of humming-relevant dynamics of air-fuel mixtures in premixed GT combustors, i.e. various versions of Rayleigh's criterion. Correspondingly, we discuss also the related well-known concepts of modal analysis and flame trasfer function. We review also a generalisation of Rayleigh's criterion to more realistic conditions, namely Myers' corollary. Secondly, we discuss the link of Rayleigh's criterion with thermodynamics, i.e. with Le Châtelier's principle, and show that formulations of the stability problem exist which are equivalent to Rayleigh's criterion. Finally, we apply our results to the description of stable, premixed, swirl-stabilised flames. As for the humming onset, we obtain also an explicit expression for a Strouhal number. As for the stabilisation of humming, we discuss the properties of some control systems, and write down some explicit prediction for future experiments.*

Part II

Dynamics

Chapter 5

The constitutive equations

We consider a viscous fluid mixture of $k = 1, \dots n$ reacting chemical species where both heat conduction and particle diffusion occur. We assume no net mass source and no body force, and invoke no detailed model of combustion.

The mass balance of the fluid mixture, the mass balance of the k-th chemical species, the momentum balance, the first principle of thermodynamics and the entropy balance read [4] [22] :

$$\frac{d\rho}{dt} + \rho \nabla \cdot \mathbf{v} = 0 \tag{5.1}$$

$$\rho \frac{dY_k}{dt} = \omega_k - \nabla \cdot (\rho Y_k \mathbf{V}_k) \tag{5.2}$$

$$\rho \frac{d\mathbf{v}}{dt} + \nabla p = \nabla \cdot \Pi \tag{5.3}$$

$$du = Tds - pd(\frac{1}{\rho}) + \sum_{k=1}^{n} g_k dY_k \tag{5.4}$$

$$\rho T \frac{ds}{dt} = Q + \Phi - \nabla \cdot \mathbf{q} - \rho \sum_{k=1}^{n} g_k \frac{dY_k}{dt} \tag{5.5}$$

respectively. Here the total time derivative is $\frac{d}{dt} = \frac{\partial}{\partial t} + \mathbf{v} \cdot \nabla$.

The quantities ρ, p, T, $\mathbf{v}$, $\mathbf{q} = -\lambda \nabla T$, and Π are the mass density, the pressure, the temperature, the velocity, the heat flow due to heat conduction with thermal conductivity λ and the viscous stress tensor of the fluid mixture respectively.

Radiation losses are often neglected in application to GT combustors; in case, they can be added to $\mathbf{q}$ with no loss of generality.

The quantities $\Phi \equiv \sum_{i,j=1}^{3} \Pi_{ij} \frac{\partial v_j}{\partial x_i}$ and $Q \equiv -\sum_{k=1}^{n} \Delta h_{f,k}^0 \omega_k$ are the viscous power density and density of *heat release* respectively, where the heat release is the amount of heat produced per unit time by combustion. We stress the point that -unless otherwise specified- our results depend on no detailed information concerning the microscopic physics ruling Q.

The quantity $-\rho \sum_{k=1}^{n} g_k \frac{dY_k}{dt}$ is the outcome of the existence of $n > 1$ chemical species in the system.

Finally, the quantities g_k, Y_k, $\mathbf{V}_k$, h_k, $\Delta h_{f,k}^0$ and ω_k are the chemical potential per unit mass, the mass fraction, the diffusion velocity, the enthalpy per unit mass, the formation enthalpy per unit mass at reference temperature 300 K and the production rate of the k-th chemical species respectively, where the identities $\sum_{k=1}^{n} Y_k \equiv 1$, $\sum_{k=1}^{n} \omega_k \equiv 0$ and $\sum_{k=1}^{n} Y_k \mathbf{V}_k \equiv 0$ hold. Together with (5.2), these inequalities lead to $n-1$ independent equations in the Y_k's.

Chapter 6

A particular case

6.1 Simplified equations and useful relationships

We start with the case where two chemical species are present and where both viscosity, heat conduction and particle diffusion are negligible, i.e.:

$$n = 2 \qquad \Pi = 0 \qquad \lambda = 0 \qquad \mathbf{V}_k = 0 \tag{6.1}$$

Furthermore, we assume *caloric perfection*, i.e. all chemical species are assumed to behave as perfect gases with the same constant values of specific heat at constant pressure and constant volume.

As we are going to see, even this simplified case allows us to identify some fundamental issues of the stability problem in thermo-acoustics. To this purpose, in this Section we are going to follow the treatment of [32] in some detail. The general case will be addressed again in the following Sections.

The mass balance (5.1) is unchanged. There is just 1 independent equation (5.2), which remains uncoupled from the other equations and will be considered no more. The balance of momentum (5.3) and the first principle of thermodynamics (5.4) reduce to

$$\rho \frac{d\mathbf{v}}{dt} + \nabla p = 0 \tag{6.2}$$

and to

$$du = Tds - pd(\frac{1}{\rho}) \tag{6.3}$$

respectively.

As for perfect gases, the equation of state, the internal energy u per unit mass and the total differential of entropy s per unit mass are:

$$p = r\rho T \tag{6.4}$$

$$\rho u = \frac{p}{\gamma - 1} \qquad du = c_v dT \tag{6.5}$$

$$\frac{ds}{c_p} = \frac{dT}{T} - \frac{\gamma - 1}{\gamma}\frac{dp}{p} = \frac{dp}{\gamma p} - \frac{d\rho}{\rho} \tag{6.6}$$

respectively, where $\gamma = \frac{c_p}{c_v}$ and c_p and $c_v = c_p - r$ are the specific heat per unit mass at constant pressure and constant volume respectively. For future reference we write here also the following auxiliary relationship:

$$\frac{\gamma - 1}{\gamma} = \frac{r}{c_p} \tag{6.7}$$

Finally, equations (5.5) and (6.4) give:

$$\frac{ds}{dt} = \frac{rQ}{p} \tag{6.8}$$

We rewrite the equations above in a more convenient form with the help of a little algebra. Dot product of both sides of equation (6.2) by $\mathbf{v}$ leads to:

$$\frac{\rho}{2}\frac{d|\mathbf{v}|^2}{dt} = -\nabla \cdot (p\mathbf{v}) + p\nabla \cdot \mathbf{v} \tag{6.9}$$

Moreover, equations (5.1) , (6.3) and (6.5) give:

$$\frac{dp}{dt} = (\gamma - 1)\rho T\frac{ds}{dt} - \gamma p\nabla \cdot \mathbf{v} \tag{6.10}$$

Together, equations (6.9) and (6.10) lead to the exact relationship:

$$\frac{\rho}{2}\frac{d|\mathbf{v}|^2}{dt}+\frac{1}{2\rho c_s^2}\frac{dp^2}{dt}+\nabla\cdot(p\mathbf{v})=\frac{\gamma-1}{\gamma}\rho T\frac{ds}{dt} \tag{6.11}$$

which we are going to invoke again and again in the following. Here $c_s \equiv \sqrt{(\frac{p}{\rho})_s}$ is the well-known Laplace's formula for the adiabatic speed of sound; in a perfect gas we have $c_s^2 = \gamma\frac{p}{\rho}$

Remarkably, equation (6.11) contains the time derivative of the square of both velocity and pressure. Suitable addition of a term which is proportional to the time derivative of squared entropy allows suitable generalisation of (6.11) for problems where entropy too undergoes perturbations. To this purpose, let us multiply each side of equation (6.8) by $\frac{ps}{rc_p}$,add the result side by side to equation (6.11) and invoke (6.7) . We obtain:

$$\frac{\rho}{2}\frac{d|\mathbf{v}|^2}{dt}+\frac{1}{2\rho c_s^2}\frac{dp^2}{dt}+\frac{p}{2rc_p}\frac{ds^2}{dt}+\nabla\cdot(p\mathbf{v})=\frac{r+s}{c_p}Q \tag{6.12}$$

Here the squares of velocity, pressure and entropy appear on the L.H.S. on an equal footing.

6.2 The unperturbed fluid is at rest

6.2.1 Energy balance of a perturbation

Further progress requires linearisation. We write $a = a_0 + \epsilon a_1$ for the generic quantity a with $\frac{\partial a_0}{\partial t} = 0$ and $0 < \varepsilon \ll 1$. Physically, this means that we consider small perturbations of a steady state. Here we assume:

$$\mathbf{v}_0 = 0 \tag{6.13}$$

i.e., the unperturbed fluid is at rest. The general case $\mathbf{v}_0 \neq 0$ will be discussed below. Furthermore, we limit ourselves to the the relevant limit for subsonic combustion: $M \ll 1$ where $M \equiv \frac{|\mathbf{v}|}{c_s}$ is the Mach number. In the same limit we neglect also ∇p_0 [4]. Equation (6.13) implies the Mach number of the unperturbed flow to vanish exactly.

We show in the Appendix on the energy balance of a perturbation in the zero Mach case that the relationships above make equation (6.12) to reduce to:

$$\frac{\partial E}{\partial t} = -\nabla \cdot \mathbf{W} + D \tag{6.14}$$

where E, $\mathbf{W}$ and the *Rayleigh index* D are defined as follows:

$$E \equiv \frac{\rho_0 |\mathbf{v}|^2}{2} + \frac{p_1^2}{2\rho_0 c_{s0}^2} + \frac{p_0}{rc_p}\frac{s_1^2}{2} \tag{6.15}$$

$$\mathbf{W} \equiv p_1 \mathbf{v}_1 \tag{6.16}$$

$$D \equiv \frac{T_1 Q_1}{T_0} - \frac{p_0}{rc_p} s_1 \mathbf{v}_1 \cdot \nabla s_0 \tag{6.17}$$

In particular, let us consider the particular case (referred to as *isentropic* in the following) where both ∇s_0 and terms $\propto O(s_1^2)$ are negligible. Then, equations (6.6) , (6.15) and (6.17) give:

$$E \equiv \frac{\rho_0 |\mathbf{v}|^2}{2} + \frac{p_1^2}{2\rho_0 c_{s0}^2} \tag{6.18}$$

$$D \equiv \frac{(\gamma - 1) p_1 Q_1}{\gamma p_0} \tag{6.19}$$

while $\mathbf{W}$ remains unaffected. It is also possible to derive equations (6.14), (6.16), (6.18) and (6.19) from (1) and the part $\propto O(\epsilon)$ of the linearised version of equation (6.2), namely:

$$\rho_0 \frac{\partial \mathbf{v}_1}{\partial t} + \nabla p_1 = 0 \tag{6.20}$$

after dot product of both sides of the latter by $\mathbf{v}_1$.

Integration on a fixed volume V of both sides of equation (6.14) leads to:

$$\frac{d}{dt}\int_V d\mathbf{x}E = -\int_{A_b} d\mathbf{a}\cdot\mathbf{W} + \int_V d\mathbf{x}D \qquad (6.21)$$

where A_b is the boundary surface of V and $d\mathbf{a}$ is its surface element vector and we have applied Gauss' theorem of divergence. The volume integral on the L.H.S. depends only on time: this is why we have replaced $\frac{\partial}{\partial t}$ with $\frac{d}{dt}$.

In the isentropic case E is given by (6.18) and the L.H.S. of equation (6.21) has the simple meaning of total energy of an acoustic perturbation, while equation (6.15) provides an additional term $\propto s_1^2$ which takes into account possible non-adiabaticity. The fact that entropy spottiness s_1 may give a contribution to a form of *energy* in the disturbance may at first seem to be a little puzzling, especially because entropy is normally taken as a measure of the unavailable energy. The important thing to be recognized is that we are speaking here of the energy in a *perturbation*; and as such, changes in entropy distribution of a gas will always induce a change in the fluid motion and hence, a change in the kinetic energy in the disturbance [33].

In contrast to popular belief, it is not at all obvious that (6.18) and (6.19) are to be preferred to (6.15) and (6.17) respectively. Generally speaking, in fact, the sound does not propagate with adiabatic velocity c_s across a fluid where propagation is far from being an adiabatic and reversible process. Should e.g. compression occur adiabatically, the fluid would be heated correspondingly, while non-vanishing heat losses (due e.g. to radiation or conduction) may induce a mismatch between compression and heating. Laplace's formula for the speed of sound applies to the former case only, and its validity is not granted [31].

On the R.H.S. of equation (6.21), the quantity $\int_A d\mathbf{a}\cdot\mathbf{W}$ is precisely the net amount of acoustic energy lost across the boundary per unit time because of sound propagation [8], and inclusion of contributions due to s_1 leaves it unaffected. If positive, it acts a sink of energy.

As for the quantity $\int_V d\mathbf{x}D$, it achieves a maximum when Q_1 and T_1 (or Q_1 and p_1, in the isentropic case) are in phase. The isentropic case has been described in detail by Rayleigh [31]. Physically, we expect such phase matching to correspond to a maximum efficiency of the transformation of heat into mechanical (here, acoustic) energy. For simple geometries, analytical formulas for the phases corresponding to stable and unstable regimes are available -see e.g. Sec. 6.6.1 of [35]. In real-life applications, however, phases are heavily affected by noise [36].

The advantage of volume integration lies in the fact that in many applications to combustion some regions inside a given combustor usually excite the oscillation by burning in phase with temperature (or pressure), while other regions damp the instability by burning out of phase. The overall effect of flame-acoustics coupling can only be predicted looking at the integrals computed on the combustor volume.

Finally, the contribution to D due to ∇s_0 (from (6.17)) tends to decrease the acoustic energy of the perturbation whenever $s_1 \mathbf{v}_1 \cdot \nabla s_0 > 0$. This means that any perturbation which tries to raise entropy where it is already large gets damped. Qualitatively at least, this conclusion seems to agree with thermodynamics. In fact, the growth of such perturbation tries to separate further the system far from thermodynamical equilibrium, where entropy is maximum and uniform everywhere; we expect therefore this growth to be prevented in agreement with the second principle of thermodynamics.

In summary, we may consider equation (6.21) as an acoustic energy balance of a perturbation, which can affect entropy too. On the R.H.S., the balance of the propagation of sound (which carries acoustic energy away from the system) and the transformation of heat into acoustic energy rules the evolution of the acoustic energy of the perturbation on the L.H.S., duly corrected for non-adiabaticity.

Finally, let us focus on combustion problems inside a combustor volume V_b, where Q s ruled by combustion processes. In this case, we derive a simple relationship which turns out to be useful in the following. Combustion occurs within the flame, whose volume V_f is usually order-of-magnitude smaller than V_b. Accordingly, Q differs from zero inside the flame only. Moreover, in many problems of lean, premixed, subsonic combustion pressure gradients are small [4], and large temperature gradients are located at the flame - see e.g. Fig. 6.1 and Fig. 6.2. The same holds therefore for ∇s_0.

As far as D is localised at the flame, we may write

$$\int_{V_b} d\mathbf{x} D = \int_{V_f} d\mathbf{x} D \tag{6.22}$$

a relationship which will turn to be useful below. Here we anticipate that (6.22) is going to allow us to discuss the impact of flame geometry (through V_f) on stability. Admittedly, combustion occurs in a small fraction of the whole flame volume, the so called *reaction zone* -see Fig. 6.3.

However, the actual value -usually referred to as Zel'dovich number Ze in the literature [6]- of the ratio between the flame thickness and the reaction zone thickness depends on the detailed microscopic description of combustion. For simplicity, it is usually taken as a constant quantity in humming research. Typically $Ze \approx 10$ in many applications.

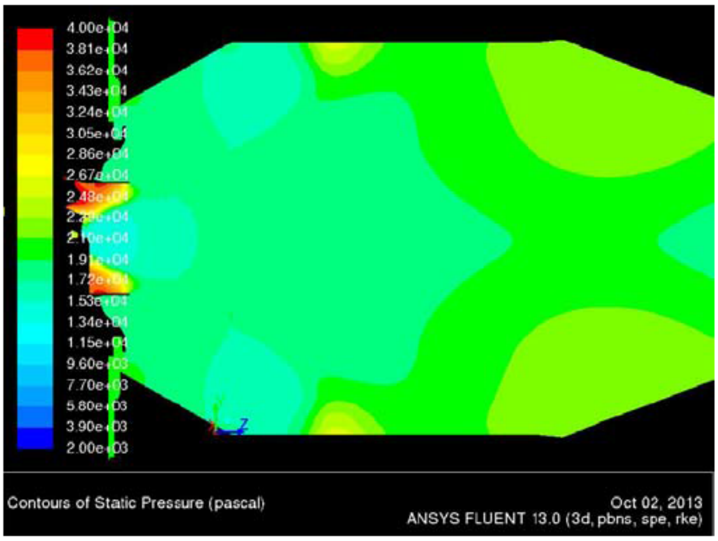

Figure 6.1: *Map of suitably normalised pressure computed in a combustor. Pressure is* $\approx$ *uniform across* V_b*. Adapted from Ref. [15].*

6.2.2 An isolated system with no dissipation

Now we may link equation (6.21) with our investigation of stability. By *stability* we mean that $|\xi|$ diverges nowhere at any time, where we have introduced [1] the vector $\xi = \xi(\mathbf{x}, t)$ such that

$$\mathbf{v}_1 = \frac{\partial \xi}{\partial t}$$

[1] Here we adapt the treatment of [37], originally conceived for stability in magnetohydrodynamics. The advantage is that no information on the spectral properties (discreteness of the spectrum, and the like) of the operators involved is required.

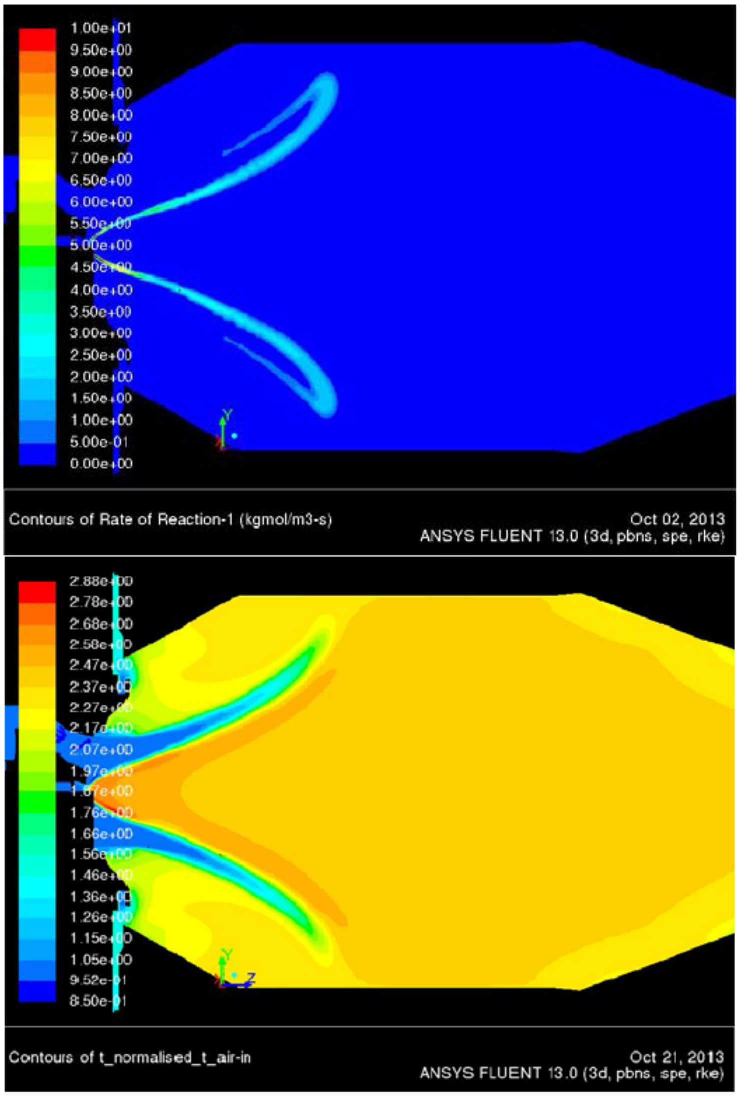

Figure 6.2: *Maps of reaction rate (top) and of suitably normalised temperature (bottom) computed in a combustor. Huge temperature gradients occur where the reaction rate is large, i.e. when combustion occurs. Adapted from Ref. [15].*

Physically, ξ is the displacement of a small element of fluid which undergoes a perturbation $\mathbf{v}_1$ of velocity. Rigorously speaking, we would better add the words *in the reference system at rest with the unperturbed small mass element of fluid* to this description of ξ; however, this addition is not relevant as far as (6.13) holds. It will be relevant in the discussion of the $\mathbf{v}_0 \neq 0$ case.

To start with, let us focus our attention on an isentropic perturbation with $\mathbf{v} \cdot d\mathbf{a} = 0$ everywhere on A_b. In this case equation (6.21) leads to:

$$\int_V d\mathbf{x} \left(\frac{\rho_0 |\mathbf{v}|^2}{2} + \frac{p_1^2}{2\rho_0 c_{s0}^2} \right) = U \qquad (6.23)$$

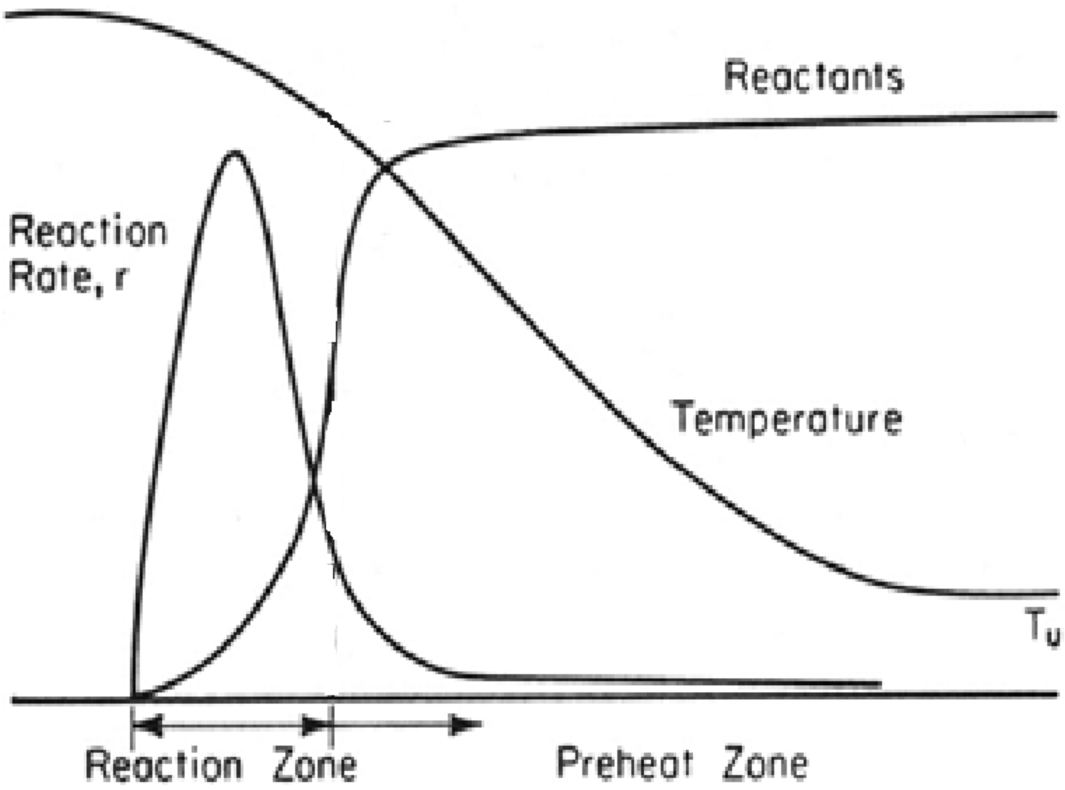

Figure 6.3: *The structure of a laminar premixed flame. The flame is made of two regions, the preheat (or diffusion) region and the reaction region. Combustion occurs in the reaction region, heat diffusion occurs from the reaction zone towards the preheat region. Here the unburnt gases impinge on the flame from the left to the right. Temperature increases considerably across the flame, starting from the upstream value* T_u*. The rate of combustion reactions is strongly peaked in the reaction zone.*

with $U =$ const. ≥ 0. Here not only (6.13) holds, but no heating process and no propagation of acoustic energy occurs, so that the total acoustic energy U of the perturbation is a constant quantity.

In order to discuss the connection between (6.23) and stability, we are going to discuss the evolution of $\xi\left(\mathbf{x},t\right)$ with the help of the linearised equations of motion. (Generalisation of this discussion will be helpful when dealing with the case $\mathbf{v}_0 \neq 0$ in the following). To this purpose, we take $\xi\left(\mathbf{x},t=0\right) = \eta\left(\mathbf{x}\right)$ as initial condition, and -in agreement with the $\mathbf{v}\cdot d\mathbf{a} = 0$ assumption of no sound propagation across the boundaries- we take also $\xi\cdot d\mathbf{a} = 0$ as boundary condition. Moreover, we rewrite the linearised balance of momentum (6.20), internal energy (1) and mass

$$\frac{\partial \rho_1}{\partial t} + \rho_0 \nabla \cdot \mathbf{v}_1 = 0 \tag{6.24}$$

(straightforwardly from equation (5.1)) as:

$$\rho_0 \frac{\partial^2 \xi}{\partial t^2} + \nabla p_1 = 0 \tag{6.25}$$

$$p_1 + \gamma p_0 \nabla \cdot \xi = 0 \tag{6.26}$$

and

$$\rho_1 + \rho_0 \nabla \cdot \xi = 0 \tag{6.27}$$

respectively. Together with the boundary condition $\xi \cdot d\mathbf{a} = 0$, equations (6.25), (6.26) and (6.27) allow us to rewrite equation (6.23) as

$$K + B = C \qquad K \equiv \frac{1}{2} \int_V d\mathbf{x} \rho_0 |\frac{\partial \xi}{\partial t}|^2 \qquad B \equiv -\frac{\gamma p_0}{2} \int_V d\mathbf{x} \xi \cdot \nabla (\nabla \cdot \xi) \tag{6.28}$$

with $C =$ const. It is easy to show that $B \geq 0$ is a necessary and sufficient condition for stability.

It is a sufficient condition, because if $B \geq 0$ then $C =$ const. prevents unbounded growth of K, hence of $|\frac{\partial \xi}{\partial t}|$.

In order to show that it is also a necessary condition, we show that $B < 0$ is a sufficient condition for instability. Suppose an initial perturbation $\eta(\mathbf{x})$ such that $B(t = 0) < 0$, $\frac{\partial \xi}{\partial t}(t = 0) = 0$. It follows that $C < 0$ at all times as $K(t = 0) = 0$. After introducing the integral $I(t) \equiv \int_V d\mathbf{x} \frac{\rho_0}{2} |\xi|^2$(which is basically $\propto$ the mass-weighted volume-average of $|\xi|^2$), straightforward computation gives both $\frac{dI}{dt}(t = 0) = 0$ and $\frac{d^2 I}{dt^2} = 2(K - B)$, and equation (6.28) leads therefore to: $\frac{d^2 I}{dt^2} = (4K - 2C) > -2C > 0$ at all times. It follows that $I(t)$ grows without bound as $t \to \infty$, indicating that $|\xi|$ increases somewhere at least as fast as t.

In spite of its rather abstract mathematical form, this result ensures stability of the unperturbed state against perturbations satisfying equation (6.23). In fact, the definition of ξ and equation (6.26) give $C = U$, $K = \int_V d\mathbf{x} \left(\frac{\rho_0 |\mathbf{v}|^2}{2} \right)$ and $B = \int_V d\mathbf{x} \left(\frac{p_1^2}{2\rho_0 c_{s0}^2} \right) > 0$ after integration by parts. Positiveness of B ensures stability.

Physically, this means that the amplitude of acoustic perturbations in a fluid initially at rest where no sound propagates across the boundary of the system and no heating occurs never diverges. An advantage of our discussion is that our results do not rely on any assumption concerning the spatio-temporal (e.g. oscillating) behaviour of the perturbation.

It is worthwhile to stress a further consequence of the positivemess of B, which admittedly is rather trivial but has far-reaching consequences. Linearity of equations (6.25) and (6.6) ensures that a system is stable (i.e., $|\xi|$ diverges nowhere at any time) if and only if E never diverges. In contrast with the former, the latter stability condition deals with a volume integral, and is therefore uniquely suitable to the evaluation of the overall effect of flame-acoustics coupling quoted above. Accordingly, we are going to identify stability with the lack of divergence of E in the following.

6.2.3 Rayleigh's criterion

Let us investigate what happens if dissipative processes occur. Together with the formula for c_{s0}, equations (6.20) and (1) lead to:

$$\frac{\partial^2 p_1}{\partial t^2} - \nabla \cdot \left(c_{s0}^2 \nabla p_1 \right) = (\gamma - 1) \frac{\partial Q_1}{\partial t} \tag{6.29}$$

Physically, this equation means that a change in the net amount of heat supplied to the small mass element (e.g. at the flame through combustion) is a source of acoustic waves, which propagate with velocity c_{s0}. Generally speaking, and in contrast with turbulence (whose impact on acoustics is described by Lighthill's analogy [38]) the flame acts as monopole source of acoustic waves [39]. Propagation of sound across the boundary is also allowed, provided that we we drop the boundary condition $\xi \cdot d\mathbf{a} = 0$. All the same, if the source is known then stability can be checked with the help of the energy balance (6.21), as E increases with increasing $|\xi|$.

For instance, suppose harmonic variations for all variables allows to write the perturbation a_1 of the generic quantity a as $a_1(\mathbf{x}, t) = \Re\{(\widehat{a}(\mathbf{x}, t) \exp\left(\frac{-2\pi i t}{\tau} \right)\}$. where $\Re\{a\}$ denotes the real part of the complex number a and $\widehat{a}$ is a real, slowly varying function of time. Whether these functions grow with time over an oscillation period τ will determine the stability of the combustor [4]. Integrating both sides of (6.21) on time over τ and dividing by τ gives

$$\frac{d}{dt}\int_{V_b} d\mathbf{x}\langle E\rangle = -\int_{A_b} d\mathbf{a}\cdot\langle\mathbf{W}\rangle + \int_{V_b} d\mathbf{x}\langle D\rangle \tag{6.30}$$

where $\langle a\rangle \equiv \dfrac{1}{\tau}\int_0^\tau dta$ is the time-average of a over τ. The growth rate of E may also be expressed may also be expressed by assuming that the amplitudes of the perturbation change slowly with time in comparison to τ, i.e. that $\widehat{a} \propto \exp(g_r t)$ with $|g_r\tau| << 1$, or, equivalently, that:

$$a_1(\mathbf{x}, t) \propto \exp(-i\omega t) \tag{6.31}$$

with complex ω, $\tau = \dfrac{2\pi}{\Re\{\omega\}}$ and $g_r = \Im\{\omega\}$ where $\Im\{a\}$ denotes the imaginary part of the complex number a and $\dfrac{|\Im\{\omega\}|}{|\Re\{\omega\}|} << 1$. In this case $\dfrac{\partial}{\partial t}\int_{V_b} d\mathbf{x}\langle E\rangle = 2\Im\{\omega\}\int_{V_b} d\mathbf{x}\langle E\rangle$ as E is quadratic in the perturbation amplitude, and equation (6.30) gives [34]:

$$\Im\{\omega\} = \frac{-\int_{A_b} d\mathbf{a}\cdot\langle\mathbf{W}\rangle + \int_{V_b} d\mathbf{x}\langle D\rangle}{2\int_{V_b} d\mathbf{x}\langle E\rangle} \tag{6.32}$$

Now, equation (6.15) ensures that if a perturbation occurs then the denominator on the R.H.S. of equation (6.32) is positive. We draw therefore the conclusion that *the system described by equations* (5.1) - (6.6) *is unstable against the growth of the amplitude of an oscillation with period* τ *if and only if:*

$$\int_{V_b} d\mathbf{x}\langle D\rangle > \int_{A_b} d\mathbf{a}\cdot\langle\mathbf{W}\rangle \tag{6.33}$$

Moreover, the cases

$$\int_{V_b} d\mathbf{x}\langle D\rangle < \int_{A_b} d\mathbf{a}\cdot\langle\mathbf{W}\rangle \tag{6.34}$$

and

$$\int_{V_b} d\mathbf{x} \langle D \rangle = \int_{A_b} d\mathbf{a} \cdot \langle \mathbf{W} \rangle \tag{6.35}$$

correspond to damped oscillation (i.e., stability) and to constant-amplitude oscillation respectively. In the latter case, if both sides vanish then the amplitude of the oscillation vanishes also identically. Together, relationships (6.33), (6.34) and (6.35) are usually referred to as *Rayleigh's criterion of thermo-acoustics* [2] .

Not surprisingly, and just as in the energy balance (6.21) it is derived from, Rayleigh's criterion predicts instability, marginal stability and stability whenever the R.H.S. of (6.33) -henceforth referred to as *destabilising term*- is larger, equal to or smaller than the L.H.S. -the *stabilising term*- respectively. The destabilising and the stabilising term are time-averages on a period τ of volume and surface integrals taking into account dissipative processes occurring in the fluid bulk (including combustion heat release) and propagation of sound across the boundaries respectively.

In particular, (6.35) may be obtained straightforwardly from time averaging of both sides of (6.21), provided that we redefine $\langle a \rangle \equiv \lim_{\tau\to\infty} \dfrac{1}{\tau} \int_0^\tau dt a$. This is far from surprising, as time-averages from 0 to τ and from 0 to ∞ give the same result for purely periodic functions $\Im\{\omega\} = 0$. Remarkably, we may replace the $\Im\{\omega\} = 0$ assumption with the assumption $E < \infty$ at all times, given the well-known fact that the time-average from 0 to ∞ of $\dfrac{da}{dt}$ vanishes for arbitrary quantity a [41].

The main difference between Rayleigh's criterion and the original (6.21) is the assumption (6.31) of periodic oscillation in time with a well defined period τ, an assumption usually satisfied in real-life applications where the combustors exhibit a discrete acoustic frequency spectrum with well-defined peaks. In a nutshell, Rayleigh' criterion is the time-averaged and volume-averaged energy balance of an acoustic perturbation, duly corrected for non-adiabaticity, with a well-peaked frequency spectrum (as $\dfrac{|\Im\{\omega\}|}{|\Re\{\omega\}|} << 1$).

Apart from that, the validity of Rayleigh's criterion relies just on the linearisation of the simple equations (5.1) - (6.6) under the constraint (6.13). The main advantage of Rayleigh's criterion is precisely its validity regardless of the detailed microscopic description of heating processes and turbulence. In fact, its proof requires no detailed information concerning combustion. As for turbulence, it plays no role as far as (6.13) holds and the detailed dependence of $\mathbf{v}_1$ on space and time is of no relevance in the low Mach approximation. This independence allows e.g. utilisation of Rayleigh's criterion in the analysis of instabilities by post processing the results of compressible CFD software packages like e.g. those based on compressible Large Eddy Simulation (*LES*) of unstable combustors [4].

[2] As for the isentropic case, ∇Q inside the flame plays a negligible role in Rayleigh's criterion provided that the upstream Mach number M is low enough, namely $M < \left(-1 + \frac{T_d}{T_u}\right)^{-2}$ where T_d and T_u are the values of temperature of the unburnt and the burnt gases respectively -see equation (6.17) of [40]. This condition is satisfied in most cases, marginally at least

For example, it is possible to start from these results and map the Rayleigh index across the fluid, in order to ascertain which regions of the fluid actually contribute to instability. Different regions of fluid may therefore trigger humming at different frequencies [5]. By far and large, Rayleigh's criterion is the only generally accepted stability criterion in the community of humming researchers.

As stated above, the first and most obvious consequence of Rayleigh's criterion is that the onset of humming is facilitated whenever the fluctuating quantities p_1, Q_1 etc. within the Rayleigh index are in phase. Dephasing such quantities is therefore the aim of most approaches to humming stabilisation, as discussed below.

Moreover, Rayleigh's index is negligible outside the flame in all combustion problems discussed below. It follows that the volume integrals of the Rayleugh's index reduce to volume integrals on the flame volume. Admittedly, such information is in implicit form only, as the flame volume appears just as the domain of integration of the destabilising term. Correspondingly, equation (6.22) allows (6.34), (6.35) and (6.33) to provide us with information on the shape of stable, marginally stable and unstable flames. Generally speaking, and in contrast with V_b, V_f may change with time, and we are just allowed to replace $\int_{V_b} d\mathbf{x}\langle D\rangle$ with $\langle\int_{V_f} d\mathbf{x}D\rangle$ (*not* with $\int_{V_f} d\mathbf{x}\langle D\rangle$!) when deriving both (6.34), (6.35) and (6.33). For example, (6.35) is equivalent to:

$$\langle\int_{V_f} d\mathbf{x}D\rangle = \int_{A_b} d\mathbf{a}\cdot\langle\mathbf{W}\rangle \tag{6.36}$$

In the following, a substantial part of the present work is concerned with in-depth discussion of this equation.

By far, the most widely known version of Rayleigh's criterion is the isentropic case, where equations (6.19) and (6.16) give D and W respectively. Even so, further modified versions are available. For example, a common (if oversimplified) approach is to neglect $\langle\mathbf{W}\cdot d\mathbf{a}\rangle$ altogether [42]. The impact of viscosity, heat conduction, mass sources and body forces (like e.g. gravity), insofar neglected, has been taken into account in [33]. It turns out that, just as for the heat release, suitable modulation of either body forces and mass sources may have a stabilising effect; both viscous dissipation and heat conduction in the bulk of the fluid are also stabilising [43]. Finally, the impact of chemical reactions on Rayleigh's criterion is discussed in [44]. It turns out that a specific chemical reaction may either raise or lower or lave unaffected the amplitude of a perturbation, depending on both the rate of the reaction and the values of the enthalpy of the chemical species involved, as both affect the heat release. Here all such effects are encompassed in the quantity Q_1.

Depending on the authors, versions of Rayleigh's criterion including non-zero $\langle\mathbf{W}\cdot d\mathbf{a}\rangle\neq 0$ and the contribution of entropy gradient are referred to as *extended* or *generalised Rayleigh's criterion*, but the fundamental structure remains the same. As for the pros and cons of Rayleigh's criterion, see Fig. 6.4

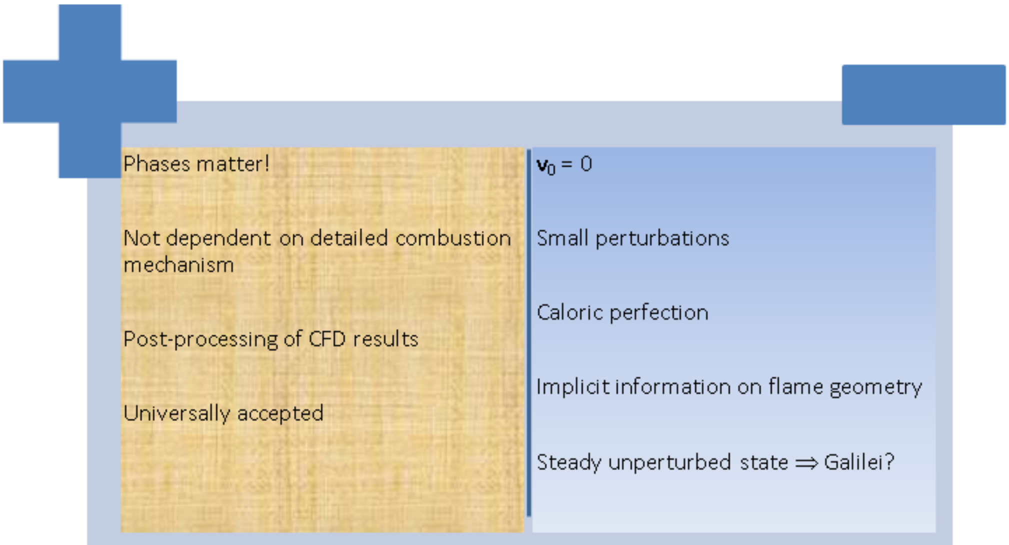

Figure 6.4: *Pros and cons of Rayleigh's criterion. See text for details.*

6.2.4 A trouble with Rayleigh

So far, we have quoted just one application of Rayleigh's criterion (the post-processing of compressible LES results) and one consequence (the relevance of relative phases of the perturbations of various physical quantities). Is it possible to make use of Rayleigh's criterion in the form (6.33)-(6.34)-(6.35) discussed above in a more straightforward manner? The answer is likely to be negative for two reasons.

Firstly, these relationships hold in the linear regime, and their validity whenever non-linear effects are relevant is doubtful. For instance, if we take the Fourier transform of both sides of (6.20) in the low Mach limit we obtain

$$\frac{|\overline{\mathbf{v}_1}|}{|\mathbf{v}_0|} = \frac{1}{\gamma M} \frac{|\overline{p_1}|}{p_0}$$

where $\overline{a}$ is the Fourier transform of the generic quantity a. Even for small humming amplitude $\frac{|\overline{p_1}|}{p_0} << 1$ the L.H.S. may be ≈ 1 (and the linearisation approximation may fail) either for $M << 1$ or for $|\mathbf{v}_0| \approx 0$; the latter condition is verified e.g. near the center of recirculation zones in real combustors. Moreover, periodic oscillations with constant amplitude are usually described with the help of limit cycles, a feature of nonlinear dynamics where the validity of (6.35) is no trivial matter. For the moment, we limit ourselves to linear theories. Nonlinear models will be discussed later.

Secondly, for all its generality Rayleigh's criterion provides just a link between perturbations of different physical quantities p_1, s_1 and the like. In particular, Rayleigh's criterion provides us with implicit information only as far as the shape of humming-free flames is concerned, through (6.22). Evaluation of the latter requires solution of the equations of motion in all cases, leaving to Rayleigh's criterion the role of stability check of the solutions.

6.2.5 Modal analysis and transfer function

Luckily, equation (6.32) ensures that the sign of $\Im\{\omega\}$ encompasses the same physical information of (6.33) - (6.35) - (6.34). In order to compute this sign, we start with the homogeneous version ($\frac{\partial Q_1}{\partial t} = 0$) of equation (6.29). Usually, it is possible to write the solution as a linear superposition

$$p_1(\mathbf{x}, t) = \sum_n c_n \varphi_n(\mathbf{x})\, exp(-i\omega_n t) \tag{6.37}$$

where $\varphi_n(\mathbf{x})$ solves the eigenvalue problem $\nabla \cdot (c_{s0}^2 \nabla \varphi_n) + \omega_n^2 \varphi_n = 0$ with eigenvalue ω_n^2 and the c_n are constant coefficients. As for the general inhomogeneous problem (with source $\frac{\partial Q_1}{\partial t} \neq 0$) where combustion is taken into account, standard Green function techniques are available for the solution in the time domain, provided that the source is known [45].

An alternative, quite popular approach is to write the Fourier transform $\overline{Q_1}(\omega)$ of $Q_1(t)$ as a function (*(flame) transfer function*, FTF) $\overline{Q_1}(\omega) = f_{FTF}\{\overline{\mathbf{v}_1}(\omega), \overline{p_1}(\omega)\}$ of the Fourier transforms $\overline{\mathbf{v}_1}(\omega)$ and $\overline{p_1}(\omega)$ of $\mathbf{v}_1$ and p_1 - see Fig. 6.5 and Fig. 6.6 [3].

Then, ω_n is found solving the eigenvalue problem given by the following couple of equations:

$$\omega_n^2 \overline{p_1} + \nabla \cdot \left(c_{s0}^2 \nabla \overline{p_1}\right) = i\omega_n (\gamma - 1) f_{FTF}\{\overline{\mathbf{v}_1}, \overline{p_1}\} \tag{6.38}$$

[3]Many authors assume the FTF to depend on $\overline{\mathbf{v}_1}(\omega)$ only. For a comprehensive review, see Chapter 2 of [46].

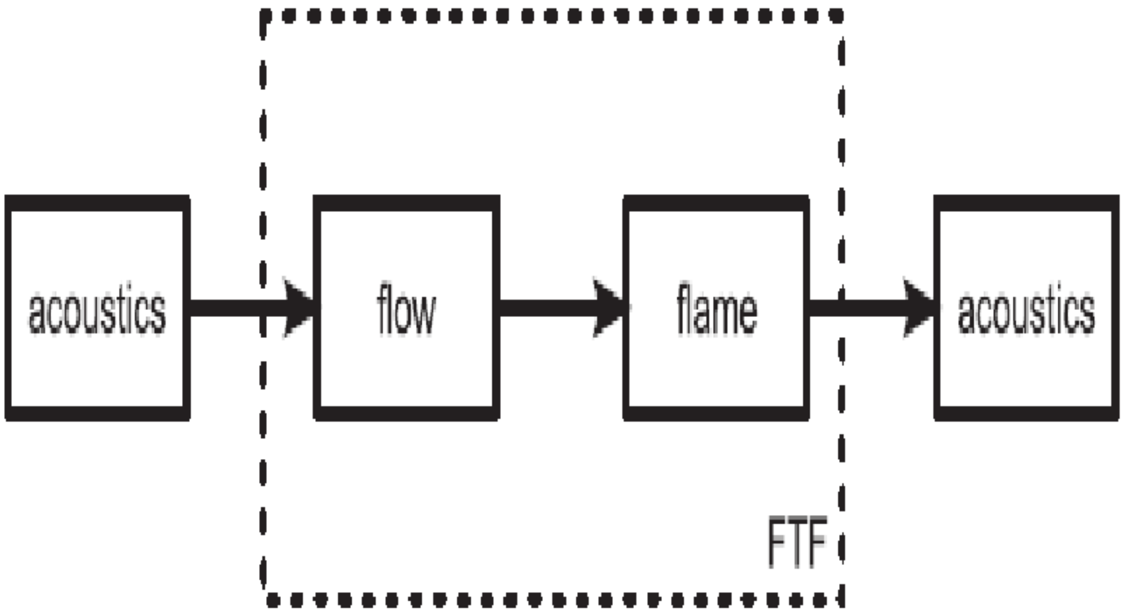

Figure 6.5: *Schematic description of a flow-flame coupling described by a FTF -from Ref. [47].*

$$-i\omega_n\rho_0\overline{\mathbf{v}_1} + \nabla\overline{p_1} = 0 \tag{6.39}$$

Equations (6.38) and (6.39) are derived from applying Fourier transform to both sides of equations (6.29) and (6.20). The system (6.38) - (6.39) is made of two equations in two unknown quantities $\overline{\mathbf{v}_1}$ and $\overline{p_1}$. Together with the definition of the FTF, equation (6.38) is basically the well-known *Helmholtz' equation* [4] [48]. In analogy with electronics, it can be said that (6.38) represents the *feedback* effect of acoustics on the fluid dynamics, represented by (6.39). This is why $f\{\overline{\mathbf{v}_1}, \overline{p_1}\}$ is called *(flame) transfer function.* FTF often depends on $\overline{\mathbf{v}_1}$ only.

Here the signal is made of perturbation of both pressure and velocity, i.e. two physical

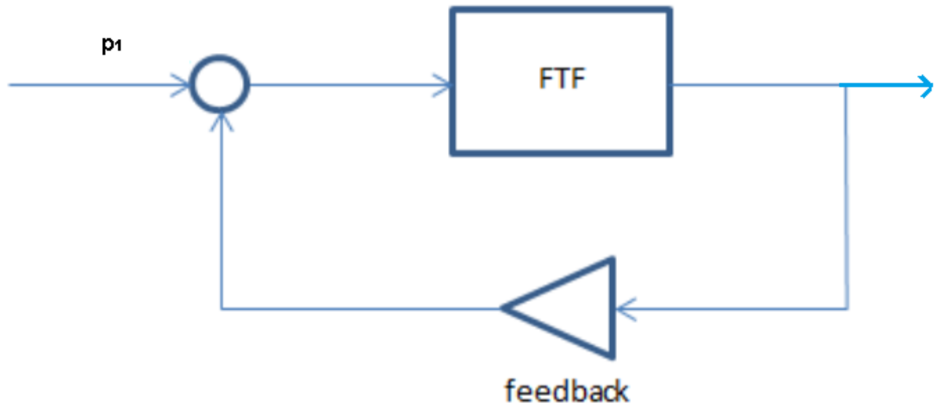

Figure 6.6: *A description of the feedback provided by* (6.38). *The small circle on the left represents equation* (6.39)*. Pressure and velocity perturbations act as input and output quantities of* (6.39) *here. The rectangle represents the FTF. Its output* $\overline{Q_1}$ *acts as input of the feedback equation* (6.38)*, displayed as a triangle here. In turn, the output of the latter equation acts as input of* (6.39).

quantities. As for the third quantity entering E in the general case, entropy, we observe that equations (6.13) and (6.8) ensure that its perturbation is localised at all times at the location of heat production (where $Q_1 \neq 0$) and does not propagate across the system.

Finally, if we take the curl of both sides of (6.20) then equation (6.13) leads to the conclusion that the perturbations of vorticity $\nabla \wedge \mathbf{v}$ vanish identically. Things are going to change when (6.13) no longer holds.

Formally, the system (6.38) (6.39) is homogeneous, so that we may still invoke (6.37). Once all ω_n's are known, we may focus our attention on that particular ω_n with the maximum imaginary part $\Im\{\omega_n\}$, say $\Im\{\omega_n\} = g_{max}$. If $g_{max} < 0$ then the imaginary parts of all other ω_n are also negative. Then (6.37) ensures that $|p_1|$ is a monotonically decreasing function of time. In this case, linearity of (6.20) , (6.6) and (6.24) ensures that E is a monotonically decreasing function of time, hence stability. In contrast, if $g_{max} > 0$ then $|p_1| \approx \exp(g_{max} t)$ diverges as $t \to \infty$, and the system becomes unstable in the same limit

$t \to \infty$. We stress the point that no instability may be predicted here but in this limit.

The approach described above (usually referred to as *modal analysis* in the literature) is currently the topic of a vigorous research effort. As for the crucial question whether a given combustor with given boundary conditions undergoes humming or not, the simple stability criterion $g_{max} < 0$ has the same physical meaning of Rayleigh's criterion in the form (6.34). With respect to the latter, it has the advantage that no explicit computation of E is ever required: for example, it does not require to decide if the isentropic formula (6.15) or the more general (6.18) is to be utilised. This is far from being trivial, as it is often difficult to ascertain which correlation is actually relevant starting from experimental data - see Fig. 6.7.

Furthermore, if instability occurs then once g_{max} is known the corresponding frequency ω_n and the corresponding eigenfunction are also known. Since the latter depends on space we know the location of the peaks of pressure perturbation p_1 Consequently, we know also the position of the location of maximum mechanical stress induced by humming on the combustor surface, a piece of information of great engineering relevance.

A further advantage of humming analysis based on FTF is that it allows quick utilisation of the measurements taken in systematic experimental campaigns at a manufacturer's test rig. To fix the ideas, let us suppose we measure oscillations on a combustor (say, I) with typical length, say, $L = 1$ m, and obtain the FTF of this combustor from the measurements [4]. Then, let us repeat the same measurements on a similar combustor (say, II) but with $L = 1.2$ m, and obtain the FTF of this combustor. When it comes to a combustor III with $L = 1.1$ m (all the rest being equal), cheap interpolation between I and II is likely to provide reliable results for III.

Moreover, once FTF is known then not only the system of equations (6.38) - (6.39) may be solved with the help of well-known software for realistic combustor geometries, but the FTF formalism allows utilisation of Bode-Nyquist stability criteria, in further analogy with electronics.

Finally, according to many authors [24] [49] [7] the value of $\Re\{\omega_n\}$ is often very near to the (real) value ω_{n0} of the same quantity computed in the much simpler case $\dfrac{\partial Q_1}{\partial t} = 0$ see Fig. 6.8. Since the propagation of the signal occurs at the speed of sound, our analogy with electronics intuitively explains why $\omega_n \approx \omega_{n0}$: humming onset relies on acoustic feedback, and the latter is particularly strong when transmission of acoustic energy across the system achieves maximum efficiency, i.e. at resonance. This fact allows us to choose $\omega_n = \omega_{n0}$ as an initial guess when solving numerically the eigenvalue problem (6.38) (6.39) in a given geometry, provided at least that $\dfrac{|\Im\{\omega\}|}{|\Re\{\omega\}|} << 1$ at all steps of the iteration procedure. Admittedly, spatial derivatives still appear in the eigenvalue problem. However,

[4]It is also possible to *compute* the FTF with the help of both CFD and acoustic codes: the latter provide us with the response of the system to perturbations of the unperturbed flow computed by the former. Comparison with experiments overcomes numerical uncertainties.

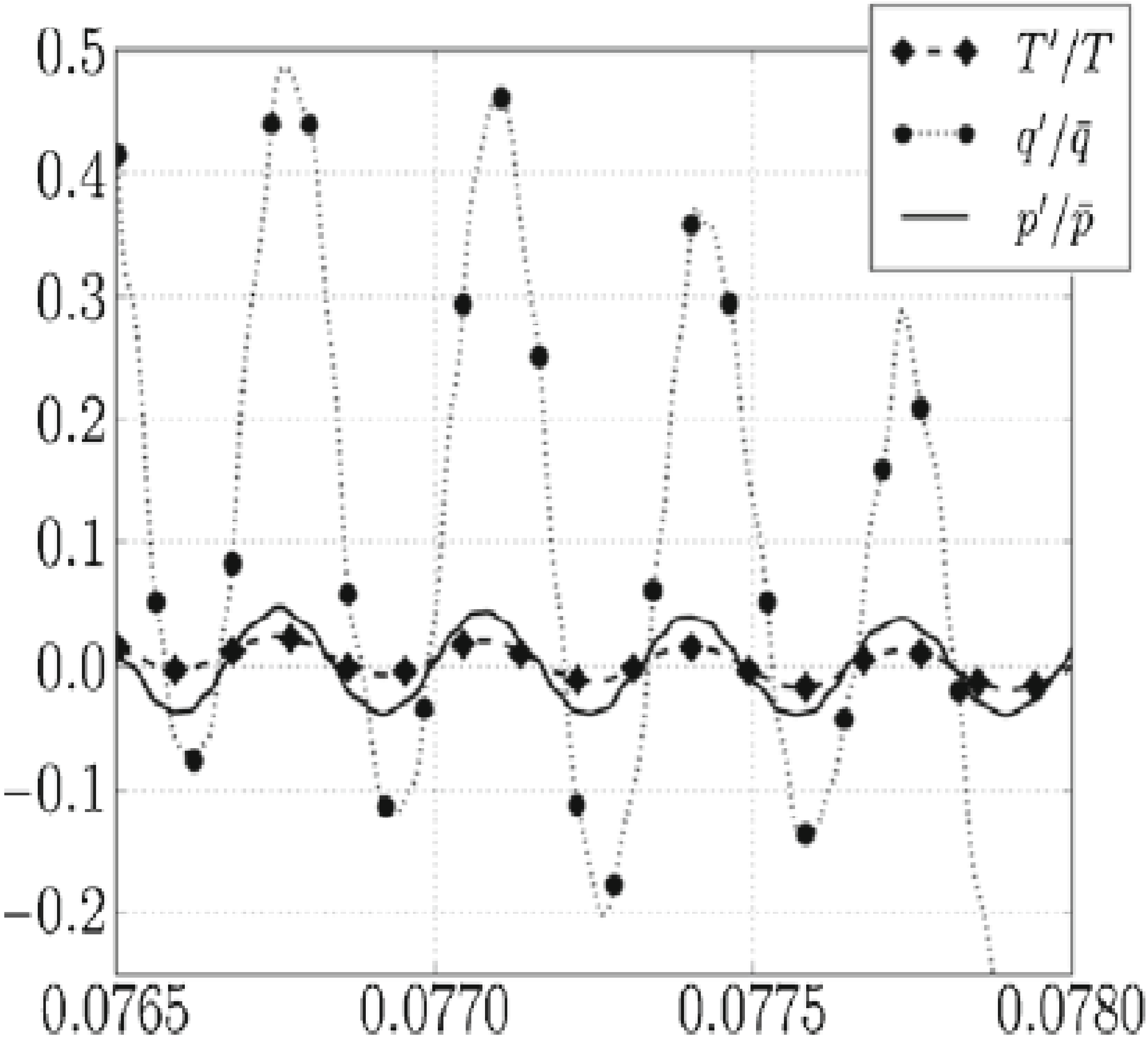

Figure 6.7: *Normalised fluctuations of temperature, heat release and pressure vs. time (s) in a ocombustor in humming - from Ref. [20]. Fluctuations of all quantities are well correlated to each pther. These data seem to make it difficult to decide if D is ruled by the correlation between e.g. fluctuations of heat release and temperature or by the correlation between fluctuations of heat release and pressure (as in the isentropic case).*

these derivatives are routinely dealt with through standard approaches like e.g. finite element methods.

From manufacturers' point of view, modal analysis seems to be promising because of the powerful and reliable numerical methods which -in principle- allow humming prediction in combustor design. Today, this goal is successfully achieved in three separate classes of problems at least -see [19], [20] and [21]- which are discussed in more detail below.

Generally speaking, in the framework of linear stability analysis the case of modal analysis is somehow complementary to Rayleigh's criterion: in contrast with the latter, the former allows humming prediction -and not just stability check *a posteriori*- but requires both validity of assumption (6.37) and knowledge of the FTF.

As for the validity of the assumption (6.37), its violation may have far-reaching consequences: it can cause algebraic growth of oscillations for a short time even though all the eigenvectors of the system could be decaying exponentially with time [50]. This means that $p_1(t)$ may include terms which scale as $t\exp(-i\omega t)$. As a consequence, even if modal analysis predicts stability ($g_{max} < 0$) E may grow at $t < \infty$ even if it goes to zero at $t \to \infty$. Moreover, this temporary growth may push the system initially at rest outside the linear regime towards a stable, constant-amplitude oscillation (a limit cycle). In this case, predictions provided by modal analysis could be over-optimistic [51]. Generally speaking, if (6.13) holds then the solutions of the system of equations (6.29) and (6.20) do satisfy (6.37): it is said that the problem is *normal*. For an overview of the pros and the cons of modal analysis from the point of view of a GT manufacturer, see Fig. 6.9.

As for the FTF, the original treatment of [49] focussed on rocket engines with liquid fuels: it linked the onset of thermo-acoustic instabilities and the dynamics of evaporation of liquid fuel droplets. Then, a simple analytical expression

$$f_{FTF} \propto n_{FTF} \cdot \exp(i\omega\tau_{FTF})$$

for the FTF (referred to as $n-\tau$ in the literature) has been introduced in formal analogy with [49] for the premixed combustion of gaseous fuels. Here n_{FTF} and τ_{FTF} describe a coupling strength and a delay time respectively.

The $n-\tau$ FTF puts in evidence the relationship between the FTF and the Rayleigh index. Let us e.g. focus our attention on a tube of length L where the pressure perturbation vanishes at both ends and where a concentrated heat source (not necessarily a flame!) is located at position x_f with $0 \leq x_f \leq L$ -see Fig. 6.10. Here we follow the discussion of Ref. [52]. An ansatz for p_1 which satisfies the boundary conditions is $p_1 \propto \sin\left(\frac{2\pi t}{\tau}\right)\sin\left(\frac{\pi x}{L}\right)$. According to the $n-\tau$ FTF model and to equation (6.20), the perturbation heat release which results from the corresponding perturbation of velocity is $\propto \sin\left[\frac{2\pi}{\tau}\cdot(t-\tau_{FTF})\right]\cdot\cos\left(\frac{\pi x}{L}\right)\cdot\delta(x-x_f)$ where the factor $\cos\left(\frac{\pi x}{L}\right)$ comes out from the one-dimensional Euler equation (6.20) linking perturbations of pressure and velocity.

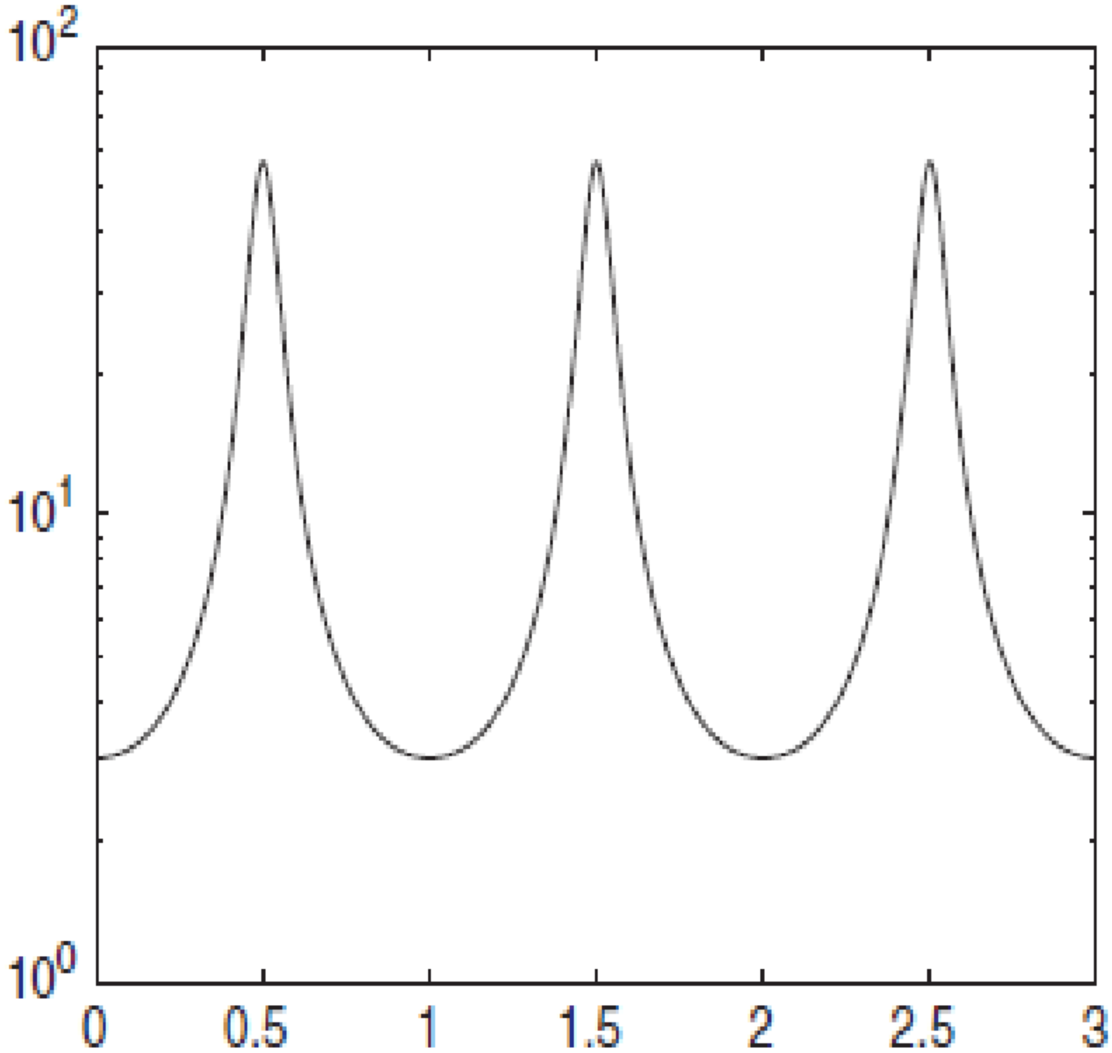

Figure 6.8: *Amplification of acoustic energy (dimensionless) vs. normalised frequency (dimensionless) in a combustor. Here the normalised values of ω_{n0} are* $0.5, 1.5, 2.5$ *etc. Near-resonance response of the flame to external excitation results in large amplification of acoustic energy - from Ref. [7].*

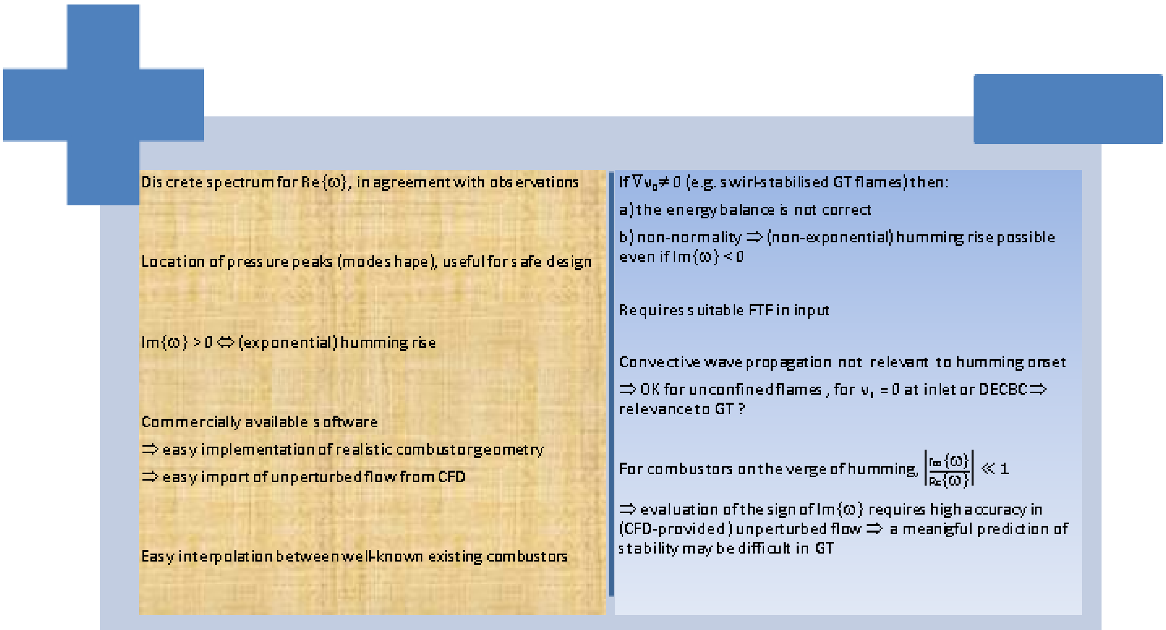

Figure 6.9: *Modal analysis for GT: pros and cons. See text for further details.*

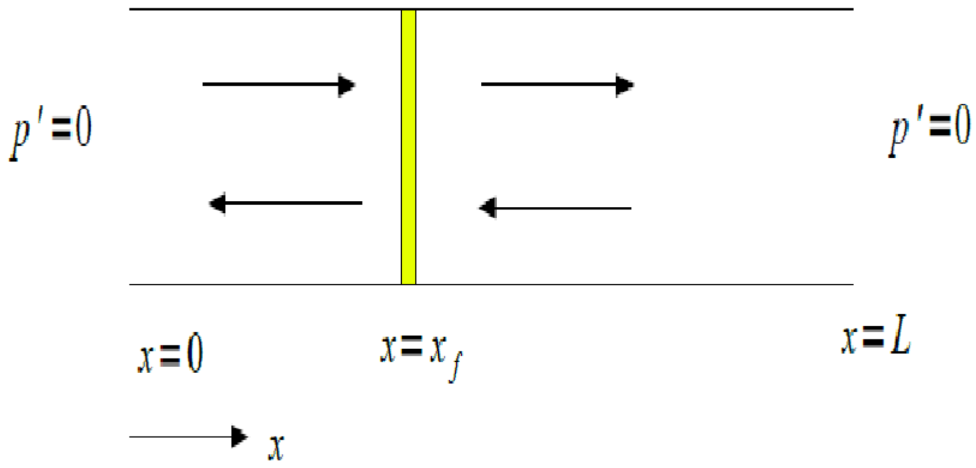

Figure 6.10: *A tube of length L with vanishing pressure perturbations at both ends and a concentrated heat source at $x = x_f$.*

In the isentropic version of Rayleigh's criterion, the resulting Rayleigh index is:

$$D \propto \cos\left(\frac{2\pi\tau_{FTF}}{\tau}\right) \cdot \sin\left(\frac{2\pi x_f}{L}\right) \tag{6.40}$$

This expression becomes greater than zero (and humming occurs, as the stabilising acoustic energy flux across the boundaries vanishes identically with these boundary conditions) in the regions of the plane $\left(\frac{x_f}{L}, \frac{\tau_{FTF}}{\tau}\right)$ plotted in red in Fig. 6.11. It is obvious that the actual occurrence of instability depends critically on τ_{FTF}.

Given its deceptively simple structure, the $n-\tau$ FTF has given birth to a vast amount of research -for a review see [53]. In particular, it allows modal analysis of an one-dimensional system with uniform unperturbed flow ($\nabla \mathbf{v}_0 = 0$) to exhibit transition from stability to instability as the phase $\Re\{\omega\} \cdot \tau_{FTF}$ exceeds some threshold values [35]. This result fits Rayleigh's original remarks concerning the relevance of relative phases in hum-

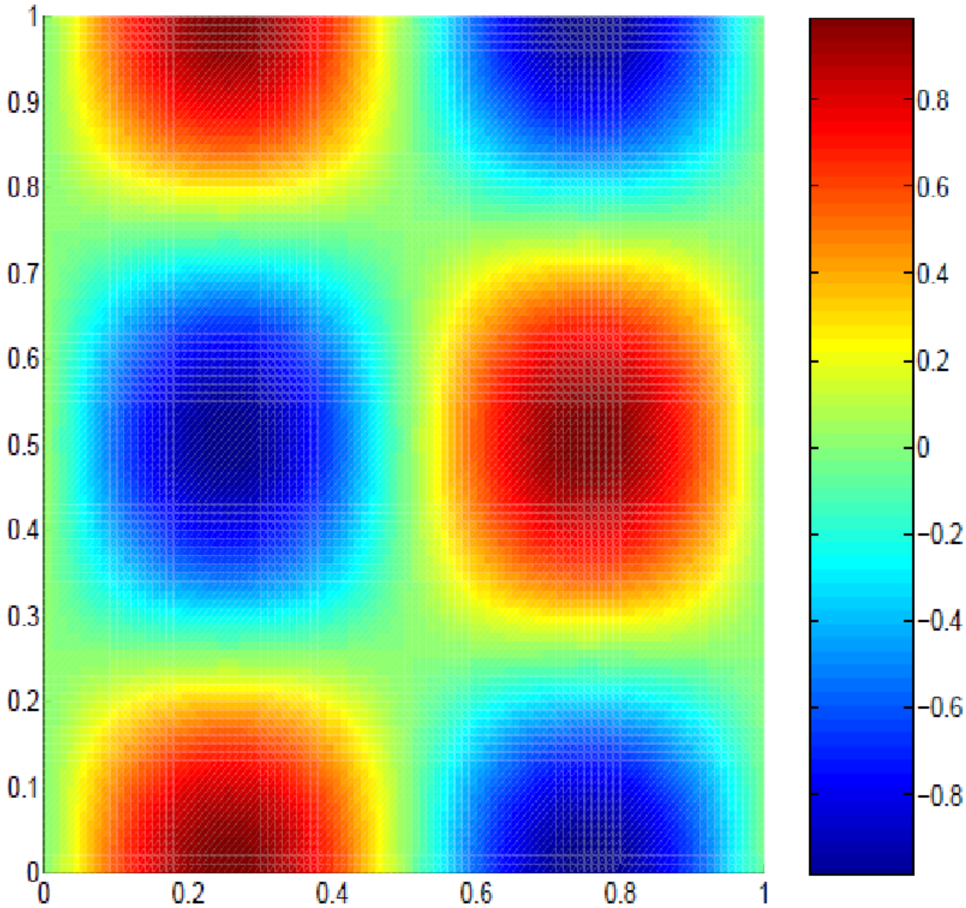

Figure 6.11: *Graphical representation of Rayleigh index in the isentropic version of Rayleigh's criterion. The horizontal and the vertical axis display* $\frac{x_f}{L}$ *and* $\frac{\tau_{FTF}}{\tau}$ *respectively. Red (blue) regions correspond to positive (negative) Rayleigh index.*

ming onset.

Moreover, in the modal analysis of [35] it turns out that $\Re\{\omega\}$ itself depends weakly on τ_{FTF}, and this result too recalls further Rayleigh's words [31]:

> *If the air be at its normal density at the moment when the transfer of heat takes place, the vibration is neither encouraged nor discouraged, but the pitch is altered. Thus the pitch is raised, if heat be communicated to the air a quarter period before the phase of greatest condensation, and the pitch is lowered if the heat is communicated a quarter period after the phase of greatest condensation.*

This success has motivated decade-long research concerning FTF in more realistic cases - for a review, see e.g. [46]. In the case of the so-called *distributed time transfer function* [54] [55], for example, the scalar quantities n_{FTF} and τ_{FTF} are replaced with scalar fields $n_{FTF}(\mathbf{x})$ and $\tau_{FTF}(\mathbf{x})$ defined at each point of the flame. As a result, many analytical expressions for the FTF are available, which usually contain adjustable parameters.

Physically, the basic idea underlying a distributed FTF is that heat release fluctuations are coupled to velocity oscillations occurring at a reference upstream section after a time lag which depends on the position on the flame, i.e. a distribution of time-delays $\tau_{FTF}(\mathbf{x})$ is to be taken into account. This distribution is computed with the help of CFD, which allows to compute the time-of-flight of a particle of fuel from the inlet to a given point $\mathbf{x}$ on the flame.

In particular, some of these models allow manufacturers to perform modal analysis of their own combustors with the help of simplified description of the combustor geometry (*low order models*). A popular example of low order model is the *(acoustic) network*. The system is descibed as a network of simple elements. Each of the latter is described by its own transfer function (possibly in multidimensional form, commonly referred to as *transfer matrix*). Pressure and velocity perturbations are the usual variables of choice. Together, the FTF, the conservation equations at the boundaries among adjacent network elements, the transfer matrices of the latter and the flame jump conditions yield a set of linearised equations in the frequency domain, to be solved to determine the frequency and the growth rate of the oscillation. For an example of acoustic network, see Ref. [56] as well as Fig. 6.12 and Fig. 6.13.

It turns out [19] that modal analysis with CFD-computed distributed FTF provide predictions concerning both the onset and the frequency of humming in agreement with experiments, where the latter have been

> *designed in order to have an acoustic behavior as closest as possible to an ideal wall*

Here the words *ideal wall* refer to a particularly simple boundary condition ($\mathbf{v}_1 = 0$) which does not involve any mean flow. For such purposedly prepared experimental set-up,

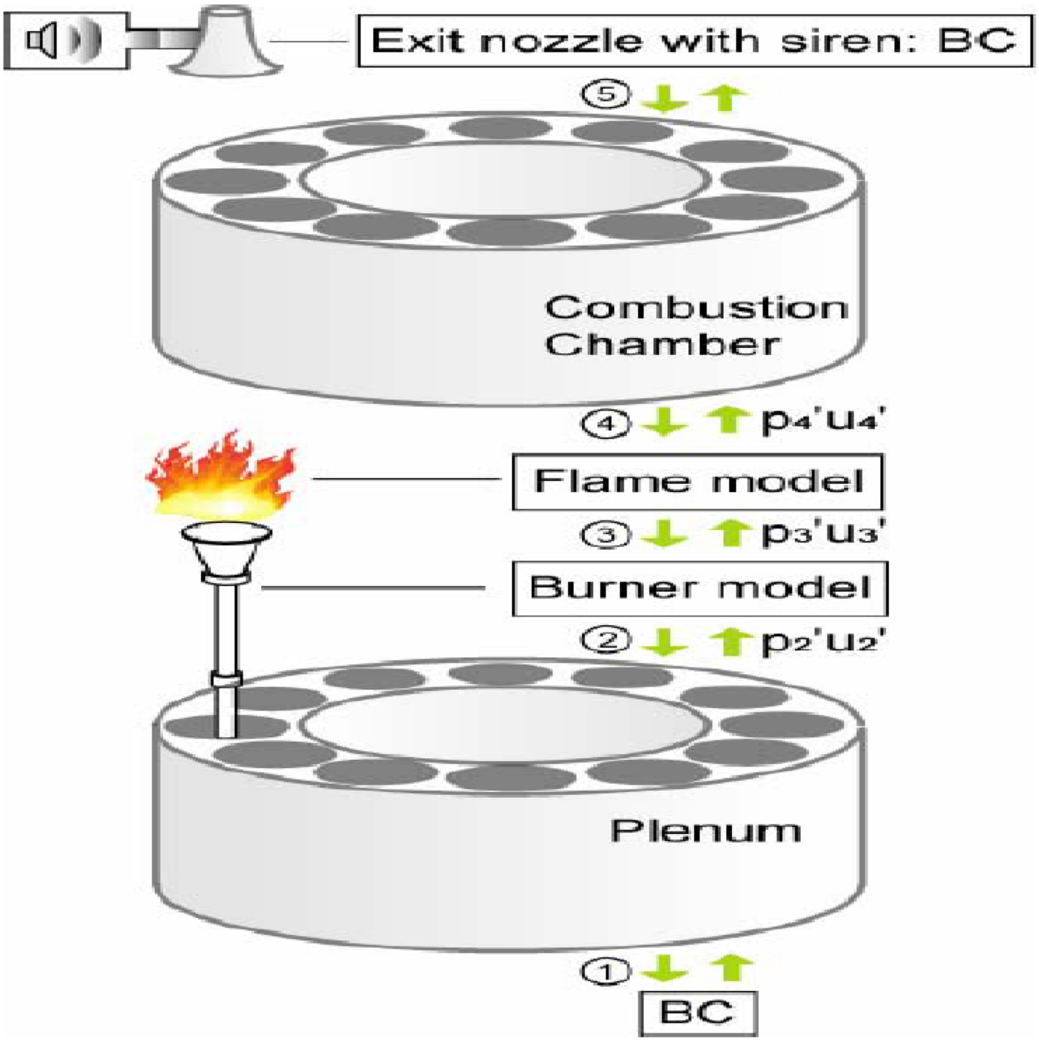

Figure 6.12: *Example of acoustic network - from Ref. [56].*

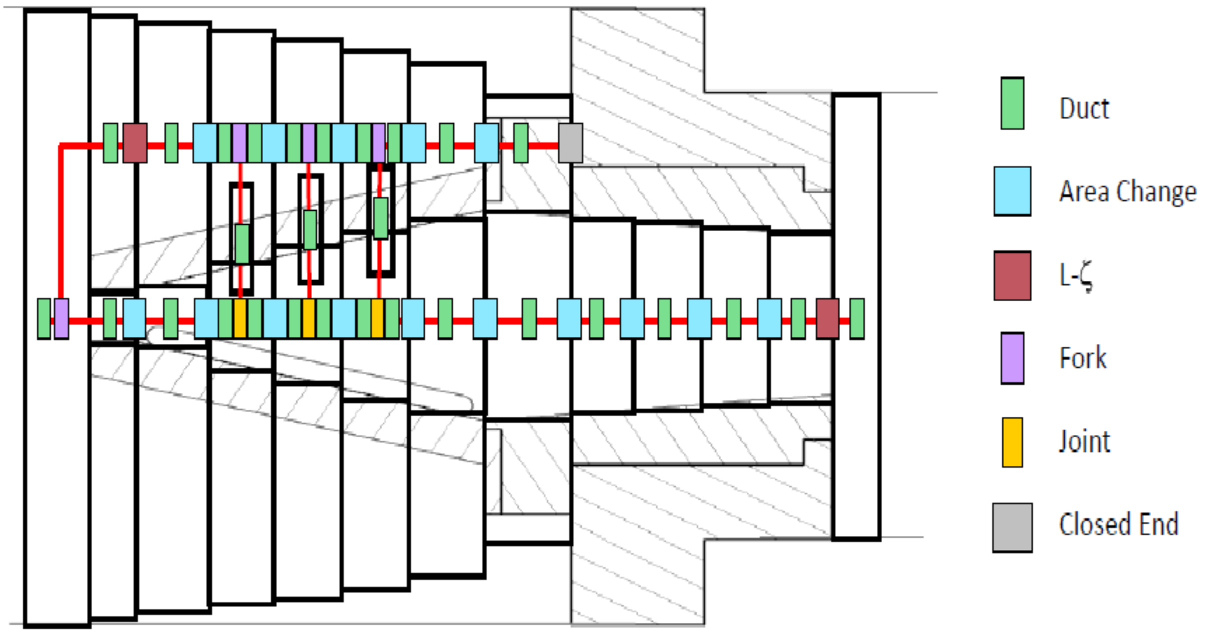

Figure 6.13: *Detail of Fig. 6.12: the burner - from Ref. [56]. Pressure losses are concentrated in $L-\zeta$ blocks.*

well-known numerical methods allow solution of (6.38) - (6.39) with the help of Dirichlet and/or Neumann boundary conditions. It remains to be seen if such approach is relevant to real-life industrial combustors. For example, ideal wall boundary condition implies that the energy of the reflected acoustic wave -as computed starting from the solutions of equations (6.38)-(6.39) above- is equal to the energy of the impinging acoustic wave. This prevents conversion of impinging acoustic waves into non-acoustic perturbations (see below), in contrast e.g. with the models of [3] and [1].

Actually, *a posteriori* comparison of numerical results with experimental data obtained from measurements either in existing combustors or in dedicated test-rigs allows manufacturers to find the values of such parameters, but then the capability of humming prediction from scratch in new combustors -obviously a feature of highest relevance to manufacturers- is lost for good.

Indeed, *a priori* computations of the FTF from first principles are available. Usually, they are:

- either limited to the low-frequency limit [57]
- or related to problems affected by quite restrictive assumptions concerning the (usually Bunsen-like, conical) shape of the unperturbed flame - see e.g. [58] and Fig. 6.14 - and/or the boundary conditions [19] and/or the direction of propagation of the wave [20]
- or the result of cumbersome LES simulations [59]. According to [13], today LES is the only current modeling strategy that correctly predicts mean statistical (i.e. mean and Root Mean Square) flow features in strongly swirled flows.

In particular, LES allows computation of FTF starting from the computation of the response of the flame to a siren located outside it (typically near the fuel inlet) ringing at a given frequency, i.e. it positions the sound source at a given location far from the flame. Implicitly, therefore, LES-assisted computation postulates -without further proof- that humming instability is of convective, not absolute nature -for a discussion, see [4].

Furthermore, even if LES provides accurate computation of FTF, the latter enters just the R.H.S. of Helmholtz' equation (6.38). Thius means that the flow computed by CFD affects the source of acoustic oscillations. But no information concerning $\mathbf{v}_0$ ever enters the L.H.S. of (6.38). This means that the unperturbed flow leaves propagation of signals across the combustor unaffected. This implicit assumption is criticised below.

Moreover, LES start from the $\omega_n = \omega_{n0}$ guess discussed above [5] (with $\Im\{\omega_{n0}\} = 0$) and lead therefore to meaningful result only if numerical errors -due e.g. to the very CFD algorithm- never exceed the small threshold $\dfrac{|\Im\{\omega\}|}{|\Re\{\omega\}|} << 1$. Fig. 6.15 displays a qualitative sketch of the incertitudes corresponding to different approaches to CFD.

[5] This requirement is somehow relaxed in [55].

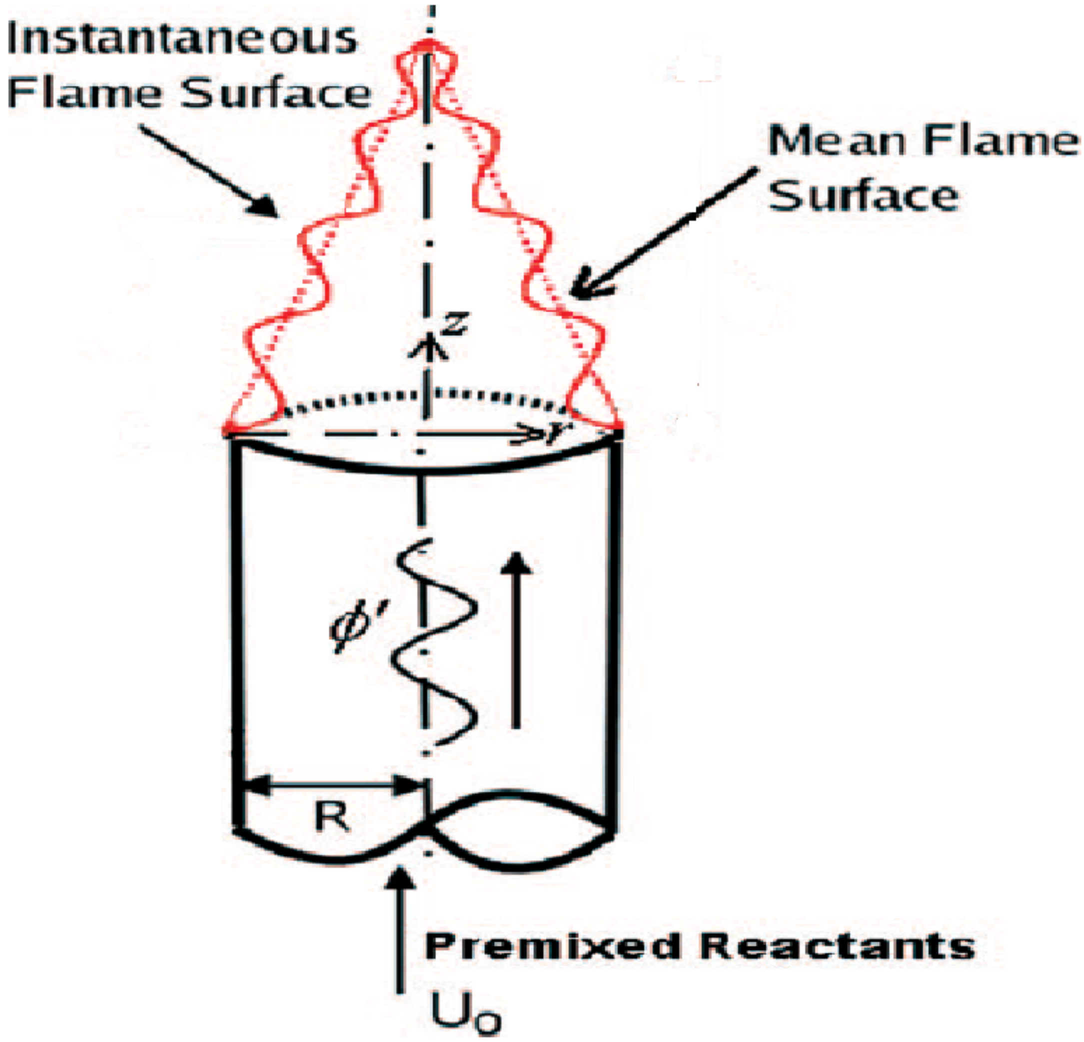

Figure 6.14: *Schematic of axisymmetric conical flame geometry for computations of FTF - abridged from Ref. [58].*

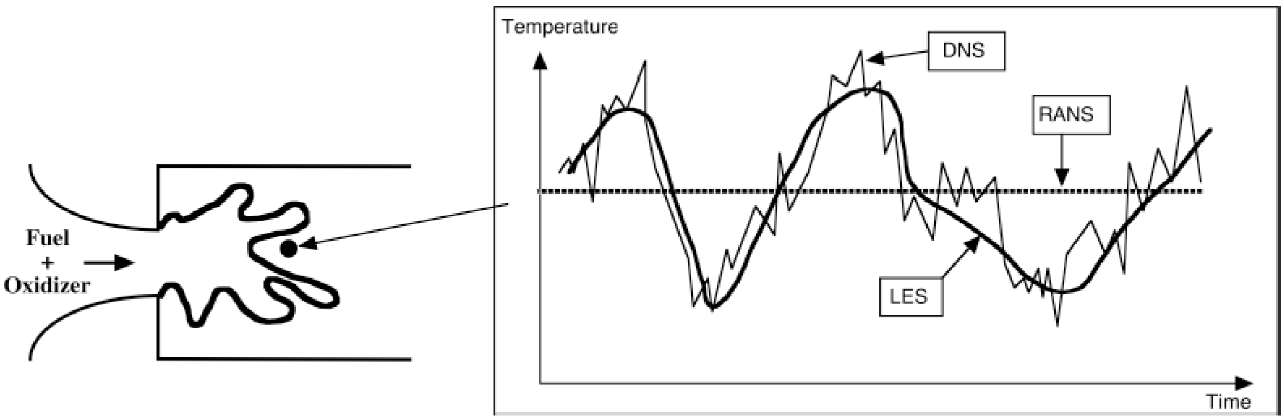

Figure 6.15: *Time evolutions of local temperature computed with DNS, RANS or LES in a turbulent flame - from Ref. [4].*

This condition should be verified for each CFD-assisted modal analysis [6]. Generally speaking, flame models obtained experimentally or numerically are known to be uncertain. Addressing the sensitivity of thermoacoustic results with respect to the input parameters is thus a necessary and important step towards reliable predictions of unstable modes in GT. Fig. 6.16 displays a typical result of modal analysis, i.e. a set of modes, each with its own frequency and growth rate. Should no uncertainty is present, each mode would correspond to a single point (black symbols) in the frequency plane.

A systematic investigation is available -Ref. [48]- which assesses the incertitude of the results of FTF-assisted modal analysis -with a $n-\tau$ FTF provided by LES- for the fundamental acoustic mode of a real, swirl-stabilised combustor. A Monte Carlo sampling is used on the two-dimensional space (n_{FTF}, τ_{FTF}). The Monte Carlo simulation relies on 4000 computations of solution of Helmholtz' equation, where 1 computation requires almost 10 minutes when using 24 processors. Admittedly, no clear, accurate analysis on the uncertainty range of n_{FTF} and τ_{FTF} is available in the literature; the authors assume a 10% uncertainty for both quantities. Each couple of values of n_{FTF} and τ_{FTF} in input corresponds to a complex frequency in output. Stability (instability) is predicted to occur when the growth rate exceeds a damping factor due to acoustic losses. (Here the condition $\frac{|\Im\{\omega\}|}{|\Re\{\omega\}|} << 1$ seems to be overlooked altogether). This damping factor is derived from comparison between experiments on one side and the results of Helmholtz' computations which assume zero losses on the other side, and is therefore also affected by uncertainty. Fig. 6.17 displays the results. Even if the uncertainty on the damping factor is neglected and if no non-normality is taken into account, it turns out that the probability that humming is triggered is 23%. To fix the ideas, a 50% value would correspond to throwing dice.

Recently, the definition itself of the variables which the FTF is built upon has been questioned [47] [7]. As we have seen, the familiar treatment of the FTF relies on the choice of the perturbations of velocity and pressure as fundamental quantities of the linearised theory. However, there is nothing special with this particular couple of variables.

[6] A more general issue concerning linearisation seems to be at stake here. When applied to a system of nonlinear equations, superposition of a small perturbation on an unperturbed state makes sense provided that no uncertainty affects our knowledge of the unperturbed state. (This is e.g. the case of thermoacosutical problems where analytical descriptions of the unperturbed state are available; an example is $\mathbf{v}_0 = 0$ everywhere. Another example is the search for local bifurcations in nonlinear dynamics [60]). In this case, in fact, we can always take the relative amplitude of the perturbation as small as we like. Thus, the error due to linearisation remains under control even as it propagates and grows with time. (Such growth occurs e.g. in chaotic systems like those occurring in fluid dynamics, with their strong sensitivity against small perturbatins of the initial conditions). It follows that linearity of the equations describing the evolution of the perturbation remains valid at all times. But if the unperturbed state itself is known up to a certain degree of confidence only (as it is customary when the unperturbed state is described with the help of CFD), then the superposition of an infinitely small perturbation is meaningless, because the evolution of the perturbation gets mixed up with the uncertainty on the unperturbed state. In summary, two basic requirements seem to be in conflict here, regardless of both the adopted solving algorithm and the available CPU computing power. On one side, the initial perturbation amplitude must be as small as we like in order to make all linearisation-induced errors negligible at all times. On the other side, the initial perturbation amplitude must be large enough to overcome the blurring due to the uncertainties affecting our description of the unperturbed state.

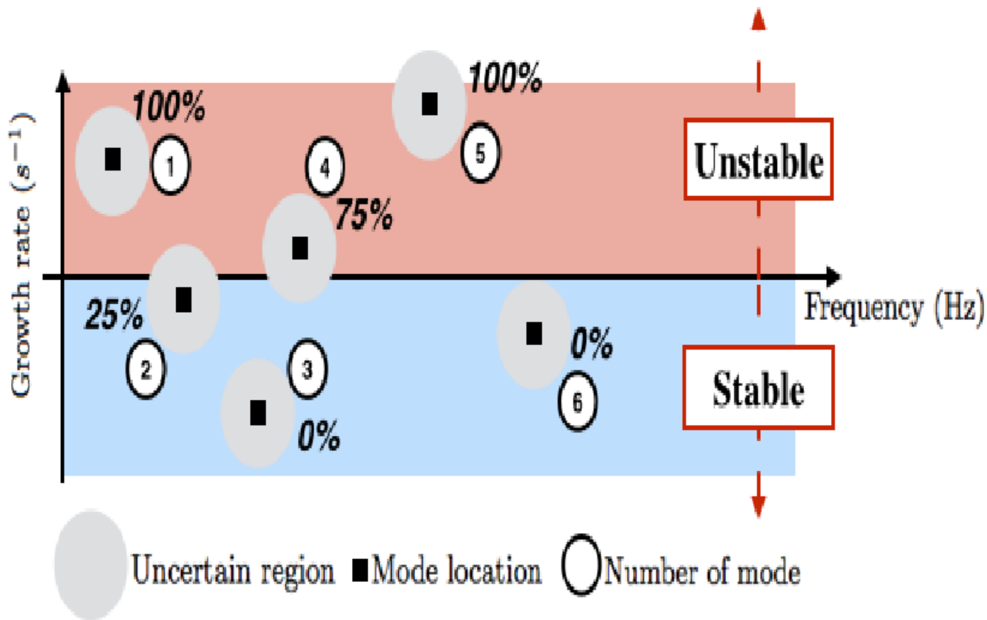

Figure 6.16: *Location of six thermo-acoustic modes in a typical combustor. Here, growth rate and frequency stand for $\Im\{\omega\}$ and $\Re\{\omega\}$ respectively. Modes 1, 4 and 5 are dangerous and should be controlled since the growth rate is positive. If uncertainties are present, each mode belongs to an admissible region of the frequency plane. Mode 2 (and maybe 6) also are somehow dangerous and should be controlled. The figure suggests that taking into account uncertainties is required for reliable predictions of combustion instabilities.- from Ref. [48].*

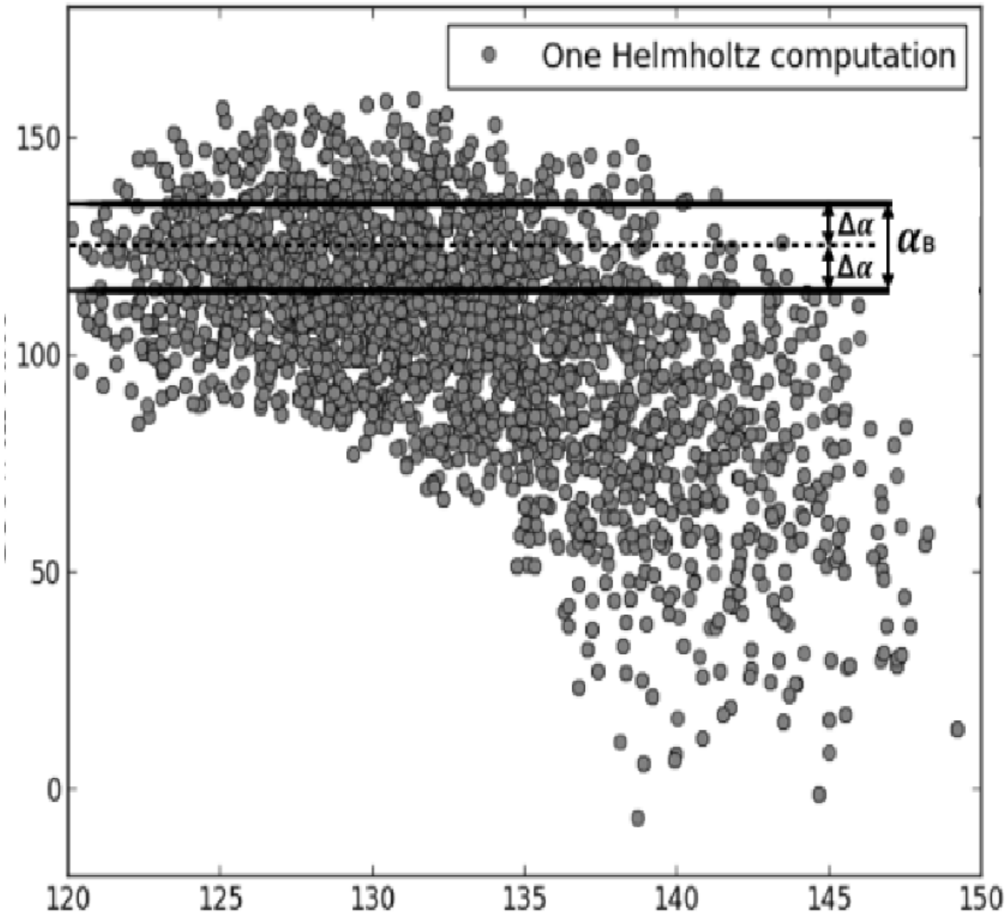

Figure 6.17: $\Im\{\omega\}$ *vs.* $\Re\{\omega\}$ *from a Monte Carlo simulation of LES-assisted modal analysis of the fundamental acoustic mode in a swirled combustor. Each grey circle coresponds to the result of one Helmholtz' computation. The horizontal line* $\Im\{\omega\} = \alpha_B = 125\ s^{-1}$ *corresponds to the damping threshold. Lack of humming and onset of humming predicted for* $\Im\{\omega\} < \alpha_B$ *and* $\Im\{\omega\} > \alpha_B$ *respectively. However,* α_B *too is affected by an uncertainty* $\Delta\alpha = \pm 10\ s^{-1}$*. Accordingly, LES-assisted modal analysis is able to provide no meaningful prediction of stability vs. instability for* $\alpha_B - \Delta\alpha < \Im\{\omega\} < \alpha_B + \Delta\alpha$*. Looking at all grey circles above the horizontal line* $\Im\{\omega\} = \alpha_B$*, moreover, it turns out that the probability that humming is triggered is 23%. Results are weakly dependent on the detailed distribution functions used for* n_{FTF} *and* τ_{FTF} *- from Ref. [48].*

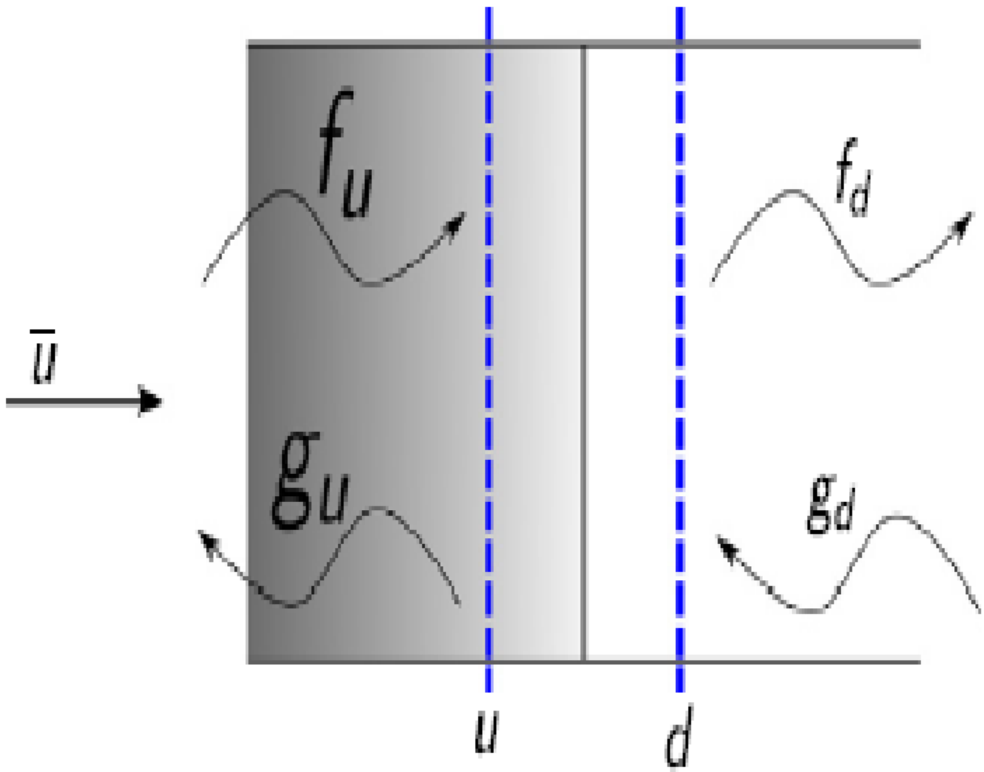

Figure 6.18: *Progressive and regressive waves in a one-dimensional model - see Ref. [7]. Labels u and d refer to upstream and downstream respectively.*

Even within a simplified, one-dimensional description of the system, if another couple is selected, namely the quantities $f = \frac{1}{2}\left(\frac{p_1}{\rho_0 c_{s0}} + u_1\right)$ and $g = \frac{1}{2}\left(\frac{p_1}{\rho_0 c_{s0}} - u_1\right)$ which correspond to progressive and regressive waves respectively and are linear combinations of the perturbations of pressure and of axial velocity, then the FTF modifies accordingly - see Fig. 6.18.

This choice has the advantage of satisfying the causality principle automatically, i.e. it allows natural distinction of causes and effects (in contrast, perturbations e.g. of velocity at a given time are always the sum of the contributions of incomping and outcoming waves, as the superposition principle holds). It turns out that with this new choice of variables modal analysis leads to a insofar undetected new class of modes (referred to as *intrinsic modes* in the literature). In contrast with the results of previous analysis, and in formal analogy with Darrieus-Landau instability outside thermo-acoustics, intrinsic modes come into existence because of the temperature jump at the flame -see Appendix C of - [7]- not just because of the phases as it could be expected when looking at Rayleigh's criterion. A new set of (*flame-intrinsic*) eigenmodes adds to the purely acoustic modes. Correspondingly, thermoacoustic instability may occur even in a perfectly anechoic environment, in agreement with experiments. This is not surprising, as the theory of intrinsic modes drops the assumption of isentropic fluids which Rayleigh's criterion relies upon [47]. It has also been shown that the linear analysis of stability based on the variables quoted above leads to a sufficient criterion for stability, namely *a system is stable if all its subsystems are stable* -see relationship (36) of Ref. [7]- or, equivalently, to a necessary criterion for instability. In analogy to Rayleigh's criterion, this criterion relies on the energy balance of an acoustic perturbation, suitably rewritten with the help of the new variables -see equation (27) of [7].

Unfortunately, this criterion is no sufficient criterion for instability -or, equivalently, it provides manufacturers with no necessary criterion for stability against humming. For practical purpose, therefore, it is likely to be just too restrictive: combustors which satisfy the criterion may as well be stable. To put it in other words, a system may be stable even if some subsystems are unstable, provided that enough damping compensates such instability in the remaining subsystems.

There is also a further, more physical reason which seems to weaken the relevance of this criterion to GT flames. The temperature jump at the flame drives both flame-intrisic modes and Darrieus-Landau instability. Both may be unstable for a perfectly flat flame of finite size (in the $He << 1$ limit, e.g. the diameter of the combustor may be much smaller than all relevant wavelengths, and the one-dimensional approach applies [7]). If suitable flame shapes (not captured in the one-dimensional approach) are able to compensate the destabilising effect of the temperature jump as far as Dariieus-Landau is concerned, it is conceivable that flame-intrinsic modes too get stabilised.

Finally, even if the FTF is known, solution of the system (6.38) - (6.39) for a real combustor requires knowledge of the relevant boundary conditions. This issue is far form trivial and its discussion lies beyond the scope of the present work. Basically, validity of simple boundary conditions (like e.g. ideal wall) involving no mean flow seems to be questionable for real combustors - see e.g. our discussion of DECBC above. Admittedly, the corrections due to $\mathbf{v}_0 \neq 0$ on (6.38) - (6.39) are just of order $\propto (M)$. Rather, it is likely that $\mathbf{v}_0 \neq 0$ affects boundary conditions. The latter should e.g. allow transformation of acoustic waves into non-acoustic waves at the wall, in contrast with the boundary conditions quoted above (for a more detailed description of non-acoustic modes, see below). Here we limit ourselves to recall that these boundary conditions are written with the help of *acoustic impedances*, complex-value functions of a complex frequency. These functions describe the acoustic coupling of the combustor with the external world. Accordingly, both the air supply system, the fuel supply system and the combustion chamber outlet have their own acoustic impedance. Both measurement of acoustic impedances in realistic environments and their computation to the degree of accuracy required by modal analysis are still an active field of research.

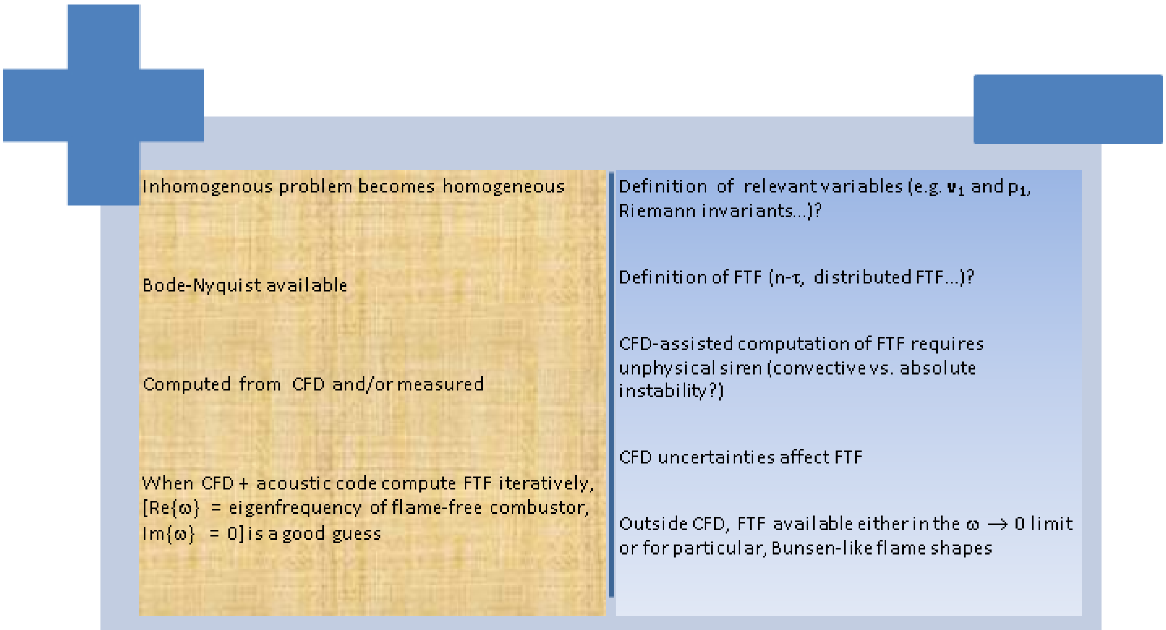

Figure 6.19: *FTF for GT: pros and cons (focussed on computational issues). See text for further details.*

To date, although many different models for the FTF have been utilized so far in order either to match a measurement or to produce the desired behaviour, it seems justified to agree with the words of Ref. [46]:

> *a clear physical explanation of the mechanism leading to an amplification has not been provided yet*

As for the pros and the cons of FTF from the point of view of a GT manufacturer, see Fig. 6.19. Admittedly, the list is somehow biased towards computational issues, and neglects questions concerning experimental techniques.

Remarkably, this very ignorance concerning the source term $\dfrac{\partial Q_1}{\partial t}$ limits also the usefulness of the rigorous approach to the solution of (6.29) based on Green function [45].

6.3 The unperturbed fluid is not at rest

6.3.1 Much ado for nothing?

We have shown that the assumption (6.13) is crucial for the validity of both Rayleigh's criterion (6.33) (6.34) (6.35) and the assumption (6.37) of modal analysis.

As far as the computation of $\Re\{\omega\}$ is concerned, indeed, (6.13) agrees well the assumption of low Mach number. In fact, if $\mathbf{v}_0 \neq 0$ then Doppler effect modifies $\Re\{\omega\}$ into $\Re\{\omega\} - \mathbf{k}\cdot\mathbf{v}_0$, where $\mathbf{k}$ wave number vector of the wave with frequency ω and $|\mathbf{k}| \approx O\left(\frac{1}{L}\right)$, $|\omega| \approx O\left(\frac{c_{s0}}{L}\right)$ for an acoustic wave propagating across a system of linear dimension L, so that the relative contribution of $\mathbf{v}_0$ to $\Re\{\omega\}$ is $\dfrac{\mathbf{k}\cdot\mathbf{v}_0}{\omega} \approx O(M) << 1$.

But we have already shown that the computation of $\Re\{\omega\}$ is only part of the story. From the point of view of Rayleigh's criterion and modal analysis, the onset or the suppression of instability depend on $\Im\{\omega\}$, which in turn depends on a balance between heating and sound propagation, i.e. a destabilising and a stabilising term respectively.

In some well-known problems of thermo-acoustics, like e.g. Rijke's tube, the heating source does not depend on $\mathbf{v}_0$, so that (6.13) is a customary assumption. Not surprisingly, original Rayleigh's work focussed on Rijke's tube. To date, Rijke tube is the experiment *par excellence* for teaching Rayleigh's criterion. We will discuss Rijke's tube in depth in the following. Here we note that the review of [43] shows that Rayleigh's criterion provides us with a fairly good description of Rijke's tube even when turbulence is present.

In combustion problems, in contrast, the heating source *does* depend on $\mathbf{v}_0$. For example, equation (6.10) gives:

$$\nabla\cdot\mathbf{v}_0 = \frac{Q_0}{(c_p\rho_0 T_0)} \tag{6.41}$$

at the order $\propto O(\epsilon^0)$ even if we neglect ∇p_0 in the low Mach limit. According to (6.41), if (6.13) holds then the unperturbed heat release density Q_0 vanishes. In this case, any oscillating perturbation Q_1 of Q with period $\dfrac{2\pi}{\omega}$ heats the fluid for half period and *cools* it during the other half period, a behaviour scarcely compatible to what is expected in combustion [22].

Admittedly, one may wonder if (6.13) is really meaningless for practical applications to unstable combustors, given the fact that combustion occurs at the flame only, hence $Q_0 \neq 0$ in a very small region only.

All the same, even if we decide to neglect $\nabla\cdot\mathbf{v}_0$ everywhere the stability problem with $\mathbf{v}_0 \neq 0$ differs significantly from the $\mathbf{v}_0 = 0$ problem discussed above in many cases. To grasp this point, let us rewrite the linearised balance of mass (6.24) and momentum (6.20) as well as the linearised equation of pressure (1) in the case $\mathbf{v}_0 \neq 0$ with $\nabla \cdot \mathbf{v}_0 = 0$ (as discussed above) and $\nabla p_0 = 0$ in the low Mach limit. We obtain:

$$\left(\frac{\partial}{\partial t} + \mathbf{v}_0 \cdot \nabla\right) \rho_1 + \rho_0 \nabla \cdot \mathbf{v}_1 = 0 \tag{6.42}$$

$$\rho_0 \left(\frac{\partial}{\partial t} + \mathbf{v}_0 \cdot \nabla\right) \mathbf{v}_1 + \nabla p_1 = -\rho_0 \mathbf{v}_1 \cdot \nabla \mathbf{v}_0 \tag{6.43}$$

and

$$\left(\frac{\partial}{\partial t} + \mathbf{v}_0 \cdot \nabla\right) p_1 = (\gamma - 1) Q_1 - \gamma p_0 \nabla \cdot \mathbf{v}_1 \tag{6.44}$$

respectively. Two cases are possible. Firstly, $\mathbf{v}_0 \neq 0$ but $\nabla \mathbf{v}_0 = 0$, i.e. $\mathbf{v}_0$ is uniform and the unperturbed fluid moves at uniform velocity as a whole, like a rigid body. Since $\frac{\partial \mathbf{v}_0}{\partial t} = 0$, in this case the frame of reference at rest with an arbitrary small mass element of the unperturbed fluid moves at the same, constant velocity $\mathbf{v}_0$ with respect to the lab frame of reference for all small mass elements of the fluid (i.e., the two frames of reference are inertial). With no need of further computation, Galileian relativity principle requires therefore physics to be the same in both frames of reference. This implies that what we observe in the lab is just what we would observe should we move at velocity $\mathbf{v}_0$, i.e. at rest with the unperturbed fluid. In particular, results of stability analysis remain unchanged. (This result lies e.g. at the core of the analysis contained in Sec. 2 of [61]). Of course, the case $\mathbf{v}_0 = 0$ discussed above is just a particular case of $\nabla \mathbf{v}_0 = 0$.

Things change considerably if $\nabla \mathbf{v}_0 \neq 0$. This latter case is relevant e.g. to combustors where the flames are sustained by recirculation zones. Physically, the frame of reference at rest with the arbitrary small mass element of unperturbed fluid and the lab frame of reference are inertial no more (Coriolis and centrifugal forces appear). Mathematically, there is no more just one transformation of coordinates which helps ut to get rid of all terms $\approx O(\mathbf{v}_0)$ in (6.42) , (6.43) and (6.44). Galileian relativity principle no longer applies. This is a far-reaching result, which deserves in-depth discussion.

Again, let us start from the discussion of the evolution of $\xi(\mathbf{x}, t)$ in the problem with no sound propagation across the boundaries and no heat production. If we take the Fourier transform in time of the L.H.S. of (6.42) then we observe that the term $\mathbf{v}_0 \cdot \nabla$ is responsible for the Doppler correction $\mathbf{k} \cdot \mathbf{v}_0$ to $\Re\{\omega\}$. The same holds for equations (6.43) and (6.44) as well. As discussed above, and in agreement with the low Mach limit, we may neglect these terms altogether. Even so, however, the term $-\rho_0\mathbf{v}_1 \cdot \nabla\mathbf{v}_0$ survives on the R.H.S. of equation (6.43) . This term differs from zero as $\nabla\mathbf{v}_0 \neq 0$. We may repeat the algebra step-by-step and obtain a modified version of equation (6.25) , namely:

$$\rho_0 \frac{\partial^2 \xi}{\partial t^2} + \nabla p_1 = -\rho_0 \left(\xi \cdot \nabla\right) \mathbf{v}_0 \tag{6.45}$$

In contrast, the other two equations ruling the evolution of $\xi\left(\mathbf{x}, t\right)$, namely equations (6.26) and (6.27) remain unchanged as we neglected the Doppler-related terms. As a consequence, in (6.28) the previous result $C = \text{const.}$ is replaced by

$$C \neq \text{const.}$$

Physically, this means that the amplitude of acoustic perturbations in a fluid initially in non-uniform motion may diverge even if no sound propagates across the boundary of the system and no heating occurs. Positiveness of B ensures stability no more.

Indeed, the implicit assumption underlying both Rayleigh's criterion and modal analysis is that an energy balance of the perturbation actually exists (equation (6.21)). However, even within the framework of a linearised, perturbative analysis of stability it is the total energy of the fluid -not the energy of the perturbation- which is conserved when no heating occurs and no energy is lost across the boundaries [8]. Generally speaking, it is not possible to decouple the contribution of the perturbation from the contribution of the unperturbed fluid. For example, if no net source of energy and no energy flow across the boundaries occurs, then energy is conserved. But it is the total energy of the fluid which is conserved, not the energy of the perturbation and of the unperturbed fluid taken as separate entities. We are going to show that, in contrast with the fundamental assumption of [33], *there is simply no such a thing as an energy of the perturbation in the general case* $\nabla\mathbf{v}_0 \neq 0$.

Admittedly, the latter statement is rather startling, to say the least. In this respect, it is worthwhile to quote Ref. [7]:

> *A definition of perturbation energy implies a decomposition of flow perturbations into acoustics, vortices and entropy, but this decomposition is not unambiguous. [...] The core issue is however that none of the norms leads to a conservative energy potential, which is needed for the construction of a rigorous stability criterion. Strictly speaking, energy provides a stability criterion only if it is monotonously decreasing for stable systems. [...] This does in general not apply to (acoustic) perturbation energy. Investigations [...] show that due to the acoustic-flow-flame-acoustic interaction even low order linear*

thermo-acoustic systems are non-normal. As a consequence (acoustic) perturbation energy may rise even if the thermo-acoustic system is asymptotically stable ("transient growth").

To fix the ideas, let us consider the velocity $\mathbf{v} = \mathbf{v}_0 + \mathbf{v}_1$ of a small mass element of fluid. The kinetic energy of this small mass element is proportional to $|\mathbf{v}|^2 = \mathbf{v}_0^2 + \mathbf{v}_1^2 + 2\mathbf{v}_0 \cdot \mathbf{v}_1$. Suppose the perturbation to be a periodic function of time with period τ , say $\mathbf{v}_1 = \mathbf{v}_{10} \sin\left(\frac{2\pi t}{\tau}\right)$, and take the time-average, so that $\langle|\mathbf{v}|^2\rangle = \langle\mathbf{v}_0^2\rangle + \langle\mathbf{v}_1^2\rangle + 2\langle\mathbf{v}_0 \cdot \mathbf{v}_1\rangle$. Now, we follow the argument of [8] and show that the total kinetic energy $\propto \langle|\mathbf{v}|^2\rangle$ unambiguously splits into the kinetic energy of the unperturbed fluid $\propto \langle|\mathbf{v}_0|^2\rangle$ and the kinetic energy of the perturbation $\propto \langle|\mathbf{v}_1|^2\rangle$ -and is therefore possible to compute the latter separately from the former- whenever $\nabla\mathbf{v}_0 = 0$. To this purpose, we take advantage of the formal relationship $\mathbf{v}_0 = \int dt \frac{d\mathbf{v}_0}{dt}$ which reduces to $\mathbf{v}_0 = \mathbf{v}_0\left(t = 0\right) + \left(\mathbf{v}_0 \cdot \nabla\right)\mathbf{v}_0 t + O\left(\epsilon\right)$ as $\frac{d}{dt} = \frac{\partial}{\partial t} + \mathbf{v} \cdot \nabla$ and $\frac{\partial \mathbf{v}_0}{\partial t} = 0$. Accordingly $\langle\mathbf{v}_0 \cdot \mathbf{v}_1\rangle \propto \left(\mathbf{v}_{10} \cdot \nabla\right)\mathbf{v}_0 \int_0^\tau dt t \cos\left(\frac{2\pi t}{\tau}\right) \neq 0$ for arbitrary $\mathbf{v}_{10}$ unless $\nabla\mathbf{v}_0 = 0$.

Physically, in the general case of non-uniform unperturbed flows the kinetic energy of the perturbation is coupled to the kinetic energy of the unperturbed fluid, i.e. the perturbation and the unperturbed fluid may exchange energy. This is why the perturbations may become unstable even if no heat is produced inside the fluid and no acoustic power is injected into the system from the external world. This additional source of instability -the available kinetic energy of the unperturbed fluid- is accounted for nowhere in Rayleigh's criterion and modal analysis.

Mathematically, problems arising from the linearised balance of momentum (6.43) are usually not normal [62] and assumption (6.37) no longer holds. As we have seen, this allows modal analysis to lead to over-optimistic predictions, and perturbations of fluids initially in non-uniform motion to achieve the status of stable oscillations of finite amplitude even if $g_{max} < 0$, the energy being supplied by the motion of the unperturbed fluid. Even if Mach number is low, its impact is far from negligible [63]. An example is given in [64] -see Fig. 6.20.

The converse is also true: unless suitable damping is added by hand (through e.g. the boundary conditions), modal analysis may predict positive growth rate even if the system is stable, i.e. if no humming occurs. Even worse, in the case discussed in Ref. [1] the damping rate is no output of modal analysis; it is estimated *a posteriori* looking at the amplitude of the saturated acoustic oscillation when instability occurs. This seems to be a further suggestion of the poor prediction capability of modal analysis -see Fig. 6.21.

Transient growth related to non-normality may allow even systems with $g_{max} < 0$ to access to nonlinear regime where linearised analysis becomes meaningless: the combined effects of non-normality and non-linearity causes the occurrence of subcritical transition to instability from initial states, even if the latter have small energy [50].

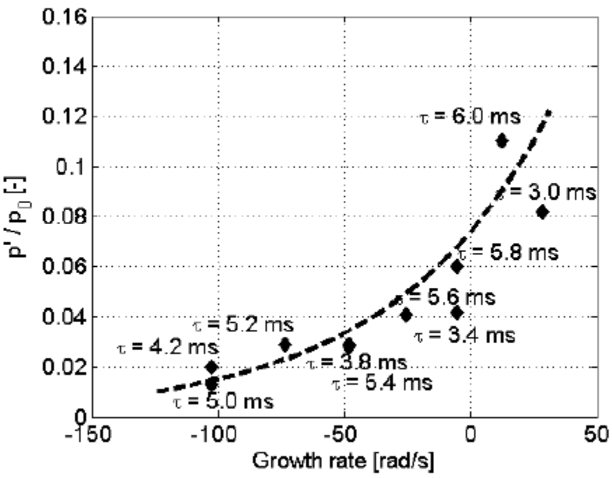

Figure 6.20: *Saturated pressure amplitude (normalised to the unperturbed pressure and computed via a limit cycle) vs. growth rate (computed via modal analysis) for different values of τ_{FTF}. Depending on the actual value of τ_{FTF}, finite humming amplitude is obtained* even for negative growth rates *[64]. Remarkably, the figure displays a correlation between the growth rate and the saturated amplitude, and the authors claim their results to be in agreement with experiments.* Per se*, however, the negative sign of the growth rate is no hallmark of lack of humming, in contrast with what we expect e.g. from equation* (6.32).

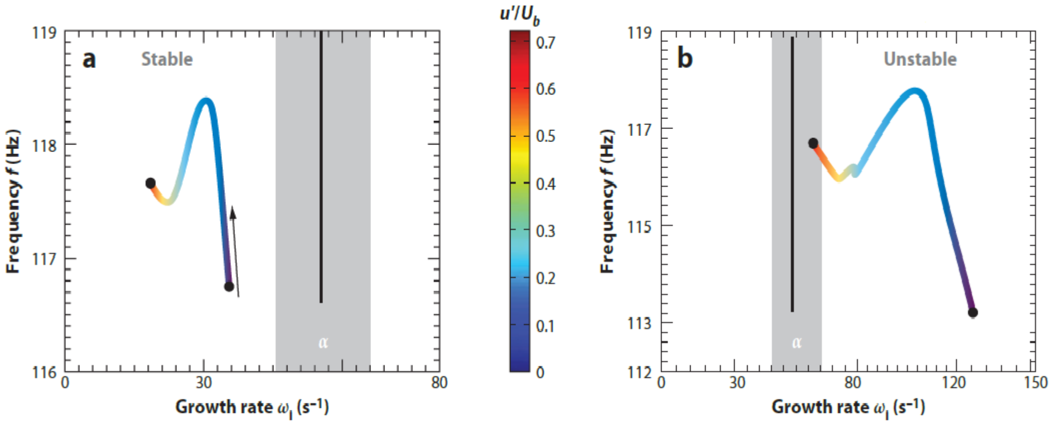

When the growth rate is below the estimated damping rate α, the system is predicted to be stable. When the growth rate exceeds the damping rate, the system is predicted to be unstable. Colors along the trajectory correspond to different levels of velocity perturbation amplitude. When the system is unstable, the oscillation level at the limit cycle corresponds to the value of u'/U_b, where $\omega_i = \alpha$.

Figure 6.21: $\Re\{\omega\}$ *vs. growth rate at different values of the perturbation amplitude [1]. We stress the point that the authors' last words in the caption of this Figure show precisely that the estimate of the damping rate relies on the amplitude of the saturated acoustic oscillation when the combustor is unstable.*

A further argument, due to [65], makes it clear how Galileian invariance prevents separability of the kinetic energy of the perturbation from the kinetic energy of the unperturbed fluid. The equation of motion (6.2) enjoys Galileian invariance, i.e. its results must be invariant when we apply the Galileian coordinate transformation $\mathbf{x}^K = \mathbf{x} - \mathbf{V}t, \quad t^K = t$ from the space-time coordinates $(\mathbf{x}, t)$ of the lab frame of reference (where a generic quantity a is measured) to the coordinates $\left(\mathbf{x}^K, t^K\right)$ of another frame of reference K moving at constant velocity $\mathbf{V}$ with respect to the lab (and where the quantity a^K is measured). Linearisation is a popular tool for solving (6.2). When linearising, we write $a = a_0 + a_1$ and assume a_1 to depend on both space and time, i.e. $a_1 = a_1(\mathbf{x}, t)$. In contrast, a_0 does not depend on time t, i.e. $\frac{\partial a_0}{\partial t} = 0$. Like all physically acceptable methods of solution of (6.2), linearisation too must satisfy Galileian invariance, hence if $a = a_0 + a_1$ then $a^K = a_0^K + a_1^K$ where a_0^K must not depend on t^K, i.e. $\frac{\partial a_0^K}{\partial t^K} = 0$. The chain rule gives

$$\frac{\partial a_0^K}{\partial t^K} = \frac{\partial a_0^K}{\partial a_0} \left[\mathbf{V} \cdot \nabla a_0 (\mathbf{x})\right] \frac{\partial t}{\partial t^K}$$

with $\mathbf{V} = \frac{\partial \mathbf{x}}{\partial t}$, $\frac{\partial a_0^K}{\partial a_0} \neq 0$ (trivially, a^K depends on a when no perturbation occurs), $\frac{\partial t}{\partial t^K} = 1$ and Galileian invariance for arbitrary $\mathbf{V}$ requires $\nabla a_0(\mathbf{x}) = 0$. This means that linearization is physically acceptable if the the unperturbed quantity is not only constant in time, but also uniform across space. In particular, if $\mathbf{v}$ plays the role of the quantity a, it follows that the linearisation invoked above leads to physically acceptable results (like e.g. the existence of an energy balance (6.21) of the perturbation) only if $\nabla a_0(\mathbf{x}) = 0$.

In agreement with this conclusion, the review work of [66] shows that none out of the many attempts to write down an explicit, physically acceptable generalisation of equation (6.15) for E to problems where $\nabla a_0(\mathbf{x}) \neq 0$ is successful, as far as premixed combustion is concerned. In fact, all available formulas lead to physically unacceptable results, like a sudden *increase* of $\int_{V_b} d\mathbf{x}E$ after switching off the flame. (Historically, it was precisely this requirement of physical soundness which has led Chu to write down equation (6.15); the latter, however, applies to the $\mathbf{v}_0 = 0$ case only). The authors claim this behaviour is to be ascribed to non-normality for $\mathbf{v}_0 \neq 0$. The role played by mutual orthogonality of different modes of excitation when deriving Rayleigh's criterion is discussed by Culick in Ref. [67] - in particular, see its equations (20) and (27). Even if written in 1987, Culick's conclusion seem still to be valid:

> *There is presently no procedure for constructing a definition of energy associated to general nonlinear motions.*

6.3.2 Convective waves: generalities

If $\mathbf{v}_0 \neq 0$ perturbations of both entropy and vorticity may propagate across the system. They are not encompassed in Rayleigh's criterion, modal analysis and the system of equations (6.38) - (6.39); the latter equations are concerned with acoustic perturbations only. Perturbations which propagate across the fluid with velocity $\mathbf{v}$ and not with the sound velocity c_s are called *convective*. Both entropy and vorticity perturbations are convective [7].

6.3.3 Entropy waves

As for entropy perturbations, equation (6.8) shows that where no heating occurs (i.e. outside the flame) the quantity s_1 satisfies the equation $\frac{\partial s_1}{\partial t} + \mathbf{v}_0 \cdot \nabla s_1 = 0$, i.e. propagates with the velocity of the unperturbed fluid $\mathbf{v}_0$. Generally speaking, the very existence of entropy perturbations cast doubts on the validity of the common identification -see Sec. 1 of [22]- of irrotational and solenoidal perturbations of $\mathbf{v}$ as acoustic and convective perturbations respectively, as entropy perturbations are both irrotational and convective. *Direct numerical simulation* (DNS, i.e. a particular kind of fluid dymnamic computation) shows that entropy perturbations propagate across a turbulent fluid with no strong dissipation

[7] Admittedly, if (6.13) holds then non-propagating perturbations of entropy and vorticity located at a fixed position at all times are possible, as a matter of principle at least. But no exchange of energy is possible between these hypothetical perturbations and the acoustic waves, in the framework of linearised treatment at least, where interacting waves must have the same frequency which in the case of convective waves at zero mean flow is zero. In fact, acoustic waves obey equation (6.29), and their amplitude is therefore proportional to a time derivative, which vanishes in the zero frequency limit.

[68]. Even in the low Mach limit, it has been shown that neglecting entropy perturbation leads to large errors [63] in the analysis of stability. For instance, in the analysis of Ref. [69]:

> *The growth rate of the acoustic mode is significantly mispredicted, suggesting that the coupling between entropy and acoustic fluctuations exhibit a strong unstable thermo-acoustic mode, while purely acoustic analysis shows a stable eigenmode.*

Such errors are $\propto O\left(M^1\right)$ and $\propto O\left(M^0\right)$ whenever the flow is perfectly premixed and is not perfectly premixed respectively [70] [8].

In this case, interaction of an acoustic wave coming from the flame at the fuel inlet in a combustor may produce perturbations of stoichiometry -hence of entropy- which in turn follow the fluid and propagate towards the flame, where they perturb the heat release and induce therefore generation of further sound waves [3]. Since stoichiometry affects heat release heavily -see Fig. 6.22- perturbations of stoichiometry leads to oscillations of heat release, which in turn produce acoustic oscillations according e.g. to (6.29) [9]. Fig. 6.23 displays some mutual relationships among perturbations of stoichiometry, flame area and flame shape (encompassed in the notion of flame stretch, a geometry-related quantity which depends on both flame speed and flame curvature - see the Appendix on flame velocity).

Interference of acoustic and entropy perturbations in premixed combustor is also possible [71]. Finally, entropy perturbations may be related to temperature variations (*hot spots*) resulting from unsteady combustion. They convect with the flow, and in the absence of acceleration (i.e. in a constant flow area downstream of the heat release zone), they do not have any acoustic waves associated with them. When the hot spots are accelerated, however, as it happens at the combustor exit/turbine inlet in a typical GT, acoustic waves are generated. The downstream propagating acoustic waves pass through the turbine, eventually appearing as a component of the exhaust noise, while the upstream propagating acoustic waves affect the flame within the combustor, and thus can influence thermo-acoustic stability [68].

[8] Here the words *perfectly premixed* denote an operation mode that generates a perfectly homogeneous fuel/air mixture without any spatial or temporal fluctuations of the mixture fraction. This is usually achieved by locating the fuel injection sufficiently far upstream of the combustor. In order to minimise the inherent risks of flame flashback and autoignition, industrial systems are usually designed with a rather short mixing section that does not provide full spatial and temporal homogenization. Usually, such a setup is called *partially premixed*.

[9] This fact is of great practical relevance. In fact, many models of humming assume a one-dimensional geometry, where the flame area A_f is a constant quantity -see e.g. Ref. [34] and Ref. [61]. In this geometry, mass conservation and equation (10.1) below require at given heat release that A_f is inversely proportional to the flame velocity. But in lean combustion any perturbation of stoichiometry, like those perturbations carried by entropy waves, modifies the flame velocity, and cannot therefore leave A_f unaffected. This fact makes it difficult for one-dimensional models to take properly into account entropy waves in lean combustion. This is far from surprising, as propagation of convective waves depends on the flow, which is intrinsically a three-dimensional quantity.

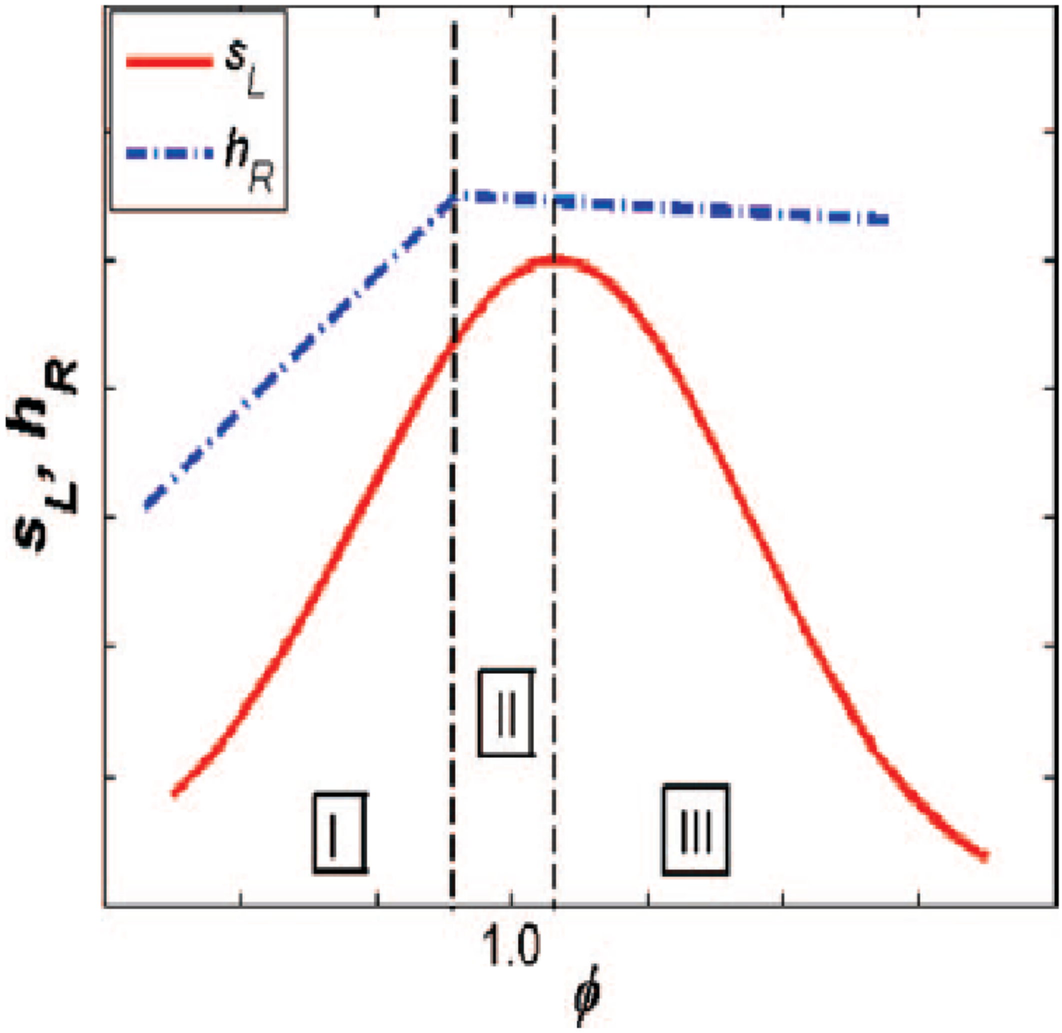

Figure 6.22: *Qualitative plot showing dependence of flame speed s_L and heat of reaction h_R on fuel/air ratio ϕ - from Ref. [58]. In the formalism of our equation* (10.1)*, $h_R = Y_{fuel} \cdot H_{LHV}$. Lean combustion corresponds to region I.*

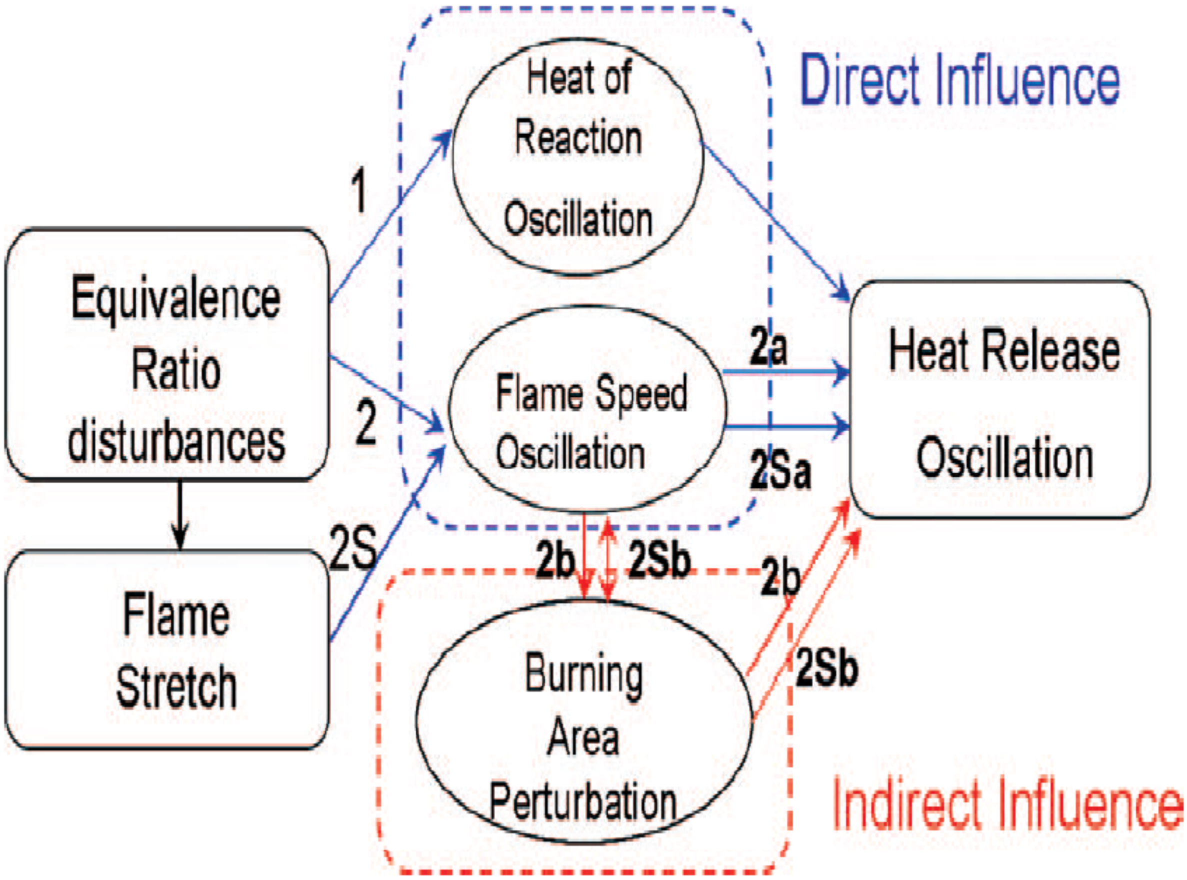

Figure 6.23: *(From Ref. [58]). Fundamental processes controlling the heat release response of premixed flames to equivalence ratio oscillations. Routes labeled S denote additional routes due to influence of flame stretch. We refer to* (10.1) *below in the text. Equivalence ratio perturbations cause fluctuations in the local flame speed (route 2a) and heat of reaction (route 1) along the flame surface. These fluctuations in the flame speed and mixture heat of reaction then cause the local heat release rate to oscillate. This is a direct route of influence. Additionally, flame speed variations also excite flame wrinkles that propagate along the flame. This leads to an oscillation in the burning area of the flame (route 2b), thereby causing the net heat release rate to oscillate. This is an indirect route of influence. It is to be noted that the indirect route of influence is also non-local, i.e. the flame area fluctuations at a given time and position are a convolution of the flame surface oscillations at all upstream locations at earlier times. Due to oscillations caused in the flame shape because of equivalence ratio perturbations, oscillations arise in the curvature of the flame front, which can perturb the flame displacement and consumption speeds [4], thereby establishing another route by which the flame speed fluctuates (route 2S). These fluctuations in flame speed can then disturb the heat release directly (route 2Sa) or indirectly through burning area fluctuations (route 2Sb). Remarkably, stretch rate oscillations are indirectly caused by equivalence ratio oscillations, i.e. equivalence ratio oscillations perturb the displacement flame speed, which causes flame wrinkles, which lead to oscillations in flame stretch, which can now perturb both the displacement and consumption speeds of the flame.*

Recently, it has been proposed that suitable boundary conditions (the so called *Delayed Entropy Coupled Boundary Condition*, or DECBC)) allow equation (6.29) to take into account also the effect of entropy waves [69]. The explicit construction of DECBC, however, relies on the choice of a particular expression for E. Now, this expression is basically equivalent to one of the generalisations of equation (6.15) ruled out as physically unacceptable in [66] for fluids where vorticity is not identically zero -to convince oneself, just compare equation (23) of [69] for the fluctuation of enthalpy (= energy + pressure · volume) with equation (21) of [66] for the energy disturbance in the same isentropic approximation. However, the authors of [69] have to be credited with the result that realistic boundary conditions for real combustors which convective waves propagate across should depend also on the unperturbed flow, i.e. on unperturbed value of Mach number -but for the above discussed articular experimental set-up at least.

Another trick which aims at describing the impact of $\mathbf{v}_0 \neq 0$ is due to Culick and Yang and is reviewed in [72]. The idea is to make use once more of equation (6.29), with the proviso that its R.H.S. is replaced by a new, scalar term which encompasses all effects related to $\mathbf{v}_0 \neq 0$ including heat release due to combustion and entropy perturbations. It turns out that this method allows perturbative algorithms to provide numerical results in good agreement with analytical results if $\mathbf{v}_0 = 0$; otherwise, according to the words of Ref. [73] the agreement remains good

> *to first order in mean flow and zeroth order in the expansion of perturbations* [...] *as long as the mean flow is kept small*

Again, this is far from surprising, as the method leaves the L.H.S. of (6.29) unchanged, so that perturbations keep on travelling across the system at velocity c_{s0} no matter how the source term on the R.H.S. is like.

6.3.4 Vorticity waves

A vorticity wave is a mode of oscillation supported by Euler equation; it is convected by the flow and features velocity disturbances in a direction perpendicular to that of the flow.

If we take the curl of both sides of equation (6.2) and invoke equation (5.1) for $\mathbf{v}_0 \neq 0$ we obtain the exact relationship [74].

$$\frac{d}{dt}\left(\frac{\nabla \wedge \mathbf{v}}{\rho}\right) = \left(\frac{\nabla \wedge \mathbf{v}}{\rho} \cdot \nabla\right)\mathbf{v} + \frac{1}{\rho^3}\nabla\rho \wedge \nabla p$$

On the R.H.S., the first and the second (*baroclinic*) term describe how the stretching of vortex lines intensifies local vorticity, and how vorticity can be created when the pressure gradient and the density gradient are not aligned respectively. The latter acts e.g. when acoustic modes propagates azimuthally across an axisymmetric flame. In the isentropic case $p = p(\rho)$, the baroclinic term vanishes and we are left with the local version of Kelvin's theorem of circuitation for inviscid fluids; integration of both sides on

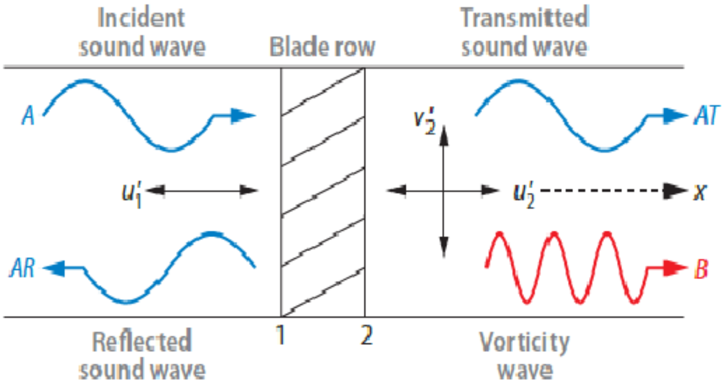

Representation of the swirler by an actuator disk, a thin discontinuity separating the (*1*) upstream and (*2*) downstream flows. An acoustic wave impinging on the swirler u_1' gives rise, on the downstream side of this unit, to an acoustic wave u_2' and to a vorticity wave characterized by transverse velocity fluctuations v_2'. This last wave is convected by the flow.

Figure 6.24: *(From Ref. [1]).*

an arbitrary surface Σ leads to $\frac{d}{dt} \int_\Sigma da \cdot \nabla \wedge \mathbf{v} = 0$, i.e. the circuitation $\int_\Sigma da \cdot \nabla \wedge \mathbf{v}$ is conserved during the fluid motion along $\mathbf{v}$ for arbitrarily chosen Σ . It follows that perturbations of vorticity travel across the fluid with velocity $\mathbf{v}$.

As an example, it can be shown [1] that an acoustic wave impinging on an inclined surface (like e.g. a blade) undergoes conversion (partially, at least) into a vorticity wave -see Fig. 6.24- of comparable amplitude -see Fig. 6.25.

All the way around, for swirl-stabilised flames perturbations of vorticity lead to perturbations of the flame shape, hence of the heat release [75]. Not surprisingly, this effect is particularly of interest in swirling flows -see Fig. 6.26.

The examples discussed above show that the sources of convective perturbations inside the combustor include the interaction between the acoustic waves originated at the flame and the combustor wall. (Generation of convective perturbations at the flame is also possible, but we are not interested in it at the moment). This suggests that if acoustic resonances occur, at whose frequencies the transmission of acoustic energy towards the combustor walls is particularly effective, then the generation of convective waves is also strong. Generally speaking, moreover, it is also noted that in many devices with a confined

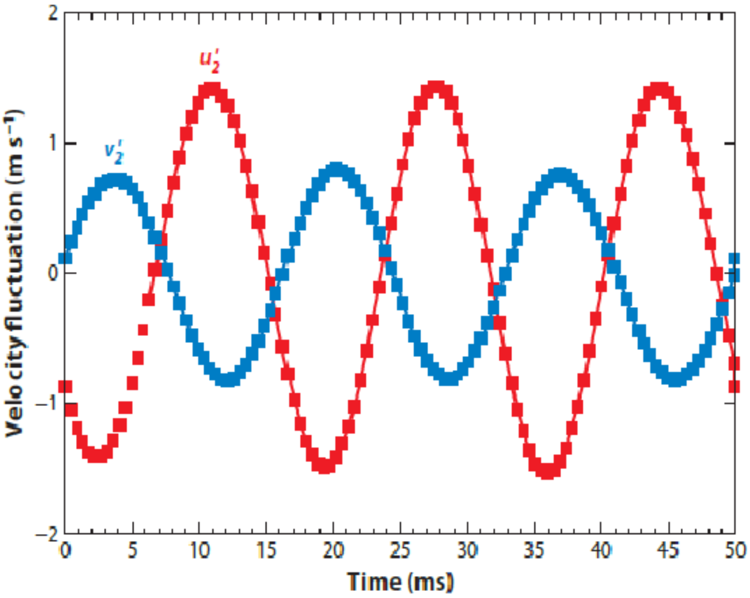

Velocity fluctuations on the downstream side of a blade row for a harmonic longitudinal perturbation $u_1' = 1$ m s^{-1} at $f = 60$ Hz. The u_2' fluctuations correspond to the transmitted acoustic wave. The transverse velocity fluctuations v_2' are linked to a vorticity wave generated by an incident acoustic wave interacting with the blade row. The amplitude of this wave is given by $|v_2'/u_2'| = \tan\theta_2$, where the trailing edge blade angle is here $\theta_2 = 25°$. Figure adapted from Palies et al. (2011a).

Figure 6.25: (*From Ref. [1]*).

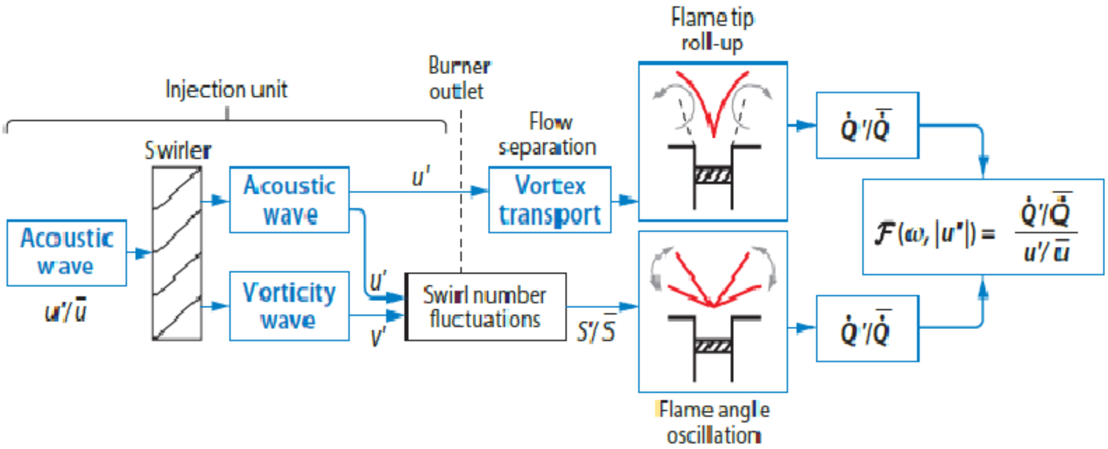

Block diagram representation of mechanisms generating heat–release rate fluctuations in swirling flows.

Figure 6.26: *(From Ref. [1]). On the right, the velocity perturbation of the acoustic wave affects the motion of vortices. This hints at the inadequacy of one-dimensional models, which are nevertheless of common use in thermo-acoustics. On the left, the transfer function (on the left) depends also on the perturbation amplitude. In this case it is referred to as* flame description function *(see text). Inside the small pictures, the red lines and the dashed rectangles represent the flames and the blades respectively. The swirl number is a dimensionless quantity, measuring the ratio of azimuthal to axial momentum fluxes in a swirling flow (see text).*

flame significant entropy and mass fraction disturbances can exist up to the combustor boundaries. In this case, the disturbance energy flux does not reduce to an acoustic energy flux within the combustor [22]. We shall see in the following that the impact on humming of convective flames may be far from negligible when the flames is confined within a combustor. In this case, neglecting $\mathbf{v}_0$ implies neglecting the energy exchange between the perturbation and the fluid, a potentially destabilising effect which adds to the effects of heat production and sound propagation already taken into account in Rayleigh's criterion.

In contrast, unconfined flames are contained by definition within no closed container, and acoustic resonances are not so well peaked. Indeed, it turns out that for unconfined flames the description provided by Rayleigh' criterion and modal analysis fits experimental data [21].

6.3.5 Convective waves and the success stories of modal analysis

It is worthwhile to recall here that, in spite of all the problems listed above, standard modal analysis based on $n - \tau$ FTF with n_{FTF} and τ_{FTF} provided by CFD has met considerably success in two different cases at least, namely the problem with ideal wall and the problem with unconfined flame discussed in Ref. [19] and Ref. [21]. In spite of their differences, both problems seem to have one feature in common: the lack of coupling between convective and acoustic modes. In [19], the boundary condition ensures that the acoustic energy of the acoustic wave impinging upon the wall is equal to the energy of the acoustic wave reflected from the wall, hence no energy is left to be converted into convective waves, unlike the situation described in [1]. In [21], there is just no wall such conversion may occur, as the flame is unconfined. If there is no coupling between convective and acoustic waves, then there is no interaction between the unperturbed flow (which carries convective waves) and sound: the acoustic perturbation evolves therefore just like in a fluid at rest (apart from a small Doppler correction on frequency), the system (6.38) - (6.39) is normal and modal analysis works fine.

This argument suggests that *every* system fluid + flame + combustor where convective waves and acoustic waves are decoupled, *no matter why*, should be correctly described with the help of the by now standard CFD-FTF-modal analysis approach.

Indeed, a recent paper [20] shows that if the acoustic modes propagate azimuthally, i.e. perpendicularly to the unperturbed flow, then modal analysis predicts humming. As usual, CFD allows to write the transfer function. According to genera consensus, such azimuthal modes are responsible for high-frequency humming, or *screech*. This results seems to strengthen our argument: convective waves propagate along the unperturbed flow only, so that their interaction with acoustic modes propagating perpendicularly to the unperturbed flow is likely to be negligible. Remarkably, however, the FTF computed in [20] for azimuthal modes differs from the FTF computed for acoustic modes which propagate along the unperturbed flow, like those modes investigated in [49] and [61], and requires separate computation.

We conclude that humming prediction from scratch is a solved problem for systems fluid + flame + combustor where convective waves and acoustic waves are decoupled. It remains to be solved for all other systems - like e.g. swirl-stabilised GT combustors where swirled blades forbid such decoupling.

Chapter 7

A more general case - Myers' corollary

7.1 Generalities

Here we discuss the more general case where both approximations (6.1) and the assumption of caloric perfection are dropped. We retain the assumptions of no net mass source and no body force, and invoke again no detailed model of combustion. Finally, we limit ourselves to small perturbations of a steady state no more, but allow large perturbations of (possibly) unsteady state to occur, i.e. we still write $a = a_0 + \epsilon a_1$ but we allow both $\epsilon \approx 1$ and $a_0 = a_0(\mathbf{x}, t)$. This is in agreement with our discussion of Galileian invariance above. So far, no detailed information on the dependence of a and a_1 on space and time is required. Remarkably, in the particular case where a is just the position of a small mass element, then the relationship $a_0 = a_0(\mathbf{x}, t)$ allows us to consider an unperturbed state with non-zero velocity, i.e. to go beyond (6.13).

In the following, we take also $a_0 = \langle a \rangle$, i.e. we identify the unperturbed value of a with the time-average on a (*slow*) time-scale much longer that the typical time-scale of the perturbation a_1, so that the time-averaging procedure erases all terms evolving on the *fast* time-scale of the perturbation ($\langle a_1 \rangle \equiv 0$). In particular, let us apply our discussion to to the time derivative $\frac{da}{dt} = \frac{d\langle a \rangle}{dt} + \frac{da_1}{dt}$. The slow term $\frac{d\langle a \rangle}{dt}$ on the R.H.S. coincides with the time-average $\langle \frac{da}{dt} \rangle$ of $\frac{da}{dt}$ because the time-average erases the fast term $\frac{da_1}{dt}$, i.e.

$$\langle \frac{da}{dt} \rangle \approx \frac{d\langle a \rangle}{dt} \tag{7.1}$$

More to the point, let us rewrite the definition of time-average $\langle a \rangle \equiv \frac{1}{\tau} \int_0^\tau dt a$ without requiring that τ is the period of humming. If we write $a(t) = a_0 + a_{10} \cos\left(\frac{2\pi t}{\tau_1}\right) + a_{20} \cos\left(\frac{2\pi t}{\tau_2}\right) + \ldots$ with $\tau_2 >> \tau >> \tau_1$ then (7.1) holds up to terms $\propto O\left(\frac{\tau_1}{\tau}\right)$. A similar result holds even if we allow a_{10} to evolve in time on a time-scale $>> \tau_1$, etc. In a combustor affected by humming with period τ, for instance, this humming period introduces a natural distinction between slow and fast time scales, $\geq \tau$ and $< \tau$ respectively. We are going to invoke (7.1) in the following. Finally, if a_0 does not depend on time then we retrieve the case discussed in the previous Sections.

With the help of cumbersome but straightforward algebra, it has been shown [22] that equations (5.1), (5.3), (5.4), (5.2) and (5.5) still lead to equation (6.14). Now, the latter equation is referred to as *Myers' corollary* in the literature, since it is a generalisation of a simpler result originally found in [76]. The definitions of E, $\mathbf{W}$ and D, however, are much more cumbersome:

$$E = \rho\left(H_1 - \langle T\rangle s_1\right) - \langle\mathbf{m}\rangle\cdot\mathbf{v}_1 - p_1 - \rho\sum_{k=1}^{n-1}\left(g_k Y_{k1} - \langle g_{k1}Y_{k1}\rangle\right) \tag{7.2}$$

$$\mathbf{W} = \mathbf{m}_1\left(H_1 - \langle T\rangle s_1\right) + \langle\mathbf{m}\rangle T_1 s_1 + \langle\mathbf{m}_1 H_1\rangle - T\langle\mathbf{m}_1 s_1\rangle + \mathbf{m}\langle T_1 s_1\rangle \tag{7.3}$$

$$D = D_\xi + D_s + D_{Q_*} + D_{Q^*} + D_\psi + D_{\psi^*} + D_{Y_k} \tag{7.4}$$

where we have defined the following quantities ($i, j = 1, 2, 3$):

$$D_\xi = -\mathbf{m}_1\cdot\zeta_1 - \langle\mathbf{m}_1\cdot\zeta_1\rangle$$

$$D_s = -\left(\mathbf{m}_1 s_1\right)\cdot\nabla\langle T\rangle + \langle\mathbf{m}\rangle\cdot\left(s_1\nabla T_1\right) - \langle\mathbf{m}_1 s_1\rangle\cdot\nabla T + \mathbf{m}\cdot\langle s_1\nabla T_1\rangle$$

$$D_{Q_*} = T_1 Q_{*1} + \langle T_1 Q_{*1}\rangle$$

$$D_{Q^*} = T_1 Q_1^* + \langle T_1 Q_1^*\rangle$$

$$D_\psi = \mathbf{m}_1\cdot\psi_1 + \langle\mathbf{m}_1\cdot\psi_1\rangle$$

$$D_{\psi^*} = \mathbf{m}_1\cdot\psi_1^* + \langle\mathbf{m}_1\cdot\psi_1^*\rangle$$

$$D_{Y_k} = g_1\nabla\cdot\mathbf{m}_1 + \langle g_1\nabla\cdot\mathbf{m}_1\rangle + \sum_{k=1}^{N-1}\left(g_{1k}\Omega_{1k} + \langle g_{1k}\Omega_{1k}\rangle\right)$$

$$H \equiv h + \frac{|\mathbf{v}|^2}{2} \qquad \mathbf{m} \equiv \rho\mathbf{v}$$

$$\Omega_k \equiv \omega_k - \nabla\cdot\left(\rho\mathbf{V}_k Y_k\right) - \nabla\cdot\left(\mathbf{m}Y_k\right)$$

$$\zeta \equiv \left(\nabla\wedge\mathbf{v}\right)\wedge\mathbf{v} \qquad \psi_i \equiv \frac{1}{\rho}\frac{\partial\Pi_{ij}}{\partial x_i} \qquad \psi^* \equiv \sum_{k=1}^{n} g_k\nabla Y_k$$

$$Q_* \equiv \frac{1}{T}\left[-\nabla\cdot(\lambda\nabla T)+\rho\nabla\cdot\left(\sum_{k=1}^{n}h_kY_k\mathbf{V}_k\right)+\Phi+Q\right]$$

$$Q^* \equiv -\frac{1}{T}\left[\sum_{k=1}^{n}g_k\omega_k+\sum_{k=1}^{n}g_k\nabla\cdot(\rho\mathbf{V}_kY_k)\right]$$

as well as the enthalpy per unit mass h and the Gibbs' free energy per unit mass g:

$$h \equiv u+\frac{p}{\rho} \qquad g \equiv h-Ts$$

7.2 Consequences

Myers' corollary (6.14) is an exact relationship, i.e. it holds for arbitrary ϵ. It is a formal consequence of the constitutive equations (5.1) - (5.5) . The same holds for its consequence (6.21) , which is obtained after volume integration of both sides of Myers' corollary on V_b. As such, the latter equation has been utilised as a self-consistency check for the results of CFD [22] [77], where E, $\mathbf{W}$ and D are computed with the help of (7.2) , (7.3) and (7.4) respectively after post-processing CFD results. The perturbations of heat release, entropy and vorticity affect the quantities D_{Q_*} ,D_s, and D_ξ straightforwardly. Other contributions to D are affected by particle diffusion.

It turns out in [77] that LES satisfies Myers' corollary quite well -see Fig. 7.1- and is therefore likely to give self-consistent results, provided that $|\int_{V_b} d\mathbf{x}D_s| \approx |\int_{V_b} d\mathbf{x}D_{Q_*}|$ -see Fig. 7.2.

This means that the terms affected by fluctuations of both mean flow and entropy (which disappear at zero Mach number, as all terms in D_s are of comparable magnitude and are also comparable with the terms affected by perturbation of heat release (which is responsible for the emission of sound) -see Fig. 7.3.

Similar results are obtained in Ref. [22] with the help of DNS -see Fig. 7.4.

Accordingly, self-consistency of both LES and DNS approaches to CFD is not compatible with the zero mean flow assumption (6.13) in the general case.

In agreement with our discussion of the previous Section, Myers' corollary is no energy balance, as equation (7.2) ensure no positiveness of E. The latter quantity is no energy density in the general case, as E is not positive-definite. It can be shown [77] that E is positive-definite only if both perturbations of Y_k and higher-order terms $\propto O(\epsilon^2)$ are negligible. Again, there is no such a thing as an energy of the perturbation in the general case.

In spite of their cumbersome structure, equations (7.2) , (7.3) and (7.4) provide relevant information on stability. In the case of a stable system, in fact, we expect the

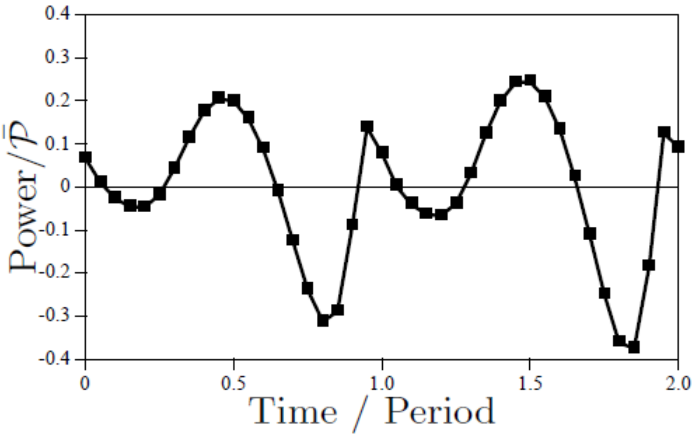

Figure 7.1: *From Ref. [77]. R.H.S.(continuous line) and L.H.S. (black squares) of* (6.21) *vs. time. Here* $\overline{\mathrm{P}}$ *is a normalisation factor.*

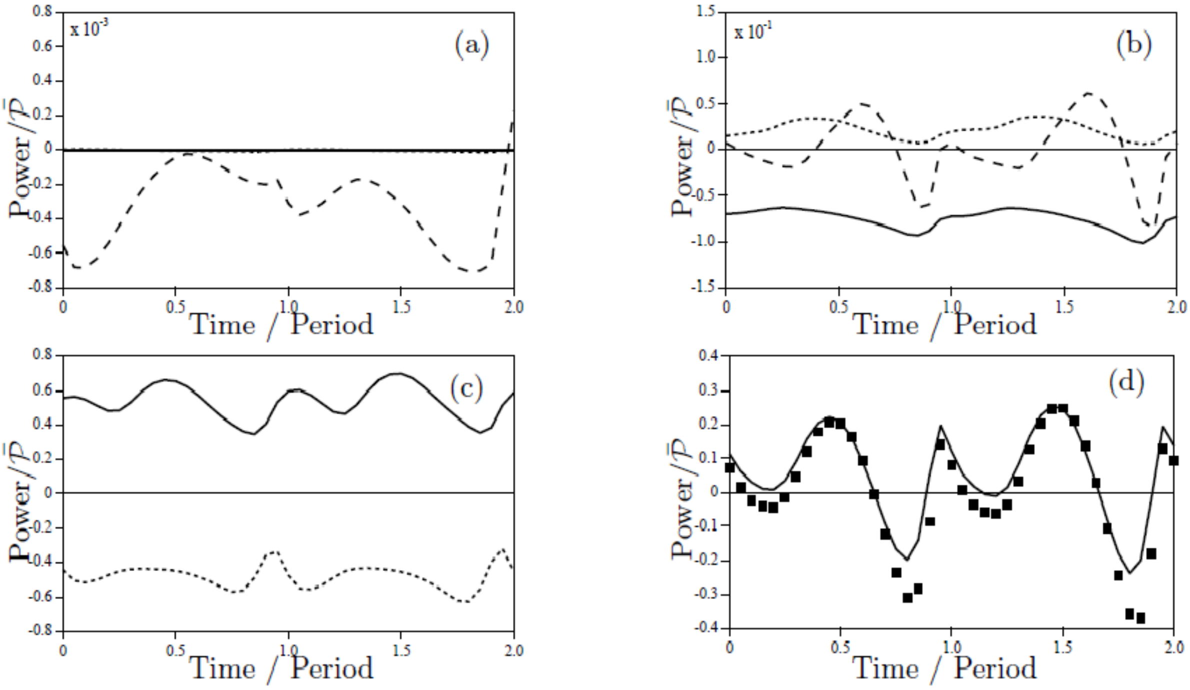

Time evolution of the volume integrals of (**a**) the boundary ($\mathcal{W}$, – – – –), D_ξ (———) and D_ψ (········) terms, (**b**) the D_{Q^*} (———), D_{ψ^*} (········) and D_{Y_k} (– – – –) terms, (**c**) the D_Q (········) and D_s (———) terms. Approximate budget (**d**) based on the heat release (D_Q) and entropy (D_s) terms only: exact time derivative of the total disturbance energy (■) and approximate spatial terms (———)

Figure 7.2: *From Ref. [77]. Here* $\overline{\mathrm{P}}$ *is a normalisation factor.*

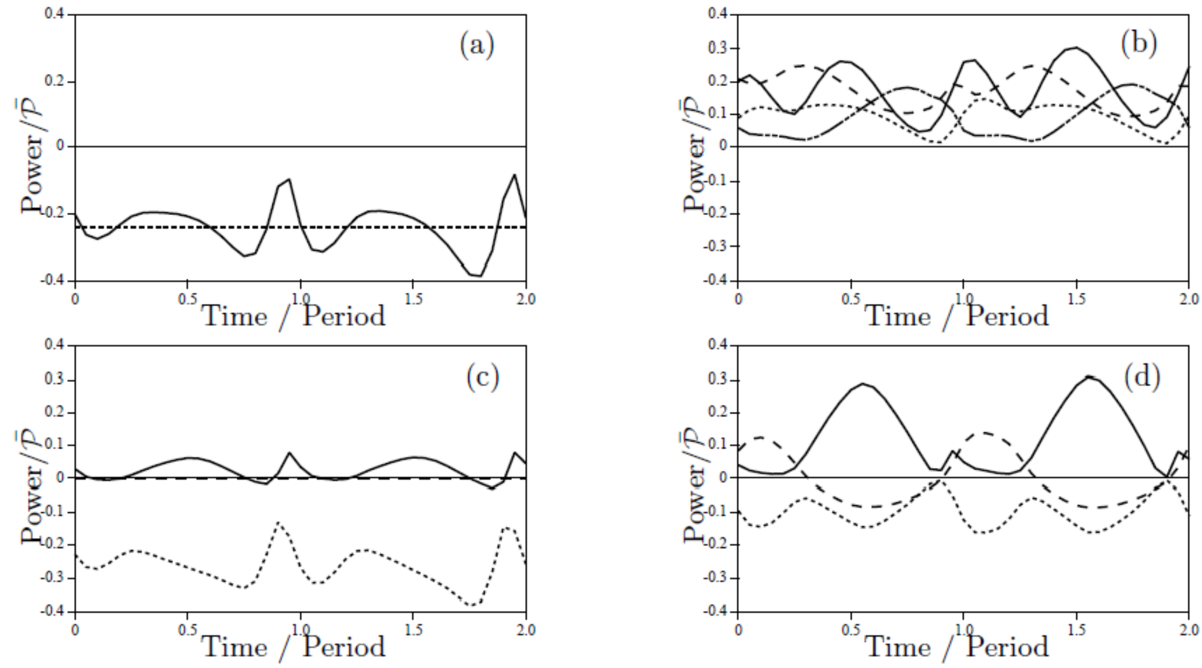

Time evolution of the volume integrals of (**a**) the terms in D_Q, viz. $T'Q'$ (———) and $\overline{T'Q'}$ (········) and (**b**) the terms in D_s, viz. $-\mathbf{m}' \cdot s'\boldsymbol{\nabla}\bar{T}$ (———), $s'\bar{\mathbf{m}} \cdot \boldsymbol{\nabla}T'$ (········), $-\overline{\mathbf{m}'s'} \cdot \boldsymbol{\nabla}T$ (– – – –) and $-\mathbf{m} \cdot \overline{T'\boldsymbol{\nabla}s'}$ (—·—), (**c**) the terms in $T'Q'$, viz. $T'(\omega_T/T)'$ (———), $-T'(\boldsymbol{\nabla}\cdot\mathbf{q}/T)'$ (········) and $T'(\phi/T)'$ (– – – –), (**d**) the terms in $T'(\omega_T/T)'$, viz. $T'\omega_T'/T$ (———), $\omega_{\bar{T}}T'(1/T - \overline{1/T})$ (········) and $-T'\overline{\omega_T'(1/T)'}$ (– – – –)

Figure 7.3: *From Ref. [77]. Here* $\overline{\mathrm{P}}$ *is a normalisation factor.*

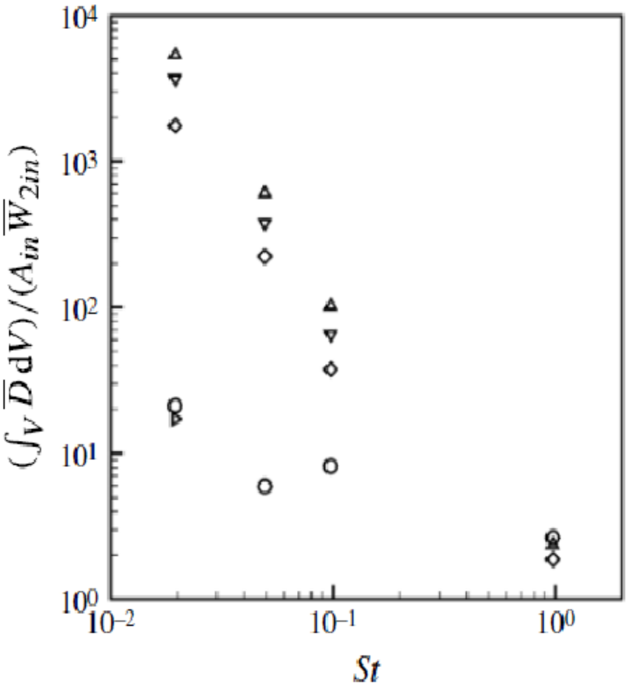

Volume-integrated and time-averaged exact source terms normalized by $A_{in}\overline{W}_{2in}$ versus St: $\triangle$, $\bar{D}_s$; $\triangledown$, -$\bar{D}_Q$; $\diamond$, -$\bar{D}_{Q*}$; $\triangleright$, -$\bar{D}_\psi$; $\circ$, $\bar{D}_Y$.

Figure 7.4: *From Ref. [22]. A flame is subject to acoustic forcing at a given forcing frequency and an ingoing acoustic power flux $A_{in}\overline{W_{2in}}$. Here various terms in Myers' corollary are displayed. All of them are a) computed by post-processing the output by a DNS code; b) integrated on the combustor volume c) time-averaged d) computed at different values of the Strouhal number St. The latter is defined in this paper as $St \equiv$ (typical length) $\cdot$ forcing frequency / speed of sound. Note that* all *terms -including those responsible for particle diffusion, usually neglected- are approximately equal as $St \to 1$.*

perturbation amplitude remains finite at all times. The definition of E ensues therefore that $|E|$ to remain finite at all times. Now, if we add the slightly more restrictive assumption that $|E|$ remains constant on the slow time scale then (7.1) allows us to write $\langle \frac{dE}{dt} \rangle = 0$. Remarkably, should we decide to drop even the slightly restrictive assumption invoked we would obtain the same result just by computing the time-average in the $\tau \to \infty$ limit, as the time-averaged time derivative of an ever-bounded quantity vanishes in this limit [41]. For all practical purposes, however, we make a small error if we neglect $\langle \frac{dE}{dt} \rangle = 0$ whenever $\tau < \infty$ is large enough. Now, after taking the time-averages of both sides of equation (6.21) we retrieve equation (6.35) -or, equivalently, (6.36)- as a necessary condition for stability.

Now, however, there are four main differences:

- The quantities D and $\mathbf{W}$ are given by (7.4) and (7.3) respectively.
- We got rid of modal analysis altogether.
- Large perturbation amplitude are allowed. This implies that both (6.35) and (6.36) apply to non-linear systems as well. If this amplitude is zero, then both sides vanish.
- The unperturbed state may depend on time. For example, it may correspond to a combustor which undergoes a periodic humming oscillation.

The fact that the unperturbed state is allowed to depend on time has far-reaching consequences. In fact, the conventional approach to humminh postulates that a system with no humming is in steady state. This postulate implies that the noise affecting the system when no humming occurs is of purely stochastic nature, and may therefore be averaged out with no impact on the self-consistency of the deterministic description of the humming-free state as provided e.g. by CFD. Recently, however, this postulate has been put in doubt in Ref. [78], where the combustion noise appears to be the outcome of deterministic chaos possibly leading to intermittency [79] [1]. If this is true, then noise in the humming-free system cannot be just averaged out without loosing essential information, and the feasibility of the conventional approach is at stake. In contrast, utilisation of Myers' corollary allows us both to consider the system in humming as the unperturbed state and to postulate nothing about the humming-free system.

In the following, we are going to take advantage of a further feature of Myers' corollary. Equations (7.3) and (7.4) show that both $\mathbf{W}$, D_ξ, D_s, D_{Q_*}, D_{Q^*}, D_ψ, D_{ψ^*} and D_{Y_k} are of the form

$$a_b = a_c + \langle a_c \rangle$$

[1] In the language of non-linear dynamical systems, indeed [60], the well-known resiliency of humming against any attempt to suppress it once triggered agrees well with the description of humming as a limit cycle with a finite basin of attraction: and a limit cycle is a non-chaotic invariant of the dynamical system which describes the physical system combustor + flame + fluid. Thus, the transition from humming-free behaviour to humming becomes a transition from chaotic to non-chaotic behaviour.

where a_b and a_c are suitably defined, bilinear quantities in the unperturbed quantities and their perturbations. For example, if $a_b = D_{Q_*}$, then $a_c = T_1 Q_{*1}$, etc. It follows that

$$\langle a_b \rangle = 2\langle a_c \rangle \tag{7.5}$$

In the particular case where the unperturbed state does not depend on time (i.e. $\dfrac{\partial a_0}{\partial t} = 0$ for the generic quantity a), comparison of equations (A.6), (A.8)-(A.10) with (2.22), (2.24)-(2.26) of [22] shows that Myers' corollary (6.14) still holds provided that we replace a_b with a_c for all the quantities listed above- in our example, D_{Q_*} becomes just equal to $T_1 Q_{*1}$. Then,

$$\langle a_b \rangle = \langle a_c \rangle \tag{7.6}$$

Together, equations (7.5) and (7.6) imply that the same necessary stability criterion (6.35) -or, equivalently, (6.36)- describes lack of instability of both steady and unsteady unperturbed states: in the latter case the factor 2 appears on both R.H.S. and L.H.S. of (6.35)-(6.36) and gets factorized. Again, should both sides of (6.35)-(6.36) vanish, this would correspond to identically vanishing perturbations. We will take advantage of this result in the following; in particular, we are going to refer to (6.35) - (6.36) as to necessary conditions of stability of unperturbed states.

Remarkably, D_s and D_{Q_*} are the dominant contributions to D in many cases of practical interest -see the order-of-magnitude estimate in Sec.2.2. of [22]. In particular, the fact that the contribution of vorticity disturbances is negligible is likely to be a clear distinction between the fundamental mechanisms involved in combustion stability and those involved in aerodynamically generated sound [38].

Finally, it can be shown [22] that if (6.1) holds and if $0 < \epsilon \ll 1$ then Rayleigh's criterion is retrieved with the quantities E, $\mathbf{W}$ and D defined as in the proof of (6.35) - (6.36), the only difference being that the unperturbed state may be an oscillating one -e.g., a combustor in humming. Admittedly, however, particle diffusion -neglected in (6.1)- seems to play a relevant role in numerical simulations -see Fig. 7.4.

For a list of pros and cons of Myers' corollary, see Fig. 7.5. For a summary of the necessary conditions for stability of both steady and unsteady unperturbed states against perturbations, as provided by dynamics, see Fig. 7.6.

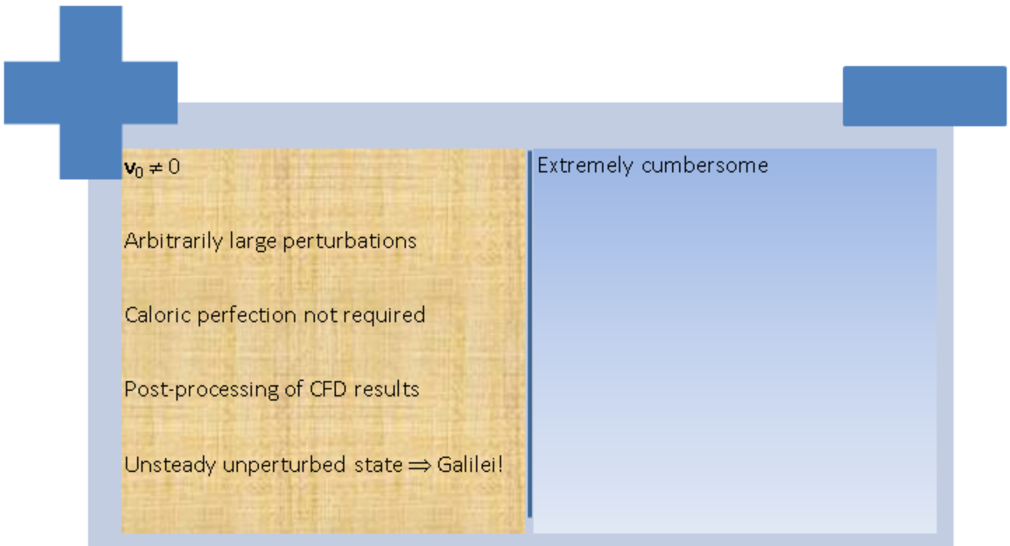

Figure 7.5: *Pros and cons of Myers' corollary for GT. See text for details.*

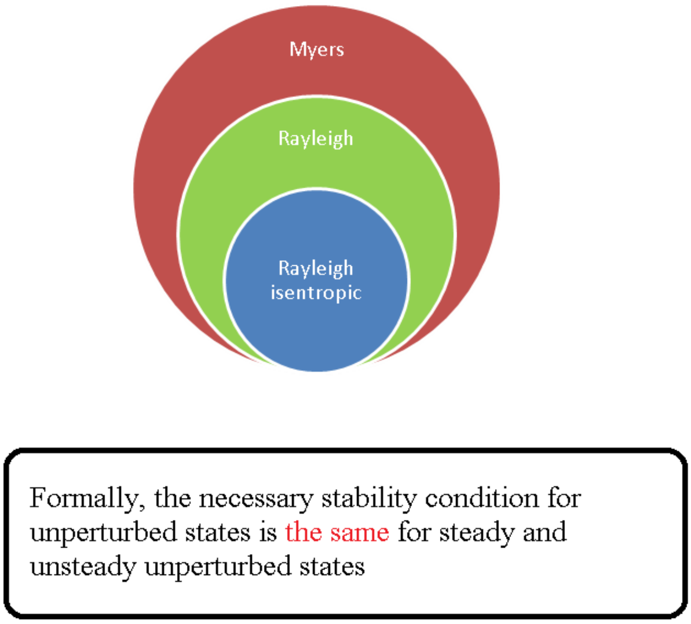

Figure 7.6: *Ranges of validity of the necessary stability criteria* (6.35) - (6.36) *as provided by Rayleigh's criterion (in the isentropic version), Rayleigh's criterion and Myers' corollary. Rayleigh's criterion (in the isentropic version) is useful for small, isentropic perturbations of unperturbed steady flows subject to no body forces and enjoying caloric perfection. Rayleigh's criterion removes the isentropic requirement. Myers' corollary removes all assumption but vanishing body forces. The words* the same *refer to the couple* (6.35) - (6.36). *Results for unsteady unperturbed states derive from the corresponding results for steady states after time-averaging.*

Chapter 8

Let a hundred flowers bloom...

8.1 The turn of the key

We have seen that linearised, modal analysis of stability is by far the most popular tool in manufacturers' efforts aiming at humming prevention, due to its powerful and reliable numerical methods, the amount of information it provides about the modes which drive humming and the conceptual simplicity of the criterion of stability it provides - in a nutshell, Rayleigh's criterion.

Nevertheless, its physical basis is difficult to assess - to say the least. This conceptual weakness weakens its looked-for prediction capabilities. The reason is that the perturbation energy balance it relies upon, basically equivalent to Rayleigh's criterion, takes into account only the flow of acoustic energy propagating across the boundaries of the combustor and the fraction of heat release which gets transformed into acoustic energy. The former and the latter are heavily affected by combustor acoustics and FTF respectively; indeed, the accurate evaluation of both has been given great care for decades.

Unfortunately, no energy exchange between the perturbation and the unperturbed fluid is taken into account when a non-trivial, realistic description of the unperturbed flow is provided. Physically, modal analysis and Rayleigh's criterion consider the contribution of acoustic waves (which propagate at the speed of sound) to the energy balance and neglect the contribution of convective (entropy, vorticity) waves, which propagate at the speed of the unperturbed fluid. In the general case, indeed, only the total energy of the fluid (unperturbed fluid + perturbation) is well-defined and may be conserved; speaking of a perturbation energy as something separated from the remaining energy of the fluid is nonsensical, because of Galileian invariance of the equations of motion. Modal analysis is therefore able to provide unambiguous descriptions of selected problems only [19] [21] [20].

To put it in other words, there is no satisfactorily definition [66] of the energy of a perturbation in a moving fluid, where according to [33] a *satisfactorily* energy should never increase when there is no combustion and no net flux at the boundary -it should rather decrease if viscous dissipation occurs. On the contrary, it seems possible for the moving fluid to feed the growth of the perturbation with its own energy even if no combustion and no sound propagation occur. As a consequence, the perturbation energy may grow at $t < \infty$ even if modal analysis predicts stability in the $t \to \infty$ limit. Mathematically, the linearised stability problem with a non-trivial unperturbed flow is non-normal.

8.2 The impact of nonlinearities

An obvious way to circumvent these difficulties is to get rid of the linearity approximation. To understand why, let us come back to the simple one-dimensional case displayed in Fig. 6.10. Should we replace the old condition for heat release perturbations $\propto \sin\left[\frac{2\pi}{\tau}\cdot(t-\tau_{FTF})\right]\cdot\cos\left(\frac{\pi x}{L}\right)\cdot\delta\left(x-x_f\right)$ provided by linear theory with the nonlinear condition [52]:

$$\propto \sin\left[\frac{2\pi}{\tau}\left(t-\tau_{FTF}\right)\right]\cos\left(\frac{\pi x}{L}\right)\delta\left(x-x_f\right)+\epsilon\left[\sin\left[\frac{2\pi}{\tau}\left(t-\tau_{FTF}\right)\right]\cos\left(\frac{\pi x}{L}\right)\right]^3\delta\left(x-x_f\right)$$

(with $|\epsilon| \ll 1$), then we would replace (6.40) with

$$D \propto \cos\left(\frac{2\pi\tau_{FTF}}{\tau}\right)\cdot\sin\left(\frac{2\pi x_f}{L}\right)\cdot\left[1+\frac{3}{4}\epsilon\cos\left(\frac{\pi}{L}\right)^2\right]$$

Noteworthy, if $\epsilon < 0$ (> 0), the new, non-linear term has a stabilising (destabilising) effect. Then, it is at least conceivable that non-linearity can help us to take into account some effects not properly dealt with in the linear approach above.

Of course, the physics of humming is somehow related to the compressible Navier-Stokes equation, which is definitely non-linear. To date, however, full numerical description of spontaneously occurring humming oscillation with the help of compressible [1] CFD in a realistic case and with the help of no unphysical, external siren seems still to be out of question. Given the huge amount of both computer resources and CPU time required, in fact, this has been done for selected cases only [4] [22] [77].

Outside the framework of linear analysis, however, the transfer function concept - renamed *(flame) describing function* (FDF), possibly in a simple, sinusoidal form- enjoys a new renaissance: in fact, if we allow f_{FTF} to be a non-linear function of its arguments [80], possibly including the perturbation amplitude itself, then the system of equations (6.29) and (6.20) may lead to a dynamical system, where the well-known results concerning limit cycles, bifurcations etc. apply [60].

[1] Admittedly, compressibility is usually neglected in subsonic motions which are typical of GT combustors. However, the divergence of $\mathbf{v}$ never vanishes at the flame, as the latter heats up the fluid even if no sound is present. Of course, compressibility is required when sound is present.

Most researchers work with a simplified one-dimensional geometry [47] [7] [61]. However, it has been shown [81] that a multi-step approach may take into account even realistic combustor geometries. Firstly, solution of the homogeneous version of equation (6.29) in a combustor filled with a fluid at rest with no flame for a given set of boundary conditions and in the frequency domain provides us with the eigenfunctions of the wave operator. The set of these eigenfunctions is an orthonormal basis for suitably chosen boundary conditions. Secondly, we look for the solution of the system (6.29) - (6.20) as a sum of a finite, properly choses, integer number of such eigenfunctions, the coefficients of this sum being functions of time. In some cases a more complicated set of equations, taking into account non-zero mean flow as well, replaces the system (6.29) - (6.20). Galerkin methods are routinely utilised [51]. Thirdly, we assign a FDF and write down a dynamical system, whose unknown quantities are the coefficients referred to above. Finally, we find the attractors and the corresponding basins of attraction of this dynamical system with the help of either brute force calculations or standard continuation analysis [81]. Remarkably, such approach takes the evolution of flame shape in time fully into account - see Fig. 8.1

In the example displayed in Fig. 8.1, the authors identify a humming oscillation with just one well-defined period and the steady state with no humming with a one-dimensional, attractive limit cycle with non-zero amplitude and zero amplitude respectively. Correspondingly, the onset of humming corresponds to a bifurcation. Usually, some feature of the impinging flow, like e.g. its Mach number, plays the role of the control parameter. Many other authors follow a similar line of reasoning.

A relevant exception is the line of research pursued by Sujith and coworkers, where the humming-free system and the humming-affected system are seen as a chaotic system and a low-dimensional attractor resectively: in this original approach, combustion noise is seen as the outcome of a deterministic, rather than stochastic, process [78] [79]. In another work [82], the authors suggest that even the familiar partition of the humming prediction problem in two parts, namely the computation of the flame transfer (or describing) function and the solution of a wave equation, fails to provide the correct bifurcation map, and the

> *describing function technique cannot be applied in general to predict the nonlinear behavior of a thermo-acoustic system.*

Far from being of purely academic relevance, the very nature of humming onset is of truly down-to-earth interest, as its prediction lies at the core of designers' efforts aiming at checking humming danger still from the drawing board.

In particular, when investigating the onset of humming, the interplay between non-normality and non-linearity rules the behaviour of the system in the neighbourhood of an initially humming-free steady state. In fact, non-normality and non-linearity tell us how much any random noise gets momentarily amplified by transient growth and how large is the minimum deviation from the humming-free state which pushes the system into the basin of attraction of a humming oscillation respectively. As a consequence, even if modal analysis predicts stability the system undergoes humming provided that either the non-normal, transient amplification of noise is large enough and/or if the minimum

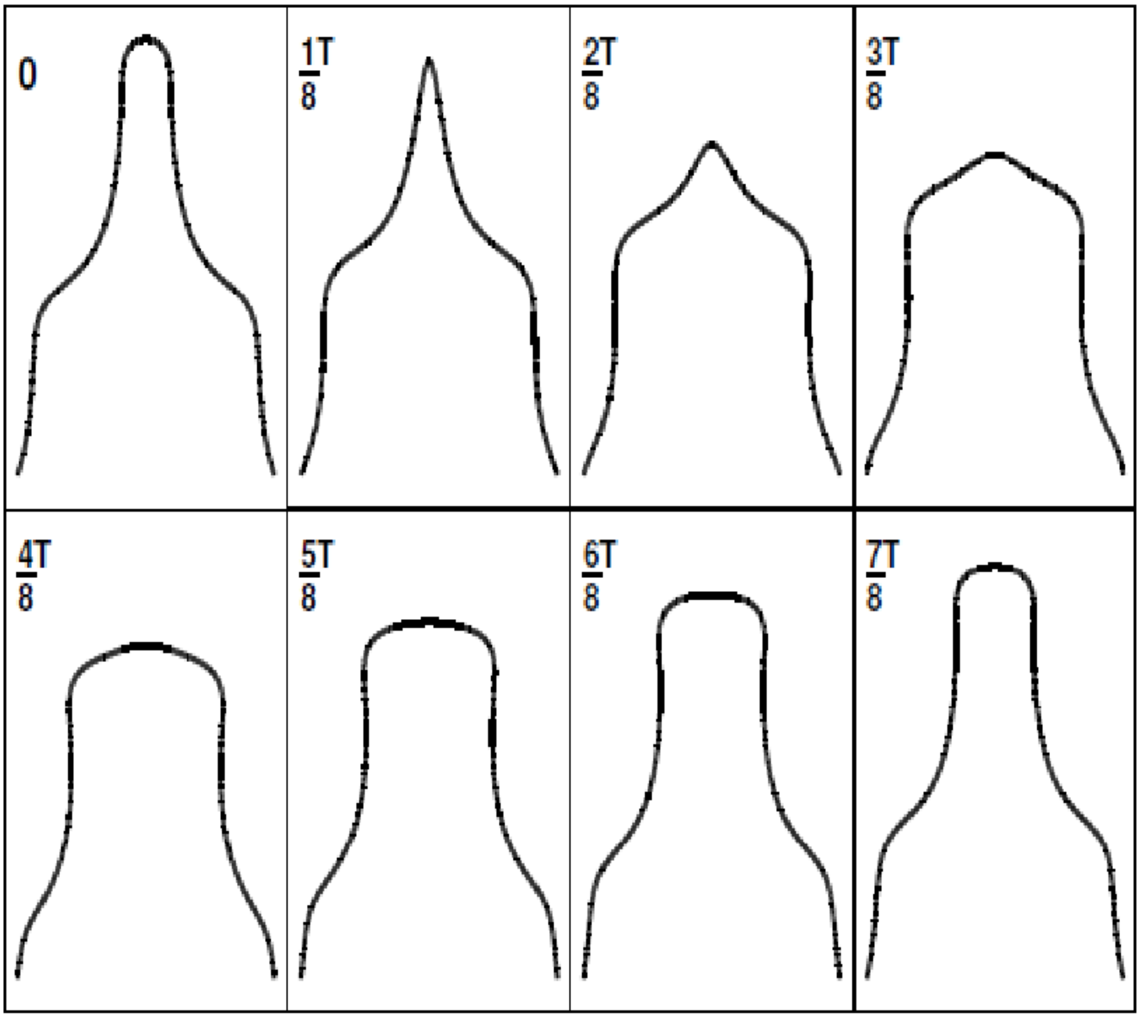

Figure 8.1: *The shape of the flame changes as (dimensionless) time goes by in the system described by Ref. [81], which oscillates with period T.*

perturbation amplitude which drives ultimately the system to fully-developed humming is low enough [51].

This approach is attractive because of its basic simplicity, as dynamic systems involve no partial differential equations -unlike modal analysis. Moreover, the structural stability of attractors like e.g. a limit cycle seems to fit well the observed resiliency of humming to any effort aimed at its suppression. Furthermore, hysteresis, a common feature found in non-linear dynamic systems, is routinely observed in real-life humming affected combustors. Finally, simultaneous utilisation of the bifurcation maps and the sensitivity analysis as provided by nonlinear analysis and nonnormal, linear analysis seems to be promising [51].

However, feasibility of a anti-humming strategy based on the description of the combustor as a dynamical system ultimately depends on how accurate the description of the flame is. This is true even in the simple case where all nonlinearities are located at the flame only [2]. In most cases, the FDF is just postulated - just like it usually happens with its linear counterpart, the FTF, in many works focussed on modal analysis and non-normality. For example, FDF neglects the effect of coupling terms between modes at different frequencies, since it is a one mode (sinusoid) approximation. Coupling between different modes in the FDF approach is a topic of current research [83]. As for an overview of linear and nonlinear approaches to thermo-acoustics, see Fig. 8.2. As for the pros and the cons of non-linear analysis from the point of view of a GT manufacturer, see Fig. 8.3.

We stress again the point that -as far as the onset of humming is concerned- the final assessment on the stability of a combustor is an outcome of both linear non-normal analysis and of non-linear analysis. Both FTF and FDF may contain arbitrary constant coefficients, to be eventually obtained after comparison with observations. Detailed computations of both functions rely once more on CFD, and are scarcely less cumbersome and more reliable than full simulation itself.

8.3 Myers vs. Rayleigh

Talking of reliability, Myers' corollary is a rigorous, Galileian-invariant generalisation of Rayleigh's criterion which gets rid of most unphysical assumption underlying this criterion -above all, linearisation and vanishing Mach number in the unperturbed flow. Even if formally similar to an energy balance, Myers' corollary is no such a thing: it is just a formal consequence of the equations of motions and of the first principle of thermodynamics. It takes a similar form regardless of the fact that the unperturbed fluid is steady or unsteady: as a consequence, a necessary criterion can be formulated, in formal analogy

[2]This case is likely to be far from realistic in GT. Nonlinearity may affect either boundary conditions or the gas dynamics itself inside the combustor. As for the former, they may couple different waves [3] and affect losses -see the discussion in [52]. As for the latter, they are usually negligible in GT, in contrast with what happens in rockets where $\frac{p_1}{p_0}$ may be larger than 20 % .

	Method	Domain	Limit Cycle Prediciton	Non-Modal Stability	Solution Type
Finite Volume Finite Element	CFD Navier - Stokes	Time	Yes	Yes	Nonlinear Partial Differential Equations
	Computational Acoustics	Time	Yes	Yes	Linearized Partial Differential Equations
Modal Based	Galerkin	Time	Yes	Yes	Delay Differential Equations
	Network Models	Frequency	No	No	Algebraic Equations
	Sinusoidal Describing Function	Frequency	Yes	No	Algebraic Equations
	Coupled Modes	Frequency	Yes	No	Algebraic Equations

Figure 8.2: *Some modeling approaches to thermo-acoustic systems - from Ref. [52].*

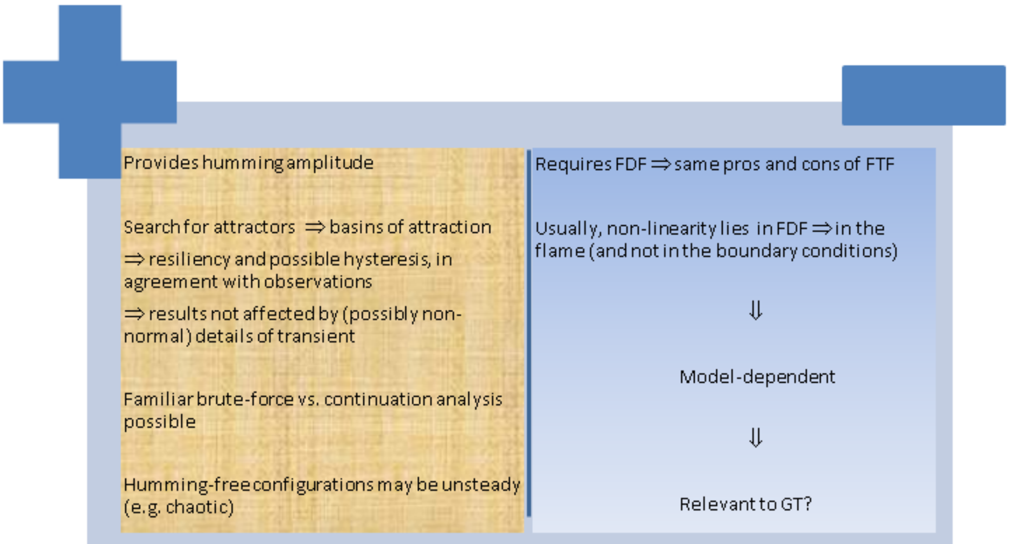

Figure 8.3: *Pros and cons of nonlinear analysis for GT. See text for details.*

with Rayleigh's criterion, for the stability of both steady and unsteady unperturbed states.

Moreover, validity of Myers' corollary does not rely on caloric perfection (according to which all gases are perfect gases with constant specific heats), nor it depends on the detailed models of combustion and turbulence. This feature is something new in our analysis so far, as both modal analysis and the approach based on dynamical systems relies on some description of the flame (FTF or FDF) where both combustion and (in realistic combustors) turbulence have to be kept into account somehow. The only exception has been precisely Rayleigh's criterion, whose generalization is Myers' corollary. Given the present uncertainties in the available models of both phenomena, this lack of dependence on a particular model is a precious advantage we would like to preserve.

Unfortunately, the extremely cumbersome structure of the terms appearing in Myers' corollary make its practical application unfeasible but for the self-consistency check of CFD results. People made such check on a confined flame for once, and it ruled out the fundamental approximation underlying modal analysis, i.e. the zero Mach approximation for the unperturbed state.

Apart from the equations of motion, the proof of both Rayleigh' criterion and Myers' corollary relies on the first principle of thermodynamics, which of course is valid regardless of any detailed model of combustion and turbulence. In particular, the first principle of thermodynamics (5.4) has been written for a small mass element of fluid. It is therefore worthwhile to ask if there is some other result of the thermodynamics of a small mass element of fluid which has not yet been invoked -explicitly at least.

8.4 A way out?

Usually, thermodynamics deals with steady states. Thermodynamic equilibrium is one of them: it is the final, stable state of the evolution of an isolated system, and the entropy of this system increases monotonically during relaxation of the latter towards thermodynamical equilibrium. Once the latter has been achieved, fluctuations are still possible, but they will relax back to equilibrium. Equilibrium is therefore a stable, steady state described by a variational principle (maximum entropy at fixed energy and volume), i.e. the *second principle of thermodynamics* [84].

Many researchers have focussed their attention on the possible existence of criteria for stability of steady states which differ from thermodynamical equilibrium. Such states may exists e.g. when suitable boundary conditions keep the steady state of a non-isolated system far from thermodynamic equilibrium. User-selected premixed flows entering a combustor are obvious example of such boundary conditions.

Admittedly, as far as fluids far from thermodynamic equilibrium are concerned, the very notion of *steady state* is rather ambiguous; all the same, we maintain -as a working hypothesis- that it still makes sense, possibly after time averaging on time scales » turbulent time scales. When it comes e.g. to real-life GT combustors, for all practical purpose *steady state* means *combustor without humming*. It has been shown that these criteria exist and take the form of variational principles in some particular cases at least [85] [86]. In these cases, if a solution of the equations of motion corresponds to a stable, steady state then it corresponds also to a minimum of some thermodynamic quantity, and any perturbation tends to increase the value of this quantity with respect to the unperturbed state. For readers who are unfamiliar with variational principles and the related topic of variational calculus, some useful results are collected in a dedicated Appendix.

Accordingly, we may discuss stability of steady states with the help of no detailed analysis of the equation of motion both at thermodynamical equilibrium and in some non-equilibrium problems. Admittedly, just as pointed out by [87], the equations of motion provide us with complete information on the evolution of the system; strictly spekimg, therefore, they make any criterion of stability redundant. All the same, availability of thermodynamical (i.e., problem-independent) criteria of stability allows us to drop cumbersome analysis of the stability of the solutions of these equations, and is useful when no detailed knowledge of the dynamics of the system is available.

Unfortunately, the very object of manufacturers' interest, humming, is definitely no steady state; it is rather a self-sustaining oscillation based on the balance of many competing processes, some of which raise entropy. It seems therefore perfectly reasonable to ask oneself if thermodynamics may provide us with some criterion of stability for oscillating fluids -for those problems at least where these thermodynamic quantities are well-defined at each time during the oscillation.

For example, Chandrasekhar's classical analysis of the onset of Benard convection cells [88] starts from the relevant equations of motion and shows that -as the small mass element moves in the rotating cell- the fluid selects the configuration which corresponds to a constrained minimum of the adverse temperature gradient -the constraint being given by the balance between time-averaged values of the dissipated power and the mechanical power delivered by buoyancy.

Unfortunately, to the author's knowledge no generally accepted answer is available in the literature to date-with the only exception of the observations of [28] discussed below. We anticipate here that the latter observations are relevant both to Rijke's tube and to the modern research on humming.

Historically, this analogy between the thermodynamics of an oscillating state and a steady state has been postulated without proof in Chapter XV of [89], where it is stated that stable oscillations in fluids minimise the time-average of the amount of entropy produced per unit time by all irreversible processes, the time-average being taken on a time-scale much longer than the oscillation period. Unfortunately, however, such minimisation requires validity of the Onsager symmetry relationships [90], which are far from being satisfied in a fluid, as they rely on a number of quite restrictive hypotheses including e.g. the assumption that all phenomenological coefficients are constant at all times and uniform across space.

Later, Glansdorff and Prigogine claimed that that the sign of the time derivative of the second-order differential of entropy provides the looked-for stability criterion [91]. But Lavenda's arguments show - see Sections 4.2 and 7.1 of [92] - that even if such sign is known, stability depends on the actual eigenvalues of the linearised equations of motion. In turn, Lavenda's *quasi-thermodynamic approach* (QTA) postulates that Onsager and Machlup's so-called *least dissipation principle* - one of the results discussed in Sec. IV.5 of [85] - holds even beyond the domain of validity of Onsager's symmetry relationships it had been originally limited to. Indeed, QTA requires that the system is ruled by the equations of motion of a generalized, forced, linear harmonic oscillator with constant coefficients. Here we refer to equations (5.2.31) and (6.4.3), to Secs. 6.4, 9.7 and to p.159 of Ref. [92], according to which the

> *interpretation of the principle of least dissipation will henceforth be mechanical in nature*

According to the same author, extension of QTA to continuum is possible, but still relies on the assumption

> *that the phenomenological coefficients are constant*

(Lucia [93] discusses the particular case of constant mass density). In spite of these limitations, however, QTA applies successfully to a particular non-linear problem, i.e. the limit cycle of a Van der Pol oscillator -provided that

> *the motion behaves as if it were periodic during any single period, whereas the effects of dissipation are only noticeable over the longer space-time of evolution*

Again, we retrieve the by now familiar assumption $|\frac{\Im\{\omega\}}{\Re\{\omega\}}| << 1$ of modal analysis.

To make things worse, two further difficulties arise. Firstly, even when thermodynamics provides us with some necessary criterion of stability in the literature, such criterion takes the form of a variational principle. In contrast, the only generally accepted neecssary stability criterion in humming research, i.e. Rayleigh's criterion in the form (6.34), is definitely no variational principle. We have therefore to find a thermodynamic description of the problem which allows us to retrieve whenever (6.1) and (6.13) hold, while allowing further necessary criteria to exist, possibly in variational form.

Secondly, no discussion of stability of some unperturbed state which deals with steady unperturbed state only leads to results which are Galileian-invariant, corresponding therefore to physically acceptable solutions of the equations of motion. A correct theory has to discuss stability of both steady and oscillating states on the same ground. Our discussion of Myers' corollary has provided us with a clue: if a criterion is available for the stability of a steady state, then suitable time-averaging may provide a corresponding criterion for the stability of the oscillating state. Indeed, we shall see that the criterion found in [28] satisfies precisely this requirement.

As we are going to show, the second principle of thermodynamics may provide us with a way out of this conundrum, through one of its corollaries, namely Le Châtelier's principle. Before discussing this point in-depth, however, it is worthwhile to review some well-known experimental results which provide us with information about the connection between thermodynamics and the problem of spontaneous oscillations in thermo-acoustics.

Part III

Thermodynamics

Chapter 9

A review

9.1 Rijke's tube

9.1.1 The experiment

We start our review with the first example of such oscillations, namely Rijke's tube. In 1859 Rijke discovered a way of using heat to sustain a sound in a cylindrical tube open at both ends [24]. He used a glass tube, about 0.8 m long and 3.5 cm in diameter. Inside it, about 20 cm from one end, he placed a disc of wire gauze -see Fig. 9.1.

Gauze friction with the walls of the tube is sufficient to keep the gauze in position. With the tube vertical and the gauze in the lower half, he heated the gauze with a flame until it was glowing red hot. Upon removing the flame, he obtained a loud sound from the tube which lasted until the gauze cooled down (about 10 s).

Instead of heating the gauze with a flame, Rijke also tried electrical heating. Making the gauze with electrical resistance wire causes it to glow red when a sufficiently large current is passed. With the heat being continuously supplied, the sound is also continuous and rather loud. Rijke seems to have received complaints from his university colleagues because he reports that the sound could be easily heard three rooms away from his laboratory. The electrical power required to achieve this is about 1 kW.

Later, Rayleigh reproduced Rijke's experiments [31]. He made use of two layers of gauze made from iron wire inserted about quarter of the way up the tube. The extra gauze is to retain more heat, which makes the sound longer lasting.

9.1.2 The model

The sound comes from a standing wave whose wavelength is about twice the length of the tube, giving the fundamental frequency. The flow of air past the gauze is a combination of two motions -see Fig. 9.2.

There is a uniform upwards motion of the air due to a convection current resulting from the gauze heating up the air. Superimposed on this is the motion due to the sound

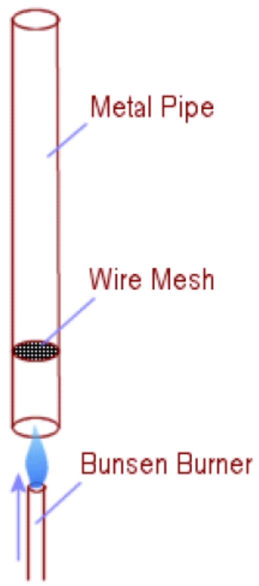

Figure 9.1: *A simple construction of the Rijke tube, with a gauze in the lower half of a vertical metal pipe. (Here wire mesh stands for gauze). The tube is suspended over a bunsen burner. The latter heats the gauze.*

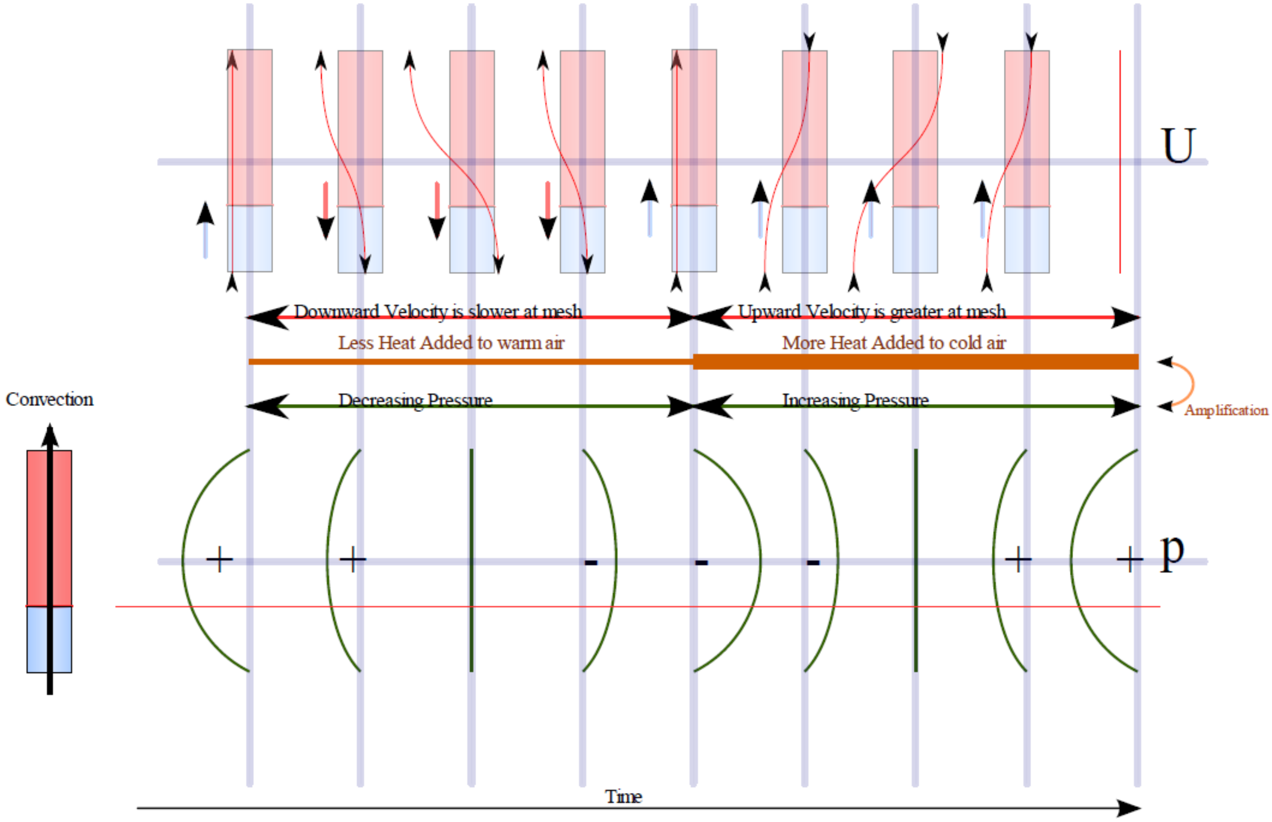

Figure 9.2: *Time is increasing from left to right. At the initial time, only upwards convection occurs (look at the left side of the figure). If a pressure perturbation occurs such that a pressure peak occurs right at the centre, then it pushes away the fluid from the centre (on the second column, look at the red arrow poynting downwards on the upper side of the figure). Accordingly, the central pressure peak lowers the upwards, convection-driven vertical motion of the fluid across the lower half of the tube* where the gauze mesh is located. *As a result, a longer time is available to heat exchange between mesh and air, the latter gets heated better and the pressure peak in enforced. As time goes by, the pressure peak flattens more and more, and even less fresh air gets heated. On the left side of the figure, things go all the other way around: there is a pressure drop on the centre, air gets sucked, there is less time available for heat exchange and air heating is less effeective, so that less heat is added by the mesh to the air, and the central pressure is further depressed. Heat exchange between air and gauze plays a crucial role.*

wave. For half the vibration cycle, the air flows into the tube from both ends until the pressure reaches a maximum. During the other half cycle, the flow of air is outwards until the minimum pressure is reached. All air flowing past the gauze is heated to the temperature of the gauze and any transfer of heat to the air will increase its temperature and its pressure, according to the gas law.

Admittedly, as the air flows upwards past the gauze most of it will already be hot because it has just come downwards past the gauze during the previous half cycle. However, just before the pressure maximum, any small quantity of cool air which comes into contact with the gauze gets heated, and its pressure is increased. This increases the pressure maximum, so reinforcing the vibration.

During the other half cycle, when the pressure is decreasing, the air above the gauze is forced downwards past the gauze again. Since it is already hot, no pressure change due to the gauze takes place, since there is no transfer of heat. The sound wave is therefore reinforced once every vibration cycle and it quickly builds up to a large amplitude. This explains why there is no sound when the flame is heating the gauze. All air flowing through the tube is heated by the flame, so when it reaches the gauze, it is already hot and no pressure increase takes place.

When the gauze is in the upper half of the tube, there is no sound. In this case, the cool air brought in from the bottom by the convection current reaches the gauze towards the end of the outward vibration movement. This is immediately before the pressure minimum, so a sudden increase in pressure due to the heat transfer tends to cancel out the sound wave instead of reinforcing it.

The position of the gauze in the tube is not critical as long as it is in the lower half. To work out its best position, there are two things to consider. Most heat will be transferred to a small mass element of air where the acceleration of this small mass element along the tube is a minimum, as heat exchange may occur in this case before the small mass element gets shifted significantly away from the pressure of the wave (for given initial position nd velocity of the small mass element). In turn, this occurs where the pressure gradient of the wave is a minimum (see equation (6.25) [1]), i.e. near the end of the tube. However, the effect of increasing the pressure (in thermodynamical jargon: the efficiency of conversion of heat into mechanical work) is greatest where there is the strongest heating, i.e. in the middle of the tube. There is therefore no perfect position for the gauze. A good compromise is obtained by placing the gauze midway between these two positions, i.e. one quarter of the way in from the bottom end.

Rijke's tube acts as a *half-wave resonator*, i.e. its length is equal to one half of the wavelength of the pressure perturbation. This means that the geometry -here, the length- fixes the oscillation period unambiguously, as the latter and the wavelength are connected

[1] When invoking (6.25), which contains no information on the chemical nature of the gas involved, we postulate that such nature is actually not relevant to the experiment. Indeed, according to [31] experiments by Chladni and Faraday successfully replicated Rijke's results with gases of different chemical composition, including hydrogen.

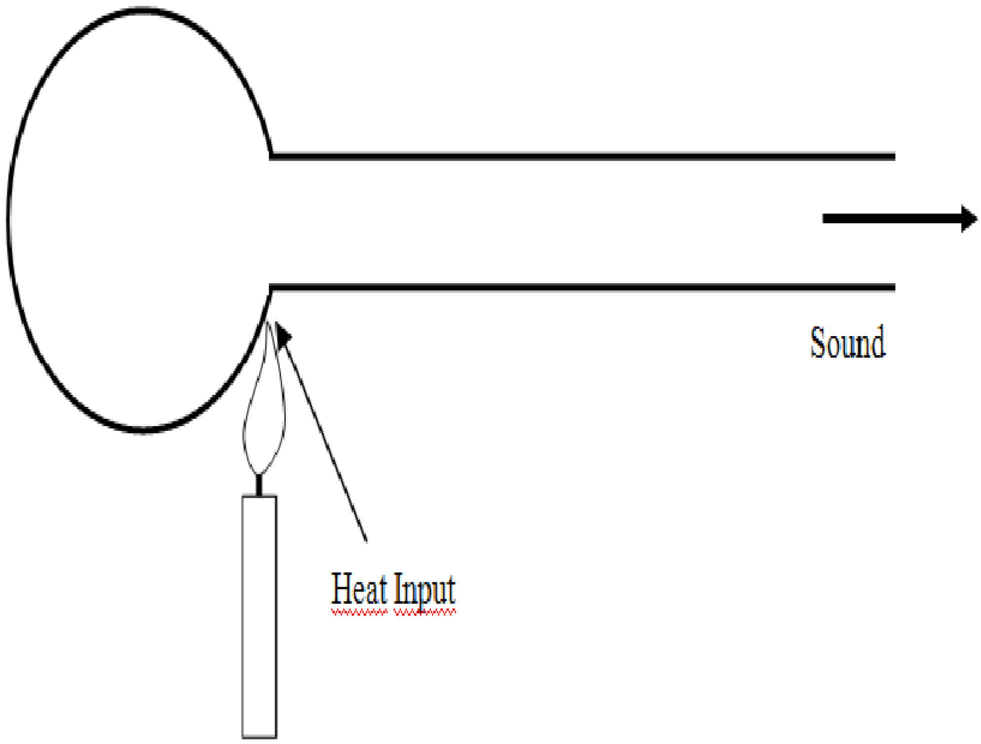

Figure 9.3: *Sondhauss' tube - from Ref. [23].*

by the distribution of the sound speed across the tube. To put in other words, the period of the oscillation is a resonant acoustic frequency of the system.

Even if seemingly trivial, we stress the point that the spontaneous production of sound depends on the exact value of the oscillation period only weakly. In fact, two Rijke's tubes with the same geometry and basically the same fundamental acoustic eigenfrequency may produce dramatically different amount of acoustic power if the gauze is located just below or above the half-length of the tube. Accordingly, the problem of computing the acoustic spectrum and the problem of predicting the actual production of sound are quite different. In the language of modal analysis, this means that accurate prediction of $\Re\{\omega\}$ guarantees no reliable prediction of humming.

9.1.3 Sondhauss' version

The fact that the period of the oscillation is a resonant acoustic frequency of the system is is no unique feature of half-wave resonators. In fact, Rijke's tube operates with both ends open. However, a tube with one end closed will also generate sound from heat, if the closed end is very hot. Such a device is called a *Sondhauss' tube* [23] after Sondhauss who described it in 1850 -see Fig. 9.3.

The phenomenon was first observed by glassblowers. Sondhauss' tube operates in a way that is basically similar to the Rijke's tube. Initially, air moves towards the hot, closed end of the tube, where it is heated, so that the pressure at that end increases. The hot, higher-pressure air then flows from the closed end towards the cooler, open end of the tube. The air transfers its heat to the tube and cools. The air surges slightly beyond the open end of the tube, briefly compressing the atmosphere. the compression propagates through the atmosphere as a sound wave. The atmosphere then pushes the air back into the tube, and the cycle repeats. Sondhauss' tube acts as a *quarter-wave resonator*, i.e. its length is equal to one fourth of the wavelength of the pressure perturbation.

Unlike Rijke's tube, Sondhauss's tube does not require a steady flow of air through it. All the same, we anticipate here for the sake of future reference that heat exchange plays a crucial role in both Rijke's tube and Sondhauss' tube. As for the former, see the caption of Fig. 9.2. As for the latter, it was discovered that placing a porous heater -as well as a *stack*, i.e. a porous plug- in the tube greatly increases the oscillation amplitude in both Rijke and Sondhauss' devices. Today, stacks are suitably designed in order to raise heat exchange between the working fluid and the material walls in modern thermo-acoustic devices [23]. This fact is to be recalled below.

9.1.4 The consequences

In spite of its apparent simplicity, Rijke's tube provides us with a lot of useful information. First of all, general consensus underlines the crucial role played by the relative phase of oscillations of pressure and heat release in Rayleigh's criterion: it is this phase which explains why sound is heard only if the gauze is located at a suitable position inside the tube [31] [53]. It turns out that both the occurrence of humming and the value of $\Re\{\omega\}$ depend on this phase [35]. As we are going to see, however, this relative phase is far from being the only quantity which is relevant to the triggering of the oscillations.

Secondly, the original Rijke's observation is that sound is spontaneously produced while the gauze cools down. In modern language, Rijke' tube is a example of those so-called *dissipative structures* where order (in this case, temporal order, i.e. an acoustic oscillation with well-defined frequency) arises from relaxation (the cooling of the gauze), i.e. from entropy growth. And where entropy is at stake, thermodynamics is likely to have a say. Outside thermo-acoustics, the Belousov-Zhabotinsky chemical reactions provide a well-known example of dissipative structures [94]. Dissipative structures are usually found in open thermodynamical systems, i.e. in systems where exchanges of energy and matter with the external world occur. This is obviously the case both of Rijke's tube - and of the flame in an industrial combustor as well. It is worthwhile to check if available results concerning dissipative structures may offer useful insight in spontaneous onset of acoustic oscillations, like in Rijke's tube -and in humming.

Thirdly, Rayleigh's original words *If heat be given [...] or be taken* quoted above [31] refer to exchanged heat, not to heat release -let alone combustion. This point is stressed again and again in many passages of Rayleigh's work. For example, when reviewing an experiment the author writes [31]:

> *in order that the whole effect of heat be on the side the side of encouragement it is necessary that previous to condensation the air should pass not*

> *merely towards a hotter part of the tube, but towards a part of the tube which is hotter than the air will be when it arrives there*

Here Rayleigh's emphasis on the words *hotter than* suggest that it was the difference of temperature, hence the heat flow, which draw his attention. It is only under the assumptions (6.1) that the proof of Rayleigh's criterion involves just the heat release. Rather than the detailed mechanism of gauze heating, it turns out that the heat exchange between the gauze and the surrounding environment is crucial to the onset of humming in Rijke's tube. For instance, sound is heard even when the gauze is cooler than the environment [26] [2].

Moreover, louder and longer sound is heard when many gauze discs are inserted inside the tube beyond the heated gauze disc, thus delaying air motion and leaving more time for heat transfer to occur. These discs play the same role of stacks in the above quoted Sondhauss' tube. In Rijke's own words [24] [3]:

> *when, instead of a single disc, several were placed in the tube, the sound lasted longer* [...] *that is because the presence of a greater number of discs, by diminishing the rapidity of the air current diminishes also the rapidity of cooling of the first disc*

This *rapidity of the air current* acts therefore as a further crucial parameter for sound generation, beyond the relative phase quoted above. This *rapidity* is just the relative velocity of the air and the hot gauze, as the hot gauze is at rest in the laboratory reference system. Together with its equivalent in the flame, it will be referred to again and again in the following. Here we anticipate that the quantity in the flame which is equivalent to this *rapidity* is the flame velocity.

Finally, we have seen that Rijke heard the sound fading away after a while in his first experiments. In order to obtain a sustained sound, Rijke heated the gauze with DC current. Sound generation starts, provided that the electric current is large enough (i.e. that the Ohmic power dissipated in the gauze is not too small). Moreover, with the heat being continuously supplied, the sound is also continuous. It is precisely the self-sustaining character of the acoustic oscillations heard by Rijke that triggered the attention of both Rayleigh and modern manufacturers of humming- affected combustors [4]. Heat released by combustion is the obvious analog to Ohmic power in Rijke's tube. Just as in the

[2] More recently, spontaneous growth of acoustic (*Taconis'*) oscillations in pipes which are partially filled with liquid helium has been reported. See e.g. Ref. [27].

[3] In his original German paper [25], Rijke refers to the *rapidity* with the term *Schnelligkeit* only when it comes to the *air current*. *Schnelligkeit* means *velocity*.

[4] In Rayleigh's words [31]

> *When a piece of fine metallic gauze, stretching across the lower part of a tube open at both ends and held vertically, is heated by a gas flame placed under it, a sound of considerable power, and lasting for several seconds, is observed almost immediately after the removal of the flame.* [...] *the generation of sound was found by Rijke to be closely connected with the formation of a through draught, which impinges upon the heated gauze. In this form of the experiment the heat is soon abstracted, and then the sound ceases; but by keeping the gauze*

latter, humming occurs in modern combustors at large heat release only. Thus, while the relative phase of pressure and heat release oscillations and the *rapidity of the air current* are crucial to decaying sound generation, such heat release is a further, third quantity which is crucial to continuous sound generation.

9.2 Biwa et al.'s selection rule

Rijke's results are retrieved and generalized by the experimental results of Biwa et al. [28]. Two solid bodies C and H, at temperature T_C and $T_H > T_C$ respectively, exchange heat with each other and a fluid -see Fig. 9.4 [5].

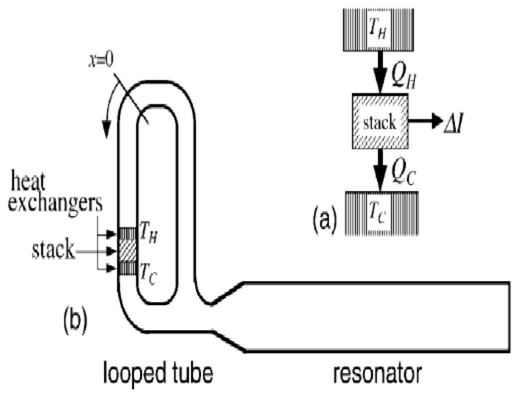

Schematic diagram of (a) the heart of a thermoacoustic prime mover and (b) the experimental setup consisting of a resonator and a looped tube containing the assembly shown in (a) inside. The origin of the coordinate x normalized with respect to the total length of the looped tube is taken at the position where the pressure amplitude for the standing-wave mode takes its maximum in the looped tube. The center of a stack is located at $x = 0.32$ in this scale.

Figure 9.4: *From Ref. [28].*

A known, total amount of heat Q_H flows out from H per unit time. The fluid, H and C correspond to the air, the hot gauze disc and the pipe wall in Rijke's tube respectively. The net amount ΔS of entropy flowing per unit time from H to C is just $\Delta S = T_C^{-1} Q_C - T_H^{-1} Q_H$ where Q_C is the total amount of heat which flows into C per unit time. Energy balance gives $Q_H = Q_C + \int_{A_b} d\mathbf{a} \cdot \langle \mathbf{W} \rangle$, where A_b is a closed surface including C and H - see equations (1) and (4) of [28]. Then,

$$\Delta S = \left(T_C^{-1} - T_H^{-1}\right) Q_H - T_C^{-1} \int_{A_b} d\mathbf{a} \cdot \langle \mathbf{W} \rangle$$

hot by the current from a powerful galvanic battery, Rijke was able to obtain the prolongation of the sound for an indefinite period. In any case from the point of view of the lecture the sound is to be regarded as a maintained sound.

[5]The figure displays a stack. See the discussion on the role of stacks in the Section on Rijke's tube.

If no sound is generated, $\int_{A_b} d\mathbf{a} \cdot \langle \mathbf{W} \rangle = 0$. If the sound is generated reversibly, then $\int_{A_b} d\mathbf{a} \cdot \langle \mathbf{W} \rangle = 0$ and Carnot formula gives the efficiency: $Q_H^{-1} \int_{A_b} d\mathbf{a} \cdot \langle \mathbf{W} \rangle = 1 - T_H^{-1} T_C$.

Experiments show that among all permissible modes of operation -either $\int_{A_b} d\mathbf{a} \cdot \langle \mathbf{W} \rangle = 0$, i.e. no humming, or $\int_{A_b} d\mathbf{a} \cdot \langle \mathbf{W} \rangle \neq 0$ - the system invariably selects the mode with the lowest ΔS -see Fig. 9.5.

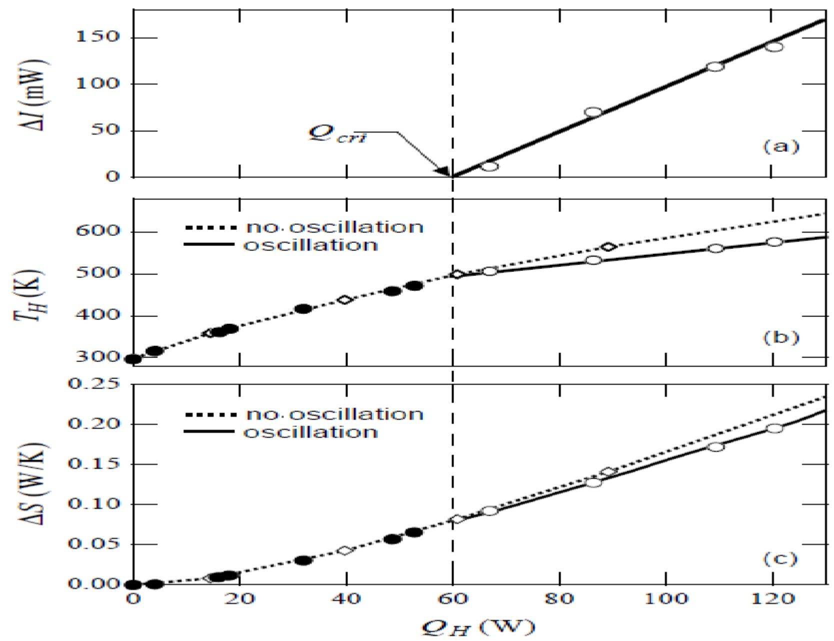

Figure 9.5: *The variation of ΔI (a), T_H (b) and ΔS (c) as a function of Q_H, when the gas oscillations are absent (solid circles) and present (open circles). Open diamonds in (b) are measured when the gas oscillations are suppressed and those in (c) represent the corresponding variation of ΔS. The vertical dashed line represents the critical heat flow Q_{cri} = 60W. From Ref. [28].*

In other words, the stable configuration satisfies

$$\Delta S = \min$$

We stress the point that this *selection rule* comes from systematic comparison of ΔS in both steady states and in various oscillating modes: in the latter case, it is the value of ΔS averaged on time on many periods of oscillations which allows such comparison with the steady-state value of ΔS -see Ref. 5 of [28].

In the following, we are going to see that this result is connected with the experimental results of Rijke's tube as well as with other relevant experimental results in humming research. We discuss the theoretical ground of this result with the second principle of thermodynamics and its connection with Rayleigh's criterion in the next Section.

9.3 From Biwa et al.'s selection rule to Rijke's tube

Since the system selects the mode with the lowest ΔS, if we want to prevent humming, i.e. to ensure stability of the $\int_{A_b} d\mathbf{a} \cdot \langle \mathbf{W} \rangle = 0$ state where $\Delta S = \left(T_C^{-1} - T_H^{-1}\right) Q_H$, we must keep the value of $\left(T_C^{-1} - T_H^{-1}\right) Q_H \geq 0$ as small as possible. In turn, this requires minimization either of Q_H or of $\left(T_C^{-1} - T_H^{-1}\right)$. As for Q_H, if the gauze is heated with a steady Ohmic power, then the latter is equal to Q_H; humming prevention requires that the heat supplied to the gauze is not too large. Furthermore, Q_H is the heat flowing from the hot gauze towards the wall and the air; in particular, humming prevention is easier at low values of heat flow towards air, hence at large *rapidity of the air current.* As for the wall temperature T_C, in Rijke's words [24]

> *the elevation of the temperature of the sides of the tube is rather injurious than otherwise to the success of the experiment* [of humming production]

Thus, humming prevention requires poor wall cooling (or even no cooling at all). In summary, humming prevention requires minimization of the heat flow from the flame towards the wall, either by reduction of heat release and/or temperature jump between flame and wall, or by increase of the *rapidity of the air current.*

9.4 From Biwa et al.'s selection rule to Rauschenbach's hypothesis

As for the relative phase, if humming occurs (i.e. $\int_{A_b} d\mathbf{a} \cdot \langle \mathbf{W} \rangle \neq 0$) then Biwa et al.'s minimization of ΔS -all the rest being equal- requires maximization of $\int_{A_b} d\mathbf{a} \cdot \langle \mathbf{W} \rangle$. This is in agreement with the following hypothesis, formulated as a rule-of-thumb by a pre-eminent Soviet rocket engineer in the Sixties, Rauschenbach -see chapter 9, Sec. 45 of [95]:

> *the development of vibrations in an oscillating combustion system evolves towards those relationships involving amplitudes and phases which maximize the amount of acoustic energy irradiated from the region where combustion occurs*

When humming occurs, therefore, phase is locked at a value which maximizes the flux of acoustic energy, just as required by Rayleigh's criterion.

9.5 Meija et al. and Hong et al.'s experiments

Now, let us come to combustion. To start with, let us consider a laminar flame. The flame is the equivalent of the hot gauze disc; both are at rest in the laboratory reference system. Thus, the *laminar flame velocity* [6] s_L is the physical quantity corresponding to Rijke's *rapidity of the air current* -see Fig. 9.6 and Fig. 9.7.

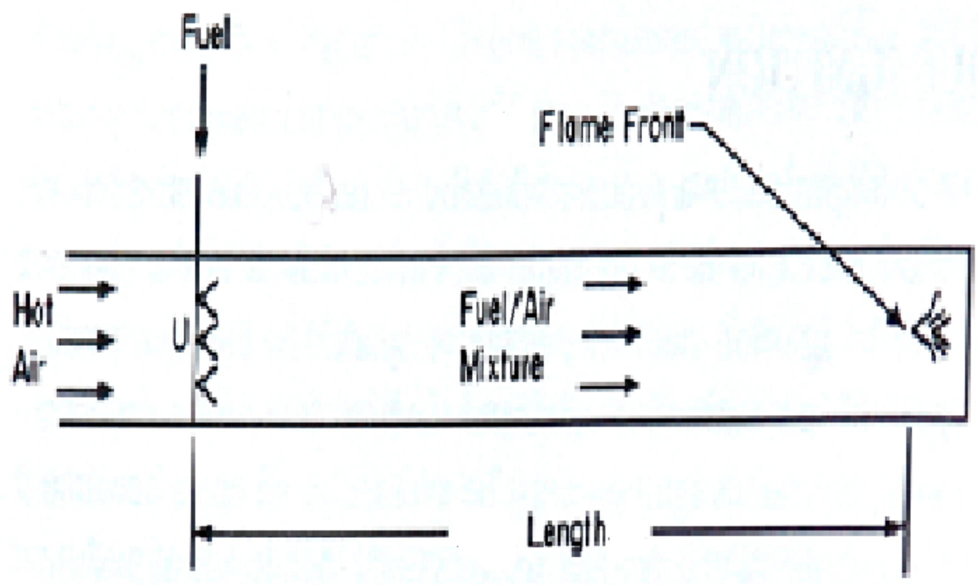

Figure 9.6: *By definition, the flame velocity is the velocity of the fuel-air mixture impinging on the flame (from left to right) when the flame front is at rest in the lab frame of reference.*

In a turbulent flame, of course, the *turbulent flame velocity* s_T plays a similar role [7]: the only difference is that s_T is always larger than s_L. Finally, the (*upstream*) flow of unburnt fuel + air mixture impinging on the flame is the equivalent of the air flow impinging from below in Rijke's tube.

Meija et al's experiments [29] with laminar premixed flames on a slot burner show that humming is triggered whenever the burner rim temperature is low enough - see Fig. 9.8 and Fig. 9.9.

In contrast, Hong et al.'s experiments [30] show that humming in a 50-kW backward facing step combustor can be prevented or significantly delayed by using a material with low thermal conductivity at the flame anchoring region; as the thermal conductivity of

[6]For a flat, laminar flame an observer riding with the flame would experience the unburned mixture approaching at the laminar flame velocity -see Chapter 8 of [2] and equation (2.24) of [4]. Basically, the latter velocity is the relative velocity of the flame at rest and the impinging fluid. It is a positive-definite quantity. If the flame is not flat, then the concept of *displacement velocity* is introduced - see the Appendix on the flame velocity.

[7]The turbulent flame velocity s_T is defined as the velocity needed at the inlet of a control volume to keep a turbulent flame stationary in the mean inside this volume -see Sec. 5.1.1 and equation (5.2) of [4].

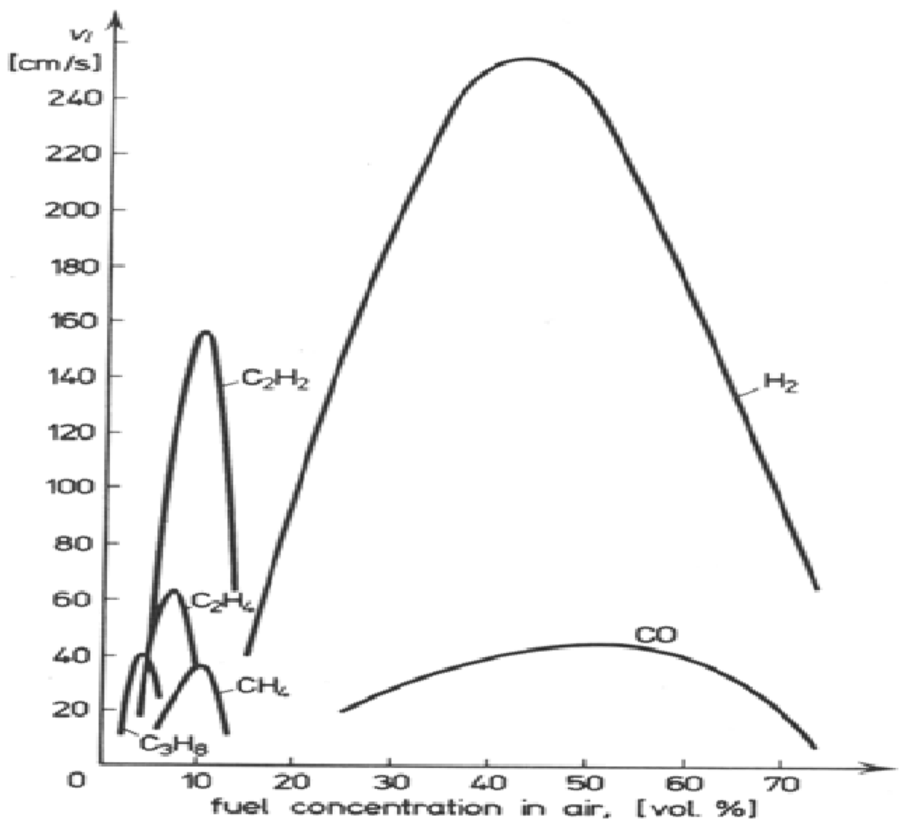

Figure 9.7: *Laminar flame velocity (cm/s) vs. fuel concentration in air (%) for various fuels.*

the flame-holder increases, the combustor becomes increasingly unstable over a range of operating conditions - seeFig. 9.10.

Finally, the upstream flow remains unaffected in both [29] and [30], just like the air flow impinging from below was unaffected in [24]. The same holds for heat release (which depends on the total amount of fuel burnt per unit time, which gets completely burnt in lean combustion at least): the corresponding quantity in [24] is the constant DC electric power supplied in order to sustain acoustic emissions. As an example of a physical quantity of the upstream flow which can be relevant to the onset of thermo-acoustic instability, and which is unaffected in [29] and [30], we quote the Mach number of the unperturbed flow, which can play a role in both liquid-propellant rocket motors [96] and GT combustors [3].

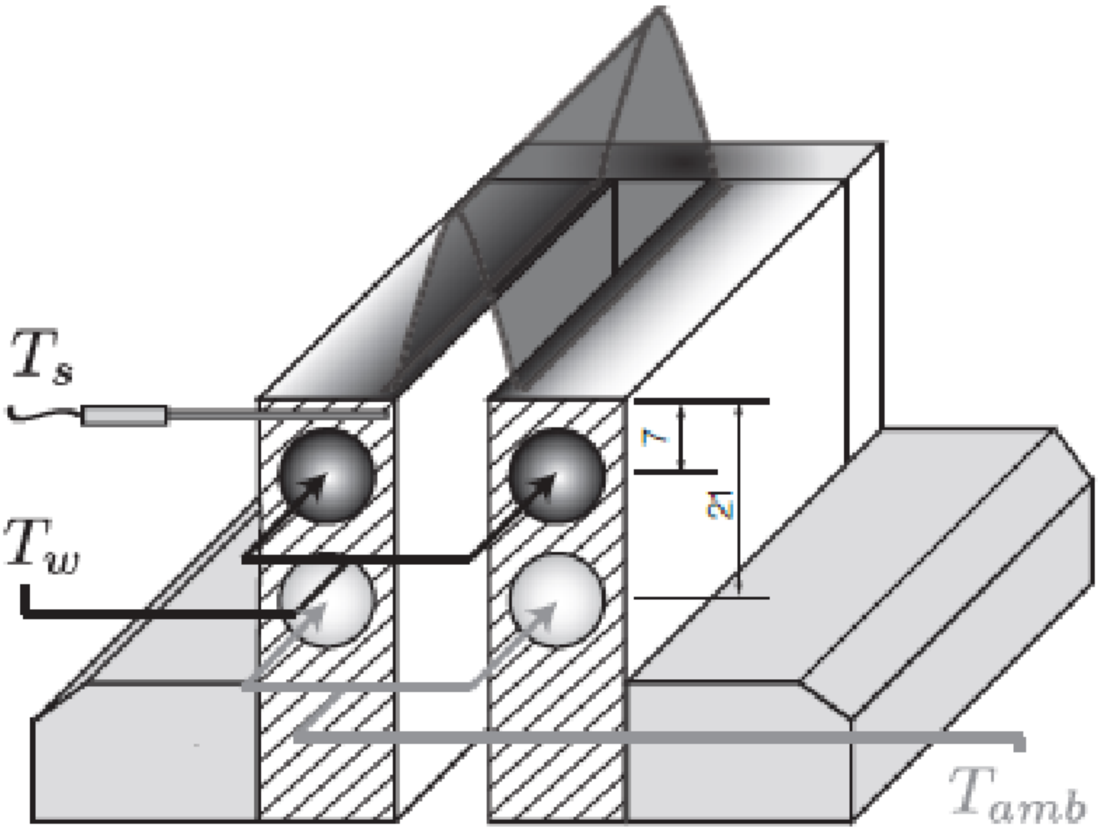

Figure 9.8: *Perspective view of the slot with the cut through the material. The upper and lower cooling channels allow a water flow at temperature T_w and T_{amb} respectively. A thermocouple meaures the slot temperature T_s - from Ref. [29].*

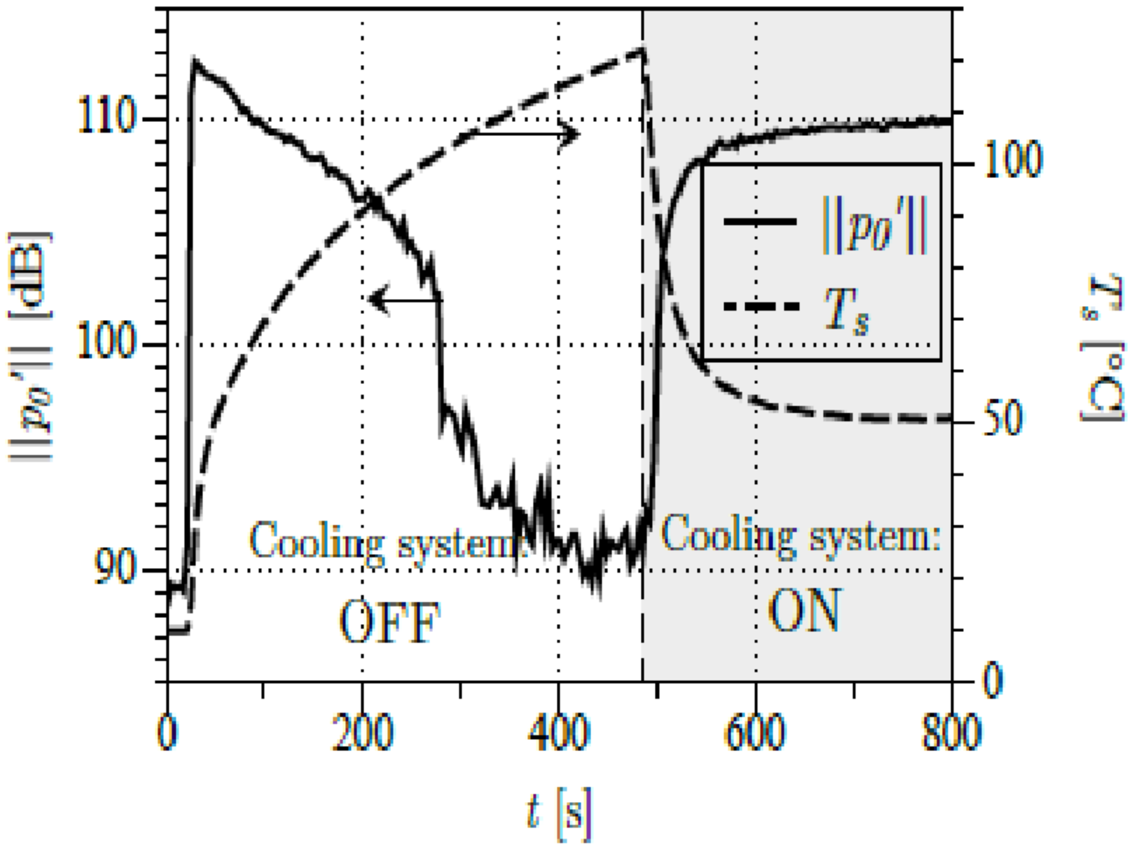

Figure 9.9: *At t = 0 the whole experiment is at room conditions. Combustion starts at t = 20 s and instabilisty develops immediately (58 Hz, acoustic mode). Pressure fluctuation amplitude reaches 113 dB and then decreases as T_s increases. Full stabilisation at t = 400 s, and T_s overcomes 100 ^oC. At t = 480 s the cooling system ($T_w = 3$ ^oC) starts, T_s decreases abruptly and instability grows up to 110 dB at t = 800 s, while T_s arrives to 50 Â°C. N.B: $p_0 = 0.993$ bar and $T_{amb} = 20$ ^oC at all times - from Ref. [29].*

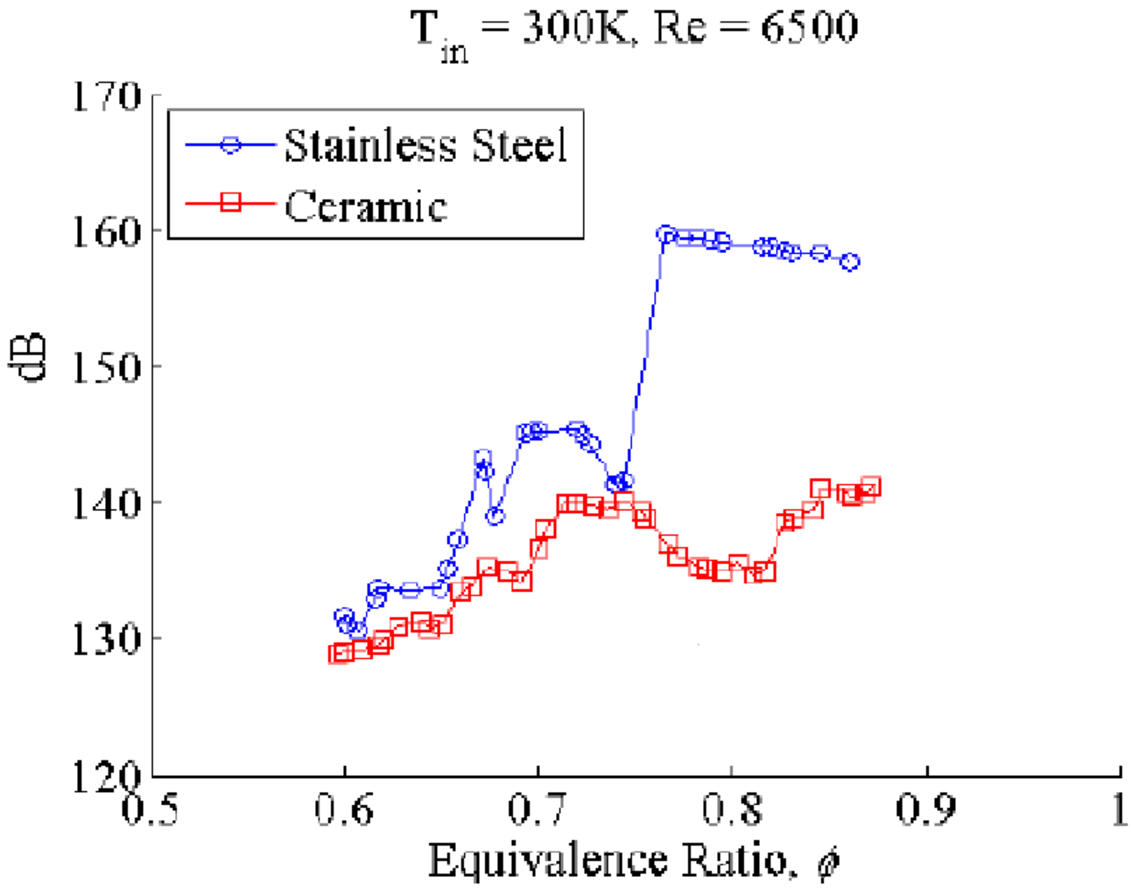

Figure 9.10: *Overall sound pressure level (dB) vs. equivalence ratio, propane/air mixture, 5.2 m/s inlet velocity, 883 kPa working pressure, 110 g/s inlet mass flow. Flameholder in stainless steel (12 W/m/K thermal conductivity) vs. ceramics (1.06 W/m/K thermal conductivity). Entropy wave at 40 Hz, acoustic mode at 70 Hz (fundamental frequency). Variations in equivalence ratio at constant inlet velocity (up to 5%) lead to corresponding variations in heat release - from Ref. [30].*

Chapter 10

Le Châtelier's principle...

10.1 Generalities and examples

The experimental results quoted above seem to confirm that -for given upstream flow at least- the onset of humming depends on the heat flow from the flame towards the surrounding environment: i.e., a way to trigger (prevent) humming is to facilitate (obstruct) such heat flow. Firstly, we give a simple (even if qualitative) explanation of some of these results. Then, a more systematic approach follows.

We start from two facts: firstly, combustion drives humming (i.e., no humming occurs without combustion); secondly, both exothermic (combustion) and endothermic chemical reactions (e.g. dissociation of CO_2) occur inside a small mass element of the flame [1].

Now, we invoke Le Châtelier's principle of thermodynamics -which, according to Secs. 22 and 103 of Ref. [84], follows straightforwardly from the second principle of thermodynamics- and apply it to our small mass element. Le Châtelier's principle reads:

> *an external interaction which disturbs the equilibrium brings about processes in the body which tend to reduce the effects of this interaction*

Le Châtelier's principle is known by all chemists, and is extensively applied in the study of chemical reactions [2]. We have already seen Le Châtelier's principle in action above: when discussing equation (6.17), we have seen that that any perturbation which tries to raise entropy where it is already large gets damped.

[1] Even in the popular approximation of one-step, infinitely fast reaction it is possible to have reactions both the exothermic and the endothermic way, the former and the latter from the unburnt gases to the burnt ones and all the other way around respectively. Neglecting the endothermic way takes a further approximation, namely *irreversible combustion* [4].

[2] It is often intuitively justified using a very simple argument: if the opposite of Le Châtelier's principle held, then equilibrium states would not be stable with respect to small fluctuations and thus they would not be observable.

Admittedly, we should not take the relevance of Le Châtelier's principle to the problem of humming for granted. Indeed, researchers have invoked the the so-called *local thermodynamic equilibrium* (LTE) either explicitly [90] or implicitly [8]. LTE means that -although the total system is not at equilibrium- the internal energy per unit mass u is the same function of the entropy s per unit mass, the pressure p, the mass density ρ, etc. as in real equilibrium; more generally, the relationships among thermodynamic quantities will be the same as in real equilibrium [94]. It is LTE which allows us to invoke the second principle of thermodynamics in any small mass element of fluid at all times, and it is the second principle -applied to the small mass element- which allows us to invoke Le Châteliers' principle to the small mass element.

We recall that *thermodynamic equilibrium* means that both chemical, mechanical and thermal equilibrium are fulfilled simultaneously [3]. Admittedly, not all chemical reactions inside the flame can actually be described with the help of LTE. In thermodynamical jargon, this is to say that chemical equilibrium is not fully realised inside the small mass element, even if mechanical and thermal equilibria are. Luckily, this fact is explicitly taken into account e.g. in the Appendix C of [22], so that it leaves the treatment of Myers' corollary unaffected.

Moreover, our LTE-based argument still seems to be valid at a rule-of-thumb level. In fact, chemical time-scales depend on the reactions of interest. In most practical combustion devices, fuel oxidation times are short. On the other hand, carbon monoxide (CO) oxidation to carbon dioxide (CO_2) is slower, and formation times of thermal nitrogen oxides (NO_x) are even longer -see Sec. 4.1 of [4]. Then, researchers concerned with detailed analysis of pollution invoke no LTE and focus their attention on chemical kinetics [4]. Analogously, the abundance of chemical species like CHO and the free electrons inside the flame rule the electric conductivity σ of the flame, so that researchers concerned with σ rely also on chemical kinetics -see the Appendix on the electrical conductivity of the flame. In all cases, however, the abundance of CO, CO_2, NO_x, CHO and free electrons is currently no larger than some parts per million. In our investigation of Rayleigh's criterion and Myers' corollary, the impact of such species on Rayleigh index and the acoustic flux $\mathbf{W}$ is therefore relatively small. Admittedly, terms like D_{Y_k} in Rayleigh's index could weaken the latter statewment; in the following, however, our results will not depend on the detailed structure of Rayleigh's index. Accordingly, we may neglect the mass fraction of those chemical species which undergo chemical reactions which in turn cannot be satis-

[3]By chemical, mechanical and thermal equilibrium we mean that no Y_k depends on time, that the sum of the external forces acting on the small mass element vanishes, and that the Boltzmann exponential rules the distribution function of the particles of each chemical species respectively

[4]For example, the simplest way to describe air-CH_4 combustion is

$$CH_4 + 2O_2 \longleftrightarrow CO_2 + 2H_2O$$

A more realistic -even if still oversimplified- description involves the couple of reactions

$$2CH_4 + 3O_2 \longleftrightarrow 2CO + 4H_2O$$

$$2CO + O_2 \longleftrightarrow 2CO_2$$

The second reaction is slow, and reliable estimate of CO_2 requires dedicated kinetic treatment.

factorily described with the equilibrium approximation, and we may safely assume LTE.

Le Châtelier's principle implies that any cooling -like e.g. the cooling due to thermal contact with a wall cooler than the flame- tends to enhance the relative importance of exothermic, humming-supporting reactions with respect to endothermic reactions, and therefore to facilitate humming. Analogously, any external heating of the flame tends to lower the relative importance of exothermic, humming-supporting reactions, and therefore to suppress humming [5]. Remarkably, on the basis of very general arguments it can be shown that a temperature increase induces a shift in the endothermic direction even outside the range of validity of LTE [97].

Now, the strategies outlined in [29] and [30] aimed at triggering the onset of humming by raising heat flow from the flame towards the combustor wall decrease also s_L while leaving the upstream flow unaffected. If the latter condition is satisfied, indeed, it can be shown that this heat loss is a decreasing function of s_L -see Fig. 10.1.

In-depth discussion is to be found in the following Sections [6].

Here we limit ourselves to stress the fact that even in the simplest model of combustion, the so called one-step, infinitely fast, combustion model [4] the laminar flame velocity is an increasing function of the combustion rate, i.e. of the number of combustion reactions occurring per second (only one chemical reaction is considered in this model). If the external world tries to raise s_L and if Le Châtelier's principle holds, then we expect the system to react in such a way to lower the reaction rate in order to compensate the external disturbance. Since it is combustion which supports humming, it is only reasonable to predict humming stabilisation. Of course, this is a qualitative discussion only: more refined treatmnet is required.

Remarkably, however, even outside the domain of humming-related research several authors show that the larger this heat loss, the lower s_L, the more likely the onset of either quenching [99] or thermo-diffusion instability (possibly coupled to Darrieus-Landau instability [100]) through increase of Le_{cr} [9]). For curved flames, investigation of equation (4.53) of [6] shows that raising or the decrease of both linear and non-linear stabilizing terms due to heat diffusion along the direction tangential to the flame surface.

[5] A common misunderstanding is lurking here. By raising the peak flame temperature, external heating fastens the kinetics of the chemical reactions which bring the small mass element of the fluid entering the flame to LTE. *Per se*, however, fastening of chemical kinetics and the relative weight of exothermic and endothermic reactions at LTE are independent of each other. For example, external heating in the Haber-Bosch synthesis of ammonia -an exothermic reaction- fastens the reaction but lowers the overall throughput. Here, Le Châtelier's principle makes the external heating to lower the the relative importance of exothermic reactions *only once* LTE is achieved. Luckily, a popular -even if oversimplifying- assumption is that combustion is infinitely fast [4], i.e. the snmall mass element achieves LTE as soon as it enters the flame, so that detailed chemical kinetics leaves the present discussion unaffected.

[6] Physically, leaving the upstream flow unaffected implies that also the speed of sound c_{s0} before the flame remains unchanged. In turn, this implies that the acoustic feedback in the electronic analogy of equations (6.38) (6.39) remains unaffected. The flows of heat and entropy quoted above refer exclusively to the flame.

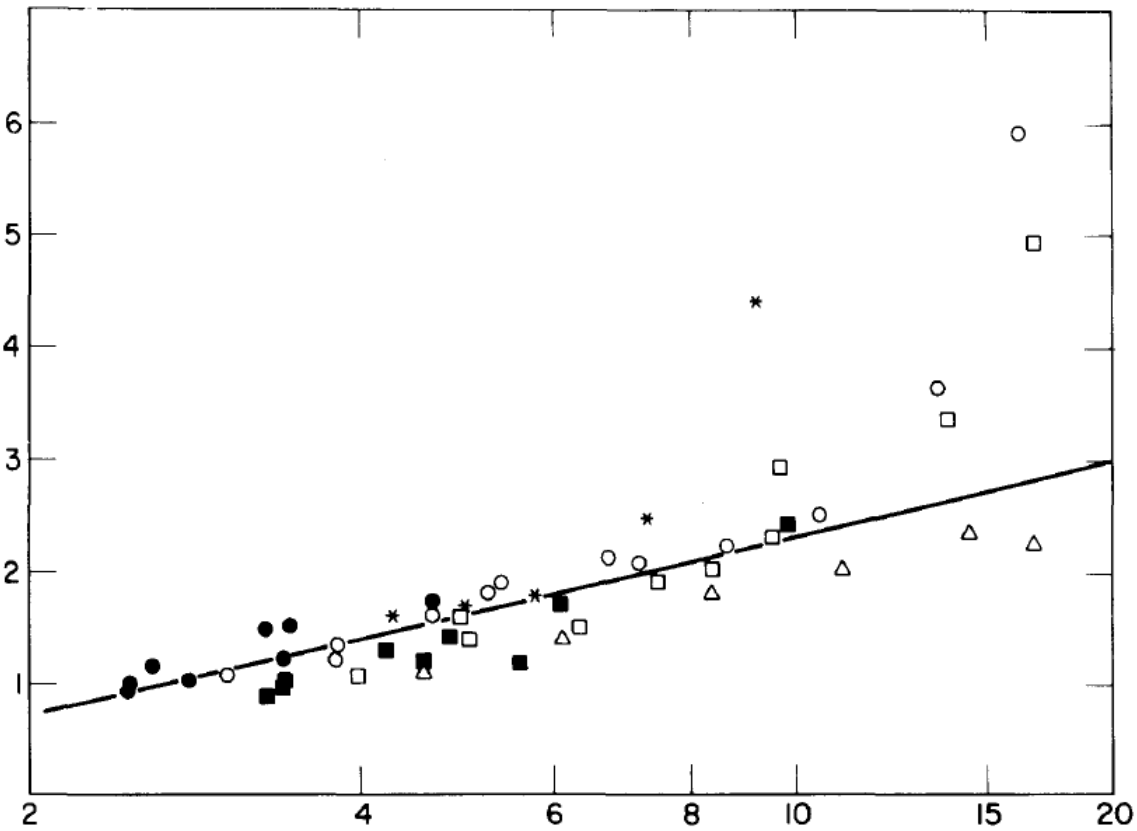

Figure 10.1: *From Ref. [98], an abridged version of Fig. 8. Normalised laminar flame velocity (y-axis) vs. ratio of the heat of combustion to the heat loss. If we lower the heat loss we raise this ratio, and s_L increases monotonically, i.e. s_L is a monotonically decreasing function of the heat loss.*

As a further example of external heating of the flame which is beneficial to humming control, we may refer to *nanosecond repetitively pulsed plasma discharges* (NRPP). NRPP stabilise a lean premixed propane-air flame at atmospheric pressure under lean conditions where it would not exist without plasma [101]; a similar result holds for laminar, premixed, lean methane-air flame [102]. Moreover, when humming occurs in a swirl-stabilized combustor at atmospheric pressure fueled with natural gas at an equivalence ratio of 0.66 and 43 kW heat release, suitably tuned NRPP with 315 W time-averaged electric power consumption induce a ten-fold decrease of pressure oscillation amplitude [103].

10.2 Beating around the bush?

Now, we may wonder if this discussion is actually relevant to flames in industrial GT combustors, or at least in any experimental set-up which resembles industrial ones more closely. Indeed, the experiments reviewed so far have little in common with real-life combustors of GT -from a manifacturer's point of view at least. For example, the lean, low-Mach combustion in GT combustors occurs very near to the blow-out point, and therefore not far from the stability line where small perturbations may produce very large responses. In this Section we are going to provide some arguments which confirm the relevance of our discussion focussed on thermodynamics to ndustrial GT combustors.

To start with, we have not yet discussed turbulence, by and large ubiquitous in GT combustors. Indeed, we expect most of our arguments still to hold -qualitatively at least- as far as the turbulent flame velocity $s_T = s_T(s_L)$ is an increasing function of s_L [4]. In particular, both Rayleigh's criterion and Myers' corollary rely on no detailed model of turbulence for the disturbances $a - < a >$ of the generic quantity a.

Generally speaking, moreover, leaner flames have lower values of flame velocity and are more prone to humming than fuel-richer flames, while the actual value of fuel mass fraction is so small that it affects upstream flow only weakly [104]. In particular, the simple model discussed in [3] for Ansaldo combustors predicts onset of humming whenever the Mach number M of the upstream unperturbed flow exceeds a threshold: the leaner the combustion, the lower the threshold, the easier the onset of humming.

All the way around, indeed, the inlet mixture temperature T_{inlet} is $\propto M^2$ all other quantities (including inlet mass flow, equivalence ratio and pressure) being equal [7]. In this case, it has been observed that even a slight increase of T_{inlet} triggers transition from stable to unstable flame in a lean-premixed swirl-stabilised combustor [105]. Physically, raising T_{inlet} implies raising the speed of sound in the region between the inlet and the flame, so that the acoustic feedback in (6.38) - (6.39) becomes more sensitive and humming gets facilitated [8].

[7] Since $M = \frac{|\mathbf{v}_0|}{c_s}$, $c_s \propto \sqrt{T_{inlet}}$ and $|\mathbf{v}_0| \propto$ (inlet mass flow) $\cdot$ (typical combustor cross section)$^{-1} \cdot \rho^{-1}$, equation (6.4) gives: $M \propto \sqrt{T_{inlet}} \cdot p^{-1}$, i.e. $T_{inlet} \propto p \cdot M^2$ at given inlet mass flow and combustor geometry.

[8] Admittedly, raising the upstream temperature $\approx T_{inlet}$ facilitates the onset of humming while *raising*

Furthermore, the region in which a swirled combustor exhibits thermo-acoustic instabilities is shifted to a lower equivalence ratio when adding a small amount of H_2 to a methane-air premixed flame [106]. Indeed, given the higher value of s_L in hydrogen-air combustion [9] such addition is likely to raise s_L: this conclusion is confirmed by the results of [107]. Remarkably, the opposite turns out to be true if water is added (e.g. in form of steam) to the inlet mixture impinging on the flame: the addition of steam notably decreases the flame velocity in both methane-air [107] and air-natural gas [108] premixed combustion.

Actually, most of the above remarks seem to find confirmation in everyday's working experience. Indeed, it is well-known that the weather affects the overall performance of a GT power plant. For instance, the hotter the external air, the larger the humming amplitude. This is in qualitative agreement with our remark about inlet temperature above. Moreover, given the temperature of the external air, the larger the air humidity the larger the humming amplitude -see Fig. 10.2.

Indeed, the larger the air humidity at the inlet (i.e. the larger the number and the mass of water droplets suspended in the air), the larger the amount of heat spent per unit time by the flame for water evaporation. But evaporation is an endothermic reaction: then, according to Le Châtelier the system tends to enhance the relative importance of exothermic, humming-supporting reactions with respect to endothermic reactions, and therefore to facilitate humming. Furthermore, addition of a tiny amount of water lowers the flame velocity as noted above, while leaving the upstream flow basically unaffected.

Our conclusion seems to be rather counter-intuitive: after all, if we pour enough water onto a flame (either a diffusion candle flame or a premixed Bunsen flame) we extinguish it altogether, thus suppressing all combustion-driven humming oscillation. Indeed, it has been reported that increased ambient humidity may *decrease* combustor acoustic oscillations -see Sec. 7.3.5 of [109]. This effect was attributed to the additional heat capacity of the water molecules which lowers the peak flame temperature and thereby reduces the reaction rate. The solution of the conundrum seems to be as follows. If we pour water onto a flame, then the heat release decreases, in agreement with the reduction of the reaction rate. In contrast, during the usual operation of a GT combustor the heat release is to be kept as near as possible to the rated value W_c sold to the final customer. Accordingly, the larger the ambient humidity the larger the required amount of heat produced by combustion in order to compensate the larger evaporation of water droplets while maintaining the net heat release, the larger the relative importance of exothermic, humming-supporting reactions.

Similar results hold for the ambient air temperature. We have seen that the hotter the external air, the larger the humming amplitude in a GT combustor *at fixed heat release.* In sharp contrast, the same Ref. [109] quoted above hints at a beneficial effect

the flame velocity [2]. Note, however, that in this case the upstream flow is *not* unchanged, and our previous remarks concerning the flame velocity do not apply.

[9] up to 5 time larger than in air-methane combustion, see Tab. 8.2 of [2].

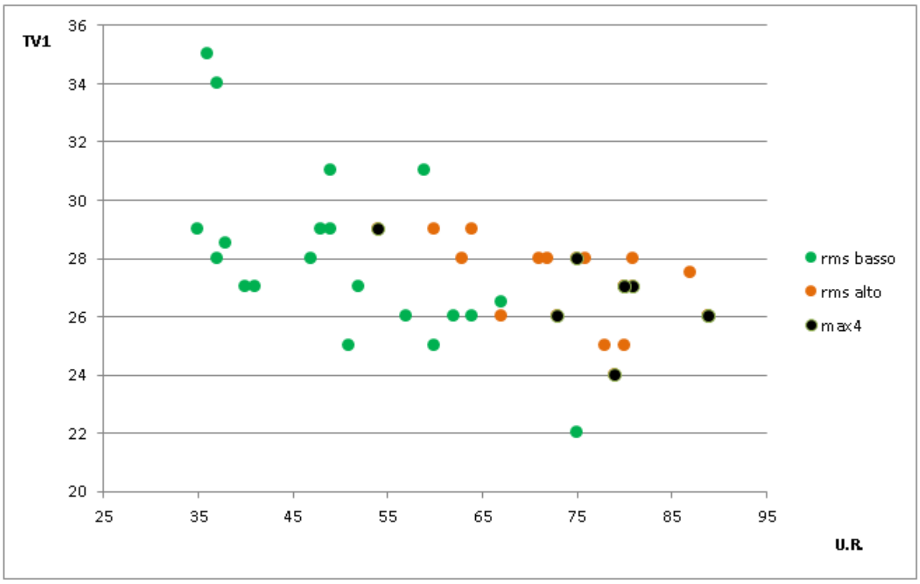

Figure 10.2: *On-field data from Ansaldo Energia. Three series of pressure r.m.s. measurements at different values of relative humidity (x-axis) and environmental temperature (y-axis). Black dots refer to cases where automatic safety systems switch on. Red dots refer to cases with dangerous pressure r.m.s. with no automatic switch-on. Other dots refer to non-dangerous cases.*

of an increase of ambient air temperature in suppressing noise. Indeed, such increase is likely to raise the flame velocity, as the latter is an increasing function of the upstream temperature [2], which in turn is an increasing function of the ambient air temperature. Thus, the impact of increasing ambient air temperature may compensate the s_L-lowering, destabilising impact of both wall cooling [29] and heat conduction across the flameholder [30], i.e. it may be stabilising, precisely as observed with [109]; but then the heat release -which depends also on s_L [35]- is not kept at a constant value, unlike the GT combustor quoted above. Again, the behaviour at fixed heat release differs from the behaviour when the heat release is not fixed.

10.3 Dynamics vs. thermodynamics

As usual in thermodynamics, the discussion in the last Section shows that the choice of what is kept fixed and what may undergo changes is of paramount importance to the solution of a given problem. We are going to show that this fact leads us to uncover a fundamental agreement between Rayleigh's criterion and its generalisation, Myer's corollary, on one side and Le Châtelier's principle and its consequences on the other side.

According to equation (33) of [75] -or, equivalently, to equation (1) of [58]- the heat release produced in a premixed combustor where all the fuel gets burnt at the flame (as it is usually assumed for practical purposes in lean combustion) and where the flame is laminar is equal to:

$$W_c = \int_{flame} d\mathrm{a} \left(H_{LHV} \cdot \rho_u \cdot Y_{fuel} \cdot s_L \right) \tag{10.1}$$

where H_{LHV}, ρ_u and Y_{fuel} are the lower heating value ($= 5 \cdot 10^7 J \cdot Kg^{-1}$ for methane) [10], the mass density and the fuel mass fraction on the upstream side of the flame respectively. Here H_{LHV} is a constant quantity. Given the upstream flow -hence both its mass density and its chemical composition - ρ_u and Y_{fuel}- if the heat relase too is fixed then the only way to raise the flame velocity is to lower the flame area. In turn, the flame area is just the ratio of flame volume and of the laminar flame thickness, and the latter is a decreasing function of s_L. It follows that any growth of flame velocity at given heat release and upstream flow corresponds to a reduction of the flame volume. But according to equation (6.22) the flame volume is just the domain of integration of the destabilising term $\int d\mathbf{x}D$ of Rayleigh's criterion -as well as of its generalisation, Myers' corollary. Now, the integrand in this term is positive (on average), as this term has to compensate the net, stabilising acoustic losses which are positive (sound is actually heard when humming occurs). Thus, reduction of flame volume leads to reduction of the destabilising term in

[10]The *lower heating value* is obtained by subtracting the heat of vaporization of the water vapor from the higher heating value. The *higher heating value* is the amount of energy released as heat by complete combustion; it is determined by bringing all the products of combustion back to the original pre-combustion temperature, and in particular condensing any vapor produced.

Rayleigh's criterion, hence is stabilising. This explains why raising the flame velocity at given upstream flow and heat release is beneficial to humming stabilisation, no matter how this growth is obtained -by preventing wall cooling, adding hydrogen of utilising less humid mixtures of unburnt gases [11]. Remarkably, the conclusions drawn from Rayleigh's criterion and Myers' corollary on one side nicely agree with the conclusions drawn from Le Châtelier's principle. This correspondence will be investigated further in the next Chapters.

Noteworthy, the price to be paid for a change in flame velocity is a change the flame shape too. In fact, flame shape and flame velocity are not independent from each other -see (13.21) below. This is why Rayleigh's criterion and Myers' corollary provide information on the shape of stable flames, even if in implicit form. An obvious corollary is that some flames are more stable than other, according on their shapes. Investigation on the shape of stable flames is the topic of one of the Chapters below.

Equation (10.1) holds for laminar flames; see equation (6.26) of Ref. [110] and Sec. 4.2 of Ref. [18] for the counterpart in turbulent flames -like those occurring in GT. Generalisation of (10.1) to turbulent flames relies on replacing s_L with s_T - see e.g. equation (2) of [111]. In particular, the flame surface area is expressed with the help of a suitably averaged flame surface density [4] and s_T replaces s_L, bot nothing changes as far as s_T is a monotonic function of s_L. Above all, it is still possible -for dimensional reasons at least- to write the ratio of flame volume and flame area as a flame thickness, which appears to depend on s_L only weakly -see equation (8) of [112]; it appears rather to depend on the typical turbulent length scales. Consequently, turbulence leaves our discussion unchanged, provided at least that the s_L-raising mechanisms leave the turbulent fluctuation spectrum unaffected.

This discussion relies on the concept of flame thickness. Unfortunately, different flame models may provide us with different estimates of this quantity, and even different definitions: the validity of our qualitative discussion is therefore somehow weakened. A more rigorous treatment is therefore desirable, which involves no detailed information concerning flame thickness. To this purpose, we take advantage of Rayleigh's criterion and Myers' corollary and present a discussion of the impact of flame velocity on humming for both laminar and turbulent, thin, premixed flames in the Appendix concerning the flame velocity. In this discussion it is also assumed that the flame is *globally concave*, i.e. that a suitably weighted average of the total curvature of the flame is positive. To put it in other words, the flame is supposed to show its concave side to the unburnt gases for most of its surface. Most flames of practical interest in Ansaldo combustors satisfy this requirement. This discussion confirms that raising flame velocity at given upstream flow is beneficial to humming stabilisation for both laminar and turbulent flames.

The main idea underlying this result is that everything oscillates periodically with period τ when humming occurs, including the flame area A_f -see Fig. 10.3 for an example

[11] Of course, making combustion slightly richer raises Y_{fuel}, and, in lean combustion, also s_L, even at a price of higher pollution

in a swirl-stabilised combustor. Now, for a sinusoidal [12] function of time $A_f = A_f(t) = A_f(t+\tau)$ with given period τ, the steeper the slope of $A_f = A_f(t)$ at a given time, the larger the maximum amplitude of $A_f(t)$ over a period. In turn, the larger the latter amplitude, the larger the absolute value of the destabiling term in of (6.36) [13], because the integration domain of this L.H.S. reduces basically to A_f for thin flames as Rayleigh's index is localised at the flame at all times. All the way around, it follows that everything which flattens the slope of $A_f = A_f(t)$ reduces the absolute value of the L.H.S. of (6.36), and is therefore stabilising. For globally convex, laminar flames, it turns out that raising s_L at given upstream flow leads to such flattening -see the Appendix concerning the flame velocity. If τ is large enough (say, $\tau >$ the longest time-scale typical of turbulent motions), then we may safely apply this discussion to turbulent flames too, as the time-scales of turbulence and of humming are decoupled [14].

Remarkably, this conclusion leads to predictions of practical interest whenever the requirement that s_T and s_L behave differently under the same perturbation of the system. For example, it is well known that in the premixed lean combustion of hydrocarbons s_T and s_L are an increasing and a decreasing function of pressure respectively -see e.g. Sec. 3.3.5 of Ref. [113]. If we are able to decrease pressure while leaving all other things unaffected, then we raise s_L and lower s_T, thus stabilising laminar flames but destabilising turbulent flames with the same heat release, stoichiometry etc. Indeed, the model of [3] -originally thought for industrial combustors with turbulent flames- predicts precisely humming onset when the Mach number -which scales as $\propto \dfrac{\sqrt{T}}{p}$ for given input mass flow- exceeds a stoichiometry-dependent threshold, i.e. it predicts that the smaller the pressure the easier the humming onset -all the rest being equal.

In the following Sections, we are going to invoke the constraint of fixed heat release W_c again and again, as this constraint is a requirement for everyday's operation of commercial GT combustors.

We suggest that dynamics and thermodynamics (i.e. Rayleigh's criterion and Myers' corollary on one side, Le Châtelier's principle on the other side, respectively) agree in predicting that raising the flame velocity at given upstream flow is beneficial to humming control. Even if in agreement with many observations, this fact has not been adequately stressed in present humming-related research. The latter focussed rather on the relative phases of the perturbations inside the Rayleigh's index, i.e. on the integrand of the destabilising term in (6.35). Our analysis of Rayleigh's criterion and Myers' corollary hints rather at the role played by the evolution of flame area when humming occurs, i.e. the

[12]If $A_f(t)$ is no sinusoidal function, we write it as a Fourier series and limit our attention to any of its sinusoidal or cosinusoidal components, with no loss of generality.

[13]The integrand of this L.H.S. is positive whenever perturbed quantities oscillate in phase, as required by Rayleigh's criterion when humming occurs. Then, this L.H.S. is an increasing function of the measure of its domain of integration. The larger the fluctuation of A_f, the larger its contribution to the time-average of the L.H.S., which is precisely the destabilising term (6.36).

[14]More generally speaking, application of thermodynamics to turbulent flames is far from surprising, as we expect turbulence to leave validity of LTE unaffected as far as the time-scale of microscopic interparticle collisions responsible for LTE are much shorter than turbulent time-scales.

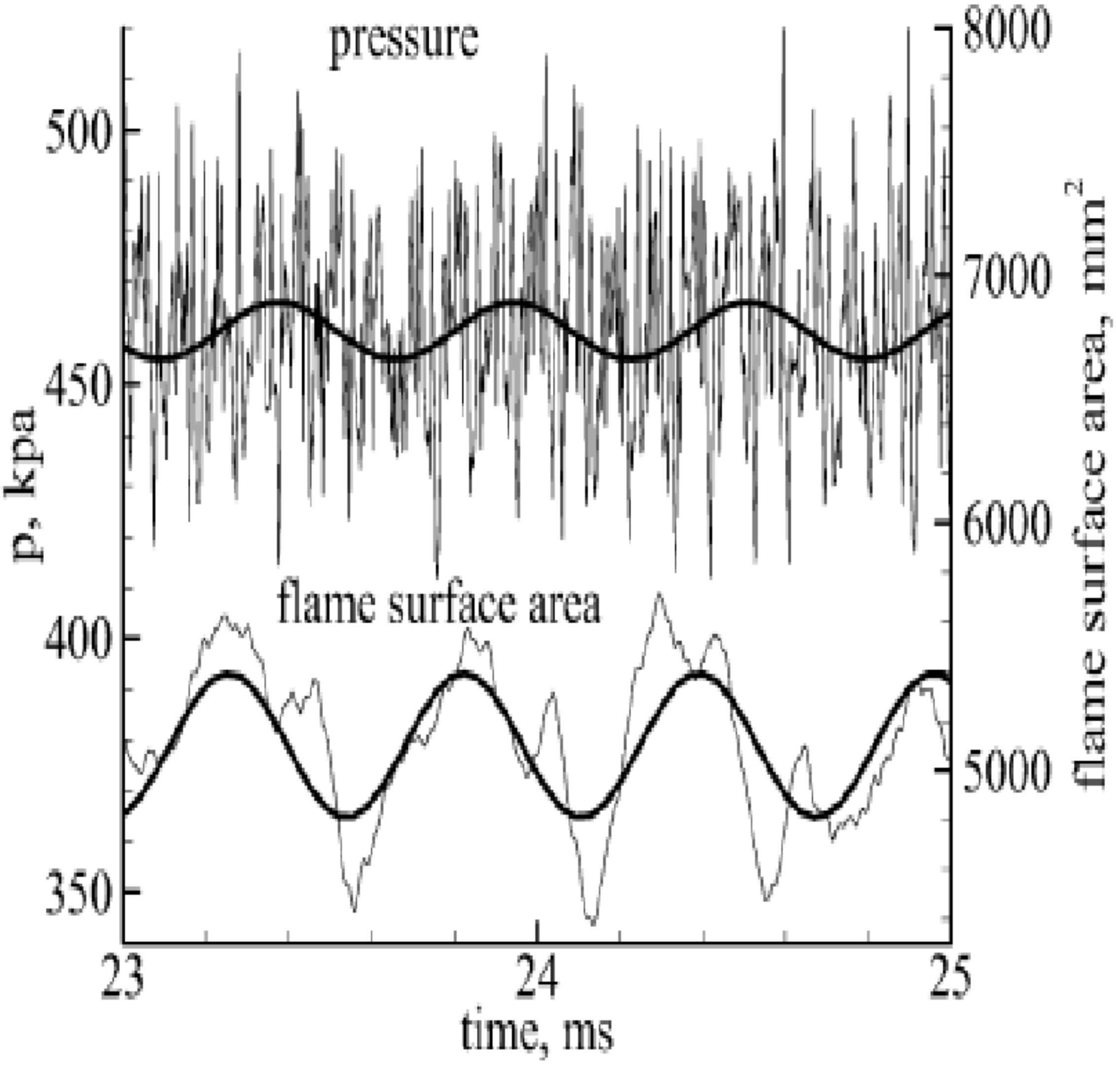

Figure 10.3: *Time histories of pressure (top) and A_f (bottom). Thick black line represent the computed contribution of the acoustic fundamental mode - from Ref. [18].*

domain of integration of the destabilising term in (6.36). This evolution affects the outcome of the time average, and is affected by the flame velocity [15].

Finally, it must be stressed that the above discussed connection between flame velocity and heat losses is no more necessarily valid if the upstream flow is not constant, e.g. when a major transition between largely different upstream flows occurs [114] [15].

[15]A simple argument shows that stability against humming is not just a matter of relative phases. Suppose humming occurs in the case described by the isentropic version of Rayleigh's principle: then, fluctuations of pressure and heat release are in phase. Accordingly, *any* modification of this relative phase should hinder humming, no matter if corresponding e.g. to increasing or decreasing fuel content. However, experience teaches us that decreasing fuel content is destabilising, in contrast with increasing fuel content. This can be explained when looking at the flame velocity, not at relative phases.

Chapter 11

... and its consequences

11.1 Generalities

In the following we are going to discuss the connections of the second principle of thermodynamics applied to a small mass element of our fluid mixture -and of its consequence, Le Châtelier's principle- with Rayleigh's criterion and the experimental results discussed in the last Section. In particular, we are going to take advantage of the results of [115] and of [116] in order:

- to derive from Le Châtelier's principle an inequality (the *general evolution criterion*) concerning the time derivatives of thermodynamic quantities in a small mass element of a fluid mixture of reacting species at LTE at all times
- to derive from the general evolution criterion three useful inequalities concerning quantites related to the entropy balance of a whole, macroscopic system
- to derive from these three inequalities a set of necessary criteria for the stability of unperturbed, steady states. These criteria include Rayleigh's criterion as a particular state. Other criteria, even if fully equivalent to Rayleigh's criterion from the point of view of their physical meaning, take the form of a variational principle.
- to generalise the result to the stability of unsteady unperturbed states. In analogy with what happens with Rayleigh's criterion and Myers' corollary, it turns out that the stability criteria for unsteady unperturbed states are formally identical to the stability criteria for steady unperturbed states, after suitable time-averaging.

As usual, we assume no net mass source, so that equation (5.1) still holds. We are going to follow the same logical path which has led us from the original version of Rayleigh's criterion to Myers' corollary, i.e. we start with the case where the unperturbed fluid is at rest and then we deal with the general case of the unperturbed fluid in motion.

11.2 The general evolution criterion

Let us describe the small mass element with the help of the thermodynamical quantities ρ, p and Y_k. Together, the well-known property of minimum Gibbs' free energy at constant

p and T (itself too a consequence of second principle) and Le Châtelier's principle lead to the following three thermodynamical inequalities involving these quantities - see [84] and Sec. XV, 5, 12 of [117]:

$$\left(\frac{\partial u}{\partial T}\right)_{\rho,n} \geq 0 \qquad \left(\frac{\partial \rho^{-1}}{\partial p}\right)_{T,n} \leq 0 \qquad \sum_{i,j}^{n} \left(\frac{\partial g_j}{\partial Y_i}\right)_{p,T} dY_i dY_i \geq 0 \tag{11.1}$$

where $i, j = 1 \ldots n$ and $()_n$ means that all Y_k's are kept fixed. Remarkably, thermodynamical inequalities(11.1) hold regardless of the detailed equation of state, of the detailed model of turbulence etc. They provide constraints on all physically acceptable deviations from thermal, mechanical and chemical equilibrium respectively.

Together, (5.4) and (11.1) lead to the so-called *general evolution criterion* [115] [116]:

$$\frac{dT^{-1}}{dt}\frac{d(\rho u)}{dt} \leq \rho \sum_i \frac{d(g_i T^{-1})}{dt}\frac{dY_i}{dt} + \left(\rho^{-1}T^{-1}\frac{dp}{dt} + h\frac{dT^{-1}}{dt}\right)\left(\frac{d\rho}{dt}\right) \tag{11.2}$$

where we write $da = \frac{da}{dt}dt$ for the generic quantity a. Inequality (11.2) is a tenet of non-equilibrium thermodynamics [94]. Even if formally trivial, the latter identity endows (11.2) with a deep physical meaning. We recall that, by definition, $\frac{d}{dt} = \frac{\partial}{\partial t} + \mathbf{v} \cdot \nabla$ where $\mathbf{v}$ is the velocity, a solution of the equations of motion which describe the trajectory of a small mass element: i.e. $\mathbf{v}$ it is a dynamical quantity. In contrast, a may be a *thermodynamical* quantity, like e.g. temperature. Formally, replacement of $da = \frac{da}{dt}dt$ in the thermodynamical inequalities leads to (11.2) ; physically, it means that these inequalities keep on being valid as the small mass element follows its trajectory according to the laws of dynamics. To put it in other words, we take for gfanted that if LTE holds within a small mass element followed along its center-of-mass-motion with velocity $\mathbf{v}$, then all relationships among total differentials of thermodynamic quantities remain valid, with the proviso that $da = \frac{da}{dt}dt$. All the way around, (11.2) is a far-from-trivial constraint to be satisfied in order that the small mass element behaves according to the second principle of thermodynamics during its trip across the system.

11.3 Three useful inequalities

Physically, relationships (5.1), (5.5) and (11.2) correspond to the balance of mass, to the first principle and to the second principle of thermodynamics respectively in a small mass element of the fluid mixture. It is possible to obtain a corresponding triplet of inequalities for a whole macroscopic system with volume $V = \int d\mathbf{x}$, total internal energy $U = \int d\mathbf{x}\rho u$ and total entropy $S = \int d\mathbf{x}\rho s$, where we allow both V, U and S to depend on time. To this purpose, we invoke the identity (*Reynolds' transport theorem*)

$$\frac{d}{dt}\int_{\Omega} d\mathbf{x} a = \int_{\Omega} d\mathbf{x}\left(\frac{\partial a}{\partial t} + \nabla\cdot(a\mathbf{u})\right)$$

- see equation (II.4.116) of [118] - for an arbitrary quantity a and a domain of integration Ω with moving boundary, where a point on the boundary moves locally at speed $\mathbf{u}$.

Moreover, it will be helpful to define in the following the quantities

$$P_h \equiv Q + \Phi \qquad P \equiv P_h - \nabla\cdot\mathbf{q}$$

The quantity P_h is just the sum of combustion and viscous power (the pedix h is for *heating*), while equation (5.5) gives $P = \rho T\frac{ds}{dt} + \rho\sum_{k=1}^{n} g_k\frac{dY_k}{dt} = \rho\frac{du}{dt} + p\rho\frac{d}{dt}\left(\frac{1}{\rho}\right)$.

Furthermore, we neglect the contribution $\propto \frac{dY_k}{dt}$ of particle diffusion (as customary in most researches on combustion [4]), so that

$$P = \rho T\frac{ds}{dt}$$

Physically, P reduces therefore to the net amount of heat delivered per unit time and volume to the small mass element, which is heated by combustion and viscous power and cooled by radiation and heat conduction. (Here we stress the point that the quantity $\mathbf{q}$ in the definition of P is a local quantity, and therefore P includes no convective transport; convection -if any- is due to flow patterns on a spatial scale $>>$ the spatial scale of a small mass element).

Moreover, we assume that an unperturbed state exists and write both $a = a_0(\mathbf{x}) + a_1(\mathbf{x}, t)$ for the generic quantity a and $P_0 = 0$.

The first relationship will allow us to retrieve Rayleigh's criterion. Admittedly, it contradicts Galileian invariance. Moreover, we have seen that Rayleigh's criterion in its original form takes into account no motion of the unperturbed flow; then, it is only self-consistent that the heat produced in the unperturbed state per unit time is removed by conduction and radiation only (as $P_0 = 0$).

All the same, suitable redefinition of the unperturbed steady state as an unperturbed time-averaged state will allow us to overcome this difficulty: after all, our discussion of Myers' corollary has shown that the necessary criterion of stability sounds the same way in both cases. In particular, once a criterion for the stability of an unperturbed state $a_0 = a_0(\mathbf{x}, t)$ has been established, it holds also for the stability of unperturbed fluid in motion as we are free to identify a_0 as the unperturbed position of moving small mass element of fluid, provided that each quantity is replaces by a time-average on a suitably chosen time-scale τ and that the time derivative of this quantity refers to its evolution on time-scales much longer than τ.

Finally, physical intuition -in agreement with Le Châtelier's principle- suggests that a state where an increase of T induces a decrease in energy losses is a bad candidate for stability, as any decrease in energy losses is likely to induce further increase of T. Analogous arguments hold for cooling processes [1].

Accordingly, we assume

$$\int d\mathbf{x}\,(\nabla\cdot\mathbf{q}_1)\left[\frac{d}{dt}\left(\frac{1}{T}\right)\right]\leq 0 \tag{11.3}$$

Under the assumptions listed above, (5.1), (5.5), (11.2) and (11.3) lead to the following three inequalities:

$$\frac{d}{dt}\int d\mathbf{x}\frac{P_h}{T}\leq c_1\frac{dV}{dt}+c_2\int d\mathbf{x}P_h \tag{11.4}$$

$$-\frac{d}{dt}\int d\mathbf{x}\left[\nabla\cdot(\rho s\mathbf{v})+\mathbf{q}\cdot\nabla\left(\frac{1}{T}\right)\right]\leq c_1\frac{dV}{dt}+c_2\int d\mathbf{x}P_h \tag{11.5}$$

$$\frac{d}{dt}\int d\mathbf{x}\frac{P}{T}\leq c_3\frac{d^2V}{dt^2}+c_4\frac{d^2U}{dt^2} \tag{11.6}$$

after volume integration on the system. For details, see the proof of the equations (3.1), (3.2) and (B.8) in [116]. Here c_1, c_2, c_3 and c_4 are constant quantities.

Physically, the quantities $\int d\mathbf{x}P_h$, $\int d\mathbf{x}\frac{P_h}{T}$ and $\int d\mathbf{x}\frac{P}{T}$ are equal to the total heating power, the total amount of entropy produced per unit time by heating (combustion +

[1] When it comes to the description of stable oscillations, Rayleigh's words are helpful again [31]:

> [...] *the heat received at this moment* (of normal density) *has no effect either in encouraging or discouraging the vibration. The same would be true of the entire operation of the heat, if the adjustment of temperature wore instantaneous, so that there was never any sensible difference between the temperatures of the air and of the neighbouring parts of the tube. But in fact the adjustment of temperature takes time, and thus the temperature of the air deviates from that of the neighbouring parts of the tube, inclining towards the temperature of that part of the tube from which the air has just come. From this it follows that at the phase of greatest condensation heat is received by the air and at the phase of greatest rarefaction is given up from it, and thus there is a tendency to maintain the vibrations*

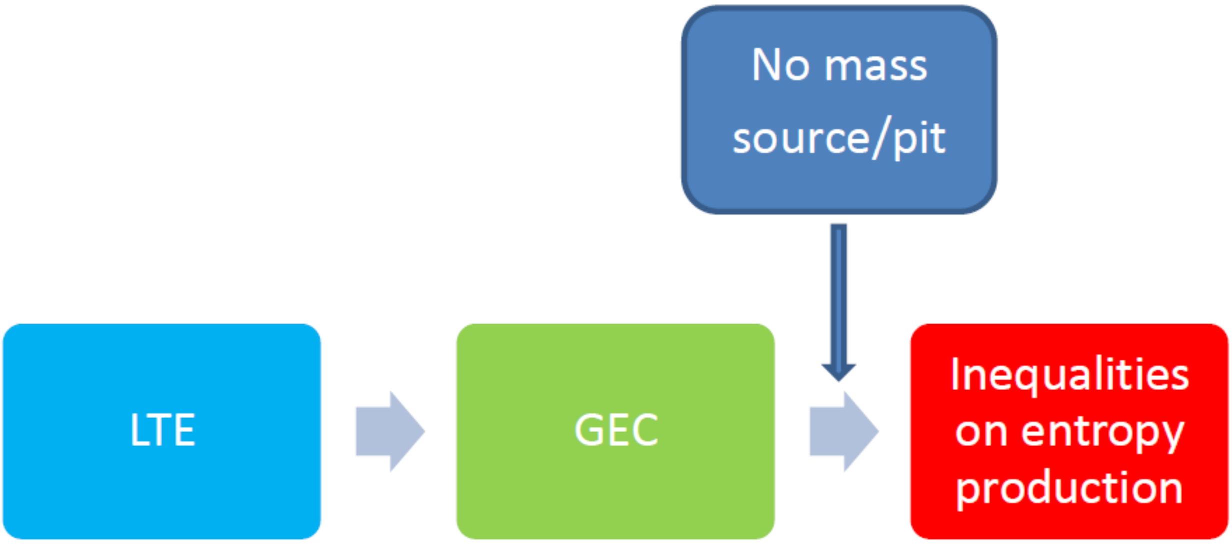

Figure 11.1: *From LTE to the inequalities concerning entropy production. See text for details.*

viscous) processes and the total time derivative $\frac{dS}{dt}$ of total entropy S respectively (the latter identity follows from both $P = \rho T \frac{ds}{dt}$, (5.1) and repeated application of Reynolds' transport theorem). The consequences of (11.4), (11.5) and (11.6) have been discussed in some detail in [116]. These inequalities are of purely thermodynamical origin and invoke no detailed model of the physical processes ruling heat production and transport. Just like the second principle of thermodynamics (in the form of Le Châtelier's principle) holds within any arbitrary smallmass element within the fluid mixture at all times, (11.4), (11.5) and (11.6) hold for the system as a whole at all times: they are constraints imposed on the evolution of the system by the second principle, and carry no further physical meaning than the original thermodynamical inequalities quoted at the beginning of this Section. For the line of reasoning leaing to these inequalities, see Fig. 11.1.

In the following, we are going to discuss the relevance of these inequalities to humming.

11.4 Variational principles and selection rules

11.4.1 Steady unperturbed state

Here we discuss (11.4) and (11.5) together as they spare the same R.H.S. and hold simultaneously. According to (11.4) and (11.5), a necessary condition for the stability of the unperturbed state is that the latter satisfies the following variational principles (we skip the subscript 0 below, unless otherwise stated):

$$\int d\mathbf{x}\frac{P_h}{T} = \min \qquad \text{with fixed} \quad V \quad \text{and} \quad \int d\mathbf{x}P_h \tag{11.7}$$

$$\int d\mathbf{x}\left[\nabla\cdot(\rho s\mathbf{v}) + \mathbf{q}\cdot\nabla\left(\frac{1}{T}\right)\right] = \max \qquad \text{with fixed} \quad V \quad \text{and} \quad \int d\mathbf{x}P_h \tag{11.8}$$

In fact, if the unperturbed state violates (11.7) , then (11.4) forbids stability against perturbations which conserve both V and $\int d\mathbf{x}P_h$ but lower $\int d\mathbf{x}\frac{P_h}{T}$. Similar arguments hold for (11.5) and (11.8). Of course, there is no warranty alytogether that our system actually relaxes to a stable state. But *if it does*, then Le Châtelier forces the stable state to satisfy both (11.7) and (11.8).

Remarkably, (11.7) has been applied to the description of a laminar flame by [119]. But in their work the utilization of (11.7) is justified because the authors choose to start from a particular, suitably chosen formula for the entropy produced per unit time and volume inside the flame -see their equations (2.1) and (2.2). Indeed, this formula allows utilisation of the well-known linearised treatment of non-equilibrium thermodynamics developed in [90], which leads precisely to minimisation of entropy production for stable steady states provided that the total entropy production due to all irreversible processes (namely, combustion and heat conduction) is taken into account, not just the contribution of conduction as in (11.7). Unfortunately, however, the treatment of [90] relies on Onsager's symmetry relationships, which are scarcely relevant to fluids (for instance,validity of Onsager's relationships requires that the heat conductivity is uniform across the flame).

Admittedly, it is possible to follow the approach of [90] and to derive from minimization of total entropy production (due to both irreversible processes of combustion and heat conduction) the conservation equations of a one-dimensional,premixed, laminar flame [120]: but the price to be paid is the introduction of the flame velocity itself into the explicit espression of both the thermodynamic fluxes and the phenomenological coefficients (see equations. (2.23) and (2.33) of [120]), a price which casts further doubt on the validity of the underlying assumption of Onsager's symmetry. In contrast with [119] and [120], we are not going to attempt derivation of the full set of consrvation equations from the results of our discussion in thermodynamics. Rather, we shall limit ourselves to make use of the results of thermodynamics in order to check stability of the solutions of the conservation equations against perturbations. Accordingly, we need no Onsager's symmetry, we do not invoke the treatment of [90] and we rely on no assumption about heat conduction but (11.3).

11.4.2 Unsteady unperturbed state

To date, we have assumed that the unperturbed state does not depend on time. If we remove this assumption, then we may consider the unperturbed state as a time-average which removes the effect of any fast time-scale. In this case the time derivative of the generic quantity a (e.g. $a = \int d\mathbf{x} P_h$, $a = \int d\mathbf{x} \frac{P_h}{T}$ etc.) refers just to evolution on a slow time-scale. Formally, we may take the time-average of both sides of the relationships (11.4) and (11.5), invoke (7.1) and obtain

$$\frac{d}{dt}\langle \int d\mathbf{x} \frac{P_h}{T} \rangle \leq c_1 \frac{d\langle V \rangle}{dt} + c_2 \langle \int d\mathbf{x} P_h \rangle \tag{11.9}$$

$$-\frac{d}{dt}\langle \int d\mathbf{x} \left[\nabla \cdot (\rho s \mathbf{v}) + \mathbf{q} \cdot \nabla \left(\frac{1}{T} \right) \right] \rangle \leq c_1 \frac{d\langle V \rangle}{dt} + c_2 \langle \int d\mathbf{x} P_h \rangle \tag{11.10}$$

In strict analogy with the above results, we may derive from (11.9) and (11.10) the following necessary criteria of stability in the form of variational principles:

$$\langle \int d\mathbf{x} \frac{P_h}{T} \rangle = \min \qquad \text{with fixed} \quad \langle V \rangle \quad \text{and} \quad \langle \int d\mathbf{x} P_h \rangle \tag{11.11}$$

$$\langle \int d\mathbf{x} \left[\nabla \cdot (\rho s \mathbf{v}) + \mathbf{q} \cdot \nabla \left(\frac{1}{T} \right) \right] \rangle = \max \qquad \text{with fixed} \quad \langle V \rangle \quad \text{and} \quad \langle \int d\mathbf{x} P_h \rangle \tag{11.12}$$

Here (11.11) and (11.12) are the obvious generalisation of (11.7) and (11.8) respectively to the general case of an unperturbed state which depends on time. The formal similarity between the stability criteria with steady unperturbed state ((11.7) and (11.8) and unsteady unperturbed state ((11.11) and (11.12) recalls the similarity observed above between the stability criteria derived from Myers' corollary for steady and unsteady unperturbed state.

Before further discussion, we remark that both (11.11) and (11.12) take the form of selection rules. According e.g. to (11.11), between a steady, humming-free state and a state affected by humming oscillation with given period the system will select the configuration which minimizes the total, time-averaged amount of entropy produced per unit time by heating. (Such choice may occur e.g. when the system is near a bifurcation). This resembles the observations of [28]. The same holds if the choice is between different limit cycles, or, in contrast, two different steady states with different flame shapes.

Before applying our discussion to the investigation of the properties of humming-free premixed, flames, in the following we are going to show that the experimental results of [28], [29], [30] and [95] discussed above confirm our findings. Moreover, we are going to invoke the -insofar neglected- relationship (11.6) in order to retrieve Rayleigh's criterion as a particular case.

Finally, the thermodynamic nature of our results makes allows them to be valid outside the domain of combustion. To show this, we shall retrieve a stability criterion -due to Eddington in its original version- for the stability of a star against spontaneous oscillations due to bistability of its opaqueness to radiation: the basic mechanism of radial oscillations in Cepheid stars.

To start with, we observe that equation (5.1), the definition of $\frac{d}{dt}$ and the formulas for P and P_h allow us to write

$$\nabla \cdot (\rho s \mathbf{v}) = -\frac{\partial (\rho s)}{\partial t} + \frac{P_h}{T} - \frac{\nabla \cdot \mathbf{q}}{T}$$

Let us replace this relationship in the maximised quantity on the L.H.S. of (11.8) in a system with constant volume and constant total heating power. Many particular cases are possible. The next Section is concerned with the discussion of these particular cases.

For a summary of the necessary stability conditions for both steady and unsteady unperturbed states -as provided by thermodynamics- see Fig. 11.2 and Fig. 11.3. For the connection between stability criteria according to dynamics and to thermodynamics, see Fig. 11.4.

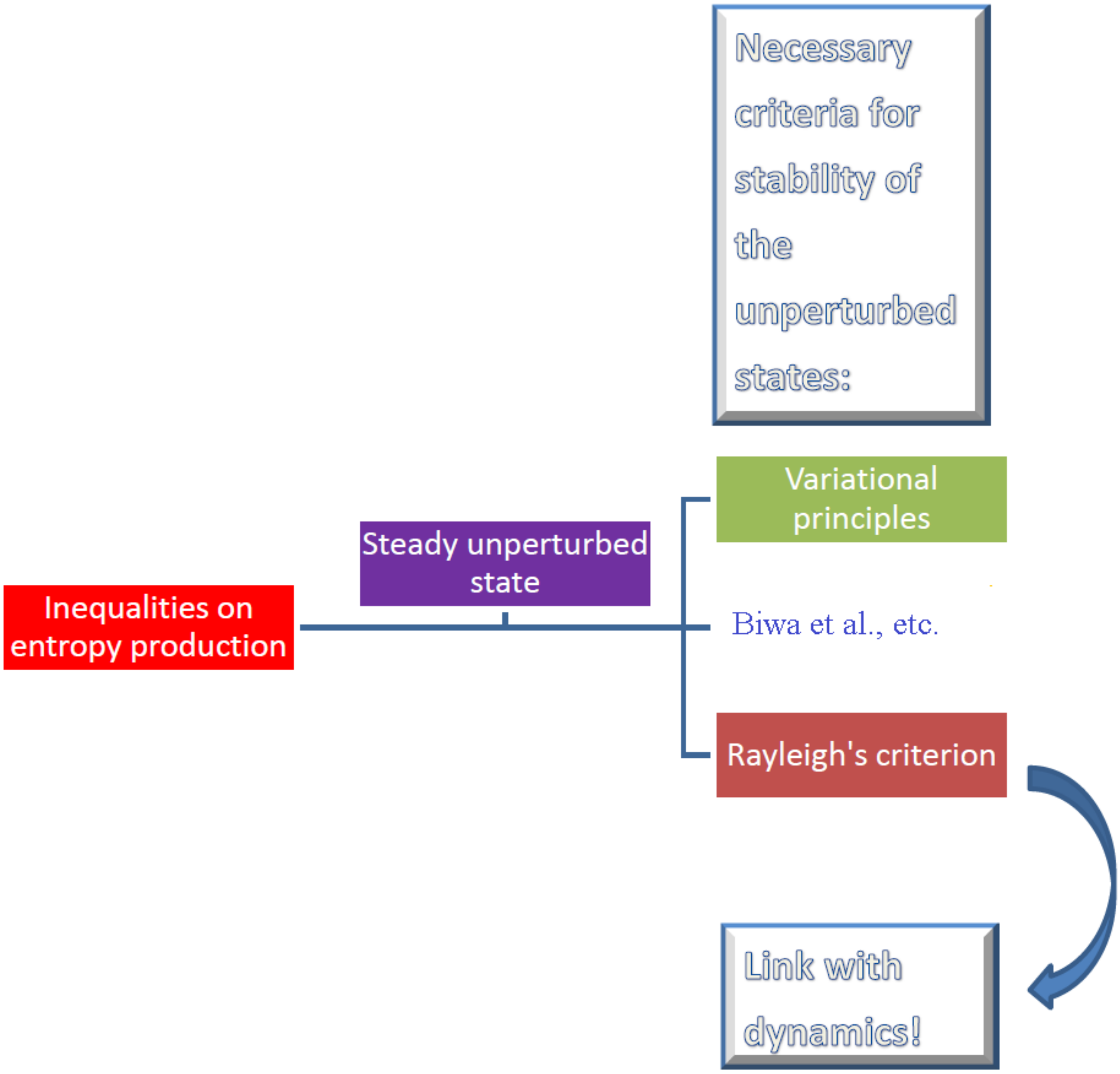

Figure 11.2: *Necessary stability conditions for steady unperturbed states, as provided by thermodynamics. The label* Biwa et al. *refers to the benchmarks discussed below. See text for details.*

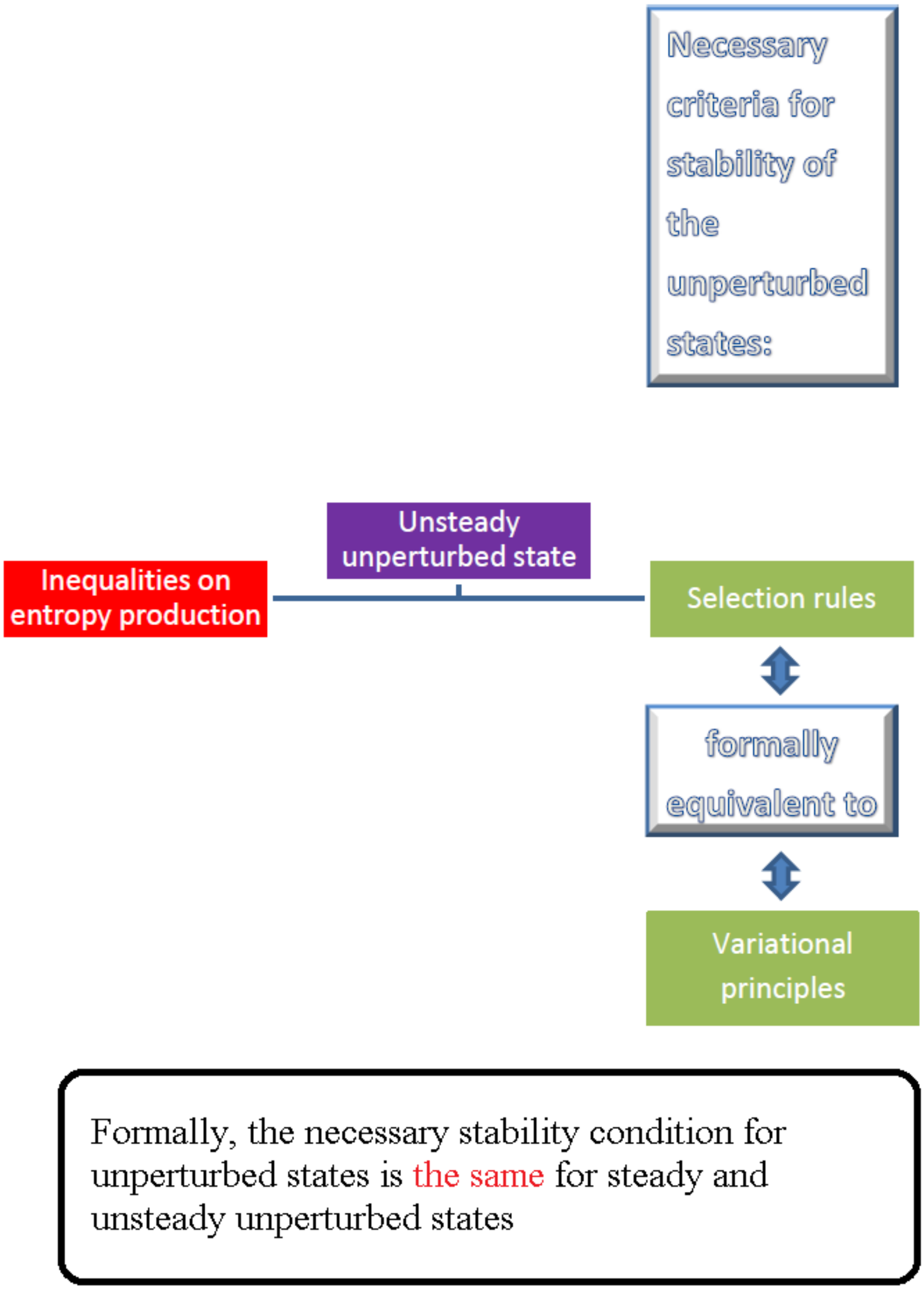

Figure 11.3: *Necessary stability conditions for unsteady unperturbed states, as provided by thermodynamics. See text for details.*

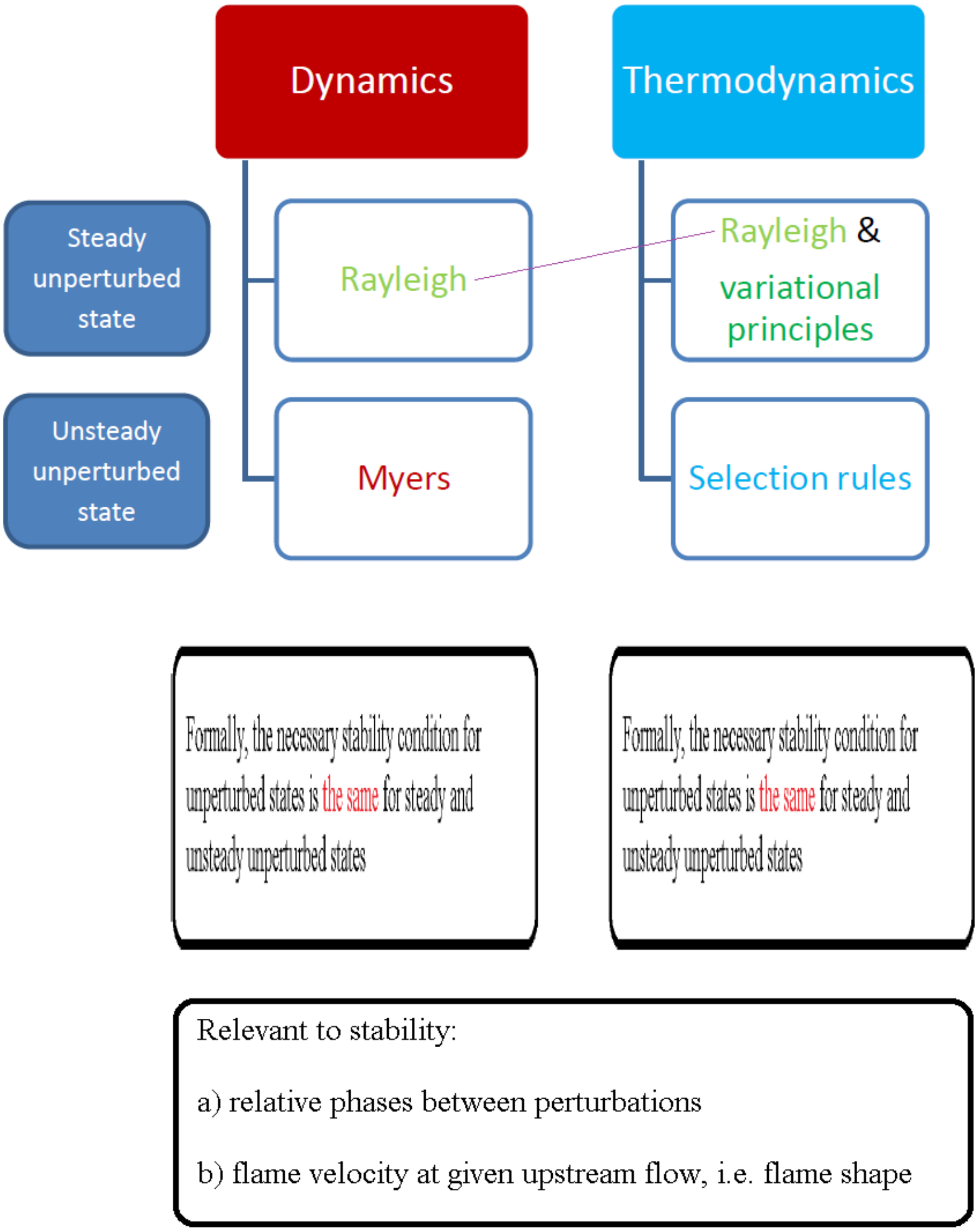

Figure 11.4: *Necessary stability conditions for steady and unsteady unperturbed states, as provided by dynamics and by thermodynamics. As for dynamics, the words* the same *refer to the couple* (6.35) - (6.36)*. As for thermodynamics, the words* the same *refer to the couples* (11.11) - (11.7) *and to* (11.12) - (11.8)*. Results for unsteady unperturbed states derive from the corresponding results for steady states after time-averaging. Rayleigh's criterion appears in both dynamic and thermodynamic column, as its isentropic version is a particular consequence of Le Châtelier's principle. See text for details.*

Chapter 12

Benchmarks

12.1 From the general evolution criterion to Biwa et al.'s selection rule

For example, we may consider a system where no combustion and no viscous heating occur, i.e. $P_h = 0$, and where no matter flows across its boundary, so that $\int d\mathbf{x}\nabla\cdot(\rho s\mathbf{v}) = \int d\mathbf{a}\cdot(\rho s\mathbf{v}) = 0$ (here and in the following we invoke both Gauss' theorem of divergence and the identity $\nabla\cdot\left(\frac{\mathbf{q}}{T}\right) = \mathbf{q}\cdot\nabla\left(\frac{1}{T}\right) + \frac{1}{T}\nabla\cdot\mathbf{q}$ again and again). An example of such a system is the couple of the solid bodies C and H in the experiment of [28], so that $\mathbf{q}$, when positive, denotes the heat flux coming out from the bodies into the fluid. In steady state we neglect the contribution $\int d\mathbf{x}\frac{\partial(\rho s)}{\partial t} = \frac{\partial}{\partial t}\int d\mathbf{x}\,(\rho s)$ of the partial time derivative. In this case, (11.8) is equivalent to maximisation of $\int d\mathbf{a}\cdot\frac{\mathbf{q}}{T} = T_H^{-1}Q_H - T_C^{-1}Q_C = -\Delta S$, i.e. to minimisation of ΔS. Note that we obtain the same result if we work with (11.12), as far as we keep on neglecting the contribution of the partial time derivative after time-averaging. We have therefore retrieved the selection rule experimentally found in [28].

12.2 From the general evolution criterion to Meija et al. and Hong et al.'s experiments...

A more general case, where both assumptions $P_h = 0$ and $\int d\mathbf{a}\cdot(\rho s\mathbf{v}) = 0$ are removed even if the constraints of constant volume and constant total heating power are retained, is also of interest. In this case we may subtract the minimised quantity in (11.7) from the maximised quantity in (11.8) and obtain maximisation of

$$\int d\mathbf{x}\left[\nabla\cdot(\rho s\mathbf{v}) + \mathbf{q}\cdot\nabla\left(\frac{1}{T}\right) - \frac{P_h}{T}\right]$$

Substitution of the expression for $\nabla\cdot(\rho s\mathbf{v})$ derived above leads to maximisation of

$-\int d\mathbf{a}\cdot\frac{\mathbf{q}}{T}+2\int d\mathbf{x}\left[\mathbf{q}\cdot\nabla\left(\frac{1}{T}\right)\right]$, i.e. to:

$$\int d\mathbf{a}\cdot\frac{\mathbf{q}}{T}-2\int d\mathbf{x}\quad \mathbf{q}\cdot\nabla\left(\frac{1}{T}\right)=\min\qquad \text{with fixed}\quad V\quad \text{and}\quad \int d\mathbf{x}P_h \tag{12.1}$$

This result applies e.g. to a flame in thermal contact with a wall at given heat release $\int d\mathbf{x}P_h$. For thin flames the volume $V = V_f$ may be safely assumed to be very small at all times. Moreover, we recall that $\mathbf{q}$ represents heat conduction and radiation, and both processes are usually assumed to play a negligible role in the cooling of the flame bulk, at least as far as GT combustors are considered. Accordingly, we may neglect the volume integral here (it will be taken into account below). In contrast, the surface integral is given a relevant contribution

$$\int_{wall} d\mathbf{a}\cdot\frac{\mathbf{q}}{T_w}$$

by the exchange of heat bewteen the flame and the wall at temperature T_w. Minimisation of this quantity is therefore a necessary condition for stability of a steady state, i.e. a configuration without humming. Any attempt to cool the wall (i.e. to raise $\frac{1}{T_w}$ or to raise the heat conductivity of the wall (hence to raise the amount of heat $d\mathbf{a}\cdot\mathbf{q}$ which flows from the flame towards the wall across a surface element $d\mathbf{a}$ per unit time) attempts at driving the system away from a minimum of the heat exchange $\int_{wall} d\mathbf{a}\cdot\frac{\mathbf{q}}{T_w}$, hence to destabilise the humming-free state and to trigger humming. (Note that in this problem the domain of integration is the flame, not the wall, so that $\mathbf{q}$ is positive when flowing into the solid wall, in contrast with the convention we have adopted for the discussion of the experiment of Biwa et al.) Our result agrees with the experimental findings of [29] and [30].

12.3 ...and beyond, to Arpaci et al.'s results on flame quenching

We may wonder what happens if we decide to neglect the surface integral and to retain the volume integral in the minimised quantity of (12.1). Physically, this decision is justified e.g. when temperature gradients are large. This the case of flames near quenching, when the flame borders on extinction due to thermal contact with a cooler wall located at the so-called *quenching distance* from the flame, and conduction rules $\mathbf{q}$. As for the order of magnitude, the quenching distance is $\approx$ the flame thickness [2], and temperature gradients are therefore huge. No flame survives at distances $<$ quenching distances.

Starting from (12.1) we obtain maximisation of

$$\int d\mathbf{x} \quad \mathbf{q} \cdot \nabla \left(\frac{1}{T} \right)$$

at given heat release and flame volume. Remarkably, this maximisation retrieves Arpaci et al.'s results about quenching - see Sec. 7 of [121], the maximised quantity being the amount of entropy produced in the flame bulk by irreversible heat transport [90]. We take this fact as a further confirmation of our arguments.

12.4 From the general evolution criterion to Rauschenbach's hypothesis

We may draw a further consequence from (11.5) in the limit of low Mach number and of caloric perfection when (6.1) holds. Equations (5.1), (6.2) and (6.3) lead to the balance of internal + kinetic energy [8]:

$$\frac{\partial}{\partial t}\left(\frac{\rho}{2}|\mathbf{v}|^2 + \rho u\right) = -\nabla \cdot \left[\rho \mathbf{v}\left(h + \frac{|\mathbf{v}|^2}{2}\right)\right] + \rho T\left(\frac{\partial s}{\partial t} + \mathbf{v} \cdot \nabla s\right)$$

Now, we invoke the definition of the total time derivative $\frac{d}{dt}$ as well as (6.4), the assumption of caloric perfection and the formula $h = c_p T$ for perfect gases and obtain:

$$\frac{\partial}{\partial t}\left(\frac{\rho}{2}|\mathbf{v}|^2 + \rho u\right) = -\nabla \cdot \left(\rho \mathbf{v}\frac{|\mathbf{v}|^2}{2} + \frac{\gamma p \mathbf{v}}{\gamma - 1}\right) + \rho T \frac{ds}{dt} \tag{12.2}$$

Finally, in the low Mach limit we take $p >> \rho \frac{|\mathbf{v}|^2}{2}$ and write

$$\frac{\partial}{\partial t}\left(\frac{\rho}{2}|\mathbf{v}|^2 + \rho u\right) = -\frac{\gamma}{\gamma - 1}\nabla \cdot (p\mathbf{v}) + \rho T \frac{ds}{dt}$$

If, furthermore, (6.13) holds, then volume integration, time-averaging, equations (6.13) and (6.16) and Gauss' theorem of divergence leads to:

$$\int_{V_b} d\mathbf{x} \langle \rho T \frac{ds}{dt} \rangle = \frac{\gamma}{\gamma - 1} \int_{A_b} d\mathbf{a} \cdot \langle \mathbf{W} \rangle$$

A dramatic simplification on the L.H.S. occurs if we neglect the contribution of $\frac{p_1}{p_0}$ to (6.6) in agreement with the $M \ll 1$ assumption, so that $s_1 = c_p \frac{T_1}{T_0}$. In this case $T = \zeta \exp\left(\frac{s}{c_p}\right)$ with ζ constant, positive quantity and then $T\frac{ds}{dt} = \frac{df}{dt}$ with $f \equiv \int^s ds'\zeta \exp\left(\frac{s'}{c_p}\right)$. We stress the point that f is a monotonically increasing function of s. It follows that

$$\rho T\frac{ds}{dt} = \rho\frac{df}{dt} = \frac{\partial(\rho f)}{\partial t} + \nabla \cdot (\rho f \mathbf{v})$$

where we have invoked (5.1). The last two relationships lead to

$$\int_{A_b} d\mathbf{a}\langle \rho f \mathbf{v}\rangle = \frac{\gamma}{\gamma - 1}\int_{A_b} d\mathbf{a} \cdot \langle \mathbf{W}\rangle \tag{12.3}$$

and the time-average allows us to get rid of the contributiuon of the partial time derivative. Since f is a monotonically increasing function of s and heat conduction is negligible for (6.1), the maximisation prescribed by the variational principle (11.8) reduces to maximisation of the L.H.S. of (12.3). Then, (12.3) implies maximisation of $\int_{A_b} d\mathbf{a} \cdot \langle \mathbf{W}\rangle$, i.e. Rauschenbach's hypothesis [95] discussed above in connection with the experiments of [28]

12.5 From the general evolution criterion to Rayleigh's criterion

So far, we have not yet utilised (11.6). Together, (11.6) and the identity $\int d\mathbf{x}\frac{P}{T} = \frac{dS}{dt}$ lead to:

$$\frac{d^2S}{dt^2} \leq c_3\frac{d^2V}{dt^2} + c_4\frac{d^2U}{dt^2} \tag{12.4}$$

For a relaxation process where both V and U are constant at all times (like, e.g., in isolated systems), (12.4) implies

$$\frac{d^2S}{dt^2} \leq 0$$

Evolution towards thermodynamic equilibrium ($S = \max$) of isolated systems ($U =$ const., $V =$ const.) provides us with a well-known example of such relaxation.

As for non-isolated systems -like e.g. the combustor of a GT- suitable boundary conditions -like e.g. a constant flow of air and fuel- may keep the relaxed state far from thermodynamic equilibrium. Now, if we focus our attention on necessary conditions of stability, then we are free to select the perturbation which we invoke in order to test stability. For example, we may wonder what happens if we apply a perturbation which leaves both V and U unaffected. In this case, both repeated utilisation of (7.1) and arguments which are similar to those discussed above allow us to derive from (12.4) the following necessary condition for stability

$$\int d\mathbf{x}\frac{P}{T} = \min$$

In the following, we are going to show that this condition includes Rayleigh's criterion (more precisely, the relationships (6.34) and (6.35) with the acoustic energy flux and the energy density defined in (6.16) and (6.17) respectively) in the zero Mach limit where the unperturbed state does not depend on time and (6.1) holds. This proof shall enable us to identify the configurations candidated to stability by Rayleigh's criterion with those candidated to stability by Le Châtelier's principle. In turn, this identification allow us to describe the combustors which are possibly free from humming according to Rayleighs' criterion with states corresponding by any of the Le Châtelier's consequences discussed so far - and in particular with those steady-state solutions of the constitutive equations (5.1) - (5.5) which satisfy the necessary condition (11.7) for the stability of steady (i.e. humming-free) states. Of course, we are perfectly free to choose (11.8) rather than (11.7), but the choice of (11.7) spares us any need for a description of the heat flux $\mathbf{q}$.

We are going to take advantage of this fact in the following Chapters. Here we anticipate that -in contrast to what happens with Rayleigh's criterion- our discussion will require no explicit knowledge of the spectrum of acoustic fluctuations.

Now, it comes to the proof. Basically, it is a generalisation of the proof contained in Appendix C of [116]. The minimum property quoted above ensures that any perturbation of the minimized quantity near a stable state is non-negative: $d\left(\int d\mathbf{x}\frac{P}{T}\right) \geq 0$. The domain of integration is the combustor volume V_b, which is a constant quantity. Taking the time-average we have $\langle d\left(\int d\mathbf{x}\frac{P}{T}\right)\rangle \geq 0$. Starting from here, we show in the Appendix on the auxiliary relationships concerning Rayleigh's criterion that the following chain of inequalities holds:

$$\int_{V_b} d\mathbf{x}\langle D\rangle + T_{0\max}\int_{V_b} d\mathbf{x}\langle(\nabla\cdot\mathbf{q}_1)\left(\frac{1}{T}\right)_1\rangle \leq K\int_{A_b} d\mathbf{a}\cdot\langle\mathbf{W}\rangle \qquad (12.5)$$

where we have defined $K \equiv F_{\max} T_{0\max}$, $T_{0\max}$ is an upper bound on the unperturbed temperature T_0, $F_{\max}$ is a suitably chosen constant and we have explicitly written down the domains of integration, i.e. the combustor volume V_b for the volume integration and the combustor surface A_b on the R.H.S. and the R.H.S. respectively. For the moment, let us neglect the contribution $\propto \nabla \cdot \mathbf{q}_1$ of heat conduction and radiation, as it is customary in premixed combustion. In the Appendix on the auxiliary relationships concerning Rayleigh's criterion we show that it is always possible to choose $F_{\max}$ in such a way that (12.5) reduces to (6.34) and (6.35) if the operator $\leq$ reduces to $<$ and to $=$ respectively.

12.6 Outside thermo-acoustics: Eddington's Cepheids

Now, let us investigate what happens if radiation and conduction are the dominant contributions to (12.5). This may happen e.g. in a system where no heating processes occur (i.e. $\langle D \rangle = 0$ and heat is mainly transported, across the system, not produced within it) and where either boundary conditions force $\mathbf{v} \cdot d\mathbf{a} = 0$ on the boundary or adiabatic processes only occur (so that $\langle \mathbf{W} \rangle \cdot d\mathbf{a} = 0$). In this case the necessary condition (12.5) for the lack of oscillations reduces to $\int_V d\mathbf{x} \langle (\nabla \cdot \mathbf{q}_1) \left(\frac{1}{T}\right)_1 \rangle \leq 0$, i.e. -not surprisingly- the time-averaged version of (11.3). Since $d\left(\frac{1}{T}\right) = -G dp$ and G is both positive-definite and lower-bounded everywhere at all times for quasi-adiabatic perturbations in a neighbourhood of a stable steady state, then

$$\int_V d\mathbf{x} \langle p_1 (\nabla \cdot \mathbf{q}_1) \rangle \geq 0 \tag{12.6}$$

The physical meaning of the stability criterion (12.6) is due to Eddington [122]:

> *Consider the mode in which thermal dissipation acts in the case of a sound wave. The air is hottest at a point of maximum compression. If this heat leaks away, the compressed fluid loses some of its spring, and the expansion which follows has diminished energy -consequently, the waves decay. If, on the other hand, the air could be persuaded to lose heat at points where it was rarified and coolest, the ensuing compression would be assisted and the waves reinforced*

The two cases correspond to the occurrence of the operator $>$ and $<$ in (12.6) respectively.

Marginal states too (oscillations with stable amplitude) which correspond to the case $=$, are also well described by Eddington:

> *Intermediately, a loss or gain of heat at a point of normal density neither dissipates nor increases the energy [...] the material relatively loses heat as it passes through its normal density expanding, and gains heat at the same stage contracting; but neither gains nor loses when most compressed or most rarified*

These words resemble closely Rayleigh's words [31]:

> *if the air be at its normal density at the moment where the transfer of heat takes place, the vibration is neither encouraged nor discouraged*

Remarkably, however, Eddington was not concerned with the onset of spontaneous acoustic oscillations in a Rijke's tube. Rather, he investigated spontaneous oscillations of a Cepheid star. A Cepheid is a member of a class of pulsating variable star. Typical Cepheids pulsate with periods of a few days to months, and their radii change by several milion Km (30 %) in the process -see e.g. Tab. III of [123]. Helium is the gas thought to be most active in Cepheid pulsation. The more helium is heated, the more ionized it becomes. But He^{++} is more opaque than He^{+}. At the dimmest part of a Cepheid's cycle, the ionized gas in the outer layers (*envelope*) of the star is opaque, and so is heated by the star's radiation, and therefore it begins to expand. As it expands, it cools, and so becomes less ionized and therefore more transparent, allowing the radiation to escape. Then the expansion stops, and reverses due to the star's own gravitational attraction. The process then repeats [124].

The mechanics of a Cepheid oscillation as a heat engine was proposed by Eddington in 1917, while Rayleigh worked with Rijke's tube in 1876. However, to the author's knowledge Eddington was no aware of Rayleigh's observations. Despite the huge differences between the two spontaneously oscillating systems, Rijke's tube and a Cepheid, Rayleigh and Eddington's arguments are quite similar, as thermodynamics is the same in both cases [1].

As for the assumptions underlying (12.6), no heating (nuclear) process occurs in the envelope, and heat is mainly transferred across the layers from the star nucleus towards the external world, Moreover, it can be safely assumed that the time-averaged speed vanish on the boundaries, provided at least that the outflow of matter has a negligible effect on the star mass balance during one oscillation. Indeed, radiation plays a crucial role in the oscillation, in contrast to oscillations involving GT flames.

The main problem left behind in our discussion is that -unlike both Rijke's tube and GT combustors- star dynamics is heavily affected by gravity, which is a body force -and we have self-consistently neglected body forces so far. According to [33], suitable modulation

[1] For example, comparison of equation (1) of Ref. [124] with our formula (6.17) shows that a source term of oscillation in Eddington's work coincides with the destabilising term of Rayleigh's criterion for $\nabla s_0 = 0$.

of body forces may be stabilising. In the particular case of gravity, however, it turns out that its modulation reduces to adding the gravitational potential to u, h and the g_j's everywhere at all times, in agreement with the small correction theorem -see equation (24.16) of [84]. Given the identity $\sum_{k=1}^{n} Y_k \equiv 1$, it follows that gravity leaves both (5.4) and (11.1) - hence the general evolution criterion (11.2) and all its consequences (11.4), (11.5) and (11.6) - unaffected, provided that by u, h etc. we keep on referring to the corresponding expressions in absence of gravity. Since gravity is a conservative force, it is far from surprising that gravity leaves both dissipation-relevant quantities P and P_h unaffected.

Part IV

Applications

Chapter 13

Absence of humming

13.1 Generalities

Rayleigh's criterion provides a necessary condition of stability for premixed flames. We have shown that if a flame is stable according to Rayleigh's criterion then it is also stable according to Le Châteliers' principle of thermodynamics, whose range of validity is far larger than the range of validity of Rayleigh's criterion and which lead to various corollaries, including variational principles and selection rules.

Accordingly, if we make use of any of the latter corollaries our results will be grounded on the same firm basis of Rayleigh's criterion itself, while getting rid of the limitations intrinsic of this criterion, including the zero mean flow approximation and the lack of explicit information concerning the shape of humming-free flames.

In this Chapter we apply our previous results to the description of premixed, lean, swirl-stabilized combustors (more precisely, of systems made of flame, fluid and combustor) which undergo no humming.

Again, we stress the point that absence of humming means no absence of combustion instability. Here we assume that, once triggered, the latter instability either relaxes back to the unperturbed state or saturates to some unoffensive, low level- and lead the system to no catastrophic failure where quantities like e.g. $|\frac{d}{dt}\int d\mathbf{x}\frac{P_h}{T}|$ diverge beyond control.

We investigate the consequences of this assumption, namely the necessary conditions for the system not to be destroyed. Hopefully, steady-state GT operation can be described as a stable steady state, where *stability* is given the meaning stated above and combustion instability is either of harmless amplitude or is averaged out on the time-scale of interest to the user (» 1 s) [1].

To this purpose, five intermediate steps are useful here and in the following.

[1]This is also why we assume the unperturbed state to be (swirl-)stabilised against flashback, lift-off and blow-off.

- We neglect viscous heating in comparison with combustion heating, so that P_h is due to combustion only.

- We remember that combustion occurs in the flame only regardless of the occurrence of humming, so that as for the domain of integration we may replace the combustor volume with the flame volume.

- We introduce a distinction between an upstream region (where no burnt gas is present) and the downstream region (where burnt gases are present). The flame separates the upstream region from the downstream region.

- Even if turbulence occurs we assume that the flame thickness is negligible with respect to the linear size of the combustor, so that the flame is a smooth mathematical surface in space. Correspondingly, we refer to s_L as to the flame velocity everywhere; fur turbulent flamess it is to be replaced by its turbulent counterpart s_T. Admittedly, this assumption is strongly unphysical. Basically, in fact, even in case of small turbulent fluctuations and large Damkoehler number for all chemical species -see [4]- we are going to identify flames without humming with flames where all other instabilities are also suppressed, so that speaking of a flame surface in steady state is meaningful. However, this strong restriction is useful for mathematical convenience, and we are going to show that it allows to obtain physically meaningful results.

- We assume for simplicity that both the temperature T_d of the downstream region and the temperature $T_u < T_d$ of the upstream region are uniform on the flame front (subscripts u and d refer to the upstream and to the downstream region respectively). This approximation corresponds to neglect high-frequency modes (see pag. 325 of [53]), and is also likely to be quite unphysical. However, it will be dropped in the following.

13.2 Shapes of stable flames

13.2.1 The absence of humming as a problem of variational calculus

A necessary condition for the absence of humming

The aim of this Chapter is to write down a necessary condition for stability which involves the flame shape explicitly, in contrast with Rayleigh's criterion which does so only implicitly.

For simplicity, we neglect both particle diffusion, heat conduction and radiation. We assume that complete combustion occurs, i.e. no fuel is present on the downstream side of the flame. Moreover, we consider just $n = 3$ chemical species, i.e. air, fuel and combustion products; this implies that we have just 2 independent equations for the Y_k's (say, for air and fuel) because of the identity $\sum_{k=1}^{n} Y_k \equiv 1$. In premixed combustion both air and fuel are present on the upstream side of the flame. Finally, we assume both caloric perfection and infinitely fast, irreversible combustion [4] where the heat release density is

$$P_h = P_0 k Y_{air} Y_{fuel} \tag{13.1}$$

while the number of combustion reactions per unit time and volume and the production rate of air and fuel are $kY_{air}Y_{fuel}$, $-AkY_{air}Y_{fuel}$ and $-BkY_{air}Y_{fuel}$ respectively, with the quantity $k = k(T) > 0$ which plays the role of an Arrhenius coefficient and A, B and P_0 positive constant coefficients. Outside the flame no combustion occurs, i.e. $k = 0$ [2].

In the last Chapter we have shown that if a system flame + fluid undergoes no humming then we may describe it as a steady-state ($\frac{\partial}{\partial t} = 0$) solution of the constitutive equations which satisfy the necessary condition (11.7) for the stability of steady states. Utilisation of (11.7) spares us the need for information on $\mathbf{q}$. Starting from both (5.1), (5.2), (6.2), (12.2) and the definitions of P and P_h we obtain the following equations in steady state:

$$\nabla \cdot (\rho \mathbf{v}) = 0 \tag{13.2}$$

$$\mathbf{v} \cdot \nabla Y_{air} + AkY_{air}Y_{fuel} = 0 \tag{13.3}$$

$$\mathbf{v} \cdot \nabla Y_{fuel} + BkY_{air}Y_{fuel} = 0 \tag{13.4}$$

$$\rho (\mathbf{v} \cdot \nabla) \mathbf{v} + \nabla p = 0 \tag{13.5}$$

$$\nabla \cdot \left(\rho \mathbf{v} \frac{|\mathbf{v}|^2}{2} + \frac{\gamma p \mathbf{v}}{\gamma - 1} \right) - P_0 k Y_{air} Y_{fuel} = 0 \tag{13.6}$$

As for the homogeneous version of (13.3) and (13.4) outside the flame, see equations (A3) and (A4) of [125]. As for (11.7), since combustion is localized at the flame the minimized

[2]Positive values of A and B mean that the number of air and fuel particles lowers as the number of combustion reactions increases. Indeed, the present treatment is a slight generalization of the treatment in Chapter 2 of [4], where the additional condition $Y_{air} \approx 1$ is included for lean combustion.

quantity $\int d\mathbf{x}\frac{P_h}{T}$ reduces to a volume integral $\int_{V_f} d\mathbf{x}\frac{P_h}{T}$ on the flame volume, in agreement with (6.22). The constraint of fixed volume $V \equiv \int_V d\mathbf{x} = V_f = \text{const.}$ plays just the role of the definition of V_f; as such it is automatically satisfied, and will be dropped below. Physically, it means that the flame is assumed to stand at rest when no humming occurs. The constraint of fixed heat release reads $\int_{V_f} d\mathbf{x}P_h = W_c$. In the following we focus our attention on the geometry of stable flames; accordingly, we are going to keep the profiles of both T and P_h across the flame fixed [3]. Then equation (13.1) makes the constraint of fixed heat release to reduce to

$$kY_{air}Y_{fuel} = P^* \tag{13.7}$$

where P^* is some known function of $\mathbf{x}$ which satisfies the property $\int d\mathbf{x}P^* = \frac{W_c}{P_0}$. Its exact structure is of no interest in the following.

Again, just like in Rayleigh's criterion, the flame volume appears as the domain of integration of a volume integral. The novelty lies in the fact that the volume integral is a minimised quantity, and that the minimisation is constrained by (13.2), (13.3), (13.4), (13.5), (13.6) and (13.7). The constrained variational principle links flame geometry and flame stability. Here and in the following, we are going to make use of tools of variational calculus, which are briefly described in the corresponding Appendix.

After introducing 8 Lagrange multipliers $\mu(\mathbf{x})$, $\zeta(\mathbf{x})$, $\vartheta(\mathbf{x})$, $\xi(\mathbf{x})$, $\nu(\mathbf{x})$ and $\lambda(\mathbf{x})$ for the constraints (13.2) - (13.7) which involve 8 physical quantities $\rho(\mathbf{x})$, $\mathbf{v}(\mathbf{x})$, $Y_{air}(\mathbf{x})$, $Y_{fuel}(\mathbf{x})$, $p(\mathbf{x})$ and $T(\mathbf{x})$, the constrained minimization in (11.7) leads to:

$$\int_V d\mathbf{x}L = \min \tag{13.8}$$

where we have introduced the Lagrangian density

[3] This makes sense even if $Y_{air} \approx 1$ as integration of the equations of motion (13.4) and (13.6) leads in this case to equations (2.35) and (5.37) of [4] (or to its generalisation to $Le \neq 1$ in Sec. 4 of Ref. [6]). In turn, these equations unambiguously link the suitably normalised profiles of T and of Y_{fuel} across the flame. Even at fixed profiles, the upstream (or equivalently, downstream) values of both T and Y_{fuel} may still undergo variation. This is why we are still allowed to consider both T and Y_{fuel} as Lagrangian coordinates in the following.

$$
\begin{aligned}
L \equiv & \frac{kY_{air}Y_{fuel}}{T} + \mu\nabla\cdot(\rho\mathbf{v}) + \zeta\left(\mathbf{v}\cdot\nabla Y_{air} + AkY_{air}Y_{fuel}\right) + \\
& + \vartheta\left(\mathbf{v}\cdot\nabla Y_{fuel} + BkY_{air}Y_{fuel}\right) + \xi\cdot\left(\rho\mathbf{v}\cdot\nabla\mathbf{v} + \nabla p\right) + \\
& + \nu\left[\nabla\cdot\left(\frac{\gamma p\mathbf{v}}{\gamma-1} + \frac{\rho\mathbf{v}\left|\mathbf{v}\right|^2}{2}\right) - P_h\right] + \lambda\left(kY_{air}Y_{fuel} - P^*\right)
\end{aligned}
$$

and we have taken into account that no combustion occurs outside the flame. (We have dropped the dependence on $\mathbf{x}$ for simplicity. Moreover, we have explicitly written the generic domain of integration V -rather than V_f of V_b- with no ambiguity, as volumes are constant quantities here). There are 16 Lagrangian coordinates in (13.8), i.e., μ, ζ, ϑ, ξ, ν, λ, ρ, p, T, $\mathbf{v}$, Y_{air} and Y_{fuel}. Correspondingly, there are $8 + 8 = 16$ Euler-Lagrange equations. The fact that we consider ρ, p and T as independent variables allows our results to depend on no particular choice of the equation of state. The Euler-Lagrange equations include the 7 balance equations (13.2), (13.3), (13.4), (13.5), (13.6) and (13.7). Steady-state configurations of the system combustor + fluid + flame solve these equations. If these steady-state solutions are also *stable*, then they solve *also* the remaining 9 Euler-Lagrange equations. The search of a stable configuration reduces therefore to a problem of variational calculus [4].

Jump conditions across a thin flame

As expected, solving the Euler-Lagrange equations explicitly in the general case turns out to be quite a formidable task. Luckily, dramatic simplification occurs if we focus our attention on the neighbourhood of a thin flame in the limit of low Mach number. In this case, in fact, the jump conditions at the flame take a simple form [8] [6]:

$$
p|_u^d = 0 \qquad \mathbf{v}_{\parallel}|_u^d = 0 \qquad \mathbf{v}_{\perp}|_u^d = \alpha\mathbf{v}_{\perp u} \tag{13.9}
$$

where $\alpha \neq 0$ is a function of T_u; moreover, $\mathbf{a}_{\perp} \equiv (\mathbf{a}\cdot\mathbf{n})\,\mathbf{n}$, $\mathbf{a}_{\parallel} \equiv \mathbf{a} - \mathbf{a}_{\perp} = (\mathbf{n}\wedge\mathbf{a})\wedge\mathbf{n}$ for an arbitrary vector $\mathbf{a}$ and $\mathbf{n}$ is the unit vector ($\mathbf{n}\cdot\mathbf{n} \equiv 1$) normal to the flame and pointing outwards, in agreement with the convention of [4] ($\mathbf{n}\cdot\mathbf{v}_d > 0$, $\mathbf{n}\cdot\mathbf{v}_u < 0$).

Further simplification occurs if we neglect $\nabla_{\parallel}a$ for the generic quantity a in the following. Admittedly, this can be taken for granted in flat, unstretched flames only, which the jump conditions (13.9) have been originally proven for, but which are also never stable because of the Darrieus-Landau instability. Luckily, if the flame is not too stretched then corrections due to flame curvature are of order $\propto O\left(\frac{1}{Pe}\right) \ll 1$ where the Peclet number

[4]Indeed, a *necessary* condition for any field to solve the extremum problem (13.8) is that this field solves the corresponding Euler-Lagrange equations. Thus, mathematics nicely fits thermodynamics.

$Pe \equiv \dfrac{\delta_L}{L}$ is » 1 for thin flames, δ_L being the laminar flame thickness [6]. In particular, neglecting $\nabla_\parallel T$ is equivalent to neglect high-frequency modes -see p. 325 of [53]- and is reasonable in steady-state analysis.

Humming vs. shape and upstream flow

We show in the Appendix on the auxiliary relationships concerning stable flames that (13.8) and (13.9) lead to a necessary condition for stability against humming which takes the form of a relationship between the upstream flow and the shape of the stable flame:

$$\int_u (\mathbf{v}_u \cdot \mathbf{n})(\nabla \wedge \mathbf{n})_\parallel d\mathrm{a} = 0 \tag{13.10}$$

where $\int_u d\mathrm{a}$ denotes surface integration on the upstream face of the flame. Since we are dealing with steady states with fixed profiles of T across the flame and negligible $\nabla_\parallel T$, we anticipate here that equations (14.1) and (14.2) below ensure that the minimized quantity $\int d\mathbf{x}\dfrac{P_h}{T}|_{steady}$ in (11.7) is equal to $\dfrac{\int d\mathbf{x} P_h}{T_f}$ with T_f constant quantity, just as $\nabla T = 0$ were uniform with $T = T_f$ everywhere across the flame. In the latter case, it is possible to show (see Sec. 3 of [126]) that the solutions of the Euler-Lagrange equations of (11.7) solve also the Euler-Lagrange equations of the variational principle

$$\int d\mathbf{x} P_h = \min \qquad \text{with fixed} \quad V \quad \text{and} \quad T = T_f \quad \text{everywhere} \tag{13.11}$$

Again, we drop the constraint of fixed volume $\int_{V_f} d\mathbf{x} = V_f$, as it plays just the role of the definition of V_f and is automatically satisfied for thin flames (see below) where it can be taken at an arbitrarily small value whose actual value is not relevant. Now, the fact that combustion occurs inside the flame only ensures that $\int d\mathbf{x} P_h = \int_{V_f} d\mathbf{x} P_h$; moreover, the constraint of fixed heat release [5] reads $\int_{V_f} d\mathbf{x} P_h = W_c$ and the facts that the profile of P_h is fixed and that $\nabla_\parallel P_h$ is negligible ensure that $\int d\mathbf{x} P_h \propto V_f$, so that minimisation of $\int d\mathbf{x} P_h$ in (13.11) implies minimisation of the flame volume. Finally, for a thin flame the flame volume is an increasing function of both the flame thickness and the flame area

$$A_f \equiv \int_u d\mathrm{a}$$

But the former is uniform across the flame as all parallel gradients of the type $\nabla_\parallel a$ are

[5] Remarkably, the constraint of fixed heat release $\int_{V_f} d\mathbf{x} P_h = W_c$ leaves the validity of (13.11) unaffected: the former gives the value of the heat release, the latter requires that this value is a minimum, i.e. that any perturbation raises it.

negligible, so that minimisation of the flame volume required by (13.11) implies minimisation of A_f. The equations of motion affect this minimisation through (13.10), and we obtain:

$$\int da = \text{min. with } \int (\mathbf{v}\cdot\mathbf{n})(\nabla\wedge\mathbf{n})_{\|} da = 0 \tag{13.12}$$

where we have dropped both the pedix 'u' (for simplicity, unless stated otherwise) and the constraint on temperature T as no quantity involved in (13.12) depends explicitly on T; let it be understood that the profile of temperature across the flame remains fixed. The reciprocity principle for isoperimetric problems of variational calculus [6] - see Sec. IX.3 of [127]- ensures that the relaxed state which satisfies (13.12) satisfies also:

$$\int (\mathbf{v}\cdot\mathbf{n})(\nabla\wedge\mathbf{n})_{\|} da = \text{max.} \quad \text{with fixed} \int da \tag{13.13}$$

Once $\mathbf{v}$ is known upstream, (13.13) provides us with information about possible shapes of stable flames. In particular, equation (13.13) is a necessary condition for the absence of humming which involves two things:

- the upstream flow
- the shape of the flame

Then, it takes still a couple of independent pieces of information concerning this flow and this shape in order to find the actual shape of a stable flame for a given upstream flow. As we are going to show, the required pieces of information are the fact that the Mach number is low and the fact that the flame is thin.

Equation (13.13) has far-reaching consequences. We are going to investigate some of these consequences in the following.

13.2.2 Axisymmetric, swirl-stabilised, thin flames...

Axisymmetric

The discussion undergoes dramatic simplification in the axisymmetric case: $\dfrac{\partial}{\partial\chi} \equiv 0$ in the cylindrical coordinate system $\{r, \chi, z\}$. We refer to Fig. 13.1.

[6] In a nutshell, and stated in non-rigorous words, the reciprocity principle says that the solution of the variational principle $A = \text{min.}$ with the constraint of fixed B solve also the variational principle $B = \text{max.}$ with the constraint of fixed A. For example, the sphere is both the solid with given surface area which encompasses the maximum volume of space and the solid with given volume which is bounded by the minimum surface area. Basically, the reciprocity principle follows from the fact that the two variational principles lead to the same Lagrangian density with different definitions of the Lagrangian multipliers.

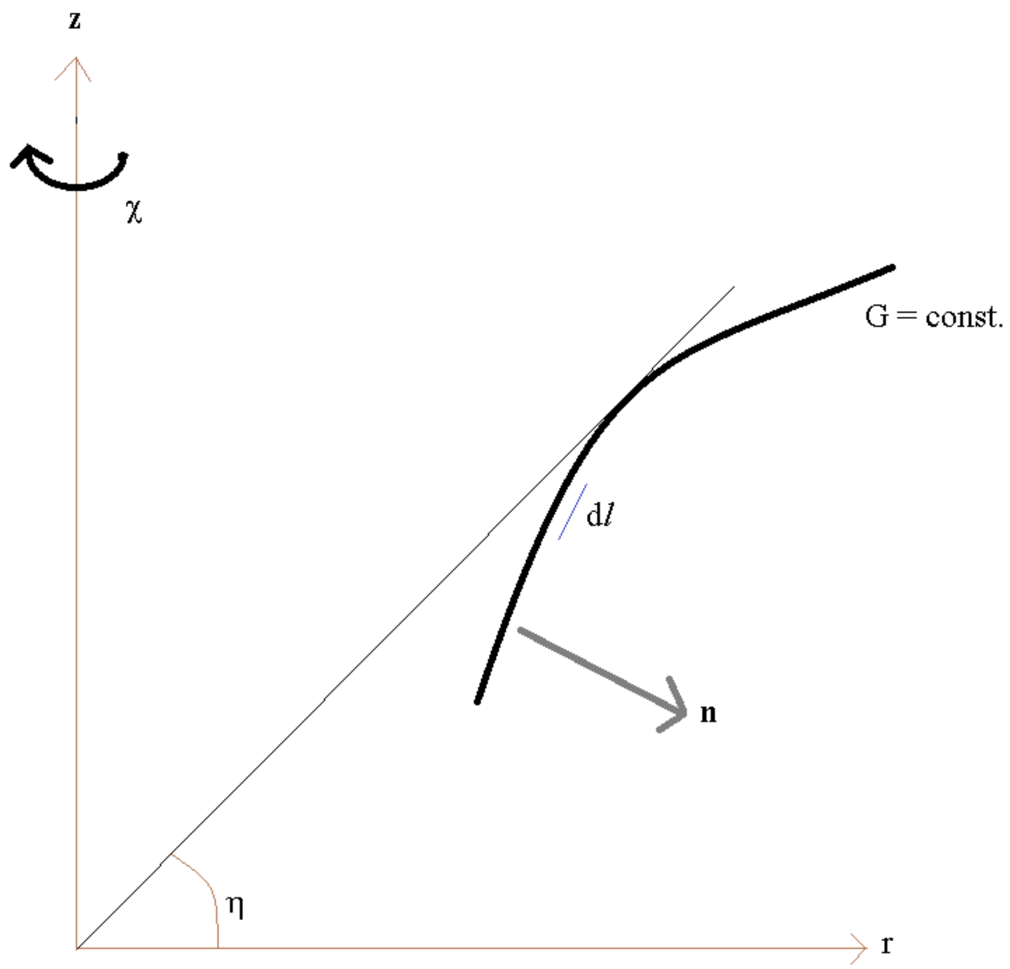

Figure 13.1: *Geometrical quantities for an axisymmetric flame surface - see text for details.*

To start with, let us write down some useful mathematical relationships, which will turn out to be useful in the following. If the boundary surface of the flame volume takes (locally at least) the form $G(\mathbf{x}) = \text{const.}$, then $\mathbf{n} = -\dfrac{\nabla G}{|\nabla G|}$. The actual value of the constant value of G on the flame has no physical meaning.

We invert $G = G(r, z)$ locally and write $G = z - f(r)$, so that $\nabla G = (-f', 0, 1)$, $f' \equiv \dfrac{df}{dr} = \tan\eta$ and $(\nabla \wedge \mathbf{n})_{\parallel} = -(0, Kf', 0)$ where $K \equiv \dfrac{f''}{(1 + (f')^2)^{3/2}} = \dfrac{d\eta}{dl}$, $\tan\eta$, $dl = \sqrt{1 + f'^2}dr$ and l are the curvature, the slope, the line element and the arc length respectively [128] of the curve $z = f(r)$ which belongs to the plane (r, z) and whose rotation generates the boundary surface of the flame volume. The area element of the flame is $d\mathrm{a} = 2\pi r dl$.

Swirl-stabilised

Streamfunction We focus our attention on the word *swirl* in this Section. The reason of the word *stabilised* will be clear in the next Section.

In the low Mach limit we write $\nabla \cdot \mathbf{v} = 0$ on the upstream side the flame [7]. The axisymmetric solution of this equation in cylindrical coordinates has the form:

$$\mathbf{v} = \frac{\nabla\psi \wedge \mathbf{e}_\chi}{r} + \frac{F(\psi)\,\mathbf{e}_\chi}{r} \tag{13.14}$$

where we have introduced the *stream function* $\psi = \psi(r, z)$ (with the dimensions of a velocity times an area) and the unit vector $\mathbf{e}_\chi$ in the azimuthal direction - see equation 12 of Ref. [129] [8] and Fig. 13.2 for a stream function map in a swirled, axisymmetric flow where no combustion occurs.

The velocity has components $v_r = -\frac{1}{r}\frac{\partial\psi}{\partial z}$ and $v_z = +\frac{1}{r}\frac{\partial\psi}{\partial r}$ on the *meridian plane* $\chi =$ const., while the azimuthal component of the velocity is just $v_\chi = \frac{F}{r}$, and F is a function of ψ. The components of $\mathbf{v}$ on the upstream side of the flame lie on $\psi =$ const. surfaces. As for the physical meaning of ψ, first of all we note that ψ and $\psi - \psi_0$, with $\psi_0 =$ const., lead to the same $\mathbf{v}$ -a fact which will turn out to be useful in the following. Moreover, equation (13.14) implies that $\mathbf{v} \cdot \mathbf{n} = -\frac{1}{r}\frac{d\psi}{dl}$, i.e.:

$$2\pi d\psi = -\mathbf{v} \cdot \mathbf{n} d\mathrm{a} \tag{13.15}$$

i.e. $d\psi$ is proportional to the mass flow $-\rho_u \mathbf{v} \cdot \mathbf{n} d\mathrm{a}$ which comes from the upstream side of the flame and impinges on the annulus of flame area $d\mathrm{a}$ [9]. In particular, equations (13.10), (13.13) and (13.15) lead both to:

$$\int K f' d\psi = 0 \tag{13.16}$$

[7] Here and in the following we focus our attention on the swirl of the *upstream* flow only, in contrast e.g. with the approach of Ref. [12] which focusses on swirled *downstream* flows. Physically, in fact, causality requires that it is the impinging flow which affects the flame shape in premixed combustion.

[8] When dealing with ψ, we are going to invoke again and again relationships taken from Ref. [37] below, where the role of $\mathbf{v}$ on the upstream side of the flame is played by an axisymmetric magnetic field at zero divergence.

[9] On the upstream side $\mathbf{v} \cdot \mathbf{n} < 0$ because $\mathbf{n}$ points outside, i.e. from the flame towards the unburnt gases -see Fig. 1

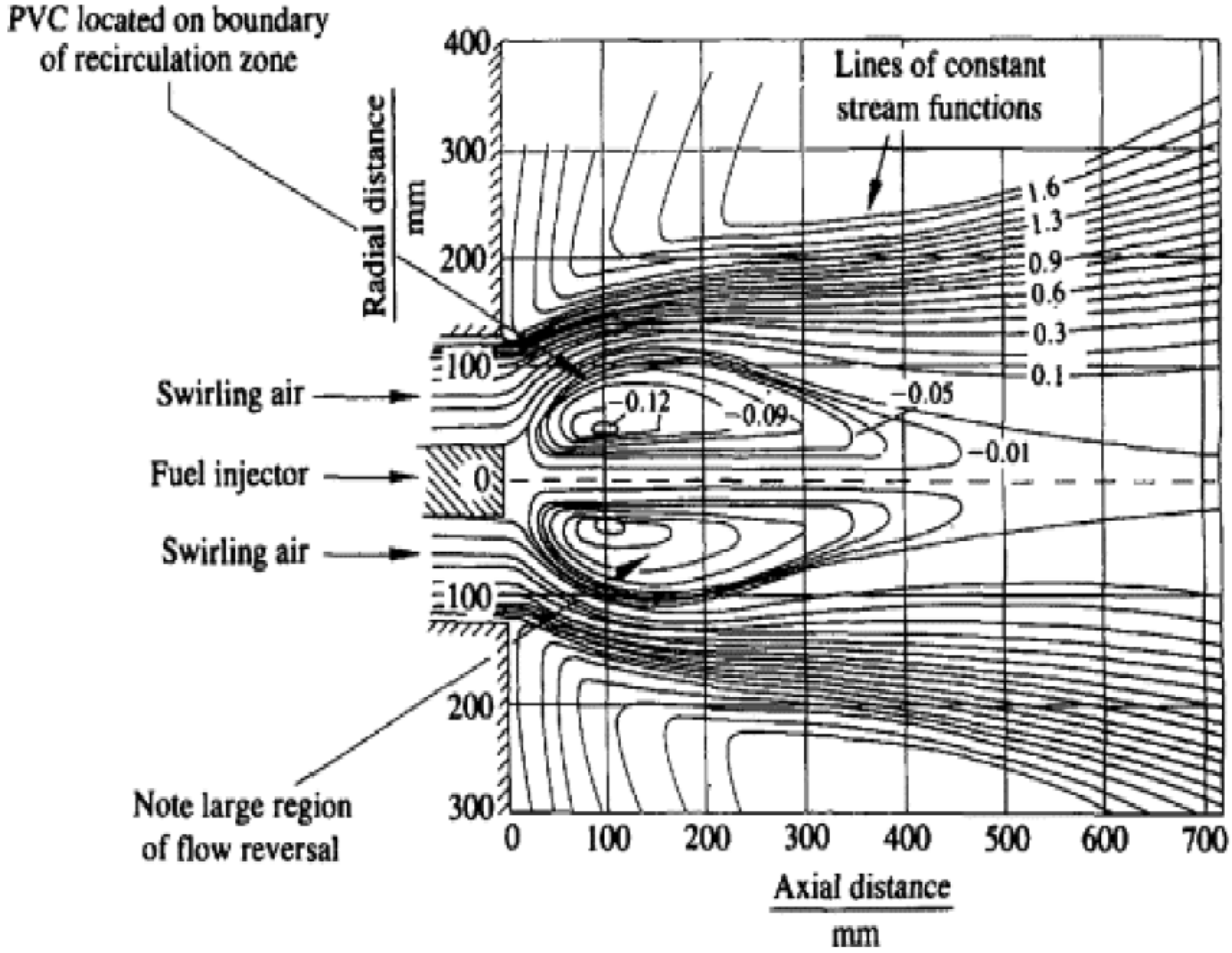

Figure 13.2: *Meridian cross-section of iso-ψ surfaces in a swirled, axisymmetric flow with PVC and no combustion -from Ref. [5].*

and to:

$$\int Kf'd\psi = \text{max.} \quad \text{with fixed} \int da \tag{13.17}$$

In turn, (13.17) implies:

$$\delta\left(\int Kf'd\psi + \int \theta da\right) = 0 \tag{13.18}$$

where θ is a Lagrange multiplier with $\nabla\theta = 0$. We are going to invoke (13.17) and (13.18) again and again in the following.

It takes no further computation, however, to show that (13.17) allows no flame with $K = 0$ everywhere (henceforth referred to as *perfectly flat flame*) to be stable [10]. In fact, (13.17) reduces to maximisation of the flame area -hence of the heat release- for such flames: and this is rather a condition for instability. Accordingly, we shall consider no perfectly flat flame as an eligible candidate to stability in the following.

The equations of motion provide us with a link of ψ and F. As usual by now, we write $p >> \rho\frac{|\mathbf{v}|^2}{2}$, $\nabla p \approx 0$ in the low Mach limit and neglect viscosity, so that equation (6.2) in steady state ($\frac{\partial}{\partial t} \equiv 0$) reduces to $\mathbf{v} \wedge \nabla \wedge \mathbf{v} = 0$. Substitution of equation (13.14) leads therefore to the following equation [11]:

$$\frac{\partial^2\psi}{\partial r^2} - \frac{1}{r}\frac{\partial\psi}{\partial r} + \frac{\partial^2\psi}{\partial z^2} + \frac{1}{2}\frac{d\left(F^2\right)}{d\psi} = 0 \tag{13.19}$$

The stream function $\psi(r, z)$ solves equation (13.19) for a given profile $\propto F(\psi)$ of the azimuthal velocity. The $\psi =$ const. surfaces are topologically similar to possibly distorted, nested tori labelled by ψ. Solution of equation (13.19) requires a boundary condition, say $\psi = \psi_b$.

Physically, the dependence of F on ψ describes the dependence of the azimuthal component of $\mathbf{v}$ on the other components of $\mathbf{v}$, or, to put it in other words, it represents the swirl in the flame-supporting upstream flow [129]. The words *flame-supporting* are given a precise meaning below, and the impact of swirl on stability is also discussed. To start with, a short discussion of the concept of *swirl* is required.

Swirl The swirl depends on the boundary conditions, including e.g. the blade pitch in the swirler at the combustor inlet. Usually, combustor designers define a swirl number S_N as a suitably normalized, dimensionless ratio of the axial flux of azimuthal momentum

[10] We recall we are dealing with premixed flames supported by a flow impinging from the side of unburnt gases. We discuss neither flames where the incoming flows of unburnt gases impinges from both sides of the flame, nor flames where fresh gases and combustion products are separately blown against the flame from opposite sides; in both cases, admittedly, flames may be both flat and stable -see Fig. 2.20 of [4]. Moreover, we should not identify our perfectly flat flame with a ***stagnation point*** flame; by definition, in fact, a stagnation point flame has zero ***total*** curvature everywhere -see eq. 2.89 and page 71 of [4]- i.e. (in our formalism) $K_{tot} = K + \frac{1}{r} = 0$ everywhere. As for the definition of total curvature, see our Appendix on flame velocity.

[11] See equation (12) in [129]. This equation is called *Grad-Shafranov* equation in [37].

and the axial flux of axial momentum, where both fluxes have been integrated on the combustor radius R_b. Generally speaking, the larger S_N, the more swirled the flow. In the case of negligible pressure jump, we have [1]:

$$S_N \equiv \frac{\int_0^{R_b} drr^2 v_z v_\chi}{R_b \int_0^{R_b} drrv_z^2}$$

Depending on the detailed combustor design, many approximate expressions of S_N are available. Usually, detailed computation of S_N is an output of full CFD computations. Generally speaking, however, and in agreement with physical intuition, it turns out that S_N is an increasing function of the angle between the direction of the flow at the exit of the swirler's blade and the axis of symmetry of the combustor, or, equivalently, of the angle β_{swirl} ($0 \leq \beta_{swirl} \leq \frac{\pi}{2}$)) between the swirler blade and the axis of symmetry of the combustor [1]. For example, if $\beta_{swirl} = 0 \left(\beta_{swirl} = \frac{\pi}{2}\right)$ then the axial flow of azimuthal momentum is negligibly small (infinitely large) with respect to the axial flow of axial momentum, and S_N goes to 0 (to ∞). Remarkably, the same holds also for the axial and azimuthal flow of mass: the larger β_{swirl}, the larger the azimuthal mass flow with respect to the axial mass flow.

In the language of equation (13.19), it is customary [37] to define the following dimensionless function of ψ:

$$q(\psi) \equiv \frac{1}{2\pi}\frac{d\varphi}{d\psi}$$

where

$$\varphi = \varphi(\psi) \equiv \int_{A_\psi} \frac{F}{r} d^2\mathrm{x} = 2\pi \int_{\psi_0}^{\psi} q(\psi')\, d\psi'$$

is the flux of the azimuthal component $v_\chi = \frac{F}{r}$ of $\mathbf{v}$ across the surface A_ψ bounded by $\psi(r,z) = \text{const.}$ in the meridian plane. Here the constant quantity ψ_0 plays the role of an extremum of integration.

Usually, regions with large *shear* (i.e. where $|\nabla \mathbf{v}|$ is large) correspond to large gradients of q. Moreover, it can be shown -see again Ref. [37]- that $q(\psi)$ is precisely the number of turns made by a flow line in the azimuthal direction per each closed loop made by the flow line in the meridian plane: as such, $q(\psi)$ goes to zero (to ∞) as S_N goes to zero (to ∞) and is a monotonically increasing function of S_N for all values of ψ. In contrast with S_N, however, $q(\psi)$ depends on ψ: it is therefore a local measure of the inclination of the flow lines. As such, it will be utilised in the following.

Thin

Now, the assumption of thin flame defined above allows us to give the words *flame-supporting flow* a precise meaning. For a thin flame, $G(\mathbf{x})$ is a steady state solution of the well-known *G-equation* [75]

$$\frac{\partial G}{\partial t} + \mathbf{v} \cdot \nabla G - s_L |\nabla G| = 0 \tag{13.20}$$

Here we have written the G-equation for a laminar flame; see [4] for its generalisation to a turbulent flame, which is essentially equivalent to (13.20) provided that we replace s_L with its turbulent counterpart s_T. Together, (13.20) in steady state [12] and the definition of $\mathbf{n}$ lead to the simple relationship [13]

$$\mathbf{v} \cdot \mathbf{n} = -s_L \tag{13.21}$$

This is the relationhip which links the flame shape (through $\mathbf{n}$), the flame velocity and the impinging flow. Stabilisation strategies against lift-off, flashback etc. refer to this relationship - and since $\mathbf{v}$ is swirled, this is also why we speak of *swirl-stabilised flames* here. Equation (13.21) satisfies the requirement of causality, as it ensures the upstream

[12] In the Appendix on the auxiliary relationships concerning stable flames we have exploited the thinness of the flame in order to reduce an integral on the flame surface to the sum of the contributions of the upstream and the downstream side of the flame. Here the flame thinness allows us to make a small error if we identify the generatrices of both the upstream and the downstream side of the flame with the same function G. This is equivalent to say that the difference between the solutions of equations (2) and (3) of [75] is small.

[13] There is a formal difficulty here. Strictly speaking, G is no Lagrangian coordinate, and equation (13.20) is therefore no allowable equation of motion in the framework of our variational problem, even in its simplified version (13.18). The fact that the constant value of G on the flame has no physical meaning allows us to overcome this difficulty. With no lack of generality, in fact, we may asusme this constant value to vanish identically on the flame. Then, straightforward algebra shows that if a function $y(\mathbf{x})$ solves (13.20) in steady state with $y = 0$ everywhere on the flame, then it solves also the Euler-Lagrange equation of the variational principle $\int d\mathbf{x} M_v = \min.$ with Lagrangian density $M_v \equiv \frac{y(\mathbf{v} \cdot \nabla y)^2}{2} - \frac{y s_L^2 |\nabla y|^2}{2}$ and Lagrangian coordinate y (here we take $\nabla s_L = 0$ for simplicity). Now, let us add $\int d\mathbf{x} \lambda M_v$ to the minimised quantity in (13.11) with λ Lagrange multiplier. We have therefore to solve the variational problem $\int d\mathbf{x}(L + \lambda M_v) = \min.$, which replaces (13.8). We retrieve (13.21) below as the Euler-Lagrange equation corresponding to λ. Moreover, all other Euler-Lagrange equations coincide with the Euler-Lagrange equations of (13.8) -so that (13.13) remains unaffected- provided that $\lambda = 0$. Physically, this agrees with the requirement of causality: in fact, it is the upstream flow which determines the shape of the flame.

flow -i.e., the flow before combustion has occurred- to rule flame shape and stabilty. This is why we focus our attention throughout this discussion on the upstream flow. Equation (13.21) has a further consequence, as it links flame stability and the impinging flow *just near the flame*. This suggests that the detailed pattern of upstream flow *far from the flame* affects the stability of the latter only weakly. It follows that even if the flame lies near a highly sheared region, we make a small error if we assume that $q \approx$ const. upstream far from the flame. We shall take advantage of this fact below.

We stress again the point that there is nothing special with s_L; in case of turbulent flame, we may just replace s_L with its turbulent counterpart s_T [2] here and in the following, provided at least that the concept of flame surface and of the related vector $\mathbf{n}$ still makes sense.

Together, (13.14), (13.21) and the definition of $\mathbf{n}$ provide us with the following equation

$$\frac{\partial \psi}{\partial r} + f' \frac{\partial \psi}{\partial z} - r s_L \sqrt{1 + f'^2} = 0 \tag{13.22}$$

Equation (13.22) holds at the flame -see Fig. 13.3. It is a connection among ψ, s_L and f, i.e. between the upstream flow, the microscopic physics of combustion and the shape of the flame respectively. This connection is of purely kinematic nature, and is satisfied at a flame with flame velocity s_L whenever the latter is fed by an upstream flow with stream function ψ. This is the looked-for meaning of the wordings *flame-supporting flow*.

Equation (13.22) is the third one out of the three above quoted, independent conditions required for the description of the shape of a stable, axisymmetric, swirl-stabilised flame: it is precisely the condition dictated by the requirement (13.20) of a thin flame.

The other two requirements are dictated by le Châtelier's principle and by the fact that the Mach number is low, i.e. by (13.18) and by (13.19) respectively.

As for (13.18), equations (13.15) and (13.21) make the variational principle to deal with a single integral with the same differential of integration variable dummy da.

As for (13.19), it links ψ and the boundary conditions -including the swirl.

Our search for a self-consistent description of the shape of stable, premixed, axisymmetric, swirled, thin flames is over. We are going to discuss some properties of such shapes in the following.

Before further discussion, however, we would like to stress an implicit but important consequence of the three conditions we have just found. Since they describe a humming-free configuration with the help of the relationships (13.21) and (13.22) which hold just at the flame, no detailed knowledge of the upstream flow far form the flame is explicitly

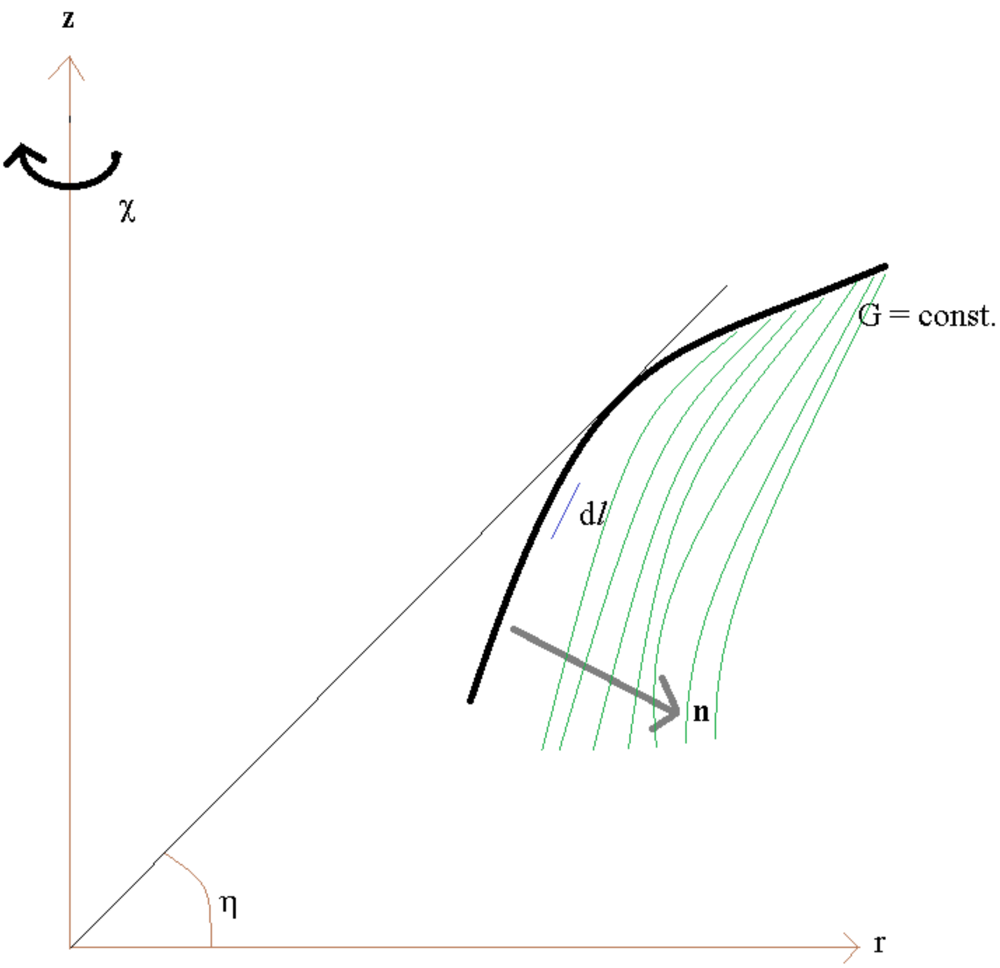

Figure 13.3: *The same as in Fig. 13.1, but with iso-ψ surfaces in addition. Green lines displays the intersection of iso-ψ surfaces with the meridian plane. At the flame, equation* (13.22) *links the derivatives of the streamfunction, the flame velocity and the slope of the flame generatrix $f(r)$. Detailed knowledge of ψ far upstream is not relevant here.*

involved. To put it in other words, knowledge of the solution ψ for (13.19) is required near to the flame only. According e.g. to (13.21), the only quantities relevant to stabilisation at each point of the flame are the local values both of flame velocity and of the angle between $\mathbf{n}$ and the tangent to the iso-ψ surfaces in the meridian plane. It follows that, far from the flame on the upstream side, we are allowed to content ourselves with approximate solutions for ψ only. We are going to take advantage of this possibility below. Finally, with the wordings *upstream flow* we are going to refer to a shortcut for *upstream flow near to the flame, which supports and stabilises it* in the following.

13.2.3 ...with non-negligible curvature

We are going to limit further our attention on two particular cases.

Firstly, we shall discuss flames with non-negligible curvature ($K \neq 0$ everywhere) and where the velocity $\mathbf{v}$ of the flow impinging on the flame is $\approx$ tangent to the flame -i.e. $\mathbf{v} \cdot \mathbf{n} \approx 0$- almost everywhere. The quantity $\mathbf{v} \cdot \mathbf{n}$ achieves its maximum value $\mathbf{v} \cdot \mathbf{n} = |\mathbf{v}|$ just at a location which we refer to as the *flame tip* in the following. Such flames are of practical interest in manufacturers' test-rigs as they resemble real GT combustors. As such, we are going to apply our result to a case of relevance to Ansaldo.

Secondly, we shall discuss stable flames with negligible curvature ($K \approx 0$ everywhere). Even if scarcely relevant to manufacturers of GT combustors, the discussion will allow us to retrieve some well-documented result of flame stability. We take this outcome as a further benchmark of our approach to flame stability focussed on thermodynamics.

13.3 Bistability...

Shapes of stable flames correspond to solutions of (13.18). In order to facilitate the search for such solution, we start with the discussion of the constraint (13.16). To this purpose, we rewrite (13.16) with the help of both (13.15) and the relationship $d\mathrm{a} = 2\pi r dl$ as follows:

$$\int K f' \mathbf{v} \cdot \mathbf{n} r dl = 0 \tag{13.23}$$

As for the flames with non-negligible curvature, the quantity $\mathbf{v} \cdot \mathbf{n}$ achieves its maximum value $\mathbf{v} \cdot \mathbf{n} = |\mathbf{v}|$ just at a location which we refer to as the *flame tip* in the following. If we denote with l_{tip} the value of the arc length at the tip, then the L.H.S. of (13.23) is ruled by the contribution of a neighbourhood of l_{tip}. Equation (13.23) is satisfied whenever Kf' is an odd function of $l - l_{tip}$. Two configurations are possible for a stable flame (*bistability*):

1. $K(l - l_{tip}) = -K(l_{tip} - l) \qquad f'(l - l_{tip}) = +f'(l_{tip} - l)$
2. $K(l - l_{tip}) = +K(l_{tip} - l) \qquad f'(l - l_{tip}) = -f'(l_{tip} - l)$

In configuration 1., $K = \dfrac{d\eta}{dl}$ changes sign at the tip, while $f' = \tan\eta$ does not. The opposite occurs in configuration 2.

Here we have written *configuration* and not just *flame* because equations (13.19) and (13.22) ensure that both the flame shape and the upstream flow differ in 1. and 2. Nevertheless, both configurations may correspond to the same value of the heat release, as the constraint (13.23) contains no explicit information on combustion.

Bistability follows straightforwardly from (13.8), i.e. from our application of Le Châtelier's principle to the description of humming-free, premixed, lean, subsonic, axisymmetric, swirl-stabilised, thin flames with non-negligible curvature. Remarkably, bistability is observed both in CFD simulation and in experiments [18] [12] [11] [15] -see Fig. 13.4. In the following, we are going to focus our attention precisely on system like those displayed in Fig. 13.4.

Finally, stability of configurations 1. and 2. implies that both correspond to a minimum of the heat release according to (13.11). Should the heat relase change then the selection rule (13.11) would dictate which configuration is selected by the system, just like in Biwa et al.'s experiment [28]. Now, two minima of the same quantity are usually separated by a maximum, which in our case corresponds to a maximally *unstable* configuration. A sharp growth of fluctuations at the commutation is therefore to be expected, in agreement with the reports of [12] and [16]. See for instance Fig. 13.5.

13.4 ...and commutation

13.4.1 A further simplification: highly elongated flames

Here we are going to discuss a possible transition (*commutation*) from configuration 1. to configuration 2. and back.

Commutation between different flame shapes, even if no humming occurs, is commonly observed in GT when raising power from ignition up to full power. It is even a good thing in some combustors, as the flame after commutation exhibits a much weaker combustion instability than the flame before commutation. It can also be said that if no commutation occurs -whatever the physical reason- then the expected amplitude of pressure fluctuations at full power is significantly larger than if commutation has occurred -compare Fig. 13.6 and Fig. 13.7. Indeed, we expect the flame to depend on a limited number of parameters, like the air flow rate, the temperature etc. But this is just a hope. In practice, there are hidden parameters -like the actual temperature of the walls of the combustion chamber, possible leaks etc.- which are beyond control today and are likely to remain beyond control in a foreseaable future. But even when all parameters are supposed to be well controlled (as in the lab), the flow itself may exhibit multiple states: bifurcations are possible. A thorough investigations of possible bifurcations in GT lies outside the scope of the present discussion. All the same, we are going to see that thermodynamics has a say.

We have seen that the selection rule which is relevant to the commutation is given by (13.11). In the discussion of (13.11) we have also shown that it is equivalent to minimisation of the flame area A_f for our problem. Generally speaking, configurations 1. and 2. share a common property: $|f'|$ is an even function of $l - l_{tip}$. Then, when it comes to compute the heat release - with the help e.g. of either the formula (10.1) or of its generalisation for turbulent flames - the integrand is the same for both the side $l < l_{tip}$ and the side $l > l_{tip}$ of the flame, provided that we neglect $\nabla_\| s_L$, or - which is the same

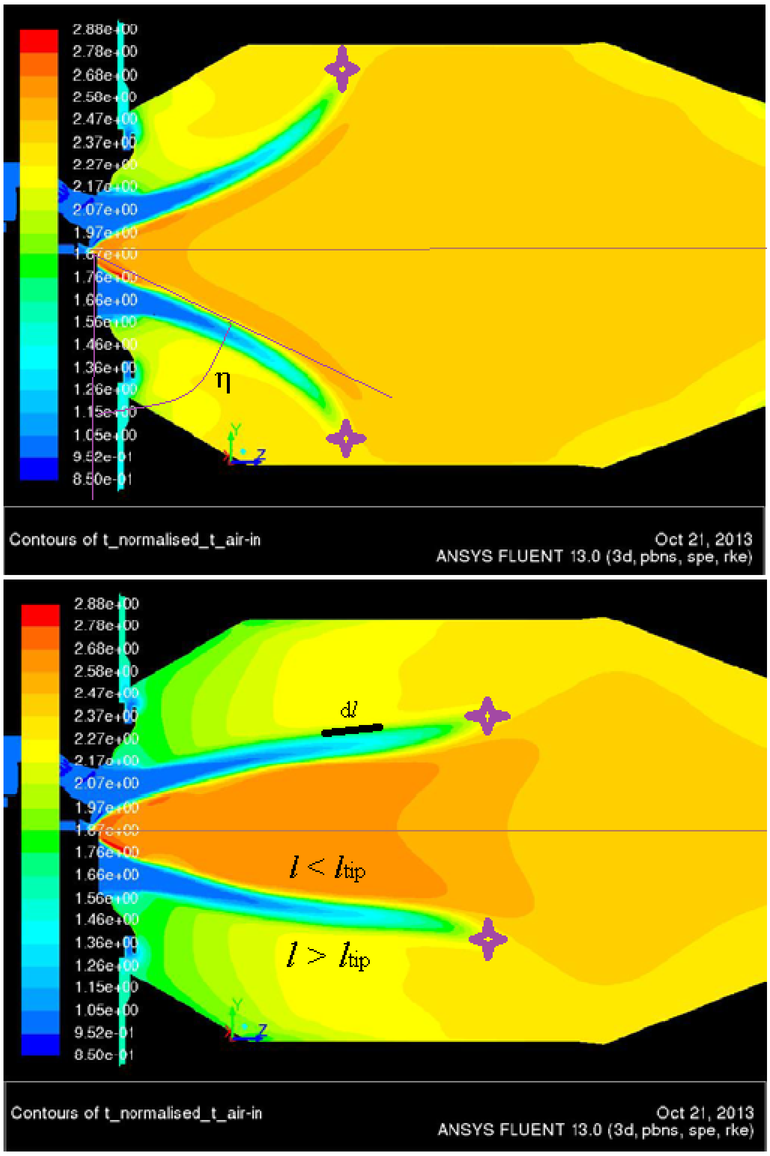

Figure 13.4: *Maps of normalised temperature computed in a axisymmetric combustor in configuration 1. (top) and configuration 2. (bottom). In both configurations: a) everything is symmetric with respect to the symmetry axis (the thin, brown, horizontal line); b) the upstream, impinging flow of unburnt gases is painted in blue and green; c) the boundary line between green and yellow represents the flame; d) violet stars shows the locations of the flame tips and correspond to* $l = l_{tip}$; *e)* $l < l_{tip}$ *on the side nearer to the symmetry axis; f)* $l > l_{tip}$ *on the side farther from the symmetry axis. The angle* η *is displayed at one point of the flame in config. 1. only for clarity. The small black segment represents an interval* dl *of curvilinear length. It is displayed in config. 2. only for clarity. As for 1., the flame shows its concavity and its convexity towards the upstream flow for* $l < l_{tip}$ *and* $l > l_{tip}$ *respectively, hence* K *changes sign at the flame tip. As for 2., the flame shows its concavity towards the upstream flow for both* $l < l_{tip}$ *and* $l > l_{tip}$*, i.e.* K *does not change sign at* $l = l_{tip}$*. Adapted from Ref. [15].*

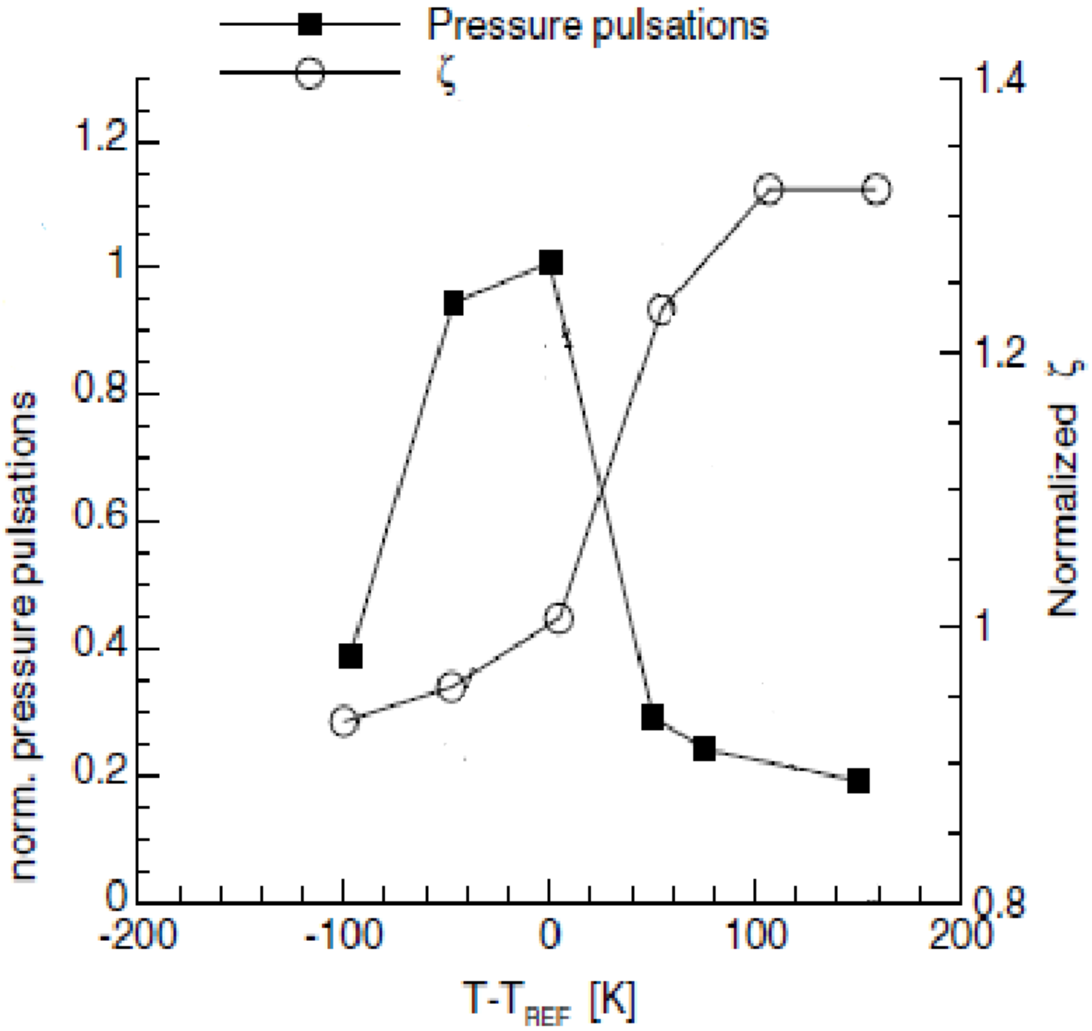

Figure 13.5: *Normalised pressure drop ζ across the flame and normalised humming amplitude vs. flame temperature, suitably rescaled with a constant additive factor $-T_{ref}$ (K). As for the meaning of* pressure drop across the flame, *see text. The values of temperature on the extreme left and the extreme right of the figure correspond to two stable configurations, with minimum humming amplitude. The latter has a maximum between them. -adapted from Ref. [12].*

because of (13.21) - provided that we neglect $\nabla_{\parallel}(\mathbf{v}\cdot\mathbf{n})$.

In turn, this makes sense because $\mathbf{v}\cdot\mathbf{n}\approx 0$ almost everywhere for *highly elongated* flames along a direction almost parallel to the axis of symmetry of the combustor for most of their surface, like those displayed in Fig. 13.4. Then, W_c reduces approximately to twice the contribution of one side of the flame (the two contributions are almost equal as the flame is thin). In the following we shall therefore consider just one side of the flame, namely the $l < l_{tip}$ side near to the *inner shear layer* (ISL) displayed in Fig. 2.9.

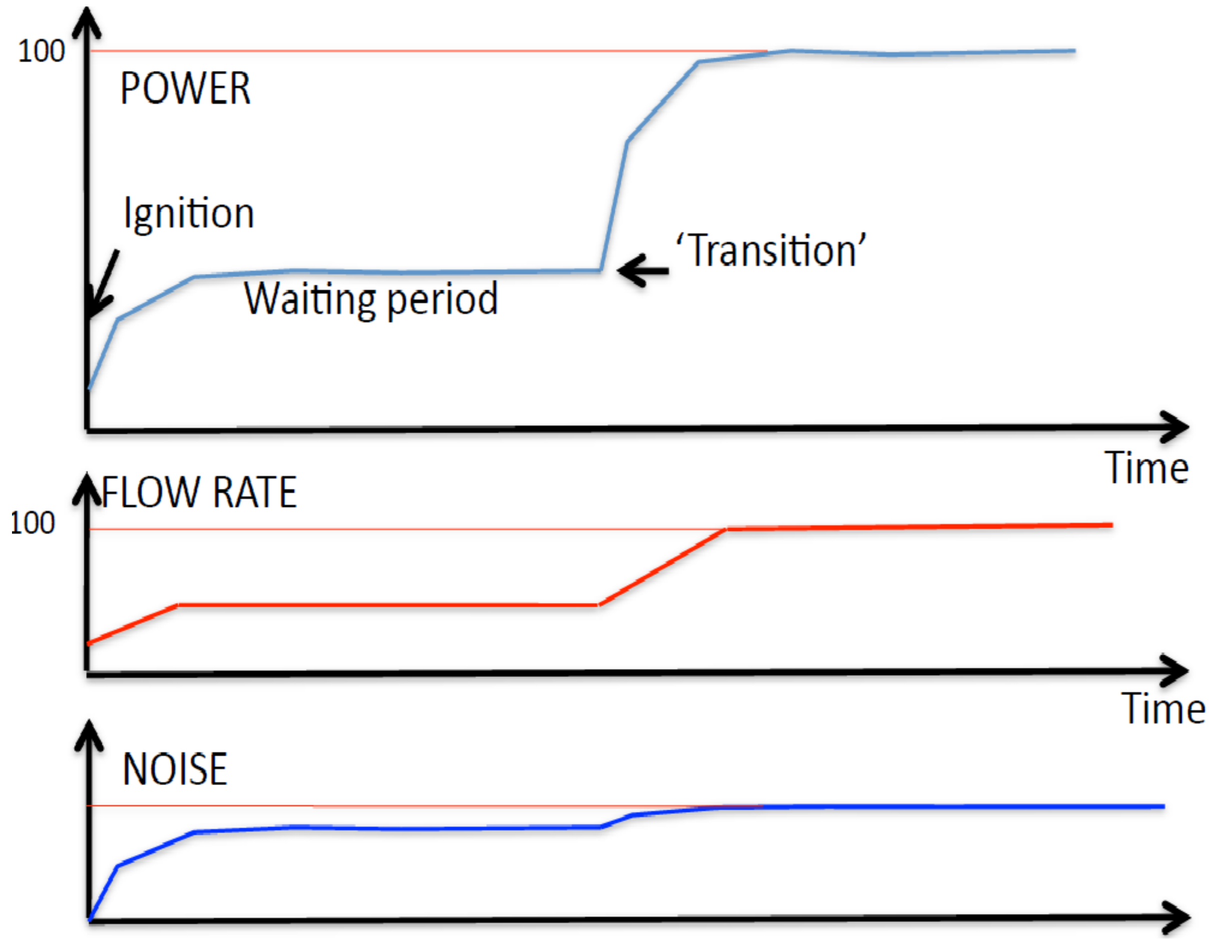

Figure 13.6: *Commutation (*transition*) occurs during load ramp up from ignition to full power in a GT - from Ref. [14].*

We select this particular side -rather than the flame side near the *outer shear layer* (OSL) displayed in the same Figure- even if the gradients of q are large at both layers, because it offers the concavity to the impinging flow, which is a common feature of configurations 1. and 2. and allows therefore meaningful comparison between them (these configurations differ from each other precisely because one of them offers concavity everywhere to the impinging flow, while the other one offers also convexity somewhere).

The price to be paid for our simplifying assumption of highly elongated flames is that we turn down full description of what happens in a neighbourhood of the flame tip. Physically, this make sense as far as the flame tip provides a small contribution to A_f, as minimisation of W_c is equivalent to minimisation of A_f. Thus, we are going to look for a minimum of the latter quantity, computed as twice the contribution of one flame side. Once we have neglected the contribution of the tip, for our elongated flames it makes sense to write $|f'| >> 1$. In turn, this leads to dramatic simplification.

Let us introduce the *opening angle* β between our flame and the direction of the axis of symmetry of the combustor, whose vertex is located at the *flame anchor point* on the

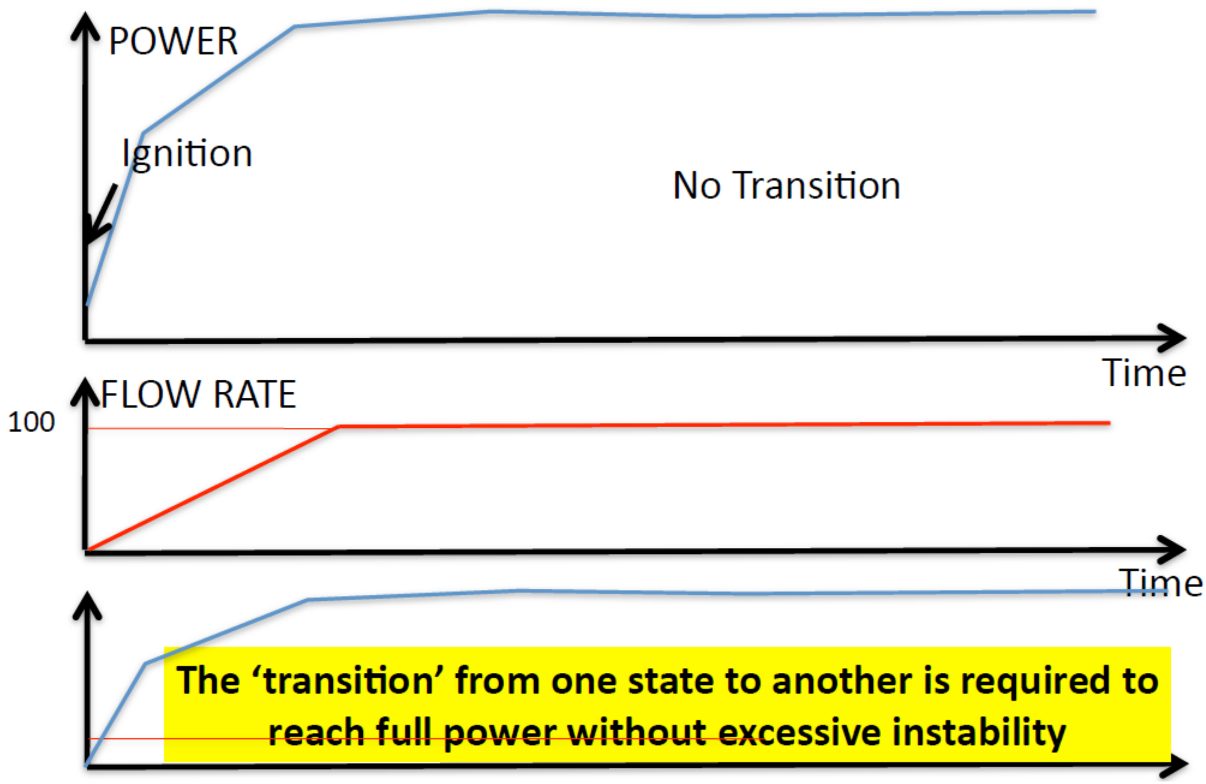

Figure 13.7: *No commutation occurs in the same GT load ramp of Fig. 13.6. All other things being equal, the fluctuation level (noise) at full power is significantly higher: the horizontal red line in the* noise *plot is the same of the* noise *plot in Fig. 13.6 - from Ref. [14].*

ISL side - we refer to Fig. 13.8, where the flame anchor point is defined as the point with coordinates $r = r_1, z = 0$. We are going to remove the ambiguity related to the words *our flame* below. Since we consider the contributions of the two sides to be essentially equal, we limit ourselves to the anchor point on the ISL side. This is equivalent to say that we consider the anchor points on the OSL and the ISL sides to be very near.

In particular, we assume that the value of the z coordinate for both anchor points is zero. Having in mind our treatment below of the commutation discussed in [15] - see Fig. 13.4 - this approximation is well justified. Admittedly, this assumption forces us to neglect the relevant case of detached flames, which can be related to PVC [14].

Accordingly, let it be clear that by *upstream region* we mean just the region embedded by ISL and OSL with black arrows in Fig. 2.9 (as the flame is located near the sheared layers) here and in the following. Correspondingly, ISL only is displayed in the following Figures (usually by a thickened, black, continuous line). Admittedly, a detailed description of the geometry of the upstream region is quite complicated, and requires full CFD treatment. Luckily, no matter how distorted and elongated the upstream region may be we need no such exact solution ψ of equation (13.19), because equation (13.21) ensures that only the upstream flow immediately near the flame is relevant to stability.

Finally, if the anchor point on the ISL side has a radial coordinate r_1 not too far from the symmetry axis $r = 0$, then we may safely write $\beta \approx \dfrac{\pi}{2} - \eta$.

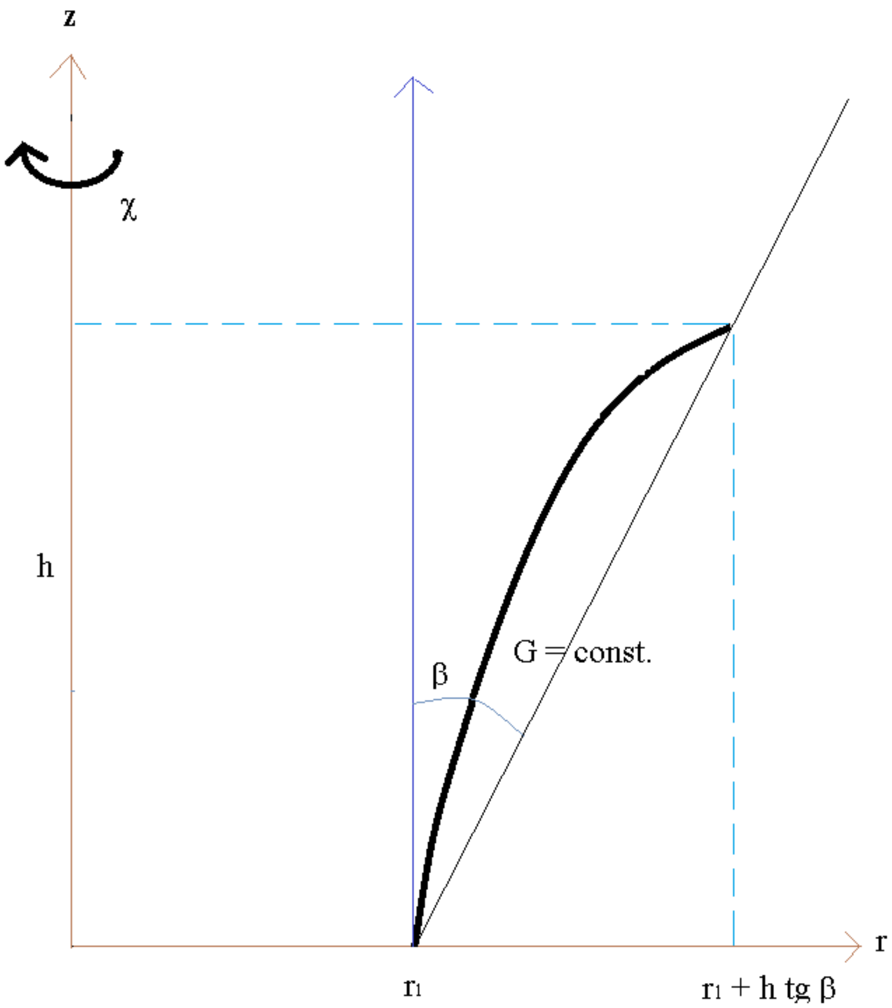

Figure 13.8: *Geometrical quantities for a highly elongated, axisymmetric flame. The ISL side of the flame referred to in Fig. 2.9 is displayed in the interval* $r_1 \le r \le r_1 + h\tan(\beta)$*, and* $\beta \approx \dfrac{\pi}{2} - \eta$ *for small* r_1 *- see both text and the Appendix on axisymmetric flames for details.*

For highly elongated flames along the direction of the symmetry axis, we may safely assume $\beta \approx \dfrac{\pi}{2} - \eta$ and $1 << |f'| = |\tan\eta| \approx \dfrac{1}{|\tan\beta|}$ provided that the radial coordinate r_1

of the flame anchor point on the ISL side of the flame is not too far from the symmetry axis $r = 0$. Accordingly, we take $\tan\beta << 1$. Axisymmetry allows us to assume $f' > 0$, hence $\tan\beta > 0$ with no loss of generality, and $0 < \beta << 1$. Since β is small, its absolute variation along the radial coordinate is also small. Accordingly, we make a small error by taking $\beta \approx$ const. along the whole flame side; we *define* it by requiring that the two points $(r = r_1, z = 0)$ and $(r = r_1 + h\tan\beta, z = h)$ in the meridian (r, z) plane belong to the flame surface $G = const.$, i.e. that:

$$f\left(r = r_1\right) = 0 \tag{13.24}$$

$$f\left(r = r_1 + h\tan\beta\right) = h \tag{13.25}$$

where we have introduced a typical elongation length of the azimuthal flow in the upstream zone

$$h \equiv \frac{\varphi}{\frac{d\varphi}{dz}}$$

which plays the role of typical length of the system flame + upstream zone along the direction of the symmetry axis [14]. Remarkably, indeed, *both* the flame and the upstream flow are quite elongated -again, see Fig. 13.4. Our strategy is to take advantage this fact in order to derive from both equations (13.19), (13.22) and from the smallness of $\tan\beta$ a single equation for $\tan\beta$. Then, we are going to show that each solution corresponds to a different solution of the Euler-Lagrange equations of the variational principle (13.18). Depending on the swirl number and other parameters, the system switches to the configuration which corresponds to a minimum of the combustion heat release, i.e. -according to (13.12)- to a minimum of A_f.

13.4.2 *Open* vs. *closed* configurations...

In agreement with our discussion on bistability, we apply equations (13.19) and (13.22) to a flame with non-negligible curvature and to the corresponding upstream flow and show in the Appendix on the auxiliary relationships concerning axisymmetric flames that two real distinct solutions for $\tan\beta$ may exist:

[14] This is definitely not to say that the flame actually extends from $z = 0$ up to $z = h\tan\beta$, as the boundary conditions (13.24) and (13.25) are only useful to find the flame shape. The actual size of the flame where combustion occurs affects the flame area and, consequently, the heat release. This point is to be discussed below, in the Section concerned with the quantity r_{max}.

$$\tan\beta_{\pm} = \frac{\Gamma \pm \sqrt{\Gamma^2 - 4\left(\Gamma + \frac{1}{2}\right)}}{2\Gamma + 1} \tag{13.26}$$

where we have defined the positive-definite dimensionless quantity

$$\Gamma \equiv \left(\frac{S_w}{h}\right)^2 \frac{(2\pi\psi_0)}{s_L}$$

Here the dimensionless quantity $S_w \equiv \sqrt{2\pi q(\psi_0)\frac{1}{\psi_b - \psi_0}\int_{\psi_0}^{\psi_b} q d\psi}$, the length $h \equiv \frac{\varphi}{\frac{d\varphi}{dz}}$ and the positive-definite quantity ψ_0 increase with increasing swirl number S_N, increasing elongation of the upstream flow along the axial direction and increasing total flux impinging on the flame respectively. For our applications, we show in the Appendix on the auxiliary relationships concerning axisymmetric flames that we can take $\psi_0 > \psi_b = 0$ with no loss of generality. We discuss in detail the connection between S_w and S_N in the following.

Equations (10.1), (13.15) and (13.21) lead to the order-of-magnitude estimates $2\pi\psi_0 = s_L A_f = \frac{W_c}{H\rho_u Y_{fuel}}$, i.e. $\Gamma = \left(\frac{S_w}{h}\right)^2 \frac{W_c}{H\rho_u Y_{fuel} s_L}$. This is equivalent to:

$$\Gamma = \frac{\pi k^2}{12}\frac{\sqrt{1+\tan^2\beta}}{\tan\beta} \tag{13.27}$$

where we have defined $k \equiv \frac{\sqrt{3}S_w D_b}{h}$ with $D_b = 2\cdot R_b$ combustor diameter, and we have invoked the identity $\sin\beta = \frac{\tan\beta}{\sqrt{1+\tan^2\beta}}$. In fact, equation (13.21) allows us to write $s_L = v_z \sin\beta$ as $\mathbf{v} \approx v_z \mathbf{e}_z$ for the upstream flow, and the typical axial velocity v_z is just equal to $2\pi\psi_0\left(\pi\frac{D_b^2}{4}\right)^{-1} = \frac{W_c}{H_{LHV}\rho_u Y_{fuel}}\left(\pi\frac{D_b^2}{4}\right)^{-1}$.

Indeed, when deriving (13.26) we have tacitly assumed $q \approx$ const. This is justified as far as we consider the bulk of the upstream flow far from both ISL and OSL, as gradients of q are relevant at shear layers by definition. Since we are allowed to content ourselves with approximate solutions for ψ far from the flame on the upstream side, our assumption $q \approx$ const. leads to a small error as far as flame stability is concerned.

Together, equations (13.26) and (13.27) link β and k. Of course only real values of β are physically allowable.

According to (13.26):

- if $\Gamma < 2 + \sqrt{6}$ there is no real solution for β, i.e. no stable configuration may exist;
- if $\Gamma > 2 + \sqrt{6}$ two real solutions β_- and $\beta_+ > \beta_-$ for β exist, i.e. two distinct configurations are candidate to stability. We refer to the configurations with β_+ and β_- as to *open* and *closed* configurations respectively in the following.

Fig. 13.9 displays the dependence of β_- and β_- on k. Physically, k increases with increasing swirl number S_N (as S_w is an increasing function of S_N), with increasing combustor diameter D_b and decreasing elongation h of the upstream zone. In turn, the lower the elongation [15] the larger β, and according to equation (13.21) the larger β the larger s_L for given impinging flow $\mathbf{v}$ [16].

Fig. 13.9 shows that no stable solution exists if the swirl is too small, in agreement with the general consensus about swirl stabilisation. We conclude that a minimum amount of swirl is required in order to allow existence of stable, premixed, thin, axisymmetric, elongated flames with non-negligible curvature. In this case, the selection rule $A_f = \min.$ - equivalent to (13.11) for the purpose of our discussion - dictates which configuration is actually stable. As we have seen, the constraints of fixed V_f and T_f on (13.11) are automatically satisfied for thin flames with given profiles of temperature across the flame. In order to compute the heat release, we need an expression for f in each case. To this purpose, we need the solutions of the variational principle (13.18) which follows from (13.11).

13.4.3 ...and the corresponding shapes

Together with the definitions of the curvature K and of the area differential da, relationships (13.15), (13.18) and (13.21) lead to:

$$\delta \int L_r dr = 0 \tag{13.28}$$

where we have neglected $\nabla_{\|} s_L$, as usual by now, we have divided everything by s_L and we have defined both $\mu \equiv \dfrac{2\pi\theta}{s_L}$ and

$$L_r \equiv \frac{f'' f' r}{1 + (f')^2} + \mu r \sqrt{1 + (f')^2}$$

[15] See the scaling $\dfrac{z}{h} = \tan\beta$ in the Appendix on the auxiliary relationships concerning axisymmetric flames for given flame position $f = z$

[16] The dependence of Γ on the square of S_w and h follows from the non-linearity of equation (13.19). It means that the actual direction of rotation (clockwise or counterclockwise)of the swirled flow around the axis of symmetry of the combustor is not relevant in the following, just as expected because of axisymmetry.

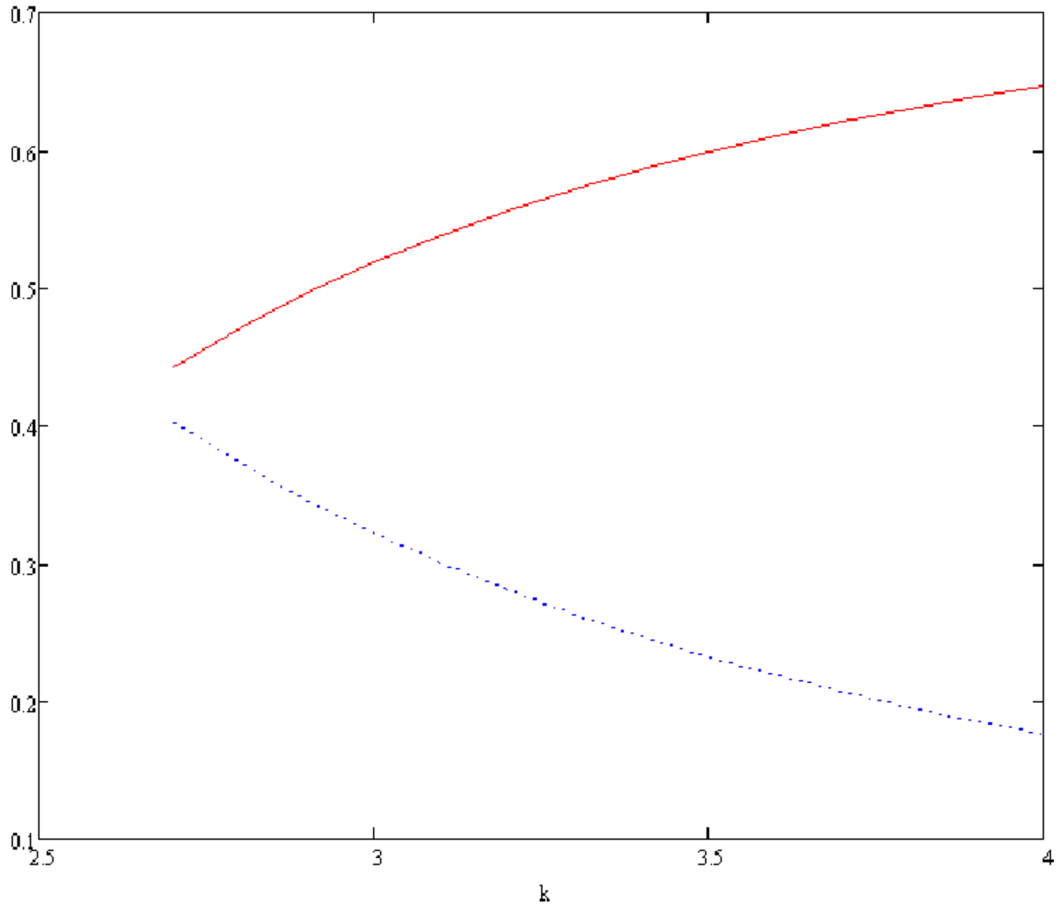

Figure 13.9: β_+ *(red) and* β_- *(dotted blue) vs.* k*. If the swirl is so small that* $k < 2.7$*, corresponding to* $\Gamma < 2 + \sqrt{6}$*, then no real solution exists.*

If the boundary conditions on the Lagrangian coordinate $f(r)$ are assigned, then the Euler-Lagrange equation of the variational problem (13.28) in the $f' >> 1$ limit reduce to

$$f'' + \mu\,(f')^2 = 0$$

As for the boundary conditions, we take (13.24) and (13.25). Then, the solution of the Euler-Lagrange equation is:

$$f(r) = \frac{1}{\mu} \ln \left[1 + \frac{r - r_1}{h \tan \beta} \left(e^{\mu h} - 1 \right) \right] \tag{13.29}$$

Equation (13.29) links $f(r)$, r_1, μ, β and h and provides us with the shape of the ISL side of a stable flame (far from the flame tip at least) [17]. We are going to refer to such shape as to the *flame shape* below, for brevity. Accordingly, the flame shape in an open configuration differs from the flame shape in a closed configurations. Correspondingly, there are different values μ_+, μ_- for μ, etc.

Remarkably, the insofar overlooked assumption of negligible viscosity provides us with a further link of μ and β. Negligible viscosity implies that commutation conserves circuitation, i.e. the flux of vorticity $\nabla \wedge \mathbf{v}$. In particular, commutation conserves the axial flux of vorticity $\approx \pi \left(\frac{D_b^2}{4} \right) \mathbf{e}_z \cdot \nabla \wedge \mathbf{v}$ in a combustor with diameter D_b. As for the order of magnitude, we may write $\mathbf{e}_z \cdot \nabla \wedge \mathbf{v} \approx \mu v_z$, because $\frac{1}{\mu}$ is the only quantity with the dimensions of a length which appears in L_r. Moreover, $s_L = v_z \sin \beta$ in highly elongated flames with small r_1 because of equation (13.21) and of $\beta \approx \frac{\pi}{2} - \eta$. Finally, as far as we are interested in flame shapes only and leave temperature profiles unaffected inside the flame, commutation leaves s_L unaffected. Then, conservation of the axial flux of vorticity implies:

$$\frac{\mu_+}{\sin \beta_+} = \frac{\mu_-}{\sin \beta_-} \tag{13.30}$$

At its face value, admittedly, this result seems to be just a meaningless trick. Indeed, we have not solved the equation of motion (6.2) - we have not even solved equation (13.19) for the stream function; all the same, we claim to link the shape of the upstream flow before and after commutation. Of course, it is perfectly possible - it is even likely - that vorticity is *not* proportional to velocity with a proportionality factor which is constant across the upstream region of the fluid, neither before nor after commutation. However, here is where our discussion of bistability turns out to be useful. The existence of two distinct configurations for flames with non-negligible curvature, as well as the existence of a selection rule of selection between them, is a result of thermodynamics. As such, it is no matter of detailed description of the flow. Such description is needed when details are investigated for a given set of operational and geometrical conditions of a particular combustor. But if we try to answer to questions concerning e.g. the impact of the swirl number on commutation, firm thermodynamical grounds spare us the trouble of computing more-or-less exact solutions of the equation of motion.

Finally, our knowledge of the flame shape -equation (13.29)- allows us to compute the value of A_f to be minimised. Free parameters are the anchor point r_1, the elongation of

[17] Starting from (13.29), it is easy to see that $|f'| >> 1$ in the limit of small $\tan \beta$, just as expected.

the supporting recirculation zone h and the quantity k, which, together with h, encompasses the effects of the swirl, the flame velocity and the combustor diameter. Once k is known, equations (13.26), (13.27) and (13.30) give both the β's (if they exist as physically acceptable, i.e. real values) and the ratio of the μ's. Once one of the μ's -say, μ_+- is known, h and r_1 allow computation of $f(r)$ for both open and closed configurations with equation (13.29). Since we are going to discuss firstly the commutation from open to closed configuration, we start from μ_+, which describes the structure of the upstream flow in open configuration, i.e. before the commutation. The stable configuration is the configuration with the lower A_f. Since the contribution of the flame tip to

$$A_f = \int \mathrm{da} = \int_{\mathrm{ISL}} \mathrm{da} + \int_{\mathrm{OSL}} \mathrm{da} = 2 \cdot \int_{\mathrm{ISL}} \mathrm{da} = 2 \cdot (2\pi) \int_{r_1}^{r_{max}} r\sqrt{1+f'^2}dr \quad (13.31)$$

is neglected, computation of A_f reduces to an integral in dr on some interval $r_1 \leq r \leq r_{max}$. (The factor 2 comes from the fact that A_f is twice the contribution of just one flame side). In the following, we are going to discuss both the physical meaning of r_{max} and an example of transition from open to closed configurations as k varies for a physically reasonable choice of r_1, r_{max} and μ_+ in a particular problem where commutation has been thoroughly investigated both experimentally and numerically [15].

13.4.4 From *open* to *closed*...

Choosing r_1, r_{max} and μ_+

Estimate of r_1 We start from the open configuration discussed in [15], which discusses premixed, lean, axisymmetric, swirled, thin flames with non-negligible curvature. In particular, we refer to Fig. 10 and 12 of this paper. Both figures show that the flame shape is basically the same on both sides of the flame tip. However, the ISL and the OSL side of the flame do not exactly coincide near the inlet, in contrast with our assumption underlying (13.31); accordingly, we take r_1 to be somehow in the middle between the two layers. Then, Fig. 12 makes it reasonable to take the radial coordinate r_1 of the anchor point at about one tenth of the combustor diameter -see Fig. 13.10. A similar estimate holds also for the closed configuration depicted in Fig. 13 of the same paper. Then, we write:.

$$r_1 = 0.1 \cdot D_b \quad (13.32)$$

Estimate of r_{max} Fig. 10 shows that the reaction rate is quite strongly peaked near the anchor point. Admittedly, this is in contradiction with our assumption of negligible $\nabla_{\|} s_L$. In order to overcome this obstacle, we make the (simplifying!) assumption that

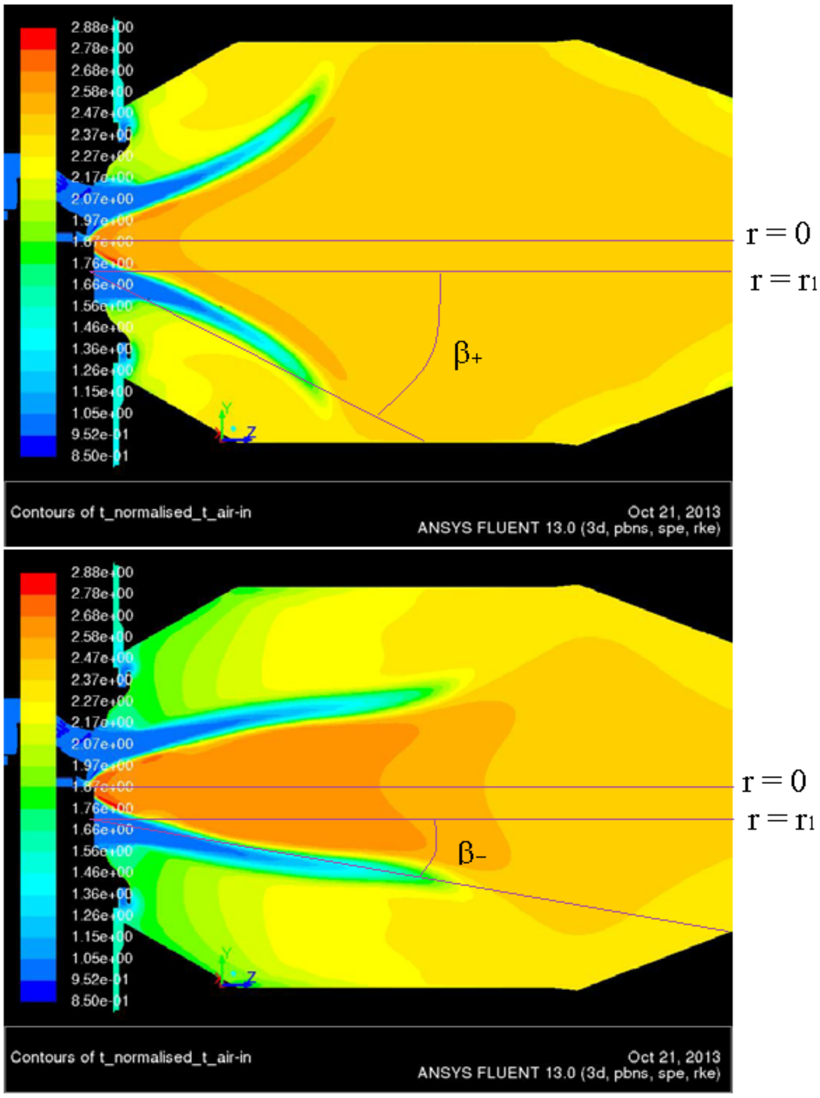

Figure 13.10: *Fig. 12 and 13 of Ref. [15]. Both r_1, β (not in scale) and the temperature map are displayed in open and closed configuration. The symmetry axis corresponds to* $r = 0$.

combustion occurs just in a small neighbourhood of the anchor point.

When looking at its face value, admittedly, this assumption seems no less devoid of physical meaning than the assumption of negligible $\nabla_{\parallel} s_L$ it is supposed to improve upon. However, we are focussing on commutation, which is a fast process [18]. It is therefore quite reasonable to take the distribution of heat release on the flame to be the same on both confiurations immediately before and after the commutation: *there is just no time available to change it during the commutation.*

In particular, if the reaction rate of the chemical reactions ruling heat release is peaked near the anchor point before commutation, the same will be true after commutation too.

[18]Indeed, when observed on Ansaldo combustors commutation is not slower than 1 second [15].

We can take into account of this fact in our formalism by taking the same value of r_{max} in (13.31) before and after commutation, i.e. for both open and close configuration. The only commutation-relevant parameter becomes therefore $\tan\beta$, whose physical meaning becomes also perfectly unambiguous: $\tan\beta$ is the flame slope at the anchor point.

The choice of not-too-large an interval of r_1 has two further advantages:

- it allows us to get rid of the unphysical assumption of uniform flame velocity all along the flame;
- it allows us to represent (qualitatively) the impact of the so called *pilot flame*, an auxiliary, non-premixed flame near the symmetry axis which helps control of the larger flame. Actually, it is the pilot mass flow rate which drives commutation in the experiments reported in [15].

In particular, when looking at the region of largest reaction rate in Fig. 10 we feel allowed to take:

$$r_{max} = 1.3 \cdot r_1 \tag{13.33}$$

A similar estimate holds also for the closed configuration depicted in Fig. 11 of the same paper - see Fig. 13.11.

Estimate of μ_+ When discussing commutation from open to closed configuration, explicit computation of A_f in open and closed configuration is needed; in turn, this requires explicit evaluation of μ_+. Physically, this is equivalent to provide information on the actual structure of the upstream flow pattern before the commutation. Equation (13.30) ensures that this structure in open configuration differs from the structure in closed configuration. Here it is worthwhile to stress once again the point that the commutation is a change in the whole structure of the configuration made of the flame and of the flow supporting it.

Once again, we take advantage of the fact that no detailed knowledge of such pattern is required far upstream, as far as equation (13.26) reflects the impact of the interaction between the upstream flow and the flame. Thus, even if the geometry of the upstream flow in Fig. 2.9 is quite compicated and distorted geometry, to our purposes it is enough to recall that the flame lies near a shear layer where $|\frac{dq}{d\psi}| >> 1$ is large, where the flow far upstream has neglibible $|\frac{dq}{d\psi}|$. It is therefore enough to provide for the upstream flow a description which satisfies the condition $|\frac{dq}{d\psi}| \approx 0$. For the sake of mathematical convenience, we neglect the distortion of the upstream flow pattern altogether, and depict it as a simple vortex with egg-like cross-section in the meridial plane - see Fig. 13.12.

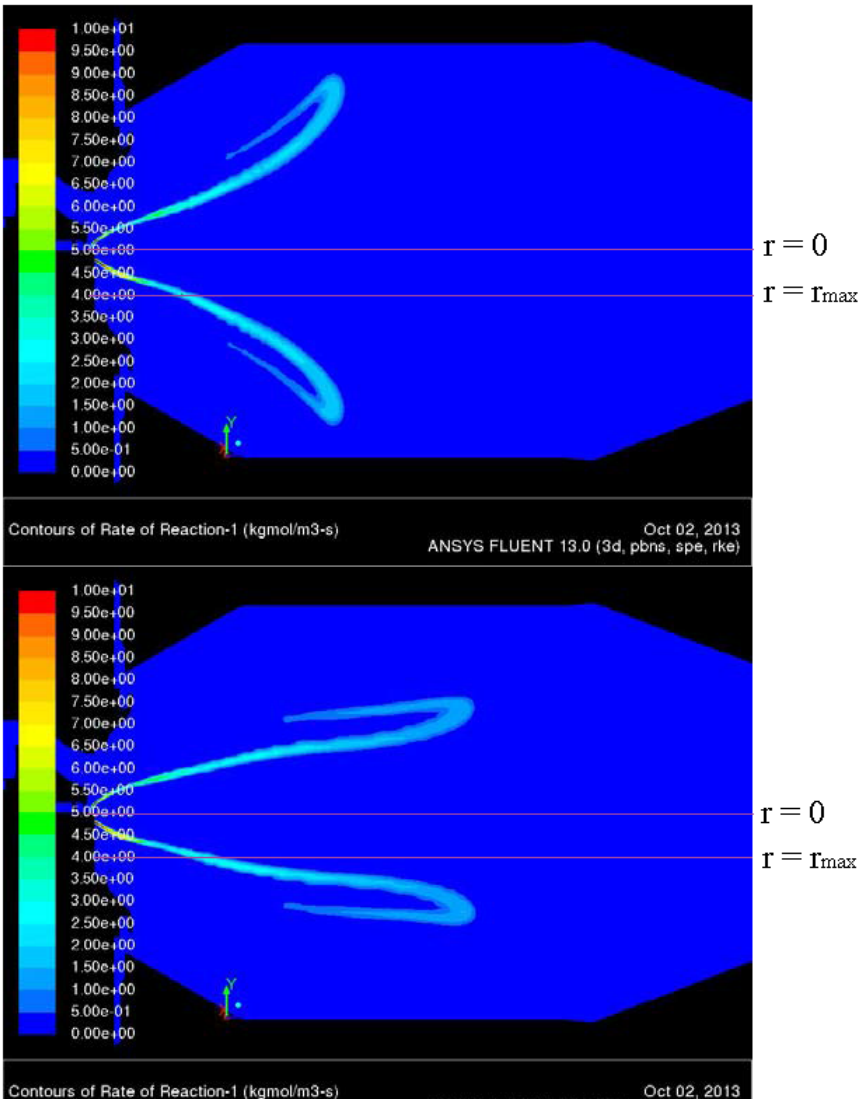

Figure 13.11: *Fig. 10 and 11 of Ref. [15]; both r_{max} (not in scale) and the map of reaction rate for air-methane combustion are displayed in open and closed configuration. The symmetry axis corresponds to $r = 0$.*

This way, admittedly, we neglect the OSL altogether. However, the resulting error seems to leave the validity of our discussion unaffected, as far as bistability (described by (13.26)) and commutation (described by minimisation of A_f in (13.31)) are concerned.

Now, our discussion includes two further steps:

- we provide some information concerning the vortex;
- we show that it satisfies the condition $|\frac{dq}{d\psi}| \approx 0$.

If we denote with $2 \cdot R_{vort}$ the radial size of the upstream flow pattern with radius R_{vort}, then an estimate of the distance R_{in} of this structure from the symmetry axis of

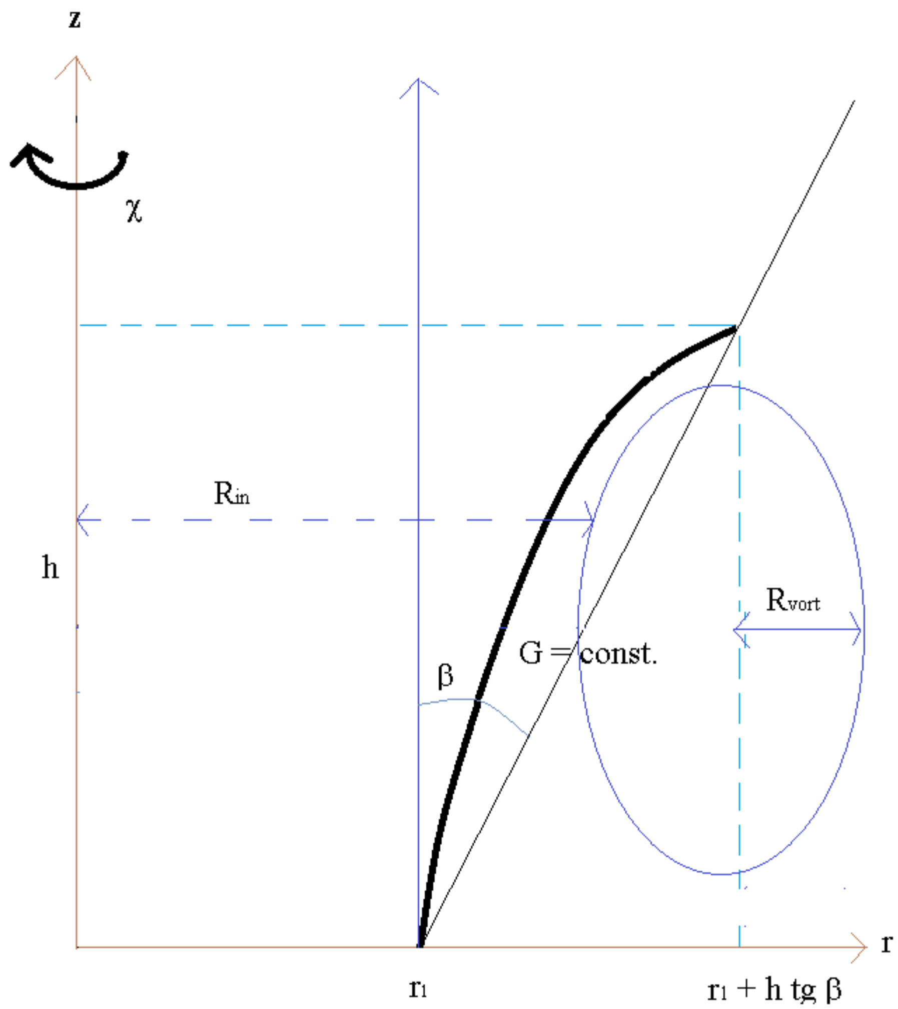

Figure 13.12: *In the meridian plane, the cross-section of an equi-ψ surface in the upstream region where* $|\frac{dq}{d\psi}| \approx 0$ *is displayed as an egg-like closed contour (blue). As for the z-dependen quantities* R_{in} *and* R_{vort}*, see text. All other things are the same as in Fig. 13.8.*

the combustor is given by:

$$2 \cdot R_{vort}(z) + R_{in}(z) = \frac{D_b(z)}{2}$$

where we have explicitly taken into account the dependence of all quantities on the axial coordinate z. This means that the combustor radius $\frac{D_b}{2}$ is the sum of the radial size of the upstream flow structure and of the distance of the latter from the symmetry axis of the combustor. Physically, this refers to the obvious (but not yet invoked) fact that the combustor embeds the upstream flow.

An expression for the z-averaged value R_v of R_{vort} is of interest, as the same dimensional reasons leading to equation (13.30) allow us to write

$$\mu = \frac{c_\mu}{R_v}$$

with c_μ constant, dimensionless quantity to be determined. To this purpose, we assume D_b = const. along z for simplicity, so that after z-averaging of both sides of the relationship above we may write:

$$2 \cdot R_v = \frac{D_b}{2} - R_i$$

where a rough estimate for the z-averaged value R_i of R_{in} is:

$$R_i = \frac{R_{in}(z=0) + R_{in}(z=h)}{2}$$

with:

$$R_{in}(z=0) = r_1 \quad \text{and} \quad R_{in}(z=h) = r_1 + h \cdot \tan^2 \beta$$

Remarkably, the latter choices for $R_{in}(z=0)$ and $R_{in}(z=h)$ recall the boundary condition on r_1 (which has led to equation (13.29)) and the scaling (33) discussed in the final lines of the Appendix on the auxiliary relationships concerning axisymmetric flames. In turn, this reflects the fact that just one quantity β describes the whole configuration in our discussion, even if the elongation of the upstream flow pattern differs from the elongation of the flame.

As for the value R_+ of R_v in the open configuration, the relationships above lead to:

$$R_+ = \frac{D_b}{4} - \frac{r_1}{2} - \frac{h \tan^2 \beta_+}{4} \tag{13.34}$$

In order to compute

$$\mu_+ = \frac{c_\mu}{R_+} \tag{13.35}$$

we have yet to evaluate c_μ. Now, according to p. 330, Sec. 12.C of Ref. [130] [19], the value

$$c_\mu = 4.493 \tag{13.36}$$

corresponds to a solution of equation (13.19) which satisfies the requirement $q(\psi) \approx$ const. stated above. In particular, we have

$$0.72 \leq q(\psi) \leq 0.82$$

everywhere across the upstream zone. Together, equations (13.26), (13.27), (13.29), (13.30) (13.31),(13.32), (13.33), (13.34), (13.35) and (13.36) allow us to look for the minimum of A_f as the latter quantity changes with varying values of the swirl-related dimensionless quantity k both in open and closed configuration.

Swirl number

For the quasi-uniform values of $q(\psi)$ found above, the definition of S_w gives:

$$S_w \approx 2.2 \cdot \sqrt{q(\psi_0)} \tag{13.37}$$

where $q(\psi_0)$ represent the actual swirl acting on the flame as the latter is stabilised near a high-shear layer. This value may differ from the values 0.72 - 0.82 inside the upstream zone, as $\psi_0 >> \psi$ inside that zone -see Appendix on axisymmetric flames.

This fact provides us with a link between the swirl-related quantities k and S_w we have introduced above and the familiar swirl number S_N. To this purpose, we recall that $q = q(\psi_0)$ is the number of turns made by a flow line in the azimuthal direction per each closed loop made by the flow line in the meridian plane. As for the open configuration before commutation, an estimate for $q(\psi_0)$ is [37]:

[19] Again, we take advantage of a formal result for $q(\psi)$ from magnetohydrodynamics. In particular, the result we refer to here holds for a solution of the equation $\nabla \wedge \mathbf{v} = \mu \mathbf{v}$, whose axisymmetric version is a particular case of equation (13.19).

$$q(\psi_0) = \frac{\text{radius of one turn in the meridian plane}}{\text{radius of one turn in the azimuthal plane}} \cdot \frac{v_\chi}{v_z} \approx \frac{R_+}{R_b} \tan \beta_{swirl} \tag{13.38}$$

where the definition of β_{swirl} allows us to write:

$$\frac{v_\chi}{v_z} \approx \tan \beta_{swirl} \tag{13.39}$$

and the simple, following relationship holds [20] [1]:

$$S_N = \frac{2}{3} \tan \beta_{swirl} \tag{13.40}$$

links $\tan \beta_{swirl} \approx \frac{v_\chi}{v_z}$ and the swirl number S_N. Relationships (13.37), (13.38) and (13.40) give:

$$S_N \approx 0.14 \cdot \frac{R_b}{R_+} S_w^2 = 0.02 \cdot \frac{D_b}{R_+} \left(\frac{h}{D_b}\right)^2 k^2 \tag{13.41}$$

Together, relationships (13.34) and (13.41) give the connection between k, S_w and S_N.

13.4.5 Commutation vs. heat release

As for the impact of heat release W_c on commutation, generally speaking W_c increases with increasing A_f. Now, Fig. 13.13 displays A_f vs. k at different values of S_N for both the open configuration $\beta = \beta_+$, $\mu = \mu_+$ and the closed configuration $\beta = \beta_-$, $\mu = \mu_-$. At fixed S_N, A_f decreases with increasing k in both open and closed configuration. Now, under the same condition $k \propto \frac{D_b}{h}$. Then, we may say that W_c is an increasing function of the normalised elongation $\frac{h}{D_b} \propto \frac{1}{k}$, i.e. both A_f and W_c decrease with increasing k. In Fig. 13.13, raising W_c corresponds therefore to going from right to left along the horizontal axis.

Note that the problem of what happens as W_c changes at fixed S_N is of great practical relevance, as the market makes the manufacturers to design GT with very low park load

[20] for axial swirlers at least. But even in radial swirlers, S_N remains proportional to the tangent of an average angle of the flow at the exit of the blades. See equations (4) and (5) of Ref. [1].

and very high ramp gradient. This means that the same combustor with the same swirler blade angle β_{swirl} (and, correspondingly, the same S_N according to (13.40)) is supposed to wrk with flames at very different values of W_c.

Let us denote with k_{cr} the value of k such that $A_{f+} = A_{f-}$. In Fig. 13.13, k_{cr} is the value of the horizontal coordinate of the point of intersection between the continuous line and the dotted line. The same figure shows that $A_{f+} < A_{f-}$ -i.e., the open configuration is stable- if and only if $k > k_{cr}$ -i.e., W_c is not too large. When W_c exceeds this threshold the situation is reverted and the closed configuration becomes stable, i.e. commutation occurs. We conclude that raising the heat release W_c at fixed swirl number S_N leads the system to commutation. Our result is in agreement with everyday GT experience, where commutation from open to closed configuration occurs during the ramp in heat release [15].

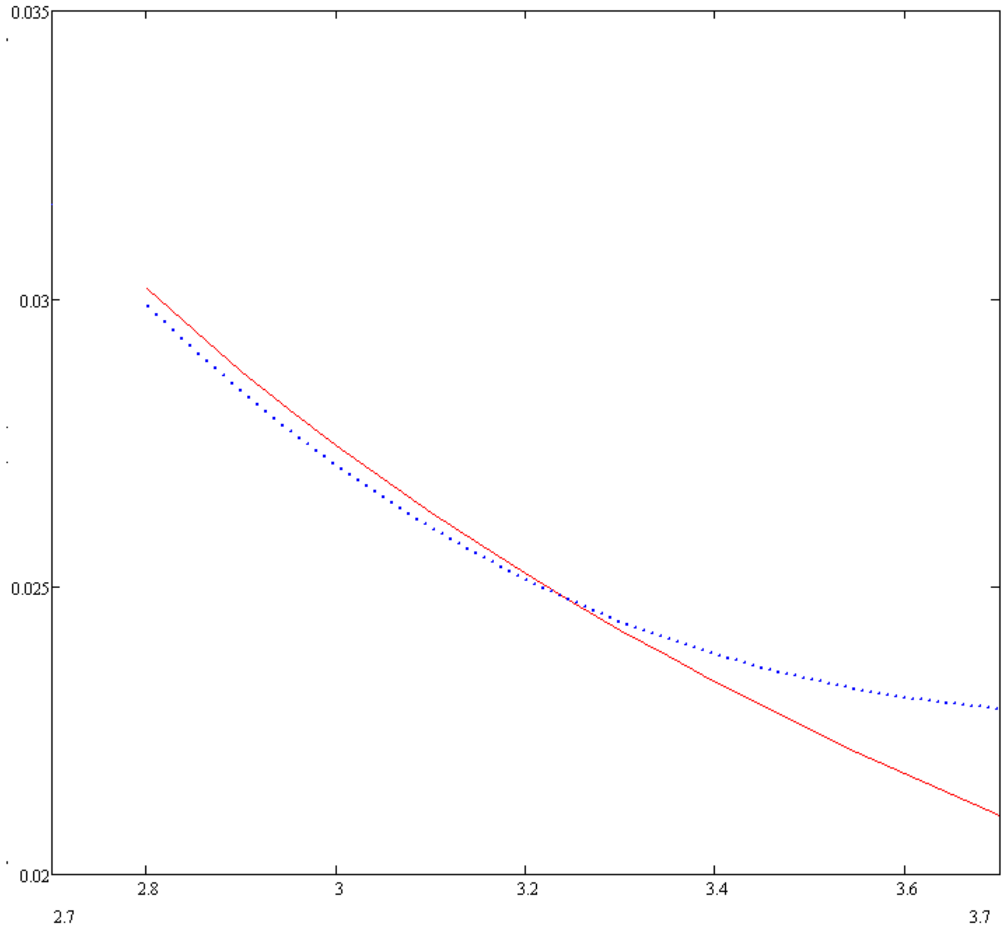

Figure 13.13: *A_f (arbitrary units, vertical axis) vs. k (horizontal axis) at S_N = 0.5 for open configuration (continuous line) and closed configuration (dotted line).*

13.4.6 Commutation vs. swirl number

As for the impact of S_N on commutation, Fig. 13.16 displays A_f vs. S_N when $k = k_{cr}$, i.e. at commutation [21]. The larger S_N, the larger the value of A_f at commutation, hence the larger the value of heat release W_c at commutation. We conclude that raising the swirl number S_N at fixed heat release W_c hinders commutation, i.e. any increase of swirl tends to stabilize the open configuration. Our result is in agreement both with observations -see Fig. 13.14- and with the results of CFD -see Fig. 13.17.

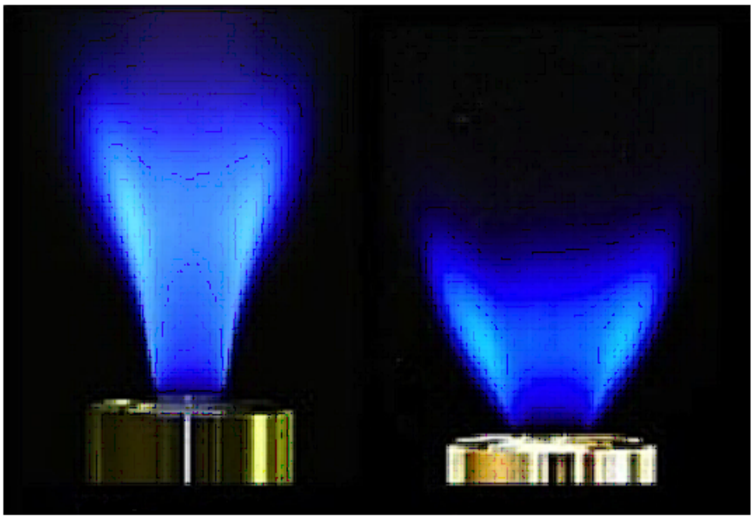

Figure 13.14: *Two premixed air-methane flames with the same stoichiometry and the same values of* p_0 *and* W_c *but with different swirl. The more swirled flame is on the right - from Ref. [131].*

[21] The commutation condition eliminates one out of the three independent quantities h, k and S_N which appear in relationships (13.34) and (13.41), so that it is possible to write e.g. $S_N = S_N(k)$ at commutation. See e.g. Fig. 13.15

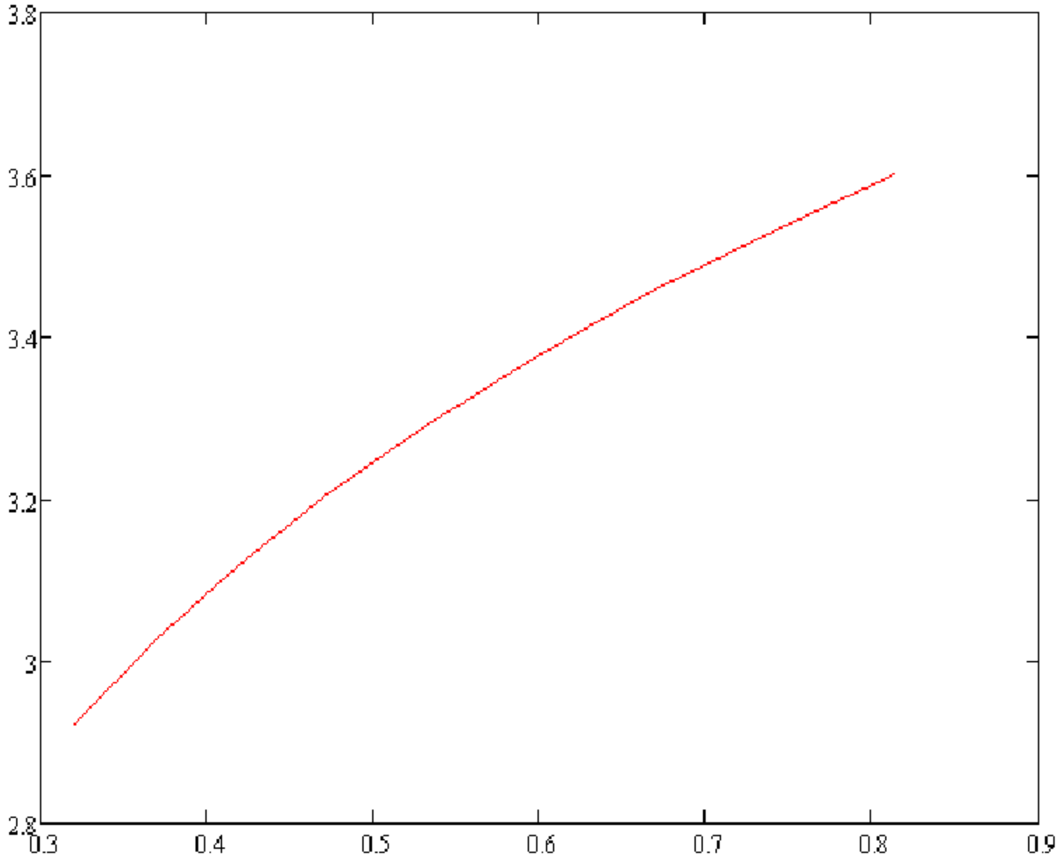

Figure 13.15: *k (vertical axis) vs. S_N (horizontal axis) at commutation. The commutation condition $A_{f+} = A_{f-}$ eliminates one out of the three independent quantities h, k and S_N which appear in relationships* (13.34) *and* (13.41).

13.4.7 Commutation vs. flame velocity

As for the impact of the flame velocity on commutation, we have seen that the larger k for given swirl and combustor diameter, the lower the elongation, the larger the flame velocity for given impinging flow [22]. Thus, raising s_L while leaving the upstream flow unaffected in a given combustor tends to delay the commutation.

Remarkably, Le Châtelier's principle seems still to be able to tell us something about commutation. Broadly speaking, if we raise W_c we push the system towards humming. According to Le Châtelier's principle, we expect that the system tries to counteract our

[22]Equation (13.29) implies that the lower h, the lower $|f'|$. In turn, the lower $|f'|$ the more negative the axial component of $\mathbf{n}$, and the larger s_L according to (13.21).

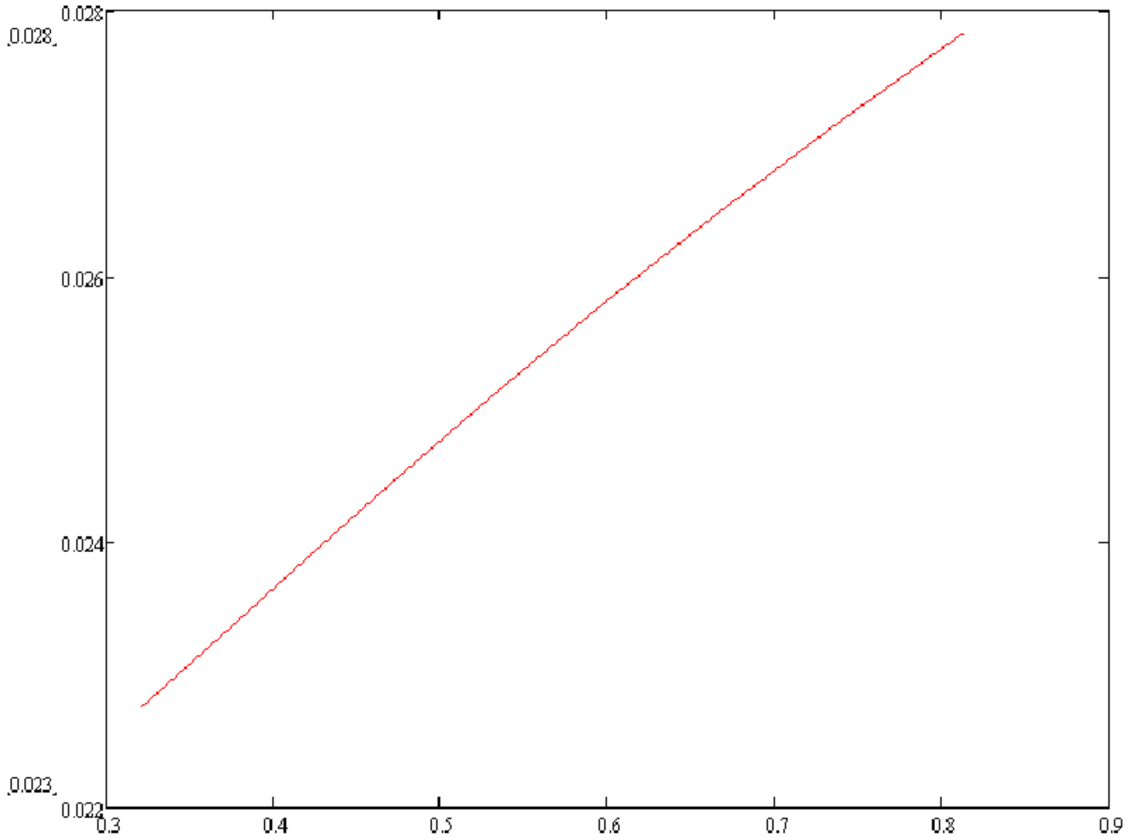

Figure 13.16: A_f *(arbitrary units, vertical axis) vs.* S_N *(horizontal axis) at commutation.*

efforts to push it towards humming. Now, we have seen that raising W_c triggers commutation from open to closed configuration. Then, we may reasonably expect that commutation is precisely the answer of the system predicted by Le Châtelier's principle, i.e. that the closed configuration shows relatively lower combustion instability amplitude than the open one no matter what the acoustic eigenfrequencies of the combustor are like.

Together, the latter results lead us to the conclusion that if we raise the fuel content -hence s_L- while leaving the upstream flow unaffected we obtain the open configuration, which has higher combustion instability amplitude than the closed configuration. This conclusion agrees -qualitatively at least- with the experimental results reported in Ref. [16] -see Fig. 13.18.

There is no contradiction with our previous conclusions concerning the beneficial effect of raising s_L at given upstream flow. In fact, s_L-raising at given upstream flow and commu-

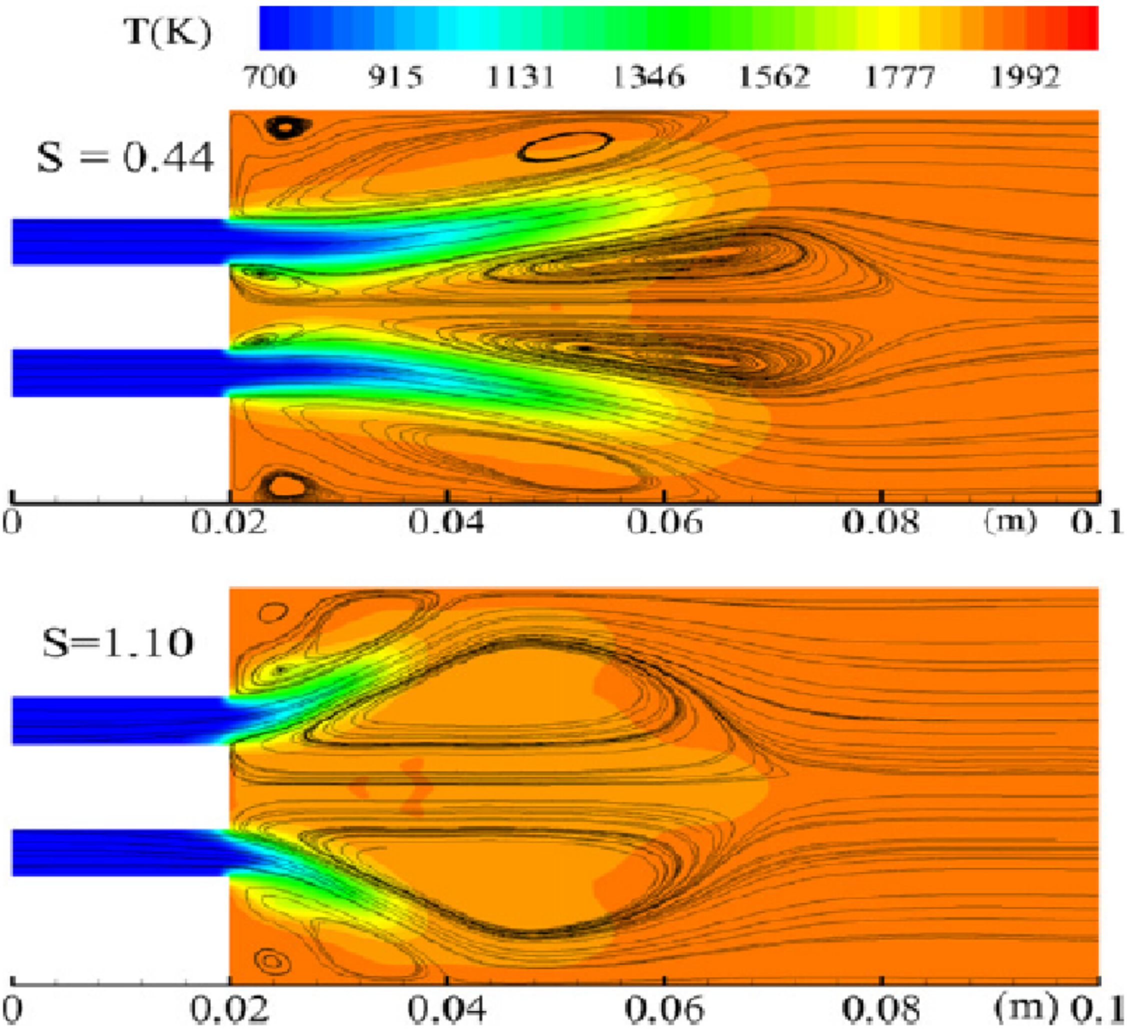

Figure 13.17: *Mean temperature fields and streamline patterns for two different swirl numbers -from Ref. [18].*

tation from 'open' to 'close' are fundamentally different processes, as the former relies on a smooth perturbation of the flame shape while the latter relies on an abrupt change of flame geometry. Neverheless, both have a stabilising effect (as for the stabilising effect of commutation, remember Fig. 13.6 and Fig. 13.7); hence -again by Le Châtelier's principle- the former hinders the latter. If we raise s_L at given upstream flow then the system answers by delaying commutation. After all commutations have occurred, s_L-raising only remains for stabilisation. As for GT, commutation occurs as W_c exceeds a threshold during load ramp. After full power has been achieved in the closed configuration, if humming still occurs then raising s_L at given upstream flow may be helpful.

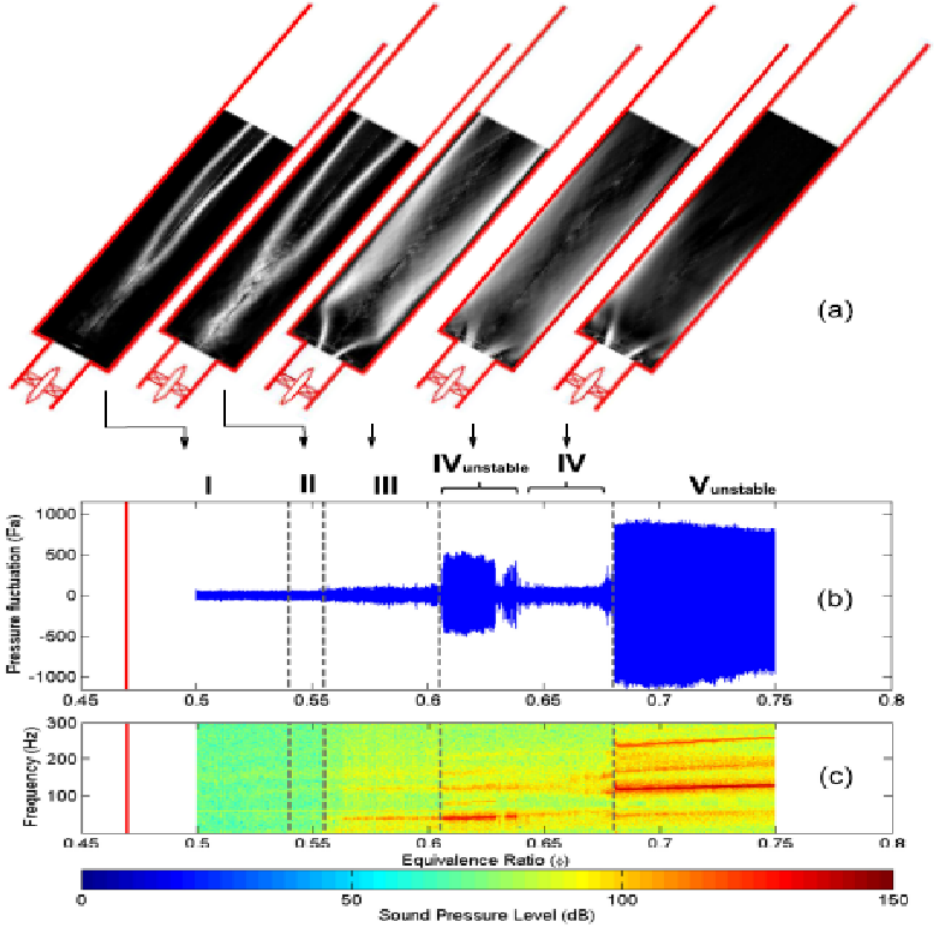

Figure 13.18: *Different swirling flame configurations in an axisymmetric air-methane combustor with constant Reynolds' number at the inlet, inlet temperature and pressure but at different values of the fuel content - from Ref. [16]. The red line on the left is the blow-out limit, which no stable flame is ignited below. At constant constant Reynolds' number at the inlet, inlet temperature and pressure the total air+fuel mass inlet inflow is constant too. Accordingly, the higher the fuel content the larger* W_c. *Broadly speaking, the higher the fuel content, the larger the level of fluctuations, the more open the flame. The word* broadly *is justified because experiments show at least six different configurations -some of them metastable- rather than just two, as in the text. Intermittence is also reported in [16], which is not displayed here. Flame shape seems therefore to be just a variable of a dynamical system [60], just like pressure [78]. Similar behaviour is reported at different lengths of the combustor, i.e. the results liste above do not depend on the detailed values of the acoustic eigenfrequencies - another blow to modal analysis.*

13.5 Numerical predictions

13.5.1 Opening angles vs. swirl number at commutation

At commutation, the opening angles β_+ and β_- are functions of the swirl number S_N [23]. Remarkably, all these quantities are observable ones, or at least can be computed by

[23] According to (13.29), the shapes of these functions depend on r_1 and on D_b.

CFD. They are therefore a matter of falsifiable predictions after rewriting the solutions of (13.26) and (13.27) as functions of S_N. Together, the results displayed in Fig. 13.9 and Fig. 13.15 lead to the results displayed in Fig. 13.19, which displays the opening angle of the open configuration and of the closed configuration vs. the swirl number. For example, if $S_N = 0.5$ then commutation occurs when the open configuration has an opening angle $\beta_+ \approx 0.57$ rad $\approx 33\ ^o$, and leads the flame to a closed configuration with opening angle $\beta_- \approx 0.26$ rad $\approx 15\ ^o$. These values are compatible with the results of Ref. [15] displayed in Fig. 13.10.

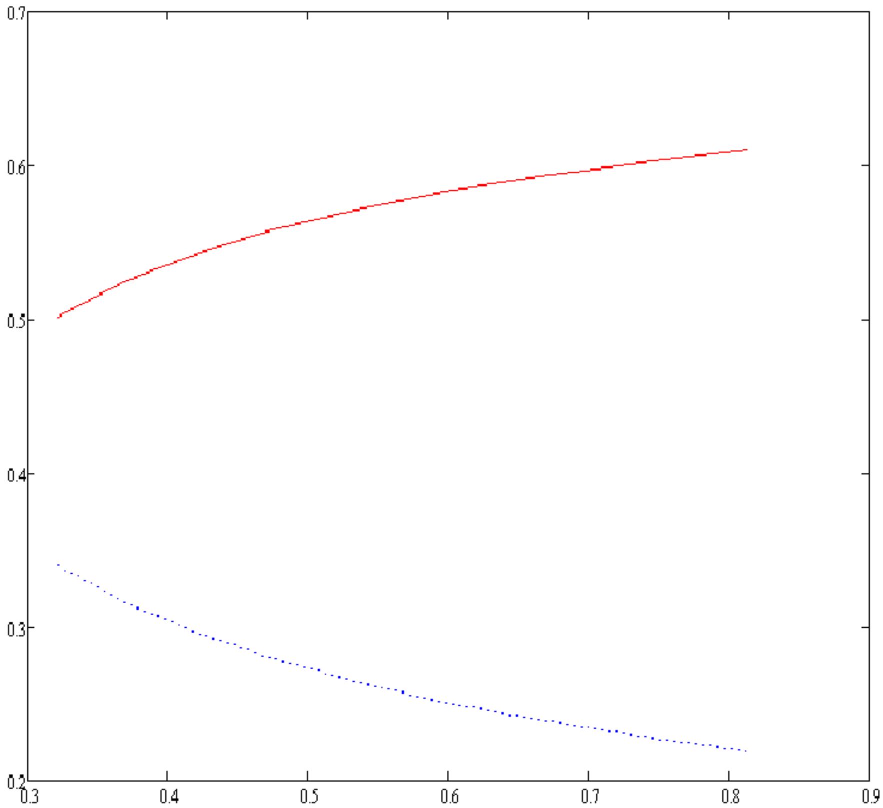

Figure 13.19: β_+ *(rad, continuous red line) and* β_- *(rad. dotted blue line) vs. swirl number (horizontal axis) for the system described in the text.*

13.5.2 Pressure drop across the flame

A further prediction concerns the pressure drop across the flame displayed e.g. in Fig. 13.5. It is customary to assume ∇p_0 to be perfectly zero across the flame in most humming-relevant research concerned with subsonic flames [4]. Indeed, this is not rigorously true: a small pressure drop across the flame is routinely measured. We are going to compute it and to compare its value before and after commutation.

According to eq. (3.53) of Ref. [6], where the momentum balance is solved across a curved flame with $Pe >> 1$ (thin flame), $M << 1$ (subsonic combustion) and $Re >> 1$ (negligible viscosity), the pressure jump reads:

$$p_N|_u^d = -Pe^{-1} \cdot I_\sigma \cdot m_N \cdot 2 \cdot c_N \tag{13.42}$$

where the following dimensionless quantities have been introduced:

- a dimensionless pressure $p_N \equiv \dfrac{p}{\rho_u s_L^2}$;
- the Peclet number $Pe \equiv \dfrac{L}{\delta_L}$ (supposed to be $>> 1$); here L is the typical combustor size, as usual by now;
- a dimensionless, monotonically increasing function I_σ of temperature (whose exact structure is not relevant in the following);
- a dimensionless impinging mass flow $m_N \equiv \dfrac{|\mathbf{m}|}{\rho_u s_L}$;
- and the dimensionless flame curvature $c_N \equiv -\dfrac{\nabla_N \cdot \mathbf{n}_N}{2}$ with dimensionless gradient operator $\nabla_N \equiv L \cdot \nabla$ and with $\mathbf{n}_N \equiv -\mathbf{n}$ unit flame surface vector poynting towards the *burnt* gases (in contrast with the definition given in [4], utilised throughout the present work). The definition of $\mathbf{n}_N$ ensures that $2c_N$ is minus 1 twice the normalised curvature.

Equation (13.42) generalises equation (13.9) to flames of finite thickness. In dimensional form, in fact, equation (13.42) reduces to:

$$p|_u^d = I_\sigma \cdot \delta_L \cdot |\mathbf{m}| \cdot s_L \cdot K \tag{13.43}$$

and equation (13.9) is retrieved in the limit $\delta_L \to 0$.

Further simplification of (13.43) is possible in the limit of elongated flames, where the impinging flow is mainly along the direction of the symetry axis because of the scaling (33) so that $|\mathbf{m}| \approx \rho_u v_z$ and $\beta \approx \dfrac{\pi}{2} - \eta$ so that equation (13.21) reduces to $v_z \approx \dfrac{s_L}{\sin\beta}$. Accordingly, (13.43) becomes:

$$p|_u^d = I_\sigma \cdot \delta_L \cdot \rho_u \cdot s_L^2 \cdot \frac{K}{\sin\beta} \tag{13.44}$$

Remarkably, commutation leaves all quantities on the R.H.S. of (13.44) unaffected but $\frac{K}{\sin\beta}$. It follows that:

$$\frac{\left(p|_u^d\right)_+}{\left(p|_u^d\right)_-} = \frac{K_+ \sin\beta_-}{K_- \sin\beta_+} \tag{13.45}$$

For small β, furthermore, equation (13.29) and the definition of K lead to:

$$K \approx -\tan\beta \tag{13.46}$$

in the limit of small h (which is the relevant limit to our problem, as we have assumed the region near the anchor point to provide the main contribution to the heat release). This way, β-lowering commutation raises the curvature radius $\frac{1}{|K|}$, i.e. the closed flame looks straighter than the open flame - in agreement with what is displayed in Fig. 13.4. Now, our choice of the ISL side for f is well justified: according to Fig. 13.4, in fact, it is this side where the maximum jump of temperature across the flame occurs, and it is therefore here that the largest pressure drop is expected.

Remarkably, according to (13.46) $K < 0$ in both open and closed configuration. Geometrically, this means that the ISL side offers its concavity towards the impinging flow in all cases. Physically, if $K < 0$ then (13.45) and (13.46) imply that the pressure in the downstream region (which the flames offers its own convexity to) is lower than the pressure in the downstream region (which the flames offers its own concavity to). This is why we have consistently spoken of pressure drop, and this is also why the L.H.S. of (13.42) is referred to as *negative surface tension* in Sec. 3.4 of Ref. [6]. Finally, we are interested in comparing the pressure drop before and after commutation. According to (13.46), the L.H.S. of (13.45) at commutation depends on the values of β_+ and β_- at commutation, i.e. on the swirl number S_N.

Experimentally, the dimensionless quantity $ALFA \equiv \frac{|\mathbf{m}|}{\pi R_b^2}\sqrt{\frac{1}{2 \cdot \rho_u \cdot |p|_{u|}^d}}$ is measured [15]. It turns out that commutation raises $ALFA$ -see Fig. 13.20.

According to (13.45) and (13.46), commutation changes the value of $ALFA$:

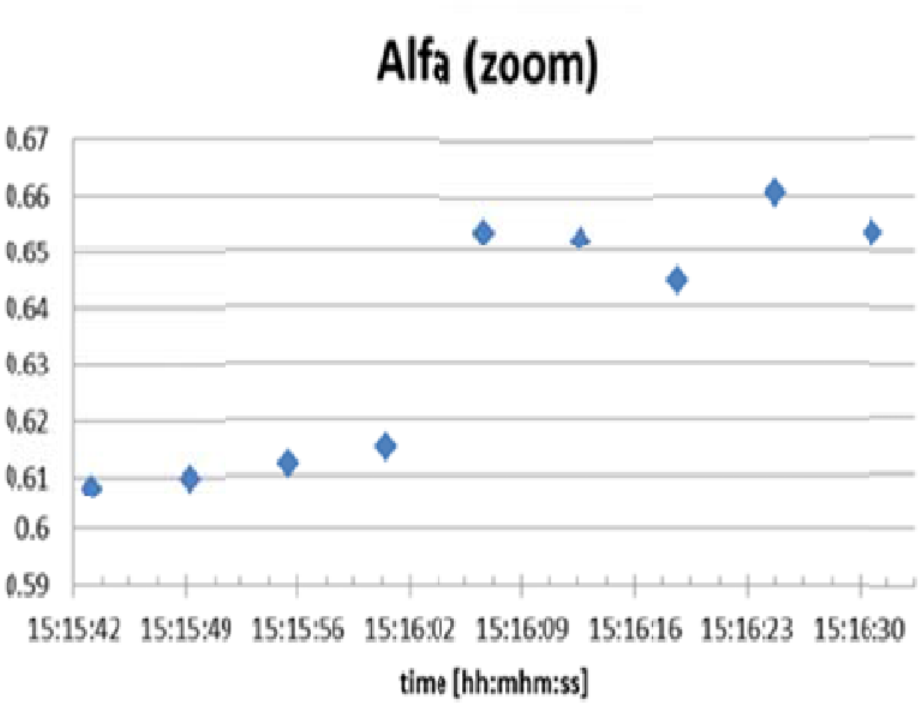

Figure 13.20: *$ALFA$ vs. time. Commutation occurs between 15.06:02 and 15.06:09. The last value of $ALFA$ immediately before commutation is ≈ 0.61. The first value of $ALFA$ immediately after commutation is ≈ 0.65.*

$$\frac{ALFA_-}{ALFA_+} = \sqrt{\frac{\cos\beta_-}{\cos\beta_+}} \tag{13.47}$$

Fig. 13.21 displays $\frac{ALFA_-}{ALFA_+}$ at commutation vs. the swirl number S_N.

Commutation raises $ALFA$, in agreement with observations. In particular, if we take $S_N = 0.5$, then the computed value of $\frac{ALFA_-}{ALFA_+}$ is 1.07. For comparison, according to Fig. 13.20 experimental data are $ALFA_+ = 0.61$ and $ALFA_- = 0.65$, hence $\frac{ALFA_-}{ALFA_+} =$ 1.065. Theory agrees well with experiments, within experimental error bars at least.

Remarkably, $S_N = 0.5$ is the same value of swirl number we have utilised in computing β_+ and β_- a tcommutation, and those computed values too were not in disagreement with

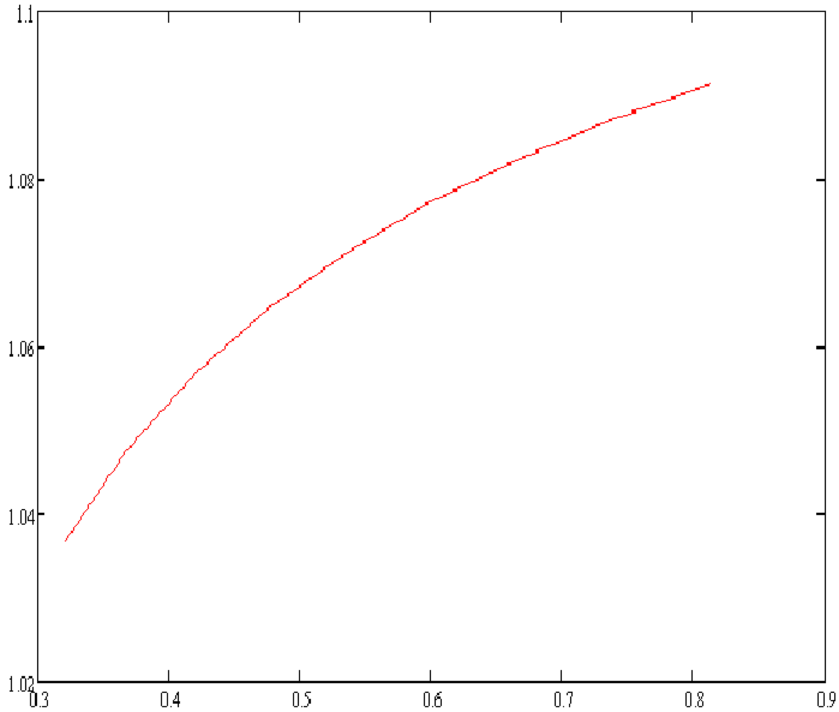

Figure 13.21: $\dfrac{ALFA_-}{ALFA_+}$ *at commutation vs. swirl number (horizontal axis) for the system described in the text.*

the output of CFD computations. We take this fact as a confirmation of the validity of our discussion.

13.6 Anticommutation and hysteresis

Anticommutation

We have shown that the system undergoes commutation from the open configuration to the closed configuration when the heat release in open configuration exceeds the heat release in closed configuration, as the system selects the configuration with the lowest value of heat release. According to Fig. 13.13, the lower k, the larger A_f (hence W_c) at given S_N.

In particular, we have also shown that a threshold value k_{cr} for k exists. If $k > k_{cr}$ ($k < k_{cr}$), then the open (close) configuration is stable. For given burner diameter D_b, the actual value of k_{cr} depends both on the location $r = r_1, z = 0$ of the flame anchor point on the $l < l_{tip}$ flame side near the ISL and on the parameter r_{max}. To put it in other words, k_{cr} depends on the flame shape in the initial (i.e.) open configuration.

As for r_1, it is the same for both open and closed configuration in our treatment, as the same boundary condition (13.24) applies to the flame shape (13.29) in both cases.

As for r_{max}, we have justified our choice (13.33) for the initial configuration of the commutation problem, i.e. the open configuration.

Usually, commutation occurs at a given time during GT load ramp, i.e. (roughly speaking) as the heat release is gradually raised up to its rated value starting from zero. The very arguments discussed above lead to the conclusion that *anticommutation*, i.e. the switching from closed to open commutation, occurs at a given time when the heat release is gradually lowered starting from its rated vale down to zero. In Fig. 13.13, anticommutation is just what happens when we go beyond the thershold, starting from the left side and moving towards the right side of the figure. Actually, anticommutation is routinely observed in Ansaldo GT.

As a matter of principle, however, there is no reason why the threshold value k_{cr-A} for k in the anticommutation case should coincide with the corresponding value k_{cr} in commutation. Physically, in fact, the initial configuration of anticommutation is the closed one, not the open one. Thus, even if both D_b and r_1 are the same, r_{max} can be different, i.e. the closed flame may violate the relationship (13.33). In particular, the closed flame is closer to the symmetry axis than the open flame; rigorously speaking, the fact that $\beta_- < \beta_+$ makes the value of r which correspond to a given $z = f$ in the equation (13.29) for the flame shape to be lower in the closed configuration than in the open configuration. Accordingly, we expect that the value of r_{max} in the closed configuration is lower than the value of r_{max} in the open configuration.

Fig. 13.22 displays A_f vs. k in both commutation and anticommutation at fixed value of the swirl number $S_N = 0.5$. As for commutation, the condition (13.33) holds for the initial configuration of commutation, i.e. the open configuration. Just as in Fig. 13.13, the continuous line and the dotted line display A_f vs. k computed for open and closed configuration respectively under this condition (13.33); k_{cr} is the value of the horizontal coordinate of the point of intersection between the continuous line and the dotted line, and represents the threshold valid for commutation. The latter occurs as k crosses k_{cr} coming from values larger than k_{cr} towards values lower than k_{cr}. In particular, the initial, open configuration is stable if and only if $k > k_{cr}$ -i.e., W_c is not too large. When W_c becomes larger than this threshold the situation is reverted and the closed configuration becomes stable, i.e. commutation occurs.

As for anticommutation, we replace (temptatively) (13.33) with the following condition, valid for the initial configuration of anticommutation, i.e. the closed configuration:

$$r_{max} = 1.25 \cdot r_1 \tag{13.48}$$

In Fig. 13.22, the XXX line and the +++ line display A_f vs. k computed for open and closed configuration respectively under this condition (13.48); k_{cr-A} is the value of the horizontal coordinate of the point of intersection between the XXX line and the +++ line, and represents the threshold valid for anticommutation. The latter occurs as k crosses k_{cr-A} coming from values lower than k_{cr-A} towards values larger than k_{cr-A}. In particular, the initial, closed configuration is stable if and only if $k < k_{cr-A}$ -i.e., W_c is not too small. When W_c becomes lower than this threshold the situation is reverted and the open configuration becomes stable, i.e. anticommutation occurs.

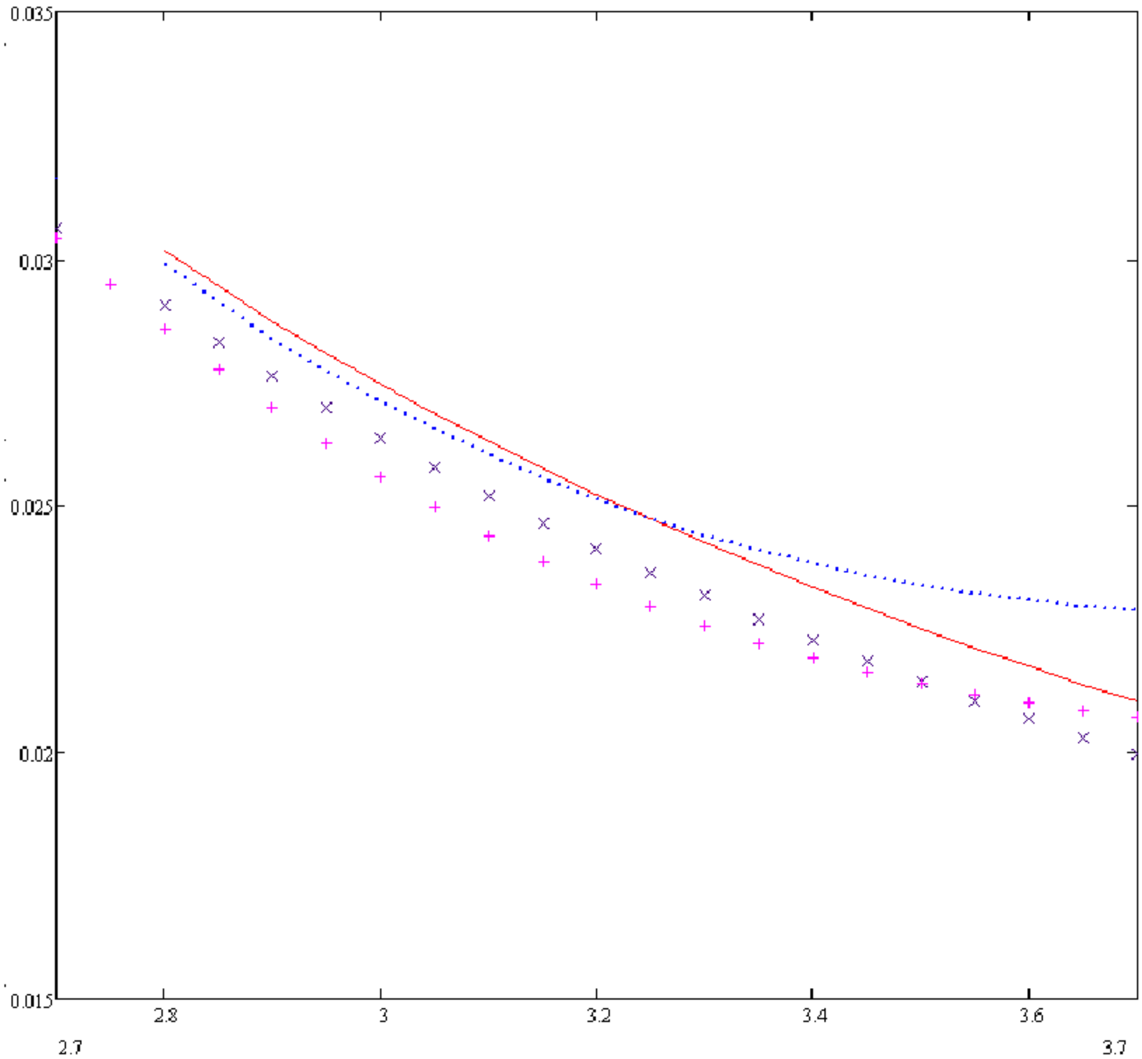

Figure 13.22: *A_f (arbitrary units, vertical axis) vs. k (horizontal axis) at S_N = 0.5 when condition* (13.33) *holds (continuous line: open configuration, dotted line: closed configuration) and when condition* (13.48) *holds (XXX line: open configuration, +++ line: closed configuration).*

Even if qualitative ((13.48) is just a reasonable guess), our discussion strongly suggests that the same selection rule -namely, minimisation of W_c- rules both commutation and anticommutation. The difference between commutation and anticommutation lies in the initial conditions, i.e. in the flame shape before the transition.

Hysteresis

Fig. 13.22 shows that $k_{cr-A} > k_{cr}$, or, equivalently, that the value of $W_c \propto A_f$ which anticommutation occurs at is lower than the value of $W_c \propto A_f$ which commutation occurs at [24].

From a practical point of view, this implies that the heat release which anticommutation occurs at in GT is lower than the heat release which commutation occurs at, i.e. that in order to retrieve the open configuration once we are in the closed one it is not enough to lower the load down to the value where commutation has occurred, but we need to lower it even further (*hysteresis*).

Hysteresis implies that different flow patterns may correspond to the same value of k, hence of the swirl number, depending on the past history of the system. Indeed, this has been observed even when no combustion occurs - see Fig. 13.23

Hysteresis too is observed in Ansaldo GT. We take this fact as a further confirmation of the validity of our results.

13.7 Kuramoto-Sivashinsky and Bunsen

As for flames with $K \approx 0$, the definition $K \equiv \dfrac{f''}{(1+(f')^2)^{3/2}}$ implies that $f'' \approx 0$, hence $|f'| \approx$ const. and $|f'|^2 \approx$ const.. (Remember that perfectly flat flames are never stable). This implies that the impinging velocity is approximately uniform all along the flame, i.e. $s_L \equiv -\mathbf{v} \cdot \mathbf{n} \approx$ const. (according to (13.21)). Finally, we assume that the radial coordinate r lies in the interval $r_A \leq r \leq r_B$. Correspondingly, in this Section by the word *everywhere* we mean *everywhere in the interval* $r_A \leq r \leq r_B$.

Under the assumptions listed above, we show in the Appendix on the auxiliary relationships concerning flames with negligible curvature that the necessary criterion of stability (13.17) takes the simple form:

$$\int_{r_A}^{r_B} dr L_R = \text{min.} \qquad L_R \equiv (F')^2 (1 - r\iota) - \frac{3}{4} (F')^4 \tag{13.49}$$

[24] The proportionality constant between W_c and A_f being essentially given by the flame velocity, the stoichiometry and the mass density upstream according to (10.1), it remains unaffected by the transition both at commutation and at anticommutation.

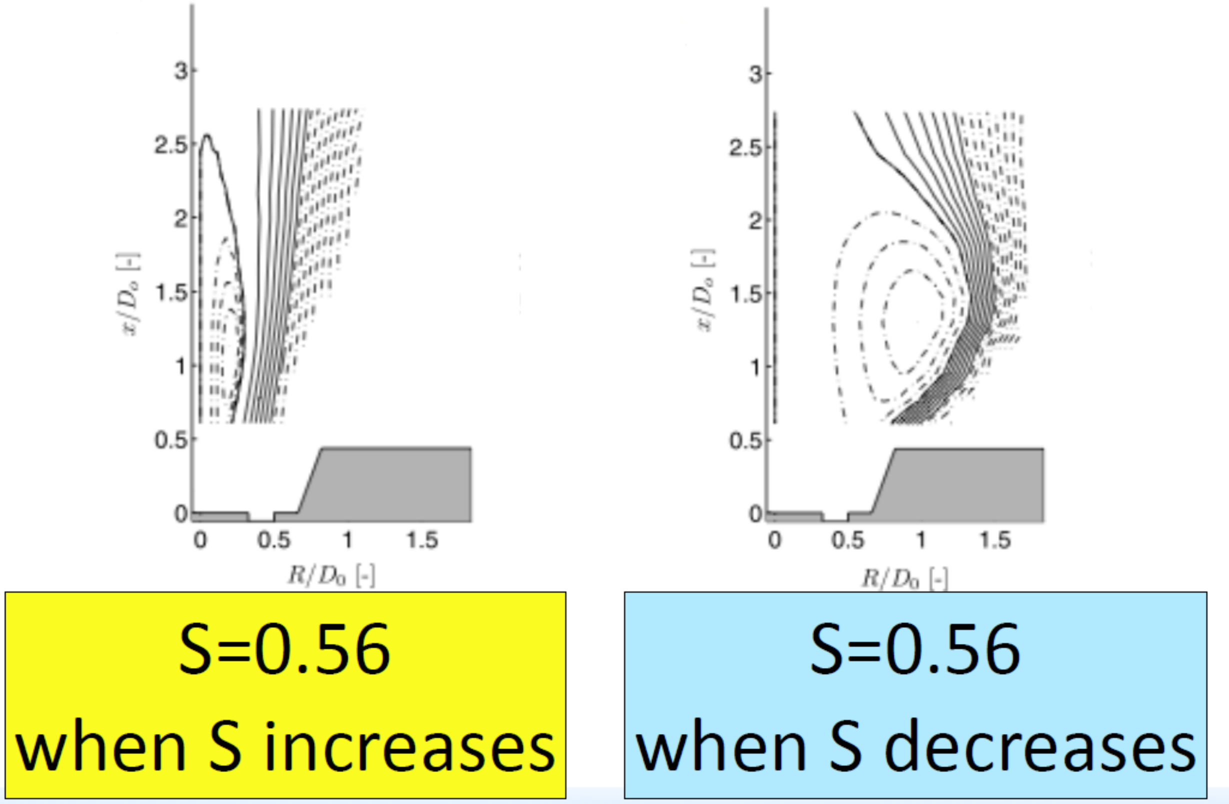

Figure 13.23: *Meridian cross section of two different swirled flows measured at the same swirl number S_N = 0.56. (S stands for S_N). On the left (right) side, S_N was increasing (decreasing) -from Ref. [14]*

where $\iota \equiv \frac{2\pi\theta}{s_L}(1+\varpi)$ and $\varpi \equiv \min\left(|f'|^2\right)$ are constant quantities everywhere, while the Lagrangian coordinate is $F = F(r) \equiv \int_{r_A}^{r} dr' \sqrt{\frac{\left(|f'|^2\right)-\varpi}{1+\varpi}} + F(r_A)$ and $F(r_A)$ is a constant quantity, whose actual value is not of interest for the moment. As usual, the prime denotes derivation on r. Physically, the quantity $F = F(r)$ represents the deviation of the flame slope from the slope of a perfectly flat flame with $K = 0$ everywhere. Typically, the scaling $(F')^2 << 1$ holds as $|f'|^2 \approx$ const. Moreover, if $K \approx 0$ then $f''\sqrt{1+(f')^2} \approx f''\cdot$ const.

We show in Appendix on the auxiliary relationships concerning flames with negligible curvature that the Euler-Lagrange equation of the variational principle (13.49) is well approximated in the limit of negligible curvature by:

$$g'' + (g')^2 + \upsilon g^{iv} - \varsigma = 0 \tag{13.50}$$

where $g = \ln F$, while υ and ς are constant quantities. Equation (13.50) is just the steady-state version of the well-known Kuramoto-Sivashinsky equation. This equation describes both the triggering and the non-linear saturation of the thermo-diffusion instability, which may affect flames with negligible curvature even if the Darrieus-Landau instability is stabilised [132]. Its steady-state version describes possible steady, stable states where thermo-diffusion instability gets saturated. As expected, here 'steady-state' means 'time-averaged on time-scales much longer than the typical time-scale of fluctuations'. Equation (13.50) describes the deviation of the shape of a flame with small curvature from the shape with exactly zero curvature everywhere.

A relevant, particular case of stable, premixed, axisymmetric flame with negligible curvature described by equation (13.50) is the well-known Bunsen flame [25] [133] [134].

[25]The shape of a Bunsen flame is almost conical, and a conical surface has $K = 0$.

Chapter 14

The onset of humming

14.1 A threshold

In this Chapter we discuss what happens when humming is triggered, i.e. when the system flame + fluid + combustor moves from a stable, steady confiuguration to humming. Given the complexity of the issue, the discussion is only qualitative.

Remarkably, the constraint of fixed $\langle \int d\mathbf{x} P_h \rangle$ (say, $\langle \int d\mathbf{x} P_h \rangle = W_c$) corresponds precisely to the operational condition of combustors in GT, which are usually set at a customer-assigned value of the heat release W_c. When choosing between a steady, humming-free flame and a flame oscillating with period τ, according to (11.11) the system selects the configuration which minimises $\langle \int d\mathbf{x} \frac{P_h}{T} \rangle$ as the stable one. Here the fixed volume is the volume V_b of the combustor, while -as we have seen- the period τ is not too far from the period of some acoustic harmonic of the combustor filled with fluid at rest without flame. In principle at least, we have therefore a tool for providing an answer to the question if humming actually occurs. Let us compute $\langle \int d\mathbf{x} \frac{P_h}{T} \rangle$ in both cases: humming-free combustor and combustor with humming.

We have assumed that both the temperature T_d of the downstream region and the temperature $T_u < T_d$ of the upstream region are uniform on the flame front. This assumption allows us to say that we make a small error if we take the temperature T out of the volume integral $\int d\mathbf{x} \frac{P_h}{T}$ provided that we replace T with some suitably-defined weighted spatial average [1]

$$T_f \equiv \frac{\int d\mathbf{x} P_h}{\int d\mathbf{x} \frac{P_h}{T}} \tag{14.1}$$

[1] In steady state at least, T_f is perfectly well-defined, as the shapes of both $T(\mathbf{x})$ and $P_h(\mathbf{x})$ inside the flame are constant

This replacement makes sense, in the framework of the present qualitative discussion at least. Accordingly, if no humming occurs then we have:

$$\langle \int d\mathbf{x} \frac{P_h}{T} \rangle |_{steady} = \int d\mathbf{x} \frac{P_h}{T} |_{steady} = \frac{W_c}{T_f} \tag{14.2}$$

What if humming occurs? Generally speaking, the constant combustor volume V_b satisfies at all times the relationship

$$V_b = V_d(t) + V_f(t) + V_u(t)$$

where $V_d = V_d(t)$ and $V_u = V_u(t)$ are the volume of the downstream region and the upstream region respectively. The flame is thin, then we neglect V_f in comparison with V_d and V_u at all times below. Let $V_d(t)$ reach its minimum value (say, V_{min}) at a time t_0. Then, $V_d(t)$ attains its maximum value $V_{max} = V_{min} + \triangle V$ at a time $t_0 + \frac{\tau}{2}$ and returns back to the value V_{min} at a time $t_0 + \tau$ [2]. Correspondingly, $V_u(t_0) = V_u(t_0 + \tau) = V_b - V_{min}$ and $V_u\left(t_0 + \frac{\tau}{2}\right) = V_b - V_{min} - \triangle V$.

Furthermore, the total amount $S_{tot}(t)$ of entropy contained in the combustor at the time t is $S_{tot}(t) = (\rho s)|_d V_d(t) + (\rho s)|_u V_u(t)$ and is *not* constant. Indeed, the entropy per unit volume $(\rho s)|_d$ in the downstream region (where burnt, hot gases are present) is larger than the corresponding quantity $(\rho s)|_u$ on the upstream side (where unburnt, cold gases only are present). Consequently, S_{tot} oscillates between a minimum value S_{min} and a maximum value S_{max}, where $S_{min} = S_{tot}(t_0) = S_{tot}(t_0 + \tau) = (\rho s)|_u (V_b - V_{min}) + (\rho s)|_d V_{min}$ and $S_{max} = S_{tot}\left(t_0 + \frac{\tau}{2}\right) = (\rho s)|_u (V_b - V_{min} - \triangle V) + (\rho s)|_d (V_{min} + \triangle V)$ In order to return back to the initial value $S_{tot}(t_0)$, at the time $t_0 + \tau$ the total amount of entropy lost by the combustor across the boundaries due e.g. to the gas flow must be equal to $S_{max} - S_{min} = (\rho s)|_u^d \triangle V$ where $(\rho s)|_u^d = ((\rho s)|_d - (\rho s)|_u)$. Here and in the following, we write $a|_u^d \equiv a|_d - a|_u$ for the generic quantity a. The combustor is given this amount of entropy by combustion inside the flame, as no entropy is produced outside the flame (for negligible viscosity at least). Thus, the time-averaged net amount of entropy produced per unit time which must be carried away is

$$\langle \int d\mathbf{x} \frac{P_h}{T} \rangle |_{oscillating} = \frac{(\rho s)|_u^d \triangle V}{\tau} \tag{14.3}$$

[2] The value of the humming period τ is near to the period of some acoustic harmonic of the combustor without the flame, hence it depends basically on the combustor geometry; as such, it will be taken as a constant quantity in the following.

According to the selection rule (11.11), the transition from steady to oscillating systems occurs when $\langle \int d\mathbf{x} \frac{P_h}{T} \rangle|_{oscillating} = \langle \int d\mathbf{x} \frac{P_h}{T} \rangle|_{steady}$, i.e.:

$$\frac{(\rho s)\,|_u^d \triangle V}{\tau} = \frac{W_c}{T_f} \tag{14.4}$$

Non-oscillating flames are stable against perturbations of amplitude $\triangle V$ and period τ when the L.H.S. of (14.4) is larger than the R.H.S., i.e. when W_c is not too large. This result is of purely thermodynamical origin, and holds therefore regardless of the detailed dynamics of the oscillation.

Let us discuss some consequences of (14.4). Firstly, as far as $\tau > 0$ equation (14.4) implies that $\triangle V > 0$ at the transition. This conclusion is in agreement with the results of the numerical simulations of [51], which suggest that the simplest mathematical model of the transition resembles the arrangement of a subcritical Hopf bifurcation and a saddle node bifurcation [60], leading just to $\triangle V > 0$ at the transition -see e.g. Figs. 1 and 13 of [51], where the value of $\triangle V > 0$ at the transition is to be computed at the value β_h of the heat release parameter. In turn, this arrangement makes hysteresis possible. In contrast, supercritical Hopf bifurcations seem to be ruled out, as they require $\triangle V = 0$ at the transition -see e.g. Fig. 1.13 of [135].

Secondly, if the flame remains within the combustor at all times, then $V_b \geq \triangle V$ and (14.4) gives:

$$\frac{(\rho s)\,|_u^d V_b T_f}{\tau} \equiv W_{threshold} \geq W_c \tag{14.5}$$

According to (14.5), no stable, humming-free flame exists for $W_c \geq W_{threshold}$. Typical order-of-magnitude estimates are $\tau \approx 10^{-2}s$, $V_b \approx 1$ m^3, $T_f \approx 1.5 \cdot 10^3 K$, $(\rho s)\,|_u^d \approx 10^2 J \cdot m^{-3} \cdot K^{-1}$ hence $W_{threshold} \approx 50MW$, i.e. just in the range of commercial combustors for energy production. Unfortunately, however, our result is just an upper bound on the actual threshold value, as $W_c \leq W_{threshold}$; moreover, it holds only as an order-of-magnitude estimate.

Thirdly, as usual by now let us keep the upstream flow (hence T_u and $(\rho s)_u$) unchanged. It follows that both T_f and $(\rho s)\,|_u^d$ are increasing functions of T_d. In turn, T_d is an increasing function of s_L in lean combustion at fixed T_u [2]. Then, $W_{threshold}$ too is an increasing function of s_L in lean combustion at fixed T_u. Just as expected from our discussion of the previous Section, it follows that raising s_L at fixed upstream flow has a stabilising effect on humming, as it raises $W_{threshold}$. We may achieve such goal e.g. by raising the fuel content; all the way around, generally speaking, the leaner the flame the more prone to instability [53].

14.2 A quality factor

We have seen that Rayleigh's criterion is connected with Le Châtelier's principle of thermodynamics, and that the latter principle leads to further necessary criteria of stability of the unperturbed, steady state of a fluid at rest; these criteria agree therefore with Rayleigh's criterion. We have also shown that the same criteria apply also to the stability of oscillating unperturbed state, after suitable time-averaging. In agreement with thermodynamics, the generalisation of Rayleigh's criterion to oscillating unperturbed states, Myers' corollary, leads after time-averaging to predictions which are formally identical to Rayleigh's ones, provided that the Rayleigh's index is suitably redefined. Accordingly, we are allowed both to invoke Myers' corollary in order to gain information about humming, and to expect that such information is in agreement with Le Châtelier's principle. This is the topic of this Section.

Starting from Myers' corollary, we show in the Appendix on the flame velocity that the following inequality:

$$\frac{1}{\tau}\left[\left\langle\left\langle K_{tot}\frac{ds_d}{ds_L}\frac{ds_L}{ds_T}s_T\right\rangle_s\right\rangle_f\right]^{-1} < 1 \tag{14.6}$$

is a rule-of-thumb necessary condition for the lack of humming in combustors with premixed, turbulent, globally concave flames. Here τ is the humming period, as usual; moreover K_{tot} and s_d are the total curvature of the flame and the flame front speed relative to the flow respectively [4]; here and in the following we refer to the Appendix for all definitions. Finally, $\langle\rangle_f$ and $\langle\rangle_s$ denote averaging on the flame surface (weighted by the Rayleigh index) and averaging on the small-scale flame surface convolutions induced locally by the turbulence, respectively. In contrast with the former averaging, the latter averaging leads to results which depend on the position on the flame, but allows us to get rid of high-frequency, small-scale, turbulence-related effects. Formally, the L.H.S. of (14.6) is positive for our flames. Reasonably, in fact, the contribution of K_{tot} is positive on average for globally concave flames. Moreover, relationship (7) ensures that the displacement speed is an increasing function of s_L everywhere, as far as no quenching occurs. Finally, s_T is an increasing function of s_L, i.e. $\dfrac{ds_L}{ds_T}$ is also positive.

Physically, each term on the L.H.S. of (14.6) takes into account the impact of a different quantity on humming. To start with, we have seen that the humming frequency $\dfrac{1}{\tau}$ is near to an acoustic eigenfrequency when no flame is present. As such, it grows with increasing function of the speed of sound c_s, which in turn is an increasing function of temperature. A simple way to raise c_s everywhere across the combustor is to raise the temperature of the unburnt fuel mixture upstream. Then, the hotter the upstream fluid mixture (all other quantities being unchanged) the larger the L.H.S. of (14.6) the more likely the onset of humming.

As for the flame velocity, the exact dependence of s_T on s_L is still matter of debate [113]; popular scaling laws predict either a linear dependence $s_T \propto s_L$ [4] or a square-root dependence $s_T \propto \sqrt{s_L}$ [112]. In both cases $\frac{ds_L}{ds_T} s_T$ is an increasing function of s_T. In turn, this fact has two consequences. Firstly, we have seen that s_T is an increasing function of pressure [113]. Then, the lower the pressure (all other quantities being unchanged), the lower s_T, the larger the L.H.S. of (14.6), the more likely the onset of humming [3]. Secondly, if we lower s_L (al other quantities being equal) -by decreasing e.g. the fuel content in lean combustion- we lower also s_T, and again we facilitate humming.

Up to now, all these results agree with the predictions of our simple model [3]. But (14.6) contains new information: the geometry of the flame. While the quantity $\frac{ds_d}{ds_L}$ depends on the flame stretch only weakly (see the Appendix on the flame velocity), the total curvature is significantly different in open configuration and in closed configuration. In the open configuration, a significant fraction of the flame exhibits its convex side towards the incoming flow, while no such convex side exists in the closed configuration. As a result, the radius of curvature changes sign along the flame in the open configuration, in contrast with the closed case. It follows that the flame-averaged curvature is larger in the closed case than in the open case, hence the commutation from open to closed flames lowers the L.H.S. of (14.6) and makes humming more difficult. Everyday working experience shows that commutation occurs as W_c grows; and when W_c exceeds a threshold, humming is triggered. Then, we can understand commutation as a further example of Le Châtelier's principle: as we push the system towards humming by raising W_c the system (which is initially in open configuration) tries to resist by commuting to a more stable, close configuration. It is therefore really possible to speak of a thermodynamics of humming onset.

Basically, the L.H.S. of (14.6) is a dimensionless quantity, i.e. the humming frequency $\frac{1}{\tau}$ normalised to the ratio of a typical velocity and a typical length, as K_{tot}^{-1} and s_T have the dimensions of a length and a velocity respectively. As such, the L.H.S. of (14.6) is much like a Strouhal number. It is customary to define a Strouhal number in problems where a fluid start oscillating, and the definition of this number depends on the particular problem -as an example of application to humming, see e.g. [22]: the larger Strouhal, the more likely the onset of humming. In our discussion, the typical length is the reciprocal of the total curvature of the flame, i.e. it is directly related to the flame geometry. Thus, inequality (14.6) is an explicit link of the flame geometry and the stability against humming. As a matter of principle, it can be expected that the dimensionless L.H.S.

[3] The reader could object that in real combustor the unburnt mixture is supplied by a compressor, so that a growth of working pressure in the combustor is unavoidably associated with a growth in the upstream temperature, hence of $c_s \propto \sqrt{T}$. All the same, for adiabatic compression $T \propto p^{1-\frac{1}{\gamma}}$, and s_T increases much faster with pressure [113], so that the L.H.S. of (14.6) is still a decreasing function of pressure.

of (14.6) may allow comparison between different configurations of the system flame + fluid + combustor as far as humming onset is concerned, just like Reynolds' number Re allows comparison between different configuration as far as turbulence is concerned. If this is true, then the L.H.S. of (14.6) plays the role of a *quality factor* for the stability against humming. Such assessment may be of practical relevance when applied e.g. to the well-defined, rated, steady-state configuration of a combustor in a real-life GT plant to be sold to customers.

Chapter 15

The control of humming

15.1 *Passive* vs. *active* strategies

Historically, Rayleigh's criterion has provided the physical basis for various strategies aiming at controlling the humming oscillation. We recall that GT manufacturers aim at such control without increasing pollution (they could otherwise make use of fuel-rich flames, which are both more stable and more polluting than lean flames).

A *passive* approach aims at maximizing the stabilizing contributions in Rayleigh's criterion through modification of the acoustics of the combustion chamber, either by increasing acoustic damping via Helmholtz-type resonators or by disturbing the propagation of sound waves via baffles. A simple, cheap (and therefore popular) passive method is just to drill holes. Long before theoretical models were available, manufactures drilled *damping holes* in the combustion chamber front plate in combustors affected by severe humming. Here the term *passive* refers to modifications of a combustion system that, during system operation, will not be changed any more and/or will require no external supply of energy. Usually. passive methods work in a small operating range only, covering a narrow frequency interval. As e.g. for damping holes, poor damping effect and frequency tuning overcompensated the advantages of simplicity and low maintenance requirements. As for Helmholtz resonators -see Fig. 15.1- they allow a safe growth of the heat release up to 20 % [136]. Generally speaking, the instability amplitude is substantially reduced if the resonator is tuned such that its resonant frequency coincides with the instability frequency. Then, a separate resonator is required for each frequency that needs to be suppressed [137].

An alternative *active* approach relies on suitably modulated injection of either fuel and/or sound [138]. Under ideal conditions, modulation is performed in a manner to have the corresponding system variable fluctuate precisely in counter-phase with the fluctuations constituting the combustion instability, thus damping them. The term *active* refers to utilization of an external power supply. Such feedback control -Fig. 15.2-works well in simple thermo-acoustic systems but is challenging in industrial systems because the sensors and actuators have to withstand very harsh environments. For example, fuel flow modulation has been considered as actuation mechanism for active control of combustion instability in practical applications, using mechanical devices such as valves. However,

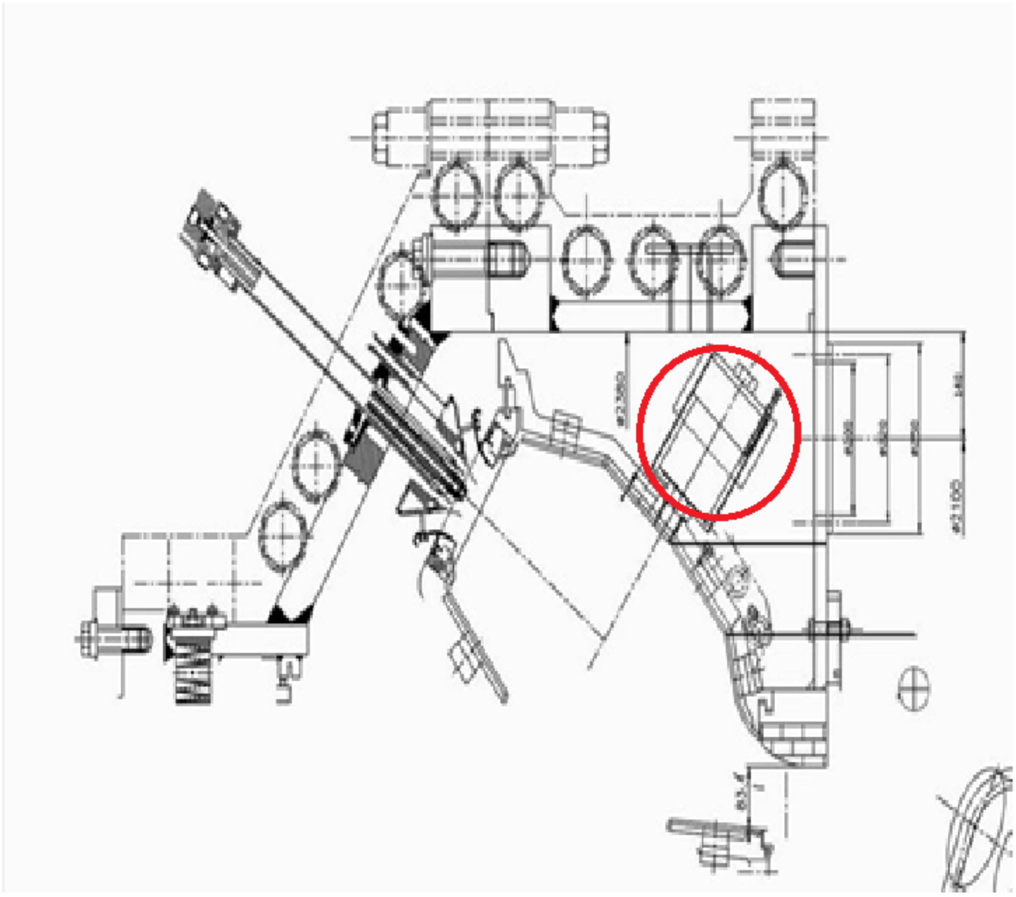

Figure 15.1: *A drawing of a combustor with a Helmholtz resonator (in the red circle).*

because these fuel valves tend to have a non-negligible space requirement and to have limited technical performance, few easily implementable solutions are currently affordable. To date, no approach seems to provide manufacturers with the ultimate solution, and suitable combination of active and passive strategies is required for each machine [139].

In the following, we are going to take advantage of our investigation on the humming-relevant thermodynamics in order to discuss the properties of a possible new class of non-mechanical actuators for the active approach.

15.2 Electromagnetic actuators: DC, NRPP...

DC

In principle, should electromagnetic fields replace mechanical actuators, wearing of the latter would be no more matter of concern in the active approach.

In particular, DC electric fields seem to affect both the flame velocity [140] and the FTF [141] of premixed methane-air flames, where the FTF is defined as the ratio of the relative heat release rate oscillation and the relative flow velocity oscillation. In the ex-

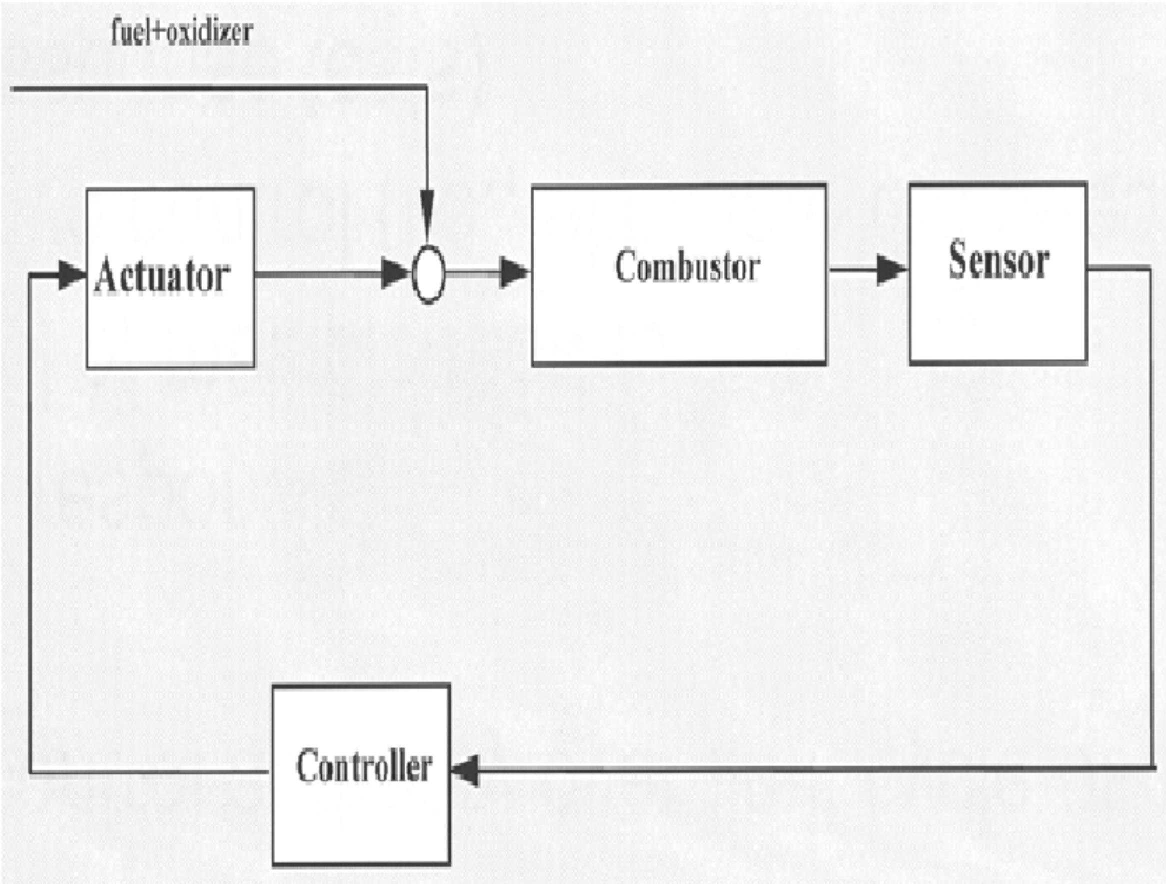

Figure 15.2: *Conceptual lay-out of an active control system.*

periment of Ref. [141], a DC electric field has been applied to a Bunsen which plays also the role of anode. It turns out that the impact of the field on a Bunsen conical (laminar) flame is much stronger than on a flat flame. Fig. 15.3 displays the measured time delay (normalised to the humming period) vs. the humming frequency for Bunsen flames with different shapes under the same DC 4 kV voltage. In all cases, the amplitude of the (artificially superimposed) velocity perturbation was $\leq 6\%$ the mean flow velocity, and the electric power delivered to the flame was $\leq 0.5\% W_c$. Negative values of the time delay correspond to the flame approaching the fuel inlet. Of course, Bunsen diffuse flames are scarcely an adequate model for realistic multi-MW premixed TG. Moreover, DC coupling e.g. to a pilot in industrial burner is far from being a trivial issue. All the same, the very fact that the absolute value of the normalised time delay is much larger than the stabilisation threshold $\frac{\pi}{2}$ in almost all cases even at such small values of the electric power suggests that flame stabilisation through electric field is worth being further investigated in detail.

In principle, charge carriers are being produced in hydrocarbon flames in the form of positive and negative ions as well as electrons. This process is called *chemionization* and happens during the oxidation of neutral particles -atoms and molecules. Usually, both the positive ions and the negative ions are rather unstable at high flame temperatures, and

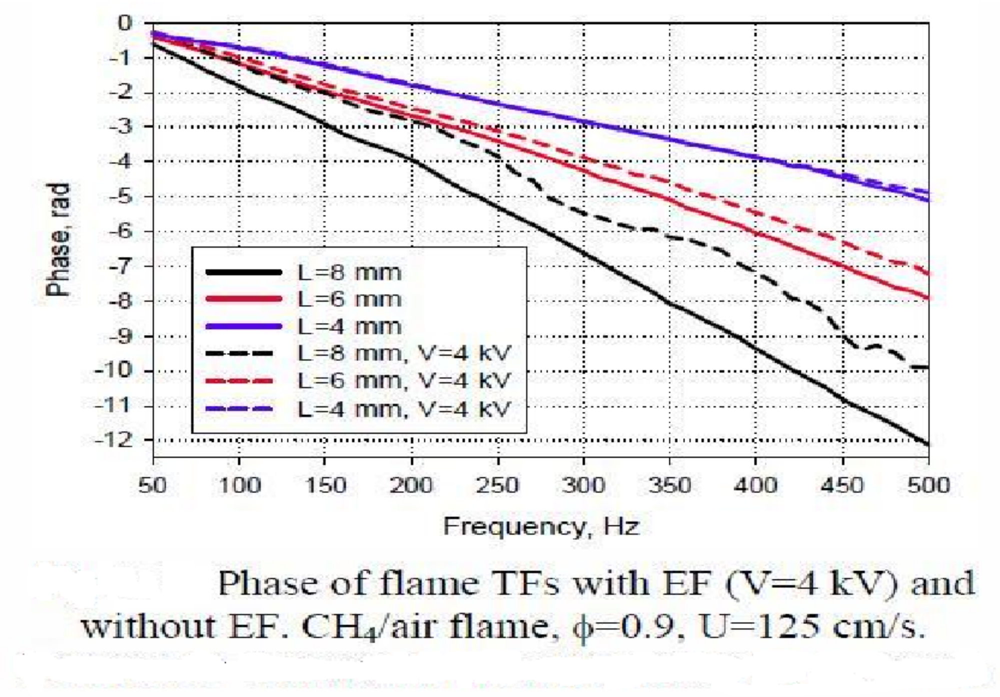

Figure 15.3: *From Ref. [141]. L and V are a typical length and the applied voltage respectively.*

therefore decay quickly into electrons and neutral particles. If an external DC electric field is applied to a flame, the most important processes will happen in the region between the reaction zone and the electrodes. Due to the applied electric field, positive and negative charge carriers are separated from each other and accelerate as they travel towards the corresponding electrode. As a result, an electric current will flow between the electrodes depending on the applied voltage. The current-voltage characteristics shown in Fig. 15.4 can be used to divide the the effects into three distinct regimes, as follows:

- At low applied voltage, the current is proportional to the voltage. Positive ions and electrons recombine. Negative ions decay. All of them form neutrals. Recombination rules physics. With increasing voltage, an increasing amount of charge carriers are removed fro the reaction zone and go the electrodes, at the expense of recombination.

- When the majority of charge carriers have been removed, further increase of voltage raise the current no more as no more charge carriers are available.

- At even larger voltage, an appreciable number of electrons extracted from the flame are accelerated on their way to the anode up to kinetic energies that are high enough to ionize neutrals. Ionization rules physics. The ionization rate is linear in the density of available free electrons, but increases exponentially with the ratio of the applied voltage to the ionisation voltage.

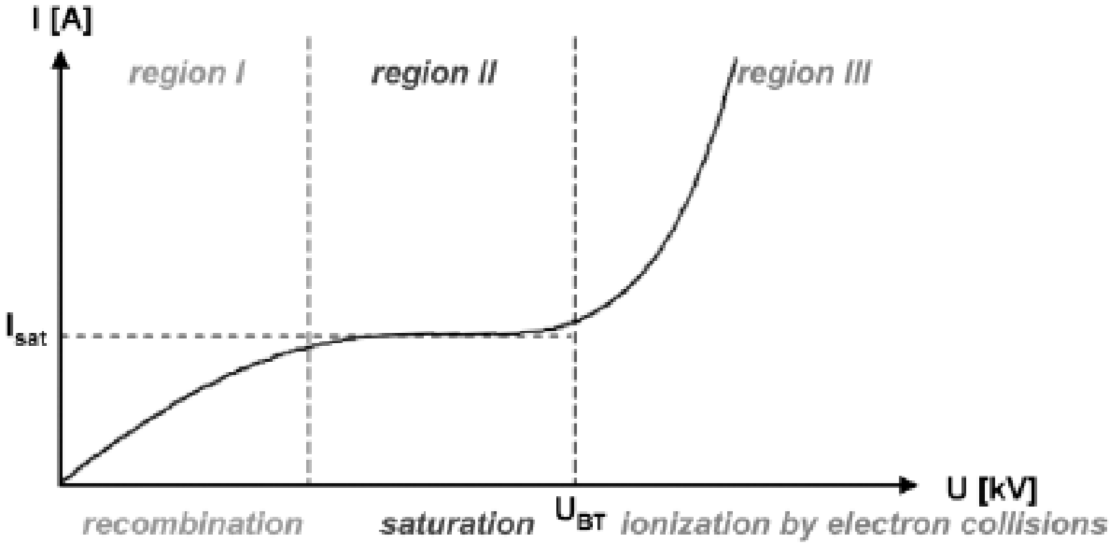

Figure 15.4: *Current-voltage characteristics for a DC electric field applied to a premixed flame (from [142]). Here U_{BT} and I_{sat} are the breakdown threshold voltage and the corresponding electric current.*

As for DC fields, the absorbed power is the product of voltage and current, then it is much larger in the ionization phase. Usually, it is ≈ 0.002 % - 0.01 % times W_c. Since $W_c \approx$ tens of MW in GT and too large values of dissipated power are far from desirable, DC actuators for active control of humming are investigated in the recombination regime.

The influence of electric fields on flames in the first regime can be explained with the help of a simple 1D schematic diagram, as shown in Fig. 15.5. A positively charged wire mesh is placed above a premixed burner with a flat, 1D flame. Due to the electric field, charge carriers are separated and accelerated towards the corresponding electrodes. The electrons and negative ions are accelerated towards the positively charged electrode, whereas the positive ions move in a counterflow to the incoming fresh gas towards the electrically grounded burner rim. In general, the ions collide with neutral molecules from the incoming mixture after passing the mean free path length. The latter is quite small and the positive ions are accelerated once more by the electric field after each collision, each positive ion undergoes a multitude of collisions with neutral molecules. Therefore, even small ion concentrations are sufficient for a noteworthy momentum transfer to the fresh gas. Unlike the ions, electrons play only a minor role in the total momentum transfer due to their low mass. Similarly, the impact of negative ions is also rather low due to their low concentration. As a result of the collisions of the fast ions with the neutral molecules within the fresh gas region, a clearly observable shift of the flame front occurs. This can be attributed to the following two different mechanisms:

- The first mechanism, usually named *the ionic wind* or *electrohydrodynamic effect*, relies solely on the transfer of momentum from the accelerated positive ions to the incoming neutral molecules. This momentum transfer to the fresh gas molecules changes the flow pattern above the burner rim. As a consequence, the flame front is shifted towards the burner exit [1].

- The second mechanism is based on the generation of radicals by the collisions of accelerated electrons with neutral molecules. Radicals are produced upstream of the effective reaction zone and increase the reactivity of the mixture. Hence, the flame also responds with a change of the reaction zone.

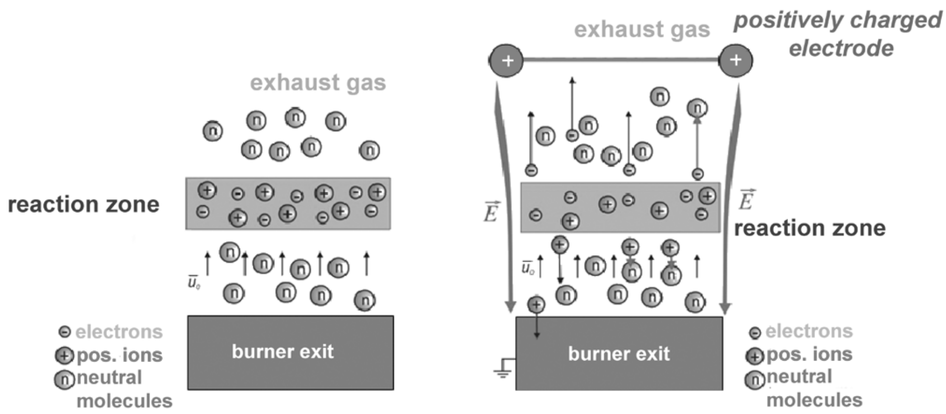

Figure 15.5: *Premixed flames without ionic wind (left) and with ionic wind (right) - from Ref. [142].*

Experiments [142] show that application of DC field in the recombination regime to a 50 kW premixed turbulent flame allows dramatic reduction of CO emissions in the range $1 \leq p_0 \leq 10$ bar. The reduction of CO emissions scaled proportionally to the ratio of voltage and pressure (This is not surprising, as electric voltages and fields in gaseous conductors below breakdown scale usually with pressure) -see Fig. 15.6. I the experiments, maximum current and voltage were 3.3 mA and 40 kV respectively.

Admittedly, the DC field leads also to slight increase in NO_x emissions. However, this increase could be inverted to a decrease using leaner mixtures, which was possible since the lean blow-off limit too was shifted to a higher air number by the stabilizing action of the electric field. The DC field allows an increase of the air-to-fuel ratio with a lean blow-off limit shift of up to 8 %. Due to this shifted lean blow-off limit, an overall 40 % decrease of NO_x emissions could be achieved with concurrent reductions of CO emissions by 60 %, compared to the case without the application of electric fields. Preheating was also favorable due to the increased reactivity of the mixture.

NRPP

In spite of its interesting features (the control of humming-relevant phases, the reduction of pollution and/or the increase of the lean blow-off limit), DC has the disadvantage that

[1]The ionic wind is a well-known effect of electricity since the XIX century.

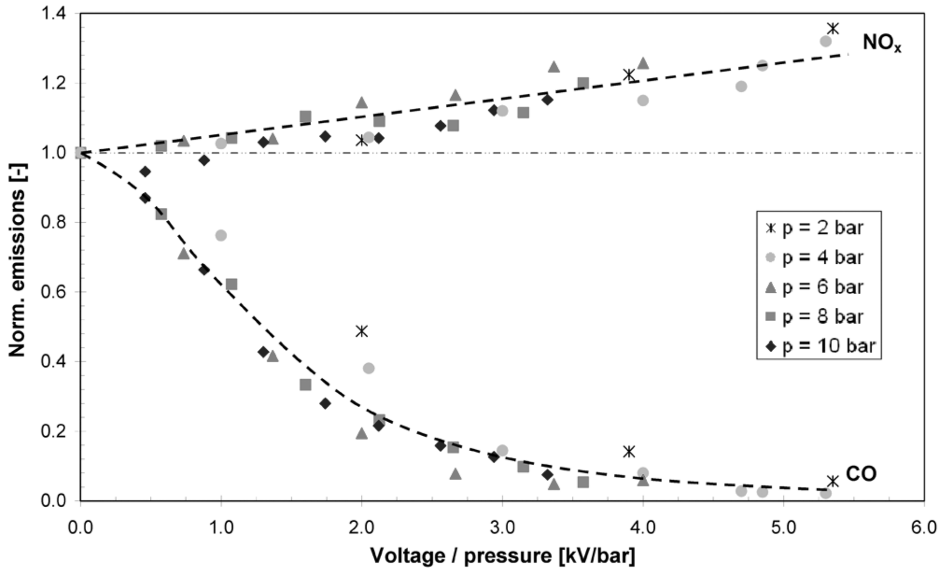

Figure 15.6: *CO and NO_x emissions vs.* $\dfrac{voltage}{p_0}$ *- from Ref. [142].*

the dissipated power increases with the applied voltage, which in turn increases with the distance between electrodes at given electric field. In order to prevent the electrodes to be too near to the flame and to shield them from the ensuing thermal stresses, the distance between them cannot be to short, and this is likely to lead to large amount of dissipated power.

It is reasonable to ask ourselves what happens if the frequency ν_{RF} of the applied electric field is not zero, like in the DC case. Intuitively, we expect that if ν_{RF} is smaller than the typical collision frequency of electrons with neutrals, i.e. if an electron undergoes at least one collision while it oscillates under the effect of the applied electric field, then things should not differ too much from the DC case, and the application of the field should be still beneficial. Approximately, this means $\nu_{RF} < 10$ GHz (see the Appendix on the RF-flame interaction). In contrast, if ν_{RF} is larger than this threshold, then electrons oscillations are basically collisionless, and the flame remains unaffected (this is why nobody expects e.g. visible light to stabilise humming).

Remarkably, oscillating electric fields propagate across vacuum (and across the gaseous mixture in GT combustors) as electromagnetic waves at the speed of light. This suggests that power may be transmitted to the flame by sources which are located far away - a fact which helps thermal shielding of the sources themselves.

Finally, electromagnetic waves at $\nu_{RF} < 10$ GHz have wavelengths > 3 cm and are emited by sources with linear size $\approx$ this wavelength. Such size is compatible with the lay-out of GT combustors.

In the following, we are going to discuss two examples of electromagnetic actuators in the GHz requency range, namely NRPP and RF.

Generally speaking, electromagnetic fields may generate a plasma near the flame [2]. In particular, plasma actuators are routinely investigated in flow control outside combustion research -see e.g. Ref. [144].

As for combustion, plasma-assisted combustion techniques have beneficial effects on flammability limits and facilitate combustion of lean mixtures; a far-from-complete list [145] includes dielectric barrier discharges and NRPP, whose beneficial effects on humming have been reviewed in the Section on Le Châtelier's principle above. Here we recall that when humming occurs in a swirl-stabilized combustor at atmospheric pressure fueled with natural gas at an equivalence ratio of 0.66 and 43 kW heat release, suitably tuned NRPP with 315 W time-averaged electric power consumption induce a ten-fold decrease of 3-mbar pressure oscillation amplitude [103]. Fig. 15.7 displays a conceptual lay-out of the epxperiment: small violet segments represent the discharge. Fig. 15.8 shows that the flame is markedly shifted bottomwards, i.e. towards the fuel inlet, by NRPP. This is agreement with an increase in the flame velocity. As for the Joule power dissipated in the discharge, Fig. 15.9 shows how suitably pulsed discharges (with repetition frequency in the range 30 - 50 KHz) allow us to achieve a large peak value even if the averaged value is relatively low. Finally, Fig. 15.10 shows the stabilising effect of NRPP. Remarkably, the higher the repetition frequency the better; this is possibly due to a NRPP power deposition time inside the flame $<$ the time of flight of the air-fuel mixture across the flame at large repetition frequency.

In a similar experiment, NRPP make a humming-affected, lean, premixed swirl-stabilised air-methane flame in open configuration to commute to a humming-free, closed configuration -see Fig. 7 of Ref. [146].

[2] By definition, a *(classical) plasma* is a gaseous medium containing unbound positive and negative electric charges whose behaviour is ruled by collective effects. The latter words mean that charged particles are so close enough together that each charged particle influences many nearby charged particles, rather than just interacting with the closest particle; these collective effects are a distinguishing feature of a plasma. More quantitatively, it can be shown under quite general assumptions that the radius of influence of a single charged particle, the so-called *Debye (screening) length* λ_D, is equal to $\lambda_D = \sqrt{\frac{\epsilon_0 k_B T}{n_e e^2}}$ where $\epsilon_0 = 8.85 \cdot 10^{-12} F \cdot m^{-1}$, $k_B = 1.38 \cdot 10^{-23} J \cdot K^{-1}$, n_e is the density of free electrons, $e = 1.6 \cdot 10^{-19} C$ and the temperature T is expressed in Kelvin degrees. It can also be shown that the definition of plasma requires that the number of free electrons available in a sphere of radius λ_D is $>> 1$, i.e. $\frac{4\pi\lambda_D^3 n_e}{3} >> 1$. Moreover, in most cases the Debye length is also much smaller than the typical linear size L, i.e. $L >> \lambda_D$. In this case, the plasma is *quasi-neutral*, i.e. i.e. the net electric charge density of a plasma is roughly zero everywhere. Any process which brings T to a large enough value (or lowers n_e correspondingly) may transform a gas or a mixture of gases -e.g. air- into a plasma. In this case, ions (electrons) play the role of positively (negatively) charged particles; even in a plasma, they may coexist with electrically neutral particles (atoms, molecules), dependng on the actual values of temperature and density. In particular, plasmas where the density of charged particles is much smaller than the density of neutrals are referred to as *weakly ionized*. Physical causes of the transformation of gases into plasmas include e.g. the application of sufficiently strong electromagnetic fields: lightning is a well-known example. Even if the external world applies no electromagnetic field, however, combustion itself may do the job: indeed, flames are quasi-neutral, weakly ionised plasmas [143]. As we shall see, a striking feature of plasmas is that their electric conductivity may be order-of-magnitude larger than the electric conductivity of gases -as it is clearly shown by the example of lightning.

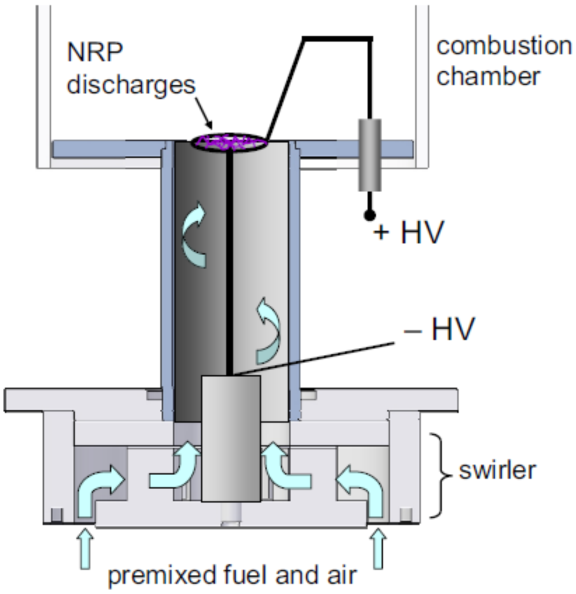

Experimental arrangement of the plasma actuator in the combustion chamber.

Figure 15.7: *From Ref. [103].*

Unfortunately, short life cycles -due to overheating and erosion of electrodes- and significant power consumption are the problems to be faced [147].

As for the electrodes, optimization of their electromagnetic coupling to the flame forces them to be located never too far from the flame itself, making their protection from the harsh conditions of the combustion chamber difficult. Similar arguments apply also to DC electrodes. In a nutshell, good electromagnetic coupling (a desirable thing) implies good thermal coupling (an undesirable thing).

As for power consumption, should 315 W be enough to suppress humming in a W_c = 43kW premixed flame, then linear extrapolation (if any) to a W_c = 50MW GT combustor would still require 366 kW electric power supply to the electrodes even for 3-mbar-amplitude humming, hardly an easy task in real-life operating conditions.

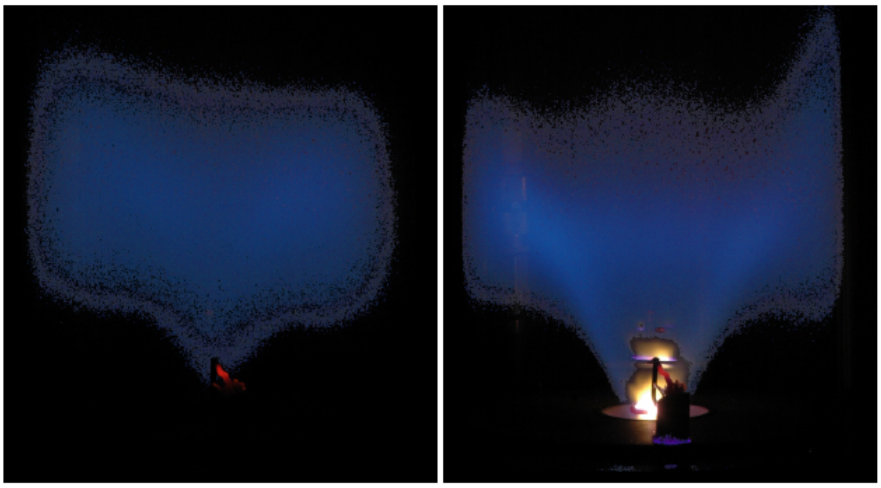

Mean images of the flame without (left) and with plasma discharges at a pulse repetition frequency of 20 kHz. Blue is enhanced in these images for an improved visualization of the flame.

Figure 15.8: *From Ref. [103].*

15.3 ..and radiofrequency (RF)

As for the problems with electrodes, bombardment [148] [149] [150] [151] [152] [153] of the flame with electromagnetic waves with frequency in the GHz range -referred to as *RF* here- seems to be an obvious answer. A conceptual lay-out of the experiment is displayed in Fig. 15.11. A more detailed lay-out is displayed in Fig. 15.12.

In fact, RF waves may propagate from the antenna across the gaseous mixture towards the flame, even if the antenna is located far from the flame. Thus, the RF antenna plays the role of an electromagnetic actuator, which could be free of the problems which affect existing electromagnetic actuators. Admittedly, this is only true in the so-called *weak field limit*, i.e. when the maximum electric field of the RF wave exceeds a given threshold nowhere. If this condition is not satisfied, the RF electric field triggers an electric breakdown which in turn leads to unwanted, parasitic electric arcs which waste RF energy and -possibly- erodes material surfaces like electrodes, combustor inner walls etc. We are going to see in the following that the weak field approximation is satisfied in all cases of practical interest.

As for the power consumption, we recall that RF power absorption occurs within the flame only [152] -unlike NRPP. In contrast with both DC fields and NRPP- RF creates

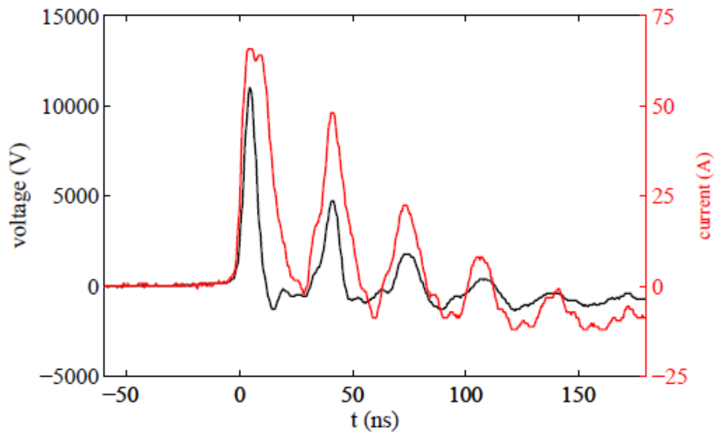

Voltage and current waveforms for a pulse repetition frequency of 50 kHz

Figure 15.9: *From Ref. [103].*

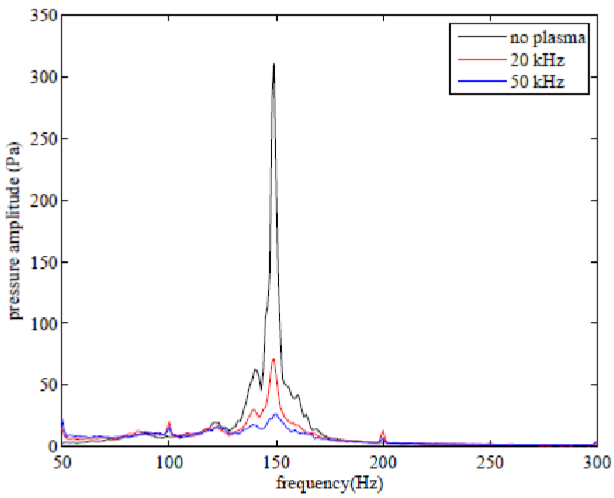

Amplitude spectra of the acoustic pressure measured in the combustion chamber without and with continuous plasma forcing at pulse repetition frequencies of 30 and 50 kHz.

Figure 15.10: *From Ref. [103].*

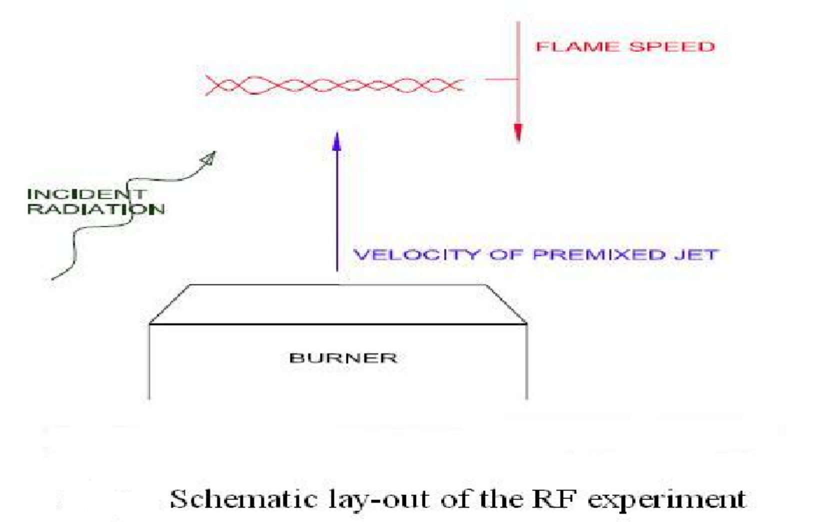

Figure 15.11: *A conceptual lay-out of the experiment - from Ref. [148].*

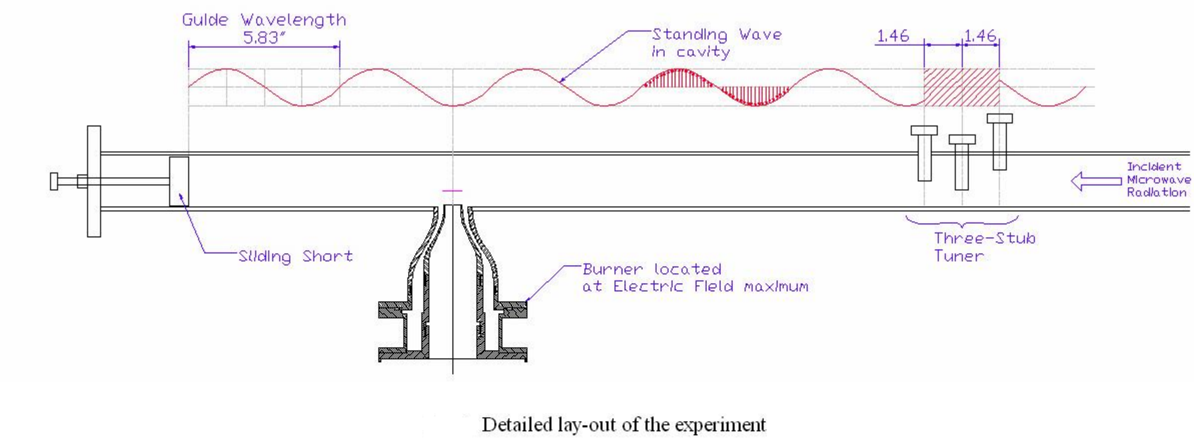

Figure 15.12: *A more detailed lay-out of the experiment. Dimensions are in inches - from Ref. [148].*

no plasma outside the flame in the weak field limit. As we shall see, RF takes rather advantage of the existence of free electrons inside the flame due to combustion even before RF. It follows that no power is wasted in the fluid around the flame. As a consequence, we expect that RF may be more efficient than NRPP.

Physically, in fact, all flames contain a tiny number of free electrons. Their number increases dramatically with increasing temperature. When RF is injected, free electrons absorb a small fraction of RF power; then, this absorbed amount of power goes to the rest of the flame because of collisions. Absorption of RF power depends on the free electron density, which in turn depends on the flame *electric conductivity* σ, a quantity which is usually overlooked in humming research. In particular, it is shown in the Appendix on RF-flame coupling that -at least if the RF frequency does not exceed tens of GHz- the density P_a of RF power absorbed inside the flame is proportional to σ, i.e.:

$$P_a \propto \sigma \tag{15.1}$$

In turn, σ vanishes for vanishing density of free electrons. Here we anticipate the result of the Appendix on electrical conductivity, that there are basically no free electrons outside the flame, while some free electrons are always available within the flame; moreover, their density is largest in the very thin reaction region of thickness $\frac{\delta_L}{Ze}$ where the combustion reaction rate peaks inside the flame.

According to the scaling (15.1), moreover, there is another reason for optimism ocncerning RF capabilities in humming control. We show in the Appendix on the electrical conductivity of the flame that σ is a monotonically, very rapidly increasing function of T: it changes by more than 10 orders of magnitude in the range 900 K $< T <$ 2200 K. Now, this very fact suggests that application of RF may trigger a positive feedback, just like a lighted match in a microwave oven: RF starts heating the flame according to (15.1), the ensuing flame heating raises σ, in turn this growth raises P_a etc., unless a large efficiency in RF absorption is achieved even if the volume of the absorbing region is tiny.

Intuitively: even if no arc is triggered and fully uncontrolled breakdown is never achieved, we are on the verge of the knee between saturation zone and ionisation zone in Fig. 15.4, just when σ starts rising, so that no large electric field is required in order to raise P_a. Even so, the impact on the flame is large precisely because the region where RF absorption occurs is tiny. Moreover, it is the field itself which raises σ, hence we retrieve the *increased reactivity* of the DC case with no need of raising T_u and with no increase in pollution (just as in the DC case). Finally, since no free electron exists outside the flame -unlike DC and NRPP- we waste no energy in accelerating them towards the electrodes. For the same reason, RF automatically couples to the flame regardless of its detailed motion (which is always much slower than the propagation of RF waves at the speed of light).

Here we anticipate that RF impact on humming is due to the capability of RF in controlling the laminar flame velocity s_L. This leads to a further argument in support of RF. Indeed, we have seen that combustion in GT combustors occurs very near to the blow-out point, and therefore not far from the stability line where small perturbations may produce very large responses. The other side of the coin is that RF-based control of humming is likely to require no large variation of s_L, hence no exceedingly lare amount of power supply to the RF antenna.

It could be objected that the proof of (15.1) in the Appendix on RF-flame coupling relies on the assumption of a flat, laminar flame. (More to the point, the validity of the proof for turbulent flame is subject to some additional conditions concerning RF and turbulence, which are justified below). In contrast, flames in GT combustors are both non-flat and turbulent. However, this lack of self-consistency is definitely not relevant. In fact, the speed of propagation of RF waves, namely the speed of light of vacuum c, is so large that we may safely assume the RF wave to reach the different parts of the flame simultaneously. This fact provides also our discussion of the impact of turbulence on RF-flame interaction below with a physical basis. Intuitively, photons are so fast that turbulent whirls seem to them like standing still. In particular, the scaling (15.1) and its consequences are perfectly reasonable for turbulent flames too. In fact, the microscopic phenomena -like electron-photon interactions, electron-neutral collisions and the like- which rule RF absorption occur on a much shorter time-scale (say, 10^{-10} s) than the typical time-scale τ_K of Kolmogorov cells in turbulent fluids ($\tau_K \approx 10^{-5}$ s, as shown in the Appendix on the flame speed).

Moreover, we expect the exact flame position to affect flame-RF wave coupling only weakly, in the weak field limit at least. In this limit, in fact, RF automatically couples only to the region of thickness $\frac{\delta_L}{Ze}$ quoted above, maintaining that coupling as the flame front oscillates during the humming [3]. Of course, in case of RF standing waves this conclusion holds provided that the flame is not located near minima of the RF electric field.

In particular, as far as the free electrons are concerned, a primary ionisation mechanism in combustion with hydrocarbons is the associative chemionisation

$$CH + O \rightarrow CHO^{+} + e$$

in collisions of CH radicals and oxygen atoms, with subsequent conversion of CHO^{+} ions into more stable H_3O^{+} ions [148] [149]. Electrons are lost primarily in two-body dissociative recombination with H_3O^{+} ions, and -to a lesser degree- in attachment accompanied by formation of negative ions. Quantitative discussion requires dedicated, detailed kinetic treatment, because these reactions are not well described by the approximation of local thermodynamical equilibrium [4]. Luckily, the mass fractions of the chemical species involved in the reactions which are responsible for σ are $\ll 1$, so that we can still apply the results based on Le Châtelier's principle to the flame which interacts with RF.

[3]Admittedly, additional coupling may occur in the downstream region due to the presence of residual ions, but this appears to be much less than in the flame front [149].

[4]For example, the associative chemionisation quoted in the text is *exothermal* -see e.g. equation (1) of Ref. [154]. Should LTE rule it, Le Châtelier's principle would make RF heating to *suppress* production of free electrons, in contrast to what happens in the microwave oven quoted above.

We discuss this kinetic treatment in the Appendix dedicated to the electrical conductivity of the flame. It has been performed by Prof. Colonna and co-workers at Consiglio Nazionale delle Ricerche in the framework of a collaboration with Ansaldo Energia, starting from data provided by the latter concerning real Ansaldo combustors (full credits are listed in the Appendix).

Finally, typical linear size of a 3 GHz antenna is $\approx$ 10 cm, i.e. the linear size of a ceramic tile in the inner wall of a combustion chamber of a GT combustor. Conceivably, therefore, there is plenty of choices for suitable antenna protection from the heat flux coming from the combustion chamber [5]. Good electromagnetic coupling does not imply good thermal coupling. This is why the GHz range is so attractive: lower and higher frequencies may lead to dimensions » 10 cm (not compatible with the lay-out of a GT combustor) and to exceedingly large power density at the antenna respectively. Engineering of flame-RF coupling may take advantage of the decade-old expertise in plasma RF heating in hostile environments -see e.g. [155]. Even small antennas may inject considerable amount of RF power, as the RF power density at the antenna may reach 25 $MW \cdot m^{-2}$ at RF wave frequency $\nu_{RF} = 3.7$ GHz [156].

Admittedly, however, nobody has tried to control humming with the help of RF -*yet*. Indeed, we have still to answer to two questions:

- Why should RF control humming?
- How much power is required at the RF antenna?

The analogies between RF and NRPP discussed above suggest that if we are able to provide an answer to the first question then we are also able to understand why NRPP stabilise humming. The fact that NRPP act on humming in agreement with Le Châtelier's principle suggests that we may take advantage of the results of our discussion of humming thermodynamics, including suitably selected versions of Rayleigh's criterion. Accordingly, we are going to utilize the latter criterion in order to provide a quantitative answer to the second question, which is crucial to possible applications on real GT combustors.

15.4 Why should RF control humming?

First of all, there are many similarities between NRPP -which *do* hinder humming- and RF:

- Just like NRPP, RF induces Ohmic heating of the flame -as shown in the Appendix dedicated to RF-flame coupling.
- RF wave period ($\approx$ ns) is similar to NRPP period.

[5] For instance, the tile itself may be helpful. A scaling similar to (15.1) ensures that the tile, whose electrical conductivity is negligible, absorbs no RF power. Moreover, no parasitic arc occurs between the RF antenna and the metallic components of the combustor, in the weak field limit at least. Finally, it has been demonstrated that electric fields can be transmitted through ceramic CC walls using capacitive coupling [142].

- Both pulsed RF and NRPP rely on commercially available, pulsed power technology.
- Both pulsed RF and NRPP lead to extension of lean combustion limit in methane-air mixtures [157].

Perhaps, the most tantalizing clue about the relevance of pulsed RF to humming is the fact that, quite unexpectedly, pulsed RF has shown the ability to generate a strong, audible sound generated from the flame region [152]. The sound follows the frequency associated with the repetition rate of the RF source and increases in intensity with power level of the incident radiation. Reasonably, if RF generates sound at the flame, it may also control it.

Indeed, many experiments unambiguously show that RF increases the laminar flame speed s_L significantly (by 70% and even more, in some cases) in lean, premixed, air-hydrocarbon, flat, laminar flames [148] [149] [150] [153] even if no humming occurs. Similar results have been obtained in Bunsen laminar flames [151] and turbulent flames [152]. This is not surprising as as s_T increases with increasing s_L and s_L is a well-known, increasing function of the flame temperature on the burnt gas side [2]; the RF wave heats the flame, hence raises s_L. However, RF-induced growth of s_L has been reported even in absence of flame heating; this is possibly due to RF-induced changes in chemical kinetics [151]. Here we refer to no detailed mechanism of RF-induced growth of s_L, and take it as an experimental fact. We refer to Fig. 15.13 and to Fig. 15.14.

for the measurements taken in the experimental lay-out photographed in Fig. 15.15.

In these experiments, the RF frequency was 2.45 GHz and the flame diameter and thickness were 1.7 cm and 0.4 cm respectively. Further operational conditions are listed in Fig. 15.16.

Not surprisingly, RF optics plays a crucial role -see Fig. 15.17.

For given inflow, raising the flame velocity is equivalent to shifting the flame towards the inlet, thus modifying the geometry of the combustion process, in analogy to what we have seen in the NRPP case (Fig. 15.8): see Fig. 15.18 and Fig. 15.19.

An independent confirmation is provided in [151], where the flame geometry is different (Bunsen conical, not flat): see Fig. 15.20 and Fig. 15.21.

Remarkably, a good efficiency in the RF absorption is a less stringent constraint than intuitively expected. In fact, it turns out [152] that with the addition of 1.2 kW of CW 2.45 GHz microwave power, flame speed enhancements of over 30 % can be achieved in a flame that only absorbs roughly 15 W of the microwave power - see Fig. 15.22.

These experimental facts allow us to write:

$$\frac{ds_L}{dP_a} > 0 \tag{15.2}$$

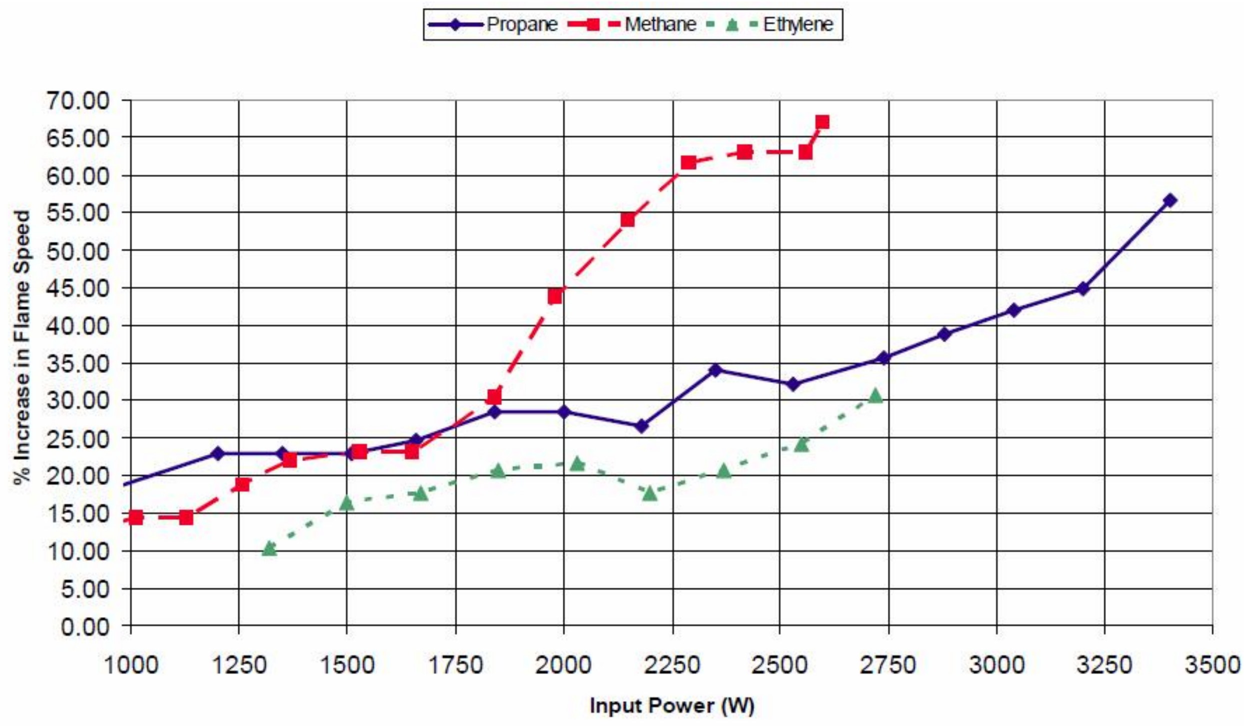

Percent increase in hydrocarbon-air flame speed as a function of microwave power.

Figure 15.13: *From Ref. [148].*

The scaling (15.1) ensures that the RF leaves the upstream fluid outside the flame (where $\sigma = 0$) unaffected. Then, RF acts just like the other approachs to humming stabilisation described above: it raises the flame velocity while leaving the upstream flow unaffected. Now, it is shown in the Appendix on the flame velocity that any physical process which raises the flame velocity while leaving the upstream flow unaffected tends to stabilise humming. This result holds both in laminar flames and in turbulent flames. Then, we are tempted to conclude that RF can stabilize humming both in laminar and turbulent flames.

All the same, the research into laminar flame enhancement allows no easy generalisation transition into studies of turbulent flame enhancement because the turbulent flames release much greater power (turbulence raises flame velocity) and have a high degree of spatial and temporal complexity. Reasonably, the larger the heat release, the larger the RF power required. Experiments [152] show that the same continuous-wave (CW) RF source effectively utilised for laminar flames affects turbulent flames only weakly (for given flows, etc.) as the turbulent heat release is much larger than the laminar one. This result is displayed in Fig. 15.23, where the impact on a turbulent flame of a RF source which has

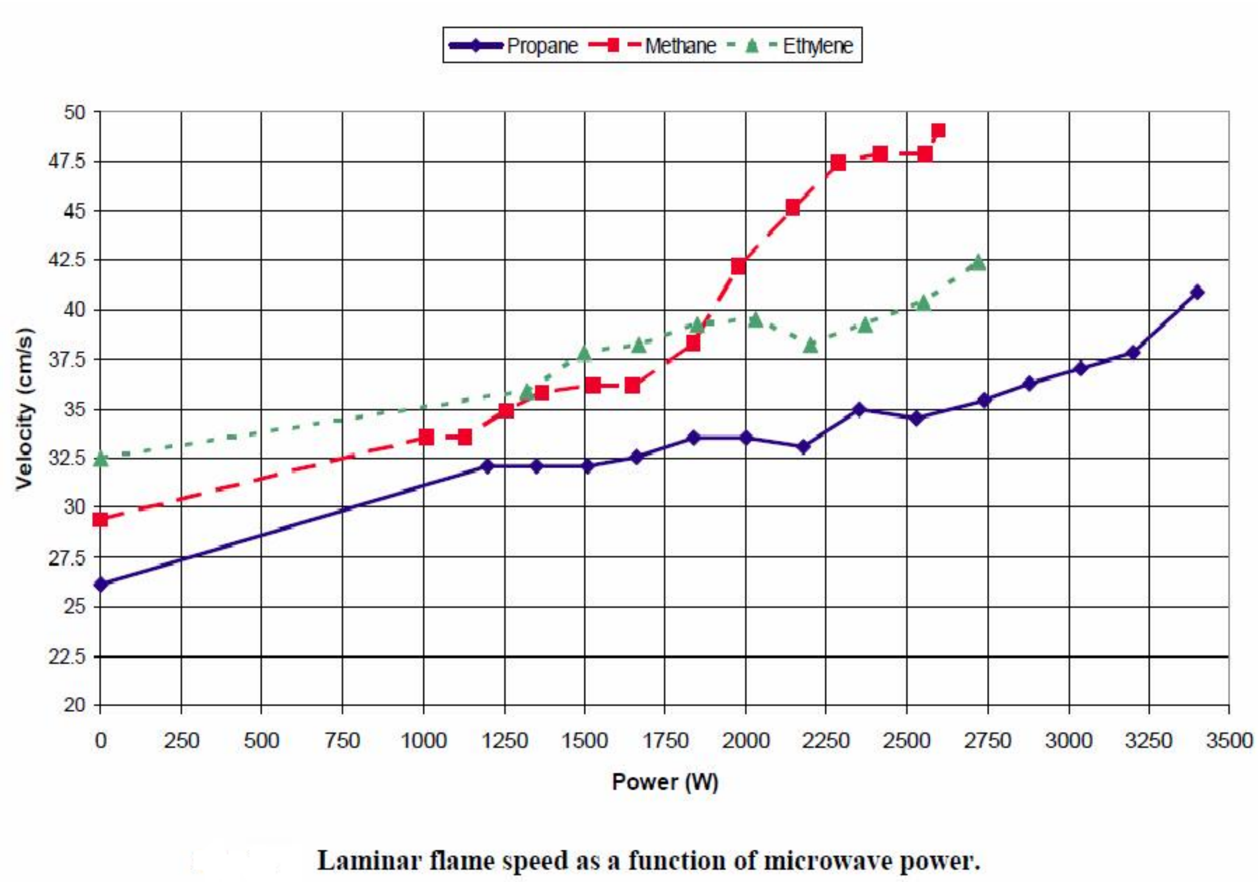

Figure 15.14: *From Ref. [148].*

previously led to a 35 % growth of flame velocity in a laminar flame appears to negligible.

However, the authors of Ref. [152] report also that *pulsed* RF may do the job effectively on turbulent flame, as the peak RF power at each pulse is order-of-magnitude larger than the averaged RF power. (At large RF power, moreover, the shorter the RF pulse the less likely the triggering of undesired parasitic discharges). In the following we display the results obtained with a 3 GHz source. This device is designed to generate $1\mu s$ pulse width at 1000 Hz repetition rates , producing 25 watts of average power and 25 kW of peak power. The air-methane flame is lean ($\phi \approx 0.7-0.8$) and the heat release is about 2 kW (the inlet mass flow is 50 standard litres per minute). Considering a flame thickness of approximately 0.5 mm and flame speeds less than 1 $m \cdot s^{-1}$, a reasonable characteristic time for reactants to pass through the preheat and reaction zone is about one millisecond. It was therefore expected that the separation between the pulses needs to be less than the flame passage time to have any potential coupling of energy into the flame front. By monitoring the microwave reflected power from the flame load and varying the pulse repetition rate of the RF source (a magnetron) a characteristic time of the interaction can be approximated -see Fig. 15.24.

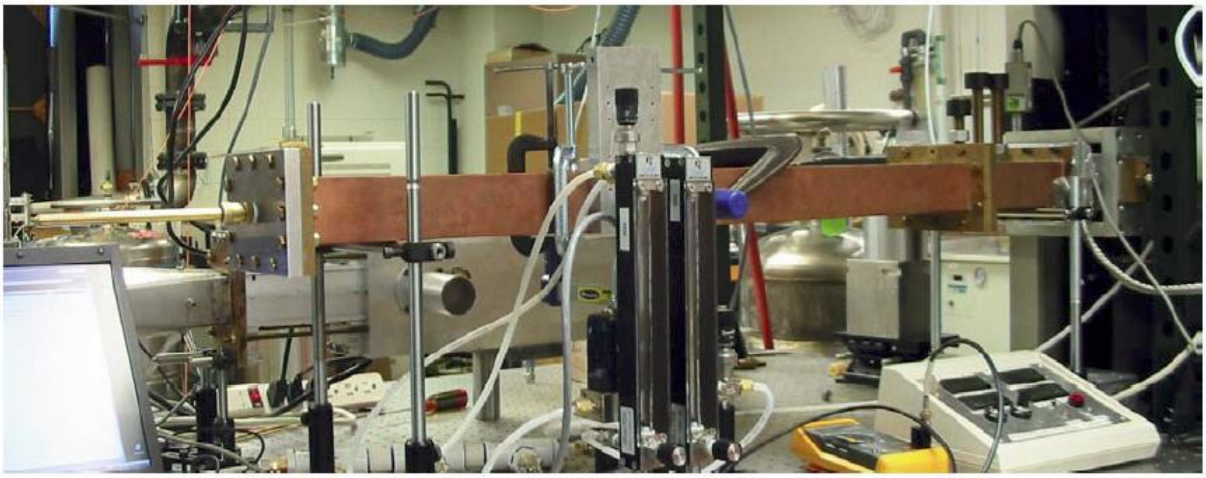

Laminar flame burner coupled to a rectangular microwave cavity operating in the TE_{01n} resonant mode. The cavity is formed from WR430 rectangular waveguide with an adjustable short forming one end wall and a 3-stub tuner forming a partially reflecting wall on the other end. The photo shows the actual laboratory set-up.

Figure 15.15: *From Ref. [148].*

It is apparent that the coupling is increasingly enhanced until 300 Hz when it levels off before rising again around 800 Hz, when the separation between pulses is less than 1.25 ms. The latter conclusion can be independently checked with the help of a laminar flame. A series of images -see Fig. 15.25- of the laminar flame enhancement at several repetition rates depicts the significant effect of this rate on the flame propagation speed. RF-induced displacement of a turbulent flame (Re = 3500, heat release ten times greater than in the laminar case) is displayed in Fig. 15.26 below. As a rule of thumb, experiments show that an average RF power of 25 W (and a peak RF power of 25 kW, each pulse $1 \mu s$ long) is needed to generate the 35 % flame speed enhancements in a lean laminar air-methane flame similar to that found with 1.4 kW of CW RF power. Ten-fold increase in flame velocity due to turbulence corresponds to an average RF power at the antenna in the kW range for a turbulent air-methane flame with 50 liters/min. inlet mass flow and $\Phi = 0.81$.i.e. $W_c \approx 2$ kW.

Not surprisingly, this conclusion is in agreement with Le Châtelier's principle: if we describe the flame as a region of space where both exothermal reactions (i.e. combustion) and endothermic reactions occur, then RF acts as a small heating due to the external world (which switches the antenna on). Here the words *small* is justified as far as we limit ourselves to the case $P_a << Q$ - see the Appendix on RF-flame coupling. Le Châtelier's

- Propane-Air
  - Mass flow rate – 5084 cc/min
  - Exit velocity – 48 cm/s
  - Equivalence Ratio – 0.6
- Methane-Air
  - Mass flow rate – 5744 cc/min
  - Exit velocity – 54 cm/s
  - Equivalence Ratio – 0.7
- Ethylene-Air
  - Mass flow rate – 4477 cc/min
  - Exit velocity – 42 cm/s
  - Equivalence Ratio – 0.5

Figure 15.16: *From Ref. [148].*

principle ensures that such heating pushes the system towards the endothermic reactions and hinders combustion, which is the ultimate energy source of humming.

Remarkably, a crucial point in our discussion is that RF leaves the upstream flow unaffected. As anticipated, RF is just one of the possible strategies aiming at humming stabilisation which are based on controlled growth of flame velocity at given upstream flow, some of which have been discussed in the Chapter about Le Châtelier's principle. We could say that as the external world tries to heat the flame, the latter tries to counteract this disturbance by shrinking the volume where RF power can be absorbed, i.e. the hot region where σ is large. But since this region coincides with the region where combustion occurs [6], the flame unavoidably shrinks also the region where combustion occurs. Since combustion feeds humming, the outcome of RF bombardment is the stabilisation of humming. Mathematically, the reduction in flame volume leads to a reduction of the domain of integration of the destabilising term in Rayleigh's criterion, whose final value gets therefore reduced [7]. Similar arguments hold if we decide to invoke Myers' corollary,

[6] As discussed in detail in the Appendix on the electrical conductivity of the flame, σ -which the absorbed RF power depends upon according to (15.1)- depends on the free electrons provided by chemical reactions in the reaction zone, where recombination is less likely due to the large values of T.

[7] We have discussed the evolution in time of the flame surface area elements in the Appendix on the flame velocity. RF acts in constrast with active approaches to humming control which are based on

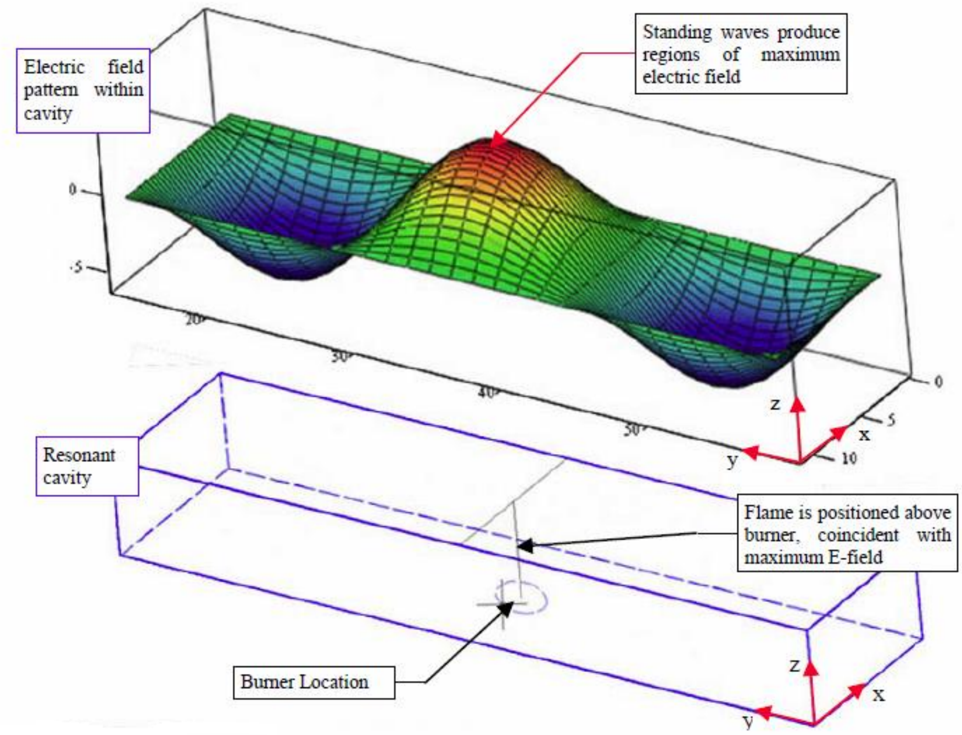

A rectangular microwave resonator formed from WR430 waveguide was used to subject the laminar flame to microwave radiation. The system was designed to make the flame location coincident with a region of maximum electric field intensity. The above figures show both the resonant cavity (note the location of the burner exit) and a contour plot of the electric field strength at each x-y location within the cavity. Also note that for the $TE_{1,0,n}$ resonant condition the electric field vector only has an E_z component.

Figure 15.17: *From Ref. [148].*

rather than Rayleigh's criterion.

Basically, *there is nothing special about RF.* Simply speaking, an advantage of RF is just that the antenna operates with no mechanical wearing at all, lies safely far from the flame and can be protected against erosion. Another advantage is that RF allows transmission of power towards the flame, and the absorption of this power inside the flame relies on free eelectrons which are already available here (and are possibly multiplied as a consequence of the absorption itself). In contrast, arcs (lke e.g. NRPP) are likely to require power just to create an electrically conducting channel across the region between the electrodes and the flame in order to allow power transmission from the former to the latter. Our discussion invokes no detailed description of RF-flame interaction; it relies rather on (15.2). As such, it applies also to NRPP stabilisation experiments. (For example, NRPP stabilises turbulent flames [101], in analogy with what has been shown for RF above). This is not surprising, as its foundation is of thermodynamical nature, hence

mechanical actuatore. Such approaches aim rather at controlling humming through modification of the relative phases in the Rayleigh index. As shown below, RF leaves such phases unaffected.

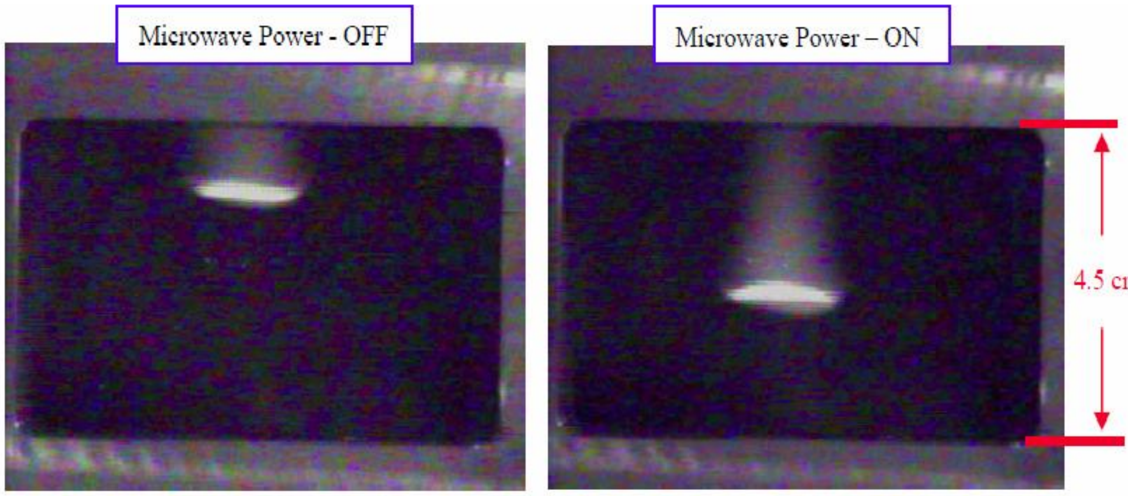

The microwave cavity contained a viewing window which was covered with wire mesh to prevent microwave leakage. This port was used to observe the behavior of the flame. Upon the introduction of microwave power into the microwave cavity, the flat flame moved down to a new stable location closer to the burner exit, thus indicating an increase in laminar flame speed.

Figure 15.18: *From Ref. [148].*

independent from the microscopic physics. Should we e.g. investigate the effect of wall cooling at given upstream flow, we could identify P_a with the density of heat supplied per unit time by the wall to the flame: P_a would therefore be a negative quantity, in contrast with the RF case where it is positive. We know that wall cooling decreases the flame velocity, hence (15.2) still holds; indeed, wall cooling triggers humming, in agreement with the experimental results quoted above [29].

15.5 How much power is required at the RF antenna?

15.5.1 Myers' corollary, again

We have shown that RF *may* stabilize humming. Up to now, however, this is just a vague possibility. Practical application requires that the power W_{ant} supplied to the RF antenna never exceeds a tiny fraction of the rated heat release W_c of the combustor. For a $1m^3$-sized, $W_c = 50MW$ combustor a conservative requirement is that W_{ant} does not exceed 100 kW [8]. The smallness of RF heating of the flame is therefore perfectly justified, as $P_a << Q$. Luckily, it is possible to show -see the Appendix on RF-flame coupling- that

[8] A 10-cm-sided square antenna still manages such power at surface power density $< 25MW \cdot m^{-2}$, but cooling could be a problem at larger values of W_{ant} in the lay-out of real combustors.

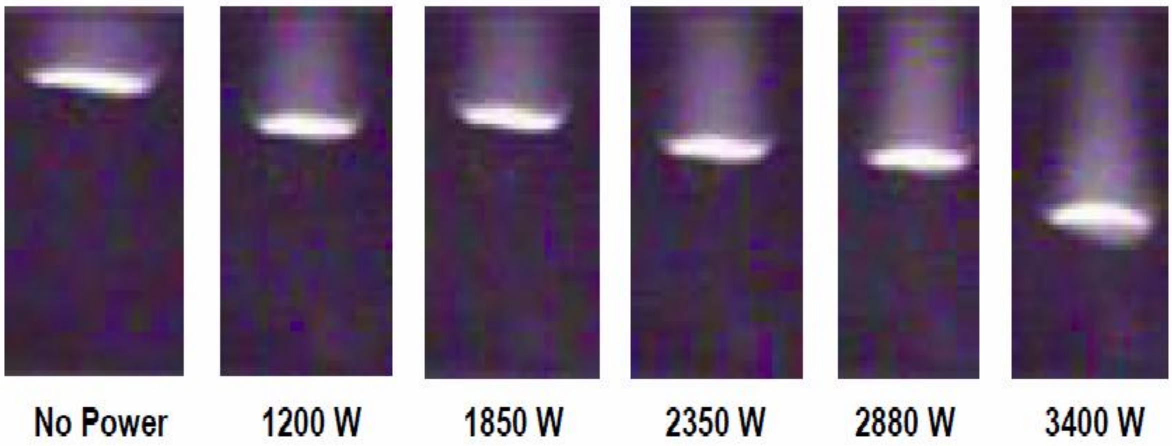

Sequence of video stills taken during a 30 minute test. The flame occupied a roughly circular volume with a diameter of 1.7 cm and a thickness of 0.4 cm. As the microwave power level was increased the flame moved downward against the flow of the fuel/air jet towards the burner exit.

Figure 15.19: *From Ref. [148].*

this case falls well within the weak field limit, and parasitic arcs are therefore less likely to occur.

We want to estimate W_{ant} in the following. To this purpose, we invoke Myers' corollary. Just like Rayleigh's criterion, indeed, the derivation of Myers' corollary from first principles depends on no detailed model of flame heating, so that RF does not weaken its validity. Rayleigh's criterion provides information on the stability of an unperturbed, steady state with zero mean flow against small perturbations. After time-averaging, Myers' corollary provides information on the stability of an unperturbed, oscillating state against perturbations, while requiring neither zero mean flow nor small perturbations. A a system flame+fluid+combustor in humming is an example of such oscillating state. Information provided by Myers' corollary and by Rayleigh's criterion are formally identical, provided that Rayleigh's index is suitably redefined. Finally, Rayleigh's criterion is connected with Le Châtelier's principle of thermodynamics. This principle leads to further necessary criteria of stability of the unperturbed, steady state which are basically equivalent to Rayleigh's criterion. We have also shown that the same criteria apply also to the stability of oscillating unperturbed state, after suitable time-averaging. Then, we are allowed both to invoke Myers' corollary in order to gain information about humming, and to expect that such information is in agreement with Le Châtelier's principle. This

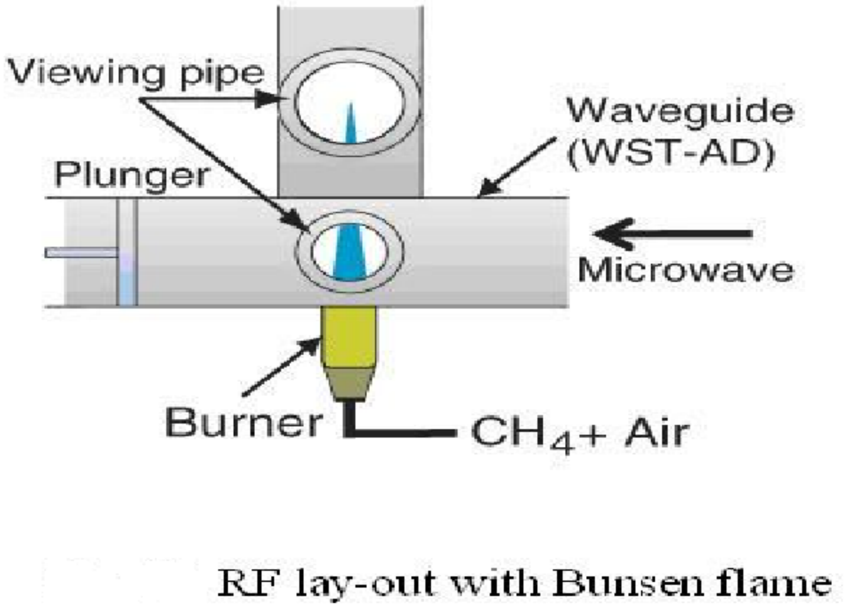

Figure 15.20: *From Ref. [151].*

is the topic of this Section.

In our approach, we start from a system flame+fluid+combustor which oscillates at a given humming amplitude, and look for the value of W_{ant} which may reduce/zero this amplitude. This approach differs from the conventional one, which analyzes stability of a system initially in steady state against small perturbations. In contrast with our approach, indeed, the conventional approach has two disadvantages.

Firstly, the conventional approach postulates that a system with no humming is in steady state. In contrast, our approach deals with the system in humming as the unperturbed state, and postulates nothing on the humming-free combustor. Indeed, the well-known resiliency of humming against any attempt to suppress it once triggered agrees well with the description of humming as a limit cycle with a finite basin of attraction. Correspondingly, a finite amount of RF power is required in order to drive the system away from this basin. Myers' corollary does the job in a model-independent way below.

Secondly, if the unperturbed state is a steady state then the humming amplitude coincides with the amplitude of the perturbation. Proper description of the latter amplitude (and of the value of RF power required to zero it) requires a detailed nonlinear model,

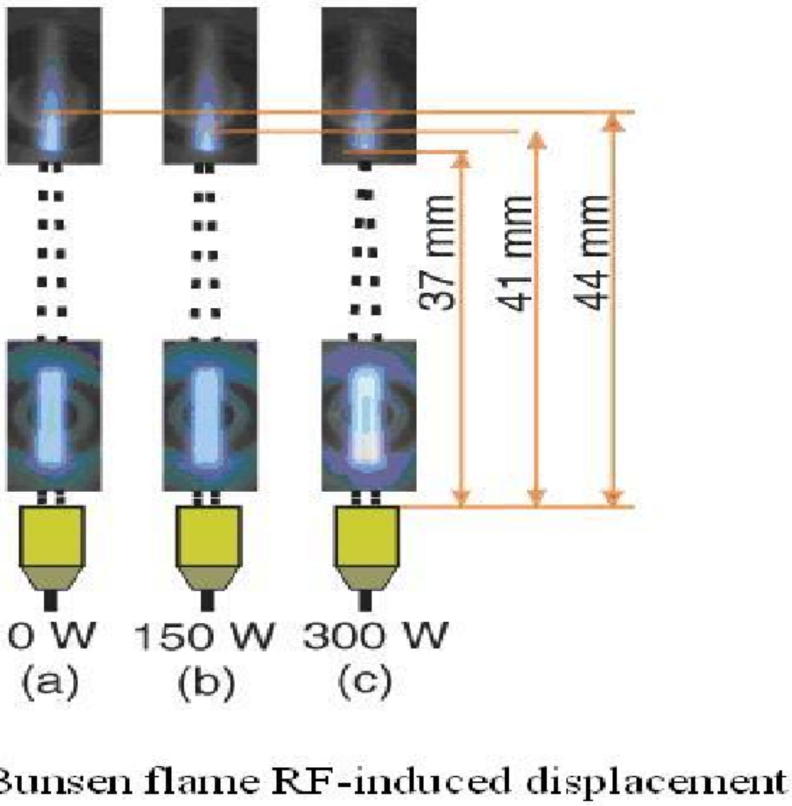

Figure 15.21: *From Ref. [151].*

as linear models provide no information on perturbation amplitides. In contrast, the main advantage of our thermodynamic discussion is that its results depend on no detailed model, even if nonlinear.

15.5.2 Preliminary steps

RF absorption and non-zero Mach number

Since we want to investigate the impact of RF on Myers' corollary, we are going to invoke the results of the Appendix on RF-wave electromagnetic coupling. Admittedly, the arguments in this Appendix ignore any impact of non-zero Mach number - i.e. of non-vanishing $\mathbf{v}_0$. Moreover, they neglect turbulence. We are going to generalise them to turbulent flames with $\mathbf{v}_0 \neq 0$ in the following.

As for the impact of $\mathbf{v}_0$ on RF-wave electromagnetic coupling, convection rules flame cooling in Ansaldo combustors. In order to see any heating, we have to apply RF power in short bursts, the duration τ_{RF} of each burst being shorter than the *residence time* τ_{res} of the flow across the flame:

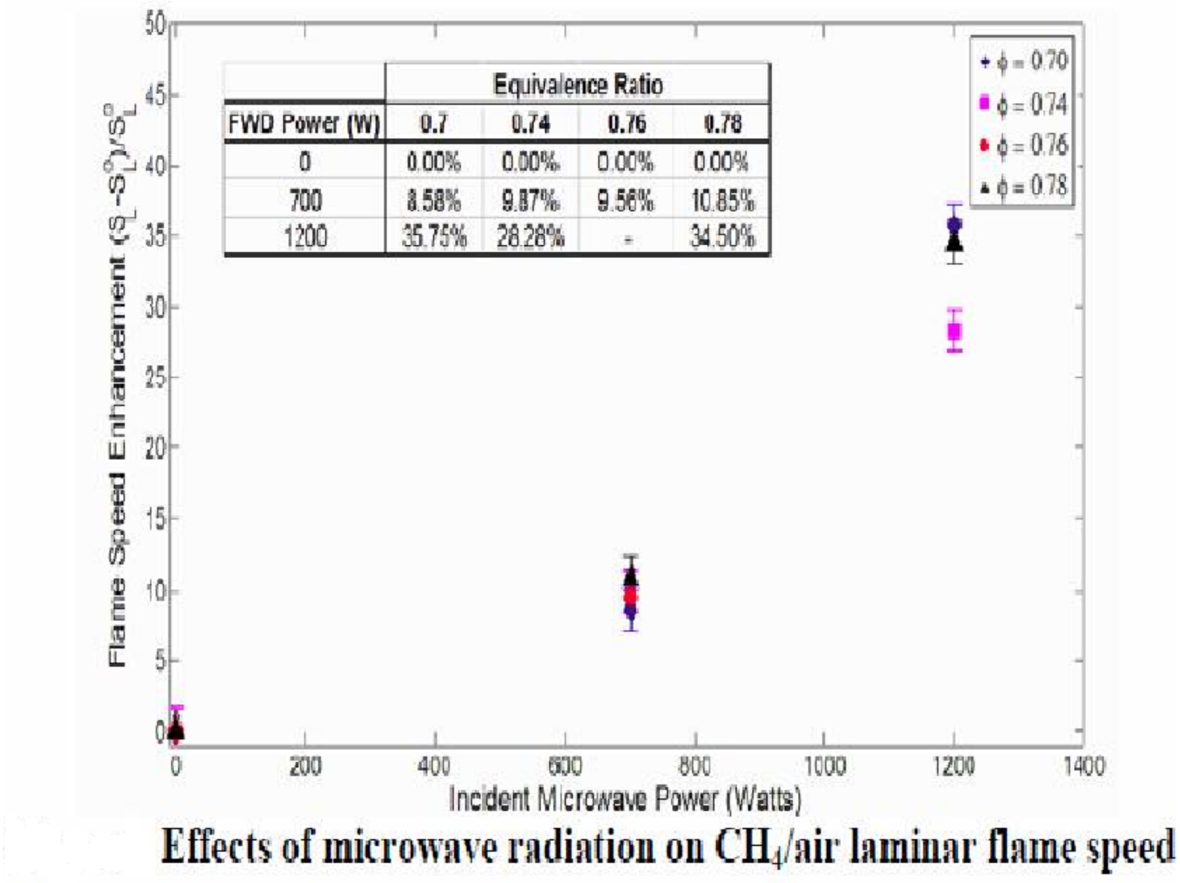

Figure 15.22: *From Ref. [152].*

$$\tau_{RF} \leq \tau_{res}$$

Now, let us compute the value τ_L of τ_{res} for laminar flames; we shall compute the value τ_T of τ_{res} for turbulent flames in the following. Since diffusion carries heat from the reaction zone of thickness $\frac{\delta_L}{Ze}$ where RF is absorbed and the rest of the flame (with thickness $\approx \delta_L$), the relevant residence time is

$$\tau_{res} = \tau_L \approx \frac{\delta_L}{|\mathbf{v}_0|}$$

The corresponding value

$$\tau_{res} = \tau_T \approx \frac{\delta_T}{|\mathbf{v}_0|}$$

for turbulent flames is value is significantly larger than τ_L, as the mean turbulent flame brush thickness δ_T is always larger than the laminar flame thickness -see Sec. 4.3 of [4]. For example, according to equation (8) of Ref. [112] we have $\delta_T \approx Da^{-\frac{3}{4}} \cdot l_T$ where Da, $l_T = \frac{Re_T \nu}{u'}$, Re_T, ν and u' are the *Damkoehler number* on the length scale l_t, a typical

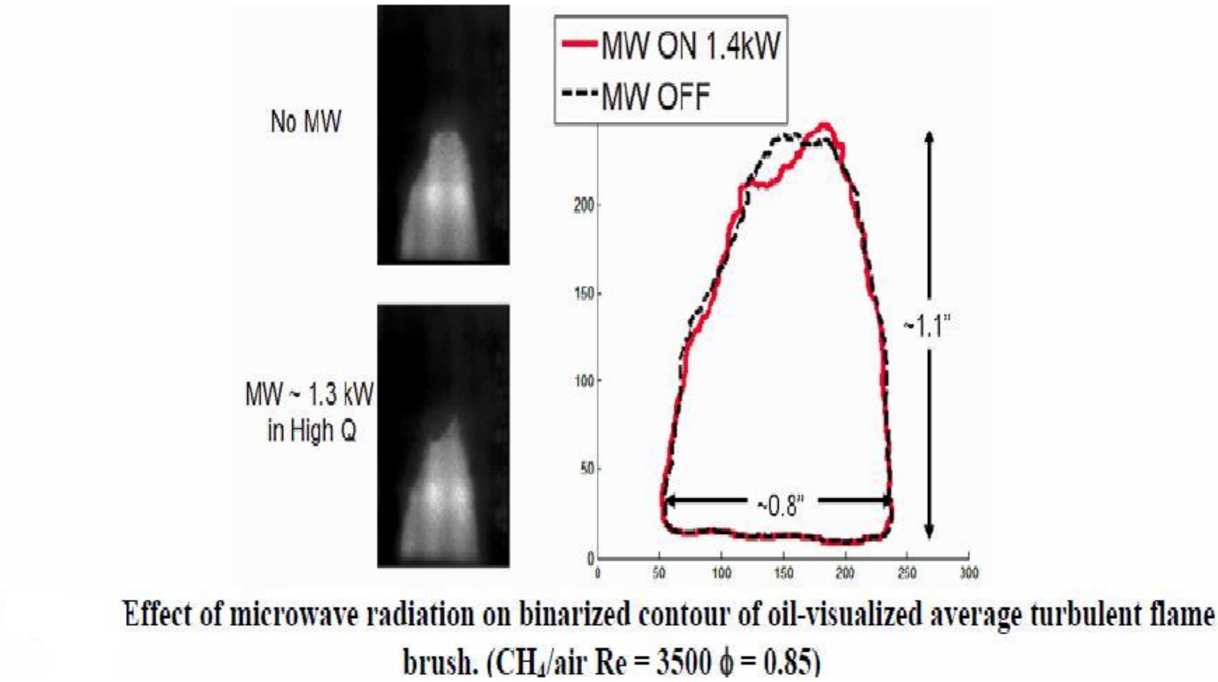

Figure 15.23: *From Ref. [152]. The wording* High Q *in the figure caption means* negligible RF power losses.

length for turbulence, the *turbulent Reynolds' number* -see equation (4.5) of [4]- the kinematic viscosity and the typical amplitude of turbulent velocity fluctuations respectively. In particular, Da is the ratio of τ_L and the typical time of chemical reactions, and is supposed to go to ∞ for infinitely fast chemistry. For turbulent flames equation (4.50) of [4] gives $Da \approx \frac{l_T^2 s_L^2}{\nu^2 Re_T}$. For typical values $\nu = 10^{-5}\frac{m^2}{s}$, $Re_T = 10^3$, $u' \approx |\mathbf{v}_0|$ for well-developed turbulence with $|\mathbf{v}_0| \approx$ some $\frac{m}{s}$ and $s_L \approx 0.2\frac{m}{s}$ -see Fig. 2.5 of [4]- we have $l_t \approx$ some mm and $Da \approx 10$, so that $\delta_T \approx$ some mm, i.e. about ten times larger than $\delta_L \approx 10^{-4}$ m. Accordingly, for turbulent flames we require $\tau_{RF} < \tau_T \approx$ some 10^{-4} s.

RF absorption and turbulence

The impact of turbulence on RF absorption Generally speaking, turbulent combustion results from the two-way interaction of chemistry and turbulence. When a flame interacts with a turbulent flow, turbulence is modified by combustion because of the strong flow accelerations through the flame front induced by heat release, and because of the large changes in kinematic viscosity ν associated with temperature changes. On

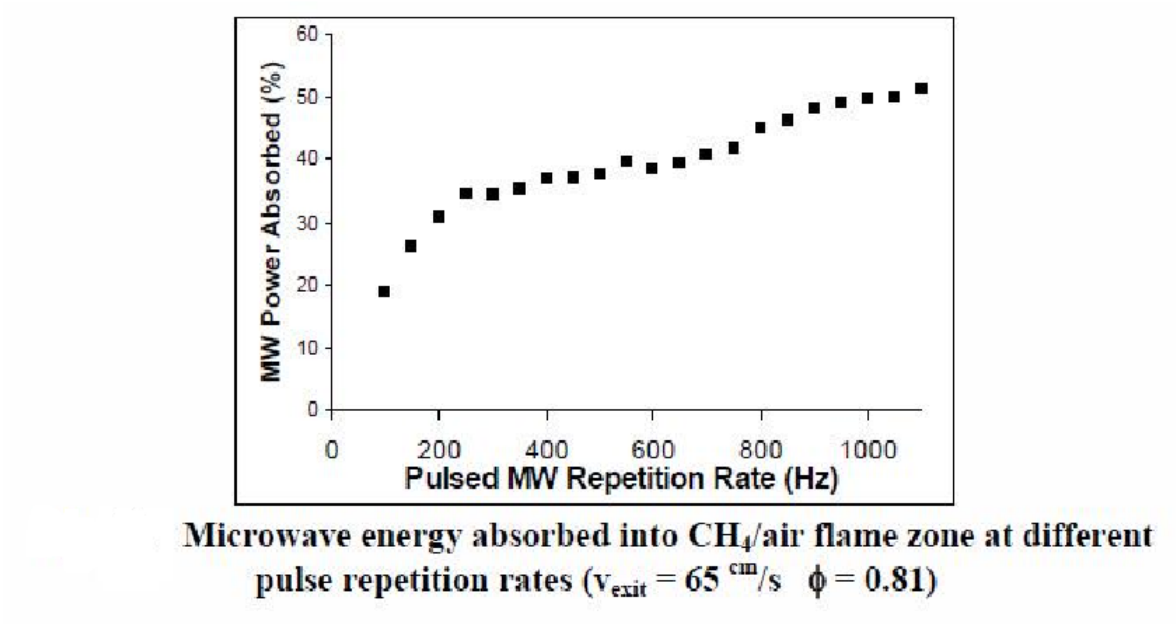

Figure 15.24: *From Ref. [152].*

the other hand, turbulence alters the flame structure, which may enhance the chemical reaction but also, in extreme cases, completely inhibit it, leading to flame quenching. It is therefore worthwhile to ask if turbulence affects RF absorption, and conversely, if RF absorption affects turbulence. Should the answer to both such questions be negative, we would be allowed to assess the impact of RF on humming stability with the help of the results of our Appendix on RF-flame coupling, which have been derived for laminar flames.

As for the impact of turbulence on RF absorption, we want to check if the absorption of RF power in the flame is slower than the transport of heat across the flame. Should it be so, heat transport would cool the flame before the RF heats it, and RF would have negligible impact on the thermodynamics of the flame. Turbulence significantly raises heat diffusion with respect to the laminar flame. While the molecular diffusion coefficient $\propto \nu$ utilised in the description of the laminar case still describes diffusion at the Kolmogorov scale, a larger diffusion coefficient $\propto \nu \cdot Re_T$ acts when turbulence occurs [9] -see the Appendix on the flame velocity. The latter coefficient is to be compared with the diffusion coefficient $\frac{c^2 \epsilon_0}{\sigma}$ which rules electromagnetic energy transfer in electric conductors

[9]For the purpose of the present, qualitative discussion we neglect the difference between the diffusion coefficient of heat and the diffusion coefficient of particles.

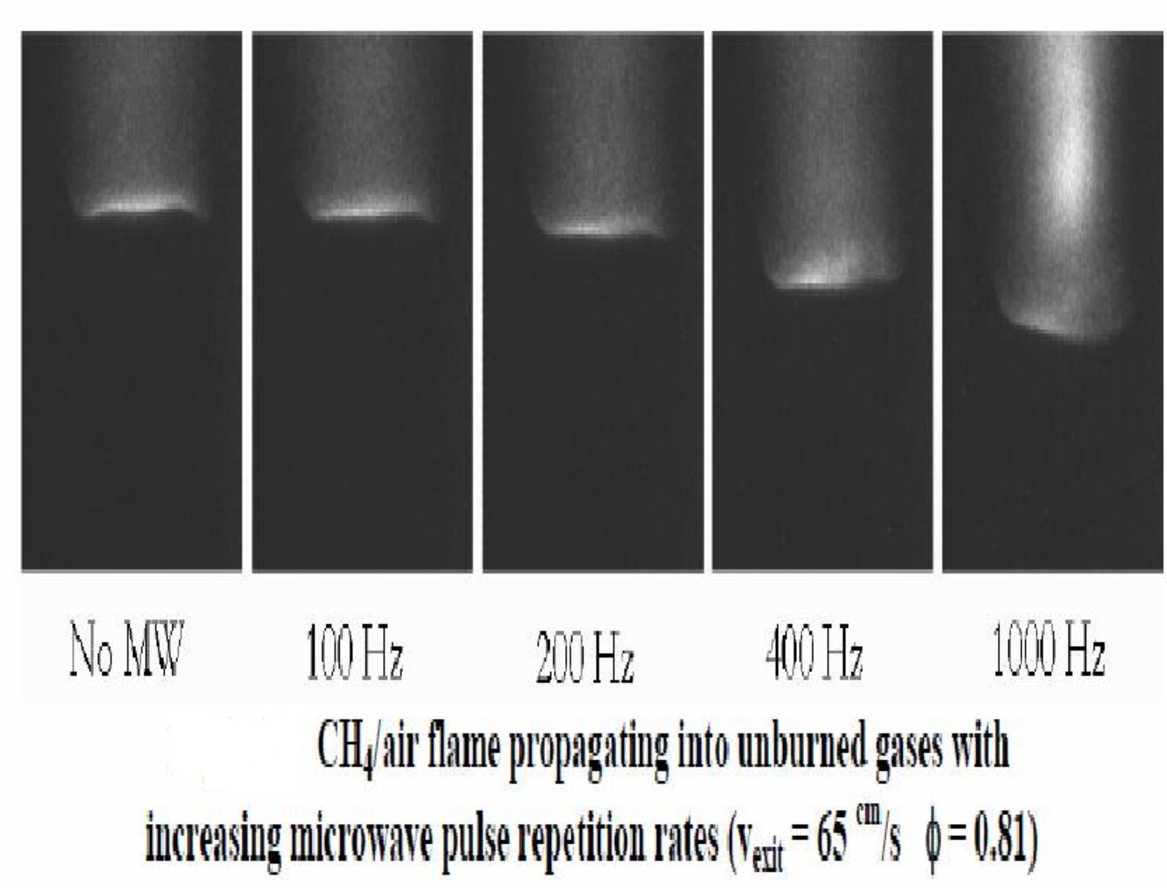

Figure 15.25: *From Ref. [152].*

[158], where $\epsilon_0 = 8.85 \cdot 10^{-12} F \cdot m^{-1}$ and $c = 3 \cdot 10^8 \frac{m}{s}$ is the speed of light in vacuum. A necessary condition for turbulence to leave RF absorption unaffected is

$$\frac{c^2 \epsilon_0}{\sigma \nu Re_T} > 1 \tag{15.3}$$

which means that turbulence-enhanced diffusion is too slow to affect RF absorption. For typical values $\nu = 10^{-5} \frac{m^2}{s}$, $Re_T = 10^3$ (see the Appendix on the flame velocity), (15.3) implies $\sigma < 10^8 \Omega^{-1} m^{-1}$, a requirement safely met in practice.

Finally, we have seen that chemical kinetics affect σ. In particular, once RF is switched off the electric field of the RF wave starts accelerating the electrons already present in the flame; in turn, the electrons trigger further ionisation, and the final outcome is a value of σ which depends on the applied electric field, on the chemical composition etc. What is relevant here is that this final outcome is achieved in a finite time $\tau_\sigma \equiv \frac{\sigma}{|\frac{d\sigma}{dt}|}$ which depends on the detailed chemical kinetics. For negligible impact of turbulence,

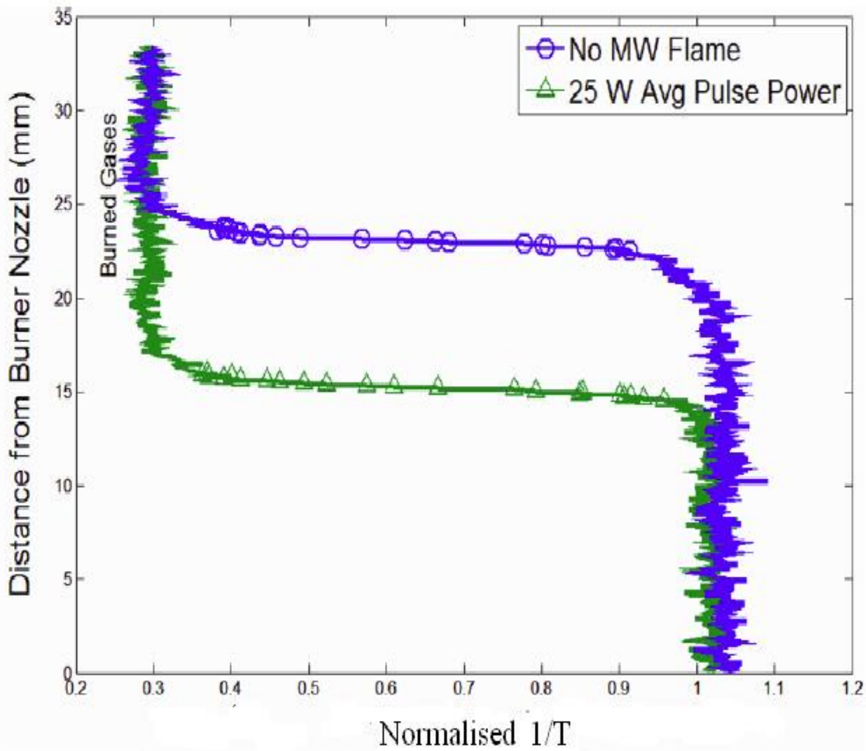

Normalised 1/T profiles of pulsed microwave enhanced flame showing no significant post or pre-flame gas heating. (Flame: CH_4/air, v_{exit}=65 $^{cm}/_{s}$, $\phi = 0.81$, MW: 25 W avg power, 1μs pulse width, 1000 Hz rep rate)

Figure 15.26: *From Ref. [152].*

we require that this time is shorter than the fastest time-scale of turbulence, namely the reciprocal τ_K of the stretch of the eddies with linear size equal to the Kolmogorov length. Should this condition be violated, it would be conceivable that the smallest turbulent eddies drag the ions of some chemical species (e.g. CHO) involved in the electron build-up ruling the evolution of σ away from the reaction zone. Typically, $\tau_K \approx 30\mu s$ -see the Appendix on the flame velocity. However, the results of chemical kinetics discussed in the Appendix on the electrical conductivity show that $\tau_\sigma << \tau_K$ but for the colder flames.

The impact of RF absorption on turbulence As for the impact of RF absorption on turbulence, an obvious requirement is that the energy density $\frac{\epsilon_0 E_{RF}^2}{2}$ of the RF wave with electric field E_{RF} exceeds the energy density $\rho\frac{(u')^2}{2}$ of turbulent eddies nowhere, where u' is a typical amplitude of turbulent fluctuations of velocity -see Appendix on the flame velocity. For typical values $u' \approx$ some $m \cdot s^{-1}$ and $\rho \approx 4.5 \cdot Kg \cdot m^{-3}$ we obtain $E_{RF} < 2 \cdot 10^6 \frac{V}{m}$, a requirement slightly stronger than the requirement of weak field $E_{RF} < E_{thr} \approx 10^7 \frac{V}{m}$ -see Appendix on the RF-flame interaction.

Another requirement is that the amount P_a of RF absorbed per unit volume exceeds the power $\rho\epsilon_{turb}$ dissipated in turbulent eddies per unit volume nowhere, where ϵ_{turb} is the mechanical power dissipated in turbulent eddies per unit mass. For typical values $\rho \approx 4.5 \cdot Kg \cdot m^{-3}$ and $\epsilon_{turb} \approx \frac{u'^4}{Re_T \nu} \approx 10^4 W \cdot Kg^{-1}$ we have $\rho\epsilon_{turb} \approx 5 \cdot 10^4 \frac{W}{m^3}$ -see Appendix on the flame velocity. Equations (41), (49) and (51) lead therefore to the following constraint on σ and E_{RF}:

$$\left[\frac{\sigma E_{RF}^2}{\rho\epsilon_{turb}}\right] < \left[\frac{4Ze}{\Xi}\right]\left[\frac{c}{\omega_{RF}\delta_L}\right] \tag{15.4}$$

for negligible reflection on the flame, where we have introduced the *wrinkling factor* $\Xi \equiv \frac{s_T}{s_L} > 1$ [4], we have defined $\omega_{RF} \equiv 2\pi\nu_{RF}$, and bracketed quantities are dimensionless. Typically $\left[\frac{4Ze}{\Xi}\right] \approx O(1)$ and $\left[\frac{c}{\omega_{RF}\delta_L}\right] \approx 5 \cdot 10^2$, so that $\sigma E_{RF}^2 < 2 \cdot 10^7 \frac{W}{m^3}$.

15.5.3 RF power required at the antenna

Myers' corollary with and without RF

Our strategy is to compare what happens to Myers' corollary -in the form (6.35)- when the system is in humming in the two cases $P_a = 0$ and $P_a > 0$.

To this purpose, we start from (6.35). When humming occurs at a period τ at a constant maximum amplitude period after period, everything in the system combustor + fluid + flame gets modulated by some periodic function of time with the same period. As usual by now, we write $a(\mathbf{x},t) = a_0(\mathbf{x},t) + \epsilon a_1(\mathbf{x},t)$ for the generic physical quantity a with $\langle a_1\rangle = 0$, i.e. $\langle a\rangle = a_0$, and we allow a_0 to depend on time. The perturbation a_1 is only useful to check the stability of the (possibly oscillating) unperturbed state a_0. Moreover, we allow $\epsilon \approx 1$. Finally, we assume (6.1) for simplicity, and recall that D_s and D_{Q_*} are [22] the dominant contributions to D. It follows that:

$$\frac{\langle D\rangle}{2} = -\langle \mathbf{m}_1 s_1\rangle \cdot \nabla\langle T\rangle + \langle \mathbf{m}\rangle \cdot \langle s_1 \nabla T_1\rangle + \langle T_1 \left(\frac{Q}{T}\right)_1\rangle = \langle T_1 \left(\frac{Q}{T}\right)_1\rangle + O\left(\epsilon^2 M\right) \tag{15.5}$$

where we have taken into account that equation (6.41) and the definitions of $\mathbf{m}$, of $\mathbf{W}$ and of the Mach number M give $|\mathbf{v}_0| \approx O(M)$, $|\mathbf{v}_1| \approx |\epsilon\mathbf{v}_0| \approx O(\epsilon M)$, $Q_0 \propto |\mathbf{v}_0| \approx O(M)$, $|\mathbf{m}_0| \propto O(M)$, $|\mathbf{m}_1| \propto O(\epsilon M)$ and $\mathbf{W} \propto O(\epsilon^2 M)$. Following Ref. [77], we observe that the relationship [10]

$$\left(\frac{Q}{T}\right)_1 = \frac{Q_1}{T} + Q_0\left(\frac{1}{T}\right)_1 - \epsilon\langle Q_1\left(\frac{1}{T}\right)_1\rangle$$

[10] It follows from the identity

(which holds exactly, i.e. at all powers of ϵ) leads to:

$$\langle T_1 \left(\frac{Q}{T}\right)_1 \rangle = \langle \frac{Q_1 T_1}{T} \rangle + Q_0 \langle T_1 \left(\frac{1}{T}\right)_1 \rangle = \langle \frac{Q_1 T_1}{T} \rangle + O\left(\epsilon^2 M\right)$$

after multiplication of all terms by T_1 and time-averaging (with $< T_1 >= 0$). Equation (6.4) gives $\frac{T_1}{T} = \frac{p_1}{p} - \frac{\rho_1}{\rho}$. Heating induces expansion, then we expect $\langle \frac{Q_1 \rho_1}{\rho} \rangle \leq 0$. It follows that $\langle T_1 \left(\frac{Q}{T}\right)_1 \rangle \geq \langle \frac{Q_1 p_1}{p} \rangle$. Finally, (6.35) and (15.5) give:

$$\int_{V_b} d\mathbf{x} \langle \frac{Q_1 p_1}{p} \rangle \leq O\left(\epsilon^2 M\right) \tag{15.6}$$

Let us denote with a_* and a_M the maximum value attained by the generic quantity $a\left(\mathbf{x}, t\right)$ in the flame and everywhere across the system on a period τ respectively. Constant maximum amplitude of humming means $|a_*| < \infty$, $|a_M| < \infty$ at all times. Finally, combustion occurs at the flame only. Then, (15.6) leads to the following chain of inequalities:

$$\begin{aligned} O\left(\epsilon^2 M\right) \geq \int_{V_b} d\mathbf{x} \langle \frac{Q_1 p_1}{p} \rangle \geq \frac{\int_{V_b} d\mathbf{x} \langle Q_1 p_1 \rangle}{p_M} = \frac{\int_{V_f} d\mathbf{x} \langle Q_1 p_1 \rangle}{p_M} = \\ = \frac{k_{Ra} V_{f*} Q_{1*} p_{1*}}{p_M} \geq \frac{k_{Ra} Q_1}{p_M} \cdot \left(V p_1\right)_f \end{aligned} \tag{15.7}$$

where k_{Ra} is a constant, dimensionless quantity encompassing all phase factors, geometrical factors etc. Its exact value depends on the detailed structure of the perturbation a_1, and is not relevant in the following. Note that $\left(V p_1\right)_f$ is the product of a volume and a perturbation of pressure, and is computed in the flame. It is therefore equal to:

$$\left(V p_1\right)_f = H_{f1} - T_{f0} S_{f1} \tag{15.8}$$

where H_f, T_f and S_f are the enthalpy, the temperature and the entropy of the flame respectively. For mathematical simplicity, we discuss here no gradient of T_f across the

---

$$\epsilon\left(ab\right)_1 = \epsilon^2 a_1 b_1 - \epsilon^2 \langle a_1 b_1 \rangle + \epsilon b_1 a_0 + \epsilon a_1 b_0$$

This identity holds for two generic quantities $a = a_0 + \epsilon a_1$, $b = b_0 + \epsilon b_1$ with $< a_1 >= 0$, $< b_1 >= 0$. We take $a = Q$ and $b = \frac{1}{T}$ in the text, then regroup all terms $\propto Q_1$ and divide by $\epsilon > 0$.

flame; we may e.g. invoke (14.1).

As for H_f, we invoke caloric perfection for simplicity, i.e. all chemical species in the flame are perfect gases with the same constant value c_p of specific heat per unit mass. Then, we write $H_{f1} = \Sigma_{i=1}^{N} H_{i1}$, $H_{i1} = (V_{f0}\rho_{i0})\, c_p T_{f1}$ and $\rho_i = \dfrac{p_i}{rT_f}$, where H_{i1} is the contribution of the i-th chemical species to H_f $(i = 1, ...N)$ and ρ_i is the mass density of the chemical species, so that $V_f\rho_i$ is the contribution of the i-th species to the flame mass. Finally, equations (6.4), (6.7) and Dalton's law of partial pressures $p = \Sigma_{i=1}^{N} p_i$ gives:

$$H_{f1} = \frac{\gamma p_0 V_{f0} T_{f1}}{(\gamma - 1)\, T_{f0}} \tag{15.9}$$

As for $T_{f0}S_{f1}$, as usual by now we neglect viscosity and radiation (which raise and lower $T_{f0}S_{f1}$ respectively). Accordingly, we may identify P_h with the combustion power density Q, so that $W_c = \int_{V_f} d\mathbf{x} Q$ and $P_a << P_h$ becomes $P_a << Q$. Generally speaking, two cases are possible.

If we apply no RF, i.e. $P_a = 0$, then $T_{f0}S_{f1}$ is due to combustion only and we may write $T_{f0}S_{f1}|_{P_a=0} = (V_f\tau_{res}Q)_1$. In fact, the unperturbed flow crosses the flame with volume $V_f$in a time τ_{res} and delivers a power density Q through combustion; the related amount of heat is $V_f\tau_{res}Q$, and the perturbation is $(V_f\tau_{res}Q)_1$. Since a_1 is only useful to check stability of a_0, we may select a_1 at will; we choose it in such a way that the flame geometry remains unaffected, and we may write $T_{f0}S_{f1}|_{P_a=0} = V_{f0}\tau_{res}Q_1$. Finally, we take advantage of the fact that heat release due to combustion is a function of temperature, and limit ourselves to small perturbations $(0 < \epsilon << 1)$, so that $Q_1 = \dfrac{dQ}{dT_f} \cdot T_{f1}$. It follows that:

$$T_{f0}S_{f1}|_{P_a=0} = V_{f0}\tau_{res}\frac{dQ}{dT_f} \cdot T_{f1} \tag{15.10}$$

Backwards substitution of (15.9) and (15.10) in (15.8) and (15.7) leads to:

$$O(M) \geq \left[\frac{\gamma p_0}{(\gamma - 1)\, p_M} - \frac{\tau_{res}}{p_M}\frac{dQ}{d\ln T_f}\right] \tag{15.11}$$

after division of all terms by $\left(\dfrac{k_{Ra}V_{f0}}{T_{f0}}\right)(T_{f1}Q_1) \propto O(\epsilon^2)$ where we have taken into account that $O(\epsilon^2) = \dfrac{O(\epsilon^2 M)}{O(M)}$; we have also written $T_{f0}\dfrac{dQ}{dT_f} = T_{f0}\dfrac{Q_1}{T_{f1}} \approx T_f\dfrac{Q_1}{T_{f1}}$ (as $\epsilon << 1$) $= T_f\dfrac{dQ}{dT_f} = \dfrac{dQ}{d\ln T_f}$. Everything in (15.11) is in dimensionless form; all square-bracketed quantities are dimensionless in this Section. Physically, (15.11) is just a particular case of (6.35), i.e. a necessary condition for stability to be satisfied at all times (as a matter of principle, all quantities but p_M and γ may depend on time). Violation of (15.11) is therefore a sufficient condition for instability.

Now, let us add to p_0 a pressure oscillation with period τ and with amplitude Δp, i.e. let us replace p_0 with $p_0 + \Delta p$. Detailed physics underlying this pressure growth is not relevant here. According to (15.9), H_{f1} becomes equal to:

$$H_{f1} = \frac{\gamma\,(p_0 + \Delta p)\, V_{f0} T_{f1}}{(\gamma - 1)\, T_{f0}} \tag{15.12}$$

If uncompensated, therefore, Δp may lead to violation of (15.11), hence to loss of stability. We have shown that RF is stabilising. Let us compute how much RF is required by stabilisation.

If we apply RF, i.e. $P_a > 0$, we may repeat step-by-step the proof of (15.11). Remarkably, RF leaves the L.H.S. of (15.11) formally unaffected. In fact, it leaves k_{Ra} unchanged, as it leaves all relative phases among fluctuating quantities unaffected -see Appendix on RF-flame interaction [11]. RF leaves also M unaffected, as it gets absorbed at the flame only, leaving therefore the upstream flow unaffected. (As for p_M, it is just an upper bound, and we are free to take for it the same value regardless of P_a). As for the R.H.S. of (15.11), RF adds the quantity $(V_f \tau_{RF} P_a)_1 = V_{f0} \tau_{RF} P_{a1}$ to $T_{f0} S_{f1}$ (in analogy to what happens with combustion), and replaces therefore (15.10) as a whole with

$$T_{f0} S_{f1}|_{P_a > 0} = V_{f0} \tau_{res} \frac{dQ}{dT_f} \cdot T_{f1} + V_{f0} \tau_{RF} \frac{dP_a}{dT_f} \cdot T_{f1} \tag{15.13}$$

Backwards substitution of (15.12) and (15.13) in (15.8) and (15.7) shows that addition of RF replaces (15.11) with:

$$O\,(M) \geq \left[\frac{\gamma\,(p_0 + \Delta p)}{(\gamma - 1)\, p_M} - \frac{\tau_{res}}{p_M} \frac{dQ}{d \ln T_f} - \frac{\tau_{RF}}{p_M} \frac{dP_a}{d \ln T_f} \right] \tag{15.14}$$

This is a link between Δp and the density of absorbed RF power required for stabilisation. Again, all quantities but p_M and γ may depend on time. As a conservative estimate, we maximise the R.H.S. and minimise the L.H.S. by taking $p_0 = p_M$ and $M \to 0$ respectively.

[11] This is in constrast with active approaches to humming control which are based on mechanical actuators. Such approaches aim precisely at controlling humming through modification of the relative phases in the Rayleigh index.

Physically, our choice on the R.H.S. corresponds to the selection of the time when unperturbed pressure achieves its maximum value. As for the L.H.S., for given upstream flow small values of M correspond to large values of c_s, hence of T_u; we have already shown that large values of T_u correspond to more unstable configurations, where stabilisation is more difficult. (Alternatively, we could say that vanishing L.H.S. corresponds to vanishing stabilising term in Myers' corollary, e.g. vanishing net flux of acoustic power propagating away from the system). Then (15.14) reduces to:

$$\left[\frac{\gamma}{(\gamma-1)}\right]\left[1+\frac{\Delta p}{p_0}\right]=\left[\frac{\tau_{res}}{p_0}\frac{dQ}{d\ln T_f}+\frac{\tau_{RF}}{p_0}\frac{dP_a}{d\ln T_f}\right] \tag{15.15}$$

RF in laminar flames

Let us apply (15.15) to flat, laminar flames (more realistic, turbulent flames are discussed below). To this purpose, we take $\tau_{res}=\tau_L$ and invoke the results of the Appendix on RF-flame interaction. Moreover, we write $W_c=\int_{V_f}d\mathbf{x}Q\approx Q\cdot V_f$. Analogously, we define the corresponding quantity for RF, i.e. the total RF power

$$W_{RF}\equiv\int_{V_f}d\mathbf{x}P_a\approx P_a\cdot V_f$$

absorbed at the flame. With the same spirit, we approximate the expression (10.1) for W_c as $W_c=A_fH_{LHV}\rho_uY_{fuel}s_L$ with $A_f=\dfrac{V_f}{\delta_L}$, $\delta_L=\tau_{res}|\mathbf{v}_0|$, $|\mathbf{v}_0|=s_L$ and $\rho_u=\dfrac{p_0}{rT_u}$ in agreement with equation (6.4). Finally, substitution of all these relationships in (15.15) allows us to write:

$$\left[\frac{\gamma rT_u}{(\gamma-1)H_{LHV}Y_{fuel}}\right]\left[1+\frac{\Delta p}{p_0}\right]=\left[\frac{d\ln s_L}{d\ln T_f}+\frac{\tau_{RF}}{\tau_L}\frac{W_{RF}}{W_c}\frac{d\ln W_{RF}}{d\ln T_f}\right] \tag{15.16}$$

after multiplication of both sides by $\dfrac{p_0s_LA_f}{W_c}=\dfrac{rT_u}{H_{LHV}Y_{fuel}}$ [12]. According to equation (15.16), W_{RF} increases with increasing Δp, just as expected. Of course, zero RF power stabilises zero pressure oscillation, i.e. $\Delta p=0$ corresponds to $W_{RF}=0$ and (15.16) leads to:

[12]When deriving (15.16) we have implicitly assumed $\dfrac{d\ln W_c}{d\ln T_f}=\dfrac{d\ln s_L}{d\ln T_f}$ as $d\ln T_f=\dfrac{dT_f}{T_f}=\dfrac{T_{1f}}{T_f}$ and T_{1f} is the perturbation. *Per se*, both Y_{fuel} and $\rho_u=\dfrac{p_0}{rT_u}$ are independent from T_{1f}.

$$\left[\frac{W_{RF}}{W_c}\right] = \frac{\left[\frac{\Delta p}{p_0}\right]\left[\frac{\tau_L}{\tau_{RF}}\right]\left[\frac{\gamma r T_u}{(\gamma-1)\,H_{LHV}Y_{fuel}}\right]}{\left[\frac{d\ln W_{RF}}{d\ln T_f}\right]} \tag{15.17}$$

Equation (15.17) provides us with the amount W_{RF} of RF power which should be absorbed by a laminar flame in order to suppress a perturbation which brings the maximum pressure in the system from p_0 to $p_0 + \Delta p$. Not surprisingly, the required W_{RF} is an increasing function of both the combustion heat release W_c and of the normalised perturbation amplitude $\frac{\Delta p}{p_0}$, and increases with decreasing τ_{RF} (as shown above, $\tau_{RF} \leq \tau_L$). It is also larger for large upstream temperature and low fuel content, as expected given the fact that leaner combustion of hotter air-fuel mixtures systems are more prone to humming. Above all, the denominator on the R.H.S. of (15.17) shows that the more strongly the absorbed RF power increases with increasing flame temperature, the easier the stabilisation. This result recalls the above quoted, positive feedback occurring in a lighted match inside a microwave oven: the larger the absorbed power by the match, the higher the heating of the latter, the larger its electrical conductivity, the larger the absorbed power in the match, and so on. This feedback raises the flame capability in absorbing RF, thus facilitating stabilisation. In particular, equation (50) gives

$$\left[\frac{d\ln W_{RF}}{d\ln T_f}\right] = \left[\frac{d\ln\overline{\sigma}}{d\ln T_f}\right] \tag{15.18}$$

provided that reflection of impinging RF waves away from the flame is negligible, as usual in most cases, i.e. that the reflection coefficient R_f is « 1 -see Appendix on the RF-flame interaction. Here $\overline{\sigma}$ is the spatial average of σ on the reaction zone of thickness $\frac{\delta_L}{Ze}$. Finally, we stress the point that equations (15.17) - (15.18) contain no more information on flame geometry. Then, their validity is scarcely affected by the oversimplified, unrealistic slab geometry of our flame.

Further information is required in order to compute the amount W_{ant} of RF power at the antenna which is required in order to feed the flame with the W_{RF} prescribed by (15.17). We provide such information in the Appendix on RF-flame interaction with the help of a much simplified treatment of RF optics. Together, equations (15.17), (15.18), (50), (52) and the definition of W_{RF} give for a laminar flame:

$$\left[\frac{W_{ant}}{W_c}\right] = \frac{\left[\frac{\Delta p}{p_0}\right]\left[\frac{c^3}{\nu_{RF}^3 V_f}\right]\left[\frac{\tau_L}{\tau_{RF}}\right]\left[\frac{\gamma r T_u}{(\gamma-1)\,H_{LHV}Y_{fuel}}\right]}{\left[\frac{d\ln\overline{\sigma}}{d\ln T_f}\right]\left[\frac{\overline{\sigma}\cdot\delta_L}{\epsilon_0\cdot c\cdot Ze}\right][q_{RF}]\,[1-R_f]} \tag{15.19}$$

where ν_{RF} and q_{RF} are the RF wave frequency and the RF quality factor. The latter is a dimensionless quantity, usually » 1, which takes into account RF losses at the walls, and the like -see Fig. 15.27.

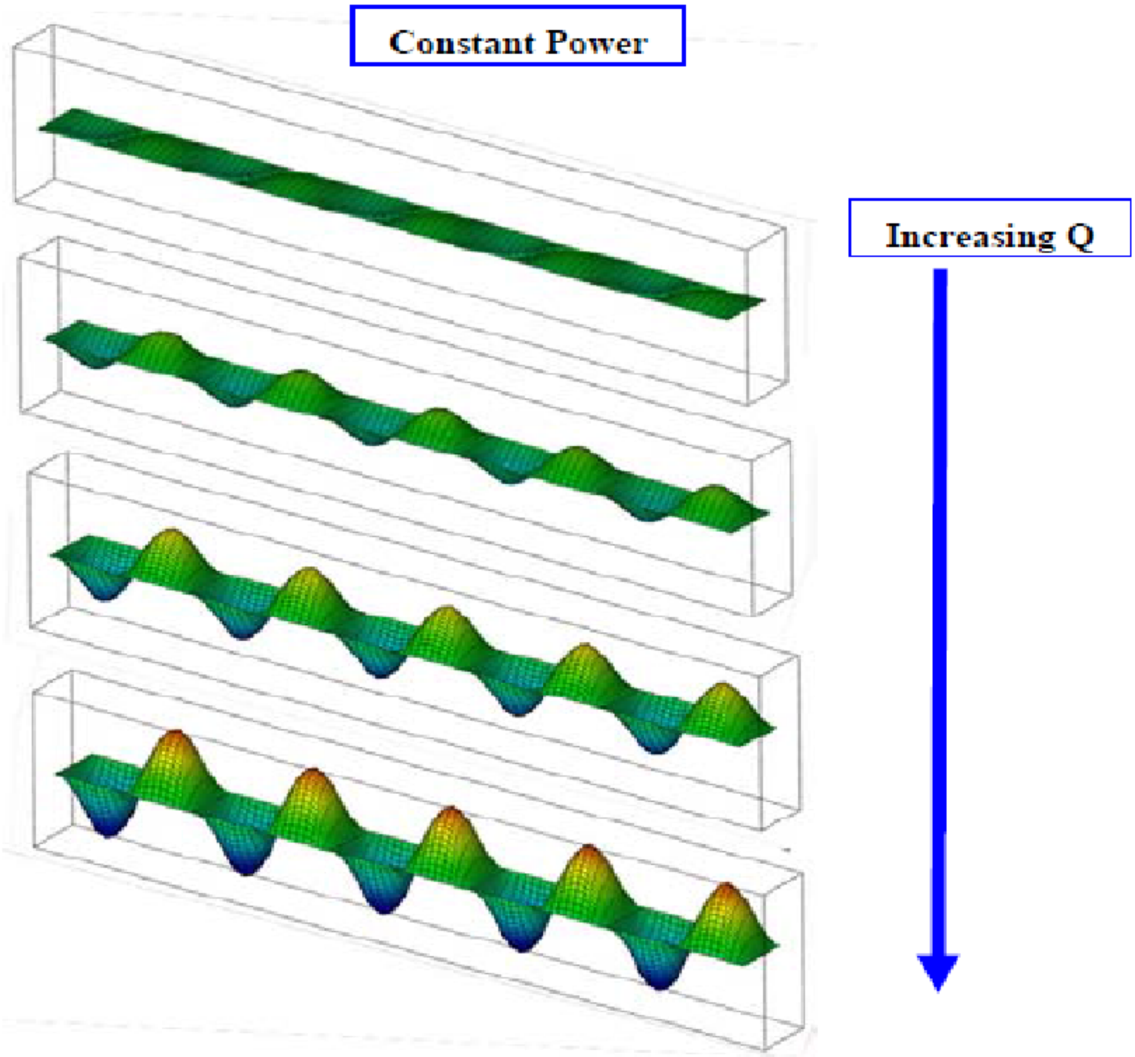

Figure 15.27: *From Ref. [148]. Electric field patterns developed within a resonant cavity embedding a flame -see Fig. 15.12- when W_{ant} is held constant and the value of q_{RF} is increased. The magnitude of the electric field increases with increasing q_{RF}, i.e. decreasing losses at the walls.*

The R.H.S. of (15.19) decreases with increasing $\overline{\sigma}$ (through the factor $\dfrac{\overline{\sigma}\delta_L}{\epsilon_0 \cdot c \cdot Ze}$), increasing number of RF photons $\dfrac{V_f \nu_{RF}^3}{c^3}$ available within the flame volume, decreasing RF reflection away from the flame (i.e. decreasing R_f) and optimising the RF cavity (i.e. increasing q_{RF}).

Finally, user-controlled quantities like T_u and Y_{fuel} replace all information on the flame speed in (15.19). This fact suggests easy generalisation to turbulent flames.

RF in turbulent flames

We have seen that turbulence and the microscopic physical processes leading to RF absorption are likely to leave each other unaffected. However, turbulence induces wrinkling of the flame surface. We show in the Appendix on RF-flame interaction that turbulence-induced flame wrinkling raises the probability of photon capture inside the flame by the wrinkling factor Ξ -see Fig. 15.28.

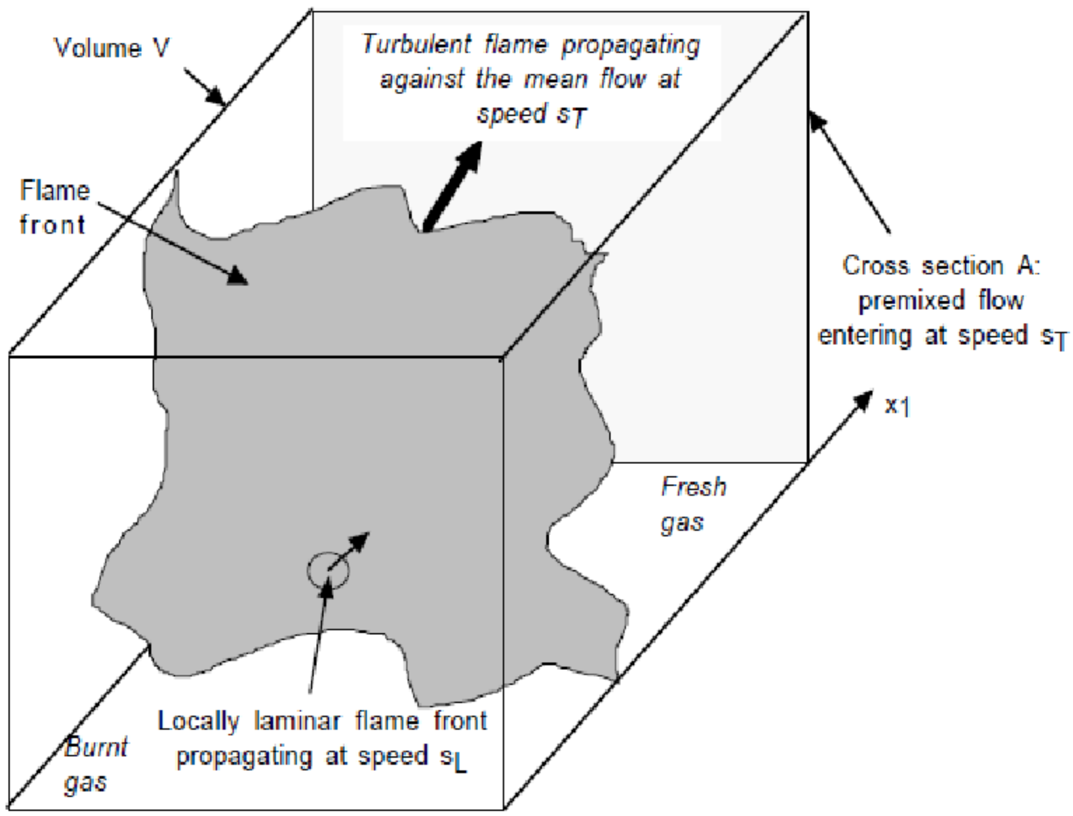

Figure 15.28: *Flame wrinkling by turbulence - from Ref. [4]. The wrinkling factor is equal to the ratio of the area of a turbulent flame and the area of a laminar flame.*

Accordingly, we may repeat the proof of equation (15.19) with the proviso that equation (51) and τ_T replace equation (50) and τ_L respectively, so that $\tau_{RF} \leq \tau_T$ and (15.19) gets replaced by:

$$\left[\frac{W_{ant}}{W_c}\right] = \frac{\left[\frac{\Delta p}{p_0}\right]\left[\frac{c^3}{\nu_{RF}^3 V_f}\right]\left[\frac{\tau_T}{\tau_{RF}}\right]\left[\frac{\gamma r T_u}{(\gamma - 1)\, H_{LHV} Y_{fuel}}\right]}{\left[\frac{d \ln \overline{\sigma}}{d \ln T_f}\right]\left[\frac{\overline{\sigma} \cdot \delta_L}{\epsilon_0 \cdot c \cdot Ze}\right][q_{RF}]\,[1 - R_f]\,[\Xi]} \tag{15.20}$$

The electrical conductivity σ of the flame is the only quantity not yet discussed in (15.20). Further discussion require detailed computation of σ.

For the sake of completeness, here we are going to write an approximate expression for the small reflection coefficient with the help of the results of the Appendix on RF-flame coupling:

$$R_f \approx \frac{1}{4}\left(\frac{c}{2\pi\nu_{RF}}\right)^2 \left(\frac{\overline{\sigma}}{2\epsilon_0 c}\right)^2 \tag{15.21}$$

15.6 Numerical predictions

Here we invoke equations (15.20) - (15.21) in order to compute $\frac{W_{ant}}{W_c}$ in Ansaldo combustors affected by humming with relative amplitude $\frac{\Delta p}{p_0}$. To this purpose, we need two things.

- we need the values of σ for Ansaldo-relevant flames. This is the topic of the Appendix on the electrical conductivity. (For historical reasons, σ is given in units $C \cdot cm^{-1} \cdot s^{-1} \cdot V^{-1}$; in order to obtain the value of σ in the correct SI unit $S \cdot m^{-1}$ all results should be multiplied by 100.).
- we have to drop the unphysical assumption of uniform T_f underlying the proof of (15.20). The temperature T_f of the flame depends on the position $\mathbf{x}$ inside the flame: $T_u \leq T_f \leq T_d$.

As for σ, it depends quite strongly on both T_f and the *progress variable* χ, i.e. the fraction of fuel which has been burnt when the fuel-air mixture has reached the position $\mathbf{x}$ inside the flame ($0 \leq \chi \leq 1$). Physically, in fact, σ increases with increasing density n_e of free electrons. In turn, n_e increases with increasing temperature, which corresponds to increasing probability of ionisation of a neutral atom or molecule. Moreover, the larger $\chi(\mathbf{x})$, the larger the number of combustion reactions which have occurred when the fuel-air mixture has reached the position $\mathbf{x}$, the larger the number of electron-producing chemical reactions which have occurred, the larger n_e. Moreover, σ depends more weakly on pressure. In the weak field limit, the dependence of σ on the applied field is also weak.

The Appendix on the electrical conductivity provide us with analytical expressions, which act as fit of the numerical output of the kinetic model which computes σ as a function of all the quantities quoted above for realistic Ansaldo flames; the relevant chemical composition has been provided by Ansaldo as an input. Such analytical expressions deal with T_f and χ as with independent variables. In real flames, however, balance equations link temperature and progress variable -see e.g. equations (2.35) and (5.37) of [4]. Typically, the smaller $T_d - T_f(\mathbf{x})$, the smaller $1 - \chi(\mathbf{x})$, i.e. the larger the fraction of burnt fuel the higher T_f, in agreement with physical intuition. As a result, σ depends on $\mathbf{x}$ through its dependence on $T(\mathbf{x})$ - or, equivalently, on $\chi(\mathbf{x})$. Rigorous computation of $\overline{\sigma}$ requires therefore detailed knowledge of $T(\mathbf{x})$, which in turn requires solution of the balance equations in the flame. For example, in a simple model of a laminar flame we should solve equation (2.43) of [4].

As for the unphysical assumption of uniform T_f, the strong dependence of σ on T and χ allows dramatic simplification. Such simplification allows us to get rid also of the need for a detailed knowledge of $T(\mathbf{x})$. Usually, σ undergoes a change of many orders of magnitude as $T_f \to T_d$ and $\chi \to 1$. This means that RF absorption is focussed on the narrow reaction zone. We make therefore a small error if we take $\chi = 1$ in the following, while keeping T_f as an independent variable, with the physical meaning of typical temperature of the reaction zone $\approx T_d$. Accordingly, we are still allowed to make use of equation (15.20), provided that we replace $\overline{\sigma}$ with $\sigma(T_f, \chi = 1)$:

$$\overline{\sigma} \to \sigma(T_f, \chi = 1)$$

Conservatively, and for the sake of self-consistency, we replace also V_f in (15.20) with $V_r \equiv A_f \cdot \dfrac{\delta_L}{Ze}$:

$$V_f \to V_r$$

This means that we consider the reaction zone, involved in RF absorption, as a region with area A_f and with thickness $\dfrac{\delta_L}{Ze}$. Finally, we are free to take

$$\tau_{RF} = \tau_T$$

in order to prevent convection to spoil the stabilising effect of RF while minimising W_{ant}.

With this proviso, we make use of the analytical fit (72) with the coefficients listed in the tables 3-14 in order to compute W_{ant} for three Ansaldo-relevant cases: AE94, ARI100a and ARI100b -see 2. Here AE94 refers to a combustor of the GT of the same name; the latter is a commercial product, successfully sold worldwide, and $W_c \approx$ tens of MW in the combustor -see Fig. 15.29 and Fig. 1.6.

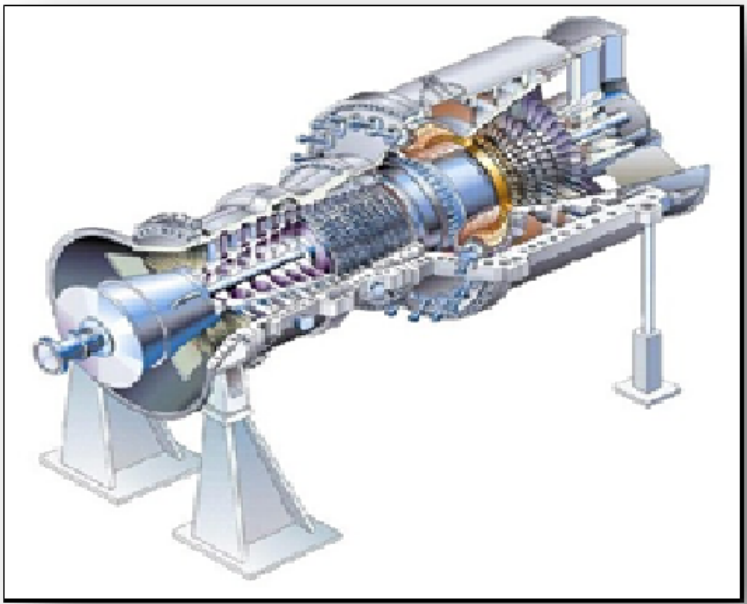

Figure 15.29: *AE94 GT (version 3a).*

In contrast, ARI100a and ARI100b refer to two different modes of operation of the same small prototype ARI100 -see Fig. 15.30- with $W_c \approx$ tens of kW [159].

Fig. 15.31 displays σ vs. temperature $\chi = 1$ for ARI100a, ARI100b and AE94. In all cases σ increases of many orders of magnitude with temperature.

Fig. 15.32 displays $\left(\frac{W_{ant}}{W_c}\right) \cdot \left(\frac{\Delta p}{p_0}\right)^{-1}$ vs. T_f for ARI100a, ARI100b and AE94. The larger the former quantity, the larger the required amount W_{ant} of RF power required in order to stabilise humming with a given amplitude Δp in a combustor at given rated pressure p_0 and heat release W_c. In all cases the larger σ the smaller W_{ant}, as expected.

Fig. 15.33 displays the predicted amount of power W_{ant} (in kW) required at the RF antenna in order to stabilise humming with amplitude Δp (in mbar) for ARI100a, ARI100b

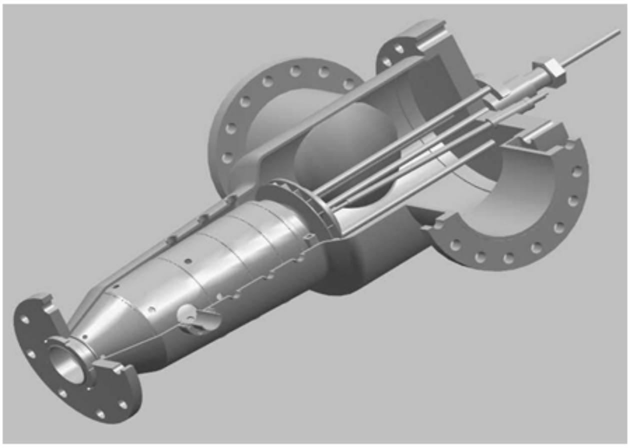

Figure 15.30: *ARI100 (single can).*

and AE94. It has been taken into account that $W_c = H_{LHV} \cdot Y_{fuel} \cdot$ total mass flow = 20 kW, 100 kW and 54 MW for ARI100a, ARI100b and AE94 respectively, in the configurations described by Tab. 2. Moreover, we have taken $\nu_{RF} = 3.7$ GHz, a reasonable value for commercially available RF sources, and $q_{RF} = 10^4$, a relatively low value which takes into account the fact that the combustor is a far-from-optimised cavity from an electromagnetic point of view. Remarkably, we obtain the same results even at quite lower values of q_{RF}, provided that we choose a slightly larger value of ν_{RF} (say, $q_{RF} = 10^3$ with $\nu_{RF} = 8$ GHz). Conservatively, we have also taken $Ze = 10$, $\Xi = 10$ and $\delta_L = 10^{-4} m$ for all combustors, so that RF absorption occurs in a 10-μm-thick region in all cases. As far as we are concerned in an order-of-magnitude estimate [13], we take $A_f = 1 m^2$ and $\gamma = 1.4$ for all cases. Finally, we have taken $T_f = 1960$ K and $T_f = 1850$ K for ARI100 and AE94 respectively, in agreement with the temperature maps of the two combustors as provided by CFD -see Fig. 15.35 and Fig. 15.34.

Fig. 15.34 displays the temperature distribution inside AE94 combustor, as provided by CFD. It shows that the choice of the value $T_f = 1850$ K is reasonable when evaluating W_{ant} for this combustor.

[13] The slab geometry assumed in the Appendix on RF-flame electromagnetic coupling for simplicity allows no higher precision

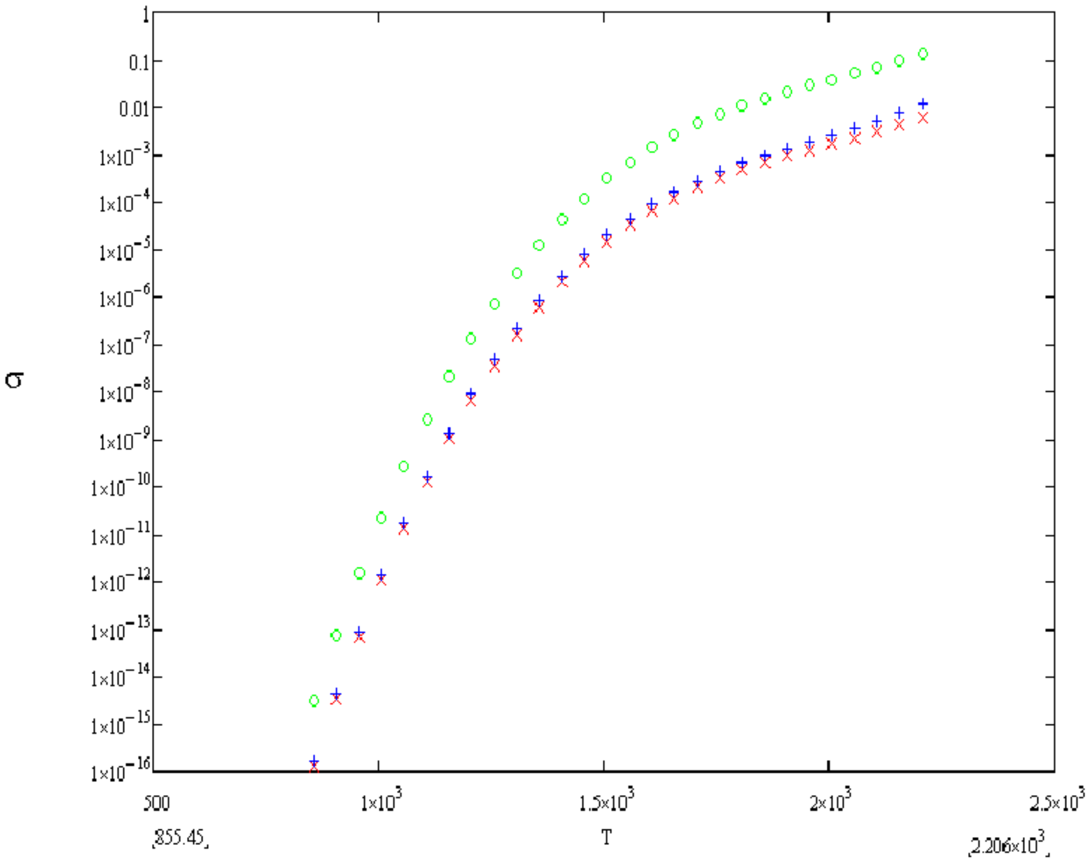

Figure 15.31: *Electrical conductivity (S/m) vs. temperature (K) @ $\chi = 1$ for ARI100a (XXXXX), ARI100b (+++++) and AE94 (OOOOO).*

Fig. 15.35 displays the temperature distribution inside ARI100, as provided by CFD. It shows that the choice of the value $T_f = 1960$ K is reasonable when evaluating W_{ant}.

In spite of the fact that the heat release W_c due to combustion is about 300 times larger in AE94 than in ARI100, the RF power W_{ant} required for stabilisation of humming at a given amplitude is only one order of magnitude larger. This result confirms the beneficial role of σ and of $\frac{d\sigma}{dT}$, as expected. Moreover, $W_{ant} << W_c$ in all cases; this confirms the applicability of the discussion in the Appendix on RF-flame electromagnetic interaction. Furthermore, out treatment of RF optics is definitely oversimplified and unduly pessimistic: suitable design of RF antenna in realistic, far-from-slab combustor geometry allows focussing of RF power on the flame and improvement of overall efficiency. Finally, our results are meaningful only if the reflection coefficient R_f is « 1 (RF wave would be otherwise reflected away from the flame, to no avail as far as humming is concerned). Fig. 15.36 displays $\log_{10}(R_f)$ vs. T @ $\chi = 1$ for ARI100a, ARI100b and AE94. The maximum value achieved by R_f in all cases is $2.8 \cdot 10^{-2}$ in AE94 at T = 2255 K. Thus, the condition R_f « 1 is satisfied in all cases.

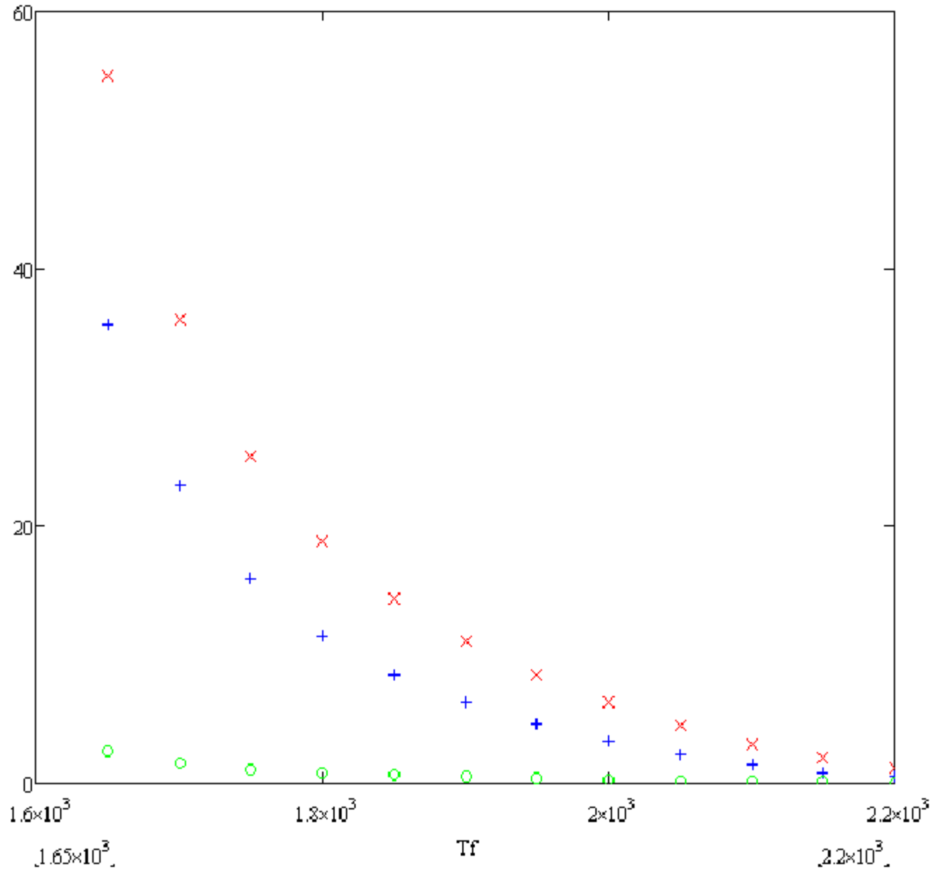

Figure 15.32: $\left(\frac{W_{ant}}{W_c}\right) \cdot \left(\frac{\Delta p}{p_0}\right)^{-1}$ *(dimensionless) vs.* T_f *(K) for ARI100a (XXXXX), ARI100b (+++++) and AE94 (OOOOO).*

The relatively low value of W_{ant} for AE94, even at relatively large values of Δp, seems encouraging. It is shown in the Appendix on the electrical conductivity that the electric field satisfies the weak field approximation even near the RF antenna for such values of W_{ant}. RF-assisted humming stabilisation is the topic of the Ansaldo patent n. AEN00495 -see Fig. 15.37.

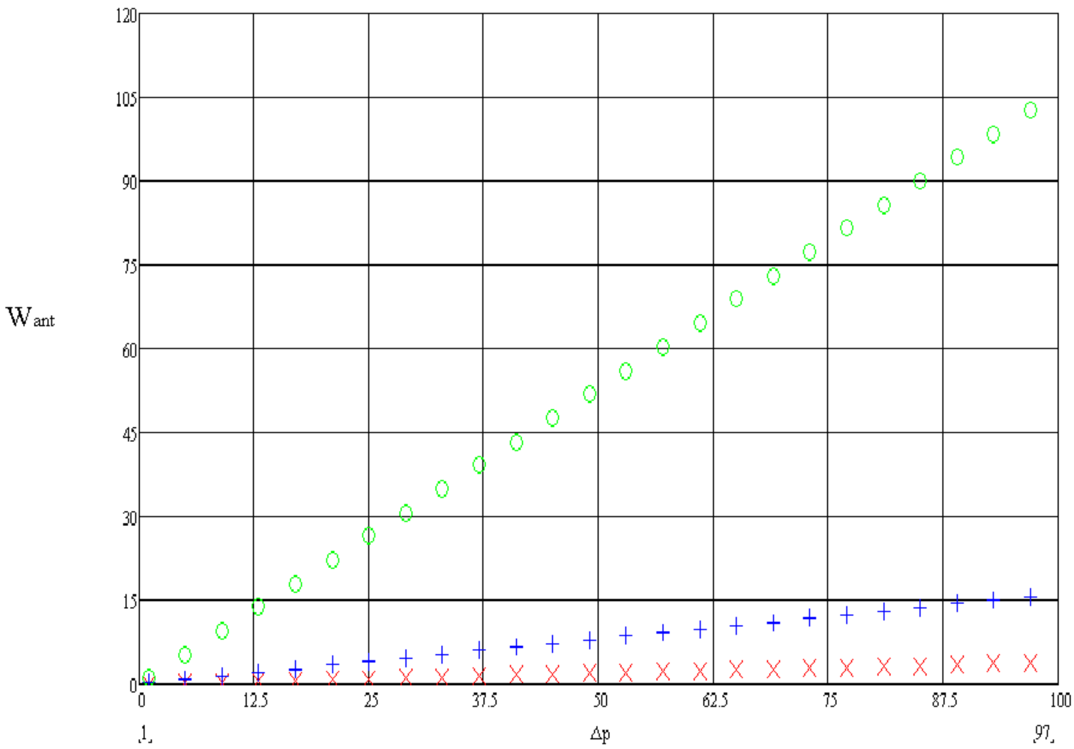

Figure 15.33: *W_{ant} (kW) vs. humming amplitude Δp (mbar) for ARI100a (XXXXX), ARI100b (+++++) and AE94 (OOOOO). Reference values for all combustors are $Ze = 10$, $\Xi = 10$, $\delta_L = 10^{-4}$ m, $A_f = 1$ m^2, $\gamma = 1.4$, $\nu_{RF} = 3.7$ GHz and $q_{RF} = 10^4$. (Same results are obtained for $\nu_{RF} = 8$ GHz and $q_{RF} = 10^3$). As for ARI100, $p_0 = 4.3$ bar and $T_f = 1960$ K. As for AE94, $p_0 = 17.7$ bar and $T_f = 1850$ K. Finally, W_c = 20 kW, 100 kW and 54 MW for ARI100a, ARI100b and AE94 respectively.*

- tempch.png

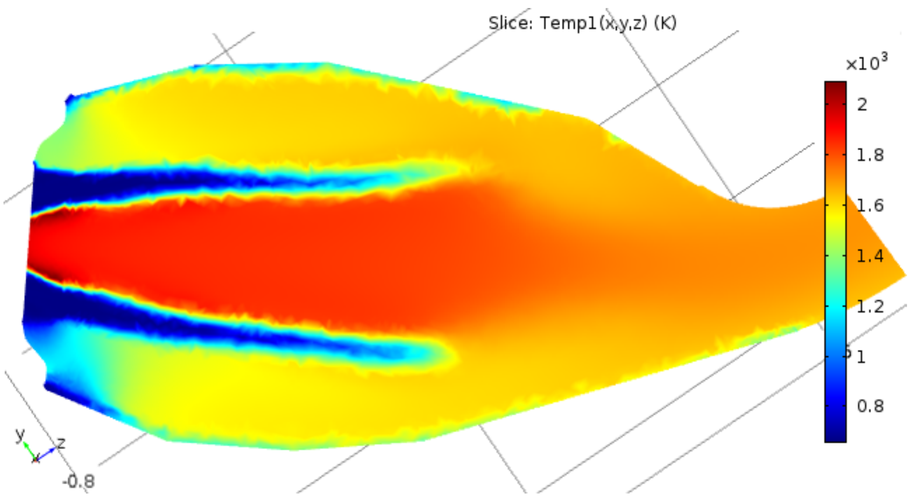

Figure 15.34: *Distribution of temperature inside AE94 combustor.*

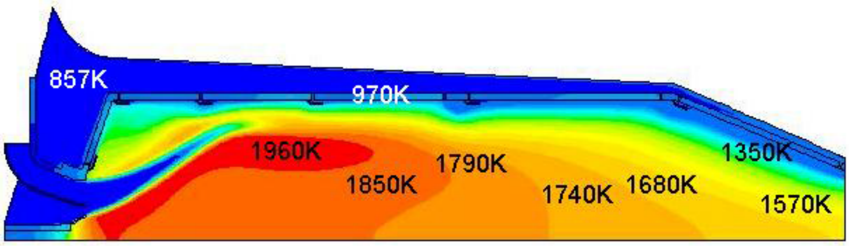

- temp.png

Figure 15.35: *Distribution of temperature inside ARI100a combustor.*

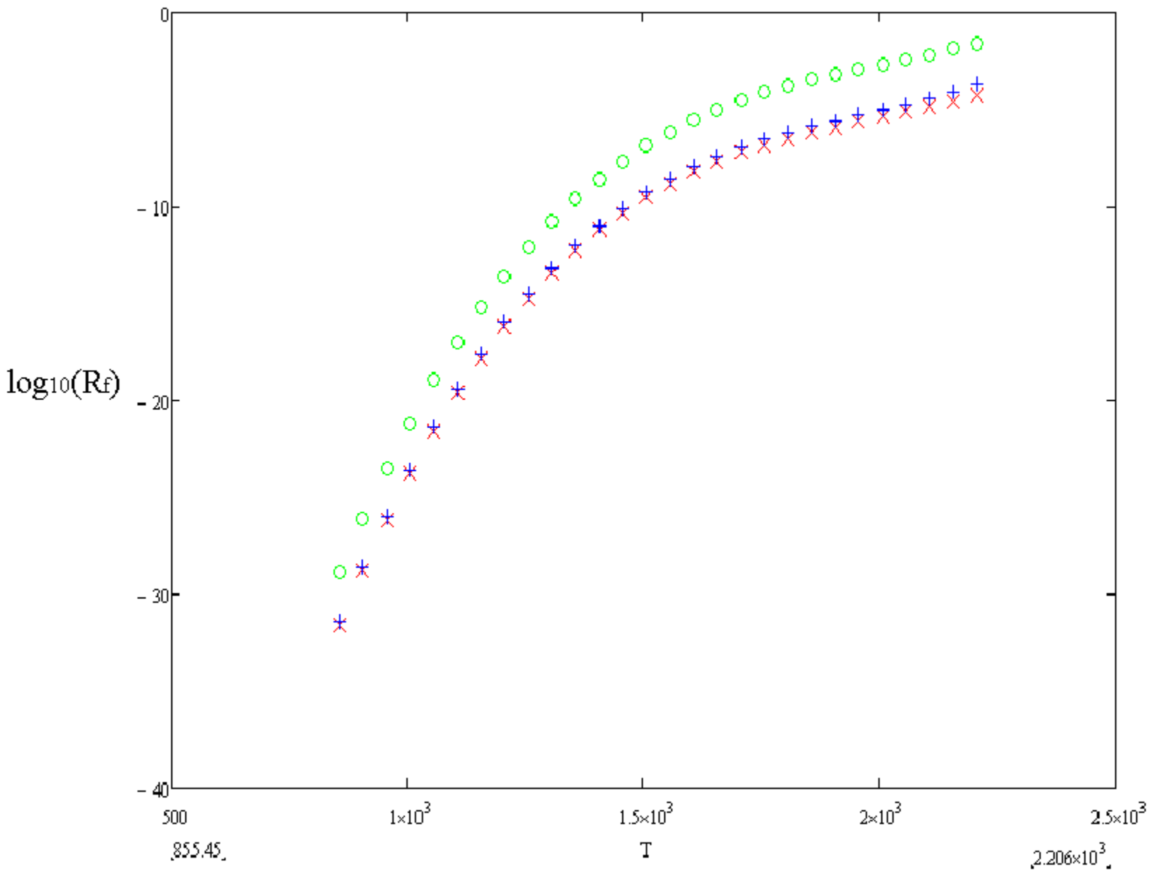

Figure 15.36: $\log_{10}(R_f)$ *vs.* T *@* $\chi = 1$ *for ARI100a (XXXXX), ARI100b (+++++) and AE94 (OOOOO).*

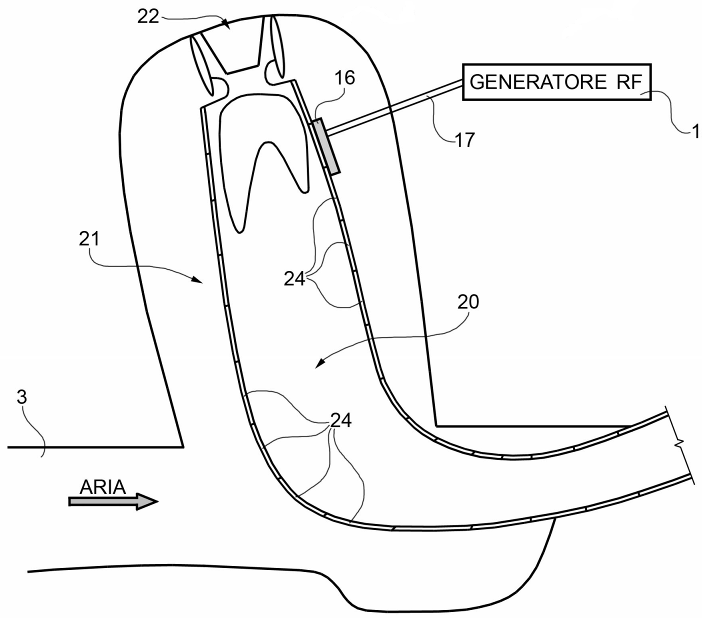

Figure 15.37: *Lay-out of RF-based stabilising system (from the Ansaldo Energia patent n. AEN00495). Combustion occurs in a combustion chamber (20) embedded in a plenum (21). The latter feeds the former with air, which comes from an air intake (3). The inner wall of the combustion chamber is coated with ceramic tiles (24). Fuel enters the system through (22). A RF power source (15) feeds a RF antenna (16) through a RF transmission line (17). The C-shaped figure inside the combustion chamber stands for the flame. Ceramic tiles shield the antenna from the hostile environment of the combustion chamber.*

Part V

Conclusions

Chapter 16

Dynamics of humming

Coupling of combustion and acoustics may lead to destructive pressure oscillations (*humming*) in lean, premixed, subsonic, swirl-stabilised combustors of heavy-duty gas turbines for power production (GT). Humming affects combustors operating at low fuel mass fraction and high heat release, regardless of the flame robustness against undesired occurences of gross instabilities like flashback, lift-off etc. Today, humming is still an issue of major concern to GT manufacturers even after decades of dedicated R & D, as it curtails precisely the performances of the most commercially attractive, i.e. high-load, low-pollution GT. Being able to predict humming would improve a manufacturer's competitiveness by making it possible to design intrinsically humming-free combustors from scratch.

Usually, manufacturers tackle the difficult problem of describing the turbulent fluid environment inside a GT combustor with the help of CFD. Unfortunately, the different orders of magnitude of acoustic and convective time-scales in subsonic combustion make it impossible to perform a full CFD treatment of humming now and -very likely- in a foreseeable future. Even if effective energy transfer between the flame (where combustion occurs) and the fluid (which sound propagates across) impies that the humming period is never too far from an acoustic eigenfrequency of the combustor, so that the humming spectrum is well peaked in the frequency domain, the answer to the crucial question *is humming going to start or not in my combustor?* is still out of reach.

Today's standard approach (*modal analysis*) aims at computing the *growth rate* of humming amplitude, which is supposed to depend exponentially on time. The growth rate is the imaginary part of a complex frequency, whose real part is connected to the humming period quoted above. Each frequency corresponds to a particular mode of oscillation -around an unperturbed state which does not depend on time- of the system made of the flame and the fluid embedding it inside the combustor, and the generic pressure perturbation is supposed to be a superposition of such modes. Humming occurs whenever the growth rate of at least one mode turns out to be positive, causing unlimited growth of the mode amplitude. In particular, those (*low order*) models which take into account just a small number of modes offer the advantage of reduced computing time. Generally speaking, the computation of growth rates relies on a linear wave (*Helmholtz'*) equation in the frequency domain for assigned boundary conditions. The latter include either standard Dirichlet-Neumann boundary conditions or, more generally, assigned linear relationships (*acoustic impedances*) between perturbations of velocity and pressure at the boundaries. Throughout the fluid, a linearised Euler equation connects such perturbations to each other. The velocity of sound depends on temperature, and the dependence of temperature on position is provided in input e.g. by CFD. Suitable jump conditions at the flame allows further partition of the system into simple modules, connected to each other in *acoustic networks* by the conservation equations of mass, momentum and energy. Indeed, low order acoustic networks are a popular application of modal analysis in manufacturers' everyday practice.

In modal analysis, the flame is represented by the flame transfer function (*FTF*), i.e. a complex-value function of frequency which provides us with the perturbation of heat release at the flame for given perturbations of velocity and pressure. (More sophisticated definitions are also available). FTF allows reduction of the system of linearised Helmholtz and Euler's equations to a homogeneous system; it allows also reduction of the computation of complex frequencies to the corresponding eigenvalue problem. Thus, once all acoustic impedances are known the whole problem of humming prediction reduces basically to the problem of finding the correct FTF for a given combustor [59].

Apart from very particular cases, however, the search for FTF is no trivial matter. Most models available in the literature are either the generalisation of simple analytical formulas with just one or two free parameters like the popular $n - \tau$ model, or postulate oversimplified, -and definitely unrealistic for GT use- shapes of the unperturbed flame. In the former case, first-principle computations of the free parameters rely once more on CFD, and are therefore affected by all drawbacks of the latter. Last but not least, unavoidable numerical uncertainties may cause the estimate of the growth rate sign to blur for combustors on the verge of humming where this growth rate almost vanishes. As an alternative, people obtain the values of these free parameters from comparison with observations on existing burners, and enter such values in some modal analysis algorithm. This approach is successful as far as we are looking for a spectrum of possible humming periods, and also for interpolation among available data. Yet, the original goal of humming prediction from scratch remains out of reach.

It is reasonable to wonder if we can get information about the occurrence of humming without previous knowledge of a FTF. The answer is affirmative, and is given by *Rayleigh's criterion of thermo-acoustics*, where *thermoacustics* investigates the interactions of sound and heat. Rayleigh's criterion, its generalisation, and its equivalent formulations are the topic of the present discussion. Rayleigh's criterion is a suitably time- and volume-averaged energy balance of an acoustic perturbation when the absolute value of its growth rate is much smaller than the absolute value of its frequency [4] [31] [32] [34] [33]. Rayleigh's criterion follows straightforwardly from the balance equations of mass, energy and momentum, as well as from the *first principle* of thermodynamics, and invokes no FTF.

Rayleigh's criterion involves a destabilising term and a stabilising term, both terms being integrals on space of time-correlations of perturbations of heat release, velocity etc. Humming is triggered (damped) when the growth rate is positive (negative), and in turn, the growth rate is positive (negative) when the destabilising term is larger (smaller) than the stabilising term. The destabilising and the stabilising terms are equal if and only if the humming amplitude is constant; in particular, if this constant vanishes then no humming occurs at all - which is precisely what manufacturers long for.

Physically, the stabilising term is the net flux of acoustic energy across the boundary of the combustor which contains the fluid and the flame: if the propagation of sound carries away from the system a positive amount of energy per unit time, then it lowers the overall amount of energy inside the combustor, hence it tends to stabilise. Conservatively, this term is often assumed to vanish altogether by some authors.

As for the destabilising term, it is the integral on the combustor volume of the so-called *Rayleigh index* D. The explicit expression of D depends on whether perturbations of entropy are allowed to or not to keep up with the perturbations of pressure. The case where no perturbations of entropy are allowed is called *isentropic*, and leads to more simple mathematical expressions [34]. However, it allows no proper discussion of heat conduction, which is properly taken into account only if entropy perturbations are allowed [32] [33]. In the isentropic case, which applies e.g. to the human voice, D is proportional to the time-correlation of perturbations of pressure and heat release; $D > 0$ (and may therefore raise the value of the destabilising term, possibly leading to the occurrence of humming) whenever the perturbations of pressure and heat release are in phase. This result has a simple thermodynamic meaning: the efficiency in transforming heat into mechanical work (here, the energy of sound) is maximum when heat is supplied to the fluid at the moment of maximum compression of the latter, in analogy to what happens in GT Brayton cycle. Remarkably, it is the phasing of the heat exchange which is relevant, not the detailed mechanism which rules heat transport and production.

Lord Rayleigh put forth this argument of thermodynamic nature when discussing the spontanenous occurrence of sound in suitably heated systems, at the very origin of thermo-acoustics in the XIX century. It is precisely this connection with thermodynamics which allows Rayleigh's criterion to hold regardless of any microscopic model of the flame response to acoustic disturbances, i.e. of FTF. Moreover, Rayleigh's argument shows the relevance of relative phases between perturbations of different physical quantities, and this result is the rationale of many modern (*active control*) strategies aiming at humming control.

If entropy perturbations are allowed, it turns out that D is the sum of two terms. The first term is proportional to the time-correlation of perturbations of temperature and heat release (and reduces to the isentropic case when the perturbations of entropy vanish): Carnot cycle replaces Brayton cycle in the arguments above. The new term is proportional to the time-correlation of the perturbations of entropy and of the component of velocity along the non-vanishing gradient of unperturbed entropy (if any exists). Remarkably, it can be shown that this term discourages modes whose propagation tends to raise entropy in regions of the system where entropy is already large in the unperturbed state. This is in agreement with Le Châtelier's principle of thermodynamics, which requires that an external interaction which disturbs the equilibrium brings about processes in the body which tend to reduce the effects of this interaction. Again, thermodynamics is at stake when it comes to Rayleigh's criterion - a point to be recalled later.

A further, often overlooked consequence of Rayleigh's criterion is that the shape of the flame affects humming. This is far from surprising, as the same shape plays a decisive role when it comes e.g. to Darrieus-Landau instability. As for humming, it is possible to show that D is strongly peaked at the flame in both isentropic and non-isentropic case. Accordingly, the destabilising term reduces to an integral on the flame, and is therefore affected by flame shape. Admittedly, such information are just implicit, but now we may reasonably wonder if there are flames whose shape make them less prone to humming than other flames.

In turn, this question leads to another question. Even if no humming occurs, stability of a premixed flame against gross instabilities like flashback, lift-off etc. puts a constraint on the flame shape: the component of the velocity of the unburnt gases impinging on the flame which is perpendicular to the flame must be equal to the flame velocity -see e.g. equation (13.21) for laminar flames, and its generalisation to turbulent flames. Given the impinging flow on a flame free from gross instabilities, therefore, all information on flame shape (even the implicit, additional constraint provided by Rayleigh's criterion against humming) involve also the flame velocity. All the way around, we may wonder if acting on the flame velocity affects stability against humming.

In spite of its general validity, unfortunately, and even if it correctly stresses the relevance of relative phases of different physical quantites to humming, Rayleigh's criterion is currently utilised in post-processing CFD results, rather than in humming prediction. The reason is that - for all its generality - Rayleigh's criterion provides just a link between perturbations of different physical quantities. Then, it allows humming prediction only once these perturbations have been computed.

Generally speaking, modal analysis is somehow complementary to Rayleigh's criterion: in contrast with the latter, the former allows humming prediction -and not just stability check *a posteriori*- but requires knowledge of the FTF. Unfortunately, both modal analysis ad Rayleigh's criterion rely on a number of simplifying assumptions. The latter include *caloric perfection*, linearity, the fact that the unperturbed state does not depend on time, and zero mean flow. Particle diffusion is also neglected, which is equivalent to assume that the Lewis number at the flame is not to small so that thermo-diffusion instability is suppressed. Most discussions include also a further assumption, namely that the body forces -like gravity- are negligible. Even if popular, it is not strictly necessary.

Caloric perfection is the more harmless assumption. It means that all chemical species inside the combustor are described as perfect gases with the same value of specific heat at constant pressure and the same value of specific heat at constant volume.

Linearity of both equations and boundary conditions is a matter of mathematical simplicity, as it allows utilisation of well-known linear algebra when dealing with the eigenvalue problem quoted above. It seems justified as the amplitude of pressure oscillations is smaller than the unperturbed pressure by orders of magnitude when humming occurs in GT. However, the same is not true when it comes to perturbations of velocity, especially near the centre of recirculation zones, which are usually present in swirl-stabilised combustion but are seldom taken into account in humming research. The price to be paid is that linear models provide us with no information about the actual value of humming amplitude. For example, it is perfectly possible that a linear theory predicts that a given mode starts growing, and then its amplitude saturates nonlinearly to a barely detectable, harmless level. Even without full CFD treatment, nonlinearity may be taken into account e.g. by introducing a dependence of FTF on the amplitude of the perturbation -in this case we speak of flame distribution function (*FDF*) [80]. Then, suitable coupling between different modes allows computation in the frequency domain. Moreover, once the nonlinearity is known at the flame and (possibly) in the boundary conditions, and starting from the conservation equations of mass, momentum and energy, Galerkin methods allow to write a system of nonlinear, ordinary differential equations in the time domain, the unknown quantities being the time-dependent coefficients of the Galerkin expansion. Standard results of nonlinear dynamical systems allow description of the bifurcations and of the basins of attraction of the combustor. The onset of humming is described either as a bifurcation leading from a steady state to a limit cycle, or as the transition from an humming-free but chaotic behaviour to a periodic orbit [81]. As far as humming is identified with an attractor with a basin of attraction of finite measure and the system remains inside this basin of attraction, humming suppression remains impossible, a concept which fits the well-known resilience of humming against any attempt to suppress it. In contrast to linear approaches, moreover, nonlinear analysis allows prediction of amplitudes. Ultimately, however, it too relies on the detailed description of the response of the flame to perturbations, and the search for FDF is affected by the same drawbacks of the search for FTF.

As for the assumption that the unperturbed state does not depend on time, it allows to identify the value of an unperturbed quantity (say, pressure) as the time-average of this quantity on many humming periods, the time-averaged perturbation being zero(this is the reason of the wording *mean flow* above). This assumption has been recently questioned by some researchers who put forth the idea that the humming-free state of a real GT combustor, far from being steady, is rather an orbit of a chaotic system [78]. Indeed, it has been shown that the very concept of *steady-state unperturbed flow* is incompatible with Galileian invariance, a fundamental requirement all meaningful solutions of the (Galileian-invariant) equations of motion have to satisfy [65]. But even if we stick to conventional wisdom and assume humming to be the time-dependent perturbation of a steady state, we recall that humming is a (far too stable) oscillating perturbation. If the unperturbed state does not depend on time, then the above quoted linearity assumption implies that the amplitude of the oscillations of all quantities involved in humming is small -which is definitely true for pressure, but not for velocity. In contrast, should we allow the unperturbed state to oscillate on its own on a time-scale much longer than the typical time-scale of the perturbation (in order to retain all essential physics of the unperturbed state after time-averaging on a time much longer than such time-scale), we could indentify the humming and its resiliency against suppression with the unperturbed state and its stability respectively -*regardless* of the actual amplitude of the oscillation.

But we are getting ourselves into real trouble when we assume that the mean, unperturbed flow vanishes, i.e. that the fluid without humming is at rest. Again, this assumption seems justified because the Mach number is much lower than 1 in subsonic GT combustion, so that Doppler corrections to the humming period are negligible. However, even if no humming occurs no flame may ever exist at a fixed location in the laboratory frame of reference without a flow supporting and stabilising the flame against e.g. flashback.

Moreover, if no unperturbed flow exists then the heat release of the unperturbed flame also vanishes, and the oscillating perturbation of heat release which the FTF is concerned with keeps on heating *and cooling* periodically the flame - an utterly unphysical result.

Finally, if the unperturbed fluid is not at rest - no matter how small its Mach number is - then an entirely new family of (*convective*) waves, related to perturbations of entropy and vorticity, may propagate across the fluid. In contrast to acoustic waves, which propagate at the speed of sound, convective waves propagate at the velocity of the unperturbed flow. Acoustic waves only may store energy and carry it across a fluid at rest. In contrast, both acoustic and convective waves may store energy and carry it across a moving fluid.

This clear difference in physics has far-reaching consequences. In both cases, for instance, if no dissipation occurs then total energy is conserved. In a fluid at rest, total energy coincides with the energy of the acoustic perturbation, which is therefore unambiguously defined if no dissipation occurs (zero growth rate of all modes) and allows derivation of Rayleigh's criterion from first principles if dissipation is weak (relatively small growth rates). In a moving fluid, total energy is the sum of the perturbation energy and of the energy of the unperturbed fluid. Even if no dissipation occurs, therefore, energy exchange between the unperturbed fluid and the perturbation is possible, and no unambiguous definition of a conserved energy of the perturbation on its own is possible. Even more so, the same is true when dissipation occurs. Every attempt to generalise the definition of energy of the perturbation -as well as the corresponding energy balance, i.e. Rayleigh's criterion- from the well-known case of zero mean flow to the realistic case of non zero mean flow (relevant to flames free of flashback) is therefore doomed to failure [66].

Non-zero mean flow affects also modal analysis. Even if the latter predicts stability (i.e. the growth rates of all modes are negative), perturbations may occur which undergo transient, non-exponential growth before decaying exponentially on the long term. Physically, the motion of the unperturbed fluid may feed the perturbation even if the stabilising term overcomes the destabilising one in Rayleigh's criterion, which does not take into account the motion of the unperturbed fluid. Mathematically, even if the FTF includes the effect of non-zero mean flow, Helmholtz' equation describes propagation of a perturbation across an unperturbed fluid *at rest*. Even if all modes described by Helmholtz' equation depend exponentially on time, therefore, it is *false* that all perturbations of a *moving* fluid are linear superpositions of such modes - the problem is said to be *non-normal* - and transient, non-exponential growth becomes possible [51]. Such growth may be large enough to trigger possibly dangerous nonlinearities. From a GT manufacturer's point of view, this means that *catastrophic humming may occur even if modal analysis predicts stability.* Finally, energy exchange between the unperturbed fluid and the perturbation may occur through interaction between acoustic and convective waves; in turn, this interaction may occur either at the flame or at the boundaries. Accordingly, modal analysis and Rayleigh's criterion may provide us with reliable humming prediction if either particular boundary conditions or particular geometries occur, which prevent coupling between acoustic and convective waves. This includes e.g. the problems of perfectly reflecting walls [19], unconfined flames [21] and azimuthal propagation of sound waves [20].

Should we be able to get rid of the unphysical assumptions underlying Rayleigh's criterion while retaining its independence from detailed modeling of flame like FTF or FDF, we would obtain more reliable information about humming prediction. Indeed, a formal generalisation of Rayleigh's criterion exists, namely *Myers' corollary*, which grants our wish [22] [76] [77]. Myers' corollary is a relationship (formally similar to an energy balance) between quantities which are bilinear in the amplitude of the perturbation of many different physical quantities. It follows from the balance equations and from the first principle of thermodynamics, and - above all - it relies on *none* of the unphysical assumptions underlying Rayleigh's criterion (the only assumption of negligible body forces is retained). If these assumptions are satisfied then Myers' corollary reduces to Rayleigh's criterion, as expected. Myers' corollary requires no caloric perfection, and takes into account the effect of heat and particle diffusion of many reacting chemical species. Myers' corollary does not require perturbations to be small, hence it applies to fully nonlinear descriptions as well - indeed, it has been utilised in benchmarking CFD codes. In spite of its similarity to Rayleigh's criterion, Myers' corollary is no energy balance, and invokes no definition of *energy of the perturbation.* Above all, Myers' corollary allows the unperturbed state to depend on time, and allows the mean flow to differ from zero. In a nutshell, Myers' corollary allows description of oscillations of arbitrary amplitude in agreement with Galileian invariance, and includes non-normality and non-linearity in a natural way.

Unfortunately, and not surprisingly given the general validity of Myers' corollary, the structure of the various terms which appear in it is extremely cumbersome. Moreover, no term seems to be negligible when humming occurs, according to CFD simulations, and no simplification is therefore possible when applying to GT. Accurate evaluation of each term requires full CFD computation, once again. Nevertheless Myers' corollary still leads to a relevant result.

If we identify stability of a (possibly oscillating) unperturbed state with the lack of divergence of the amplitude of a perturbation, where the latter is suppose to evolve on a time-scale which is much shorter than the evolution time-scale of the unperturbed flow, then *the necessary condition for stability -equation* (6.36)- *is the same for both steady and unsteady unperturbed flow*, namely the equality between a destabilising term and a stabilising term. (For a steady unperturbed flow the typical evolution time-scale of the unperturbed flow is infinite). Both terms are time-averages of integrals over space, the time-average being computed on a time-scale much longer than the evolution time-scale of the perturbation and much shorter than the evolution time-scale of the unperturbed state. The common value of the destabilising and the stabilising term vanishes as the perturbation amplitude relaxes to zero. Many phenomena, including combustion, affect the destabilising term. The latter is still an integral of a suitably generalised Rayleigh index D. For small Mach number, the stabilising term is basically the flux of acoustic energy across the boundaries, with corrections due to the unperturbed flow. If the assumptions underlying Rayleigh's criterion are satisfied, then the necessary condition of stability reduces to the corresponding condition as obtained from Rayleigh's criterion.

When asking dynamics for information about humming prediction, it turns out that a list of relevant issues should include not just the role of proper phasing of heat exchange and entropy fluctuations, as expected from Rayleigh's criterion, but also the role of the flame shape and flame velocity, a necessary condition for stability (understood as lack of divergent perturbation amplitude) which is common to both steady and unsteady unperturbed states, and -last but not least- the connection with thermodynamics. In particular, the latter would ensure that the most desirable feature of Rayleigh's criterion, the independence from the detailed flame model, remains valid even beyond the all too restricted domain of validity of Rayleigh's criterion itself.

Chapter 17

Thermodynamics of humming

Myers' corollary and its particular case, Rayleigh's criterion, follow from both the balance equations of mass, momentum and energy and the first principle of thermodynamics. The latter is cast in local form, i.e. it is applied to a small mass element of the fluid. Implicitly, therefore, whoever invokes Myers' corollary or Rayleigh's criterion assumes that local thermodynamic equilibrium (*LTE*) holds everywhere at all times inside the fluid, which means that all thermodynamical quantities (pressure, temperature, internal energy etc.) can be defined and are connected to each other by the same familiar relationships which hold at thermodynamical equilibrium [94]. Should a particular chemical species not satisfy LTE, then its description would require dedicated kinetic treatment. Admittedly, some chemical species involved in premixed combustion (like e.g. those responsible either for pollution or for the electrical conductivity of the flame) violate LTE. However, their mass fraction is usually no larger than few millionths, and their presence leaves therefore the validity of our results above unaffected.

Together with the first principle, LTE implies also validity of the (usually overskipped) *second principle* of thermodynamics inside the small mass element. A familiar consequence of second principle is Le Châtelier's principle [84]. We have already hinted at the role played by Le Châtelier's principle when discussing the contribution of entropy fluctuations to Rayleigh's criterion. Furthermore, the fact that the second principle holds inside a small mass element all along the evolution of the latter in time puts a constraint on this evolution, the so called general evolution criterion (*GEC*) [115]. The latter takes the form of an inequality involving total time derivatives of thermodynamic quantities inside the small mass element. To understand the relevance of GEC and Le Châtelier's principle to humming, three remarks are useful.

First of all, GEC involves total time derivatives which express the rate of change of quantity in a small fluid element as seen from an observer at rest with respect to the fluid elemet itself. Consequently, we expect GEC-based results to satisfy the requirement of Galileian ivariance.

Secondly, since GEC deals with time derivatives of physical quantities including entropy, then we expect it to apply to *relaxation* processes, i.e. to spontaneous, irreversible evolution of the system towards some stable configuration. If there is no exchange of matter and energy with the external world, then relaxation leads to global thermodynamic equilibrium of the system as a whole (and not just to LTE). If such exchange occurs -as it is obviously the case with GT combustors- then well-ordered patterns (*dissipative structures*) may arise from relaxation. Humming is an example of time-ordered dissipative structure. Rijke's tube [24], Sondhauss' tube [23], Taconis' oscillations [27] and Eddington's model of Cepheid stars [122] provide us with further examples of dissipative structures in thermo-acoustics, even beyond the domain of combustion. In all these examples, irreversible heat exchange triggers a time-ordered pressure oscillation in a fluid. The role of heat exchange has been already put in evidence when discussing Rayleigh's criterion.

Finally, in contrast to GEC (which applies to a small mass element) Myers' corollary and Rayleigh's criterion apply to the combustor as a whole. Together, however, GEC, Reynolds' transport theorem, Le Châtelier's principle and two reasonable assumptions (namely, no net source of matter inside the volume of the system and negligible particle diffusion) lead to three inequalities involving various terms of the balance of the total entropy of the fluid inside the system (e.g., a combustor). No matter what the microscopic physics is like, LTE makes the system to satisfy these three inequalities simultaneously at all times [116].

As for small perturbations of a steady state with zero mean flow of a fluid enjoying caloric perfection, it is possible to show that satisfying Rayleigh's criterion (or the equivalent Eddington's condition when radiation rules energy transport) is a sufficient condition for satisfying one of the inequalities quoted above, and -as a consequence- also the other two inequalities as the three LTE-related inequalities hold together. These latter two inequalities lead to two necessary conditions for stability of the unperturbed steady state. Both conditions are cast in form of variational principles. These principles involve both the amount of entropy produced within the system and the amount of entropy produced by transport processes inside the system and across its boundaries; the former and the latter are e.g. ruled by combustion and convection respectively in GT. As far as LTE rules relaxation, a stable, steady state and its perturbations satisfy the two variational principles and the necessary condition derived from Rayleigh's criterion respectively. Thus, rather than applying Rayleigh's criterion to check *a posteriori* the stability of a given solution of the equations of motion (full CFD, FTF-assisted Helmholtz' equation, etc.), we may solve for a solution (if any exists) of the variational principles which satisfies the constraints provided by the balance equations of mass, momentum and energy. This way, rather than looking for possible causes of humming by changing e.g. the FTF and then check the stability of the results, we look straightforwardly for the humming-free flames made possible by a given upstream flow.

In strict analogy to what happens when discussing Myers' corollary, generalisation to unsteady unperturbed state requires just replacement of a steady unperturbed state with a suitably time-averaged state, the time-average being taken on a time-scale much longer than the time-scale of the perturbation. The variational principles which describe stable steady state are particular cases of more general selection rules, according to which the system selects the configuration which satisfies a given extremum property among many configurations.

The actual extremum property of relevance depends on the particular problem, according to which the variational principles reduce to minimisation or maximisation of this and that quantity. As for a thin flame in thermal contact with a wall, for example, it is minimization of the heat flow pouring out of the heat source which facilitates selection of a humming-free, steady state as the stable state, in contrast with a humming-affected, oscillating state. Experiments with flames either attached to a suitably cooled burner rim [29] or to flameholders made of materials with different thermal conductivity [30] confirm this conclusion. (For steady-state flames whose linear size is not much larger than the quenching distance, in contrast, the large temperature gradients make the variational principles to reduce to maximisation of entropy produced by irreversible heat transport, in agreement with the result of [121]). Outside combustion, the esperiments of [28] on thermo-acoustic stacks in thermal contact with a working fluid lead to the same result; moreover, we have shown the equivalence between the thermodynamic foundations of Rayleigh's criterion we have dscussed and Eddington's results on spontaneous oscillatons of Cepheid stars [122]. Finally, humming in a perfect, subsonic gas corresponds to a configuration which maximises the emitted acoustic power, in agreement with a hypothesis about thermo-acoustics in rockets, put forward in the Sixties [95].

The minimization of heat flow hinted at above recalls Rijke's observation that sound production is suppressed (enhanced) whenewer we hinder (facilitate) the heat flow pouring out of the heat source by shortening (extending) the time available to heat exchange with the surrounding fluid. In particular, if the heat source is the combustion occurring in a flame which propagates across a fluid at rest while in thermal contact with a wall, then lowering the time available for the heat exchange between the flame and the wall is equivalent to raise the flame velocity -the relative velocity of the flame and the fluid- while leaving the upstream fluid unaffected. (Here we speak of laminar flame velocity s_L, for reasons which will become clear below; turbulent flame velocity is an increasing function of the laminar one. Admittedly, moreover, the time available to heat exchange increases with increasing flame thickness. But the latter is either a decreasing function of s_L or depends on it only weakly, in laminar [2] and turbulent flames [112] respectively. Accordingly, we keep on focussing our attention on s_L.). Galileian invariance ensures that the fluid speed far from the flame is not relevant, hence our conclusion concerning the flame velocity holds also for a flame at rest in a moving fluid. This discussion suggests that raising s_L -all other things being equal- stabilises humming.

This conclusion agrees with a number of well-known facts. Firstly, s_L is a monotonically decreasing function of the heat losses due to conduction towards the wall [98]: hence, raising s_L (again, all other things being equal) is equivalent to reducing such losses, as discussed above. Secondly, it is well-known that leaner flames -where the value of s_L is lower than the value of s_L in stoichiometric combustion- are more prone to humming. Thirdly, addition of a small percentage of hydrogen to a air-methane flame has the twofold effect of raising s_L [107] and to stabilise humming [106].

The beneficial effect of raising s_L on humming stabilisation is another topic where thermodynamics agrees with dynamics. As for thermodynamics, if we describe the flame as a system where both exothermic reactions (combustion) and endothermic reactions act simultaneously, then Le Châtelier's principle ensures that any attempt to enhance exothermic reactions inside the flame triggers counter-reaction through enhancement of endothermic reactions, at the expense of humming-supporting combustion. In the particular model of one-step, infinitely fast reaction combustion [4], for example, s_L is an increasing function of the reaction rate; if we try to raise (lower) s_L then the flame reacts in order to lower (raise) the reaction rate of those combustion reactions which feeds humming with energy. As shown above, in order to raise s_L while leaving other things like the upstream flow, the heat release etc. unaffected, we may decide either to raise the relative abundance of fuel (in lean combustion) at the price of increased pollution, or to add some hydrogen (in the case of air-methane combustion). Similarly, Joule heating of flames with the help of an electric arc stabilise humming [103]. In contrast, when the external world enhances endothermic reactions then further humming is excited. Indeed, it is a matter of manufacturer's everyday experience that the larger (lower) the environmental humidity the larger (lower)the humming amplitude in GT: in fact, the higher the water mass fraction in the unburnt mixture the larger the amount of water vaporised per second at the flame in an endothermic vaporisation process. Experimentally, the larger the amount of steam added to the unburnt gases the lower s_L for both air-methane [107] and air-natural gas [108] combustion. Remarkably, turbulence -e.g. in GT- leaves this argument unaffected, as far as Damkoehler number is large at least: this is why we have focussed our attention on s_L.

As for dynamics, every physical mechanism leading to reduction of the destabilising term is going to stabilise humming, as such term is proportional to the acoustic power irradiated away from the system (duly corrected for finite values of Mach number). But D is localised at the flame too, and its volume integral on the combustor volume reduces to the volume integral on the flame volume; for thin flames, the latter integral reduces further to a surface integral on the flame area A_f. Fluctuations of A_f (usually overlooked with no further justification) and of heat release are in phase with each other, as the heat release is proportional to A_f at all times. Fluctuations of A_f contribute therefore to the destabilising term in Myers' corollary (or Rayleigh criterion) just like the fluctuations of heat release. It turns out that raising s_L at given upstream flow lowers the contribution of the fluctuations and is therefore stabilising -for concave flames at least (like most GT flames). In fact, for such flames it is possible to show that raising s_L at given upstream flow acts upon the flame stretch in such a way that the slope of $A_f(t)$ gets flattened. Now, when humming occurs with a given period τ, A_f too oscillates with the same period. In this case, the steeper (flatter) the slope of $A_f(t)$ the larger (smaller) the maximum amplitude of flame area oscillations, the larger (smaller) their contribution to the destabilising term, the larger (smaller) the humming amplitude. (Intuitively, but not rigorously, we note that fuel mass balance in lean combustion forces any growth of flame velocity at given impinging flow to correspond to a reduction of A_f, hence of the domain of integration of the destabilising term, thus limiting the amplitude of humming). Remarkably, turbulence leaves this argument unaffected as far as $\tau >>$ all turbulent time-scales, provided that we replace the flame stretch with its average on turbulent wrinkling.

By now, dynamics and thermodynamics are in full agreement. Inclusion of flame area oscillations in the computation of the destabilising term of Myer's corollary leads to a prescription for humming onset, i.e. lowering of flame velocity at given upstream flow - in agreement with Le Châtelier's principle. Rayleigh's criterion is a particular case of Myers' corollary, and is also one of the necessary conditions for the stability of an unperturbed steady state provided by LTE - which in turn are particular cases of the corresponding selection rules. If oscillations of A_f are neglected altogether and we are in the isentropic case of Rayleigh's criterion, then humming is sustained by suitable relative phasing of the oscillations of heat relase and pressure, in agreement with what thermodynamics tells us on the efficiency of a Brayton cycle. To date, humming-related research has focussed precisely on such phasing. If oscillations of A_f are neglected altogether and we are *not* in the isentropic case of Rayleigh's criterion, then humming is sustained by suitable relative phasing of the oscillations of heat relase and temperature, in agreement with what thermodynamics tells us on the efficiency of a Carnot cycle. Even so, however, modes are discouraged whose propagation tends to raise entropy in regions of the system where entropy is already large in the unperturbed state - again in agreement with Châtelier's principle. The agreement of the results provided by Rayleigh' criterion and Myers' corollary with thermodynamics confirms their independence from detailed microscopic models of combustion and turbulence.

Chapter 18

Applications

18.1 Absence of humming

We have shown that Myers' corollary leads to a necessary condition for stability. This criterion involves a destabilising term, which reduces to an integral on the flame, and is therefore affected by flame shape. In stabilised flames, moreover, the flame velocity is equal to the normal component of the upstream velocity impinging on the flame -see (13.21). Accordingly, stability links the shape of humming-free flames, the flame velocity and the upstream flow. This fact provides the physical ground for the search of a necessary condition for stability which involves flame shape explicitly, and non just explicitly like in Myers' corollary and Rayleigh's criterion.

To this purpose, we limit ourselves to infinitely fast, irreversible, one-step, subsonic, premixed combustion occurring in a thin flame, and neglect both viscosity, radiation, particle diffusion and heat conduction. The assumption of thin flame allows us to neglect the gradient of all physical quantity along the flame [6]. Since we focus our attention on the flame shape, we take the temperature profile inside the flame as fixed. Then, the variational principles which -according to thermodynamics- provide a necessary condition for stability equivalent to Rayleigh's criterion- reduce just to constrained minimisation of the heat release due to combustion, the constraints being given by the relevant conservation equations for mass, momentum and energy in steady state. Thus, the vaiational problem takes the simpified form (13.13), which involves both the upstream flow and the shape of the flame, as expected.

Dramatic simplification follows from the further assumption of axisymmetric, swirl-stabilised, highly elongated flames. Analysis of (13.21) and (13.13) shows that no stable flame exists if the swirl number is too low. Otherwise, two possible stable configurations exist, *open* and *close*, corresponding to a larger and a smaller opening angle with respect to the direction of the axis of symmetry respectively. Given the swirl number, the flame switches from the open to the close configuration (*commutation*) when the heat release related to the close configuration becomes larger than the heat release related to the open confugiuration, i.e. when the heat release overcomes a threshold a result in agreement with [15] and with manufacturers' experience. It turns out that the latter threshold increases with increasing swirl number and with increasing relative fuel abundance -in agreement with the results of [18] and [16] respectively. In the subsonic limit, the pressure jump across the flame is small; however, rigorous treatment of the momentum balance across a curved flame [6] shows that it depends on the flame curvature, and is therefore different for the open and close flame. It follows that this pressure jump undergoes a discontinuous drop when commutation occurs, and this drop can be measured. The computed values of both the opening angles and of the drop agree with the results of [15]. Finally, after commutation has occurred, if we lower the heat release then the flame switches back from the close configuration to the open configuration (*anticommutation*) as the heat release becomes lower than a threshold. Generally speaking, however, *hysteresis* occur, i.e. the anticommutation threshold is lower than the commutation threshold. Both anticommutation and hysteresis are commonly observed in manufacturers' experience.

As a final benchmark, we apply (13.21) and (13.13) to flames with small curvature - a case which is not relevant to GT, but which includes well-known examples as the conical-shaped, Bunsen premixed flames. It is shown that the Euler-Lagrange equation of the variational problem reduces to the steady-state version of Kuramoto-Sivashinsky equation, which describes saturation of thermo-diffusion instability in flames with negligible curvature. Solutions of Kuramoto-Sivashinsky equation include Bunsen flames, which appear therefore to be stable, as expected.

18.2 Onset of humming

18.2.1 A threshold

We have dealt with humming-free systems so far. When it comes to the onset of humming, a selection rule (namely, minimisation of time-averaged amount of entropy produced per unit time by combustion) decides if the system remains in steady state or starts oscillating. With no further computation, it turns out that this very fact leads to the following conclusions:

- the onset of humming occurs when the heat release overcomes a threshold, $\approx$ tens of MW in GT combustors;
- the humming amplitude goes from zero below threshold to a non-zero value above threshold, with a discontinuity at the threshold. This agrees with the results of [51];
- raising s_L at given upstream flow raises the threshold, i.e. delays the onset of humming (in agreement with our previous discussion).

18.2.2 A quality factor

When discussing the impact of flame velocity on Myers' corollary, it turns out that a necessary condition exists for the absence of humming - the inequality (14.6). The latter implies that a suitably defined, dimensionless *quality factor* is lower than 1, where the quality factor involves both the total curvature of the flame, the flame velocity and the period of humming. Basically, this quality factor plays the role of a Strouhal number, the typical length in the latter being the reciprocal of the flame curvature.

It turns out that the quality factor increases (i.e., humming onset becomes easier) with increasing temperature of the unburnt gases (which corresponds to a growth of flame velocity while *not* leaving all other things, including the heat release, unchanged), with decreasing pressure and with decreasing s_L(again, all other things being unchanged).

18.3 Stabilisation of humming

Once humming has started, Myers' corollary and Rayleigh's criterion suggest possible humming stabiisation by acting either on the stabilising term or on the detsabilising term. In the former (*passive approach*) case, the exchange of acoustic energy with the external world is modified, either by drilling suitable damping holes or by applying additional devicee to the combustor chamber like Helmholtz' resonators; as for their dimensions, however effective solutions of this kind do not fit always the lay-out of existing combustors. In the latter (*active approach*) case, we may either try to lower D by changing the relative phase of the release and pressure (or temperature) or to raise s_L at given upstream flow. In contrast with the passive approach, the active approach may require utilisation of an external power supply. Acting on phases relies usually on mechanical modulation of fuel injection. Under ideal conditions, modulation is performed in order to have the corresponding system variable fluctuate precisely in counter-phase with the fluctuations constituting the combustion instability, thus damping them. In turn, however, this requires a feedback control, and this feedback control is challenging in GT because the sensors and actuators have to withstand very harsh environments for very long time (years of operation). Acting on s_L is precisely what is routinely done by raising the fuel content, but at the expense of raising pollution.

(An even simpler way, of course, is just to strenghten the walls of the combustor with suitably applied mechanical supports. But this obvious solution requires the non-trivial knowledge of where the antinodes, i.e. the pressure peaks, of the mode which is responsible for humming are located, a far-from-trivial task in GT as many different modes can be unpredictably excited. Moreover, the overall dimension itself of such supports may be a relevant issue for the lay-out of GT combustors. As a matter of principle, it is also possible to damp sound with baffles inside the combustor, but again at the expense of heavy modifications of the lay-out).

Now, experiments [148] [149] [150] [151] [152] [153] unambiguously show that bombardment of the flame with electromagnetic waves with frequency in the GHz range -referred to as *RF* here- raises s_L while leaving the upstream flow unaffected. Admittedly, no one has yet tried to stabilise humming with the help of RF. However, we are right to believe that such stabilisation is possible and is also a promising alternative.

Physically, the flame is a weakly ionised plasma, where a tiny fraction of free electrons is always present. As far as the frequency ν_{RF} of an applied electric field is smaller than the typical collision frequency ν of electrons with neutrals ($\approx$ tens of GHz in GT flames), i.e. if an electron undergoes at least one collision while it oscillates under the effect of the applied electric field, and the energy of the electron accelerated by the electric field can be transmitted to the other particles in the flame. This is a far-reaching fact, and its consequences include Joule heating of the flame, production of further (*secondary*) free electrons which can carry electric current, growth of the electrical conductivity σ of the flame, new chemical reactions etc.

As far as $\nu_{RF} < \nu$, intuitively, things should not differ too much from the $\nu_{RF} = 0$ (DC) case. Experiments [142] show that DC fields broaden the flammability limit and reduce CO emissions. As for the GHz range, we may refer to *nanosecond repetitively pulsed plasma discharges* (NRPP). NRPP stabilise a lean premixed propane-air flame at atmospheric pressure under lean conditions where it would not exist without plasma [101]; a similar result holds for laminar, premixed, lean methane-air flame [102]. Moreover, when humming occurs in a swirl-stabilized combustor at atmospheric pressure fueled with natural gas at an equivalence ratio of 0.66 and 43 kW heat release, suitably tuned NRPP with 315 W time-averaged electric power consumption induce a ten-fold decrease of pressure oscillation amplitude [103]. The fact that both NRPP and RF act with the help to the same physical quantity (an applied electromagnetic field) and in the same frequency range, together with the observed stabilising properties of NRPP, suggest that RF too may stabilise. Perhaps, the most tantalizing clue about the relevance of RF to humming is the fact that, quite unexpectedly, pulsed RF has shown the ability to generate a strong, audible sound generated from the flame region [152]. The sound follows the frequency associated with the repetition rate of the RF source and increases in intensity with power level of the incident radiation. Reasonably, if RF generates sound at the flame, it may also control it. (In contrast, if $\nu_{RF} > \nu$ then electrons oscillations are basically collisionless, and the flame remains unaffected. This is why nobody expects e.g. visible light to stabilise humming). Indeed, it is also likely that RF is *more* efficient than NRPP when it comes to stabilise humming.

First of all, as far as RF power is much less than the heat release due to combustion, the energy balance of the flame is affected only weakly. All the same, even small modifications of flame velocity may have a significant impact on humming, as the relative amplitude of humming-related perturbations of pressure in GT is often small with respect to the unperturbed pressure. Moreover, it turns out that the absorption of RF power depends on σ. The latter quantity is zero outside the flame, and undergoes an extremely large growth, by many orders of magnitude, as the RF starts being absorbed within the flame and starts therefore producing more and more secondary electrons, in a positive feedback. This result recalls the positive feedback occurring in a lighted match inside a microwave oven: the larger the absorbed power by the match, the higher the heating of the latter, the larger its electrical conductivity, the larger the absorbed power in the match, and so on. This feedback raises the flame capability in absorbing RF, i.e. reduces the required power supply to the RF source (the *antenna*) for given RF power absorbed at the flame, then facilitating stabilisation. Moreover, and in contrast with what happens with DC and NRPP, RF power crosses the space between the antenna and the flame without being absorbed as $\sigma = 0$ outside the flame, and RF absorption occurs in the flame only no matter how the flame motion is like (it will be always extemely slower than RF photons). Furthermore, suitably pulsed RF power - with pulses no longer than 0.1 ms - prevents excessive cooling due to convection, which would otherwise impede RF absorption inside the flame. Finally, and again in contrast with DC and NRPP, the antenna for a GHz RF wave has a linear size ≈ 10 cm; as such, it may be located behind one of the ceramic tiles of a GT wall, which are transparent to RF photons but protect from heat. Unlike DC and NRPP, therefore, RF requires no electrodes near the flame.

We have investigated the effect of RF on humming with the help of Myers' criterion. The derivation of Myers' corollary from first principles depends on no detailed model of flame heating, so that RF does not weaken its validity. The investigation is made of many steps.

When assessing the feasibility of RF-assisted humming control, σ plays a key role. The chemical species involved in the physical processes underlying σ violate LTE, and computation of σ requires therefore dedicated kinetic treatment. Computations have been performed by Prof. G. Colonna, A. Laricchiuta, L. D. Pietanza and A. D'Angola of Consiglio Nazionale delle Ricerche [1] in the framework of a collaboration with Ansaldo Energia, starting from data relevant to real GT combustors.

Once σ is known, a simplified description of RF optics (in slab-like geometry) links the amount of RF power which is absorbed at the flame and the corresponding power supply to the antenna. This description is linear, and linearity puts an upper threshold on the maximum amplitude of RF electric field. In particular, no electric arc should be triggered (*weak field approximation*). We neglect also the impact of RF absorption on turbulence and -all the way around- the impact of turbulence on RF absorption. The former assumption requires that the absorption of RF in the flame is faster than the transport of heat across the flame,m and that the characteristic ramp-up time of σ is shorter than the fastest time-scale of turbulence, i.e. the reciprocal of the stretch of the turbulent eddies with linear size equal to Kolmogorov length. The latter assumption requires that both RF energy density and RF absorbed power are no larger than the energy density and the dissipated power density in turbulent eddies. Indeed, the RF electric fields corresponding to the values RF absorbed power computed below seem to satisfy all these requirements, so that our discussion is self-consistent at least.

In order to compute the amount of RF power absorbed at the flame which is required for stabilisation of humming with given amplitude, we compare Myers' corollary with and without RF and require that the new term due to RF compensates the term due to finite amplitude of pressure oscillations. Given the latter, equations (15.20)-(15.21) provide a conservative estimate for the required power supply at the antenna. Fig. 15.33 displays the results for three GT combustors. For AE94, e.g., which works at 17.7 bar with 54 MW heat release, we predict a 105 kW power supply to a 3.7 GHz RF antenna to stabilise 100 mbar humming. RF-assisted stabilisation of humming has been patented.

[1] The full address is CNR-IMIP, via Amendola 122D, Bari, Italy

18.4 Future work

Hopefully, the present investigation on multifaceted Rayleigh's criterion, its generalisation -Myers' corollary- and their connection with thermodynamics conveys the richness of information in the older literature that still can have significant value and implications for present day research. It also helps to remind us that our depth of understanding is much less than we would generally like to conceive.

Many items need further investigation. A far-from-complete list includes:

- The impact of the attachment point on commutation. We have discussed commutation and anticommutation for just one location of the attachment point of the flame, for the sake of mathematical simplicity. However, the attachment point may change, and different configurations become possible.

- The role of the distribution of s_L on commutation. For the sake of mathematical simplicity, we have neglected the gradient of flame velocity along the flame: firstly, we assumed it to be uniform, then we have focussed our attention on the flame area near the attachment point in order to take into account the relevant role of the auxiliary pilot flame. Of course, more refined treatment is required.

- Computation of the quality factor in GT combustors with and without humming. If, as we expect, it is larger in humming-affected combustors, then too large values of this quality factor may alert designers since the early phases of the design of a new GT combustor.

- It is worthwhile to ask if this quality factor may act on humming-relevant experiments just like Reynolds' number acts on turbulence-related experiments, i.e. as a dimensionless similarity factor which allows both comparison between different experiments and search for possible scaling laws.

- Improvement in RF optics. Here we made use of a slab-like geometry, which is useful just for order-of-magnitude estimates. Our treatment of power losses in the combustor walls was also oversimplified. Detailed description of RF optics is required for more realistic assessment of RF feasibility.

- Detailed description of RF source lay-out and power supply is required in order to assess feasibility of experiments on RF-assisted stabilisation of humming.

Part VI

Bibliography

Bibliography

[1] S. Candel, D. Durox, Th. Schuller, J. F. Bourgouin and J. P. Moeck, Annu. Rev. Fluid Mech. **46**:147-173 (2014)

[2] S. R. Turns, *An Introduction To Combustion - Concepts and Applications* McGraw-Hill, New York (2000)

[3] A. Di Vita, F.Baccino, E. Cosatto, *A limit cycle for pressure oscillations in a premixed burner* Proc. AIA-DAGA Merano Italy (2013)

[4] T. J. Poinsot and D. Veynante, *Theoretical and Numerical Combustion* R. T. Edwards (2001)

[5] M. Emadi, *Flame Structure And Thermo-Acoustic Coupling For The Low Swirl Burner For Elevated Pressure And Syngas Conditions*, PhD Thesis, December 2012, University of Iowa http://ir.uiowa.edu/etd/4968

[6] A. G. Class, B. J. Matkowsky and A. Y. Klimenko, JFM **491**, 11-49 (2003)

[7] T. Emmert, S. Bomberg and W. Polifke, Combustion and Flame **162**, 75-85 (2015)

[8] L. D. Landau and E. Lifshitz *Fluid Mechanics* Pergamon, Oxford, UK (1960)

[9] G. I. Sivashinsky, Ann. Rev. Fluid Mech. **15**, 179-199 (1983)

[10] Y. Kortsarts, I. Brailovsky and G. I. Sivashinsky, Combust. Sci. and Technol. **123**, 207-225 (1997)

[11] F. Biagioli, Combustion Theory and Modelling, **10**, 3, 389-412 (2006)

[12] F. Biagioli, F. Guethe, and B. Schuermans, Experimental Thermal and Fluid Science **32**, 1344-1353 (2008)

[13] L. Gicquel, G. Staffelbach and Th. Poinsot, Progress in Energy and Combustion Science, **38**, 6, 782-817 (2012)

[14] M. Falese, S. Hermeth, G. Staffelbach and L. Gicquel, *Bifurcations In Combustors* http://www.princeton.edu/cefrc/Files/2013%20 Lecture%20Notes/Poinsot/10b-Bifurcations-in-swirling-flames.key.pdf

[15] V. Anisimov, A. Chiarioni, F. Dacca', L. Rofi and C. Ozzano, *Bi-Stable Flame Behaviour Of Heavy Duty Gas Turbine Burner* GT2014-25546, Proceedings of ASME Turbo Expo 2014, June 16-20, 2014, Duesseldorf, Germany

[16] S. Taamallah, Z. A. LaBry, S. J. Shanbhogue and A. F. Ghoniem, *Correspondence Between Uncoupled Flame Macrostructures And Thermoacoustic Instability In Premixed Swirl-stabilized Combustion* GT2014-27316, Proceedings of ASME Turbo Expo 2014: Turbine Technical Conference and Exposition, June 16-20, 2014, Duesseldorf, Germany

[17] N. Syred, Progress in Energy and Combustion Science **32**, 2, 93-161 (2006)

[18] Y. Huang and V. Yang, Proc. Combustion Inst. **30** 1775-1782 (2005)

[19] D. Laera and S. M. Camporeale, *Coupling a Helmholtz solver with a Distributed Flame Transfer function (DFTF) to study combustion instabilities of a longitudinal combustor equipped with a full-scale burner* XXXVIII Meeting of the Italian Section of the Combustion Institute, 20-23 Sept. 2015, Lecce, Italy

[20] A. Ghani, Th. Poinsot, L. Gicquel and J. D. Mueller, *LES Study of Transverse Acoustic Instabilities in a Swirled Kerosene-Air Combustion Chamber*, Flow Turbulence Combust., DOI 10.1007 s10494-015-9654-9

[21] D. Durox, T. Schuller, N. Noiray, A. L. Birbaud and S. Candel, Combustion and Flame **156** 106-119 (2009)

[22] M. J. Brear, F. Nicoud, M. Talei, A. Giauque and E. R. Hawkes, J. Fluid Mech. **707**, 53-73 (2012)

[23] I. Girgin and M. Turker, J. Naval Science and Engineering, **8**, 1, 14-32 (2012)

[24] P. L. Rijke, Philosophical Magazine **17**, 419-422 (1859) http://books.google.com/books? id=yVEwAAAAIAAJ&pg=PA419 #v=onepage&q&f=false

[25] P. L. Rijke, Annalen der Physik **183**, 339-343 (1859) (in German) http://gallica.bnf.fr/ark:/12148/bpt6k151924.pleinepage. r=Annalen+der+Physic.f349.langFR

[26] P. Riess, Annalen der Physik **185**, 145-147 (1860) (in German) http://gallica.bnf.fr/ark:/12148/bpt6k15194t.pleinepage. r=Annalen+der+Physic.f157.langFR

[27] H. A. Kramers, Physica **15**, 11-12, 971-984 (1949)

[28] T. Biwa, Y. Ueda, T. Yazaki and U. Mizutani, EPL **60**, 363 (2002)

[29] D. Meija, L. Selle, R. Bazile and T. Poinsot, Proc. Comb. Inst. **35**, 3201-3208 (2014)

[30] S. Hong, S. J. Shanbhogue, A. F. Ghoniem *Impact Of The Flameholder Heat Conductivity On Combustion Instability Characteristics* GT2012-70057 Proceedings of ASME Turbo Expo 2012 June 11-15, 2012, Copenhagen, Denmark

[31] J. W. S. Rayleigh, Nature **18**, 319-321 (1878)

[32] F. Nicoud, T. J. Poinsot, Combustion and Flame **142**, 153-159 (2005)

[33] B. T. Chu, Acta Mech. **1**, 3, 215-234 (1965)

[34] S. Akamatsu and A. P. Dowling, *Three Dimensional Thermo-acoustic Oscillation In A premixed Combustor* Proceedings of ASME TURBO EXPO 2001 June 4-7, 2001, New Orleans, Louisiana 2001-GT-0034

[35] T. C. Lieuwen, *Unsteady Combustor Physics* Cambridge University Press, Cambridge, UK (2012)

[36] T. C. Lieuwen, J. of Sound and Vibration **242**(5), 893-905 (2001)

[37] J. P. Freidberg, *Ideal Magnetohydrodynamics* Plenum Press, New York (1987)

[38] M. J. Lighthill, Proc. R. Soc. Lond. A **211**, 564-587 (1952)

[39] P. Subramanian and R. I. Sujith, *Non-normality and internal flame dynamics in premixed flame-acoustic interaction*, AIAA 2010-1153, 48th AIAA Aerospace Sciences Meeting Including the New Horizons Forum and Aerospace Exposition, 4-7 January 2010, Orlando, Florida

[40] A. P. Dowling J. Sound and Vibration, **180** (4), 557-581 (1995)

[41] L. D. Landau and E. Lifshitz *Mechanics* Pergamon, Oxford, UK (1960)

[42] A. A. Putnam and W. R. Dennis, J. Acoustic Society of America, **26** 5, 716-725 (1954)

[43] K. R. Sreenivasan and S. Raghu, Current Science **79** 6, 867-883 (2000)

[44] A. Laverdant, D. Thevenin, Combustion and Flame **134**, 11-19 (2003)

[45] M. Heckl, A. Bigongiari, *Coupling Of Heat Driven Modes In The Rijke Tube* Proc. XXI Intl. Congress on Sound And Vibration, Beijing, China, 13-17 July 2014

[46] E. Freitag, *On The Measurement And Modelling Of Flame Transfer Functions At Elevated Pressure* PhD Thesis, April 2009, TUM, Munich https://www.td.mw.tum.de/fileadmin/w00bso/www/Forschung/Dissertationen/freitag.pdf

[47] S. Bomberg, T. Emmert and W. Polifke, *Thermal versus acoustic response of velocity sensitive premixed flames* 35th Comb. Symp., Proc. Combustion Inst. (2014)

[48] A. Ndiaye, M. Bauerheim, S. Moreau and F. Nicoud, *Uncertainty Quantification Of Thermo-acoustic Instabilities In A Swirled Stabilized Combustor*, GT2015-44133, Proceedings of ASME Turbo Expo 2015: Turbine Technical Conference and Exposition, GT2015, June 15-19, 2015, Montreal, Canada

[49] L. Crocco, J. Am. Rocket Soc. **21** 6, 163-178 (1951)

[50] R. I. Sujith, *Non-normality And Non-linearity In Thermo-acoustic Instabilities* Proceedings of the 13th Asian Congress of Fluid Mechanics, 17-21 December 2010, Dhaka, Bangladesh

[51] M. P. Juniper, JFM **667**, 272-308 (2011)

[52] F. Selimefendigil, *Identification and Analysis of Nonlinear Heat Sources in Thermo-Acoustic Systems*, PhD Thesis, TUM Institut fuer Energietechnik, Lehrstuehl fuer Thermodynamik, Munich, Germany (2010) https://www.tfd.mw.tum.de/fileadmin/w00bsb/www/Forschung/Dissertationen/

[53] T. C. Lieuwen, V. Yang eds. 2005 *Combustion Instabilities in Gas Turbine Engines: Operational Experience, Fundamental Mechanisms, and Modeling* Prog. Astronaut. Aeronaut. 210. Reston, VA: Am. Inst. Aeronaut. Astronaut.

[54] S. Kato, T. Fujimori, A. P. Dowling and H. Kobayashi Proceedings of the Combustion Institute **30**, 1799-1806 (2005)

[55] P. Subramanian, R. S. Blumenthal, W. Polifke and R. I. Sujith, *Distributed time lag response functions for the modelling of combustion dynamics, Combustion Theory and Modelling* (2015), DOI 10.1080 13647830.2014.1001438

[56] S. Bade, M. Wagner, Ch. Hirsch and Th. Sattelmayer, *Design For Thermoacoustic Stability: Modeling Of Burner And Flame Dynamics* Proceedings of ASME Turbo Expo 2013 - Turbine Technical Conference and Exposition June 3-7, 2013, San Antonio, Texas, USA GT2013-95058

[57] W. Polifke and C. Lawn, Combustion And Flame **151** 3, 437-451 (2007)

[58] H. S. Shreekrishna and T. Lieuwen, Combustion Theory and Modelling, **14**, 5, 681-714 (2010)

[59] L. Tay Wo Chong, R. Kaess, T. Komarek, S. Foeller and W. Polifke, *Identification of Flame Transfer Functions Using LES of Turbulent Reacting Flows*, in S. Wagner et al. (eds.), *High Performance Computing in Science and Engineering* Garching-Muenich, Springer Verlag (2009) DOI $10.1007978-3-642-13872-022$

[60] Y.A. Kuznetsov, *Elements of Applied Bifurcation Theory* Springer New York (2004)

[61] M. A. Ferreira and J. A. Carvalho Jr., J. of Sound and Vibration **203** (5), 889-893 (1996)

[62] K. Balasubramanian, R. I. Sujith, Phys. Fluids **20** 044103 (2008)

[63] K. Wieczorek, C. Sensiau, W. Polifke and F. Nicoud, Phys. Fluids **23** 107103 (2011)

[64] W. Krebs, H. Krediet, E. Portillo, S. Hermeth, Th. Poinsot, S. Schimek and O Paschereit, J. Eng. Gas Turbines and Power, **135** 081503 (2013); *Comparison of Nonlinear to Linear Thermo-acoustic Stability Analysis of a Gas Turbine Combustion System*, GT2012-69477 Proc. ASME Turbo Expo 2012, June 11-15 2012, Copenhagen, Denmark

[65] A. T. Fedorchenko, J. Sound and Vibration **232** (4), 719-782 (2000)

[66] K. J. George and R. I. Sujith, J. Sound and Vibration **330** 5280-5291 (2011)

[67] F. E. C. Culick, Combust. Sci. and Technol. **56**, 159-166 (1987)

[68] A. S. Morgans and Ch. S. Goh, *Analytical Modelling of the Dissipation and Dispersion of Entropy Waves in Combustor Thermo-acoustics*, Proc. AIA-DAGA 2013 Merano Italy (2013)

[69] E. Motheau, L. Selle and F. Nicoud, J. Sound and Vibration **333** (1), 246-262 (2014)

[70] L. S. Chen, S. Bomberg and W. Polifke, *Propagation and Generation of Acoustic and Entropy Waves Across a Moving Flame Front* Preprint submitted to Combustion and Flame, 2015

[71] W. Polifke, Ch. O. Pascherheit and K. Doebbeling, Intl. J. Acoustics and Vibration, **6** 3, 1-12 (2001)

[72] D. You, V. Yang and X. Sun, *Three-Dimensional Linear Stability Analysis Of Gas Turbine Combustion Dynamics* in T. C. Lieuwen, V. Yang eds. 2005 *Combustion Instabilities in Gas Turbine Engines: Operational Experience, Fundamental Mechanisms, and Modeling* Prog. Astronaut. Aeronaut. 210. Reston, VA: Am. Inst. Aeronaut. Astronaut.

[73] J. E. Portillo, J. C. Sisco, Y. C. Yu, W. E. Anderson, and V. Sankaran *Application of a generalized instability model to a longitudinal mode combustion instability* AIAA Paper, **5651** 8-11 (2007)

[74] A. P. Dowling and S. R. Stow, *Acoustic Analysis Of Gas Turbine Combustors*, in T. C. Lieuwen, V. Yang eds. 2005 *Combustion Instabilities in Gas Turbine Engines: Operational Experience, Fundamental Mechanisms, and Modeling* Prog. Astronaut. Aeronaut. 210. Reston, VA: Am. Inst. Aeronaut. Astronaut.

[75] T. Lieuwen, J. Propulsion and Power, **19** 5, 765-781 (2003)

[76] M. K. Myers, J. Fluid Mech. **226** 383-400 (1991)

[77] A. Giauque, T. Poinsot, M. Brear and F. Nicoud, *Budget of disturbance energy in gaseous reacting flows* Center for Turbulence Research Proceedings of the Summer Program 2006

[78] V. Nair, G. Thampi and R. I. Sujith, J. Fluid Mech. **756**, 470-487 (2014)

[79] V. Nair and R. I. Sujith, *Intermittency on the Dynamics of Turbulent Combustors* GT2014-26018, Proceedings of ASME Turbo Expo 2014: Turbine Technical Conference and Exposition, GT2014, June 16-20, 2014, Duesseldorf, Germany

[80] B. Cosic, J. P. Moeck and Ch. O. Paschereit, Combustion Sci. and Technol. **186**, 6, 713-736 (2014)

[81] I. C. Waugh, K. Kashinath and M. P. Juniper, *Matrix-Free Continuation Of Limit Cycles And Their Bifurcations For A Ducted Premixed Flame* n^3l Intl. Summer School And Workshop On Non-Normnal And Non-Linear Effects In Aero- And Thermo-acoustics, June 18-21, 2013, Muenich

[82] P. Subramanian, V. Gupta, B. Tulsyan and R. I. Sujith, *Can Describing Function Technique Predict Bifurcations in Thermo-acoustic Systems?* AIAA 2010-3860 16th AIAA/CEAS Aeroacoustics Conference, 7-9 June 2010, Stockholm, Sweden

[83] F. Selimefendigil and W. Polifke, Intl. J. Spray and Combustion Dynamics, **3**, 4, 303-330 (2011)

[84] L. D. Landau and E. Lifshitz *Statistical Physics* Pergamon, Oxford, UK (1960)

[85] I. Gyarmati, *Non-equilibrium Thermodynamics* Springer, Berlin (1970)

[86] L. M. Martyushev and V. D. Seleznev, Chemistry And Biology Phys. Rep. **426**, 1 (2006)

[87] E. T. Jaynes, Ann. Rev. Phys. Chem. **31**, 579 (1980)

[88] S. Chandrasekhar, *Hydrodynamic and Hydromagnetic Stability* Oxford University Press, New York (1961)

[89] R. J. Tykodi, *Thermodynamics of Steady States* Macmillan, New York (1967)

[90] S. R. DeGroot and P. Mazur, *Non-Equilibrium Thermodynamics* North Holland, Amsterdam (1962)

[91] P. Glansdorff and I. Prigogine, *Thermodynamic Theory Of Structure, Stability, And Fluctuations* Wiley- Interscience, New York, (1971)

[92] B. H. Lavenda, *Thermodynamics of Irreversible Processes* Macmillan, London (1978)

[93] U. Lucia, Physica A **376** 289-292 (2007)

[94] I. Prigogine and G. Nicolis, *Non-equilibrium Systems* Wiley & Sons New York (1977)

[95] B. V. Rauschenbach, *Vibrational Combustion* State Editions of Physico-Mathematical Literature, Moscow, URSS (1961) (in Russian)

[96] W. A. Sirignano, Combustion Science and Technology, **187**:1-2, 162-205 (2015)

[97] P. Dasmeh, D J. Searles, D. Ajloo, D. J. Evans and S. R. Williams, J. Chem. Phys. **131**, 214503 (2009)

[98] C. R. Ferguson and J. C. Keck, Combustion And Flame **34**, 85-98 (1979)

[99] G. Joulin and P. Clavin, Combustion and Flame **35**, 139-153 (1979)

[100] S. H. Kang, S. W. Baek and H. G. Im, Combustion Theory And Modelling **10**, 4, (2006) 659-681

[101] G. Pilla, D. Galley, D.A. Lacoste, S. Ducruix, F. Lacas, D. Veynante and C.O. Laux, IEEE Transactions on Plasma Science, **34**, 6 2471-2477 (2006)

[102] M. S. Bak, H. Do, M. G. Mungal and M. A. Cappelli, Combustion and Flame, **159**, 10, 3128-3137 (2012)

[103] J. P. Moeck, D. A. Lacoste, Ch. O. Laux and Ch. O. Paschereit, *Control Of Combustion Dynamics In A Swirl -Stabilized Combustor With Nanosecond Repetitively Pulsed Discharges* 51st AIAA Aerospace Sciences Meeting Including The New Horizons Forum and Aerospace Exposition, 07-10 Jan. 2013, Grapevine (Dallas/Ft. Worth Region), Texas, USA

[104] T. C. Lieuwen and K. MacManus, J. Propulsion And Power, **19**, 5 (2003) 721-721

[105] Y. Huang and V. Yang, Combustion and Flame, **136**, 383-389 (2004)

[106] R. W. Schefer, D. M. Wicksall and A. K. Agrawal, Proceedings of the Combustion Institute, **29**, 843-851 (2002)

[107] T. Bouschaki, Y. Dhué, L. Selle, B. Ferret and Th. Poinsot, Intl. J. Hydrogen Energy, **37**, 9412-9422 (2012)

[108] B. Z. Dlugogorski, R. H. Hichens, E. M. Kennedy and J. W. Bozzelli, Process Safety and Environmental Protection **76** 2, 81-89 (1998)

[109] A. H. Lefebvre and D. R. Ballal *Gas Turbine Combustion: Alternative Fuels and Emissions*, (3rd edition) CRC Press, Boca Raton, FL, USA (2010)

[110] W. Polifke, *Six Lectures on Thermo-acoustic Combustion Instability*, 21st CISM-IUTAMInternational Summer School on Measurement, Analysis and Passive Control of Thermo-acoustic Oscillations, June 29 - Jul 3 2015, Udine, Italy

[111] A. N. Lipatnikov and P. Sathiah, Combustion and Flame **142**, 130-139 (2005)

[112] V. Zimont, W. Polifke, M. Bettelini and W. Weisenstein, Trans. ASME **526** 120, (1988)

[113] A. N. Lipatnikov and J. Chomiak, Progress in Energy and Combustion Science, **28** 1-74 (2002)

[114] J. Faerber, R. Koch, H. J. Bauer, M. Hase and W. Krebs *Effects Of Pilot Fuel And Liner Cooling On The Flame Structure In A Full Scale Swirl-Stabilized Combustion Setup*, GT2009-59345 Proceedings of ASME Turbo Expo 2009: Power for Land, Sea and Air June 8-12, 2009, Orlando, FL, USA

[115] P. Glansdorff and I. Prigogine, Physica **30**, 351 (1964)

[116] A. Di Vita, Phys. Rev. E **81**, 041137 (2010)

[117] I. Prigogine and R. Defay, *Chemical Thermodynamics* Longmans-Green, London (1954)

[118] V. I. Smirnov *A Course in Higher Mathematics* Mir, Paris, 1977

[119] A. V. Kudrin, A. I. Karpov, Vestn. Udmurtsk. Univ. Mat. Mekh. Komp. Nauki, **4** 80-85 (2011) (in Russian)

[120] A. I. Karpov, Vestn. Udmurtsk. Univ. Mat. Mekh. Komp. Nauki, **3** 61-68 (2008) (in Russian)

[121] V. S. Arpaci and A. Selamet, Prog. Energy Combustion Sci. **18** 429-445 (1992)

[122] A. S. Eddington, *The Pulsation Theory Of Cepheid Variables* The Observatory **40**, 290-293 (1917)

[123] A. W. Rodgers, Monthly Notices of the Royal Astronomical Society **117** 84-94 (1956)

[124] S. A. Zhevakin, Annual Review of Astronomy and Astrophysics **1**, 367-400 (1963)

[125] Th. C. Lieuwen, H. Torres, C. Johnson, B. T. Zinn, Transactions of the ASME **123** 182-189 (2001)

[126] A. Di Vita, Proc. R. Soc. London, Ser. A **458**, 21 (2002)

[127] I. V. Elsgolts, *Differential Equations and Variational Calculus*, Mir, Moscow, URSS (1981)

[128] G. A. Korn and Th. A. Korn, *Mathematical Handbook For Scientists And Engineeers*, McGraw- Hill, New York (1968)

[129] A. Naso, R. Monchaux, P. H. Chavanis and B. Dubrulle, Phys. Rev. E **81**, 066318 (2010)

[130] Th. J. Dolan, *Fusion Research* Pergamon Press, New York (1982)

[131] M. S. Sweeney, S. Hochgreb, M. J. Dunn and R. S. Barlow, Combustion and Flame, **159**, 9, 2912-2929 (2012)

[132] G. I. Sivashinsky, Phil. Trans. R. Soc. Lond. A **332**, 135-148 (1990)

[133] D. Michelson, SIAM Journal on Mathematical Analysis **23**, 2, 364-386 (1992)

[134] S. Gutman, R. L. Axelbaum, G. I. Sivashinsky, Combustion Sci. and Technol. **98**, 57-70 (1994)

[135] Th. C. Lieuwen, *Physics Of Premixed Combustion-Acoustic Wave Interactions*, in T. C. Lieuwen, V. Yang eds. 2005 *Combustion Instabilities in Gas Turbine Engines: Operational Experience, Fundamental Mechanisms, and Modeling* Prog. Astronaut. Aeronaut. **210**, Reston, VA: Am. Inst. Aeronaut. Astronaut.

[136] J. Lepers, W. Krebs, B. Prade, P. Flohr, G. Pollarolo and A. Ferrante, *Investigation of Thermo-acoustic Stability Limits of an Annular Gas Turbine Combustor Test Rig With and Without Helmholtz Resonators* GT200568246, ASME Turbo Expo 2005 Power for Land, Sea, and Air, Volume 2, Reno, Nevada, USA, June 6-9, 2005

[137] T. C. Lieuwen, *Combustion Driven Oscillations in Gas Turbines* Turbomachinery International, January/February 2003, 16-18

[138] A. M. Annaswamy, A. F. Ghoniem, IEEE Control Systems Magazine **22**, 6 37-54 (2002)

[139] J. Hermann, A. Orthmann, S. Hoffmann, P. Berenbrink, *Combination of Active Instability Control and Passive Measures to Prevent Combustion Instabilities in a 260MW Heavy Duty Gas Turbine*, RTO MP-051, RTO AVT Symposium on Active Control Technology for Enhanced Performance Operational Capabilities of Military Aircraft, Land Vehicles and Sea Vehicles, Braunschweig, Germany, 8-11 May 2000

[140] J. D. B. J. van den Boom, A. A. Konnov, A. M. H. H. Verhasselt, V. N. Kornilov, L. P. H. de Goey, H. Nijmeijer, Proceedings of the Combustion Institute **32**, 1237-1244 (2009)

[141] E. N. Volkov, V. N. Kornilov, L. P. H. de Goey, Proceedings of the Combustion Institute **34**, 1, 955-962 (2013) http://www.sciencedirect.com/science/article/pii/S1540748912002830

[142] F. Altendorfner, F. Beyrau, A. Leipertz, Th. Hammer, D. Most, G. Lins and D. W. Branston, Chem. Eng. Technol. **33**, 4, 647-653 (2010)

[143] A. Von Engel and J. R. Cozens, *Flame Plasmas* in Marton L. (ed.) Advances In Electronics And Electron Physics vol. 20, Academic Press, New York (1964) p.99

[144] R. Erfani, H. Zare-Behtash, C. Hale, K. Kontis, Acta Astronautica, **109**, 132-143 (2015)

[145] S. M. Starikovskaia, J. Phys. D Appl. Phys. **39** R265 (2006)

[146] D. A. Lacoste, J. P. Moeck, D. Durox, C. O. Laux and T. Schuller, J. Engineering for Gas Turbines and Power **135**, 101501-1-7 (2013)

[147] A. A. Nikipelov, I. B. Popov, G. Correale, A. E. Rakitin, and A. Y. Starikovskii, *Ultra-Lean And Ultra-Rich Flames Stabilization By High-Voltage Nanosecond Pulsed Discharge* 48th AIAA Aerospace Science Meeting, AIAA Vol. 1341. (2010)

[148] D. J. Sullivan, S. H. Zaidi, S. O. Macheret, Y. Ju and R. B. Miles *Microwave Techniques for the Combustion Enhancement of Laminar Flames* 40th AIAA/ASME/SAE/ASEE Joint Propulsion Conference AIAA-2004-3713, Fort Lauderdale, FL, 11-14 July 2004

[149] S. H. Zaidi, S. O. Macheret, Y. Ju, R. B. Miles and D. J. Sullivan, *Increased Speed Of Premixed Laminar Flames In A Microwave Resonator* 35th AIAA Plasmadynamics and Lasers Conference AIAA 2004-2721, Portland, OR 28 June - 1 July 2004

[150] J. Yiguang, S. O. Macheret, M. N. Schneider, R. B. Miles and D. J. Sullivan *Numerical Study Of The Effect Of Microwave Discharge On The Premixed Methane-Air Flame* AIAA 2004-3707, 40th AIAA/ASME/SAE/ASEE Joint Propulsion Conference and Exhibit 11 - 14 July 2004, Fort Lauderdale, Florida

[151] K. Shinohara, N. Takada and K. Sasaki, J. Appl. Phys. D **42** 182008 (2009)

[152] E. S. Stockman, H. Sohail, S. H. Zaidi and R. B. Miles *Pulsed Microwave Enhancement of Laminar and Turbulent Hydrocarbon Flames* AIAA-1348 , Miami FL (2007)

[153] S. H. Zaidi, E. Stockman, X. Qin, Z. Zhao, S. Macheret, Y. Ju , R. B. Miles, D. J. Sullivan and J. F. Kline *Measurements of Hydrocarbon Flame Speed Enhancement in High-Q Microwave Cavity* AIAA-1217, Reno Nevada (2006)

[154] K. Schofield, Progress in Energy and Combustion Science **34**, 3,330-350 (2008)

[155] M. Porkolab, *RF Heating Of Magnetically Confined Plasmas* in E. Teller, (ed.) Fusion, vol. I B , p. 151 Academic Press, New York (1981)

[156] Ph. Bibet , G. Agarici, M. Chantant, J. J. Cordier, C. Deck, L. Doceul, A. Durocher, A. Ekedahl, Ph. Froissard, L. Garguiolo, L. Garampon, M. Goniche, P. Hertout, F. Kazarian, D. Lafon, C. Portafaix, G. Rey, F. Samaille, F. Surle and G. Tonon, *New Advanced Launcher For Lower Hybrid Current Drive On Tore Supra* Fusion Engineering and Design **51**-**52**, 741-746 (2000) (DOI: 10.1016/S0920-3796(00)00450-6)

[157] J. B. Michael, R. B. Miles, *Ultra-Lean Combustion Sustained By Pulsed Subcritical Microwaves* in 42nd AIAA Plasma Dynamics And Lasers Conference (No. 3446) (2011, June)

[158] L. D. Landau and E. Lifshitz *Electrodynamics of Continuous Media* Pergamon, Oxford, UK (1960)

[159] J. Parente, V. Anisimov, G. Mori and G. Croce, *Micro Gas Turbine Combustion Chamber Design And CFD Analysis* GT2004-54247, Proceedings of ASME Turbo Expo 2004, Power for Land, Sea and Air, Jule 14-17, 2004, Vienna, Austria

[160] Th. H. Stix, *The Theory Of Plasma Waves* McGraw-Hill New York (1962)

[161] I. Kosarev, N. Aleksandrov, S. Kindysheva, S. Starikovskaia and A. Y. Starikovskii, Combustion and Flame **154**, 3, 569-586 (2008)

[162] N. Popov, Journal of Physics D: Applied Physics **44**, 28, 285201 (2011)

[163] E. Mintoussov, S. Pendleton, F. Gerbault, N. Popov and S. Starikovskaia, Journal of Physics D: Applied Physics **44**, 28, 285202 (2011)

[164] C. Pintassilgo, V. Guerra, O. Guaitella and A. Rousseau, Plasma Sources Science and Technology **23**, 2, 025006 (2014)

[165] H. Teitelbaum, Journal of Physical Chemistry **94**, 8, 3328-3332 (1990)

[166] A. Starik, A. Sharipov and N. Titova, Combustion Science and Technology **183**, 1, 75-103 (2010)

[167] A. Starikovskiy, *Plasma Assisted Combustion Mechanism for Small Hydrocar- bons* American Institute of Aeronautics and Astronautics, 2015. doi: 10.2514/6.2015-0158.

[168] V. Smirnov, O. Stelmakh, V. Fabelinsky, D. Kozlov, A. Starik and N. Titova, Journal of Physics D: Applied Physics **41**, 19, 192001 (2008)

[169] T. Ombrello, S. H. Won, Y. Ju and S. Williams, Combustion and Flame **157**, 10, 1906-1915 (2010)

[170] T. Ombrello, S. H. Won, Y. Ju and S. Williams, Combustion and Flame **157**, 10, 1916-1928 (2010)

[171] A. Starik, N. Titova and A. Sharipov, *Kinetic mechanism of H_2-O_2 ignition promoted by singlet oxygen $O_2(a^1\Delta_g)$*, in *Deflagrative and Detonative Combustion*, Torus Press, Moscow (2010), pages 19-42

[172] A. Starik, B. Loukhovitski and A. Chernukho, Plasma Sources Science and Technology **21**, 3, 035015 (2012)

[173] M. Capitelli, G. Colonna, O. De Pascale, C. Gorse, K. Hassouni and S. Longo, Plasma Sources Science and Technology **18**, 1, 014014 (2009)

[174] M. Capitelli, G. Colonna, G. D'Ammando, V. Laporta and A. Laricchiuta, Physics of Plasmas **20**, 10, 101609 (2013)

[175] G. D'Ammando, G. Colonna, M. Capitelli and A. Laricchiuta, Physics of Plasmas **22**, 3, 034501 (2015)

[176] G. Colonna, G. D'Ammando, L. Pietanza and M. Capitelli, Plasma Physics and Controlled Fusion **57**, 1 014009 (2015)

[177] G. Colonna and M. Capitelli, Journal of Physics D: Applied Physics **34**, 12, 1812 (2001)

[178] M. Capitelli, G. Colonna, L. Pietanza and G. D'Ammando, Spectrochimica Acta Part B: Atomic Spectroscopy **83**, 1-13 (2013)

[179] G. Colonna and M. Capitelli, Journal of Thermophysics and Heat Transfer **22**, 3, 414-423 (2008); DOI:10.2514/1.33479

[180] A. Bourdon and P. Vervisch, Journal of thermophysics and heat transfer **14**, 4, 489-495 (2000)

[181] V. Guerra, P. Sa' and J. Loureiro, The European Physical Journal Applied Physics **28**, 02, 125-152 (2004)

[182] V. Laporta, R. Celiberto and J. Wadehra, Plasma Sources Science and Technology **21**, 5, 055018 (2012)

[183] V. Laporta, C. Cassidy, J. Tennyson and R. Celiberto, Plasma Sources Science and Technology **21**, 4, 045005 (2012)

[184] G. Colonna, V. Laporta, R. Celiberto, M. Capitelli and J. Tennyson, *Nonequilibrium vibrational and electron energy distributions functions in atmospheric nitrogen ns pulsed discharges and μ-s post-discharges: the role of electron molecule vibrational excitation scaling laws* Plasma Sources Science and Technology (in press)

[185] G. P. Smith, D. M. Golden, M. Frenklach, N. W. Moriarty, B. Eiteneer, M. Goldenberg, C. T. Bowman, R. K. Hanson, S. Song, W. C. Gardiner Jr., V. Lissianski and Z. Qin, *GRI-Mech database* (1999) http://www.me.berkeley.edu/

[186] T. Pedersen and R. C. Brown, Combustion and Flame, **4**, 94, 433-448 (1993)

[187] S. M: Aithal, A. R. White, V. V. Subramaniam, V. Babu, G. Rizzoni, *A chemichal kinetic model of current signatures in an ionization sensor* unpublished

[188] Y. Ju, S. O. Macheret, M. N. Shneider and R. B. Miles *Numerical study of the effect of microwave discharge on the premixed methane-air flame* AIAA 2004-3707, 40th AIAA/ASME/SAE/ASEE Joint Propulsion Conference and Exhibit Fort Lauderdale. Florida 11-14 July 2004

[189] I. A. Kossyi, A. Y. Kostinsky, A. A. Matveyev, V. P. Silakov, Plasma Sources Science and Technology **1**, 3, 207 (1992) http://stacks.iop.org/0963-0252/1/i=3/a=011

[190] G. Colonna and M. Capitelli, Journal of Physics D:Applied Physics **34**, 12, 1812 (2001)

[191] M. Capitelli, I. Armenise, E. Bisceglie, D. Bruno, R. Celiberto, G. Colonna, G. D'Ammando, O. De Pascale, F. Esposito and C. Gorse, Plasma Chemistry and Plasma Processing 1-24 (2012)

[192] G. Colonna, M. Tuttafesta and D. Giordano, Computer Physics Communications **138**, 213-221 (2001)

[193] G. Colonna, L. Pietanza and G. d'Ammando, Chemical Physics **398**, 37-45 (2012)

[194] M. Perrin, G. Colonna, G. D'Ammando, L. Pietanza, P. Riviere, A. Soufani and S. Surzhikov, The Open Plasma Physics Journal **7**, 114-126 (2014)

[195] I. Armenise and E. Kustova, Chemical Physics **415**, 269-281 (2013)

[196] M. Capitelli, G. Colonna, G. D'Ammando, V. Laporta and A. Laricchiuta, Chemical Physics **438**, 31-36 (2014)

[197] G. Colonna, M. Capitelli, S. Debenedictis, C. Gorse and F. Paniccia, Contributions to Plasma Phys. **31**, 6, 575-579 (1991)

[198] G. Capriati, G. Colonna, C. Gorse and M. Capitelli, Plasma Chemistry and Plasma Processing **12**, 3, 237-260 (1992)

[199] R. K. Janev and D. Reiter, Collision processes of hydrocarbon species in hydrogen plasmas: I. the methane family, Juel-Report 3966.

[200] The LXcat database, http://www.lxcat.laplace.univ-tlse.fr/

[201] H. C. Straub, D. Lin, B. G. Lindsay, K. A. Smith and R. F. Stebbings, The Journal of Chemical Physics **106**, 4430 (1997)

[202] M. T. Lee, M. F. Lima, A. M. C. Sobrinho and I. Iga, Journal of Physics B: Atomic, Molecular and Optical Physics **35**, 11, 2437 (2002)

[203] Y. K. Kim, M. Asgar Ali, M. Eugene Rudd, Journal of Research - National Institute of Standards and Technology **102**, 693696 (1997)

[204] K. L. Baluja and A. Z. Msezane, Journal of Physics B: Atomic, Molecular and Optical Physics **34**, 15, 3157 (2001)

[205] R. K. Janev and D. Reiter, *Collision processes of hydrocarbon species in hydrogen plasmas: II. ethane & propane families*, Juel-Report 4005.

[206] A. Jain, Journal of Physics B: Atomic, Molecular and Optical Physics **26**, 24, 4833 (1993)

[207] S. H. Zheng and S. K. Srivastava, Journal of Physics B: Atomic, Molecular and Optical Physics **29**, 14, 3235 (1999)

[208] M. Hoshino, *Elastic Differential Cross Sections for Electron Collisions with Polyatomic Molecules*, Vol. 101 of NIFS DATA, National Institute for Fusion Science, 2008.

[209] W. Hwang, Y. K. Kim and M. E. Rudd,The Journal of Chemical Physics **104**, 2956 (1996)

[210] Y. Itikawa and N. Mason, Journal of Physical and Chemical Reference Data **34**, 1, 122 (2005)

[211] A. M. C. Sobrinho, N. B. H. Lozano and M. T. Lee, Phys. Rev. A **70**, 3, 032717(2004)

[212] V. Tarnovsky, H. Deutsch and K. Becker, The Journal of Chemical Physics **109**, 932 (1998)

[213] M. Rao and S. K. Srivastava, Journal of Physics B: Atomic, Molecular and Optical Physics **25**, 9, 2175 (1999)

[214] J. S. Rajvanshi and K. L. Baluja, Physical Review A **82**, 6, 062710 (2010)

[215] K. N. Joshipura, M. Vinodkumar and U. M. Patel, Journal of Physics B: Atomic, Molecular and Optical Physics **34**, 4, 509 (2001)

[216] Y. Itikawa, Journal of Physical and Chemical Reference Data **31**, 3, 749768 (2002)

[217] P. C. Cosby, The Journal of Chemical Physics **98**, 7804 (1993)

[218] H. Munjal, K. L. Baluja and J. Tennyson, Phys. Rev. A **79**, 3, 032712(2009)

[219] P. Bhatt and S. Pal, Chemical Physics **327**, 2, 452456 (2006)

[220] J. Lopez, V. Tarnovsky, M. Gutkin and K. Becker, International Journal of Mass Spectrometry **225**, 1, 2537 (2003)

[221] S. Kaur and K. L. Baluja, Phys. Rev. A **85**, 5, 052701 (2012)

[222] S. K. Srivastava, H. Tanaka and A. Chutjian, The Journal of Chemical Physics **69**, 1493 (1978)

[223] A. Jain and S. S. Tayal, Journal of Physics B: Atomic and Molecular Physics **17**, 1, L37 (1984)

[224] O. May, D. Kubala and M. Allan, Phys. Rev. A **82**, 1, 010701 (2010)

[225] S. H. Pandya, F. A. Shelat, K. N. Joshipura and B. G. Vaishnav, International Journal of Mass Spectrometry, **323**-**324**, 28-33 (2012)

[226] M. A. Khakoo, J. Blumer, K. Keane, C. Campbell, H. Silva, M. C. A. Lopes, C. Winstead, V. McKoy, R. F. Da Costa and L. G. Ferreira, Phys. Rev. A **77**, 4, 042705 (2008)

[227] R. T. Sugohara, M. G. P. Homem, I. P. Sanches, A. F. de Moura, M. T. Lee and I. Iga, Phys. Rev. A **83**, 3, 032708 (2011)

[228] R. Rejoub, C. D. Morton, B. G. Lindsay and R. F. Stebbings, The Journal of Chemical Physics **118**, 1756 (2003)

[229] S. Kaur and K. L. Baluja, Journal of Physics B: Atomic, Molecular and Optical Physics **38**, 21, 3917 (2005)

[230] A. A. Sobrinho, L. E. Machado, S. E. Michelin, L. Mu-Ta and L. M. Brescansin, Journal of Molecular Structure: THEOCHEM **539**, 1, 6574 (2001)

[231] M. Vinodkumar, K. N. Joshipura, C. Limbachiya and N. Mason, Phys. Rev. A **74**, 2, 022721 (2006)

Part VII

Appendices

Energy balance of a perturbation in the zero Mach case

Once terms $\approx O(M), O(\epsilon^3)$ are neglected, straightforward algebra gives $\frac{\rho}{2}\frac{d|\mathbf{v}|^2}{dt} \approx \frac{\rho}{2}\frac{\partial|\mathbf{v}|^2}{\partial t}$ and $\nabla \cdot (p\mathbf{v}) = \nabla \cdot (p_0\mathbf{v}_1) + \nabla \cdot (p_1\mathbf{v}_1)$. Moreover, equation (6.10) reduces to

$$\frac{\partial p_1}{\partial t} = (\gamma - 1)Q_1 - \gamma p_0 \nabla \cdot \mathbf{v}_1 \tag{1}$$

so that

$$\frac{1}{2\rho c_s^2}\frac{dp^2}{dt} \approx \frac{1}{2\rho_0 c_{s0}^2}\frac{\partial p_1^2}{\partial t} + \frac{rQ_1}{c_p} - \nabla \cdot (p_0\mathbf{v}_1)$$

We are left with the discussion of the term $\propto \frac{ds^2}{dt}$ on the L.H.S. of equation (6.12). To this purpose, we recall that $s = s_0 + s_1$ and $\frac{\partial s_0}{\partial t} = 0$, so that

$$\frac{ds_0}{dt} = \mathbf{v}_1 \cdot \nabla s_0$$

and

$$\frac{ds_1}{dt} = \frac{ds}{dt} - \frac{ds_0}{dt} = r(Q/p)_1 - \mathbf{v}_1 \cdot \nabla s_0$$

In agreement with the $M \ll 1$ assumption, we neglect the contribution of $\frac{p_1}{p_0}$ to equation (6.6). In fact, this contribution scales as M because $p_0 \approx c_{s0}^2$ and the linearised version of equation (6.2) (see (6.20) below) makes p_1 to be linear in $\mathbf{v}_1$. As a consequence, we write

$$s_1 = \frac{c_p T_1}{T_0}$$

and

$$\frac{ds_1}{dt} = r\frac{Q_1}{p_0} - \mathbf{v}_1 \cdot \nabla s_0$$

It follows that

$$\frac{sQ_1}{c_p} = \frac{s_0 Q_1}{c_p} + \frac{s_1 Q_1}{c_p} = \frac{s_0 Q_1}{c_p} + \frac{T_1 Q_1}{T_0}$$

and that

$$\frac{ds}{dt} = \frac{rQ_1}{p_0}$$

because $\dfrac{ds}{dt} \approx O(\epsilon)$. Finally, we invoke the identity

$$\frac{ds^2}{dt} = \frac{ds_0^2}{dt} + \frac{ds_1^2}{dt} + 2\frac{ds_0 s_1}{dt}$$

and obtain:

$$\frac{p}{2rc_p}\frac{ds^2}{dt} = \frac{p_0}{2rc_p}\frac{\partial s^2}{\partial t} + \frac{s_0 Q_1}{c_p} + \frac{p_0}{rc_p} s_1 \mathbf{v}_1 \cdot \nabla s_0$$

These relationships make equation (6.12) to reduce to (6.14).

Auxiliary relationships concerning Rayleigh's criterion

We recall that $da = \frac{da}{dt}dt$ for the generic quantity a. Since $\langle a_1 \rangle = 0$, the only non-zero contributions to $\langle d\left(\int d\mathbf{x}\frac{P}{T}\right)\rangle$ will be of second-order. Let us compute such contributions.

Reynolds' transport theorem (for $\mathbf{u} = \mathbf{v}$) and Gauss' theorem of divergence allow us to write:

$$0 \leq \langle \left(\int d\mathbf{x}\frac{P}{T}\right)_1 \rangle = \langle dt\frac{d}{dt}\int d\mathbf{x}\frac{P}{T}\rangle = \langle dt\int d\mathbf{x}\frac{\partial}{\partial t}\left(\frac{P}{T}\right)\rangle + \langle dt\int d\mathbf{a}\cdot\mathbf{v}\frac{P}{T}\rangle$$

Substitution of both the definition of $P = \rho\frac{du}{dt} + p\rho\frac{d}{dt}\left(\frac{1}{\rho}\right)$ and of the assumption (6.13) leads to:

$$-\langle \int d\mathbf{x}dt\frac{\partial}{\partial t}\left(\frac{P}{T}\right)\rangle \leq \langle \int d\mathbf{a}\cdot\frac{\mathbf{v}_1}{T}\left[\rho du + p\rho d\left(\frac{1}{\rho}\right)\right]\rangle \tag{2}$$

Further progress requires finding a lower (upper) bound for the L.H.S. (R.H.S.) of (2). To this purpose, we observe that stability of the unperturbed state requires that the perturbation amplitude never diverges, i.e., it remains upper-bounded everywhere across the system at all times. Then, $a(\mathbf{x}, t) \leq A_M(t)$ everywhere for the generic quantity a , where $A_M(t) \leq A_{\max}$ for arbitrary t. Analogous arguments hold for the lower bound $A_{\min}$ ($a(\mathbf{x}, t) \geq A_m(t) \geq A_{\min}$). We are e.g. free to take $A_{\min} = -A_{\max}$. Accordingly, stability of the unperturbed state imply that for a generic $a(\mathbf{x}, t)$ two positive constant quantities $A_{\max}$, $A_{\min}$ and two functions of time $A_M(t)$ and $A_m(t)$ exist such that the following inequality holds:

$$A_{\max} \geq A_M(t) \geq a(\mathbf{x}, t) \geq A_m(t) \geq A_{\min}$$

Finally, we invoke the definition of $\frac{d}{dt}$ and write $dt\frac{\partial}{\partial t}\left(\frac{P}{T}\right) = dt\frac{d}{dt}\left(\frac{P}{T}\right)|_{\mathbf{v}=0}$ where

$$dt\frac{d}{dt}\left(\frac{P}{T}\right)|_{\mathbf{v}=0} = d\left(\frac{P}{T}\right)|_{\mathbf{v}=0} = \frac{dP|_{\mathbf{v}=0}}{T} + Pd\left(\frac{1}{T}\right)|_{\mathbf{v}=0} + (dP)\,|_{\mathbf{v}=0}d\left(\frac{1}{T}\right)|_{\mathbf{v}=0}$$

The relationships listed above allow us to find a lower bound for the L.H.S. of (2) with the help of the following chain of inequalities:

$$\begin{aligned}
&-\langle\int d\mathbf{x}dt\frac{\partial}{\partial t}\left(\frac{P}{T}\right)\rangle \geq -\frac{1}{T_{\min}}\int d\mathbf{x}\langle(dP)\,|_{\mathbf{v}=0}\rangle - P_{\max}\int d\mathbf{x}\langle d\left(\frac{1}{T}\right)_{\mathbf{v}=0}\rangle + \\
&-\int d\mathbf{x}\langle(dP)\,|_{\mathbf{v}=0}d\left(\frac{1}{T}\right)_{\mathbf{v}=0}\rangle = -\int d\mathbf{x}\langle(dP)\,|_{\mathbf{v}=0}d\left(\frac{1}{T}\right)_{\mathbf{v}=0}\rangle = \\
&= \int d\mathbf{x}\langle(P)_{1(\mathbf{v}=0)}\left(\frac{-1}{T}\right)_1\rangle = \int d\mathbf{x}\langle\left(\rho T\frac{ds}{dt} - \rho T\mathbf{v}\cdot\nabla s\right)_1\frac{T_1}{T_0^2}\rangle = \\
&= \int d\mathbf{x}\langle(P_h - \nabla\cdot\mathbf{q} - \rho T\mathbf{v}\cdot\nabla s)_1\frac{T_1}{T_0^2}\rangle = \int d\mathbf{x}\langle\frac{(P_{h1} - \nabla\cdot\mathbf{q}_1)\,T_1}{T_0^2} - \frac{\rho_0 T_1\mathbf{v}_1\cdot\nabla s_0}{T_0}\rangle = \\
&= \int d\mathbf{x}\langle\frac{(P_{h1} - \nabla\cdot\mathbf{q}_1)\,T_1}{T_0^2} - \frac{p_0 s_1\mathbf{v}_1\cdot\nabla s_0}{rc_pT_0}\rangle \geq \frac{1}{T_{0\max}}\int d\mathbf{x}\langle D\rangle + \int d\mathbf{x}\langle(\nabla\cdot\mathbf{q}_1)\left(\frac{1}{T}\right)_1\rangle
\end{aligned} \tag{3}$$

Here we have invoked the vanishing of the time-average of first-order perturbations, we have invoked the definition of P, we have invoked (6.4), (6.6), (6.17) and (6.13) and we have neglected the contribution of $\frac{p_1}{p_0}$ to (6.6) in agreement with the $M \ll 1$ assumption, so that $s_1 = c_p\frac{T_1}{T_0}$.

Now, let us look for an upper bound on the R.H.S. of (2). In order to select the perturbation of interest, we take advantage of the smallness of P_1. According to $P_0 = 0$ and to $P = \rho T\frac{ds}{dt}$ $P_1 \approx 0$ is satisfied whenever $ds \approx 0$. Since the perturbation is almost adiabatic and we are dealing with a mixture of perfect gases, we make a small mass error if we assume that relationships $\frac{p}{\rho^\gamma} = c_5$ hold together with (6.4) with c_5 constant quantity, and that (6.5) is sligthly corrected as follows:

$$\rho u = \frac{(1+c_6)\,p}{\gamma - 1}$$

where $|c_6| << 1$ expresses the deviation from purely adiabatic behaviour. To the author's knowledge, the impact of this deviation on the evolution of our soundlike perturbation in the zero Mach limit has been explicitly stressed for the first time in [33], where some preliminary remarks of [31] have been developed. Basically, c_6 represents the difference bewteen the values of E as computed according to equations (6.15) and (6.18). It follows that $d\left(\frac{1}{T}\right) = -Gdp$ and $\frac{\rho}{T}du + \frac{p\rho}{T}d\left(\frac{1}{\rho}\right) = Fdp$ where $F \equiv \frac{c_6 G p_0}{\gamma - 1}$ and $G \equiv \frac{r}{c_5^{\frac{1}{\gamma}}}\left(1 - \frac{1}{\gamma}\right) p_0^{\frac{1-2\gamma}{\gamma}} > 0$. We have seen that near a stable state a quantity $F_{\max}$ exists such that $F \leq F_{\max}$, then substitution in the R.H.S. of (2) with the notation $p_1 = dp$ together with equation (6.16) give

$$\langle \int d\mathbf{a} \cdot \frac{\mathbf{v}_1}{T}\left[\rho du + p\rho d\left(\frac{1}{\rho}\right)\right]\rangle \leq F_{\max} \int d\mathbf{a} \cdot \langle \mathbf{W} \rangle \tag{4}$$

Together, (2), (3) and (4) give (12.5).

Finally, we stress the point that the fact that $|c_6| << 1$ allows us to choose $F_{\max}$ in such a way that (12.5) reduces to (6.34) and (6.35) if the operator $\leq$ reduces to $<$ and to $=$ respectively.

On the impact of flame velocity on humming

Here we start from equation (6.36). We are going to refer to a particular expression for the Rayleigh's index D nowhere in the following; depending on the selected expressions for D and for $\mathbf{W}$, we may refer either to Rayleigh's criterion or to Myers' corollary.

The R.H.S. of (6.36) is non-negative as far as we supply the system with no net acoustic power (i.e., we ring no external bell, siren and the like. Now, both equation (6.36) and the inequality $\int_{V_f} d\mathbf{x}D \leq |\int_{V_f} d\mathbf{x}D| \leq \int_{V_f} d\mathbf{x}|D|$ lead to the following inequality:

$$\langle \int_{V_f} d\mathbf{x}|D|\rangle \geq \langle \int_{V_f} d\mathbf{x}D\rangle = \int_{A_b} d\mathbf{a} \cdot \langle \mathbf{W} \rangle \geq 0$$

This inequality ensures that if we are able to reduce the positive-definite quantity $\langle \int_{V_f} d\mathbf{x}|D|\rangle$ then we are able to reduce the destabilising L.H.S. of equation (6.36), hence to stabilise humming. We are going to show that this is precisely the effect of raising the flame velocity (Rijke's *rapidity of the air current* [24]) at given upstream flow $\mathbf{v}$.

To this purpose, we limit ourselves to thin flames, which are described as a 2-dimensional *flame surface* $G(\mathbf{x}, t) = 0$ in the 3-dimensional space. Since the surface is 2-dimensional we are free to denote each point on it with a couple of coordinates (x_1, x_2). Since the Rayleigh index is peaked at the flame (just like the combustion power density and the entropy jump) we may write $|D| = D_f \delta(G)$ with δ denoting Dirac's delta and $D_f > 0$. The relationship

$$\int_{V_f} d\mathbf{x}|D| = \int_{A_f} |J|^{-1} dx_1 dx_2 D_f$$

follows therefore from (6.22), where J is the Jacobian of the coordinate transformation $(x, y, z) \to (x_1, x_2, G)$ and $|J|^{-1} dx_1 dx_2$ is the area element. In turn, the surface integral $\int_{A_f} |J|^{-1} dx_1 dx_2 D_f$ is equal to $\lim_{N\to\infty} \sum_{q=1}^{q=N} D_f \Delta A_q$ by definition, where $\Delta A_q > 0$ is the flame area element centered at the point $(x_1, x_2) = (x_{1q}, x_{2q})$ on the flame. (Here and in the following we drop the dependence of each term on x_{1q}, x_{2q} and t for simplicity). In summary, we write:

$$\int_{V_f} d\mathbf{x}|D| = \lim_{N\to\infty} \sum_{q=1}^{q=N} D_f \Delta A_q \tag{5}$$

For further analysis, we focus our attention on laminar flames for the moment. The flame velocity is s_L. Turbulent flames will be dealt with in the following. The flame area oscillates when humming occurs, and the same obviously occurs to each flame area element ΔA_q. The relevant equation of motion [2] reads [4]:

$$\kappa_{st} \equiv \frac{1}{\Delta A_q}\frac{d\Delta A_q}{dt} = \frac{d\ln \Delta A_q}{dt} = (\delta_{ij} - n_i n_j)\,\frac{\partial v_i}{\partial x_j} + s_d \frac{\partial n_i}{\partial x_i} \tag{6}$$

where $i, j = 1, 2, 3$, summation on repeated indices is assumed, both the *stretch* κ_{st} and the unit surface vector $\mathbf{n}$ perpendicular to the flame and pointing towards the unburnt gases depend on both on x_{1q}, x_{2q} and t, and we denote the Kronecker's delta with δ_{ij}. Following Chapter 5 of [4], we define the *displacement speed* s_d in such a way that $\mathbf{v} + s_d\mathbf{n}$ is the velocity of the point x_{1q}, x_{2q} on the flame surface in the laboratory system of reference; it is also possible to show that

$$\frac{ds_d}{ds_L} > 0 \tag{7}$$

and depends weakly on κ_{st} in most cases where no flame quenching occurs under the assumptions of single-step chemistry and high activation energy - see Sec. 2.7.3 of [4]. (Usually $\frac{ds_d}{ds_L} \approx 1$). Finally, the relationship

$$\nabla \cdot \mathbf{n} \equiv \frac{\partial n_i}{\partial x_i} = -K_{tot} \tag{8}$$

links the flame shape and the *total curvature* K_{tot} of the flame, i.e. the sum of the reciprocals of the principal curvature radii of the flame. Equations (6) and (8) give:

$$\Delta A_q = \Delta A_q\,(t = 0) \cdot \exp\left[\int_0^t dt'\,(\delta_{ij} - n_i n_j)\,\frac{\partial v_i}{\partial x_j}\right] \cdot \exp\left[-\int_0^t dt' s_d K_{tot}\right] \tag{9}$$

[2]In the formalism of Sec. 2.6 of [4] the quantities ΔA_q and κ_{st} are referred to as A and κ respectively.

Equations (5) and (9) give:

$$\langle \int_{V_f} d\mathbf{x}|D|\rangle = \langle \lim_{N\to\infty} \sum_{q=1}^{q=N} D_f \Delta A_q \left(t=0\right) \exp\left[\int_0^t dt' \left(\delta_{ij} - n_i n_j\right) \frac{\partial v_i}{\partial x_j}\right] \exp\left[-\int_0^t dt' s_d K_{tot}\right]\rangle \tag{10}$$

after time-averaging all quantities. In turn, derivation of both sides of (10) on s_L at fixed $\mathbf{v}$ implies:

$$\left(\frac{\partial}{\partial s_L}\right)_{\mathbf{v}=const.} \langle \int_{V_f} d\mathbf{x}|D|\rangle = \langle \lim_{N\to\infty} \sum_{q=1}^{q=N} D_f \Delta A_q \left[-\int_0^t dt' K_{tot} \frac{ds_d}{ds_L}\right]\rangle \tag{11}$$

All terms on the R.H.S. of (11) are positive definite but the last one in square brackets. According to (5), (7), (9) and (11), $\left(\frac{\partial}{\partial s_L}\right)_{\mathbf{v}=const.} \langle \int_{V_f} d\mathbf{x}|D|\rangle < 0$ -i.e., a small increase of s_L at fixed $\mathbf{v}$ is stabilising- if and only if $\langle\langle \int_0^t dt' K_{tot} \frac{ds_d}{ds_L}\rangle_f\rangle > 0$, where we have defined the average $\langle a\rangle_f \equiv \frac{\int_{A_f} |J|^{-1} dx_1 dx_2 D_f a}{\int_{A_f} |J|^{-1} dx_1 dx_2 D_f}$ of the generic quantity a taken on the flame surface and weighted by the Rayleigh index. A simpler, sufficient condition is that the flame is globally concave ($\langle K_{tot}\rangle_f > 0$) at all times, where we have taken into account that $\frac{ds_d}{ds_L} \approx 1$.

So far, we have discussed laminar flames. When it comes to turbulent flames, a vast range of length scales and time scales (down to the Kolmogorov length scale η_k) is relevant. Locally and instantaneously, the combustion process may undergo quenching and re-ignition again ad again and the very concept of flame surface may be meaningful in a statistical sense only. Depending on the particular case of interest, the sign of both the flame stretch and the total curvature may change in space and time. In particular, in the laminar case the flame is like a smooth surface in the neighbourhood of the point (x_{1q}, x_{2q}) within the flame surface element ΔA_q, the flame thickness being very small.

In contrast, turbulence leads to many convolutions of the flame front near (x_{1q}, x_{2q}); correspondingly, in the neighbourhood of this point the available flame surface area per unit volume may be much larger than ΔA_q. Locally, it is possible to introduce in the neighbourhood of (x_{1q}, x_{2q}) the average $\langle a\rangle_s$ of the generic quantity a along the flame surface. As for the rigorous definition of this turbulent flame surface average -which, in spite of its misleading name, is still a function of (x_{1q}, x_{2q})- see both equation (5.79) and note (xvi) in Sec. 5.3.6 of [4]. Physically, the main advantage of this approach is to separate turbulence-combustion interactions (ruled by the available flame surface area per unit volume) from the chemistry and the thermodynamics of combustion, incorporated in the average flame speed.

Since we are interested in the impact of the flame speed on humming, the obvious question if it is possible to generalise our results (9), (10) and (11) to the turbulent flame by replacing the relevant quantities κ_{st}, etc. with their turbulent flame surface averages $\langle\kappa_{st}\rangle_s$ and the like.

The answer is likely to be affirmative, provided e.g. that we are able to show that the period τ of humming oscillations which we are concerned with ($\approx 10^{-2}s$) is much longer than the characteristic time-scales of turbulence. There is a continuous range of such time-scales. In the case of homogeneous and isotropic turbulence, equations (4.5), (4.7), (4.9) and (4.11) of [4] ensure that the lower bound $\tau_K = \sqrt{\frac{\nu}{\epsilon_{turb}}}$ on this range is the reciprocal of the stretch of the eddies with linear size η_K; the upper bound is $\tau_K \cdot \sqrt{Re_T}$ where ν, $\epsilon_{turb} = \frac{(u')^4}{Re_T \cdot \nu}$, $Re_T = \frac{u' l_T}{\nu} > 1$ and u' are the kinematic viscosity, the mechanical power dissipated per unit mass in turbulent eddies, the turbulent Reynolds number and the integral length, i.e. the typical amplitude of turbulent velocity fluctuations on the length-scale $l_T = Re_T^{\frac{3}{4}} \eta_K$ respectively. Physically, $\nu Re_T = u' l_T$ acts as a turbulent diffusion coefficient, larger than the molecolar diffusion coefficient $\propto \nu$. For typical values $\nu = 10^{-5}\frac{m^2}{s}$, $Re_T = 10^3$ and $u' \approx |\mathbf{v}_0| \approx \text{some}\frac{m}{s}$ we have indeed $\tau \approx 10^{-2}s > \tau_K \cdot \sqrt{Re_T} \approx 10^{-3}s > \tau_K \approx 3 \cdot 10^{-5}s$.

Admittedly, this is just an order-of-estimate analysis. Firstly, turbulence is far from homogeneous e.g. near the walls. Secondly, Re_T lies in the range $10^2 < Re_T < 2 \cdot 10^3$ in many combustors -see Sec. 4.2 of [4]. Finally, the very definition of u' is far from unambiguous near a premixed turbulent flame - see Secs. 4.2 and 5.2.1 of [4]. However, the requirement $\tau > \tau_K \cdot \sqrt{Re_T}$ is likely to be too restrictive. In fact, our discussion on the thermodynamical meaning of the impact of s_L (and of the corresponding turbulent quantity s_T, which is an increasing function of s_L) on humming makes it unlikely that turbulence affects such impact, as the time-scale of the inter-particle collisions ($\approx 10^{-10}s$) which ensure the validity of LTE is much shorter than τ_K. We are going to refer to this separation of time-scale in the following. Of course, when investigating the impact of the perturbation of Rijke's *rapidity of the air current* we have to apply a perturbation to the turbulent flame velocity s_T here.

In particular, equations (5.31) and (5.78) of [4] provides us implicitly with a definition of $\langle\kappa_{st}\rangle_s$ which is just the straightforward generalisation of (6):

$$\langle \kappa_{st} \rangle_s = \frac{d \ln \langle \Delta A_q \rangle_s}{dt} = \left\langle (\delta_{ij} - n_i n_j) \frac{\partial v_i}{\partial x_j} \right\rangle_s + \left\langle s_d \frac{\partial n_i}{\partial x_i} \right\rangle_s \tag{12}$$

where the separation of time-scales quoted above allows us to exchange the quantities $\frac{da}{dt}$ and $\langle a \rangle_s$ for the generic quantity a. Here s_d is still an increasing function of s_L; in the following, we take advantage of the fact that s_T is a monotonically increasing -hence invertible- function of s_L, so that s_d is an increasing function of s_T, with $\frac{ds_d}{ds_T} = \frac{ds_d}{ds_L} \frac{ds_L}{ds_T} > 0$. We may repeat the proof of (11) step-by-step and write:

$$\left(\frac{\partial}{\partial s_T} \right)_{\mathbf{v}=const.} \langle \int_{V_f} d\mathbf{x} |D| \rangle = \langle \lim_{N \to \infty} \sum_{q=1}^{q=N} D_f \Delta A_q \left[- \int_0^t dt' \left\langle K_{tot} \frac{ds_d}{ds_L} \frac{ds_L}{ds_T} \right\rangle_s \right] \rangle \tag{13}$$

Finally, we show that (13) leads to an appoximate necessary condition for the absence of humming, namely the inequality (14.6). To start with, we compute the perturbation of $\langle \int_{V_f} d\mathbf{x} |D| \rangle$ in a combustor affected by humming with period τ due to a tiny increase $\delta s_T > 0$ of s_T. Such small perturbations leave τ unaffected and -if small enough- cannot suppress humming. For the sake of simplicity, we choose a δs_T localised at a given point (x_{1q}, x_{2q}) on the flame surface. According to (13), D_f gets multiplied by a factor

$$1 - \left\langle \int_0^t dt' \left\langle K_{tot} \frac{ds_d}{ds_L} \frac{ds_L}{ds_T} \delta s_T \right\rangle_s \right\rangle_f > 0$$

This factor is positive whenever humming occurs, as $D_f > 0$ both before and after the application of $\delta s_T > 0$. Our result holds to first-order, and is therefore valid provided that δs_T is not too large and is not applied for too long time. Finally, we expect to grasp all essential physics in a combustor affected by humming with period τ by taking $\delta s_T \neq 0$ in the time interval $0 \leq t \leq \tau$ only. A longer time interval would lead to exceedingly large values of $\left\langle \int_0^t dt' \left\langle K_{tot} \frac{ds_d}{ds_L} \frac{ds_L}{ds_T} \delta s_T \right\rangle_s \right\rangle_f$; a shorter one would prevent us from taking into account the relevant physics. Accordingly, we write

$$0 < 1 - \left\langle \int_0^t dt' \left\langle K_{tot} \frac{ds_d}{ds_L} \frac{ds_L}{ds_T} \delta s_T \right\rangle_s \right\rangle_f \approx 1 - \tau \left\langle \left\langle K_{tot} \frac{ds_d}{ds_L} \frac{ds_L}{ds_T} \delta s_T \right\rangle_s \right\rangle_f$$

whenever humming occurs. Approximately, therefore, a sufficient condition for the occurrence of humming is $1 - \tau \left\langle \left\langle K_{tot} \frac{ds_d}{ds_L} \frac{ds_L}{ds_T} s_T \right\rangle_s \right\rangle_f > 0$ as $s_T > \delta s_T > 0$, and the violation of this inequality, i.e. (14.6), is a necessary condition for the absence of humming. In (14.6) $\left\langle K_{tot}\frac{ds_d}{ds_L}\frac{ds_L}{ds_T}s_T\right\rangle_s$ does not depend on time, so that no time-averaging occurs.

Auxiliary relationships concerning stable flames

First of all, we write down explicitly the remaining 9 Euler-Lagrange equations. To this purpose, let us introduce an auxiliary vector field $\mathbf{\Theta}(\mathbf{x})$ such that $P_h = \nabla \cdot \mathbf{\Theta}$. Then, the Lagrange multiplier ν in L multiplies the divergence of the vector $\frac{\gamma p \mathbf{v}}{\gamma - 1} + \frac{\rho \mathbf{v} |\mathbf{v}|^2}{2} - \mathbf{\Theta}$. Now, we take advantage of the well-known property of a variational problem like (13.8): no Euler-Lagrange equation changes if we replace L with $L' = L + \nabla \cdot \mathbf{a}$ with $\mathbf{a}$ arbitrary vector. We choose $\mathbf{a} = -\nabla \cdot \left[\nu \left(\frac{\gamma p \mathbf{v}}{\gamma - 1} + \frac{\rho \mathbf{v} |\mathbf{v}|^2}{2} - \mathbf{\Theta}\right)\right]$ so that the new Lagrangian density L' is:

$$
\begin{aligned}
L' \equiv\ & \frac{kY_{air}Y_{fuel}}{T} + \mu \nabla \cdot (\rho \mathbf{v}) + \zeta \left(\mathbf{v} \cdot \nabla Y_{air} + AkY_{air}Y_{fuel}\right) + \\
& + \vartheta \left(\mathbf{v} \cdot \nabla Y_{fuel} + BkY_{air}Y_{fuel}\right) + \xi \cdot \left(\rho \mathbf{v} \cdot \nabla \mathbf{v} + \nabla p\right) + \\
& + \left[\mathbf{\Theta} - \frac{\gamma p \mathbf{v}}{\gamma - 1} - \frac{\rho \mathbf{v} |\mathbf{v}|^2}{2}\right] \cdot \nabla \nu + \lambda \left(kY_{air}Y_{fuel} - P^*\right)
\end{aligned}
$$

With this form of the Lagrangian density, the Euler-Lagrange equation for ν is still eqaution (13.6), while all other 15 Euler-Lagrange equations contain ν just in additive terms $\propto \nabla \nu$. It is enough to set

$$\nu = \nu_0 \tag{14}$$

with $\nu_0 =$ const. and all these terms vanish, so that ν appears elsewhere no more. Other Euler-Lagrange equations are:

$$\frac{kY_{air}}{T} + \zeta AkY_{air} + \vartheta BkY_{air} + \lambda kY_{air} - \nabla \cdot (\vartheta \mathbf{v}) = 0 \tag{15}$$

$$\frac{kY_{fuel}}{T} + \zeta AkY_{fuel} + \vartheta BkY_{fuel} + \lambda kY_{fuel} - \nabla \cdot (\zeta \mathbf{v}) = 0 \tag{16}$$

$$\nabla \cdot \xi = 0 \tag{17}$$

$$\xi \cdot (\mathbf{v} \cdot \nabla) \mathbf{v} - \mathbf{v} \cdot \nabla \mu = 0 \tag{18}$$

$$Y_{air} Y_{fuel} \left[-\frac{k}{T^2} + \frac{dk}{dT} \left(\frac{1}{T} + \zeta A + \vartheta B + \lambda \right) \right] = 0 \tag{19}$$

$$\zeta \nabla Y_{air} + \vartheta \nabla Y_{fuel} + \rho \left[\xi \wedge \nabla \wedge \mathbf{v} + \xi (\nabla \cdot \mathbf{v}) - \nabla \wedge (\xi \wedge \mathbf{v}) - \nabla \mu \right] = 0 \tag{20}$$

Together, equations (14), (15), (16), (17), (18), (19) and (20) are the looked-for 9 remaining equations. Equation (14) is decoupled from the other equations, and will therefore invoked no more in the following [3]. Equation (19) is solved by $\lambda = \Lambda^{-1} - T^{-1} - \zeta A - \vartheta B$ where $\Lambda \equiv -d (\ln k) / d (1/T)$. Physically, the flow is incompressible ($M \ll 1$) everywhere *outside* the flame; combustion heating induces expansion on the flame. Mathematically, we write $\zeta = \zeta_0$ where ζ_0 is uniform across the system so that (16) reduces to:

$$\nabla \cdot \mathbf{v} = \frac{P^*}{\zeta_0 \Lambda Y_{air}} \quad (\neq 0 \quad \text{at the flame only}) \tag{21}$$

Now, let us look for the solution of (17) in the form

$$\xi = \beta_c \mathbf{v} - \nabla \phi \tag{22}$$

(β_c constant scalar quantity, ϕ scalar field). Physically, $\nabla \phi$ and ξ are $\propto$ the irrotational and the rotational part of $\mathbf{v}$ respectively. Together, equation (21) and the condition of

[3] Further investigation requires utilisation of the following identities $\boldsymbol{a} \wedge (\nabla \wedge \boldsymbol{b}) = (\nabla \boldsymbol{b}) \cdot \boldsymbol{a} - \boldsymbol{a} (\nabla \cdot \boldsymbol{b})$, $\nabla (\boldsymbol{a} \cdot \boldsymbol{b}) = \boldsymbol{a} \wedge (\nabla \wedge \boldsymbol{b}) + \boldsymbol{b} \wedge (\nabla \wedge \boldsymbol{a}) + (\boldsymbol{a} \cdot \nabla) \boldsymbol{b} + (\boldsymbol{b} \cdot \nabla) \boldsymbol{a}$, $\nabla \wedge (\boldsymbol{a} \wedge \boldsymbol{b}) = \boldsymbol{a} (\nabla \cdot \boldsymbol{b}) - \boldsymbol{b} (\nabla \cdot \boldsymbol{a}) + (\boldsymbol{b} \cdot \nabla) \boldsymbol{a} - (\boldsymbol{a} \cdot \nabla) \boldsymbol{b}$ and $\nabla \wedge \nabla a = 0$ for arbitrary vectors $\boldsymbol{a}$ and $\boldsymbol{b}$ and scalar a.

negligible $\nabla_{\|}a$ for the generic quantity a make ϕ to satisfy Poisson's equation of the electrostatic potential created by an electric conductor charged with uniform charged density $\propto \zeta_0^{-1}\Lambda^{-1}Y_{air}^{-1}P^*$. Equations (13.5), (18), (20), (22) and the smallness of pressure gradients in the subsonic limit [4] correspond therefore to:

$$\nabla\phi = \text{const. } \mathbf{n} \text{ (at the flame surface)} \tag{23}$$

$$\mu = \frac{\beta_c \left|\mathbf{v}\right|^2}{2} \tag{24}$$

$$2\left(\mathbf{v}\cdot\nabla\right)\left(\nabla\phi\right) = +\nabla\left(\mathbf{v}\cdot\nabla\phi\right) - \rho^{-1}\zeta_0\nabla Y_{air} - \rho^{-1}\vartheta\nabla Y_{fuel} \tag{25}$$

Now, equations (13.2), (13.3), (13.4), (13.9) and (15) ensure that $\nabla\rho \parallel \nabla Y_{air} \parallel \nabla Y_{fuel} \parallel \nabla\vartheta \parallel \mathbf{n}$. It follows that the R.H.S. of (25) is curl-free. Moreover, both T_u and $\alpha = \alpha\left(T_u\right)$ are uniform behind the flame for negligible $\nabla_{\|}a$. (Now, equation (15) is decoupled from other equations, and will therefore invoked no more in the following). Then, it follows from (23) and (25) that

$$\nabla \wedge \left[\left(\mathbf{v}\cdot\nabla\right)\nabla\phi\right] = 0 \tag{26}$$

The identity $\int d\mathbf{x}\nabla\wedge\boldsymbol{b} = \int d\mathbf{a}\wedge\boldsymbol{b}$ holds for arbitrary $\boldsymbol{b}$, where $d\mathbf{a} = \mathbf{n}\ d\mathrm{a}$. Moreover, if we perform a surface integration on the boundary surface of the flame volume, then the result is basically a sum of the contributions of the downstream and the upstream side, because the flame is thin. After volume integration on the flame volume, equation (26) gives therefore equation (13.10). In fact, we take $\boldsymbol{b} = \left(\mathbf{v}\cdot\nabla\right)\nabla\phi$, invoke equation (23) and obtain:

$$\begin{aligned}
0 &= \int d\mathrm{a}\ \mathbf{n}\wedge\left(\mathbf{v}\cdot\nabla\right)\mathbf{n} = \int_d d\mathrm{a}\ \mathbf{n}\wedge\left(\mathbf{v}_d\cdot\nabla\right)\mathbf{n} + \int_u d\mathrm{a}\ \mathbf{n}\wedge\left(\mathbf{v}_u\cdot\nabla\right)\mathbf{n} = \\
&= -\int_u d\mathrm{a}\ \mathbf{n}\wedge\left(\mathbf{v}_\perp|_u^d\cdot\nabla\right)\mathbf{n} = -\alpha\int_u d\mathrm{a}\left(\mathbf{v}_u\cdot\mathbf{n}\right)\mathbf{n}\wedge\left(\mathbf{n}\cdot\nabla\right)\mathbf{n} = \\
&= \alpha\int_u d\mathrm{a}\left(\mathbf{v}_u\cdot\mathbf{n}\right)\mathbf{n}\wedge\left(\mathbf{n}\wedge\nabla\wedge\mathbf{n}\right) = -\alpha\int_u d\mathrm{a}\left(\mathbf{v}_u\cdot\mathbf{n}\right)\left(\nabla\wedge\mathbf{n}\right)_{\|}
\end{aligned} \tag{27}$$

In the proof of the last chain of relationships we have done three things:

- we have denoted by $\int_u d\mathrm{a}$ and $\int_d d\mathrm{a}$ the surface integration on the upstream side and the downstream side of the flame respectively -see Fig. 1;
- we have invoked both the identity $\mathbf{n} \cdot \mathbf{n} = 1$ and the fact that $\nabla_{\parallel}\alpha$ is negligible;
- we have taken advantage of the fact that

$$\left[\int_d d\mathrm{a} + \int_u d\mathrm{a}\right] \; \mathbf{n} \wedge (\mathbf{v}_d \cdot \nabla)\, \mathbf{n} = 0$$

because the integrand is a pseudo-vector [4]; thus, for a thin flame the contribution of any surface element $d\mathrm{a}$ to the integral on the downstream side of the flame has equal absolute value and opposite sign of the corresponding contribution to the integral on the upstream side because they can be obtained from each other through reflection across a median surface between the two sides, and pseudo-vectors change sign under such reflection.

[4]We recall that $\mathbf{n} \cdot \mathbf{v}_u$ and $\mathbf{n} \cdot \mathbf{v}_d$ have opposite sign, even if both $\mathbf{v}_u$ and $\mathbf{v}_d$ are directed downstream. Accordingly, the direction of $\mathbf{n}$ is overturned when going from the downstream side to the upstream side. However, $\mathbf{n}$ appears *twice*, so that this overturning has no effect. It is the $\wedge$ which makes the integrand to be a pseudo-vector, even if $\mathbf{v}_d$ is a true vector.

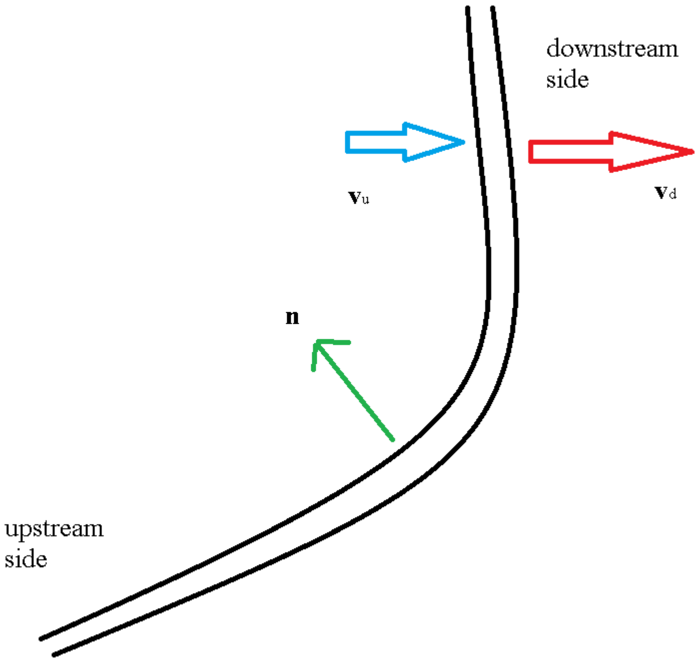

Figure 1: *Nomenclature of quantities relative to a thin flame. See text for details. The unit vector* $\boldsymbol{n}$ *is displayed on one side only.*

Auxiliary relationships concerning axisymmetric flames

Here we refer to Fig. 13.8. First of all, we write down a simplified version of equation (13.19) for the upstream flow which supports our flame with non-negligible curvature. Basically, the idea is that highly elongated flames are supported by highly elongated upstream flows. This idea is suggested by equation (13.21), which ensures that the angle between the upstream velocity and the normal to the flame is $\approx$ constant for negligible $\nabla_{\parallel} s_L$.

We start with the non-linear term $\frac{1}{2}\frac{d\left(F^2\right)}{d\psi}$. Since our flame is elongated along the axis of symmetry of the combustor, we make a small error if we write $A_\psi = rz$ with area differential $d^2\mathrm{x} = rdz$. As for the azimuthal flow, this implies $\varphi = \int Fdz$, or, equivalently, $F = \frac{d\varphi}{dz}$.

It follows from the definition of h that $F = \frac{\varphi}{h}$; then, the non-linear term in (13.19) becomes $\frac{1}{2}\frac{d\left(F^2\right)}{d\psi} = F\frac{dF}{d\psi} = \frac{\varphi}{h^2}\frac{d\varphi}{d\psi} = \frac{2\pi\varphi q}{h^2} = \frac{4\pi^2\kappa q\left(\psi-\psi_0\right)}{h^2} = \left(\frac{S_w}{h}\right)^2\left(2\pi\right)\left(\psi-\psi_0\right)$ where $\varphi = 2\pi\int_{\psi_0}^{\psi} qd\psi = 2\pi\kappa\left(\psi-\psi_0\right)$ and we have done the following things:

- we have defined the dimensionless quantities $S_w \equiv \sqrt{2\pi\kappa q\left(\psi_0\right)}$, $\kappa = \kappa\left(\psi\right) \equiv \frac{1}{\psi-\psi_0}\int_{\psi_0}^{\psi} qd\psi \approx \kappa\left(\psi_b\right)$;
- we have invoked the definition of $q\left(\psi\right)$
- and we have assumed $q\left(\psi\right) \approx q\left(\psi_b\right)$, i.e. $q \approx$ const. The latter approximation is justified in the text.

Note that S_w increases with increasing swirl number S_N because of its dependence on q.

Now, equation (13.14) ensures that $\mathbf{v}$ depends explicitly only on the components of the gradient of ψ. We can therefore take $\psi_b = 0$ with no loss of generality. Remarkably, regardless of the actual value ψ_b of ψ at the boundary (which includes the symmetry axis of the combustor at $r = 0$) the inequality $\psi_0 > \psi$ corresponds to a increasing ψ with increasing r from $r = 0$ up to the location of $\psi = \psi_0$. In this case $v_z = +\frac{1}{r}\frac{\partial\psi}{\partial r} > 0$ in this region, i.e the upstream flow is actually impinging from behind on the flame near the symmetry axis of the combustor, which makes sense; we take therefore $\psi_0 > 0$ for $\psi = 0$. Finally, since the region near the boundary occupies the largest part of the upstream region of the combustor, we make a small error if we approximate

$$\frac{1}{2}\frac{d\left(F^2\right)}{d\psi} \approx -\left(\frac{S_w}{h}\right)^2 (2\pi\psi_0)$$

As for the other terms in equation (13.19), we recall that

$$v_r = -\frac{1}{r}\frac{\partial\psi}{\partial z}$$

and

$$v_z = +\frac{1}{r}\frac{\partial\psi}{\partial r}$$

It follows that

$$\frac{\partial^2\psi}{\partial r^2} = \frac{\partial}{\partial r}\frac{\partial\psi}{\partial r} = \frac{\partial}{\partial r}(rv_z) = v_z + r\frac{\partial v_z}{\partial r}$$

As for the upstream flow, we make a small error if we write $r\frac{\partial v_z}{\partial r} \approx v_z$, so that

$$\frac{\partial^2\psi}{\partial r^2} \approx 2v_z$$

Moreover, we have

$$\frac{\partial^2\psi}{\partial z^2} = \frac{\partial}{\partial z}(-rv_r) = -r\frac{\partial v_r}{\partial z}$$

and

$$-\frac{1}{r}\frac{\partial\psi}{\partial r} = -v_z$$

The above relationships allow us to rewrite equation (13.19) as follows:

$$v_z - r\frac{\partial v_r}{\partial z} = \left(\frac{S_w}{h}\right)^2 (2\pi\psi_0) \tag{28}$$

Further simplification is possible. In fact, we may write $\beta \approx \frac{\pi}{2} - \eta$, $f' = \tan\eta$ and $\frac{1}{\tan\beta} \approx f' = \frac{dz}{dr}$ as $G =$ const. at the flame, and $\frac{dz}{dr} \approx \frac{z}{r}$ as the flame is elongated [5], so that $\tan\beta \approx \frac{r}{z}$. But the upstream flow has an axial length $\approx h$, hence $\frac{v_z}{v_r} \approx \frac{h}{r}$, or, equivalently:

$$v_r \approx \frac{z}{h} v_z \tan\beta \tag{29}$$

In turn, this leads to: $\frac{\partial v_r}{\partial z} \approx \frac{v_z}{h}\tan\beta$ as we may safely neglect $\frac{\partial v_z}{\partial z}$ in an elongated upstream flow where $v_z \approx$ uniform. Substitution in (28) gives:

$$\left(1 - \frac{r}{h}\tan\beta\right) v_z = \left(\frac{S_w}{h}\right)^2 (2\pi\psi_0) \tag{30}$$

Similar arguments lead to a simplified version of equation (13.22) for elongated flames. Again, we have $\frac{\partial\psi}{\partial r} = r v_z$ and $\frac{\partial\psi}{\partial z} = -r v_r$ with $v_r \approx \frac{z}{h} v_z \tan\beta$, $z = f$ at the flame with $G = 0$ and $f' = \frac{1}{\tan\beta}$, hence $f'\frac{\partial\psi}{\partial z} = -r\frac{f v_z}{h}$ and equation (13.22) reduces to:

$$v_z\left(1 - \frac{f}{h}\right) = s_L\sqrt{1 + \frac{1}{(\tan\beta)^2}} \tag{31}$$

[5] Admittedly, this relationship requires $f(r = 0) = 0$; however, this requirement is going to leave our final result unaffected, as the latter does not depend on r. Basically, our discussion applies to flames whose length in the axial direction is much longer than their typical radial distance from the symmetry axis of the combustor. This fits well our starting assumption of elongated flames. Note that axisymmetry allows us to assume $f' > 0$ here, hence $\tan\beta > 0$.

Together, equations (30) and (31) give:

$$\Gamma\left(\tan\beta\right)\frac{\left(1-\dfrac{f}{h}\right)}{1-\dfrac{r}{h}\tan\beta}=\sqrt{1+\left(\tan\beta\right)^2} \tag{32}$$

But $v_r \approx \dfrac{z}{h} v_z \tan\beta$ and $\dfrac{v_z}{v_r} \approx \dfrac{h}{r}$, hence $\dfrac{r}{h}\tan\beta \approx \dfrac{z}{h}\tan^2\beta$ is of order $\approx O\left(\tan^2\beta\right) << 1$ as $|\tan\beta| << 1$. In the same limit we write also $\sqrt{1+\left(\tan\beta\right)^2} \approx 1+\dfrac{\left(\tan\beta\right)^2}{2}$.

Moreover, $z = f$ as $G = 0$ at the flame, so that $\dfrac{f}{h} = \dfrac{z}{h}$ at the numerator of the L.H.S. of equation (32). We justify below the scaling $\dfrac{z}{h} = \tan\beta$. Thus, (32) reduces to:

$$\Gamma\left(\tan\beta\right)\left(1-\tan\beta\right)=1+\frac{\left(\tan\beta\right)^2}{2}$$

which leads to equation (13.26).

As for the justification of the scaling $\dfrac{z}{h} = \tan\beta$, equation (13.21) with $\mathbf{n} = (\sin\eta, -\cos\eta) \approx (\cos\beta, -\sin\beta)$ and the scaling (29) make this scaling $\dfrac{z}{h} = \tan\beta$ to be equivalent to

$$s_L \approx v_z\sin\beta - v_r\cos\beta = v_z\left(\tan\beta\right)\frac{1-h^{-1}\cdot z\cdot\tan\beta}{\sqrt{1+\left(\tan\beta\right)^2}} = v_z\left(\tan\beta\right)+O\left(\tan^2\beta\right)$$

This agrees with the idea of an elongated upstream flow. Indeed, the relationships $\dfrac{r}{h}\tan\beta \approx \dfrac{z}{h}\left(\tan\beta\right)^2$ and $\dfrac{v_z}{v_r} \approx \dfrac{h}{r}$ make the scaling $\dfrac{z}{h} = \tan\beta$ to be equivalent to

$$\frac{v_r}{v_z} \approx \tan^2\beta \tag{33}$$

i.e., the upstream flow is more elongated than the flame (whose inclination with respect to the axis of symmetry of the combustor is $\dfrac{r}{z} \approx \dfrac{1}{f'} \approx \tan\beta$). This fits physical intuition as, no matter how large its elongation, the upstream flow actually impinges upon the upstream side of the flame according to equation (13.21).

Some useful results of variational calculus

Generally speaking [127], the search for an unconstrained extremum (minimum or maximum) of the quantity

$$\int_V d\mathbf{x} L\left(q_i, \frac{\partial q_i}{\partial x_j}, \frac{\partial^2 q_i}{\partial x_j^2}, \cdots\right)$$

where the *Lagrangian density* L depends on the $i = 1, \cdots D$ *Lagrangian coordinates* $q_i(x_j)$ and where the Lagrangian coordinates depend on the $j = 1, 2, 3$ components of $\mathbf{x}$ and satisfy a given set of boundary conditions on the boundary of a given domain V requires that the Lagrangian coordinates solve the system of D *Euler-Lagrange equations*

$$\frac{\partial L}{\partial q_i} - \sum_{j=1}^{3} \frac{\partial}{\partial x_j} \frac{\partial L}{\partial\left(\frac{\partial q_i}{\partial x_j}\right)} + \sum_{j=1}^{3} \frac{\partial^2}{\partial x_j^2} \frac{\partial L}{\partial\left(\frac{\partial^2 q_i}{\partial x_j^2}\right)} - \cdots = 0$$

Remarkably, addition of the divergence of a vector field to the Lagrangian leaves the Euler-Lagrange equations unaffected. In the particular case of a 1D problem ($j = 1$) this means that two Lagrangians which differ by a total derivative lead to the same Euler-Lagrange equations, i.e. describe the same physics.

The search described above is an example of *variational principle*, and the related branch of mathematics is referred to as *variational calculus*. Usually, the variational principle discussed above is denoted with the notation $\delta \int_V d\mathbf{x} L = 0$.

If, furthermore, the extremum is constrained by a number $r = 1, \cdots B$ of constraints $R_r\left(q_i, \frac{\partial q_i}{\partial x_j}, \cdots\right) = 0$ then the necessary condition for the existence of an extremum is the same of the uncontrained case, provided that we replace L with $L + \sum_{r=1}^{B} \Upsilon_r(\mathbf{x}) R_r$ where we have introduced B additional degrees of freedom $\Upsilon_r(\mathbf{x})$, the so-called *Lagrange multipliers*. Now, the resulting system of Euler-Lagrange equations is made of $D + B$

equations and has to be solved in both the $q_i(\mathbf{x})$'s and the $\Upsilon_r(\mathbf{x})$'s.

In most problems, it is tacitly assumed that the variational principle refers to a minimum. It is usually overlooked that the Euler-Lagrange equations are just the necessary condition for an extremum.

In the particular case $L = L(r, q, q')$ -where the prime denotes derivation on r and the latter quantity is defined in a range $r_A \le r \le r_B$- a *sufficient* condition for

$$\int_{r_A}^{r_B} dr L = \min$$

is that two conditions are simultaneously satisfied (see pages 366, 367 and 371 of [127]):

- $\dfrac{\partial^2 L}{\partial q'^2} > 0$ everywhere in the range $r_A \le r \le r_B$ (*Legendre's condition*);
- A solution $u = u(r)$ of the equation

$$\left[\frac{\partial^2 L}{\partial q^2} - \left(\frac{\partial^2 L}{\partial q \partial q'}\right)'\right] u - \left(u' \frac{\partial^2 L}{\partial q'^2}\right)' = 0$$

  exists and vanishes nowhere in the range $r_A \le r \le r_B$ (*Jacobi's condition*);

In particular, if $\dfrac{\partial L}{\partial q} = 0$ and Legendre's condition is satisfied then Jacobi's condition is satisifed too as the general expression for u is

$$u = c_A \int^r \frac{dr}{\dfrac{\partial^2 L}{\partial q'^2}} + c_B$$

with integration constant quantities c_A and c_B; we may always ensure $u > 0$ everywhere $r_A \le r \le r_B$ with the help of a suitable choice of c_A and c_B.

Finally, if the operator $<$ replaces $>$ in Legendre' condition then we have the sufficient condition for $\int_{r_A}^{r_B} dr L = \max$

Auxiliary relationships concerning flames with negligible curvature

First of all, let us start with the proof of (13.49). Relationships (13.15), (13.17) and (13.21) lead to:

$$\int_{r_A}^{r_B} dr \left[\frac{1}{2} \left(|f'|^2 \right)' \frac{r}{\left(1 + (f')^2\right)^{3/2}} + \frac{4\pi^2 \theta}{s_L} r \sqrt{1 + f'^2} \right] = \max. \tag{34}$$

where we have taken into account that $da = 2\pi r dl$, $dl = \sqrt{1 + f'^2} dr$, $f' f'' = \frac{1}{2} \left(|f'|^2 \right)'$ and $(\nabla \wedge \mathbf{n})_{\|} = -(0, K f', 0)$. The quantity $\frac{4\pi^2 \theta}{s_L}$ acts as Lagrange multiplier, and is uniform all along the flame. We may rewrite each term in (34) as follows:

$$\frac{1}{2} \left(|f'|^2 \right)' \frac{r}{\left(1 + (f')^2\right)^{3/2}} = \frac{1}{\sqrt{1 + \varpi}} \frac{r}{2} \frac{y'}{(1 + y)^{3/2}}$$

$$\frac{4\pi^2 \theta}{s_L} r \sqrt{1 + f'^2} = \frac{1}{\sqrt{1 + \varpi}} \iota r \sqrt{1 + y}$$

where the definition of F makes the quantity $y = y(r) \equiv \frac{(|f'|^2) - \varpi}{1 + \varpi}$ to satisfy the identity $(F')^2 = y$. Accordingly, after multiplication of both sides by the positive quantity $\sqrt{1 + \varpi}$ equation (34) gives:

$$\int_{r_A}^{r_B} dr \left[\frac{r \left(|F'|^2 \right)'}{2 \left(1 + |F'|^2\right)^{3/2}} + r \iota \sqrt{1 + |F'|^2} \right] = \max. \tag{35}$$

Further simplification is possibile. In fact, $|K| \approx 0$ implies $|F'| << 1$, and Taylor expansion in powers of $|F'|$ in (35) leads to:

$$\int_{r_A}^{r_B} l_R dr = \text{max.} \quad ; \quad l_R \equiv \frac{r\left(|F'|^2\right)'}{2}\left(1 - \frac{3}{2}|F'|^2\right) + r\iota\left(1 + \frac{1}{2}|F'|^2\right) \tag{36}$$

Finally, straightforward algebra shows that

$$l_R = -\frac{L_R}{2} + \left[\frac{r|F'|^2}{2} + \frac{r^2\iota}{2} - \frac{3r|F'|^4}{8}\right]'$$

so that (36) reduces to (13.49) as the total derivative provides no contribution to the variational problem.

As for the proof of equation (13.50), we observe that the derivatives of F do not vanish identically for flames with negligible curvature. Then, the Euler-Lagrange equation of the variational principle (13.49) leads to the following relationship

$$F'' = \frac{F'\iota}{1 - r\iota - \frac{9}{2}\left(F'\right)^2} \tag{37}$$

Equation (37) allows to us possible extrema of $\int_{r_A}^{r_B} drL_R$; *stable* flames correspond to minima of this quantity. We invoke both Legendre and Jacobi's sufficient conditions for a minimum from our Appendix on variational calculus. Since $\frac{\partial L_R}{\partial F} = 0$, both conditions are automatically satisfied and $\int_{r_A}^{r_B} drL_R$ is actually a minimum provided that $\frac{\partial^2 L_R}{\partial F'^2} > 0$ everywhere, i.e. $1 - r\iota > \frac{9\left(F'\right)^2}{2}$ everywhere. In the $\left(F'\right)^2 << 1$ limit which holds for flames with negligible curvature we obtain

$$|r\iota| << 1 \quad \text{everywhere} \tag{38}$$

as a sufficient condition for the solution of (37) to describe a stable flame with negligible curvature. Not surprisingly, (38) is satisfied whenever s_L is not too small. Both (38) and the $\left(F'\right)^2 << 1$ scaling allow Taylor expansion of the R.H.S. of (37) in powers of $r\iota + \frac{9}{2}\left(F'\right)^2$. Neglecting higher-order terms, we obtain:

$$\frac{F''}{\iota} - F' - \frac{9}{2}\left(F'\right)^2 - \frac{81}{4}\left(F'\right)^5 = 0 \tag{39}$$

It is possible to rewrite (39) in a more convenient form taking advantage from the fact that -up to now- we have not yet chosen any particular value for the additional constant $F(r_A)$ in the definition of F. Now, we limit ourselves to take a large, positive value for $F(r_A)$, so that $F > 0$ everywhere and we are allowed to introduce the logarithm $g \equiv \ln F$. After lengthy algebraic manipulation, and neglecting terms $\approx O\left(F^{iii}, F^{iv}\right)$, equation (39) reduces to:

$$\left[g'' + (g')^2\right]\left[1 - \frac{81}{2}F(g')^3\iota\right] - \varsigma\left[1 + \frac{9}{2}F^2(g')^2\right] + \upsilon g^{iv} - \frac{81}{8}F'F^3\iota\left[g'' + (g')^2\right]^2 = 0 \quad (40)$$

where we have introduced the quantities $\upsilon \equiv \dfrac{27}{8}\varsigma F^4$ and $\varsigma \equiv \dfrac{\iota F'}{F}$. For large enough values of $F(r_A)$ we can both raise $|F|$ and lower $|F'|$, and we may therefore safely neglect both ς' and υ'. Since F is large, terms $\approx O\left(F^2\right)$ are much smaller than terms $\approx O\left(F^4\right)$. Finally, F has the dimension of a length; then, the scaling (38) makes it reasonable to take also $|\iota F| << 1$ Thus, equation (40) leads to (13.50).

RF-flame electromagnetic coupling

Here we discuss the electromagnetic interaction of a RF wave with a flame. For simplicity, we limit ourselves to a slab geometry, and assume the RF wave to impinge normally onto a flat, laminar flame.

Let a RF wave at frequency $\nu_{RF} \approx$ GHz propagate in the $\mathbf{x}$ direction perpendicular to the flame front and impinge on the flame with electric field $E_{RF}\exp(i\mathbf{k}_{RF}\cdot\mathbf{x} - i\omega_{RF}t)$, where $\omega_{RF} \equiv 2\pi\nu_{RF}$, $\mathbf{k}_{RF} = k_{RF}\mathbf{x}$ and $k_{RF} = \Re\{k_{RF}\} + i\Im\{k_{RF}\}$. Its power density is

$$P_i = \frac{\epsilon_0\omega_{RF}E_{RF}^2}{4} \tag{41}$$

i.e. P_i scales as the square of the maximum electric field. Noteworthy, the assumption of perpendicular incidence in slab geometry is due to mathematical simplicity only. The price to be paid is that we drop all details related to RF optics. Remarkably, optimisation of the latter may raise P_i considerably, given the RF power at the antenna. Correspondingly, we expective our discussion to be quite a conservative one.

We make use of the fact that the flame is a weakly ionized plasma [143] with free electron density n_e « the density n_n of neutral particles (atoms and molecules; $n_n \approx \dfrac{\rho N_{Av}}{m_{air}}$ for lean combustion, where $N_{Av} = 6.023\cdot10^{23}$ is the Avogadro number and $m_{air} = 28\cdot10^{-3}$ Kg plays the role of air molar mass). RF waves crossing the flame are weakly absorbed. Electrons are the lightest free charged particles in the flame. As such, they are well accelerated by RF fields and absorb RF energy. The absorption rate depends on both n_e and the electrical conductivity $\sigma = \dfrac{n_e e^2}{m_e\nu}$ through the electron plasma frequency $\omega_p \equiv e\sqrt{\dfrac{n_e}{\epsilon_0 m_e}}$ and the electron collision frequency $\nu = n_n\sigma_{coll}v_{ave}$, where $m_e = 9.11\cdot10^{-31}Kg$, $e = 1.6\cdot10^{-19}C$, $\epsilon_0 = 8.85\cdot10^{-12}F\cdot m^{-1}$, σ_{coll} and v_{ave} are the electron mass, the elementary electric charge, the electric permittivity of vacuum, the total electron-neutral cross section and the averaged electron velocity respectively. No electric breakdown occurs -i.e., the weak field approximation is correct- provided that E_{RF} does not exceed a threshold value E_{thr}, where $\dfrac{E_{thr}}{n_n} \approx 1.1\cdot10^{-19}V\cdot m^2$ [148]. We anticipate here the following inequalities:

$$\nu > \sqrt{\frac{eE_{RF}k_{RF}}{m_e}} \tag{42}$$

$$\nu > \omega_{RF} \quad , \quad \omega_p \tag{43}$$

Self-consistency of (42) and (43) is discussed below. Inequality (42) implies that the wave-plasma interaction is linear. Then, according to the result of Chapter 2 of Ref. [160] the dispersion relation for electromagnetic waves reads:

$$\left(\frac{k_{RF}c}{\omega_{RF}}\right)^2 = 1 - \frac{\omega_p^2}{\omega_{RF}\left(\omega_{RF} + i\nu\right)} \tag{44}$$

Here $c = 3 \cdot 10^8 \frac{m}{s}$ is the speed of light in vacuum. Linearity implies also that propagation leaves ω_{RF} unaffected. Relationships (43) and (44) imply:

$$\Re\{k_{RF}\} \approx \frac{\omega_{RF}}{c} \tag{45}$$

$$\Im\{k_{RF}\} \approx \frac{\sigma}{2\epsilon_0 c} \tag{46}$$

According to (45), $\Re\{k_{RF}\}$ has the same value in the flame and in the vacuum, i.e. the flame leaves the value of $\lambda_{RF} \equiv \frac{2\pi}{\Re\{k_{RF}\}} = \frac{2\pi c}{\omega_{RF}}$ unaffected, and the *phase speed* (i.e., the velocity of propagation of the RF wave front) across the flame of the RF wave across the flame is c with excellent approximation, i.e. it is extremely larger than all other velocities (c_s, $|\mathbf{v}|$ discussed so far. It follows that, as far as RF photons are involved, the flow in the flame and near the flame appears frozen, no matter how complicated its detailed structure.

RF power absorption in the flame induces flame heating: the RF electric field accelerates the electrons, which collide with neutrals and other particles inside the flame. The absorbed RF power density

$$P_a = P_i - P_r - P_t$$

adds therefore to the heat release density P_h, where P_r and P_t are the power density of the reflected and the transmitted RF wave respectively. For normal incidence, equation (86.9) of Ref. [158] gives:

$$P_r = R_f P_i \quad ; \quad R_f = \frac{\left(n_{flame} - 1\right)^2 + \kappa_{flame}^2}{\left(n_{flame} + 1\right)^2 + \kappa_{flame}^2} \quad ;$$

$$n_{flame} = \frac{c\Re\{k_{RF}\}}{\omega_{RF}} \quad ; \quad \kappa_{flame} = \frac{c\Im\{k_{RF}\}}{\omega_{RF}} \quad ;$$

Equation (45) gives $n_{flame} \approx 1$; relationships (43), (46) and the definitions of σ and ω_p give $\kappa_{flame} << 1$, hence $R_f \approx \frac{\kappa_{flame}^2}{4} << 1$. After reflection, a power density $(1 - R_f) P_i$ is available for transmission across the flame. Generally speaking, the electric field of a RF wave transmitted across a layer of thickness d_0 and uniform electric conductivity σ is damped by a factor $\exp(-d_0 \Im\{k_{RF}\})$, hence $P_t = \exp(-2d_0 \Im\{k_{RF}\}) (1 - R_f) P_i$ (the factor 2 is due to the fact that the power is quadratic in the electric field) and:

$$\left[\frac{P_a}{P_i}\right] = \left[1 - \exp\left[-\frac{\sigma d_0}{\epsilon_0 c}\right]\right][1 - R_f] \approx \left[\frac{\sigma d_0}{\epsilon_0 c}\right][1 - R_f] \tag{47}$$

where we have assumed $\frac{\sigma d_0}{\epsilon_0 c} << 1$, i.e. $P_a << P_i$. (Here and in the following, bracketed quantites are dimensionless). Inside a flame, this assumption seems to be reasonable [6].

If we drop the assumption of uniform σ across d_0, then we may generalise equation (47) as follows. The electric field of a RF wave transmitted across a layer of thickness $\Delta x << d_0$ (where Δx is so small that we may safely assume σ to be uniform across it) is damped by a factor $\exp(-\Delta x \cdot \Im\{k_{RF}\})$ where we may still invoke (46). Thus, the electric field gets damped by a factor $\exp\left[-\frac{\overline{\sigma} d_0}{2\epsilon_0 c}\right]$ after crossing a layer of thickness d_0, where $\overline{\sigma} \equiv \frac{1}{d_0}\int_0^{d_0} \sigma \mathrm{dx}$ is the spatial average of σ on d_0 and $0 \leq \mathrm{x} \leq d_0$. As far as we neglect the lack of uniformity of the small reflection coefficient $R_f << 1$, equation (47) is easily generalised to:

$$\left[\frac{P_a}{P_i}\right] = \left[1 - \exp\left[-\frac{\overline{\sigma} d_0}{\epsilon_0 c}\right]\right][1 - R_f] \approx \left[\frac{\overline{\sigma} d_0}{\epsilon_0 c}\right][1 - R_f] \tag{48}$$

[6] For instance, both inequalities $P_a << P_i$ and $R_f << 1$ agree with the fact that fire-fighters *do* make use of radios when fighting fire.

In particular, RF absorption may occur where chemical reactions make free electrons available. We identify therefore the RF absorption zone with the reaction zone inside the flame, so that in a laminar flame we may write:

$$d_0 \approx \frac{\delta_L}{Ze} \tag{49}$$

and we may safely assume that RF leaves Ze unaffected as far as $P_a << P_h$. Equations (48) and (49) give:

$$\left[\frac{P_a}{P_i}\right] = \left[1 - \exp\left[-\frac{\overline{\sigma}\delta_L}{\epsilon_0 c Ze}\right]\right][1 - R_f] \approx \left[\frac{\overline{\sigma} \cdot \delta_L}{\epsilon_0 \cdot c \cdot Ze}\right][1 - R_f] \tag{50}$$

Generalisation of (49) and substitution in (48) in order to describe RF interaction with turbulent flames is possible, provided that we show that turbulence leaves the basic mechanism of RF-flame interaction unaffected. For this proof, we refer to the chapter on the RF power required at the RF antenna, in the text. In the following, we limit ourselves to invoke Damkoehler's discussion of the differences between turbulent and laminar flames, which leads to equation (5.4) of [4].

Damkoehler explains the well-established experimental result $s_T > s_L$ (i.e. $\Xi > 1$) by a simple phenomenological model assuming that each point of the flame surface moves locally at the laminar flame velocity s_L, so that equation (10.1) and its generalisations to turbulent flames still apply and the amount of fuel consumed by combustion per unit time remains proportional to the flame area in both laminar and turbulent flames. In contrast with the laminar case, however, turbulence induces wrinkling of the flame surface, thus raising the flame area by a factor $\Xi > 1$ and the fuel consumption. Accordingly, if we want to keep the flame stationary (in the mean at least) then we have to raise the amount of fuel supplied to the flame per unit time by the same factor Ξ. This is equivalent to say that $s_T = \Xi \cdot s_L > s_L$.

Exactly the same argument applies to RF. In fact, RF absorption occurs where combustion occurs, i.e. in a thin reaction zone inside the flame. Just as for combustion, the larger the flame area, the larger the overall volume occupied by this thin reaction zone (all other things being equal), the larger the fraction $\left[\frac{P_a}{P_i}\right]$ of RF power which gets actually absorbed by the flame. To put it in other words, the larger the turbulent wrinkling, the larger both the flame velocity and the total cross section of photon capture inside the flame, hence $P_a \propto$ flame velocity. Accordingly, turbulence raises $\left[\frac{P_a}{P_i}\right]$ by a factor Ξ, so that we may replace (50) with:

$$\left[\frac{P_a}{P_i}\right] = \left[\frac{\overline{\sigma} \cdot \delta_L \cdot \Xi}{\epsilon_0 \cdot c \cdot Ze}\right] [1 - R_f] \tag{51}$$

Finally, as a rule-of-thumb (50) and (51) lead to the scaling $P_a \propto \sigma\delta_L$ for laminar and turbulent flames respectively, all other things being equal [7]. Since the gases outside the flame carry no electric current, $\sigma = 0$ outside the flame, then $P_a = 0$ too outside the flame. Admittedly, σ and δ_L are an increasing and a decreasing function of T respectively. However, δ_L changes with T much less than σ for all values of T of practical interest -to convince oneself, it is enough to compare equation (8.30) of [2] with the results of the Appendix on the electrical conductivity of the flame. Accordingly, we may safely consider P_a as an increasing function of σ and of T, and the scaling (15.1) follows.

Remarkably, the scaling (15.1) is the same scaling which rules electromagnetic braking: a change of electromagnetic field induces Faraday currents in a conductor, which get dissipated though Ohmic heating -and, as a consequence, the flame gets heated by the external world. Just as in brakes, σ plays a crucial role: no braking occurs in insulators. And -again in analogy with brakes- the low-frequency approximation (43) is of paramount relevance: light waves (whose ω_{RF} violates (43)- cross the flame unabsorbed.

Typical orders of magnitude for our RF are $\nu \approx 40$ GHz, $\omega_{RF} \approx 10^{10}\frac{rad}{s}$, $\omega_p \approx 10^9\frac{rad}{s}$, $E_{thr} \approx 10^7 V \cdot m^{-1}$ and $\lambda_{RF} \approx 0.1$ m. Accordingly, both (42) and (43) are satisfied in the weak field limit. Here we have assumed a flame temperature $\approx 1500K$, so that $v_{ave} = \sqrt{\frac{k_B T}{m_e}} \approx 10^5\frac{m}{s}$. Moreover we have taken $\sigma_{coll} = \pi R_{air}^2$ with R_{air} typical radius for a neutral in air; this is equivalent to neglect all collisions but elastic electron-neutral collisions, which is reasonable because $n_e \ll n_n = \frac{p}{k_B T}$ and $p \approx 20$ atm in a typical combustor, so that $n_n \approx 10^{26} m^{-3}$, $\rho = 4.5 Kg \cdot m^{-3}$ and $E_{thr} \approx 10^7 V \cdot m^{-1}$. Finally, we have taken $R_{air} \approx 10^{-10} m$ as a reasonable value for the order of magnitude of the radius of a neutral. This is a quite conservative choice indeed: larger, more realistic values of R_{air} lead to even larger values of ν.

In turn, according to equation (41) the weak field limit holds if $P_i << 10^{12} W \cdot m^{-3}$ in the GHz range. This allows to provide a qualitative estimate on the maximum value of the RF power at the antenna W_{ant} allowed by the weak field limit, i.e. by the requirement that there is no arc.

To this purpose, we recall that the combustor embedds the flame at all time, and that an optimum combustor-cavity electromagnetic coupling reuires that the linear size L_{ant} of the antenna is $L_{ant} \approx \lambda_{RF}$. It happens that -as for the order-of-magnitude at least- $\lambda_{RF} \approx 0.1m \approx$ the typical linear distance between the flame and the wall in front of it. Thus, a *very* rough approximation allows us to describe the flame-antenna system as a resonant cavity of linear size λ_{RF} and volume $V_{RF} = \lambda_{RF}^3$, where an antenna supplies

[7] We show in the text that RF leaves turbulence-related quantities like Ξ unaffected.

a power W_{ant}. This power must compensate the power losses W_{loss}, i.e. $W_{ant} = W_{loss}$. In turn, W_{loss}, ω_{RF} and the total RF energy in the resonant cavity $U_{RF} = \frac{V_{RF}\epsilon_0 E_{RF}^2}{4}$ are linked by a dimensionless, geometry-dependent quality factor $q_{RF} \equiv \frac{\omega_{RF} U_{RF}}{W_{loss}}$ of the resonant cavity. Together, the above relationships, equation (45), equation (41) and the definitions of ω_{RF} and of λ_{RF} lead to:

$$P_i = \frac{q_{RF}\nu_{RF}^3 W_{ant}}{c^3} \tag{52}$$

Then, the weak field limit requires $W_{ant} < \frac{10^9}{q_{RF}}$ W. Since the combustor is by no means an optimized electromagnetic resonant cavity, q_{RF} achieves no particularly large value (say, $q_{RF} \leq 10^4$) and the weak field limit is satisfied for all values of W_{ant} of practical interest (i.e., not larger than $\approx 10^5$ W). In this case, moreover, RF heating is always much weaker than combustion heating. As for the electric field $\approx \sqrt{\frac{2W_{ant}}{\epsilon_0\omega_{RF}V_{RF}}}$ at the antenna, it is $\approx 3 \cdot 10^4 \frac{V}{m}$ for $W_{ant} = 10^5$ W, $\omega_{RF} = 2 \cdot \pi\nu_{RF}$, $\nu_{RF} = 3$ GHz and $V_{RF} = \lambda_{RF}^3$ with $\lambda_{RF} = \frac{c}{\nu_{RF}} = 10$ cm.

Finally, we may further identify P_h with the combustion power density Q for negligible viscous heating, so that $W_c = \int_{V_f} d\mathbf{x}Q$ and $P_a << P_h$ becomes $P_a << Q$. Then, a consequence of (15.1) is that perturbations T_1 of T correspond to fluctuations P_{a1} of P_a which are always in phase with T_1. If, furthermore, Q_1 too is in phase with T_1, P_{a1} is also in phase with Q_1. Generally speaking, if $P_a << Q$ then the impact of RF on the relative phases of T_1 and fluctuations of other quantities -like e.g. pressure- is negligible.

The electrical conductivity

Credits and generalities We have anticipated that the chemical reactions ruling σ are not well described by LTE. Such reactions are not dealt with by commercially available software packages like e.g. CHEMKIN, and require therefore dedicated kinetic treatment. The present Appendix describes this treatment.

Computations have been performed by Prof. G. Colonna, A. Laricchiuta, L. D. Pietanza and A. D'Angola of Consiglio Nazionale delle Ricerche [8] in the framework of a collaboration with Ansaldo Energia. Here we limit ourselves to discuss some relevant physics. Results are to be found in the following Section.

Since free electrons are by far the lightest electrically charged particles in a flame, they rule its conduction of electric current, and σ depends crucially on them. An applied electric field may induce ionisation, thus making a small number of free electrons available. Such electrons are accelerated by the same field and hit neutrals (atoms and molecules). Collisions make further electrons available, and so on. The electrical conductivity is an increasing function of the density of free electrons and a decresing function of their cross section with neutrals.

The commonly used kinetic models in plasma-assisted combustion consider the amplitude of the applied field high enough so that the electron density is controlled by the electron induced ionization [161]. Due to the short discharge time, the rate coefficients of processes induced by electron impact are calculated at fixed composition, in the so-called cold plasma approximation, and only depend on the reduced electric field [102] [9].

When a short electric pulse with high power density is applied to the gas mixture, the temperature increases initially of few degrees [162] [163] [164]. More important contribution comes from the radicals, such as atoms and ions, that in this kind of discharges are produced in relatively large quantities, initiating the oxidation chain. Another important aspect is the role of excited states, and in particular vibrationally excited molecules [165] [166] [167] and electronically excited states of oxygen [168] [169] [170] [171] [172], whose main effect is to reduce the activation energy.

[8] The full address is CNR-IMIP, via Amendola 122D, Bari, Italy

[9] Here by the wording *reduced electric field* we mean the ratio between the electric field and the particle density of neutrals. Historically, the reduced electric field is measured in Townsend (1 Td = $10^{-21}\dfrac{V}{m^2}$. The reduced electric field is usually referred to as E/N.

Vibrationally and electronically excited states also significantly affect the free electron kinetics. In a cold gas, inelastic collisions dominate and as a consequence, part of the energy supplied by the electric field is transferred to the excitation of heavy particles. Superelastic collisions may transfer energy from excited states to electrons resulting in peculiar structures in the electron energy distribution function (EEDF) [173] [174] [175].

To take into account the mutual interaction between electrons and internal states the self-consistent model [176] [177] [178] should be considered, coupling the kinetics of excited states with a Boltzmann equation for the EEDF [179]. The main difficulty of this approach is the lack of data for elementary processes, i.e. cross sections and rate coefficients, involving the whole spectrum of the internal states.

Different scaling laws have been used to extend available reduced set of electron-impact cross sections to the complete vibrational spectrum [180] [181]. Recently, new cross sections have been calculated to cover the whole vibrational spectrum of different diatomic species[182] [183]. The results obtained with different data sets [184] have been compared showing the relevance of using accurate cross sections in discharge modeling and that the self-consistent approach is necessary also to model nanosecond atmospheric discharges.

It should be pointed out that free electrons are also produced by chemical processes in the flame, making necessary to construct an adequate kinetic scheme when the applied field is not very high. One application of this discharge condition is precisely the control of humming by DC electric discharge [141]. Similar problem can be found in electrical measurements in flames [154].

We are going to present the model for the estimation of the electrical conductivity of the air-methane mixture, from the unburnt gas to complete combustion. The model uses a chemical kinetic code coupled self-consistently with a Boltzmann solver for free electron kinetics [179]. In this way it is possible to calculate σ as the combustion process evolves, relating the relevant quantities to a progress variable χ. Here by the wording *progress variable* we mean the molar fraction of fuel which has been burnt when the fuel-air mixture has reached a position $\mathbf{x}$ inside the flame.

We have applied the model in order to calculate σ as a function of pressure, temperature and applied electric field. The combustion model is based on the database GRI-Mech 3.0 [185], which is one of the most used combustion model for methane/air mixture, completed with electron induced processes and ion kinetics. Input data are taken from Ansaldo, and refer to flames in commercial products. Finally, analytical fits are provided. The latter allow fast computation of σ in Ansaldo flames.

Kinetic model Here we discuss the kinetic model used to calculate the electrical conductivity of an air/methane flame. The model consists in 351 reactions for 53 neutral species, 7 ions and electrons. The kinetic scheme combines methane oxidation mechanisms in the database GRI-Mech 3.0 [185] with a series of chemi-ionization, ion-molecule, and dissociative-recombination reactions.

GRI-Mech 3.0 rates are expressed either as constant or by a single or double Arrhenius

$$K^f(T) = AT^m \exp\left(-E^a/RT\right) \tag{53}$$

The rate coefficients K^b of reverse reactions are related to the forward rate constant through the equilibrium constants K_{eq} by

$$K^b = K^f/K^{eq} \tag{54}$$

The model includes the following ionic species (H_3O^+, HCO^+, O^-, O_2^-, $C_3H_3^+$, CH_3^+, $C_2H_3O^+$) plus free electrons. For chemionization and electron molecule reactions, the kinetic data have been taken from references [186] [187]. The major chemionization reaction is:

$$\mathrm{CH} + \mathrm{O} \rightarrow \mathrm{HCO}^+ + e^- \tag{55}$$

whose rate, as suggested by [188], is raised by 10% respect to the data reported in [186] to yield a better agreement with experimental data at fuel lean condition. Moreover, as suggested by [186], the reaction of electronically excited CH ($CH^*(A^2\Delta)$) with oxygen atoms:

$$\mathrm{CH}^*(A^2\Delta) + \mathrm{O} \rightarrow \mathrm{HCO}^+ + e^- \tag{56}$$

is 2000 times faster than the same reaction with ground-state (eq. 55). As a consequence, reaction (56) may also be an important source ions in the flame and cannot be neglected. Moreover, beside the process (56), a simplified kinetic model for the CH^* has been considered by including also the kinetic processes listed in Tab. 1.
The HCO^+ ion is not the dominant ion in hydrocarbon flames since it is quickly consumed by H_2O to produce H_3O^+ via [186]:

$$\mathrm{HCO}^+ + \mathrm{H_2O} \rightarrow \mathrm{H_3O}^+ + \mathrm{CO} \tag{57}$$

Table 1: Chemistry reactions involving the first excited electronic level of the CH ($CH^*(A^2\Delta)$), the corresponding rate coefficients are in the form $K = AT^B \exp(-E_a/RT)$
.

CH^* reactions	A (cm-mole-s)	B	E_a (cal/mole)
$C_2 + OH \rightleftharpoons CH^* + CO$	$3.39e^{-12}$	0.0	0.0
$C_2H + O \rightleftharpoons CH^* + CO$	$6.2e^{12}$	0.0	0.0
$CH^* \rightarrow CH$	$1.85e^{6}$	0.0	0.0
$CH^* + N_2 \rightleftharpoons CH + N_2$	$3.03e^{2}$	3.4	−381.0
$CH^* + O_2 \rightleftharpoons CH + O_2$	$2.48e^{6}$	2.1	−1720.0
$CH^* + H_2O \rightleftharpoons CH + H_2O$	$5.30e^{2}$	0.0	0.0
$CH^* + H_2 \rightleftharpoons CH + H_2$	$1.47e^{14}$	0.0	1361.0
$CH^* + CO_2 \rightleftharpoons CH + CO_2$	$2.41e^{-1}$	4.3	−1694.0
$CH^* + CO \rightleftharpoons CH + CO$	$2.44e^{12}$	0.5	0.0
$CH^* + CH_4 \rightleftharpoons CH + CH_4$	$1.73e^{13}$	0.0	167.0

The H_3O^+ ion can form other flame ions by a series of ion-molecule reactions or it can undergo dissociative recombination [186]:

$$H_3O^+ + e^- \rightarrow H_2O + H \tag{58}$$

whose rate has been fixed to 1.30 10^{18} cm^3/mole/s, as suggested by [188], to fit experimental electron number density distribution at stoichiometric condition. Another dissociative recombination channel included into the model is [186]:

$$CH_3^+ + e^- \rightarrow CH_2 + H \tag{59}$$

Other processes involving ions are [186]:

$$H_3O^+ + C_2H_2 \rightarrow C_2H_3O^+ + H_2 \tag{60}$$

$$HCO^+ + CH_2 \rightarrow CH_3^+ + CO \tag{61}$$

$$H_3O^+ + CH_2 \rightarrow CH_3^+ + H_2O \tag{62}$$

$$CH_3^+ + C_2H_2 \rightarrow C_3H_3^+ + H_2 \tag{63}$$

$$C_3H_3^+ + H_2O \rightarrow C_2H_3O^+ + CH_2 \tag{64}$$

$$CH_3^+ + CO_2 \rightarrow C_2H_3O^+ + O \tag{65}$$

Finally the following two collision detachment reactions, with the corresponding rate coefficients, are added to take into account of the equilibrium of O_2^- [189]

$$O_2^- + N_2 \rightarrow e^- + O_2 + N_2 \tag{66}$$

$$O_2^- + O_2 \rightarrow e^- + O_2 + O_2 \tag{67}$$

$$\begin{aligned} &K = 6.6\ 10^{10} T^{0.5}\ \exp(-E_a/R_0 T)\ \ \mathrm{cm^3/mole/s} \\ &E_a = 9920.0\ \ \mathrm{cal/mole} \end{aligned} \tag{68}$$

$$\begin{aligned} &K = 9.4\ 10^{12} T^{0.5}\ \exp(-E_a/R_0 T)\ \ \mathrm{cm^3/mole/s} \\ &E_a = 11113.0\ \ \mathrm{cal/mole} \end{aligned} \tag{69}$$

The kinetic processes described in above have been included into the numerical code described in [190] [179] [191] [173]. The code calculates simultaneously and self-consistently global plasma properties such as composition and electrical conductivity, and internal distribution of diatomic species and electron energy distribution function. The code solves the equations describing heavy particle and electron kinetics under the effect of electromagnetic fields [179]. In the present paper we have considered an homogeneous plasma [191] [173]. The kinetic model is also coupled with a steady flow solver in quasi-1D geometries solving Euler equation [192] and applied to the description of shock waves, expansions through nozzle and in general to 1D reactive fluxes.

The heavy particle kinetics consists in solving the master equations considering separately species in each internal state, in such a way it is possible to calculate internal energy distributions. This approach is called *State-to-State* (StS) and require complete sets of rate coefficients and electron impact cross sections. Commonly, StS approach is applied to vibrational and electronic states of diatomic molecules, to account for non-equilibrium vibrational distributions, while rotational levels are usually considered in equilibrium with the gas temperature. The StS kinetics has also been applied to atoms, including the transport of photons to calculate radiative properties [176] [178] [193] [194]. However this approach can hardly be extended to polyatomic molecules being the number of internal levels too large [195]. Alternatively, thermal non-equilibrium can be solved in the *Multi-Temperature* (MT) assuming that each internal degree of freedom is described by a Boltzmann distribution at a given temperature.

To calculate the rate coefficients of electron induced processes, the electron Boltzmann equation is solved. Calculating the electron energy distribution function (EEDF), the

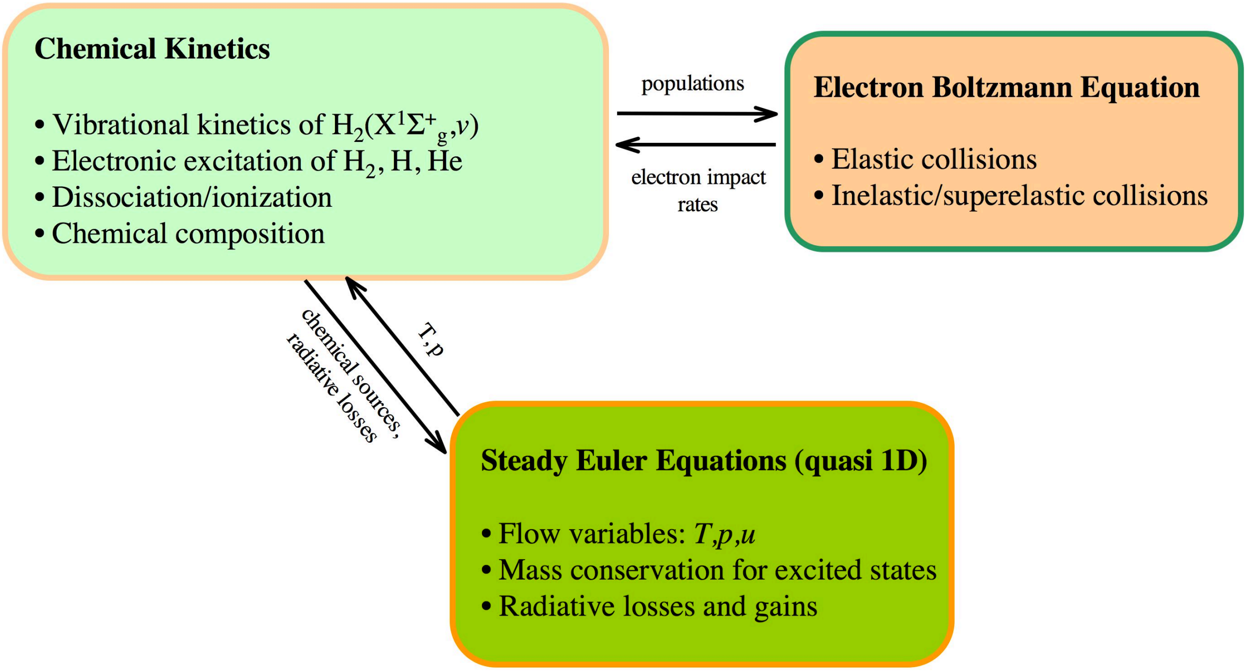

Figure 2: *Kinetic model. Postprocessing of output quantities (free electron population and impact rates) give* σ.

rate coefficients are calculated integrating the relative cross section over the EEDF. This expect is particularly interesting in the presence of excited states, where the superelastic collisions, transferring energy from internal states to electrons, produce long plateaux in the EEDF increasing the rates of endothermic electron induced processes [174] [175] [184] [196] [197]. The Boltzmann equation is solved self-consistently with the master equations for heavy particles, i.e. exchanging information at each time step, because the Boltzmann equation takes as input the gas composition and internal distributions, while the master equations need the rates of electron impact processes. From the EEDF it is possible to calculate some macroscopic properties of the electron gas [198] such as the diffusion coefficient, electron mobility and electrical conductivity. See Fig. 2.

Electron cross sections

Generalities A large number of processes are promoted in electron-molecule collisions, the elastic collisions always representing the channel characterized by the higher probability. However also inelastic channels, including vibrational and electronic excitations, and high-threshold dissociation and ionization are relevant to the microscopic dynamics.

The rate coefficients for electron-impact induced processes in non-equilibrium plasmas are calculated by integration of corresponding cross sections on the actual electron energy distribution function (EEDF), obtained by the solution of the Boltzmann equation for free electrons, shaped by the collisional dynamics under the action of the external electric field.

The dynamic information for electron-molecule collisions has been retrieved in the literature, combining knowledge obtained by experiments and theoretical approaches, the references for different processes being reported in the following, grouping chemical species by family.

To date, the database is incomplete due to the large number of chemical species in the flame and where unavailable the effective elastic (momentum transfer) cross section, representing the minimal information, has been assumed equal to that for species having similar molecular structure.

It should be stressed that this is usually the case of minority species, giving a small contribution to the flame properties, and weakly affecting the accuracy in the estimation of the electrical conductivity.

CH_4, radicals and short-chain hydrocarbons A wide literature exists on the methane family, also for the relevance in the modeling of fusion devices, and the dynamic information for CH_y and CH_y^+ (with $1 \leq y \leq 4$) has been recently collected in the report [199] and also available through the LXcat database [200].

The CH_4 ionization actually can proceed through different fragmentation paths, sketched as

$$e + \mathrm{CH_4} \rightarrow \begin{cases} 2e + \mathrm{CH_4^+} \\ 2e + \mathrm{CH_3^+} + \mathrm{H} \\ 2e + \mathrm{CH_2^+} + \mathrm{H_2} \\ 2e + \mathrm{CH^+} + \mathrm{H_2} + \mathrm{H} \\ 2e + \mathrm{C^+} + 2\mathrm{H_2} \\ 2e + \mathrm{H_2^+} + \mathrm{CH_2} \\ 2e + \mathrm{H^+} + \mathrm{CH_3} \end{cases} \tag{70}$$

For these processes results in [201] have been considered, where the absolute value for partial cross sections of different channels, determined by time-of-flight experiments, have been reported.

In Ref. [202] electron-methylidyne elastic collisions have been studied theoretically, combining the Schwinger variational iterative method and the distorted-wave approximation, using a complex optical potential.

For the CH ionization, theoretical BEB (Binary-Encounter-Bethe model) cross section of Ref. [203] has been considered. Moreover for the CH species also inelastic excitations to electronic states $(a^4\Sigma, A^2\Sigma, B^2\Sigma, C^2\Sigma)$ have been considered [204].

For short-chain alcanes C_xH_y, with different carbon hybridizations, the information, more fragmentary, has been reviewed in Ref. [205].

For the ethine (C_2H_2) momentum transfer has been theoretically investigated in Ref. [206] adopting a local, non-empirical potential for electron-exchange, while the ionization considering different fragmentation channels has been experimentally investigated with a pulsed electron beam in Ref. [207], obtaining absolute cross sections from threshold to rather high electron-impact energies.

The momentum transfer and non-dissociative ionization cross sections for electron impact on C_2H_4, C_2H_6 and C_3H_8 molecules have been considered in Refs.[208] and [209].

As for the radicals $C_2H_{1||3||5}$ and C_3H_7 the momentum transfer cross sections have been set equal to those for the corresponding parent molecules.

As for the reactions taken into account, see Fig. 3 and Fig. 4.

$$
\begin{array}{ll}
e + \mathrm{CH_4} & \text{momentum transfer} \\
e + \mathrm{CH_4} \rightarrow \begin{cases} 2e + \mathrm{CH_4^+} \\ 2e + \mathrm{CH_3^+} + \mathrm{H} \\ 2e + \mathrm{CH_2^+} + \mathrm{H_2} \\ 2e + \mathrm{CH^+} + \mathrm{H_2} + \mathrm{H} \\ 2e + \mathrm{C^+} + 2\mathrm{H_2} \\ 2e + \mathrm{H_2^+} + \mathrm{CH_2} \\ 2e + \mathrm{H^+} + \mathrm{CH_3} \end{cases} & \text{ionization} \\
e + \mathrm{CH_3} & \text{momentum transfer} \\
e + \mathrm{CH_3} \rightarrow \begin{cases} 2e + \mathrm{CH_3^+} \\ 2e + \mathrm{CH_2^+} + \mathrm{H} \end{cases} & \text{ionization} \\
e + \mathrm{CH_2} & \text{momentum transfer} \\
e + \mathrm{CH_2} \rightarrow \begin{cases} 2e + \mathrm{CH_2^+} \\ 2e + \mathrm{CH^+} + \mathrm{H} \end{cases} & \text{ionization} \\
e + \mathrm{CH} & \text{momentum transfer} \\
e + \mathrm{CH}(X^2\Pi) \rightarrow \begin{cases} e + \mathrm{CH}(a^4\Sigma) \\ e + \mathrm{CH}(A^2\Sigma) \\ e + \mathrm{CH}(B^2\Sigma) \\ e + \mathrm{CH}(C^2\Sigma) \end{cases} & \text{electronic excitation} \\
e + \mathrm{CH} \rightarrow 2e + \mathrm{CH^+} & \text{ionization} \\
e + \mathrm{C} & \text{momentum transfer} \\
e + \mathrm{C} \rightarrow 2e + \mathrm{C^+} & \text{ionization}
\end{array}
$$

Figure 3: *Reactions involving electrons, C, CH_2, CH_3 and CH_4.*

H_2O family In the case of water molecule a quite comprehensive review of data for electron-impact induced processes is available [210], including the momentum transfer, the dissociation following all the different fragmentation channels, the dissociative attachment, leading to the formation of negative ions (OH^- and O^-), and both non-dissociative and dissociative ionizations also considering the further ionizations.

As for the hydroxyl radical, momentum transfer [211] and non-dissociative ionization [212] have been considered. The electron elastic scattering from H_2O_2 and HO_2 has been modeled with the elastic cross section for H_2O.

As for the reactions taken into account, see Fig. 5.

$$
\begin{array}{ll}
e + C_2H_2 & \text{momentum transfer} \\
e + C_2H_2 \rightarrow \left\{ \begin{array}{l} 2e + C_2H_2^+ \\ 2e + C_2H^+ + H \\ 2e + C_2^+ + H_2 \\ 2e + CH^+ + CH \\ 2e + C^+ + CH_2 \\ 2e + H^+ + C_2H \end{array} \right. & \text{ionization} \\
e + C_2H_4 & \text{momentum transfer} \\
e + C_2H_4 \rightarrow 2e + C_2H_4^+ & \text{ionization} \\
 & \\
e + C_2H_6 & \text{momentum transfer} \\
e + C_2H_6 \rightarrow 2e + C_2H_6^+ & \text{ionization} \\
 & \\
e + C_3H_8 & \text{momentum transfer} \\
e + C_3H_8 \rightarrow 2e + C_3H_8^+ & \text{ionization} \\
 & \\
e + C_2H & \\
e + C_2H_3 & \\
e + C_2H_5 & \\
e + C_3H_7 & \text{momentum transfer} \\
e + C_2H_2 & \\
e + C_2H_4 & \\
e + C_2H_6 & \\
e + C_3H_8 &
\end{array}
$$

Figure 4: *Reactions involving electrons and other hydrocarbons.*

NH_3 family The ammonia momentum transfer cross section [200] and the ionization channels, experimentally investigated with a crossed-beam apparatus [213], have been included in the kinetic scheme. The cross sections for different electron-impact induced processes in NH species have been calculated [214]. For NH_2 the missing cross section for the elastic channel has been modeled with that for NH_3, while for the ionization theoretical data in [215] have been considered.

As for the reactions taken into account, see Fig. 6.

$$
\begin{array}{lll}
e + \mathrm{H_2O} & & \text{momentum transfer} \\
e + \mathrm{H_2O} \rightarrow & \left\{ \begin{array}{l} e + \mathrm{OH} + \mathrm{H} \\ e + \mathrm{O}(^1S) + \mathrm{H_2} \end{array} \right. & \text{dissociation} \\
e + \mathrm{H_2O} \rightarrow & \left\{ \begin{array}{l} 2e + \mathrm{H_2O^+} \\ 2e + \mathrm{OH^+} + \mathrm{H} \\ 2e + \mathrm{O^+} + \mathrm{H_2} \\ 3e + \mathrm{O^{2+}} + \mathrm{H_2} \\ 2e + \mathrm{H_2^+} + \mathrm{O} \\ 2e + \mathrm{H^+} + \mathrm{OH} \end{array} \right. & \text{ionization} \\
e + \mathrm{H_2O} \rightarrow & \left\{ \begin{array}{l} \mathrm{OH^-} + \mathrm{H} \\ \mathrm{H^-} + \mathrm{OH} \\ \mathrm{O^-} + \mathrm{H_2} \end{array} \right. & \text{dissociative attachment} \\
e + \mathrm{OH} & & \text{momentum transfer} \\
e + \mathrm{OH} \rightarrow 2e + \mathrm{OH^+} & & \text{ionization} \\
e + \mathrm{H_2O_2} & & \\
e + \mathrm{HO_2} & & \text{momentum transfer} \\
e + \mathrm{H_2O} & &
\end{array}
$$

Figure 5: *Reactions involving electrons and the H_2O family.*

CO_2 & CO For electron-CO_2 processes reference is made to the compilation of recommended cross sections in Ref. [216].

The carbon monoxide elastic electron scattering cross section from the LXcat database [200] has been used, with the relevant dissociation channel, experimentally measured in [217], and with the ionization cross section from [209].

$$
\begin{array}{ll}
e + \mathrm{NH_3} & \text{momentum transfer} \\
e + \mathrm{NH_3} \rightarrow \left\{ \begin{array}{l} 2e + \mathrm{NH_3^+} \\ 2e + \mathrm{NH_2^+} + \mathrm{H} \\ 2e + \mathrm{NH^+} + \mathrm{H_2} \\ 2e + \mathrm{N^+} + \mathrm{H_2} + \mathrm{H} \\ 2e + \mathrm{H_2^+} + \mathrm{NH} \\ 2e + \mathrm{H^+} + \mathrm{NH_2} \\ 3e + \mathrm{NH_3^{2+}} \end{array} \right. & \text{ionization} \\
e + \mathrm{NH} & \text{momentum transfer} \\
e + \mathrm{NH} \rightarrow 2e + \mathrm{NH^+} & \text{ionization} \\
e + \mathrm{NH_2} \rightarrow 2e + \mathrm{NH_2^+} & \text{ionization} \\
\left. \begin{array}{l} e + \mathrm{NH_2} \\ e + \mathrm{N_2H} \\ e + \mathrm{NH_3} \\ e + \mathrm{N_2} \end{array} \right. & \text{momentum transfer}
\end{array}
$$

Figure 6: *Reactions involving electrons and the NH_3 family.*

As for the reactions taken into account, see Fig. 7.

$$
\begin{array}{ll}
e + \mathrm{CO_2} & \text{momentum transfer} \\
e + \mathrm{CO_2} \rightarrow e + \mathrm{CO} + \mathrm{O}(^1S) & \text{dissociation} \\
e + \mathrm{CO_2} \rightarrow \begin{cases} 2e + \mathrm{CO_2^+} \\ 2e + \mathrm{CO^+} + \mathrm{O}(^3P) \\ 2e + \mathrm{O^+} + \mathrm{CO} \\ 2e + \mathrm{C^+} + \mathrm{O_2} \end{cases} & \text{ionization} \\
e + \mathrm{CO} & \text{momentum transfer} \\
e + \mathrm{CO} \rightarrow e + \mathrm{C}(^3P) + \mathrm{O}(^3P) & \text{dissociation} \\
e + \mathrm{CO} \rightarrow 2e + \mathrm{CO^+} & \text{ionization}
\end{array}
$$

Figure 7: *Reactions involving electrons, CO_2 and CO.*

NO_2 & N_2O The NO_2 momentum transfer cross section with inelastic electronic excitations have been calculated in [218]. The dissociative ionization channels have been investigated in [219] within a semi-empirical formulation well-comparing with experiments.

For N_2O the momentum transfer cross section is available in the LXcat database [200] and the experimental partial ionization cross sections of different fragmentation paths, obtained with a fast-neutral-beam technique, are available in [220].

As for the reactions taken into account, see Fig. 8.

$$
\begin{array}{lll}
e + \mathrm{NO_2} & & \text{momentum transfer} \\
e + \mathrm{NO_2} \rightarrow & \left\{ \begin{array}{l} 2e + \mathrm{NO_2^+} \\ 2e + \mathrm{NO^+} + \mathrm{O} \\ 2e + \mathrm{O^+} + \mathrm{NO} \\ 2e + \mathrm{N^+} + \mathrm{O_2} \\ 2e + \mathrm{O_2^+} + \mathrm{N} \end{array} \right. & \text{ionization} \\
e + \mathrm{N_2O} & & \text{momentum transfer} \\
e + \mathrm{N_2O} \rightarrow & \left\{ \begin{array}{l} 2e + \mathrm{N_2O^+} \\ 2e + \mathrm{NO^+} + \mathrm{N} \\ 2e + \mathrm{N^+} + \mathrm{NO} \\ 2e + \mathrm{O^+} + \mathrm{N_2} \\ 2e + \mathrm{N_2^+} + \mathrm{O} \end{array} \right. & \text{ionization}
\end{array}
$$

Figure 8: *Reactions involving electrons, NO_2 and N_2O.*

NCO, HCN, CN and related species Cross section data for electron-impact induced elastic and inelastic channels in NCO molecule have been calculated in [221].

For the momentum transfer cross section of HCN, experimental values are available for energies below 50eV [222], while in the intermediate and high energy range theoretical data have been derived in [223]. In this system also the dissociative electron attachment channel leading to the formation of CN^- ion is of particular relevance; the corresponding cross section is experimentally determined in [224]. The ionization of HCN, as well as for CN, have been estimated by complex potential ionization contribution method in [225].

For the species H_2CN, HCN_2, HCNO, HNCO, HOCN the elastic momentum transfer cross section has been assumed equal to that of NCO or HCN, while for the CN molecule the elastic cross section of CO has been used.

As for the reactions taken into account, see Fig. 9.

$e + \mathrm{NCO}$	momentum transfer
$e + \mathrm{NCO} \to 2e + \mathrm{NCO}^+$	ionization
$e + \mathrm{HCN}$	momentum transfer
$e + \mathrm{HCN} \to \mathrm{CN}^- + \mathrm{H}$	dissociative attachment
$e + \mathrm{HCN} \to 2e + \mathrm{HCN}^+$	ionization
$e + \mathrm{CN}$	momentum transfer
$e + \mathrm{CN} \to 2e + \mathrm{CN}^+$	ionization
e+CO	momentum transfer

Figure 9: *Reactions involving electrons, NCO, HCN, CN and related species.*

CH_2O, CH_3OH and related species The momentum transfer for methanol has been obtained merging the integrated experimental differential cross section in the energy range 1-100 eV [226] with higher-energy (200-1000 eV) values found in [227]. The absolute partial cross section values for each fragmentation path

$$e + \mathrm{CH_3OH} \rightarrow \begin{cases} 2e + \mathrm{CH}_n\mathrm{O}^+ + (4-n)\mathrm{H} \\ 2e + \mathrm{CH}_n^+ + \ldots \text{ or } \mathrm{H}_n\mathrm{O}^+ + \ldots \\ 2e + \mathrm{H}^+ + \mathrm{CH_3O} \end{cases} \tag{71}$$

have been experimentally detected by a time-of-flight mass spectrometer in [228].

For e+CH_2O again the momentum transfer cross section has been reconstructed combining the low-energy (0.01-21 eV) calculations [229] with theoretical results [230] at higher energies. For the ionization the cross section in [231] has been considered.

For the species CH_2CHO, CH_2OH, CH_3CHO, CH_3CO, CHO, HCCO, CH_2CO dynamical data for electron induced processes are not available, therefore only the momentum transfer process is accounted and the corresponding cross sections are assumed equal to those of the specie CH_3OH or CH_2O.

To complete the discussion of this class of processes, also the electron-electron collisions, relevant to the efficiency of the EEDF thermalization, and the collisions of electrons with ionic species are to be considered, these processes being described in the model by Coulomb cross sections.

As for the reactions taken into account, see Fig. 10.

$$
\begin{array}{lll}
e + \mathrm{CH_3OH} & & \text{momentum transfer} \\
e + \mathrm{CH_3OH} \rightarrow & \left\{ \begin{array}{l} 2e + \mathrm{CH}_n\mathrm{O}^+ + (4-n)\mathrm{H} \\ 2e + \mathrm{CH}_n^+ + \ldots \text{or } \mathrm{H}_n\mathrm{O}^+ + \ldots \\ 2e + \mathrm{H}^+ + \mathrm{CH_3O} \end{array} \right. & \text{ionization}
\end{array}
$$

$$
\begin{array}{ll}
e + \mathrm{CH_2O} & \text{momentum transfer} \\
e + \mathrm{CH_2O} \rightarrow 2e + \mathrm{CH_2O}^+ & \text{ionization}
\end{array}
$$

Figure 10: *Reactions involving electrons, CH_2O, CH_3OH and related species.*

How σ depends on pressure, temperature and applied field The model has been used to calculate the electrical conductivity (σ) of methane/air mixture during combustion, at different values of temperature, pressure and applied electric field. Initial composition are those reported in the Section on Ansaldo combustors (Tab. 2) at the column $AE94$.

For historical reasons, σ is given in units $C \cdot cm^{-1} \cdot s^{-1} \cdot V^{-1}$; in order to obtain the value of σ in the correct SI unit $S \cdot m^{-1}$ all results should be multiplied by 100.

The first case study is characterized by E=0 Td, the pressure $P = 1$ Bar or $P = 10$ Bar and temperature between 500 K e 3000 K. The electrical conductivity time evolution, in this first study case, is reported in Fig. 11. As it can be seen, the electrical conductivity is negligible for $T \leq 1500$ K and rapidly increases with the temperature due to the increase of the exothermic reaction velocity with the temperature.

Another important aspect is the presence of the peak during σ time evolution. This behavior can be explained by taking into account that $\sigma \propto N_e \mu_e$ and the principal factor is the electron density. Combustion produces electrons, which can be partially lost as the end of the process is approached.

Time is no convenient variable to be chosen, in order to build up a model for σ. We need a more meaningful variable connected to time and σ. We have picked out the CH_4 molar fraction. Fig. 12 shows the electrical conductivity as a function of the percentage of CH_4 molar fraction ($\Delta CH_4(\%)$) consumed during the combustion in the same conditions of Fig. 11. Results show a good correlation between σ and $\Delta CH_4(\%)$, even if there is a slight correlation loss after the maximum has been achieved (right figure side). These results suggest to use a function dependent on pressure, temperature and CH_4 lost molar fraction.

Let us consider the impact of the oscillating electric field on σ. Fig. 13 displays σ as a function of time, for $T = 2000$ K and two pressure values $P = 1$ Bar e $P = 10$ Bar, in absence of electric field (E=0) and by applying different electric fields. It can be noted that there is an active contribution of the electric field over the conductivity and this effect is pronounced at lower pressure.

At the beginning, the electric field reduces the electron density, since, by increasing the electron energy, the dissociative attachment process is activated (O_2+e$\rightleftharpoons$ O^-+O). When the steady condition is achieved, the conductivity follows the applied electric field period: the peaks correspond to zero electric field, while the minima to electric filed maxima. By increasing the electric field frequency, the peak number is reduced, while the oscillation amplitude is proportional to the amplitude of the electric field. At very high field frequencies, oscillations are no more observed since sample points are not enough dense. All the electric fields are considered under the breakdown threshold, which is approximately $E/N \approx 30$ Td [188] [148] [149]. This condition is satisfied e.g. by an electric field $3 \cdot 10^4 \frac{V}{m}$, like the electric field at the antenna estimated above.

Previous results have shown that by using weak electric field, without exceeding the breakdown threshold, the field effect is small. To understand the effect of electric field frequency over electrical conductivity, Fig. 14 represents the EEDF and the electron density at time step $t = 10^{-4}$ and $P = 10$ Bar and $T = 2000$ K in the case of zero electric field (E=0) and at different electric field frequencies. The EEDF is weakly influenced by the frequency unless for $\nu_{RF} = 10^8$ Hz.

Slightly more evident is the effect of electric field frequency over electron density. Electron density decreases by increasing the frequency with a maximum change of 10%. It can be noted that the field frequency acts in a opposite way on the EEDF and on the electron density, leading to a balance. Moreover, the electron density does not decrease in a substantially way at the end of combustion process. This happens since electron are not lost with volume processes since electron density is too low to have a relevant velocity. Electron loss is general due to the interaction with the walls, but this process is not taken into account and depends on the combustion chamber geometry.

Fig. 15 shows the electric conductivity as a function of temperature at fixed pressure ($P = 1$ Bar, $P = 10$ Bar and $P = 18$ Bar) and for different residual CH_4 molar fractions. Fig. 16, instead, shows the electric conductivity as a function of temperature at fixed residual CH_4 molar fractions (χ_{CH_4}= 0.0 and 0.011) for different pressures.

Analytical expressions for n_e and σ in Ansaldo combustors Here we present the analytic expressions of n_e and σ vs. T and χ in the flame at fixed pressure and in different conditions. Three Ansaldo combustors are taken into account, namely AE94, ARI100a and ARI100b. As for the chemical composition of the gaseous mixture at the inlet and their operational conditions, we refer to Tab. 2.

We invoke the following expression:

$$f\left(\hat{\chi}, \hat{T}\right) = \sum_{i=0}^{N_\chi} \sum_{j=0}^{N_T} \alpha_{ij} \hat{\chi}^i \hat{T}^j \tag{72}$$

where $f = \ln\left(n_e\right), \ln\left(\sigma\right)$ is the natural logarithm of density or electrical conductivity. (In this Section we refer to n_e as to *density*, as a shortcut). The analytical expression are given for two different pressure values:

$$\begin{aligned} p_A &= 1 \text{ bar} \\ p_C &= 17.7 \text{ bar} \end{aligned} \tag{73}$$

in the following temperature and molar fraction intervals:

$$\begin{aligned} T &= [855.45, 2200]\text{K} \\ \chi &= [0, 1] \end{aligned} \tag{74}$$

where

$$\chi = 1 - \frac{\chi(t)}{\chi(t_0)} \tag{75}$$

and $\chi(t_0)$ is the initial methane molar fraction.

The variables $\hat{T}$ e $\hat{\chi}$ to be used in eq. 72 are scaled and centered as the following expressions:

$$\begin{aligned} \hat{T} &= \frac{T - \bar{T}}{\sigma_T} \\ \hat{\chi} &= \frac{\chi - \bar{\chi}}{\sigma_\chi} \end{aligned} \tag{76}$$

with $\bar{\chi}, \bar{T}, \sigma_\chi, \sigma_T$ average values and standard deviations.

The set of fitted coefficients for α_{ij} is reported in the following tables (3-14). Relative error is $< 10\%$.

Fig. 17 and 18 display a comparison between the analytical expressions and the results of the kinetic model for the reactor AE94 at pressure p_A.

Table 2: Composition and operative conditions for different ANSALDO reactors.

	Reactors		
Specie	AE94	ARI100a	ARI100b
O_2	$1.83\ 10^{-1}$	$1.95\ 10^{-1}$	$1.80\ 10^{-1}$
H_2	$2.98\ 10^{-7}$	$3.24\ 10^{-7}$	$2.02\ 10^{-5}$
H	$9.39\ 10^{-9}$	$1.80\ 10^{-8}$	$3.14\ 10^{-6}$
O	$7.39\ 10^{-7}$	$9.29\ 10^{-7}$	$2.82\ 10^{-5}$
OH	$3.00\ 10^{-5}$	$2.19\ 10^{-5}$	$1.42\ 10^{-4}$
H_2O	$1.75\ 10^{-2}$	$6.52\ 10^{-3}$	$1.81\ 10^{-2}$
HO_2	$1.94\ 10^{-7}$	$6.67\ 10^{-8}$	$3.06\ 10^{-6}$
H_2O_2	$1.46\ 10^{-8}$	$3.30\ 10^{-9}$	$6.84\ 10^{-8}$
C	$1.03\ 10^{-21}$	$7.43\ 10^{-23}$	$1.95\ 10^{-14}$
CH	$6.55\ 10^{-16}$	$1.01\ 10^{-17}$	$3.83\ 10^{-11}$
CH_2	$2.41\ 10^{-12}$	$1.90\ 10^{-14}$	$2.94\ 10^{-8}$
$CH_2(S)$	$2.20\ 10^{-13}$	$1.81\ 10^{-15}$	$3.07\ 10^{-9}$
CH_3	$1.18\ 10^{-9}$	$5.14\ 10^{-12}$	$3.41\ 10^{-6}$
CH_4	$3.74\ 10^{-2}$	$3.61\ 10^{-2}$	$4.57\ 10^{-2}$
CO	$1.55\ 10^{-6}$	$6.32\ 10^{-7}$	$3.34\ 10^{-4}$
CO_2	$8.73\ 10^{-3}$	$3.27\ 10^{-3}$	$8.77\ 10^{-3}$
HCO	$1.87\ 10^{-12}$	$1.14\ 10^{-14}$	$2.24\ 10^{-8}$
CH_2O	$1.12\ 10^{-9}$	$3.66\ 10^{-12}$	$2.62\ 10^{-6}$
CH_2OH	$4.97\ 10^{-13}$	$2.50\ 10^{-15}$	$4.15\ 10^{-9}$
CH_3O	$5.28\ 10^{-13}$	$1.88\ 10^{-15}$	$2.93\ 10^{-9}$
CH_3OH	$4.93\ 10^{-10}$	$7.59\ 10^{-13}$	$4.81\ 10^{-7}$
C_2H	$5.73\ 10^{-15}$	$1.36\ 10^{-16}$	$1.01\ 10^{-12}$
C_2H_2	$1.21\ 10^{-10}$	$1.35\ 10^{-12}$	$4.95\ 10^{-9}$
C_2H_3	$1.06\ 10^{-13}$	$1.07\ 10^{-15}$	$2.33\ 10^{-10}$
C_2H_4	$6.55\ 10^{-11}$	$4.01\ 10^{-13}$	$3.96\ 10^{-8}$
C_2H_5	$1.04\ 10^{-13}$	$2.51\ 10^{-16}$	$1.68\ 10^{-9}$
C_2H_6	$3.12\ 10^{-12}$	$6.24\ 10^{-15}$	$1.19\ 10^{-8}$
HCCO	$2.38\ 10^{-13}$	$4.95\ 10^{-15}$	$3.67\ 10^{-10}$
CH_2CO	$8.08\ 10^{-11}$	$7.89\ 10^{-13}$	$3.14\ 10^{-8}$

continued on next page ...

Tables and figures

. . . continued from previous page

	Reactors		
Specie	AE94	ARI100a	ARI100b
HCCOH	$4.00\ 10^{-9}$	$4.12\ 10^{-11}$	$8.62\ 10^{-10}$
N	$5.79\ 10^{-14}$	$1.14\ 10^{-13}$	$2.06\ 10^{-12}$
NH	$3.39\ 10^{-14}$	$2.38\ 10^{-14}$	$1.77\ 10^{-11}$
NH_2	$9.84\ 10^{-13}$	$9.70\ 10^{-14}$	$2.67\ 10^{-11}$
NH_3	$1.23\ 10^{-11}$	$6.73\ 10^{-13}$	$5.04\ 10^{-11}$
NNH	$3.26\ 10^{-13}$	$1.57\ 10^{-13}$	$2.48\ 10^{-11}$
NO	$5.28\ 10^{-7}$	$1.09\ 10^{-6}$	$1.33\ 10^{-6}$
NO_2	$4.66\ 10^{-9}$	$4.33\ 10^{-9}$	$1.08\ 10^{-8}$
N_2O	$9.45\ 10^{-8}$	$2.11\ 10^{-8}$	$3.76\ 10^{-7}$
HNO	$1.11\ 10^{-12}$	$1.85\ 10^{-12}$	$4.83\ 10^{-11}$
CN	$3.21\ 10^{-16}$	$3.70\ 10^{-17}$	$1.57\ 10^{-13}$
HCN	$7.43\ 10^{-12}$	$4.26\ 10^{-13}$	$8.44\ 10^{-10}$
H_2CN	$3.62\ 10^{-18}$	$9.02\ 10^{-20}$	$1.25\ 10^{-14}$
HCNN	$1.55\ 10^{-17}$	$5.08\ 10^{-20}$	$2.73\ 10^{-13}$
HCNO	$7.22\ 10^{-10}$	$1.05\ 10^{-10}$	$1.42\ 10^{-9}$
HOCN	$6.30\ 10^{-11}$	$2.72\ 10^{-12}$	$5.87\ 10^{-11}$
HNCO	$9.13\ 10^{-11}$	$8.96\ 10^{-12}$	$3.42\ 10^{-9}$
NCO	$4.59\ 10^{-13}$	$8.07\ 10^{-14}$	$9.18\ 10^{-11}$
N_2	$7.54\ 10^{-1}$	$7.59\ 10^{-1}$	$7.46\ 10^{-1}$
C_3H_7	$1.09\ 10^{-17}$	$1.10\ 10^{-19}$	$9.89\ 10^{-14}$
C_3H_8	$1.97\ 10^{-15}$	$1.56\ 10^{-17}$	$4.78\ 10^{-12}$
CH_2CHO	$3.42\ 10^{-14}$	$1.80\ 10^{-16}$	$8.33\ 10^{-11}$
CH_3CHO	$6.74\ 10^{-13}$	$1.18\ 10^{-14}$	$4.84\ 10^{-9}$

continued on next page . . .

. . . continued from previous page

Missing specie in GRIMECH3.0			
	Reactors		
Specie	AE94	ARI100a	ARI100b
C_2	0.0	0.0	0.0
N^+	0.0	0.0	0.0
O_2^+	0.0	0.0	0.0
O^+	0.0	0.0	0.0
H_3O^+	0.0	0.0	0.0
HCO^+	0.0	0.0	0.0
O^-	0.0	0.0	0.0
O_2^-	0.0	0.0	0.0
$C_3H_3^+$	0.0	0.0	0.0
$C_3H_3O^+$	0.0	0.0	0.0
CH_3^+	0.0	0.0	0.0
$C_2H_3O^+$	0.0	0.0	0.0
N_2^+	10^{-15}	10^{-15}	10^{-15}
El	10^{-15}	10^{-15}	10^{-15}
Operative conditions at the reactor entrance			
T [K]	882.55	856.07	975.11
P [Bar]	17.7	4.30	4.30
$\dot{m}$ [kg/s]	28.2	$2.03\ 10^{-2}$	$1.21\ 10^{-1}$

Table 3: α_{ij} coefficients for calculating the density in the reactor AE94 by means of eq. 72 at pressure p_A with $\hat{\chi} = 0.5001, \hat{T} = 1705, \sigma_\chi = 0.3038, \sigma_T = 300.7$.

	i=0	i=1	i=2	i=3
j=0	16.98	3.583	-0.2292	0.4993
j=1	3.675	0.4123	-0.8537	-
j=2	-0.6004	-0.4642	-	-
j=3	-0.0229	-	-	-

Table 4: α_{ij} coefficients for calculating electrical conductivity in the reactor AE94 by means of eq. 72 at pressure p_A with $\hat{\chi} = 0.5001, \hat{T} = 1705, \sigma_\chi = 0.3038, \sigma_T = 300.7$.

	i=0	i=1	i=2	i=3
j=0	-16.99	3.526	-0.2159	0.4933
j=1	3.807	0.4145	-0.8503	-
j=2	-0.6139	-0.4648	-	-
j=3	-0.02131	-	-	-

Table 5: α_{ij} coefficients for calculating the density in the reactor AE94 by means of eq. 72 at pressure p_C with $\hat{\chi} = 0.499, \hat{T} = 1705, \sigma_\chi = 0.3031, \sigma_T = 300.7$.

	i=0	i=1	i=2	i=3
j=0	16.71	2.721	-0.2026	0.2715
j=1	4.926	1.317	-0.4925	-
j=2	0.1076	-0.4859	-	-
j=3	-0.4761	-	-	-

Table 6: α_{ij} coefficients for calculating electrical conductivity in the reactor AE94 by means of eq. 72 at pressure p_C with $\hat{\chi} = 0.499, \hat{T} = 1705, \sigma_\chi = 0.3031, \sigma_T = 300.7$.

	i=0	i=1	i=2	i=3
j=0	-18.02	3.487	-0.1642	0.418
j=1	4.328	0.8982	-0.6677	-
j=2	-0.5365	-0.7205	-	-
j=3	-0.1354	-	-	-

Table 7: α_{ij} coefficients for calculating the density in the reactor ARI100a by means of eq. 72 at pressure p_A with $\hat{\chi} = 0.5001, \hat{T} = 1705, \sigma_\chi = 0.3038, \sigma_T = 300.7$.

	i=0	i=1	i=2	i=3
j=0	16.94	3.463	-0.2749	0.4984
j=1	3.483	0.4244	-0.8048	-
j=2	-0.6021	-0.4318	-	-
j=3	0.006091	-	-	-

Table 8: α_{ij} coefficients for calculating electrical conductivity in the reactor ARI100a by means of eq. 72 at pressure p_A with $\hat{\chi} = 0.4986, \hat{T} = 1705, \sigma_\chi = 0.3029, \sigma_T = 300.7$.

	i=0	i=1	i=2	i=3
j=0	-17	3.406	-0.2606	0.4922
j=1	3.613	0.4264	-0.801	-
j=2	-0.6152	-0.4326	-	-
j=3	0.007697	-	-	-

Table 9: α_{ij} coefficients for calculating the density in the reactor ARI100a by means of eq. 72 at pressure p_C with $\hat{\chi} = 0.4989, \hat{T} = 1705, \sigma_\chi = 0.3031, \sigma_T = 300.7$.

	i=0	i=1	i=2	i=3
j=0	16.68	2.634	-0.2236	0.2709
j=1	4.867	1.304	-0.485	-
j=2	0.09674	-0.4572	-	-
j=3	-0.4747	-	-	-

Table 10: α_{ij} coefficients for calculating electrical conductivity in the reactor ARI100a by means of eq. 72 at pressure p_C with $\hat{\chi} = 0.4989, \hat{T} = 1705, \sigma_\chi = 0.3031, \sigma_T = 300.7$.

	i=0	i=1	i=2	i=3
j=0	-20.14	2.573	-0.2114	0.265
j=1	4.994	1.306	-0.4808	-
j=2	0.08434	-0.4573	-	-
j=3	-0.4727	-	-	-

Table 11: α_{ij} coefficients for calculating the density in the reactor ARI100b by means of eq. 72 at pressure p_A with $\hat{\chi} = 0.5001, \hat{T} = 1705, \sigma_\chi = 0.3038, \sigma_T = 300.7$.

	i=0	i=1	i=2	i=3
j=0	16.93	3.63	-0.1207	0.5464
j=1	3.835	0.4008	-0.8895	-
j=2	-0.5551	-0.4833	-	-
j=3	-0.05881	-	-	-

Table 12: α_{ij} coefficients for calculating electrical conductivity in the reactor ARI100b by means of eq. 72 at pressure p_A with $\hat{\chi} = 0.5001, \hat{T} = 1705, \sigma_\chi = 0.3038, \sigma_T = 300.7$.

	i=0	i=1	i=2	i=3
j=0	-17.06	3.57	-0.1001	0.5324
j=1	3.971	0.4051	-0.8881	-
j=2	-0.5687	-0.4834	-	-
j=3	-0.05721	-	-	-

Table 13: α_{ij} coefficients for calculating the density in the reactor ARI100b by means of eq. 72 at pressure p_C with $\hat{\chi} = 0.4986, \hat{T} = 1705, \sigma_\chi = 0.3029, \sigma_T = 300.7$.

	i=0	i=1	i=2	i=3
j=0	16.77	2.803	-0.1464	0.2971
j=1	4.92	1.324	-0.4879	-
j=2	0.1094	-0.5209	-	-
j=3	-0.4587	-	-	-

Table 14: α_{ij} coefficients for calculating electrical conductivity in the reactor ARI100b by means of eq. 72 at pressure p_C with $\hat{\chi} = 0.4986, \hat{T} = 1705, \sigma_\chi = 0.3029, \sigma_T = 300.7$.

	i=0	i=1	i=2	i=3
j=0	-20.09	2.736	-0.1286	0.2844
j=1	5.052	1.328	-0.4861	-
j=2	0.09627	-0.5202	-	-
j=3	-0.4565	-	-	-

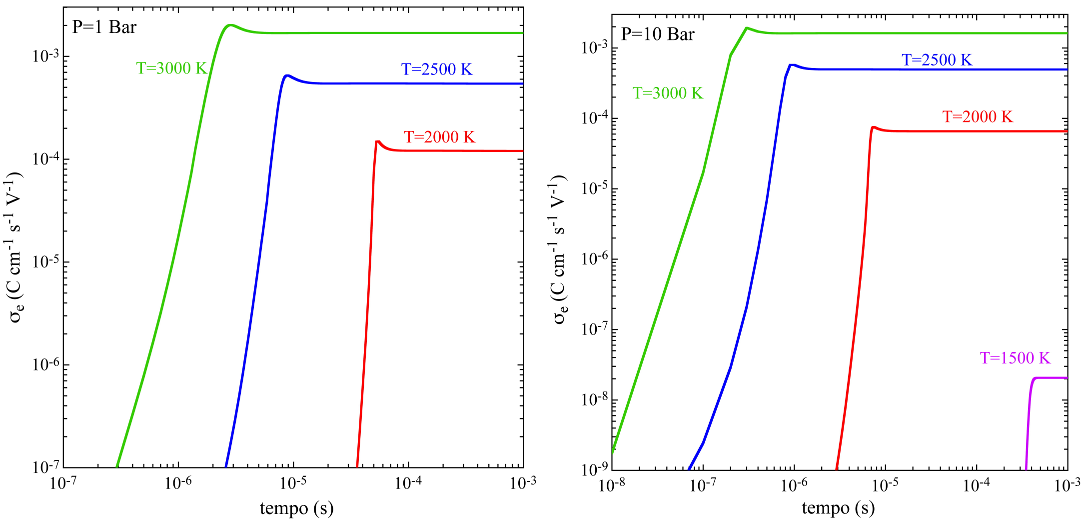

Figure 11: *Time evolution of the electrical conductivity at different temperature values [500-3000] K and pressure ($P = 1$ Bar and $P = 10$ Bar) with electric field E=0 Td.*

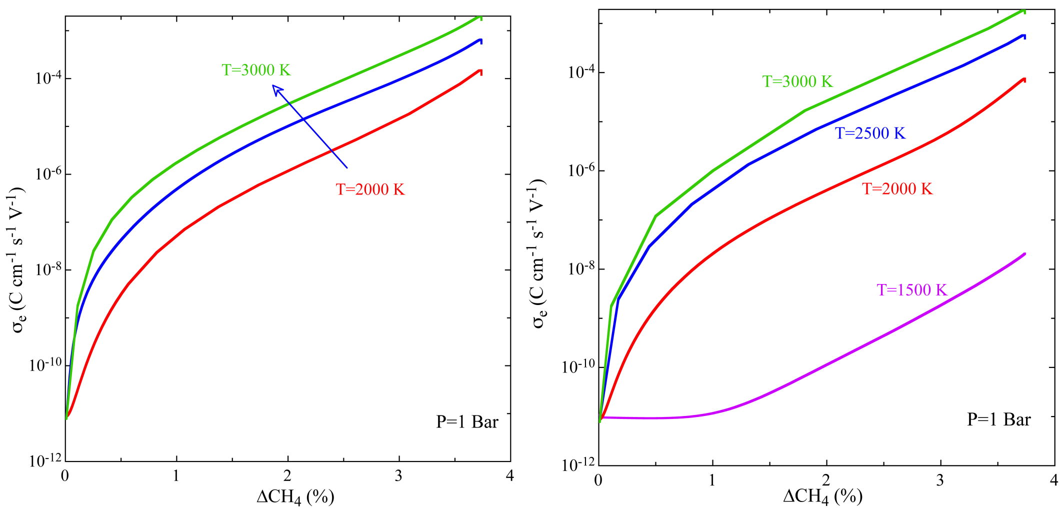

Figure 12: *Electric conductivity as a function of the percentage of CH_4 molar fraction loss for different pressures ($P = 1$ Bar e $P = 10$ Bar) and for different temperature values.*

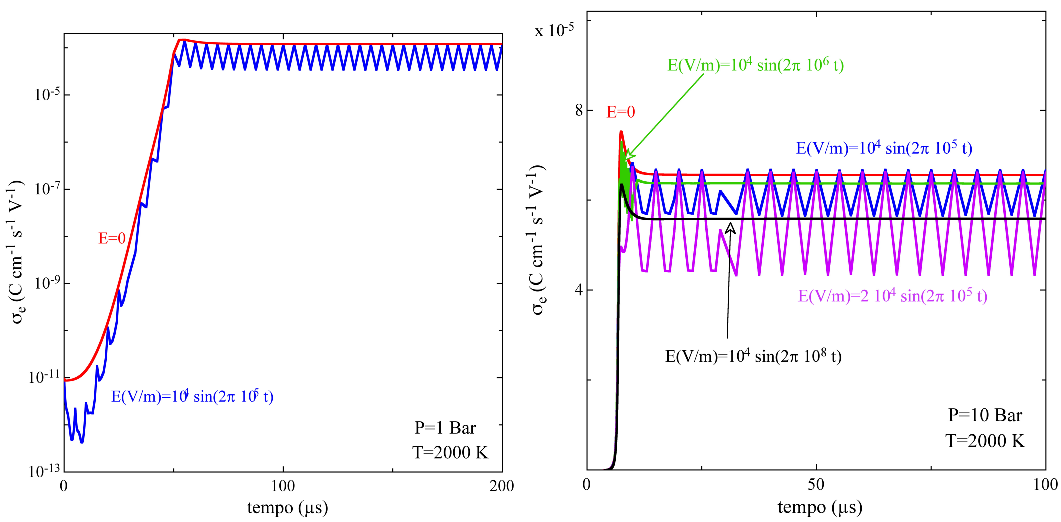

Figure 13: *Electric conductivity as a function of time for different electric field frequencies and amplitude in the case for $T = 2000$ K and for two different pressure values $P = 1$ Bar and $P = 10$ Bar.*

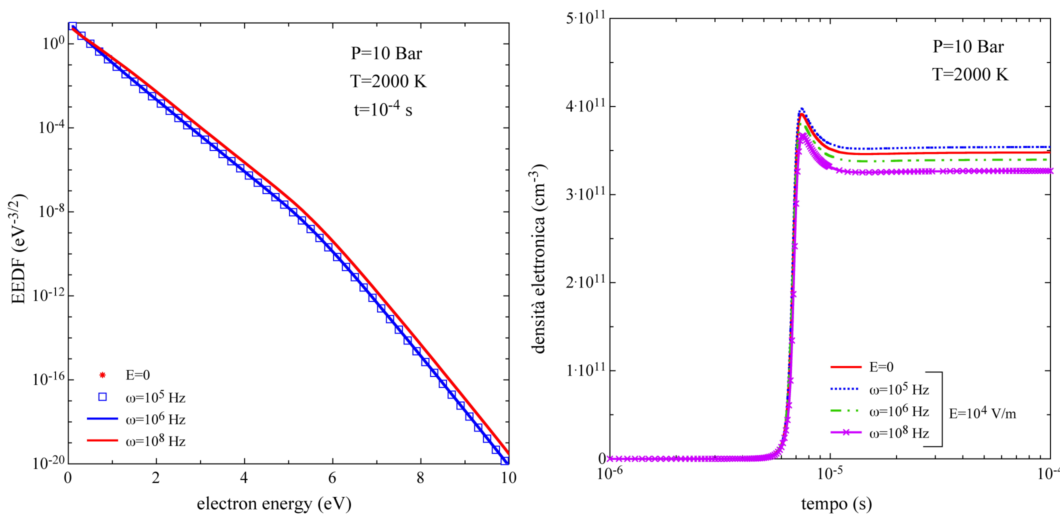

Figure 14: *EEDF and electron density at $t = 10^{-4}$ s as a function of time for different values of electric field frequencies (ν_{RF}) and for $E = 10^4$ V/m for $P = 10$ Bar and $T = 2000$ K.*

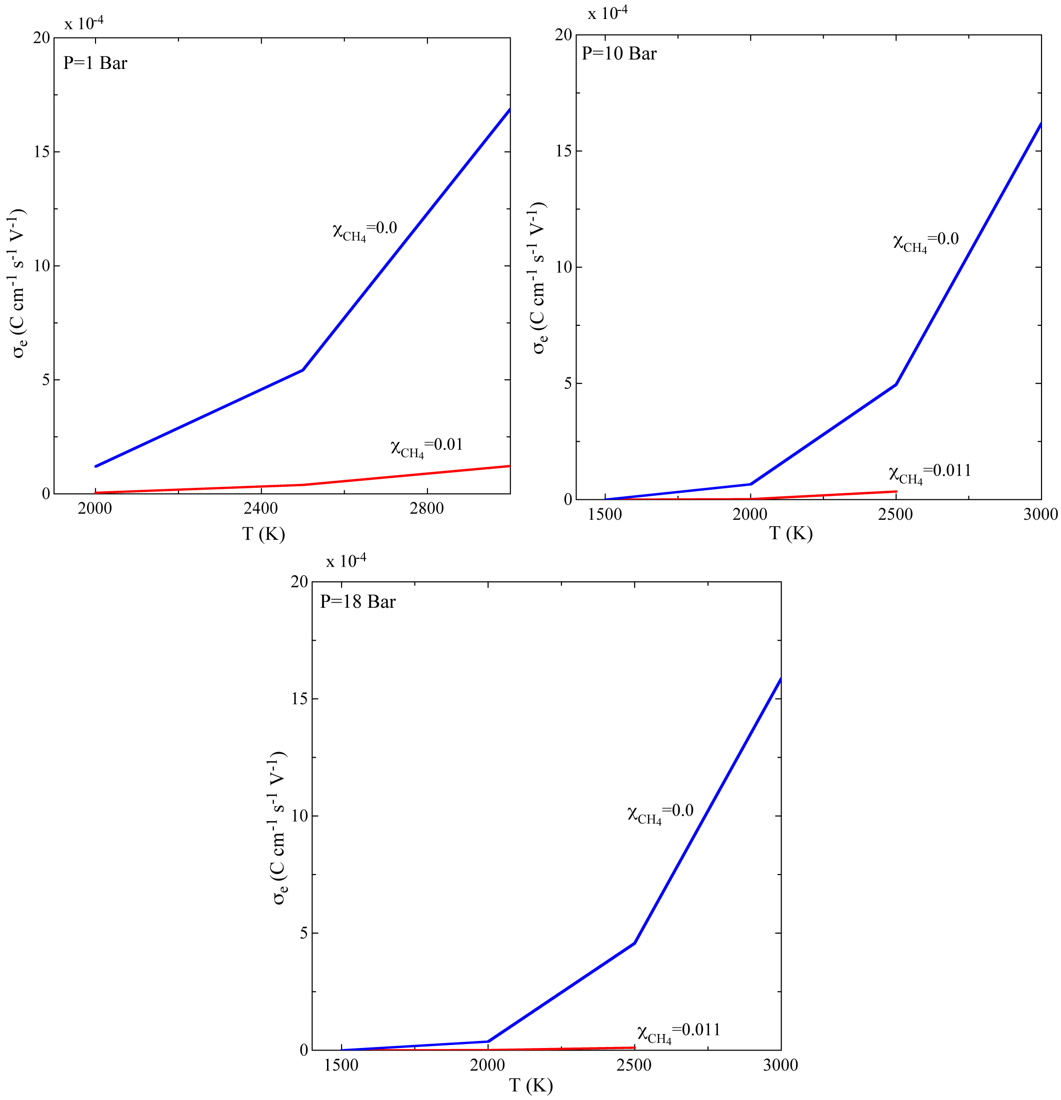

Figure 15: *Electric conductivity as a function of temperature at different pressures ($P = 1$ Bar, $P = 10$ Bar and $P = 18$ Bar) for two different values of residual CH_4 molar fractions.*

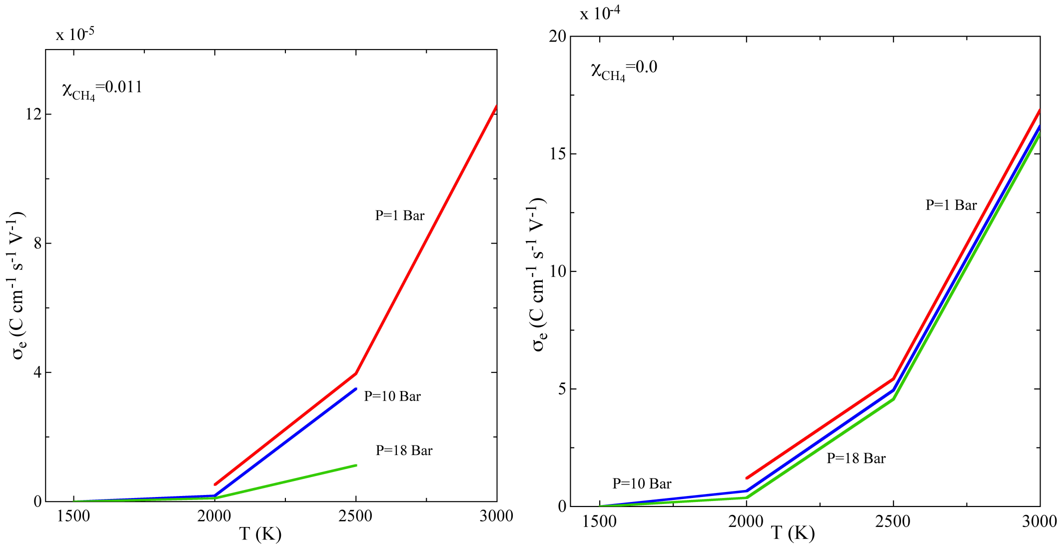

Figure 16: *Electric conductivity as a function of temperature at fixed values of residual CH_4 molar fractions (χ_{CH_4}= 0.0 and 0.011) and for different pressure values ($P = 1$ Bar, $P = 10$ Bar e $P = 18$ Bar).*

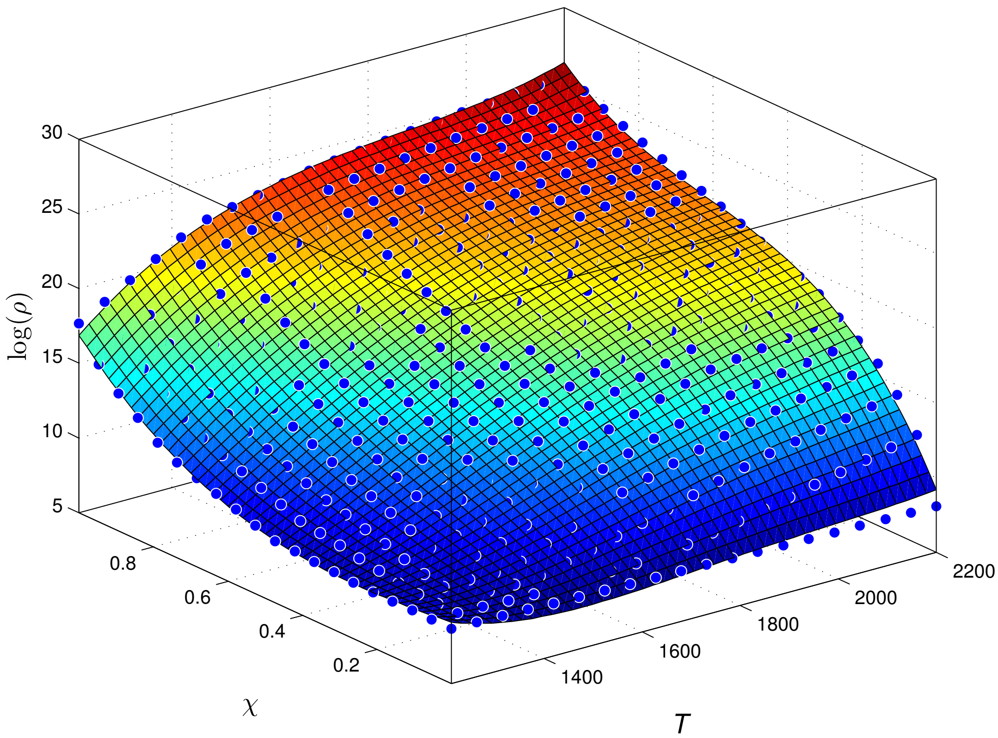

Figure 17: *Natural logarithm of density (points) and corresponding analytical values (surface) at pressure p_A in the reactor AE94.*

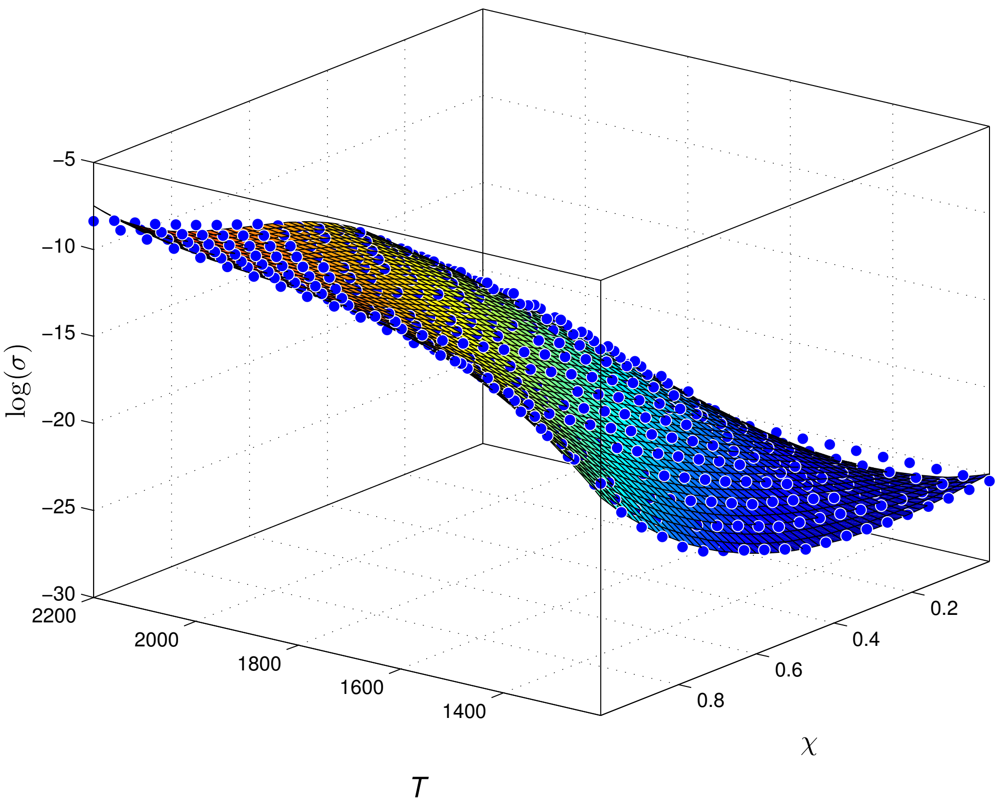

Figure 18: *Natural logarithm of the electrical conductivity (points) in the flame and corresponding analytical values (surface) at pressure p_A in the reactor AE94.*